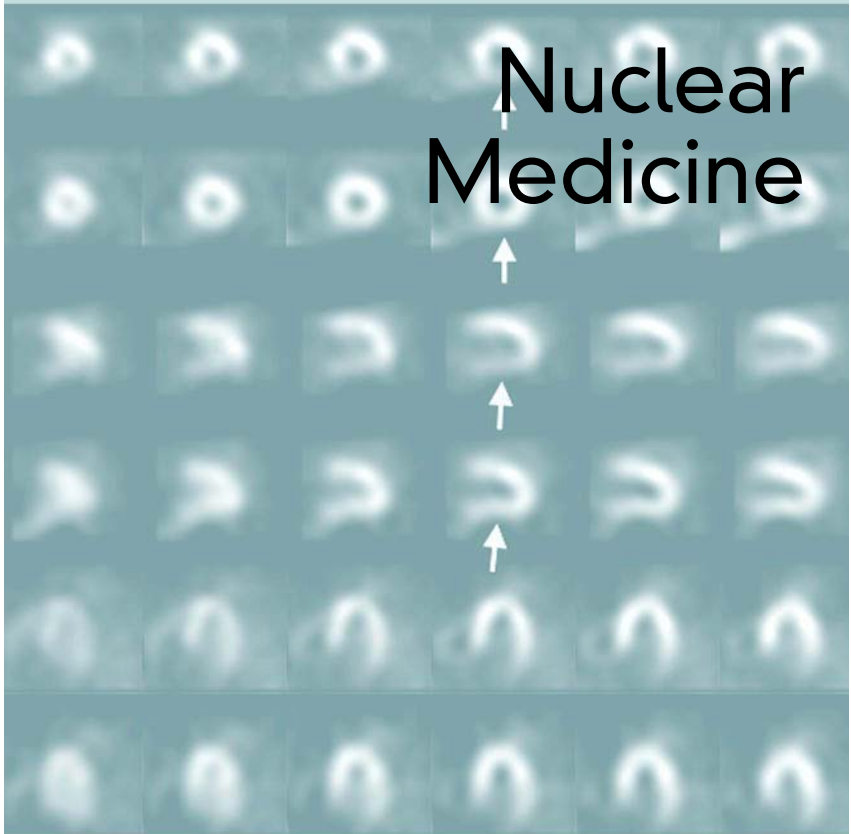# Nuclear Medicine

William D. Leslie
I. David Greenberg

Nuclear Medicine

William D. Leslie, MD, FRCPC, ABNM, MSc
University of Manitoba
Winnipeg, Manitoba, Canada

I. David Greenberg, MDCM, FRCPC, ABR, ABNM
University of Manitoba
Winnipeg, Manitoba, Canada

VADEMECUM
Nuclear Medicine
LANDES BIOSCIENCE
Georgetown, Texas U.S.A.

Library of Congress Cataloging-in-Publication Data

Contents

Editors

William D. Leslie, MD, FRCPC, ABNM, MSc
Associate Professor of Medicine and Radiology
University of Manitoba
Winnipeg, Manitoba, Canada
Chapters 6 and 12

I. David Greenberg, MDCM, FRCPC, ABR, ABNM
Associate Professor of Radiology
University of Manitoba
Winnipeg, Manitoba, Canada
Chapters 3 and 4

Contributors

Keevin Bernstein
Associate Professor of Medicine
University of Manitoba
Winnipeg, Manitoba, Canada
Chapter 9

Ford Bursey
Associate Professor of Medicine
Memorial University of Newfoundland
St. John's, Newfoundland, Canada
Chapter 10

Anna Celler
Medical Imaging Research Group
Nuclear Medicine
University of British Columbia
Vancouver, British Columbia, Canada
Chapter 1

Michael J. Chamberlain
Professor of Radiology
University of Ottawa
Ottawa, Ontario, Canada
Chapter 2

Robert Corne
Associate Professor of Medicine
  and Radiology
University of Manitoba
Winnipeg, Manitoba, Canada
Chapters 3 and 4

Albert A. Driedger
Professor of Nuclear Medicine
  and Oncology
University of Western Ontario
London, Ontario, Canada
Chapters 13 and 14

David Gilday
Professor of Radiology
University of Toronto
Chapter 17

Peter Hollett
Professor of Radiology
Memorial University of Newfoundland
St. John's, Newfoundland, Canada
Chapter 10

Michael Hoskinson
Nuclear Medicine
University of Alberta
Edmonton, Alberta, Canada
Chapter 9

Catherine Kissel
Associate Professor of Medicine
Université de Montreal
Montreal, Quebec, Canada
Chapter 16

Reinhard Kloiber
Clinical Professor of Radiology
University of Calgary
Calgary, Alberta, Canada
Chapter 11

Denis Lacroix
Assistant Professor of Psychiatry
Université de Montreal
Montreal, Quebec, Canada
Chapter 16

Brian Lentle
Emeritus Professor
Radiology
University of British Columbia
Vancouver, British Columbia, Canada
Chapter 1

Peter MacDonald
Associate Professor of Orthopedic Surgery
University of Manitoba
Winnipeg, Manitoba, Canada
Chapter 7

Gary R. May
Clinical Associate Professor of Medicine
University of Calgary
Calgary, Alberta, Canada
Chapter 11

Thomas J. McDonald
Professor of Medicine
University of Western Ontario
London, Ontario, Canada
Chapters 13 and 14

A. J. B. McEwan
Professor, Department of Oncology
University of Alberta
Edmonton, Alberta, Canada
Chapter 15

Pierre Plourde
Associate Professor of Medical
  Microbiology
University of Manitoba
Winnipeg, Manitoba, Canada
Chapter 12

Bruce E. Roe
Associate Professor of Medicine
University of Manitoba
Winnipeg, Manitoba, Canada
Chapter 6

Leonard Rosenthall
Professor of Radiology
McGill University
Montreal, Quebec, Canada
Chapter 7, 8

Jean-Paul Soucy
Professor of Nuclear Medicine
University of Ottawa
Ottawa, Ontario, Canada
Chapter 16

Philip S. Wells
Medicine
University of Ottawa
Ottawa, Ontario, Canada
Chapter 5

Ralph Wong
Assistant Professor of Hematology
  and Oncology
University of Manitoba
Winnipeg, Manitoba, Canada
Chapter 8

Daniel F. Worsley
Assistant Professor of Radiology
University of British Columbia
Vancouver, BC, Canada
Chapter 5

Preface

> "*The expert at anything was once a beginner.*"
> -Hayes

In an era of spectacular medical advances, it is easy to become immune to the announcement of new "breakthroughs". This in no way lessens the remarkable achievements of diagnostic imaging over the last few years in which the field of Nuclear Medicine has shared. To the outsider the specialty of Nuclear Medicine can appear confusing and esoteric since it operates in a world of invisible radioactive emissions, nuclear decay charts and obscure elements. In reality, the distance from the cyclotron to the bedside is a short one and this young specialty has matured and been integrated into many aspects of patient care. In fact, the array of agents and techniques that can be used for diagnosis and therapy is so broad that only the most commonly used and widely available can be covered in this handbook. The material covers traditional aspects of Nuclear Medicine as well as the newest advances in the field. In this handbook, the role of Nuclear Medicine techniques in diagnosis and treatment is presented in conjunction with the essential elements of radiopharmacology, instrumentation and radiation protection. This handbook is not intended to be as comprehensive as a nuclear medicine textbook but will provide a more thorough presentation of the specialty than is afforded when it shares the stage with other diagnostic imaging modalities. It was designed to be a practical and accessible handbook for trainees in both imaging and clinical sciences.

Junior physicians and trainees will learn how to take this imaging science and apply it to the real-life problems encountered in clinical medicine. Most clinical chapters are jointly authored by a Nuclear Medicine specialist and an experienced clinician, an approach that is unique among Nuclear Medicine texts. The individuals selected are clinical practitioners, not ivory tower researchers, which gives them a firsthand appreciation of the challenges of clinical medicine. For readers that find that they have a thirst to learn more about Nuclear Medicine, this handbook will serve as a guide to the specialty and to more comprehensive textbooks listed below. Perhaps others will be stimulated to consider Nuclear Medicine as an exciting career opportunity. Certainly the future is bright for a specialty that has come so far in so short a time.

William D. Leslie
I. David Greenberg

Comprehensive References

1. Harbert JC, Eckelman WC, Neumann RD, eds. Nuclear Medicine Diagnosis and Therapy. New York: Thieme Medical Publishers, Inc., 1996.
2. Wagner HN, Szabo Z, Buchanan JW, eds. Principles of Nuclear Medicine. Second Ed. Philadelphia: W.B. Saunders Company, 1995.
3. Murray ICP, Ell PJ, Strauss HW, eds. Nuclear Medicine in Clinical Diagnosis and Treatment. Second Ed. Edinburgh: Churchill Livingstone, 1994.
4. Sandler MP, Patton JA, Coleman RE, Gottschalk A, Wachers FJT, Hoffer P. Diagnostic Nuclear Medicine. Third Ed. Baltimore: Williams & Wilkins, 1996.
5. Henkin RE, Boles MA, Dillehay GL, Halama JR, Karesh SM, Wagner RH et al, eds. Nuclear Medicine. St. Louis: Mosby, 1996.

An Introduction to Nuclear Medicine

Brian Lentle and Anna Celler

Introduction

Nuclear medicine is defined as that medical specialty concerned with the use of unsealed sources of radiation in the diagnosis and treatment of disease.

Disease usually begins as disordered function. While an exception to this might be trauma, many accidents also may be due to altered behavior. Thus altered function often anticipates structural or morphological change by months or even years. Other techniques used in diagnostic imaging (e.g., radiography, computed tomography [CT] and magnetic resonance imaging [MRI]) largely focus on the identification of disordered structure although with the emergence of advanced MRI methods this is beginning to change. The power of nuclear medicine in clinical diagnosis rests with its ability to detect altered function with great sensitivity. For this reason nuclear medicine has contributed not only to clinical diagnosis but, to a degree unmatched by other imaging methods, to an understanding of disease mechanisms.

History

Modern clinical radiology began with one seminal event, namely Wilhelm Röntgen's discovery of X-rays in November 1895. Nuclear medicine had not one but many parents. Bequerel discovered radioactivity in early 1896. Both of these discoveries were serendipitous. Röntgen, a German physicist, was experimenting in his laboratory in Würzburg. While working with cathode-ray tubes in a darkened room he noticed, by chance, fluorescence at a distance. He went on to discover that this fluorescence was caused by penetrating, but hitherto undiscovered, radiations from the cathode-ray tubes. He called these X-rays, using the algebraic symbol "x" for an unknown. Before the end of that year Röntgen had used the new rays to image the internal structure of the body—the bones of his wife's hand.

Subsequently Henri Becquerel (Fig. 1) discovered natural radioactivity in February 1896. The story has it that he placed lumps of pitchblende on sealed photographic film in sunlight, intent on finding out if the rays of the sun induced any penetrating fluorescence in the mineral. By chance, on developing the film after a cloudy day he was surprised to find as much blackening of the photographic emulsion as had occurred in bright sunlight. He realized that the pitchblende itself was a source of the energetic rays.

Later Mme. (Dr.) Marie and Dr. Pierre Curie working in Paris described natural radioactivity and discovered radium. Subsequently Mme. (Dr.) Irène Curie was to observe the artificial induction of radioactivity. Rutherford, a British-educated, New Zealand physicist working at McGill University in Montreal went on to discover the structure of the atom. All won Nobel prizes—Becquerel and Curie jointly.
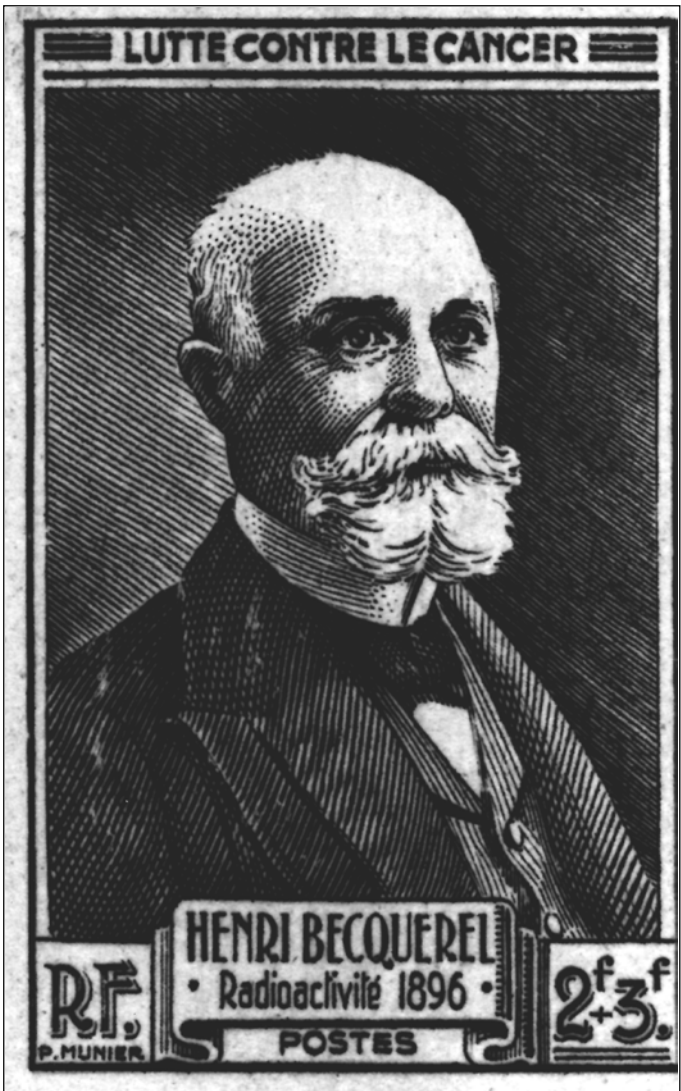
Figure 1. A stamp commemorating Becquerel's discovery of radioactivity for which he received a Nobel Prize.

Another important insight came when a Hungarian scientist—George de Hevesy (a former student of Rutherford)—first used the tracer principle (Fig. 2). He experimented with a plant having its roots in a water bath containing a radioactive isotope of lead. Hevesy was able to follow the rate of passage of the tracer through
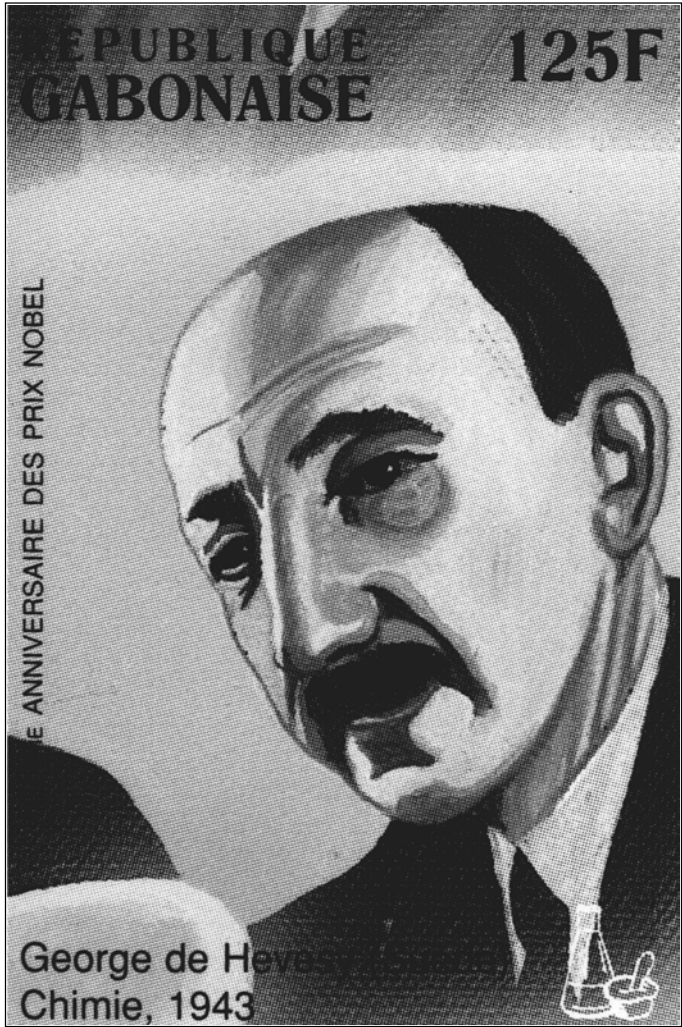
Figure 2. A stamp celebrating the anniversary of the Nobel Prize awarded to de Hevesy for the discovery of the tracer principle.

the stem of the plant with an instrument capable of detecting and measuring radioactivity. This use of radioactive atoms, present in minute amounts but acting as a marker of other, non-radioactive atoms came to be called the tracer principle. It only required that Hevesy's insight be translated to people instead of plants, and for the tracer to be administered by injection instead of through a plant's root system, for the power of nuclear medicine to become clear.

Without a capacity to image the distribution of radiotracers in the body, however, there might be little to remark upon concerning the importance of nuclear medicine. Dr. Benedict Cassen developed the first rectilinear scanner to image tracers by virtue of the gamma rays they emit. This was followed by the development of the gamma camera, able to image both static and changing distributions of radioactive tracers in the body, by Dr. Hal Anger. He, Dr. David Kuhl and others went on to develop the concept of tomographic sectional imaging in nuclear medicine.

Nuclear medicine, while beginning in the late nineteenth century, gained momentum through the twentieth. Medicine in the twenty-first century will continue to be fundamentally changed by the insights it provides.

Comparative imaging and the Role of Nuclear Medicine

Classical radiology had been rooted in studies of structure. That is changing as physiological images and sometimes measurements are being made with CT and, especially, functional MRI and spectroscopy. Nevertheless, from first principles it will be difficult to match the power of nuclear medicine in, for example, detecting receptor binding.

Another decisive advantage of nuclear medicine is its capacity to be used in whole body imaging. The idea of whole body MRI "screening" has been mooted but its value is speculative and it would be expensive. In contrast, nuclear medicine body imaging is unsurpassed in the search for disease not causing local symptoms, such as metastatic tumor spread or occult infections.

As we have seen, the first technique which allowed us to "see" the inside of the human body was X-ray imaging. Very soon, however, it was followed by other techniques such as nuclear medicine, ultrasound (US), CT and, more recently, MRI. In order to realize the possibilities and limitations of each technique and to better understand their place in the diagnostic process it is important to consider the physical process that each modality employs. In differing degrees most methods are capable of anatomical and functional imaging and almost all techniques can examine both when special contrast agents or other modifications are used.

Attenuation of electromagnetic radiation (which depends on the electron density of the material) is the physical principle used in X-ray imaging or CT. The resulting images represent differences in transmission of the X-rays (a form of electromagnetic radiation) or, indirectly, differences in their attenuation by tissues and, thereby, the anatomy of the subject. If a special contrast agent is introduced any images made will reflect the distribution of this agent and such images may depict a particular organ's function. Similarly, from the physical point of view, US measures sound wave transmission and reflection in the body and MRI is sensitive to body water contents because hydrogen atoms in water molecules are responsible for the majority of the magnetic signal detected by MRI. Again, in both situations, the images display more particularly the anatomy, not function. Recently developed functional MRI (fMRI), however, is sensitive to the flow of the blood in the body while doppler US can additionally measure the movement, for example of blood, within an imaged organ.

Nuclear medicine, by contrast, is a technique that is intrinsically functional because it measures radiation emitted by a tracer which has been introduced into a patient's body, usually by injection, and for which the location and concentration are directly

related to the function of an organ. The term "nuclear medicine" encompasses several different imaging techniques ranging from positron emission tomography (PET) and single photon emission computed tomography (SPECT) through whole body planar images or "scans."

There are several ways in which the analysis of nuclear medicine data can be done ranging from a simple and qualitative visual inspection of planar images up to a full numerical and quantitative analysis of the three- or even four-dimensional (including temporal) data sets. Creation of these quantitative images is quite complex and usually requires application of several corrections to the data (attenuation, scatter, normalization, for example) as well as iterative reconstruction methods. Also the use of quantitative analytical methods usually involves kinetic modeling and sophisticated computer-based operations. The information obtained from such analyses can be directly related, however, to physiological processes and may provide a very useful and comprehensive picture of a disease. At present this type of data analysis is available mostly in centers with strong research programs because only the most advanced nuclear medicine systems using modern image reconstruction techniques are able to realize fully quantitative data. Therefore, diagnostic applications of this approach remain in development.

The relative sensitivities of PET and MRI for the detection of metabolic changes in vivo are such that PET can detect concentrations of metabolites several orders of magnitude smaller than those detectable with MRI. Thus, while functional and anatomic imaging are converging, the methods each have strengths and weaknesses which suggest that both will have a role to play in the future. Indeed there is growing interest not only in fusing anatomical and functional images but also in obtaining such images with hybrid technology combining, for example, PET and CT.

Radionuclide production

Radioactive atoms (radionuclides) are fundamental to the tracer principle. Thus their production is an important step in the clinical practice of nuclear medicine.

The radionuclides used in imaging usually emit gamma (γ) rays. Occasionally a particle is emitted as well. X-rays and γ-rays are both part of the electromagnetic spectrum. Visible light, radiowaves and microwaves are also part of this spectrum. However, X-rays and γ-rays are of short wavelength and thus are energetic and can penetrate tissues. The penetrating power of X-rays and γ-rays is a function of their energy usually measured in electron volts—the gamma rays from technetium-99m are of 140 thousand electron volts (140 keV). While γ-rays are in general more energetic than X-rays the real distinction between them stems from their origins: γ-rays are produced in nuclear decay processes whereas X-rays derive from orbital electron perturbations produced, for example, by electrons accelerated in an X-ray tube.

Radionuclides may be created by one or other of the following methods.

Cyclotron Irradiation

Radionuclides may be made by irradiation of stable atoms with cyclotron-accelerated particles—usually protons. This method of production is especially important for those radioactive atoms used in PET since these usually have very short half-lives and must be manufactured where they are to be used. The reaction
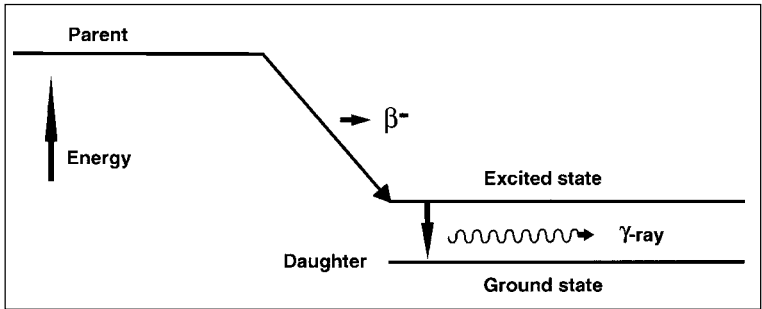
Figure 3. Beta-minus decay with the emission of a γ-ray (iodine-131 decays in this way).

can be represented as follows, where the oxygen atom is stable, *p* is the accelerated proton, *n* is the neutron produced and fluorine-18 is the resulting tracer (half-life about 2 hours):

$$^{18}O + p = {}^{18}F + n$$
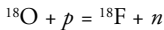
In this reaction oxygen has eight protons and fluorine nine in the respective nuclei. The superscripts used throughout this volume refer to the atomic mass of the atom, essentially the sum of the protons and neutrons in the atomic nucleus since electrons and other particles have negligible mass.

Reactor Irradiation

Atomic nuclei may be made radioactive by the flux of neutrons in a nuclear reactor or from the fission of heavier atoms. Molybdenum, for example, may be made by either of the following reactions:

$^{98}Mo \; (n, \gamma) \rightarrow {}^{99}Mo$ (low specific-activity)

$^{235}U \; (n, \text{fission}) \rightarrow {}^{99}Mo$ (high specific activity)
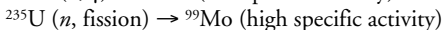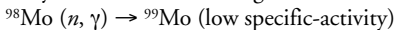
In these reactions *n* stands for a neutron and γ for a gamma ray. Specific activity is a measure of the fraction of radioactive atoms present of the total in the sample—important to consider in the preparation of some radiopharmaceuticals.

Reactor produced atoms are often rich in neutrons and thus decay by β⁻ emissions (e.g., iodine-131) (Fig. 3). β⁻ particles (energetic electrons) give large local radiation doses which may be destructive. This may make them important in therapy as in the use of radioactive iodine to treat Graves' disease and thyroid cancer.

Generator Production

A common strategy in nuclear medicine practice is to take delivery, at a hospital or clinic, of a generator containing a long-lived precursor of a short-lived daughter isotope. The precursor may be made in either a reactor or cyclotron. Molybdenum-99/technetium-99m generators (Fig. 4) are very widely used in nuclear medicine, the molybdenum most often being reactor produced. Technetium-99m has many useful features (short half-life, no particulate emissions to cause large radiation exposures to patients and a γ-ray energy ideal for gamma-camera detection) and is
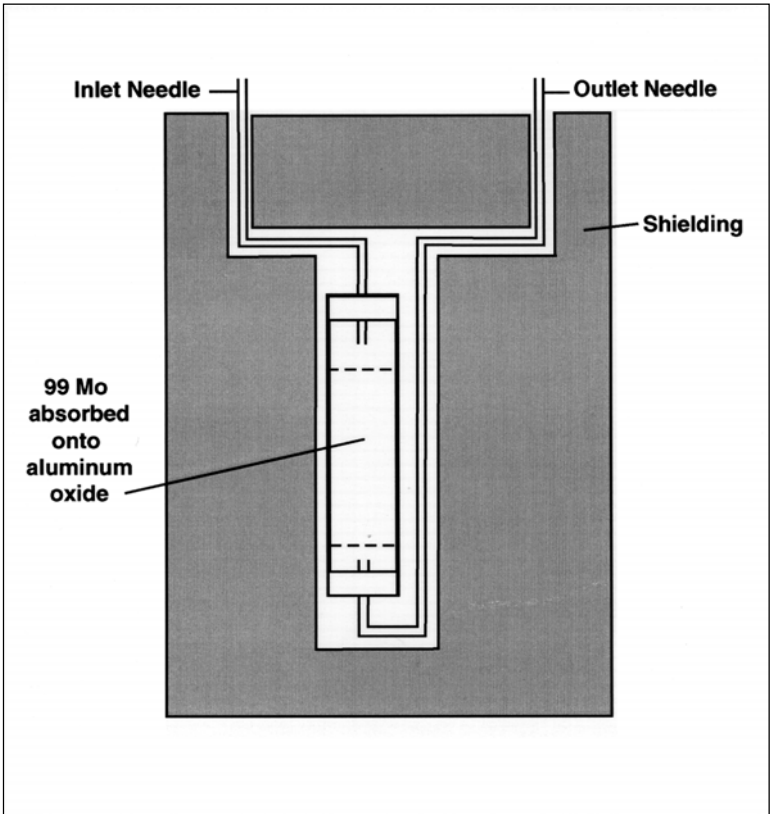
Figure 4. A section through a generator (diagrammatic). Saline is introduced through the inlet needle and extracted at the outlet needle containing technetium-99m as sodium pertechnetate. The technetium-99m is not absorbed on the aluminum oxide as is the molybdenum-99.

more widely used than any other radionuclide at present. Yet with a half-life of about six hours it would not be readily available on the scale on which it is used were it not for its availability from a generator. The generator contains a long-lived molybdenum-99 parent absorbed onto a column and, as this radionuclide decays, technetium (which being different chemically is not so absorbed) is eluted (milked) from the column in the generator on a daily or twice-daily basis. The molybdenum decays as follows:

$$^{99}Mo \rightarrow {}^{99m}Tc + \beta^- + \overline{\nu}$$
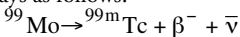
and the technetium used in preparing the radiotracer then decays as follows (Fig. 5):

$$^{99m}Tc \rightarrow {}^{99}Tc + \gamma$$
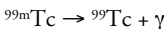
with the γ-rays being used for imaging.
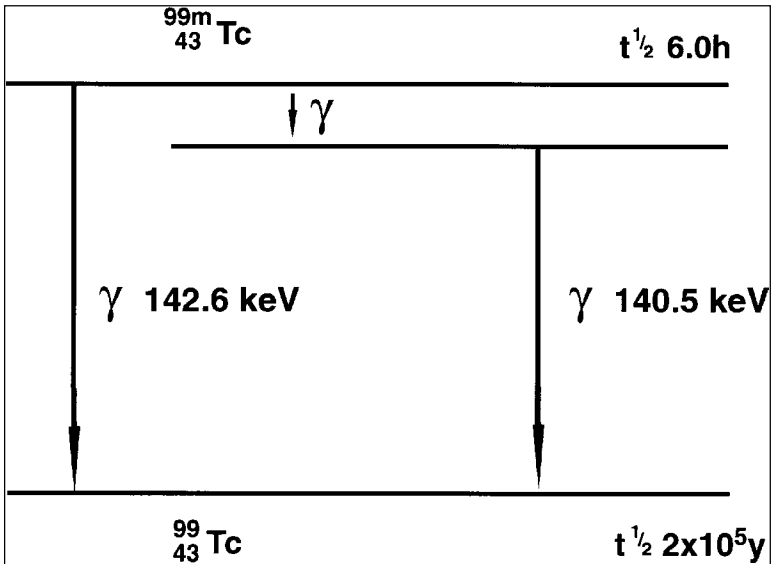
Figure 5. Decay of technetium-99m.

Radionuclide Decay

Some nuclei are unstable and decay at a rate described by the half-life (the time taken for 50% of the nuclei of a given radioactive sample to decay). The life expectancy of an individual atom is impossible to predict but in the large numbers in which they are produced the whole-population characteristic half-life can be described by bulk averaging. Radioactive instability is related to the excess of energy contained in a given "excited" nucleus and often results from an imbalance of the numbers of protons and neutrons in the nucleus. Radioactive atoms decay by a number of processes each with different implications for nuclear medicine practice. Decay processes may be classified according to whether in the atoms in question the imbalance leads to a neutron-rich nucleus (usually reactor produced) or proton-rich nucleus (usually accelerator produced). The commoner forms of decay are described. Half-lives and principal emissions from common radionuclides are summarized in Appendix I.

Electron (or Beta-) Particle Emission (Fig. 3)

Neutron-rich atoms decay by the transformation of a neutron into a proton and electron. The proton remains in the nucleus but the electron is emitted, and for historical reasons, it is in this context called a β-minus particle:

$n \rightarrow p + e^- + \bar{\nu}$
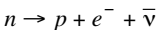
where the *n* is a neutron, *p* a proton, *e⁻* the negative electron (beta particle) and *v* an antineutrino (an undetectable and nearly mass-less particle). In this reaction

the daughter atom has the same mass number as the parent but an increase in one of the atomic number because of the increase in number of protons in the nucleus.

Isomeric Transition (Gamma Decay) (Fig. 5)

This method involves an internal rearrangement of the nuclear structure with minimal change in atomic weight. However, an alteration in the energy state of the nucleus results in the emission of γ-rays. Such γ-rays are very energetic forms of electromagnetic radiation, like light, and lose little of their energy in the body. Thus little radiation damage results to the tissues while the gamma rays are well-suited to imaging the distribution in the body of the physiological molecule-of-interest to which they are attached. For such reasons technetium-99m which decays by this mechanism is widely used in nuclear medicine, the decay schematic being as follows:

$$^{99m}Tc \rightarrow {}^{99}Tc + \gamma$$
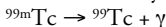
Electron Capture

If a nucleus is not sufficiently energetic to decay by positron emission (see below) it may capture an orbital electron. A proton is then transformed into a neutron and a neutrino emitted. Since a vacancy is created in the inner electron shell, this is filled from outer rings and a succession of so-called characteristic X-rays result (characteristic because of their specific and recognizable energies). Examples used in nuclear medicine are indium-111 and iodine-123. The decay schematic is as follows:

$$p^+ + e^- \rightarrow n + \nu$$
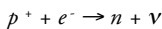
Internal Conversion

This type of decay occurs in parallel to γ-decay. It is the result of an energetic radioactive nucleus transferring its energy to an orbital electron which is ejected, rather than a γ-ray. The result is again characteristic X-rays (as the orbital vacancy is filled) and the electron (called an Auger electron) of discrete energy. This process is particularly important in calculations of radiation doses resulting from radioactive decay.

Positron (Beta+) Emission

Positrons (or positive electrons) are an example of anti-matter so beloved of science fiction writers. However, positrons have a very important role in nuclear medicine. They result from the decay of proton-rich nuclei. It so happens that the only externally detectable isotopes of carbon, hydrogen, oxygen and nitrogen (which make up a major part of bodily tissues) are carbon-11, oxygen-13 and nitrogen-15, all proton rich. All three decay by positron-emission albeit with very short half-lives. Add in fluorine-18, which can substitute for hydroxyl groups and which is also a positron-emitting radionuclide, and it is apparent that detection of positron emissions might be a very powerful tool for studying disease. Indeed positrons might also be used to study the mechanisms of disease and the behavior and localization of important molecules in the body.

Positrons do not decay themselves but are extremely short-lived. When they lose their kinetic energy after collision(s) with electrons they finally meet a negative electron and the particles mutually annihilate. The energy associated with their rest mass appears as two high-energy electromagnetic photons (each of an energy of 0.511
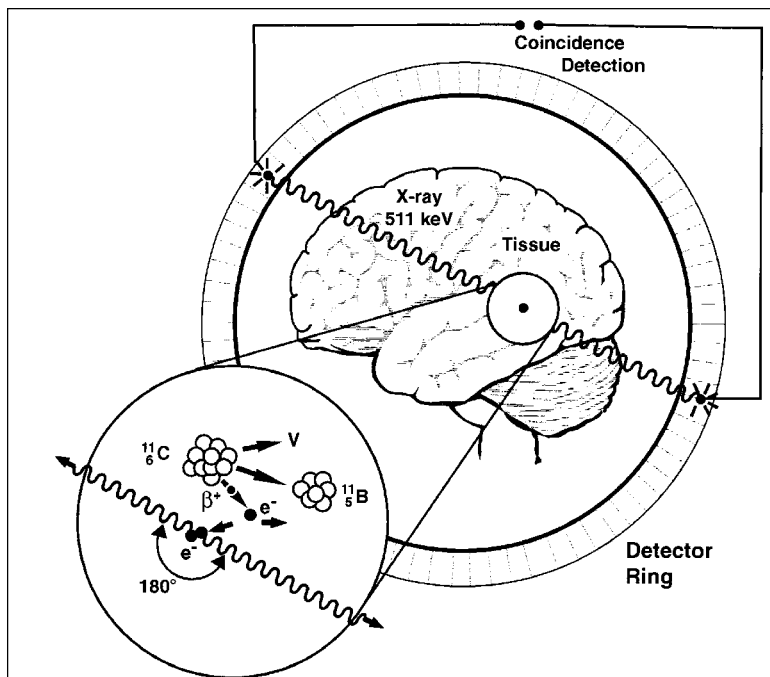
Figure 6. Positron decay and the principle of positron emission tomography. The positron, after a short path and scattering off negative electrons, interacts with such an electron. As both annihilate, their rest mass results in two photons detected as coincidental events in the detector ring.

MeV) propagated in nearly opposite directions—following Einstein's famous equation describing the equivalence of mass and energy: $E = mc^2$. Their detection is central to the technique of PET (Fig. 6), but may also be done with gamma cameras.

Alpha-Particle Decay

Alpha (α) particles (consisting of two protons and two neutrons - the nuclei of helium atoms) usually result from the decay of heavier nuclei. Their large mass and short range make them virtually undetectable outside the body as they are usually absorbed in close proximity to the site at which they decay. This mechanism of decay is not used, for that reason, in radionuclide imaging. On the other hand, the large local radiation damage produced in tissues makes molecules labeled with α-particles of great potential interest in the treatment of cancers.

Detection Systems

We have seen that the strength of nuclear medicine lies in the use of radioactive atoms to detect disease, analyze physiological processes (the tracer principle), treat cancers, and a myriad of other applications. It remains, therefore, for us to explore the systems used to detect and localize high-energy radiations. The machines in use
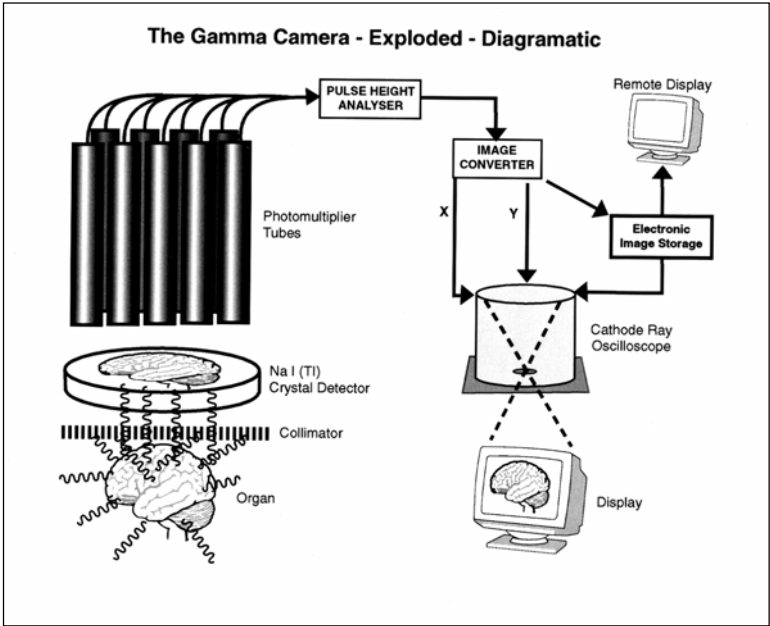
Figure 7. A diagrammatic representation of the gamma camera imaging chain. Those gamma rays passing through the collimator cause the sodium iodide crystal to scintillate. The light is detected by photomultiplier tubes and analyzed in sum for the energy of the interaction and differentially for its position. The sum of many such interactions form the image projected on an oscilloscope or stored electronically.

all combine detectors with electronic amplification and analysis of the signal. The detectors in gamma cameras (Fig. 7) are scintillators made of sodium iodide crystals, whereas in positron emission detection bismuth germinate is often used but other materials are being explored for both applications including semi-conductor detection systems. A discussion of the relative advantages and disadvantages of these materials is beyond the scope of this chapter.

The electronic processing firstly involves pulse height analysis. This determines if the parcel of energy associated with each detected γ-ray of electromagnetic radiation corresponds with the energy anticipated knowing the radionuclide injected. If it does not, and it might, for example, come from cosmic radiation or the naturally occurring radioactive tracer potassium-40 present in each of us, then that signal is rejected as having the potential to degrade the image. Secondly the electronic processing involves giving the signal an "address" which describes the coordinates of the interaction in the crystal. The collimator in the imaging system makes the image coherent much as the lens in a camera focuses light. The vertical perforations in the collimator between the patient being studied and the crystal make the radiation

reaching the crystal reflect the distribution of the nuclide in the patient's body. In this way an image of that distribution can be built up.

It is important to note that since the data acquired are inherently digital (the positional address is computed) then nuclear medicine readily lends itself to quantitative methods. Several specific detection methods exist.

Static Imaging

The gamma camera is used to image a single organ within its field-of-view, such as heart or lung, after injection of an appropriate tracer. An example is a map of lung perfusion obtained after injection of ^{99m}Tc-protein aggregates which trap in lung capillaries.

Dynamic Imaging

This technique is often combined with static imaging. The arrival and uptake of tracer in an organ as well as its washout may be imaged or analyzed from repeated images taken over a span of time.

Gated Imaging

To "arrest" body motion during the time it takes to make an image, and thus reduce image blurring, the image may be gated by linking image acquisition to particular times in the cardiac or respiratory cycles. Images from the same segment of many such cycles are thus combined into what is in effect a ciné loop of the organ in motion.

Whole-Body Imaging

Among other imaging techniques involving exposure to ionizing radiation, such as computed radiography, the radiation exposure to the patient increases with each additional image made. This is not the case in nuclear medicine. In nuclear imaging the radiation exposure is determined by the injection of the tracer and additional images take time but do not otherwise expose the patient to risk. Radionuclide imaging is a particularly powerful method to search the whole body for disease, the distribution of which is unknown. Examples are bone scans done to detect metastases, tumor scans (for example with ^{18}F-fluoro-deoxyglucose [FDG]) and scans with labeled white cells to detect occult infections.

Region-of-Interest (ROI) Analysis

Because, as we have seen, the data acquired in nuclear medicine images are inherently digital, it is easy to obtain quantitative information about organ function. From the gamma camera image the organ, or a part of it, is defined by a computer-generated outline—the "region-of-interest"—and the activity within this area measured, either as total uptake or rate-of-uptake in an activity-time plot. At present much research is being done to ensure that these measurements are accurately corrected for scattered radiations and attenuation of activity because of the depth of the organ in the body.

Single-Photon Emission (Computed) Tomography (SPECT or SPET)

The burgeoning of imaging methods in the second half of the twentieth century owes much to computer developments. These have made it possible to reconstruct sectional body images in CT, MRI, SPECT and PET. Sectional images avoid the superimposition of structures and reveal inner structure just as the slices of a loaf of bread reveal structure not apparent from merely looking at the loaf. Applied to nuclear medicine the sectional imaging method is called SPECT and is used almost invariably in brain and cardiac imaging and often in bone and tumor imaging. The detector system in SPECT, unlike PET in which a ring of crystal detectors is used, usually consists of two or three rotating gamma-camera heads. When not used for SPECT these are then available for other imaging methods (whole-body imaging, static imaging, etc.).

Positron-Emission Tomography (PET)

This technique images the radiations resulting from radionuclides decaying by positron emission (Fig. 6). The positrons (positive electrons) interact with negative electrons to yield two photons in opposite directions. Since this radiation is directional and simultaneous (the two rays arriving virtually simultaneously at the detector ring are identified as a single "coincidence" event) they must originate from a point on a line joining the sites of detection. In this way the use of a collimator may be avoided. PET is powerful in research and practice because it images the distribution in the body of compounds labeled with such biologically important atoms as carbon, nitrogen and oxygen.

As radiological methods have developed and multiplied in the last half century it sometimes has seemed that nuclear medicine might be overtaken by other technologies. That this has not occurred is an eloquent comment on the power of the tracer concept and the technology that supports it. Molecular biology and its offshoots such as the human genome project are poised to change medicine more in the next three decades than the previous thirty centuries. Indeed as medicine moves increasingly from descriptive science into an era of fundamental understanding, the molecular biological revolution, like the communications one, will present enormous opportunities for the promise of nuclear medicine to be fully realized.

Clinical Practice

While nuclear medicine is a clinical specialty practiced by physicians with specialty education, the development and practice of nuclear medicine owes a great deal to scientists of many disciplines:

Physics, Engineering and Computing Science

Not only have the imaging tools in nuclear medicine been developed by basic scientists in physics and engineering but these scientists continue to refine the use of gamma cameras by developing increasingly sophisticated techniques for image analysis.

Radiopharmacy

The science of nuclear- or radio-pharmacy has provided a series of very effective tracers for diagnostic purposes. Many of these have been labeled with technetium-

99m. No stable form of this element is found on earth and it has no role in human metabolism. However, it is cheaply available from a generator, has advantageous physical properties as noted above, and has proved to be the work-horse for nuclear medicine for the past three decades. This fact owes a great deal to the innovations by radiopharmacists in finding ways to label biologically interesting molecules with technetium-99m.

A Perspective on the Future

Diagnostic imaging, by any method, does not exist in isolation but must respond to the changing context in which medicine is practiced. Several trends in healthcare stand out as the twentieth century gives way to the twenty-first:

• The high cost of care, and societal imperatives to contain such costs, and re-align spending for other social purposes;

• The focus on the patient (sometimes called the client in this context) as a partner in health promotion rather than as the passive recipient of care;

• The public's increasing interest in and use of "complementary" medicine - either traditional methods such as acupuncture, or new techniques such as Bach flower therapy. By implication, this interest seems to be a measure of public skepticism about allopathic medicine and certainly represents a use of resources that might otherwise be used in conventional care;

• A further change in the traditional relationships between physicians and patients dictated by the accessibility of information, good and bad, about health from sources such as the world-wide-web;

• Increasing emphasis on the public health and the social determinants of illness as distinct from the "medical" view of illness;

• A requirement that any medical interventions be evidence-based. Again modern information technology will impact on this as decision support tools are developed and on-line records become a tool for audit and outcomes analyses; and

• Against this pattern of social change in the context in which medicine is practiced, medicine itself is also poised on the threshold of revolution. The insights afforded by molecular biology and the unfolding of the human genome project are about to change forever the human view of disease and the ability to treat it.

• Nuclear medicine methods are, by the standards of technology-intensive medicine, relatively low-cost, safe and minimally invasive as well as often able to be done for people as out-patients. This makes them likely to be important to the future of care.

• Nuclear medicine clearly will not and should not be expected to respond to every change in the social context in which medicine is practiced. Nevertheless it is capable of being made user-friendly. At the same time images are intrinsically an effective way to communicate with patients and might be used more often for this purpose.

• In the longer view the movement to an evidentiary basis for practice will serve nuclear medicine well given its rich tradition of intellectual inquiry. A considerable literature has already emerged, for example, to show that positron emission tomography with ^{18}F-fluoro-deoxyglucose is, while expensive, both a cost-effective technique in cancer diagnosis and staging and one which positively influences patient outcomes.

Additional Reading

The following articles supply more information on the roots of nuclear medicine:

1. Brucer M. A Chronology of Nuclear Medicine. St. Louis: Heritage Publications Inc., 1990:piii.
2. Brucer M. Nuclear Medicine Begins with a Boa Constrictor. New York: Society of Nuclear Medicine, 1979:v-xxvi.
3. Cohen M. Ernest Rutherford at McGill University. In: Aldrich JE, Lentle BC, eds. A New Kind of Ray: The Radiological Sciences in Canada. 1895 - 1995. Montreal: The Canadian Association of Radiologists, 1995.
4. Levi H. George Hevesy and his concept of radioactive indicators—In retrospect. Eur J Nucl Med 1976; (1):3-7.
5. Röntgen WC. On a new kind of rays (English translation). Nature 1896; 53:274-276.
6. Mould RF. Discovery of radioactivity and radium. In: A Century of X-rays and Radioactivity in Medicine. London: The Institute of Physics Publishing, 1993:10.

1

Radiation Effects and Safety

Michael J. Chamberlain

Introduction

The International Commission on Radiological Protection (ICRP) declares that "the primary aim of radiological protection is to provide an appropriate standard of protection for man without unduly limiting the beneficial practices giving rise to radiation exposure." Nuclear medicine professionals have a duty to fellow healthcare workers, patients and their families, research volunteers, the general public and the environment to ensure the safe and responsible handling of radioactive materials used diagnostically, therapeutically and in research. Radiation protection, the observance of these safe practices, is the responsibility of every nuclear medicine professional in conjunction with the local Radiation Safety Officer (RSO), Radiation Safety Committee, government regulatory agencies and scientific advisory groups (Table 1).

Radiation Dosimetry

Types of Radiation

As seen in Chapter 1, different types of radiation can be emitted from radioactive materials. Alpha particles are basically the nuclei of helium atoms and consist of two protons and two neutrons. Beta particles are either electrons (with a negative charge) or positrons (positive electrons). Energetic photons emitted during radioactive decay from the nucleus of an atom are termed gamma rays. They are identical to X-rays except for their origin. An X-ray originates from the electron shell of the atom while a gamma ray originates from its nucleus.

Energy emitted during the radioactive decay process interacts with the matter it encounters and is the basis for its detection, therapeutic effect and any biological hazard it poses. Alpha, beta (including positron), gamma and X-ray radiations emitted from radioactive materials are of sufficiently high energy to ionize the atoms and molecules which they encounter. These different forms of energy can be in the form of particles (alpha or beta) or electromagnetic radiation (gamma or X-ray) each with different abilities to penetrate animal tissue and shielding materials. Alpha radiation will penetrate less than one mm of tissue and an external source may be shielded by a sheet of cardboard or by the surface layer of the skin. Higher energy beta particles can penetrate up to 10 mm of tissue and may be blocked by a thin layer of metal or plastic. Due to this limited penetrance, alpha and beta emitters are only hazardous to human health if ingested, injected, inhaled or deposited on the skin and are not useful labels for imaging of internal organs. Conversely, gamma and X-ray radiations have the potential to penetrate more than a metre of tissue. These more penetrating

Table 1. Radiation protection bodies

Regulatory agencies	United States: Nuclear Regulatory Commission (NRC)
	Canada: Canadian Nuclear Safety Commission (CNSC)
	United Kingdom: British Health & Safety Executive—Nuclear Safety Directorate
	Europe: Commission of the European Communities (CEC)—Euratom Treaty
Advisory groups	International Commission on Radiological Protection (ICRP)
	National Council on Radiation protection and Measurements (NCRP)
	United Nations Scientific Committee on the Effects of Atomic Radiation (UNSCEAR)
	Committee on the Biological Effects of Ionizing Radiations (BEIR)

emissions, while suitable labels for external imaging of radionuclide distribution within the body, require relatively thick shielding with dense materials such as lead or concrete or they will otherwise pose an external radiation hazard.

Equal absorbed doses of different types of radiation do not produce equal biological effects. The relative biological effectiveness (RBE) of the different radioactive emissions is related to their energy and their tissue penetrance. Thus the RBE of alpha radiation is high because a large amount of energy is given up over a short distance, causing a dense cluster of ionizations and potentially irreparable DNA damage. The related concept, linear energy transfer (LET), describes the energy transferred to the absorbing medium per unit length of track. This can vary from 2 keV/μm for gamma-radiation used in nuclear medicine imaging to 2000 keV/μm for heavy charged particles. Alpha radiation is therefore termed "high LET" as compared with the "low LET" gamma radiation (Fig. 1).

Units of Radiation Exposure

Nuclear medicine uses units of measure which are unfamiliar to most non-physicists (Table 2). These are used to describe the amount of radioactive material (often known as its activity), how much energy this ionizing radiation imparts to a mass of irradiated material (absorbed dose) and the biological impact of an absorbed dose that considers the quality of the radiation (dose equivalent). The fact that an older system of measures (curie, rad, rem) and the newer Système International (becquerel, gray, sievert) are both in widespread use adds to the confusion.

For Nuclear Medicine purposes the becquerel is an inconveniently small unit and the curie is inconveniently large. Activities are therefore usually stated as megabecquerels (MBq) or milli-curies (mCi). Absorbed dose is expressed in units of rad or gray (Gy) while dose equivalent is expressed as rem or sievert (Sv). Rad is an acronym for Radiation Absorbed Dose and rem is an acronym for Roentgen Equivalent Man.

2
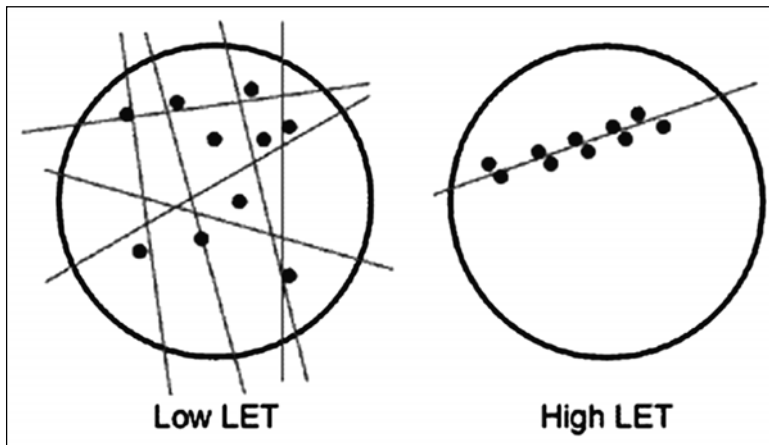
Figure 1. Linear energy transfer (LET). Individual ionization events (small circles) occur along paths followed by the radiation (lines). The large circles contain equal numbers of ionizations for low LET and high LET radiation. In the case of high LET radiation, all energy deposition occurs along a single short ionization track With low LET radiation it takes a larger number of radiation emissions as each one has a relatively small chance of tissue interaction.

Dose equivalent was developed in an effort to incorporate biology into the physics of radiation exposure. Not all forms of radiation (alpha, beta, neutron, gamma, X-ray) produce the same biological effect for equal absorbed doses. For example, neutron irradiation has five times the biologic effect of X-rays while alpha radiation has twenty times the biologic effect of X-rays. This is denoted by the Quality Factor (1 for X-ray, gamma and beta irradiation; 5 for neutron and 20 for alpha irradiation). The dose equivalent is the absorbed dose multiplied by the radiation's Quality Factor. For instance, 0.01 Gy (1 rad) of beta radiation produces a dose equivalent of 0.01 Sv (1 rem) while 0.01 Gy (1 rad) of alpha radiation produces a dose equivalent of 0.2 Sv (20 rem).

Effective Dose

In order to be able to compare different radiation doses with differing forms of radiation affecting different parts of the body it is necessary to express each radiation dose as if it had been distributed evenly throughout the body. This uses information on the radionuclide's biodistribution, tissue weighting factors which adjust for the varying susceptibility of different tissues and organs to radiation damage, and quality factors which reflect the RBE of different forms of ionizing radiation. A radiation dose expressed in this way is termed an effective dose equivalent (or simply an "effective dose"). These principles are illustrated in the effective doses shown in Table 3 which compare a thyroid radioiodine uptake (assuming a 24-hour uptake of 25%) with a bone scan (assuming normal renal function). Despite considerable differences in the radiation emissions, activities and biodistributions (critical organs) it is possible to see that the bone scan should result in about twice the biologic effect of the uptake

Table 2. Units of measurement used in nuclear medicine

	SI Unit	Older Unit	Conversions
Activity	1 becquerel= 1 nuclear decay per second	1 curie (Ci) = 3.7 x 10^{10} nuclear decays per second = activity producing the same number of nuclear decays as 1 gram of radium-226	MBq = 37 x mCi mCi = 0.027 x MBq
Absorbed dose	1 gray (Gy) = 1 Joule per kg	1 rad = 100 erg per gram	Gy = 0.01 x rad rad = 100 x Gy
Dose equivalent*	1 sievert (Sv) = 1 gray x Quality Factor 1	1 rem = 1 rad x Quality Factor 1	Sv = 0.01 x rem rem = 100 x Sv

* Quality Factor = 1 for all X-, gamma, and beta radiations; 5 for neutrons; 20 for alpha radiation.

measurement. Effective dose from common radiologic and nuclear medicine procedures are summarized in Appendix 2.

Background Radiation

Living on Earth has always meant continuous exposure to natural background radiation including cosmic radiation, radiation from naturally-occurring minerals in natural surroundings and construction materials as well as internal radiation from radionuclides within our own bodies. Finally there is the inevitable but highly variable inhalation of the ubiquitous radioactive gas radon, a decay product of the uranium-238 which is a component of the Earth's crust.

In Eastern North America typical natural background radiation is in the order of 1.0 mSv per year with exposure to radon contributing a further 1-2 mSv. Natural background radiation varies by a factor of five to eight times from place to place in the world and the variation is even greater when differences in inhaled radon are taken into account. Numerous large surveys have compared cancer incidence and deaths in high and low background regions in an attempt to measure the presumed carcinogenic effect of low level radiation. No association between cancer incidence and level of background radiation has been found. It is ironic that for radiation safety purposes we may struggle to regulate and reduce radiation exposures which are less than those which may be incurred by moving from one city to another because of the geographic variation in background radiation levels!

Table 3. Sample effective doses for bone and thyroid scans

	Bone Scan	Thyroid Uptake
Radiopharmaceutical	^{99m}Tc-MDP	^{131}I-Sodium iodide
Physical half-life	6.02 hours	8.1 days
Radionuclide emissions	gamma (140 keV)	gamma (364 keV) and beta (mean 192 keV)
Activity	740 MBq (20 mCi)	0.185 MBq (5 µCi)
Critical organs	bone, bladder	thyroid, bladder
Effective dose	5.9 mSv (0.59 rem)	2.8 mSv (0.28 rem)

Radiation Effects and Carcinogenesis

Biological Effects of Radiation

Cellular DNA is the critical target for the biological effects of ionizing radiation, both as direct target and as a secondary target of the diffusible radiolytic products of water and possibly other cellular constituents. Radiation induced damage may occur within each of the chemical components of DNA. Spontaneous chemical reversal of the damage may occur but if it does not then the site undergoes enzyme-mediated repair. This either restores the DNA to its original state or results in stable DNA damage. Ionizing radiation and other genotoxic agents such as ultraviolet radiation and numerous chemicals can damage DNA nucleotide bases or cause single strand and double strand breaks in the sugar-DNA backbones and DNA-protein cross links. Of these it is the DNA double strand lesions which are most important in the induction of lethal cell events, chromosomal abnormalities and gene mutations.

At high dose rates the natural repair mechanism can be overwhelmed. Lowering the dose rate (e.g., by fractionation of the radiation dose) is likely to diminish its RBE because of the possibility of simultaneous DNA damage and repair at low dose rates. Exposure to natural background radiation is an important example of how low dose rate radiation might be expected to exhibit a lesser biological effect than the equivalent high dose rate exposure.

Stochastic and Deterministic Effects

The clinical manifestations of unrepaired DNA damage caused by ionizing radiation are conventionally divided into those which are "stochastic" and those which are "deterministic" (formerly called "non-stochastic").

With deterministic effects the probability of causing harm will be zero at doses up to some known threshold (usually hundreds or even thousands of mSv) and then will increase steeply and proportionately to dose above the threshold (for clinical effect). Radiation burns, decreased salivary gland secretion, lens opacities (cataracts) and loss of fertility from gonadal irradiation are deterministic effects. Because the threshold levels are relatively high, such effects will not be seen in the practice of diagnostic nuclear medicine. In radionuclide therapy however deterministic effects are deliberately sought but may also be encountered as side effects. For example when iodine-131 is administered to treat hyperthyroidism we deliberately seek to reduce thyroid gland function while with the larger doses used in the treatment of thyroid carcinoma radiation sialadenitis may be encountered as a side effect. Similarly,

when treating painful bony metastases with an agent such as radioactive strontium-89 bone marrow depression may occur as a side effect.

With stochastic effects the probability of the event increases with radiation dose with the assumption that there is no threshold (i.e., no dose too small not to have an effect). In practice there may well be a point below which the effect is imperceptible or so small as to be negligible. Examples of stochastic effects are the increased probability of developing leukemia or a solid cancer following radiation exposure.

Linear No Threshold Hypothesis

This hypothesis states that the stochastic dose/response effects (e.g., cancer induction) observed at high doses and dose rates can be extrapolated in a straight line passing through the origin (zero dose and zero effect). This implies that there is no dose so low that it does not have an adverse effect even though no effect is directly observable. This is a perfectly valid scientific and safety device providing it is appreciated that it is not proven or provable, and that other hypotheses may fit the observable phenomena such as a linear/quadratic relationship between dose and effect for low doses and even that there is indeed a threshold (Fig. 2).

Sources of Radiation

Along with natural background radiation there comes exposure to man-made radiation. Some of this is unavoidable such as the fall-out from nuclear weapons testing (now at very low levels), the generation of electricity by nuclear power, and the radiation from luminous dials and signs. By far the greatest contribution to the man-made radiation in the developed world comes from medical uses in diagnostic radiology and nuclear medicine. When distributed over the adult North American population this is approximately equivalent to two-thirds of natural background.

Radiation-Induced Cancer

The clinical presentation of leukemia induced by ionizing radiation is likely to be delayed by several years from the time of exposure. In the case of solid tumours the latent period may be several decades. It is believed that excess cancers are still arising in Japanese atomic bomb survivors. The risk of inducing additional neoplasms is generally quoted as the average for an adult population. The additional lifetime risk of developing a fatal cancer is generally taken as 1 in 4,000 for an effective dose of 10 mSv. Lifetime risk from radiation exposure is relatively less in elderly individuals (due to limited life expectancy from other illness) and relatively greater in healthy children.

Atomic bomb survivor data show an excess of leukemias and solid cancers over the expected spontaneous occurrence but the excess of solid cancers only exceeds 95% confidence limits for victims with estimated doses in the range 50-250 mSv and higher with no excess demonstrable for exposures below 50 mSv.

Effects of Ante-Natal (in utero) Radiation Exposure

The effects of radiation exposure of the conceptus depends upon the time of exposure relative to conception (Table 4). Prior to the beginning of organogenesis (three weeks after conception) damage to the small number of relatively undifferentiated cells is most likely to result in failure of implantation or undetectable death of the conceptus rather than a damaged liveborn child. When major

2
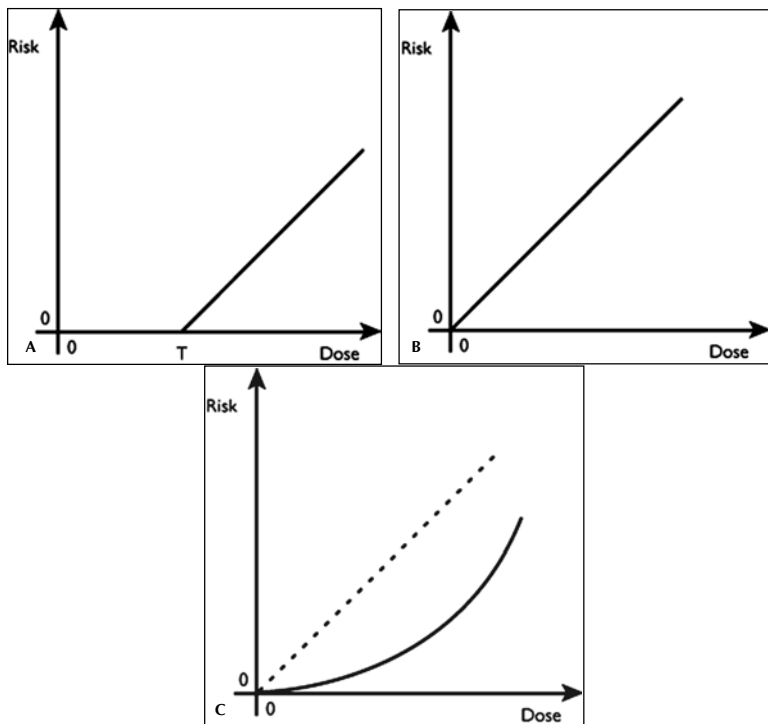
Figure 2. Possible mathematical relationships between radiation dose and cancer risk: (a) threshold, (b) linear no threshold and (c) quadratic models. The threshold model (a) suggests that there is a threshold below which stochastic effects such as cancer induction do not occur. Above this threshold, cancer induction is predicted to be proportional to dose. The linear no threshold model (b) assumes no such threshold. The quadratic (c) model assumes a low rate of cancer induction at lower radiation doses and a higher rate at higher doses.

organogenesis is underway irradiation may cause congenital malformations. These effects are deterministic with an estimated threshold in humans of 10 to 25 mSv. Mental retardation, sometimes associated with microcephaly, has been seen in the children of atomic bomb survivors. The threshold for this effect is estimated at 60 to 300 mSv.

The fetal thyroid gland does not concentrate iodide (or radioiodide) until after 12 weeks of gestation. Radioiodine administered to the pregnant woman after this time has the potential to cause radiation damage to the fetal thyroid including the induction of congenital hypothyroidism. Cases have been reported in the literature in which therapeutic doses of iodine-131 administered to thyrotoxic pregnant women have caused hypofunction of the fetal thyroid. This has happened sufficiently often for it to be known that during intra-uterine existence the fetus survives and develops normally on maternal thyroxine of either endogenous or exogenous (supplemental)

Table 4. Human fetal developmental milestones in weeks

Implantation	1-2 weeks
Neural plate formation	1-3
Organogenesis	3-7
Upper limb bud formation	4
Heart septation	7
Palate closure	8
Concentration of iodine in fetal thyroid	12

origin. Providing that the possibility of congenital hypothyroidism is recognized and treated within a few weeks of birth, normal post natal development can occur.

The evidence for the stochastic effect of intrauterine irradiation conferring an increased probability of developing cancer or leukemia in childhood or in adult life is not consistent but it is generally thought reasonable to assume that in utero sensitivity may be several times that of the adult population.

The possibility of pregnancy or breast feeding should always be excluded when a nuclear medicine procedure is contemplated in a female of reproductive age. Most departments post a notice in waiting rooms and washrooms asking any woman who knows or suspects herself to be pregnant, who has missed an expected menstrual period or who is breast feeding to report this to the receptionist or a technologist before starting the procedure. It is also the duty of the technologist to ask the patient concerning pregnancy and breastfeeding prior to administering a radiopharmaceutical. Many departments will record that the question has been asked and record the response and some may require the patient to sign a declaration. Once the woman's status is known the nuclear medicine specialist and the referring physician can decide to go ahead, cancel, modify or postpone the procedure according to a risk/benefit analysis. Clearly a proposed ventilation/perfusion lung scan for suspected pulmonary embolism at 32 weeks of pregnancy requires different consideration from a speculative bone scan at 8 weeks in a woman with a tentative diagnosis of fibromyalgia. The risk/benefit analysis must consider radiation dose to the fetus, including that due to any transplacental passage of the radiopharmaceutical, and its residence time in maternal organs adjacent to the uterus (particularly the bladder).

Practice Point

Exclusion of pregnancy is particularly important when therapeutic radiopharmaceuticals are to be administered. Serum beta-HCG becomes detectable about two weeks after ovulation (around the time of implantation) and should be tested whenever pregnancy cannot be reliably excluded otherwise. Particular tact may be required when dealing with a thyrotoxic teenage candidate for radioiodine therapy accompanied by a parent.

Genetic Disorders

Theoretically genetic disorders may occur in first and subsequent generation children born to parents with radiation exposure prior to conception due to radiation-induced mutation in gamete precursors. This effect has never been demonstrated to occur in human populations (including the atomic bomb survivors) but its occurrence

is predicted from plant and animal work. By extrapolation, it has been estimated that a doubling of the spontaneous mutation rate (non-radiation induced plus background radiation induced) requires on the order of 50 to 250 mSv.

Principles of Radiation protection

Increased Distance from the Source

Increasing the distance from a point source of radiation causes the exposure rate to drop off rapidly according to the Inverse Square Law. For example moving from 10 cm to 30 cm from a point source will decrease exposure rate by a factor of nine. You can illustrate this effect by warming your hands at an open fire and then taking a step backwards.

Practice Point

Increasing distance from the source brings major benefits in reducing radiation exposure in nuclear medicine but the major source of radiation exposure, the patient, is not a point source. Simple inverse square law calculations do not apply when the distance from the patient is less than 3 m. This principle can be easily demonstrated by taking a survey meter and measuring exposure rates at increasing distances from a patient recently injected with a ^{99m}Tc agent for a bone or myocardial perfusion scan.

Minimize Time of Exposure

Carefully plan procedures to require the least time handling or in the vicinity of a radiation source.

Shielding

Gamma and X-ray radiation is attenuated by the material through which it passes to an extent determined by the energy of the radiation, the density of the material and its thickness. The thickness of a shielding material required to reduce radiation exposure from a given radionuclide by half is called its half value layer (HVL). The HVL of lead for ^{99m}Tc is 0.3 mm whereas for the more energetic emission of ^{131}I a thickness of 3.0 mm is needed (Table 5). Lead is frequently used for shielding because its high density minimizes the thickness and hence the volume occupied by the shielding needed to provide a required attenuation. Where space is available, concrete, compacted earth or water may provide effective and economical shielding.

Practice Point

The wearing of lead or lead equivalent (usually 0.25 mm lead equivalent) aprons to shield the trunk is popular among technologists and mandated in some jurisdictions. These are effective shields at typical diagnostic X-ray energies but the theoretical attenuation achieved for ^{99m}Tc is < 50%, while for ^{131}I it is negligible. The risk of wearing the heavy device may not be negligible in terms of back strain.

Elements of distance, time and shielding are often used together to achieve the desired reduction in radiation exposure. Occasionally over emphasis on one principle can have a net negative effect. For example particularly heavy and clumsy shielding of a radioactive source may increase the time needed to handle it and increase the possibility of a spill.

Table 5. Common half-value layers (HVL)

	^{99m}Tc	^{131}I
Photon energy keV	140	364
HVL in tissue (cm)	4.6	6.3
HVL in lead (mm)	0.3	3.0

As low as reasonably achievable (ALARA)

The adoption of the linear no threshold hypothesis, with its implication that no level of exposure no matter how small can be considered safe, logically led to the adoption of the imperative that exposure should always be as low as reasonably achievable—ALARA. This had its beginning more than 40 years ago with ICRP and NCRP. The phrase "reasonably achievable" is open to misinterpretation, and to avoid preoccupation with inconsequentially small amounts of radiation has been qualified by the phrase—too often forgotten or ignored—"social and economic factors taken into account." ALARA remains a valuable principle for radiation protection, providing it is interpreted with common sense and does not become a tyranny. In the institutional setting that common sense may be provided by a broadly representative Radiation Safety Committee.

Practical Aspects of Radiation protection

Expression of Radiation Risk

For most nuclear medicine diagnostic procedures the risk comes down to the stochastic risk of a small increment in the individual's pre-existing risk of developing a fatal leukemia or cancer at some time in their remaining lifespan. The radiation dose is determined by the radiopharmaceutical injected, body size and anything influencing biodistribution and is independent of the actual imaging procedure ie. once a patient is injected with the radiopharmaceutical the radiation dose will be identical regardless of whether one image is taken or twenty.

A radiation dose of 10 mSv is estimated to confer a lifetime risk of fatal malignancy in the order of 1 in 4,000, a small increment to the lifetime risk of cancer death of 1 in 5 for every newborn child (rising to 1 in 3 for an adult of 65 years). Thus a bone scan following the injection of ^{99m}Tc- MDP 750 MBq results in an effective dose of 6 mSv and an estimated lifetime risk of fatal cancer of 1 in 6,700. A rest/stress myocardial perfusion scan with each component receiving ^{99m}Tc-sestamibi 1100 MBq results in a total radiation dose of 25 mSv and a lifetime cancer risk of 1 in 1,600. In the first case the procedure will have increased the probability of the dreaded event from 0.25000 to 0.25015 for a young adult and in the second from 0.33333 to 0.33396 for an elderly man.

These risks will appear small to the informed physician and very small when set against the possible benefit to be obtained from the bone scan and the myocardial perfusion scan to which they relate. Yet how are they to be expressed to the patient and his or her relatives who may find it difficult to accept any risk and be unfamiliar with thinking in epidemiological terms and dealing with the concept of stochastic risk? When told the odds of death are 1 in 10,000 the expert concentrates on the

odds and dismisses the risk. Conversely the layperson concentrates on the dread event, ignores the odds and is concerned by the risk. (If you doubt the above consider the person who dreams the afternoon away planning how he will spend a lottery prize while ignoring the odds against winning.)

Equivalent risks may be helpful in putting radiation risks in context but be warned that your attempt to be helpful may be counterproductive. Expressing the risk of a nuclear medicine procedure in terms of an equivalent number of chest radiographs may be thought helpful in that the latter is more familiar to most patients. Anyone told that a bone scan is equivalent to 60 chest X-rays or that a rest/stress myocardial perfusion scan equates to 250 chest X-rays is unlikely to know that annual natural background radiation is equivalent to 30 chest X-rays or focus on the safety of chest X-rays rather than the apparent danger of the nuclear medicine procedure. Describing the risk of nuclear medicine procedures in terms of cigarettes smoked, slices of cream pie eaten or minutes of mountain climbing is more likely to make the physician look foolish than to educate the patient. It may be more acceptable to relate risk to that of a fatal accident when driving a car since that is such a familiar, recurrent and difficult to avoid activity.

The risk of a fatal accident during a working lifetime in a "safe" occupation, such as a bank manager or sales assistant, is approximately 1 in 10,000. This is equivalent to a 4 mSv radiation dose. For many people this will help to put a bone scan in context. The Health Physics Society recommends against quantitative estimation of health risks below an individual dose of 50 mSv in one year or a lifetime dose of 100 mSv in addition to background radiation.

Dose limits

Legislation changes over time and differs between countries and the reader should consult local authorities for the current dose limits. Current radiation effective dose limits in Canada, Britain and Europe are 1 mSv (0.1 rem) annually for the general public and 20 mSv (2 rem) annually for someone who is occupationally exposed. The corresponding limits for the United States are 1 mSv (0.1 rem) and 50 mSv (5 rem) respectively. At these limits it can be seen that nuclear medicine technologists with a typical exposure of 1.5-2.0 mSv annually exceed the limit for the general public but fall far short of that for the occupationally exposed.

Dose limits for pregnant women are less uniform. In Canada the dose limit for the occupationally-exposed pregnant worker is 4 mSv (0.4 rem) effective dose to the worker from the summed internal and external sources of radiation exposure for the remainder of the pregnancy after the pregnancy has been declared. In the United States the dose to an embryo/fetus during the entire pregnancy due to occupational exposure of a declared pregnant woman must not exceed 5 mSv (0.5 rem). There is no dose rate restriction on this maternal exposure. In Europe and the United Kingdom the dose limits for the pregnant worker are 2.0 mSv to the surface of the abdomen and 1.0 mSv to the fetus for the remainder of the pregnancy after the pregnancy has been declared. The rate of fetal exposure must not exceed 0.06 mSv in any two week period in the remainder of the pregnancy. In practical terms this means that pregnant women who wish to carry out the normal work of a nuclear medicine technologist may generally do so.

The "Ten Day Rule"

It has been advocated that elective nuclear medicine procedures should be carried out only during the first ten days following the first day of menstruation in women of reproductive capacity because of the relative certainty that the patient is not pregnant during that time. This "Ten Day Rule" is theoretically sound but is not enforced in many nuclear medicine departments for diagnostic procedures on grounds of the administrative difficulty of its implementation and with the knowledge of the relative radiation insensitivity of the pre-implantation and pre-organogenesis embryo and the unlikely event of congenital defects in liveborn survivors. All female patients of childbearing potential referred for radionuclide therapy should have a pregnancy test performed to prevent inadvertent exposure to the embryo/fetus.

Breast feeding

Breast feeding by a woman who has recently received a radiopharmaceutical for therapeutic or diagnostic purposes may pose a risk to the child because of the proximity of the woman to the child during the time of breast feeding and/or because of the excretion of certain radiopharmaceuticals or their labelled breakdown products in the breast milk. In these circumstances an elective procedure may be cancelled or postponed. Alternatively complete cessation or temporary interruption of breast feeding may be advised (Table 6). A major consideration is the woman's desire to continue breast feeding and the age of the infant in question. With temporary interruption of breast feeding it should be borne in mind that the woman may be able to express and "bank" her milk prior to the procedure so that it may be used to bottle feed the infant during the interruption. It is also likely that the woman will need to express and discard her milk during the interruption. In practice the interruption of breast feeding for more than a few days is likely to become its complete cessation. The objective is to reduce the maximum radiation dose to the infant to under 1.0 mSv.

Safe Handling of Radiopharmaceuticals

Radioactive materials must be stored in a secure, shielded location that has appropriate warning signs and that is appropriate to the physical and chemical nature of the material. For example, solutions of potentially volatile radioiodine should be stored in a fume hood directly vented to the exterior. Materials awaiting disposal should be clearly marked and securely stored while awaiting decay to a safe activity level.

Always wear surgical gloves when handling radioactive materials. Never eat, drink or smoke in a place where radioactive materials are stored or handled. Never mouth pipette. Whenever possible manipulate radioactive material behind a barrier which shields the trunk. Use metal syringe shields with heavy lead glass for all injections of radiopharmaceuticals Ensure that face masks and mouth pieces are tightly fitting when administering radioaerosols and gases. Remember that the injected patient is in effect an unshielded container and as such the greatest source of technologist radiation exposure. Therefore minimize close contact with the patient to what is clinically and technically required. Know how to clean up radioactive spills including those of bodily fluids of patients who have received radiopharmaceuticals.

Disposal of radioactive materials may be by venting to the outside air, to the sewer or as solid garbage. In each case measurements must be made to ensure that

---

Table 6. Breast feeding restrictions following administration of common radioactive nuclear medicine materials

Material	Breast feeding Restriction
99mTc-labelled agents for renal scans (MAG$_3$, DMSA, glucoheptonate, DTPA), bone scans (MDP, PYP), cardiac perfusion scans (sestamibi), red blood cells, liver scans (colloids, biliary materials such as disofenin, mebrofenin); 123I-sodium iodide; 111In-leukocytes	no interruption
99mTc-labelled agents for lung scans (MAA)	interruption for 12 hours
99mTc-pertechnetate, leukocytes	interruption for 24 hours
67Ga-gallium citrate, 201Tl-thallium chloride	interruption for at least one week
131I-sodium iodide administered diagnostically or therapeutically	complete cessation

---

quantities and concentrations of the particular radionuclides permitted by regulatory authorities are not exceeded. Such responsibility is not avoided when a commercial waste disposal organization is employed.

Frequently Asked Questions (FAQs)

Is radiation exposure dangerous to nuclear medicine technologists and other professionals?

Figures from the Canadian National Dose Registry based on readings from thermoluminescent dosimeter badges show that a nuclear medicine technologist may expect to receive approximately 1.5 mSv annually as a result of occupational exposure. Patients injected with 99mTc-based imaging radiopharmaceuticals are the major source of this exposure. By comparison the radiation dose received by diagnostic radiology technologists is approximately one-tenth of that received by their nuclear medicine counterparts. However neither group is exposed to significant risk as compared with the numerous stochastic and non-stochastic risks cheerfully accepted as part of everyday living.

Radiation doses for nuclear medicine physicians are no greater than those of other radiologists and are significantly smaller than those received by technologists because of the limited exposure to patients.

What do you do if a woman mistakenly undergoes a nuclear medicine procedure at a time when she is at an early stage of

pregnancy?

Occasionally, despite all precautions, it will be discovered that a procedure has been performed on a woman who is subsequently found to have been pregnant at the time. The question of performing a therapeutic abortion may then be raised. In such cases as much factual information as possible must be supplied as quickly as possible to what will inevitably be an anxious situation. This will include calculation of the radiation dose likely to have been received by the products of conception (taking a worst case scenario), consideration of the stage of the pregnancy and the threshold considerations for deterministic effects as discussed above. These must be seen in the context of the rates of spontaneous occurrence of the effects it is feared that radiation may induce and all the other risks of pregnancy. Consideration should also be given to the opportunities for detection of fetal abnormalities by ultrasound and amniocentesis. Rarely if ever will the additional risk to an unborn child resulting from in utero irradiation alone justify interruption of the pregnancy. The nuclear medicine physician can be a helpful resource to the woman, her family and her obstetrician/gynecologist by dispassionately presenting them with the facts and the risks.

Why is explaining radiation risk so difficult?

Nuclear medicine professionals may sometimes think that radiation risks are somehow unfairly magnified in comparison with all the other threats to continuing health and happiness. They may wonder why they seem to be so bad at explaining this. The following factors may have something to do with it.

1.   The Hiroshima and Nagasaki legacy. The atomic bombing of these Japanese cities and their largely civilian populations was such a dramatic and horrifying event that the general perception of the scale of their long term radiation consequences is greatly magnified. Consequently the risks of radiation generally are exaggerated.. Visitors to the Radiation Effects Research Foundation official web page may be surprised by the figures for excess cancers and leukemias among atomic bomb survivors with average exposure of 200 mSv The 428 excess cancer deaths attributable to radiation in the survivor population studied represented 8.8% of the total cancer deaths observed in 1950-1990.

2.   The difficulty in explaining the small incremental risk of death from cancer seen against a several thousand fold greater pre-existing risk.

3.   Obsessional concentration on the feared (anticipated) event rather than the remote odds of it happening (lottery syndrome).

4.   The ALARA principle and linear no threshold hypothesis preclude a 'safe" radiation dose making it difficult to reassure an anxious patient

5.   The difficulty in explaining stochastic risk.

6.   Dependence on thermoluminescent dosimetry which provides only delayed reassurance rather than using a direct reading device whenever concern over radiation exposure is expressed.

7.   Irresponsible colleagues who either treat radiation in a cavalier fashion describing the radiation dose received from a rest/stress myocardial perfusion scan as

"about equivalent to a chest X-ray" (whereas it is equivalent to approximately 250 chest X-rays) or who by their actions exaggerate radiation dangers.

8.   The extreme sensitivity with which radioactive emissions can be detected.

9.   The long delay (latency) in the presentation of radiation-induced cancer which indicates a lurking danger still present 40 years after a bone scan.

Additional Reading

http://www.radscice.com/dowd.html/
An Extensive Listing of Radiation protection Resources on the Internet
Hall EJ. Radiobiology for the Radiologist. 5th ed. JP Lippincott Company, 2000.
A perennial classic that takes the reader from the basic principles of radiobiology to practical aspects of radiation protection and carcinogenesis.
ICRP Publication 52, "Protection of the patient in nuclear medicine". 1987.
ICRP Publication 53, "Radiation dose to patients from radiopharmaceuticals". 1987.
ICRP Publication 80, "Radiation doses to patients from radiopharmaceuticals: Addendum 2 to ICRP Publication 53". 1998.
Selected monographs from the International Commission on Radiological Protection (ICRP) listings at http://www.icrp.org/.

Myocardial Perfusion Imaging

Robert Corne and I. David Greenberg

Introduction

Coronary artery disease (CAD) is the leading cause of death in North America. Atherosclerosis is by far the major cause of CAD. CAD can range from asymptomatic luminal irregularities to sudden total occlusion leading to myocardial infarction.

Atherosclerotic CAD involves an intimal inflammatory reaction. Endothelial cell injury associated with coronary risk factors (smoking, hypertension, diabetes mellitus, hyperlipidemia) results in the entry into the subendothelial space of cellular elements (monocytes) and plasma constituents (notably LDL cholesterol). Monocytes transform into macrophages which engulf LDL cholesterol that has been oxidized in the subendothelial space ("minimally modified" LDL). Activated macrophages produce cytokines which direct smooth cell proliferation and migration into the subendothelial space and produce metalloproteinases and tumor necrosis factor (TNF). Both of these substances can lead to connective tissue degradation, plaque rupture (Fig. 1) and acute coronary syndromes (unstable angina, acute myocardial infarction).

Plaque growth results in progressive coronary stenosis which may cause transient myocardial ischemia (clinically manifested as angina pectoris) when there is an increase in myocardial oxygen demand such as with exercise or emotional stress. The detection of coronary stenosis by nuclear medicine techniques is based on the assessment of relative coronary blood blow at rest and during stimuli that normally increase coronary flow.

Physiologic and Technical Considerations

Physiologic Evaluation of Coronary artery disease

Whereas coronary angiography provides information about the anatomic extent and severity of CAD, myocardial perfusion imaging (MPI) assesses the physiologic or hemodynamic significance of coronary stenosis by inducing heterogeneity in coronary flow. Resting coronary flow is maintained until there is approximately a 90% reduction of coronary arterial diameter. However, the ability to attain maximum flow (termed coronary flow reserve) is impaired with approximately a 50% coronary stenosis (Fig. 2). Increases in coronary flow can be achieved by increasing oxygen demand with exercise (treadmill or bicycle) or beta adrenergic agonists (dobutamine) and by direct vasodilators (adenosine, dipyridamole).

Treadmill Exercise

Graded exercise testing (GXT) in conjunction with myocardial perfusion imaging is most commonly performed on a treadmill. GXT is preferred over pharmaco-

---

3
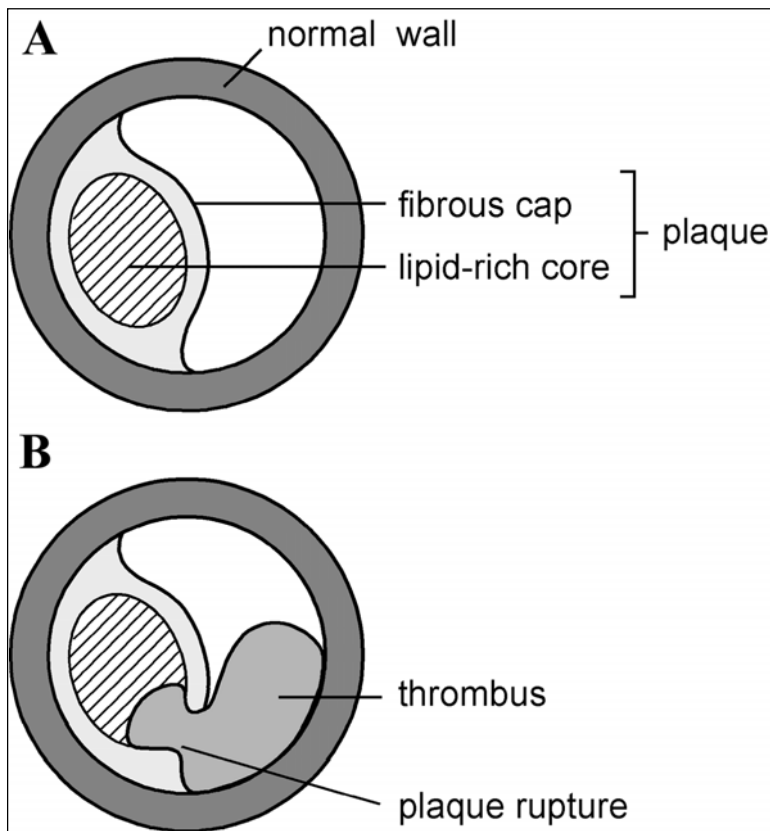
Figure 1. Cornoary artery plaque and plaque rupture. (A) Plaque is made up of a lipid-core containing free lipid and foam cells covered by a fibrous cap denuded of normal endothelium. (B) Unstable plaque may rupture exposing circulating blood to underlying thrombogenic material with the consequent formation of a thrombus.

logic testing in patients able to exercise adequately because it provides an assessment of well validated prognostic markers such as workload, ST segment depression, anginal symptoms and heart rate/blood pressure response.

Maximal exercise results in a 3-4-fold increase in coronary blood flow secondary to (1) an increase in myocardial oxygen consumption due to an increase in heart rate and contractility and (2) flow-mediated vasodilatation from release of endothelial derived relaxing factor (EDRF = nitric oxide) from normal endothelial cells in response to shear stress from increased flow. In the presence of a hemodynamically significant coronary stenosis, there is a submaximal increase in coronary flow resulting in flow heterogeneity. The radiopharmaceutical is injected at peak exercise and the patient
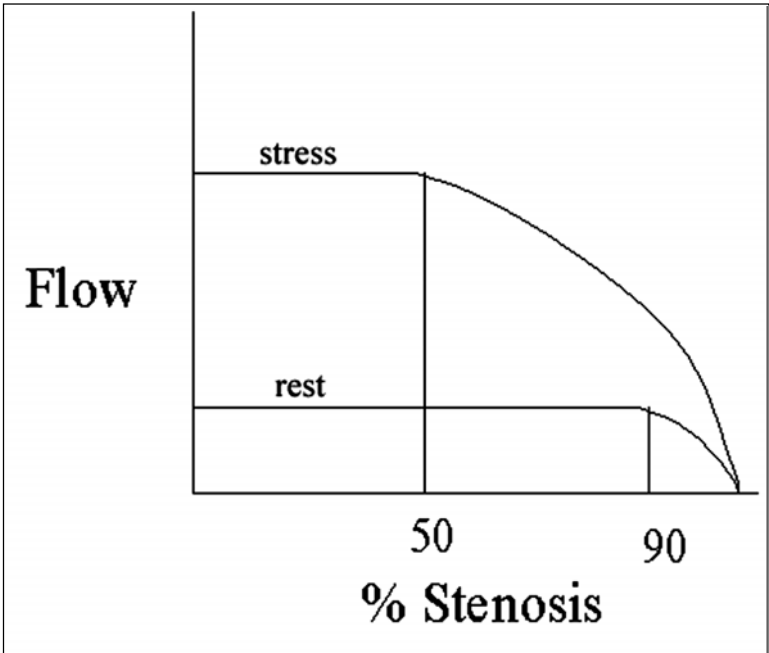
Figure 2. The effect of stenosis on mycocardial flow. At rest (curve A), flow is maintained until a critical stenosis of approximately 90% is reached. With stress (curve B), flow increases by a factor of 4. As the degree of stenosis increases, flow is maintained until approximately a 50% stenosis is reached. In this example, at rest there is no difference in flow between myocardium supplied by a normal artery and that supplied by an artery with a 70% stenosis. However, at stress flow will be reduced to myocardium supplied by the stenotic artery.

is encouraged to continue exercising an additional 1-2 minutes to allow tracer uptake during the time of maximal coronary flow.

The diagnostic accuracy of the examination is dependent on the ability of the patient to exercise sufficiently to induce maximal vasodilatation. A frequently used index to determine if the patient has exercised adequately is whether the patient has attained his target heart rate (THR). The THR is 85% of the predicted maximum heart rate (PMHR) where the PMHR = (220 – age) beats per minute.

Pharmacologic Agents

Pharmacologic vasodilatation with adenosine or dipyridamole is indicated for patients who are unable to exercise or are unable to increase their heart rate (rate-limiting medications) and patients with a left bundle branch block (LBBB) or paced ventricular rhythm.

Due to delayed septal activation in patients with LBBB, there is a corresponding delay in relaxation of the septum resulting in less time for diastolic flow. At rest, this

effect is negligible but as the heart rate increases (and diastole shortens) flow to the septum may be compromised in the absence of coronary stenosis. Vasodilator stress is preferred in this circumstance because it is not associated with a significant increase in heart rate.

Vasodilator stress with adenosine or dipyridamole is contraindicated in patients with significant reactive airway disease. Methylxanthines such as caffeine and theophylline competitively block adenosine receptors and must be avoided for 24 hours prior to the examination.

Exercise and dobutamine increase myocardial oxygen demand and in the presence of hemodynamically significant coronary stenosis result in myocardial ischemia. Vasodilator stress with dipyridamole or adenosine usually creates flow heterogeneity by causing a greater increase in coronary blood flow in normal coronary arteries compared with coronary arteries with significant stenosis. Although myocardial ischemia occurs much less commonly with these agents, there is the potential for the development of ischemia due to a decrease in distal perfusion pressure and/or the development of a coronary steal. Side effects occurring with vasodilator stress can be rapidly reversed by the intravenous administration of aminophylline (100-200 mg over 2-5 min).

Adenosine

Adenosine activates specific receptors in vascular smooth muscle resulting in smooth muscle relaxation and vasodilatation. This results in approximately a fourfold increase in coronary flow. Adenosine is administered intravenously at 140 µg/kg per minute for three minutes followed by radiotracer injection into a different vein and continuation of the adenosine infusion for an additional three minutes.

Dipyridamole

Dipyridamole blocks the cellular re-uptake of endogenously produced adenosine. It is administered as an intravenous infusion of 0.56 mg/kg over 4 minutes. The radiotracer is injected after an additional 4 minutes (i.e., 8 minutes after the start of the dipyridamole infusion) when there is maximal increase in coronary flow. The use of low-level supplemental exercise (e.g., Bruce stage I) following the infusion is used in some centers. It serves to lessen symptoms as well as to improve image quality by reducing infradiaphragmatic splanchnic activity.

Dobutamine

Dobutamine is a beta adrenergic agonist with both positive chronotropic and inotropic effects resulting in coronary arteriolar dilatation secondary to an increase in myocardial oxygen demand. Dobutamine is given as an intravenous infusion in incremental doses starting at 5 µg/kg/min and gradually increasing, at three-minute intervals, to 40 µg/kg/min. If there is a submaximal increase in heart rate, atropine is often administered during maximal dobutamine infusion. Dobutamine is less potent than either adenosine or dipyridamole for maximizing coronary blood flow (two to threefold increase in coronary flow) and may be associated with a lower sensitivity in the detection of CAD. It is primarily used for patients with reactive airway disease in whom adenosine and dipyridamole are contraindicated.
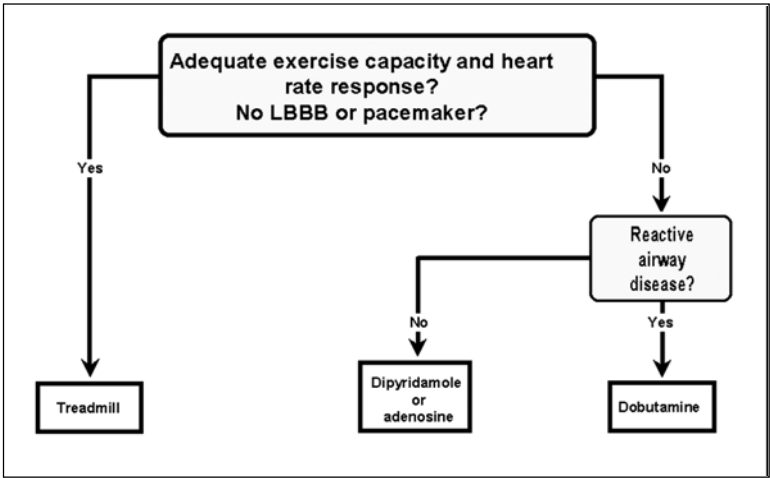
Figure 3. Flow-chart outlining the criteria for the selection of treadmill, dipyridamole/adenosine or dobutamine stress.

Contraindications to the use of dobutamine include acute coronary syndromes (recent MI or unstable angina), significant LV outflow obstruction (hypertrophic cardiomyopathy, severe aortic stenosis), arrhythmia (atrial tachyarrhythmia with uncontrolled ventricular response, complex ventricular ectopy), Wolff-Parkinson-White (WPW) syndrome and severe hypertension.

A flow-chart outlining the approach to selecting a stress technique is shown in Figure 3. A comparison of the various stress modalities with regard to indications, contraindications, mechanisms of action, stopping conditions and treatment of side effects is presented in Table 1.

Radiopharmaceuticals

In MPI, the injected radiopharmaceutical will be delivered to the myocardium in proportion to flow. There will be reduced tracer uptake in regions with reduced blood flow and increased tracer uptake in regions with increased blood flow. The perfusion imaging agents most commonly used are ^{201}Tl-thallium chloride (^{201}Tl), ^{99m}Tc-sestamibi and ^{99m}Tc-tetrofosmin. Table 2 compares the properties of ^{201}Tl and the ^{99m}Tc-perfusion agents.

^{201}Tl-thallium Chloride

Thallium is a metal with properties similar to potassium. The uptake of thallium is primarily an active process involving the Na-K ATPase pump. The extraction efficiency of thallium (i.e., the percentage of thallium extracted by the heart in one circulation through the coronary vessels) is 85%. In the physiologic flow range, uptake is proportional to flow. At higher flow rates the extraction efficiency decreases modestly (Fig. 4). While the initial distribution of thallium is proportional to flow, over the next few hours there is a net washout of activity from the heart so that the late distribution of thallium reflects the potassium pool (i.e., viable myocytes).

ss interventions

	Contra- indication	Mechanism	Stopping Condition	D
	- unstable angina - recent MI - complex ventricular ectopy	– ↑ O_2 demand	- angina - >2mm ST depression - hypotension - complex ventricular ectopy - SVT	
lus exercise	- as for treadmill - severe hypertension - hypertrophic cardio-myopathy - arrhythmia - WPW syndrome	- ↑ O_2 demand	- as for treadmill - BP> 220/120	- l i - k
lus exercise thm increase e	- as for treadmill - asthma - 2nd and 3rd degree AV block - +/- sinus node dysfunction	- coronary vaso-dilatation	- severe angina - marked hypotension	- 1 c

Table 2. Comparison of ^{201}Tl-chloride and ^{99m}Tc-perfusion agents

	^{201}Tl-chloride	^{99m}Tc-perfusion agents
Physical properties		
decay mode	electron capture	isomeric transition
physical half life	72 hours	6 hours
emission	63-80 keV	140 keV
Effective dose	23 mSv (2.3 rems) for 100 MBq	13 mSv (1.3 rems) for 750 MBq x 2 (stress & rest)
Blood flow		
Extraction efficiency	85%	65%
Tracks high flow rates	good	moderate
Temporal distribution	washes out from heart	no significant washout
Image quality	satisfactory	good
Accuracy	good	good

^{201}Tl is the radioactive form of thallium used for scanning. It has a half-life of 72 hours and decays by electron capture. Characteristic x-rays (range of 63-80 keV) produced during electron capture in addition to low abundance 135 and 167 keV gamma rays are imaged. ^{201}Tl has relatively poor imaging characteristics. Its low photon energy makes it subject to attenuation by overlying soft tissues while its long half life limits the activity that can be administered rendering the images relatively count poor.

^{99m}Tc-sestamibi

This tracer is the most commonly used ^{99m}Tc-perfusion agent. It is a lipophilic monovalent cation that is passively taken up by myocytes along an electochemical gradient (and therefore requires cell membrane integrity). The extraction efficiency is approximately 65%. In the physiologic flow range, uptake is proportional to flow. However the deposition of the tracer does not increase linearly with flow but rather tends to level off at higher flow rates (Fig. 4). The distribution of ^{99m}Tc-sestamibi remains relatively fixed for several hours. This allows imaging to be delayed up to several hours after injection thereby facilitating the evaluation of patients presenting with acute chest pain (who can be injected during pain and imaged several hours later once stabilized).

Separate injections are required at stress and rest. These may be done on the same day (e.g., rest injection of 300 MBq and several hours later a stress injection of 1000 MBq) or as a two day protocol (e.g., 750 MBq injections at rest and stress on separate days). A third option is to administer ^{201}Tl for the rest study and ^{99m}Tc-sestamibi for the stress study.
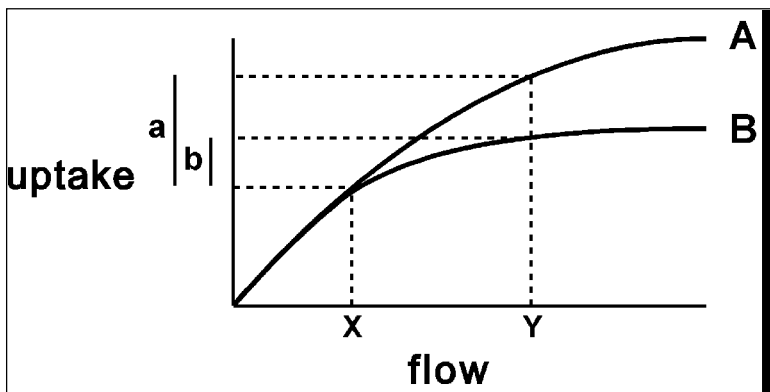
Figure 4. Schematic representation of myocardial uptake versus flow for ^{201}Tl and ^{99m}Tc-sestamibi. Uptake increases linearly with flow at low-flow rates for both tracers. At higher flow rates, there is a "roll-off" which is less marked for ^{201}Tl (curve A) than for ^{99m}Tc-sestamibi. For two areas of the heart with flows of 'x' and 'y', there is a greater difference in uptake with ^{201}Tl ('a') than with ^{99m}Tc-sestamibi ('b').

Hepatobiliary excretion of tracer may result in liver and/or gut activity obscuring the inferior wall of the left ventricle. To minimize adjacent infra-diaphragmatic activity imaging is delayed for at least 30 minutes after a stress injection and 60 minutes after a rest injection.

^{99m}Tc-tetrofosmin
^{99m}Tc-tetrofosmin is another commonly used ^{99m}Tc-perfusion agent with properties similar to ^{99m}Tc-sestamibi. While its extraction efficiency is somewhat lower than that of ^{99m}Tc-sestamibi there is less hepatobiliary extraction potentially decreasing interference with inferior wall assessment.

PET Tracers
While not available in many centers, PET radiopharmaceuticals can be used to assess myocardial flow and viability. ^{18}F-fluorodeoxyglucose (FDG) is a glucose analogue. In the fasting state the myocardium normally uses fatty acids as its metabolic substrate. In ischemic myocardium, glucose is used preferentially. Increased uptake of FDG (in comparison to flow which is assessed with a separate radiopharmaceutical) in an ischemic segment indicates sustained metabolic activity and implies myocardial viability.

PET tracers to assess myocardial blood flow include ^{13}N-ammonia and rubidium-82 (^{82}Rb). ^{13}N-ammonia has a high extraction efficiency of 90%. The energy of the positron and consequently its path range is low yielding improved resolution. Because of its short half-life of ten minutes, an on-site cyclotron is needed to produce ^{13}N. ^{82}Rb has properties similar to potassium and thallium. Since it is produced from a strontium-82 generator, an on-site cyclotron is not required. ^{82}Rb has a short half life of 1.3 minutes with an extraction efficiency lower than that of ^{13}N-ammonia. Its positron energy is greater than that of ^{13}N-ammonia and hence resolution is poorer.
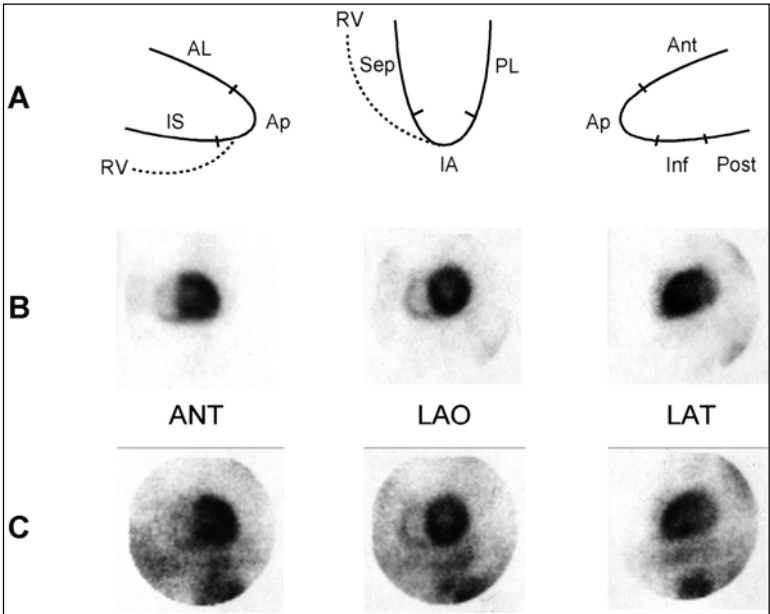
Figure 5. Normal planar ^{201}Tl scan with images in the anterior, LAO and LAT projections. Panel A shows the nomenclature of the myocardial segments. There is uniform uptake of tracer in all segments of the left ventricle on the immediate post-stress images (panel B) and on the delayed images 4 hours post injection (panel C). Typically, the counts in the heart decrease by approximately 50% over 4 hours. For the purpose of comparison, however, the intensity of uptake within the heart is normalized to the same brightness as the stress images and therefore the decrease in counts is not apparent. (Ant-anterior; AL-anterolateral; Ap-apex; Inf-inferior; IA-inferoapical; IS-inferoseptal; Post-posterior; PL-posterolateral; Sep-septum; RV-right ventricle)

Planar, SPECT and Gated SPECT Imaging

Planar imaging usually consists of three views of the heart obtained in the anterior, LAO and steep LAO projections (Fig 5). While SPECT imaging (Figs. 6 and 7) is technically more demanding than planar imaging, advantages to its use include higher lesion contrast and an improved ability to localize defects. Conventionally a 180° acquisition (from the right anterior oblique to the left posterior oblique projection) is utilized for cardiac imaging rather than a full 360° acquisition since few cardiac photons are detected in the posterior projections.

SPECT was originally performed with single-head gamma cameras. These have largely been replaced with multi-head gamma cameras which increase counting efficiency. A common configuration used for cardiac imaging is a two-headed camera with the heads oriented at right angles. The gantry need only rotate 90° in order to obtain a 180° acquisition.

The principle of R-wave synchronized cardiac gating is discussed in Chapter 4. In the same way, cardiac SPECT data can be gated to obtain eight sets of tomographic
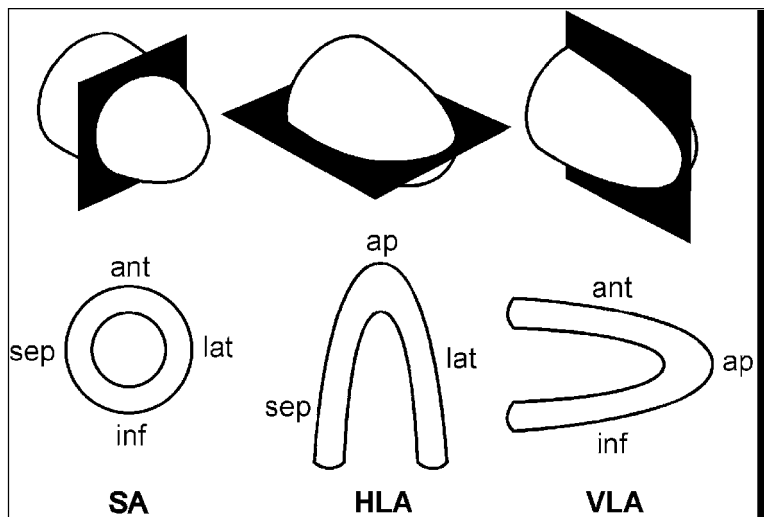
Figure 6. Schematic showing the three orthogonal planes used for SPECT myocardial imaging and segmental nomenclature. The short-axis (SA) slices can be considered as "cucumber" slices through the left ventricle. The horizontal long axis (HLA) slices are similar in orientation to the echocardiographic four chamber view. The vertical long axis (VLA) slices can be thought of as viewing the heart from a lateral projection. (ant-anterior; ap-apex; inf-inferior; lat-lateral; sep-septal)

data spanning the R-R interval. This allows for assessment of wall motion and using commercially available software the determination of the left ventricular ejection fraction (Fig. 8). Gated SPECT has become the standard technique for MPI.

Interpretation and Quantification

The interpretative approach to myocardial perfusion imaging is illustrated in Figure 9. A defect at stress which improves or normalizes at rest is termed a reversible defect and indicates ischemia. An infarct will result in diminished or absent uptake of tracer at stress and at rest. This pattern is termed a fixed defect.

The distribution of radiotracer in the heart is assessed qualitatively by examining the tomographic slices in orthogonal planes. It is also possible to generate a polar plot that condenses the three-dimensional information into a two-dimensional image (Fig. 10). Tracer distribution in the myocardium for a group of patients with a low likelihood of CAD can be used to generate a normal database. In a polar plot, segments of the myocardium below the normal range can be highlighted (Fig. 11).

A semi-quantitative method of representing the extent and severity of the perfusion abnormalities at stress has become popular. The heart is divided into 17 or 20 segments (Fig. 12). Each segment is graded on a five-point scale from normal (0) to absent uptake (4). The sum of these values is the 'summed stress score' (SSS) and is a useful index of cardiac risk. In a similar manner a summed rest score (SRS) can be generated as well as a summed difference score (= SSS-SRS).
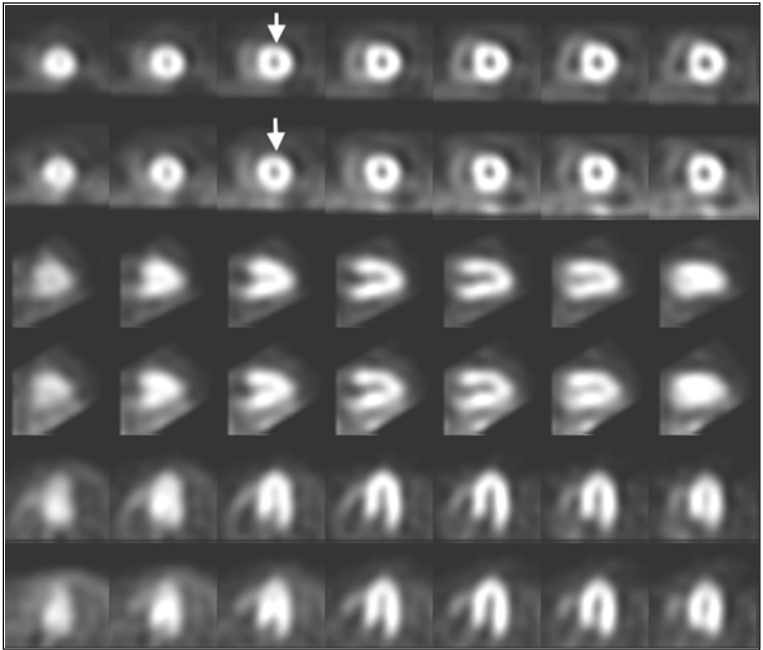
Figure 7. Normal MPI study in a 54 year old woman referred because of a positive GXT. There is mildly diminished activity anteriorily both at stress and rest (arrow) attributable to breast attenuation. No other fixed or reversible abnormalities are identified. The top row are short axis (SA) images of the left ventricle at stress and the second row are corresponding SA slices at rest going from apex (on the left) towards the base of the heart (on the right). The next two rows are vertical long axis images (VLA) at stress and rest going from septum to lateral wall. The bottom two rows are horizontal long axis (HLA) at stress and rest going from inferior to superior slices. For subsequent MPI studies the same format has been used.

Two ancillary findings, increased lung thallium activity and transient ischemic dilatation are useful in defining patients at high risk for subsequent events. Increased lung activity is related to increased LV filling pressure and accumulation of ^{201}Tl in the pulmonary interstitial space is a marker for patients with multivessel coronary disease and/or LV dysfunction. It is assessed quantitatively in the anterior view performed immediately after the injection of ^{201}Tl during stress, by comparing activity in lung to that in the hottest area of the myocardium. The lung/heart ratio is less useful with ^{99m}Tc-sestamibi and tetrofosmin, partly because of the 30-60 minute delay before imaging begins. Dilatation of the LV cavity at stress compared to rest is variously termed transient ischemic dilatation or stress-induced dilatation. It is caused by subendocardial ischemia at stress (causing an apparent increase in LV size) or by true dilatation of the LV cavity post-stress.

3
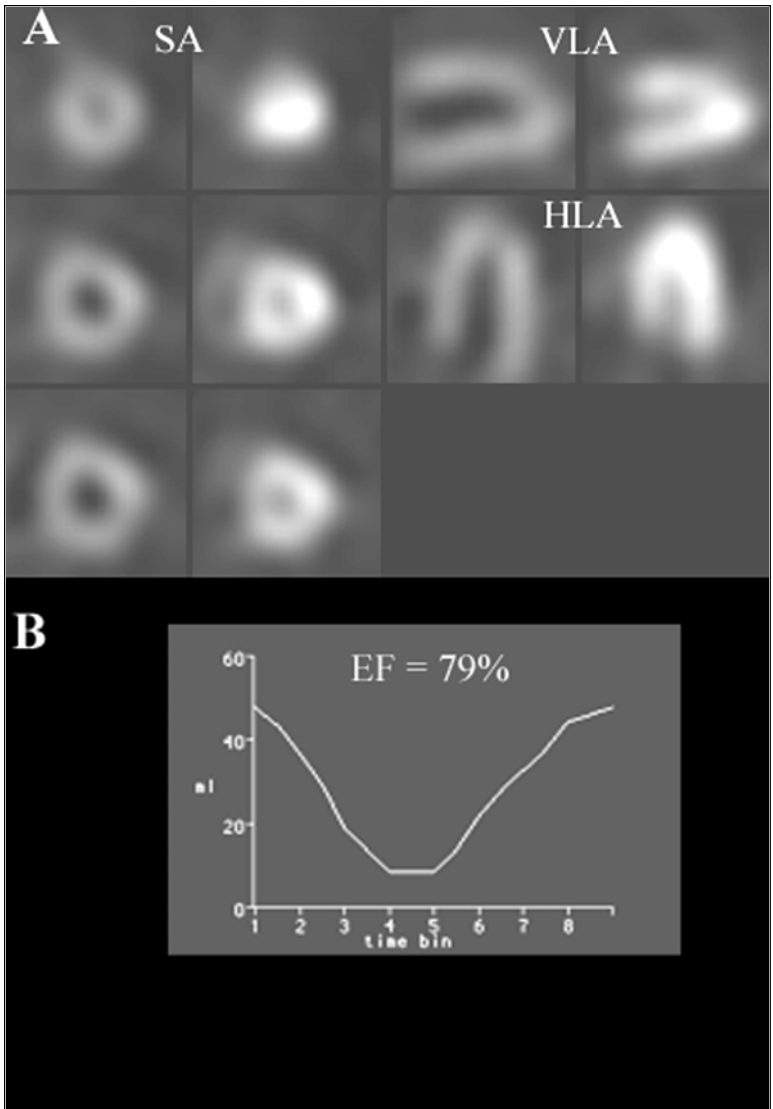
Figure 8. Gated SPECT. (A) 3 short axis slices are shown at ED on the left and ES on the right. Note that the ventricle is smaller and brighter at ES. The increase in brightness is related to systolic thickening of the ventricular wall. On the right hand side of the panel, single VLA and HLA mid-ventricular slice are shown at ED and ES. (B) A program identifies the endocardial margins of the left ventricle for all frames and generates a volume curve from which the ejection fracture (EF) is derived.
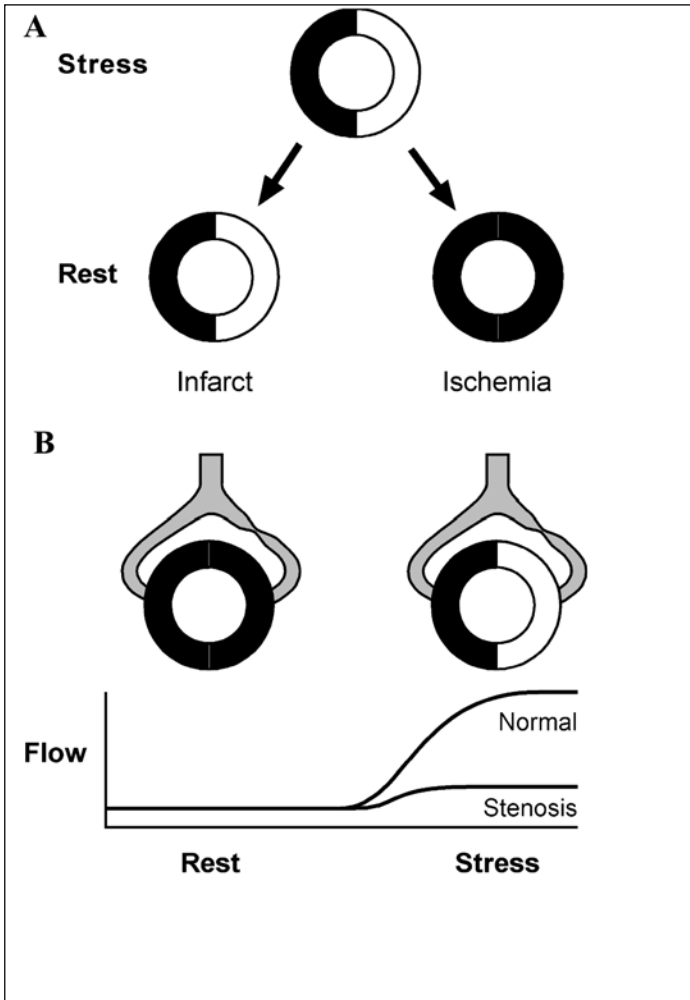
Figure 9. (A) Fixed and reversible defects. A defect (light area) present at stress and rest is termed a fixed defect and typically represents an area of infarction. A defect present at stress but not at rest is termed a reversible defect and implies ischemia. (B) Schematic showing induction of a perfusion defect at stress. One segment of the ventricle is supplied by a normal artery and a second segment by a stenoic artery. At rest, there is equal flow to both myocardial segments and equal uptake of tracer. At stress, flow to the myocardium supplied by the patent artery increases markedly. Flow to the myocardium supplied by the stenoic artery increases marginally. Less tracer will be taken up in the myocardium supplied by the stenotic vessel than in normally supplied myocardium, i.e., a perfusion defect is induced at stress.

3
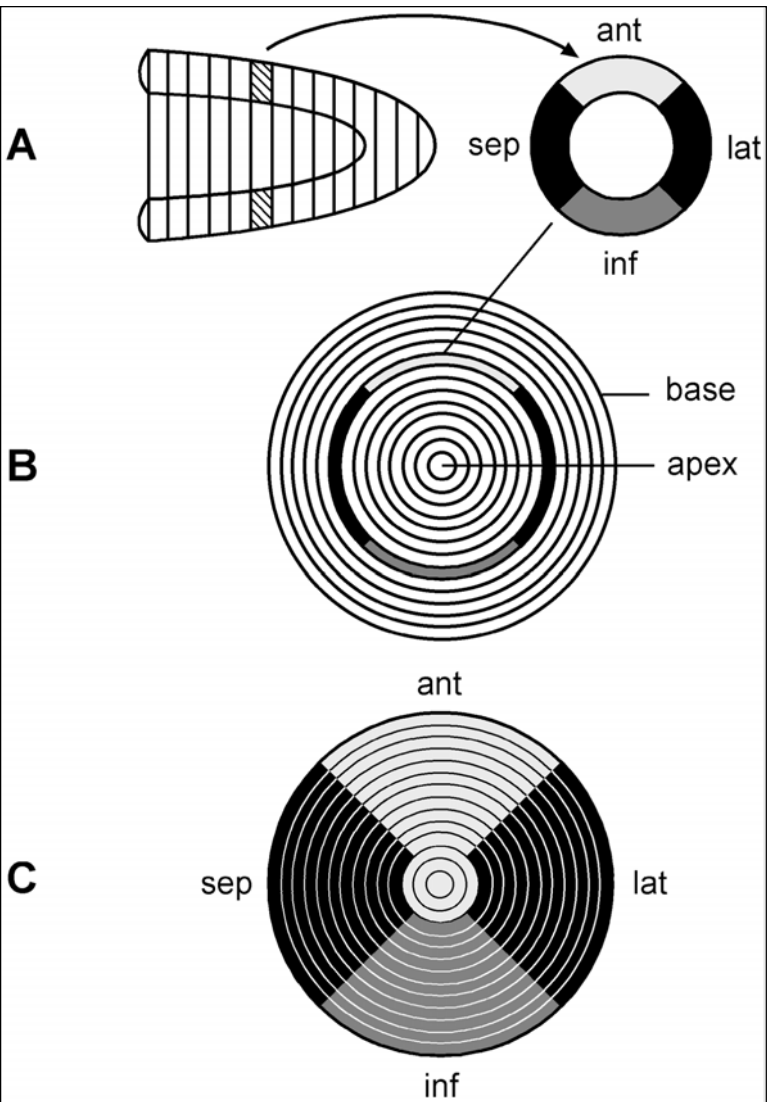
Figure 10. Schematic showng derivation of the polar plot. The heart is divided into one pixel slices (A). A single slice is shown on the right side of panel A. The septum and lateral wall show normal uptake while the inferior wall shows a mild defect and the anterior wall a severe defect. Information from this slice (B) and all other slices is inserted into a polar plot (C). In this example, the septum and lateral wall are normal. The entire inferior wall shows mildly diminished activity while the entire anterior wall and apex show markedly dimished uptake.
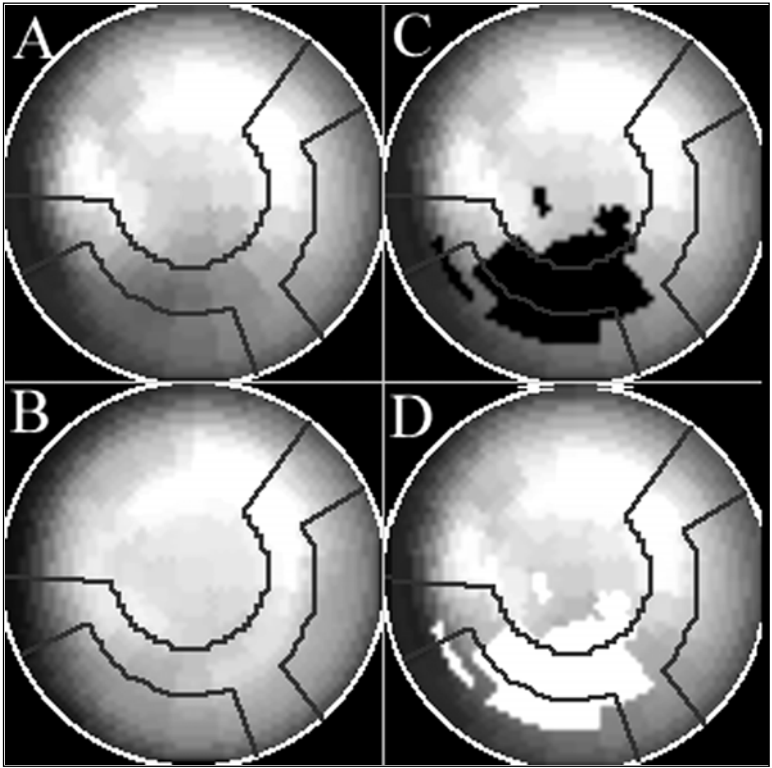
Figure 11. Polar plot of study shown in Figure 17. (A) Stress polar plot showing diminished activity (darker area) in the inferior wall. (B) Rest polar plot showing improved uptake in the inferior wall. (C) Using the stress polar plot, areas considered to be abnormal (based on normal population database) are highlighted in black. (D) Using this "blackout" image, areas considered to improve significantly between stress and rest (i.e., the reversible inferior wall defect) are highlighted in white.

Clinical Role in the Diagnosis of Coronary Artery Disease

Indications

One of the major applications of MPI is the detection of hemodynamically significant CAD in patients with an intermediate pre-test likelihood of coronary disease. In most institutions, a GXT is the initial diagnostic test unless there are resting electrocardiographic abnormalities or the patient is on digoxin (since inducible ST segment depression in this population is of uncertain diagnostic significance). MPI is also indicated in patients who have a non-diagnostic GXT because they were unable to reach their target heart rate and did not have angina or ST segment depression (Table 3). In accordance with Bayes' theorem the predictive accuracy of a test depends not only on its sensitivity and specificity but also on the prevalence of

3
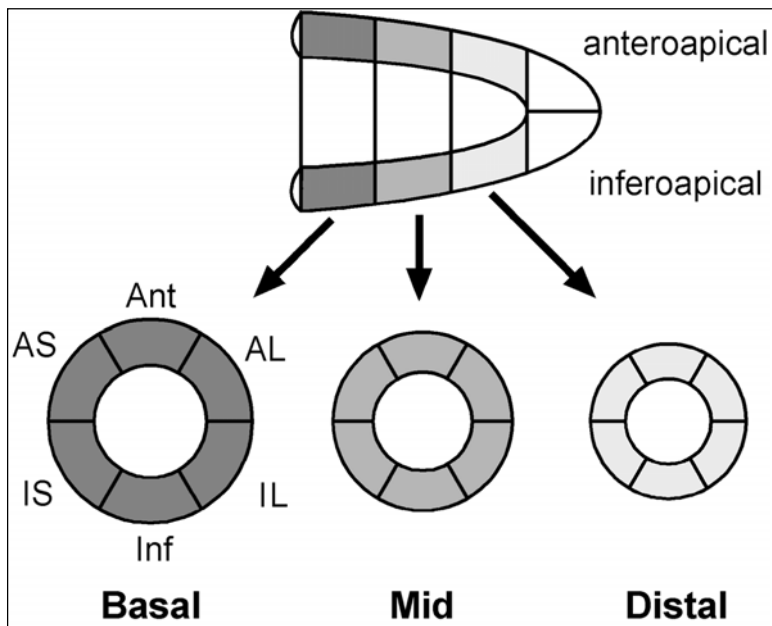
Figure 12. Twenty segment model used for calculation of the stress severity score (SSS). The left ventricular apex is divided into two segments (anteroapical and inferoapical). The remainder of the ventricle is divided into three cylindrical slices representing the distal, mid and basal thirds of the ventricle. Each of these thirds is divided into six segments (Ant-anterior; AL-anterolateral; PL-posterolateral; Inf-inferior; IS-inferoseptal; AS-anteroseptal) for a total of 20 segments. To calculate the SSS, each segment is assigned a score from 0 (normal) to 4 (absent) uptake. The sum of the scores for all 20 segments is the SSS.

disease in the population under study (for a simplified approach to Bayes' theorem see FAQs). Diagnostic testing is most effective in patients with an intermediate prevalence of disease estimated from the patient's age, gender and chest pain history, together with consideration of coronary risk factors (Fig. 13).

Sensitivity

The overall sensitivity of SPECT imaging using either ^{201}Tl or ^{99m}Tc-sestamibi is 85-90%. SPECT detects stenosis in individual vessels with a sensitivity for the left anterior descending artery of 80%, right coronary artery 80% and circumflex 70%. In those patients in whom SPECT cannot be performed (unable to lift left arm, unable to lie still, body weight considerations), quantitative planar studies yield a similar sensitivity (on a per patient basis) although the identification of individual vessel stenoses is reduced.

Sensitivity varies depending upon:

Table 3. Indications for MPI for detection of coronary artery disease (CAD)

Intermediate Pretest Probability of CAD
Abnormal Resting Electrocardiogram
  • Non-specific ST-T Abnormalities
  • Left Ventricular Hypertrophy
  • Conduction Disturbance
  • Ventricular Pacing
  • Pre-excitation (WPW syndrome).
Non-diagnostic Treadmill Stress Test
  • Inability to Reach ≥ 85% Maximal Predicted Heart Rate
  • Digoxin

• Extent of Coronary Disease

The sensitivity of detecting CAD increases from 80% in patients with single vessel disease to 90% in double vessel disease and 95% in triple vessel disease. The ability to correctly identify a patient as having multivessel disease (by detecting perfusion defects in two or more coronary artery territories) is 65% (Fig. 14).

• Severity of Coronary Disease

Angiographically, stenoses are classified as moderate if they compromise 50-70% of the lumen and severe if >70%. Since impairment of coronary flow reserve is related to the severity of coronary stenosis, the sensitivity of perfusion imaging will vary with stenosis severity and ranges from 60% with moderate stenosis to 90% with severe stenosis.

• Workload

The identification of inducible ischemia with perfusion imaging depends upon creating coronary flow heterogeneity. Patients who are only able to perform a low workload on the treadmill have a submaximal increase in coronary flow. The sensitivity of detecting CAD is reduced in patients unable to attain 70% of their predicted maximum heart rate. In those able to exceed 70% but unable to reach 85% of predicted maximum, it appears that the detection of individual coronary stenoses is decreased while sensitivity (on a per patient basis) is maintained. If patients cannot perform adequate exercise, pharmacologic vasodilatation with dipyridamole or adenosine should be employed. In patients with significant reactive airway disease dobutamine is an alternative with similar sensitivity to exercise.

• Drugs

Sensitivity may also be adversely affected by drugs which reduce myocardial oxygen demand and/or improve coronary flow (nitrates, beta blockers, calcium channel blockers). Beta blockers and non-dihydropyridine calcium channel blockers (verapamil, diltiazem) decrease myocardial oxygen demand and reduce the sensitivity of MPI with treadmill exercise and dobutamine whereas nitrates and dihydropyridine calcium channel blockers (nifedipine, amlodipine) may lower the sensitivity of all stressors because they dilate conductance arteries. If possible, nitrates should be withheld on the day of the stress test and in clinically stable patients rate-limiting drugs should be held for 24-36 hours prior to a treadmill or dobutamine test. As indicated earlier, since methylxanthines block adenosine receptors, patients undergoing perfusion scintigraphy with either dipyridamole or adenosine must be
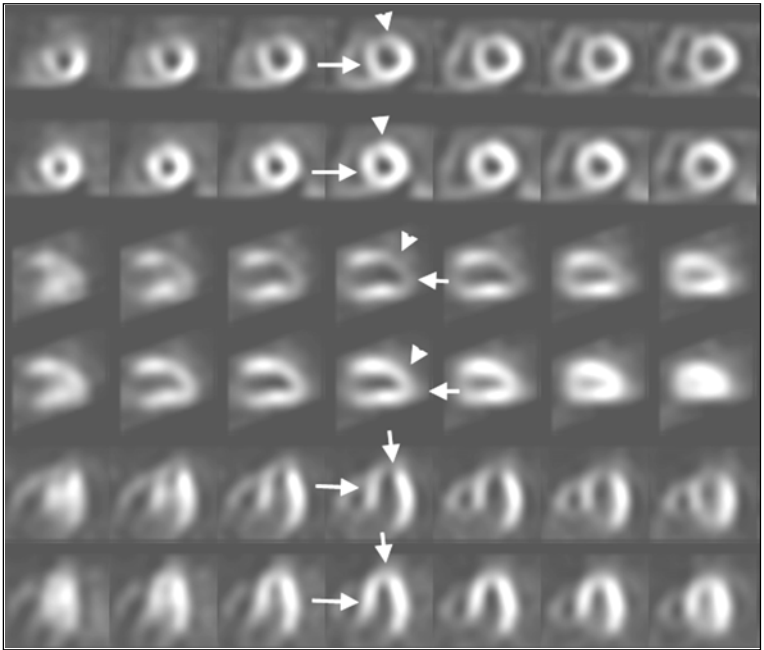
Figure 13. 85 year old male with atypical chest pain. The MPI study was performed for diagnostic purposes. There is extensive severe reduction of activity in the septum (long arrow), anterior wall (arrowhead) and apex (short arrow) at stress with normalization at rest. A subsequent angiogram showed an occluded LAD with filling of the LAD via collaterals from the RCA. Note the dilation of the LV cavity at stress (transient ischemic dilation) which is evident in all three planes.

on a caffeine-free diet for approximately 24 hours and avoid methylxanthine containing medications during this time.

• Gender

The sensitivity of MPI in detecting CAD in women is reduced compared to men. Reasons for this include: (1) left ventricular cavity size in women tends to be smaller. Small lesions may therefore be harder to resolve with SPECT. (2) Women are less likely to perform an adequate level of treadmill exercise. (3) Disease severity in women is generally less than in men and, therefore, sensitivity will decrease as stenosis severity decreases. (4) Breast attenuation causes greater variability in the appearance of the anterior wall. True anterior wall defects may be attributed to breast attenuation thus reducing sensitivity.

While the "gold standard" for the detection of CAD is coronary arteriography, it is important to appreciate that the anatomic data from angiography may not always be concordant with the physiologic data provided by perfusion imaging. Coronary flow reserve using Doppler flow velocity technique correlates better with SPECT
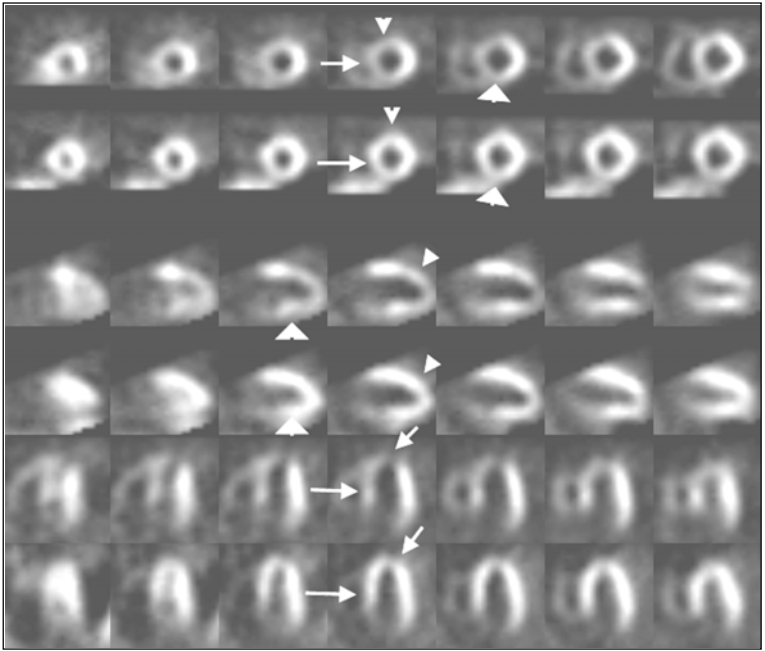
Figure 14. 70 year old male with stable angina. The MPI study was performed for risk assessment. There is reduced activity in the anterior wall (narrow arrowhead), apex (short arrow) and septum (long arrow) at rest with improvement at rest. There is reduced activity inferiorly at stress with improvement of the distal inferior wall at rest (broad arrowhead). There is evidence of both LAD and RCA disease.

perfusion imaging than with quantitative coronary angiography. An additional limitation of coronary angiography relates to the considerable variability in the extent of jeopardized myocardium in patients with stenosis of similar anatomic severity and location (Fig. 15).

Specificity

The specificity of perfusion imaging is between 70 and 80%. One potential explanation for the apparent low specificity is referral bias i.e., the selective referral of patients with an abnormal perfusion study for coronary angiography. It has been suggested that the "normalcy rate" (the percentage of patients with a low pre-test probability of coronary disease with normal images) should be used instead of specificity. The normalcy rate for SPECT imaging is approximately 90%.

False positive studies may be due to technical factors (e.g., patient motion), soft tissue attenuation and left bundle branch block (septal hypoperfusion at rapid heart rates). Patient motion during acquisition of a study may cause apparent myocardial defects on the reconstructed images. To ensure that there was no significant patient
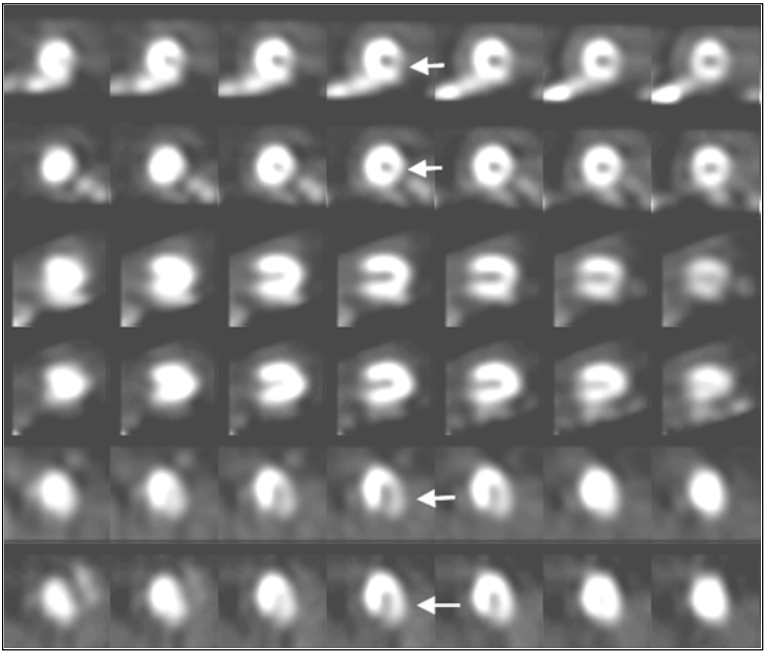
Figure 15. 71 year old male with post MI angina. An angiogram showed moderately severe stenosis of the proximal RCA and severe stenosis of the circumflex artery. The MPI study was performed to identify the "culprit" artery prior to revascularization. At stress, severe reduction of activity is seen in the lateral wall on the short axis and HLA images (arrows) with improvement at rest. Based on the finding of a reversible lateral wall abnormality, the patient underwent a PTCA of the circumflex artery with excellent results.

motion the projection images are examined. This is typically done by reviewing the images in cine mode looking for evidence of vertical or horizontal movement of the heart. Another cause of an apparent myocardial defect is attenuation from overlying soft tissue structures. In women breast tissue frequently overlaps the anterior myocardial wall on many of the SPECT projections. In these projections fewer anterior wall counts will be detected and consequently, upon reconstruction of the data, the anterior wall will show apparently diminished uptake (Fig. 7). Attenuation of the inferior wall is frequently seen in men with a protuberant abdomen and an elevated left hemidiaphragm.

Clinical Role in Prognosis and Risk Stratification

MPI provides important prognostic information in a wide spectrum of patients with CAD. The ability to identify patients at high and low risk has been validated for both planar and tomographic techniques using ^{201}Tl or ^{99m}Tc-sestamibi with exercise or pharmacologic stress.

Patients with Known or Suspected Coronary Disease

A normal myocardial perfusion study in patients with angiographically documented coronary artery stenosis as well as in patients with suspected coronary disease identifies a low risk group with a rate of cardiac death or non-fatal myocardial infarction less than 1% per year which is similar to the general population. On the other hand (a) reversible or fixed perfusion abnormalities representing jeopardized viable or infarcted myocardium particularly in multiple vascular territories (b) increased lung thallium uptake or (c) transient ischemic dilatation identify patients at increased risk of future cardiac events. There is a significant relation between the extent and severity of the perfusion abnormality and cardiac death or non-fatal infarction. Importantly, MPI provides independent and incremental prognostic information to that already available from clinical and exercise variables.

A cost-effective strategy (Fig. 16) is to use perfusion imaging in patients who have an intermediate probability of coronary disease after a GXT. Patients at low risk after clinical assessment and stress testing have a low event rate and may not require additional investigation. Patients with a high risk GXT (based on a low workload, angina, exercise induced hypotension, ST segment depression that is severe, occurs at a low workload and persists into the recovery period) warrant coronary angiography while those considered at intermediate risk after GXT should be evaluated with a myocardial perfusion study. While significant increases in cardiac death and/or myocardial infarction (MI) occur as a function of worsening scan results, patients with mildly abnormal perfusion studies (SSS = 4-8) are at intermediate risk for MI but low risk for cardiac death. Since myocardial revascularization (CABG or PTCA) has not been shown to reduce the rate of subsequent MI, patients with a mildly abnormal perfusion study can be managed with medical therapy unless they have disabling symptoms. Similarly patients with an intermediate risk treadmill test but a normal exercise perfusion study are at low risk for subsequent cardiac death and can be managed medically without coronary angiography until they develop disabling symptoms requiring revascularization.

Following Myocardial Infarction

MPI is ideally suited to identify the presence and extent of jeopardized viable myocardium after acute myocardial infarction thereby identifying patients at risk for future cardiac events (Fig. 17). Compared with exercise stress testing, MPI has an increased sensitivity for detecting multi-vessel coronary disease and identifying patients at risk for subsequent cardiac events. MPI can also localize ischemia, identify viable jeopardized myocardium and determine global left ventricular systolic function with gated acquisition.

Pre-discharge post-infarction myocardial perfusion imaging with either ^{201}Tl or ^{99m}Tc-sestamibi in conjunction with submaximal exercise or vasodilator stress (dipyridamole or adenosine) stratifies patients into low, intermediate and high risk. The extent and severity of the perfusion defect and the degree of reversibility are predictors for in-hospital and late cardiac events whether or not patients receive thrombolytic therapy.

Early risk stratification is important, since most early (< 1 year) post-MI cardiac events (e.g., unstable angina, recurrent infarction, cardiac death) occur within 4-6
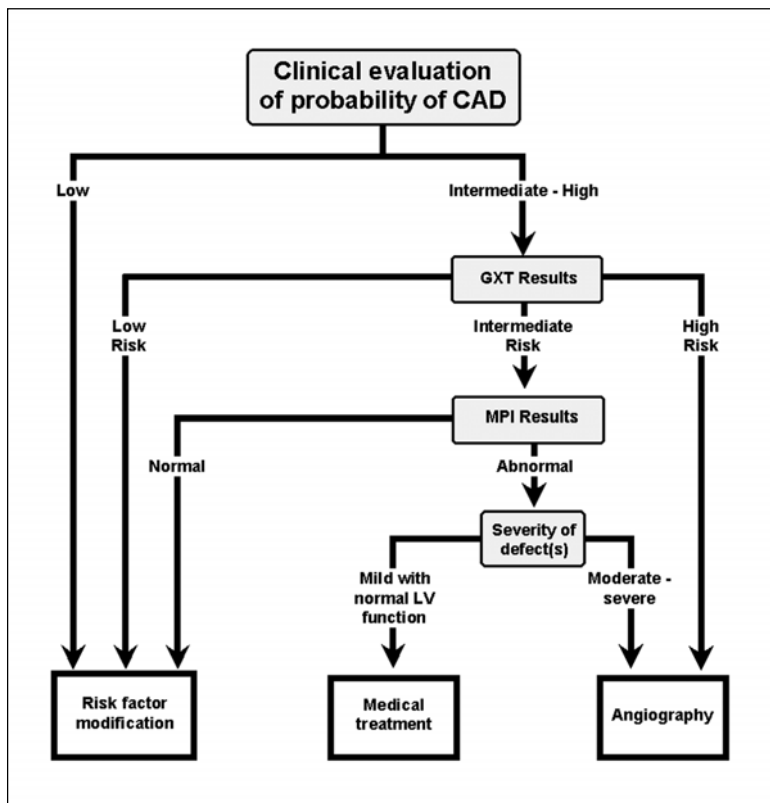
Figure 16. Flow chart outlining a cost-effective strategy for the evaluation of coronary artery disease (MPI-myocardial perfusion imaging; GXT-graded exercise stress test).

weeks of the acute event. The ability to perform vasodilator stress imaging safely two to four days following acute infarction with greater separation of low and high risk patients compared with submaximal exercise imaging makes this an attractive strategy. Patients identified as low risk can be considered for early discharge whereas those at high risk can be referred for early angiography and possible revascularization.

Unstable Angina

Patients with an acute non-ST segment elevation coronary syndrome (unstable angina or non-Q wave myocardial infarction) who have recurrent angina, ST segment depression or elevated troponin should be considered for early coronary angiography. Patients with unstable angina without ST segment depression or biochemical markers of myocardial injury who respond to initial medical treatment can be effectively risk stratified with perfusion imaging. In the latter group, there is no reduction in hard cardiac events with early coronary angiography and revascularization compared with
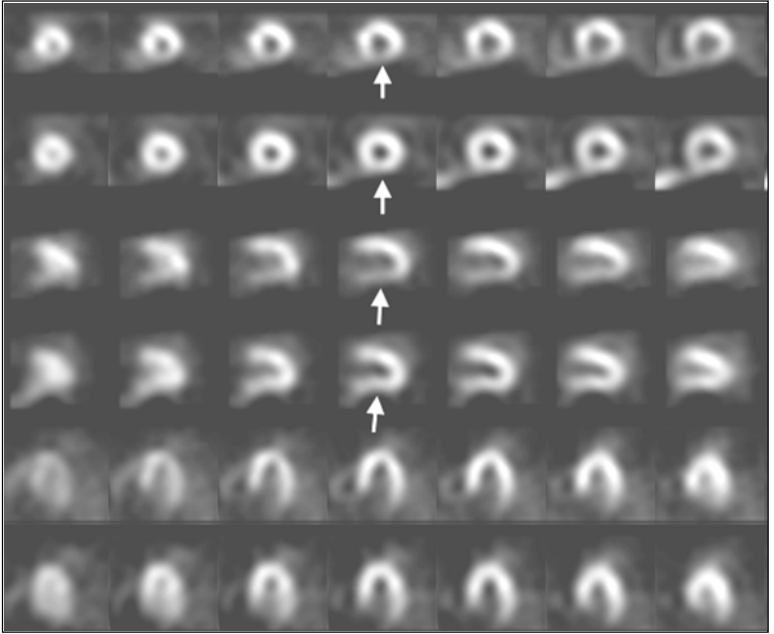
Figure 17. 50 year old male with previous inferior MI. A GXT demonstrated mild ST segment depression at a high workload without angina. The MPI study was done for risk stratification. A large area of severely decreased uptake is seen in the inferior wall at stress (arrows). This area normalizes at rest. Subsequently, angiography demonstrated an occlusion of the RCA which was dilated and stented.

a non-invasive strategy reserving angiography for patients with recurrent angina or evidence of inducible ischemia. The presence of jeopardized viable myocardium identifies patients at high risk for cardiac death or non-fatal infarction whereas the absence of a reversible defect identifies patients at low risk.

Pre-operative Cardiac Risk Assessment

Pre-operative MPI can help identify patients at high risk for perioperative cardiac complications by identifying jeopardized viable myocardium.

Patients undergoing vascular reconstructive surgery including repair of an abdominal aortic aneurysm have a high prevalence of CAD and are at an increased risk of perioperative cardiac ischemic complications including death and non-fatal myocardial infarction. Age greater than 70 years, history of myocardial infarction, cardiac failure, angina pectoris and diabetes help stratify patients into low, intermediate (one to two factors) and high risk (three or more factors). Patients considered by clinical assessment to be at intermediate risk can be further risk stratified with dipyridamole MPI based on the extent and severity of reversible defects. Patients at high clinical risk may be referred for coronary angiography although we prefer an

initial strategy of MPI in both intermediate and high risk patients reserving angiography for those with extensive inducible ischemia.

The negative predictive value of a normal scan is approximately 99% while approximately 30% of intermediate risk vascular surgical patients with scintigraphic evidence of inducible ischemia will have a perioperative cardiac ischemic complication. Perioperative beta-blockers reduce cardiac death and non-fatal infarction in high-risk patients. Alternatively patients considered to have a high probability of multivessel CAD and left ventricular dysfunction by non-invasive assessment can selectively be referred for coronary angiography and possible myocardial revascularization (CABG or PTCA) with a view to improving their long-term survival.

Clinical Role in Defining Myocardial viability

Impaired left ventricular function is an important determinant not only of symptoms but also of survival. Regional LV dysfunction may result from (a) a transmural myocardial infarction (b) a non-transmural (subendocardial) myocardial infarction (c) a transient period of myocardial ischemia ("stunning") causing a wall motion abnormality for a variable length of time after the transient ischemic insult or (d) a prolonged period of resting myocardial hypoperfusion ("hibernation"). It has been suggested that hibernating myocardium may actually represent the effects of repetitive stunning i.e., patients with hibernating myocardium have reduced coronary flow reserve without reduced resting coronary blood flow.

If the myocardium in the abnormally contracting region is viable i.e., has sustained metabolic activity, left ventricular dysfunction in patients with CAD may be potentially reversible with restoration of coronary blood flow for those patients with stunned or hibernating myocardium. On the other hand regional left ventricular dysfunction due to myocardial infarction (scar) is irreversible after revascularization. Recovery of regional left ventricular dysfunction may occur (a) after thrombolytic therapy or PTCA for acute myocardial infarction (b) after exercise induced ischemia (c) in patients who have experienced unstable angina and (d) in the setting of chronic "silent" ischemia (when overt or compensated cardiac failure may be the dominant clinical finding) after CABG or PTCA.

There are a number of non-invasive techniques available for the assessment of myocardial viability (Table 4). Metabolic imaging with ^{18}F-FDG is often considered the gold standard for assessing myocardial viability. ^{18}F-FDG uptake in a region of decreased perfusion (mismatch pattern) supports a determination of myocardial viability. Presently, few centers have the capacity to perform PET studies.

^{201}Tl and ^{99m}Tc-sestamibi myocardial perfusion imaging assess perfusion and cell membrane integrity and therefore provide information regarding myocardial viability. Both defect reversibility and severity are important markers of viable myocardium (Fig. 18). With quantitative analysis of regional tracer activity, a threshold of ^{201}Tl or ^{99m}Tc-sestamibi activity greater than 50% of maximal regional activity as a criterion for viability has a positive predictive accuracy of approximately 70% and a negative predictive accuracy of 90% for improved regional left ventricular function after revascularization. The predictive accuracy of myocardial perfusion imaging for functional recovery can be improved by considering the level of regional tracer activity as a continuum and documenting whether there is inducible ischemia.

Table 4. Non-invasive assessment of myocardial viability

---

^{201}Tl imaging
- Stress and 4 hour redistribution
- Stress, 4 and 24 hour redistribution
- Stress and 4 hour redistribution and reinjection
- Rest and 4 Hour redistribution

^{99m}Tc-perfusion imaging
- Stress and rest
- Rest (± after nitrate)

^{18}F-Fluorodeoxyglucose

The appropriate "gold" standard for determining the benefit of revascularization of viable myocardium should be the improvement in symptoms and survival. Because of the established relationship between left ventricular dysfunction and mortality, improvement in left ventricular function after revascularization has been considered the only important benefit of revascularization. It is possible, however, that by (a) attenuating left ventricular remodeling (b) reducing ventricular arrhythmias and (c) reducing the risk of subsequent fatal ischemic events that symptoms and event-free survival may improve with successful revascularization of viable myocardium even without a significant change in left ventricular function.

Frequently Asked Questions (FAQs)

I keep hearing about Baye's theorem and Bayesian analysis. What is it?

Essentially Baye's theorem states that if one uses an imperfect test, the likelihood of an individual having the disease for which he/she is being tested will vary with the prevalence of disease in the population. The best way to understand this is to work through an example (Table 5). Let us consider that based on a patient's gender and symptomatology, the likelihood (or "prevalence" or "pre-test probability") of CAD is 60%. Let us also assume that the patient will undergo a myocardial perfusion scan for which the sensitivity and specificity are 90%.

We know that in a population of 100 with a 60% disease prevalence 60 patients would be expected to have CAD and 40 patients would be expected to be free of CAD. Assuming a sensitivity of 90%, the myocardial perfusion study would detect disease in 54 (true positive) patients and miss disease in 6 (false negative) patients.

Given a specificity of 90%, one can anticipate that of the 40 patients without disease 36 would be correctly labeled (true negatives) and four patients would be incorrectly labeled as having CAD (false positive). Combining this information, we can see that of 58 patients with a positive scan, 54 patients will be correctly identified as having CAD. In other words the positive predictive value = 54/58 = 93%. Similarly of 42 patients with a negative study, 36 will indeed not have disease (i.e., the negative predictive value = 36/42 = 86%). In summary, the 60% pre-test probability of CAD will be increased to 93% with a positive scan and decreased to 14% (or 100%— 86%) with a negative scan. These same calculations can be applied to any pre-test
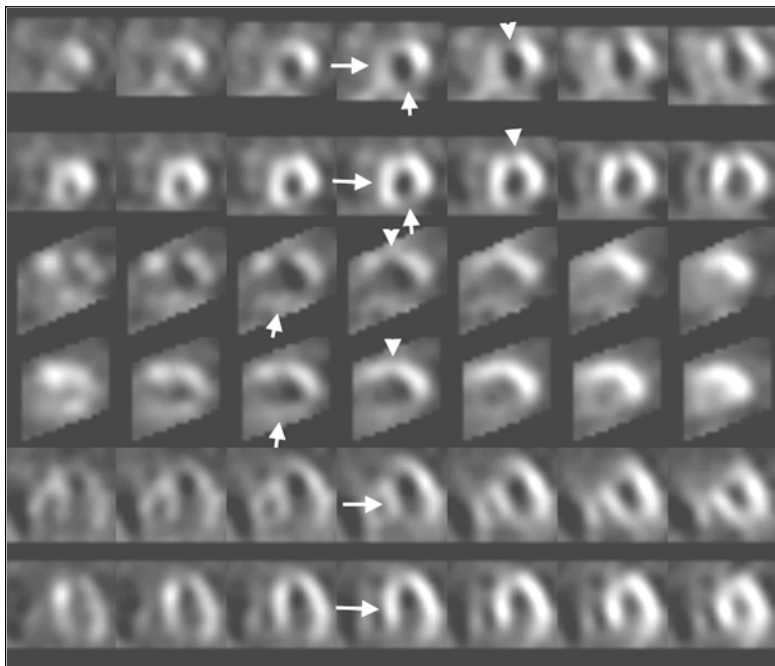
Figure 18. 53 year old male with a previous history of an inferior MI being considered for revascularization. Both a ventriculogram and an equilibrium radionuclide angiocardiogram showed widespread wall motion abnormalities and global decrease in systolic function (ejection fraction = 28%). The study was performed as a dipyridamole ^{201}Tl stress study with additional images at four hours and following reinjection. Only the stress and reinjection images are shown. There is severe (<50% of peak) fixed reduction of activity in the inferior wall (short arrow), a reversible septal abnormality (long arrow) and a partially reversible anterior wall abnormality (arrowhead). In summary, the examination demonstrates extensive ischemia and, with the exception of the inferior wall, viability of all segments.

probability (Fig. 19). As can be seen the greatest changes in probability occur when applying this test to patients who have an intermediate pre-test probability of disease.

Sequential Bayesian analysis refers to the situation where the post-test probability after a diagnostic test becomes the pre-test probability for the next test. Suppose that on the basis of risk factors a patient is assigned a pre-test probability of 20%. He then undergoes a GXT after which the (post-test) probability is raised to 60%. This 60% probability now becomes the pre-test probability for any subsequent examination such as a myocardial perfusion study.

Why is it necessary to have polar maps based on a normal database? Shouldn't perfusion to all portions of the heart be

Table 5. Derivation of post-test probability of coronary artery disease (CAD) with positive and negative test results from myocardial perfusion imaging (MPI).

		CAD		
		yes	no	
MPI	+ve	54	4	58
	-ve	6	36	42
		60	40	

equal?

With a perfect imaging system the answer would be 'yes'. However, there are certain factors that prevent this. Firstly, activity in the heart will be attenuated to a greater or lesser extent by soft tissues. For instance in women, photons arising from the anterior myocardial wall will in many SPECT projections have to traverse the breast. A certain number of photons will be absorbed or scattered in the breast and will not be detected by the gamma camera. Because fewer anterior wall counts will be detected, the reconstructed images will contain fewer counts in the anterior wall (i.e., there will be an apparent anterior wall defect). In men, the inferior wall often demonstrates decreased activity because of attenuation from infra-diaphragmatic structures. Secondly scattered photons emanating from outside the heart will be detected as originating from within the heart causing inhomogeneity of uptake. Lastly, resolution in deeper structures is poorer than resolution of more superficial structures contributing to non-uniformity. There are various approaches to correct for this non-uniformity.

Transmission imaging with an external radioactive source can be used to correct for the effects of variable attenuation (Fig. 20). A gadolinium-153 sealed source(s) is mounted on the gamma camera. The camera is rotated about the patient and a transmission map (which can be thought of as a low resolution CT scan) is reconstructed from the projection data. With the transmission data in hand the emission (SPECT) data can be corrected for variable attenuation. This technique is not as yet being used on a widespread clinical basis.

Additional Reading

1. Beller GA, Zaret BL. Contributions of nuclear cardiology to diagnosis and prognosis of patients with coronary artery disease. Circulation 2000; 101:1465-1478.
   Excellent review of myocardial perfusion imaging.
2. Bergmann SR. Cardiac positron emission tomography. Semin Nucl Med 1998; 28(4):320-340.
   A review of cardiac PET applications.
3. Berman DS, Germano G, Shaw LJ. The role of nuclear cardiology in clinical decision making. Semin Nucl Med 1999; 29(4):280-297.
   An excellent article focusing on risk stratification.
4. Botvinick EH, ed. Unit 2: Pharmacologic stress and associated topics. In : Nuclear
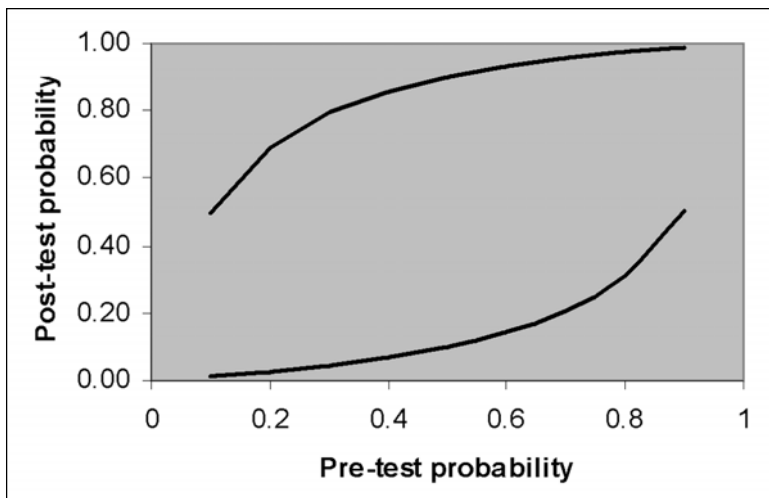
Figure 19. The relationship of pre- and post-test probability is shown for a test with 90% sensitivity and specificity. For example, if the pretest probability of disease is 0.6 and the test is positive, the post-test probability of disease will be 93% (top curve). If the test is negative, the likelihood of disease is 14% (bottom curve).
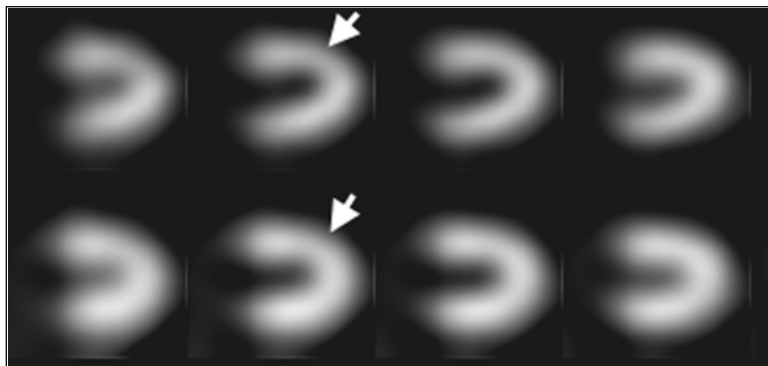
Figure 20. (A) Vertical long axis image shows decreased activity in the anterior wall in this 74 year old female. (B) With attenuation correction, the anterior wall normalizes, suggesting that the reduction is due to breast attenuation.

Medicine: Self-Study Program III: Nuclear Medicine Cardiology. Society of Nuclear Medicine, 1998.

A self-study program with illustrative cases, problems and answers.

5. DePuey EG, Garcia EV, eds. Updated imaging guidelines for nuclear cardiology procedures, Part 1. J Nucl Cardiol 2001; 8(1):G1-G58.

An expert consensus on how to perform nuclear cardiology studies.

6. Epstein FH, Wijns W, Vatner SF et al. Mechanisms of disease: Hibernating myocardium. NEJM 1998; 339(3):173-181.
   A review of the clinical and pathophysiologic basis of hibernating myocardium.

7. Iskandrian AE, Verani MS. Bar Harbor panel summaries. J Nucl Cardiol 2001; 8(2):224-316.
   A current review of the "state of the art" by leaders in the field of nuclear cardiology.

8. Ritchie JL et al. ACC/AHA guidelines for clinical use of cardiac radionuclide imaging. J Am Coll Cardiol 1995; 25:521-547.
   Guidelines on the use of nuclear cardiology procedures published by the American College of Cardiology and the American Heart Association.

9. Siebelink HJ, Blanksma PK, Crijns HJ et al. No difference in cardiac event-free survival between positron emission tomography-guided and single–photon emission computed tomography-guided patient management. J Am Coll Cardiol 2001; 37:81-88.
   The name says it all. Also look at the well-written accompanying editorial by Udelson "Testing our tests: surrogate end points versus driving patient management and outcomes".

10. Travin MI. Use of myocardial perfusion imaging to assess viability. J Nucl Cardiol 2000; 7(1):72-80.
    A nice review of the techniques used to assess myocardial viability with emphasis on ^{201}Tl and ^{99m}Tc-sestamibi.

3

Equilibrium Radionuclide Angiocardiography

I. David Greenberg and Robert Corne

Introduction

A quantitative evaluation of ventricular function gives an objective assessment of ventricular performance in asymptomatic patients and provides prognostic information in patients with ischemic and valvular heart disease. The technique of radionuclide angiography provides an accurate and reproducible method of non-invasively assessing global left ventricular systolic function in patients receiving cardiotoxic chemotherapy. The extent and severity of regional left ventricular wall motion abnormalities including ventricular aneurysm can be defined. Right ventricular function can also be evaluated.

Technical Considerations

The nuclear medicine technique most commonly used to assess ventricular function is termed equilibrium radionuclide angiocardiography (ERNA). The first ERNA program was developed by Medical Data Systems which coined the term MUGA (multiple gated acquisition). This proprietary term is still frequently used as is the generic description "gated blood pool imaging". The American Society of Nuclear Cardiology has suggested that ERNA be adopted as standard terminology. In this technique a tracer is administered that remains in the intravascular compartment. After allowing several minutes for equilibration (hence the term equilibrium), the heart—the largest blood containing structure in the body—can be imaged. While planar images could identify the cardiac chambers, they would not provide information on cardiac function. "Gating" the studies allows for the generation of a series of images representing the heart through the entire cardiac cycle. This is achieved by attaching electrodes to the patient and using the R wave to synchronize image acquisition with the cardiac cycle (Fig. 1). Effectively one acquires information over several hundred heartbeats to produce a composite cardiac cycle consisting of 16 to 24 images. These images can then be viewed in an "endless loop format" allowing wall motion to be assessed. The left ventricular ejection fraction will also be derived from these images.

Typically image sets are obtained in three projections: anterior, left anterior oblique and steep left anterior oblique (or left lateral). In this way the various walls of the left ventricle can be seen tangentially and regional wall motion evaluated (Fig. 2). The LAO view is not taken at a specific angle but rather the technologist will adjust the projection to maximize separation between the left and right ventricles. The camera is angled caudally to separate left ventricle and left atrium. This modi-
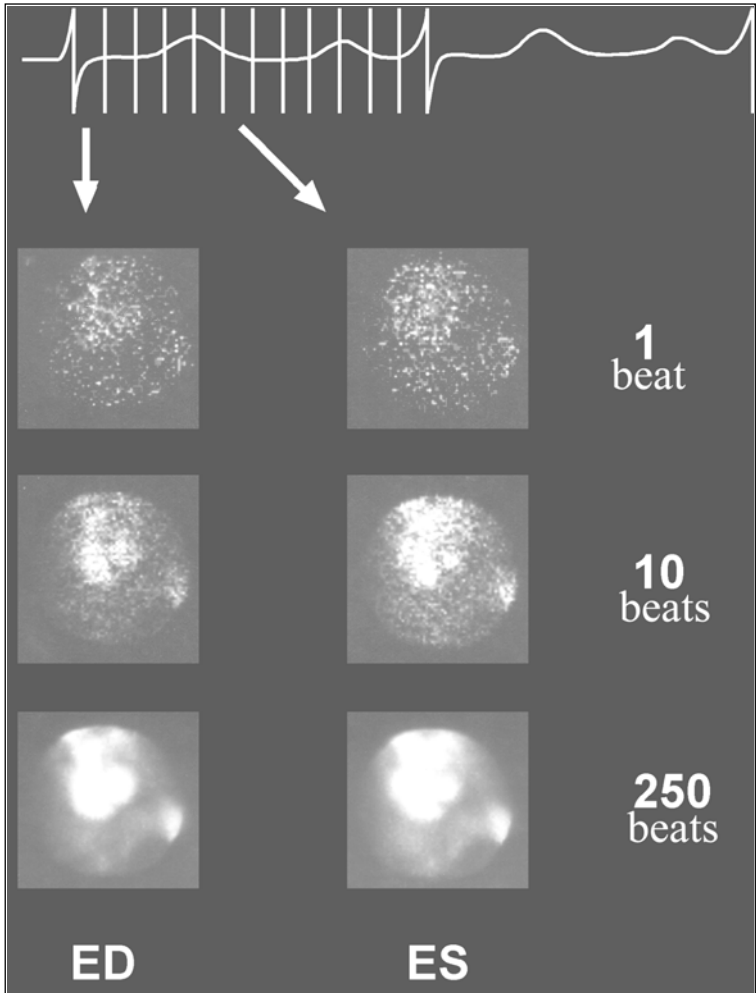
Figure 1. Principle of equilibrium radionuclide angiocardiography (ERNA). Three ECG leads are attached to the patient. The QRS complexes are detected by the computer and used for gating. In this example, each R-R interval is divided into 12 frames. Data collected during the first 1/12th of the R-R interval is collected in computer bin 1, the second 1/12th in bin 2 and so on for all 12 fractions of the R-R interval. Typically, the first bin is the end diastolic frame (ED). In this patient, the sixth bin represents the end-systolic frame (ES). If acquisition were stopped after one beat, only a few counts would be collected in each of the 12 frames. The computer senses the next QRS complex and divides the next R-R interval in the same fashion, adding data from the first 1/12th of the cardiac cycle into bin 1, second 1/12th into bin 2 and so on. After 10 beats, anatomic structure becomes discernible. After 250 beats, the right and left ventricles are clearly seen.
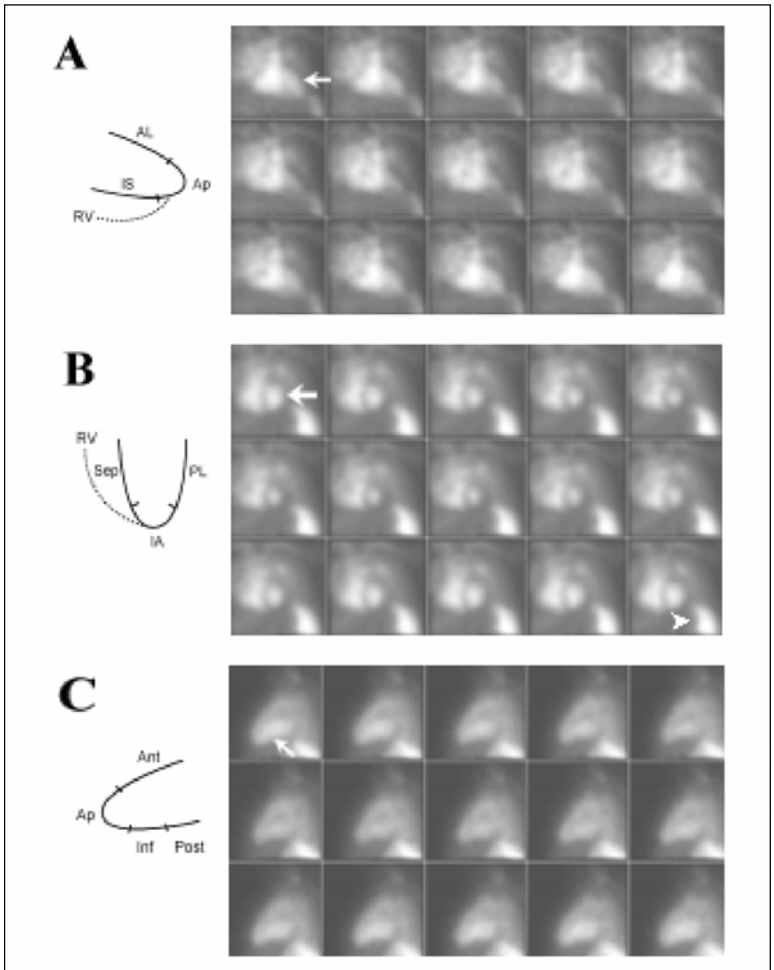
Figure 2. Normal ERNA. Typically, three projections are obtained: anterior (A), best-septal (B) and steep LAO or lateral (C). The left ventricle is seen in all three projections (arrow). When describing wall motion, the same segmental nomenclature is used as that for planar ^{201}Tl or ^{99m}Tc-sestamibi studies (AL-anterolateral; Ap-Apex; IS-inferoseptal; PL-posterolateral; IA-inferoapical; Sep-Septum; Ant-Anterior; Inf-Inferior; Post-Posterior). The spleen (arrowhead) is often seen.

fied LAO projection, termed the "best septal" view, separates the left ventricle from other structures and is used for determination of the ejection fraction. In our center, the best-septal view is acquired first. The "anterior" view is obtained by rotating the camera head 40° counter-clockwise from the best septal view while the "steep LAO"
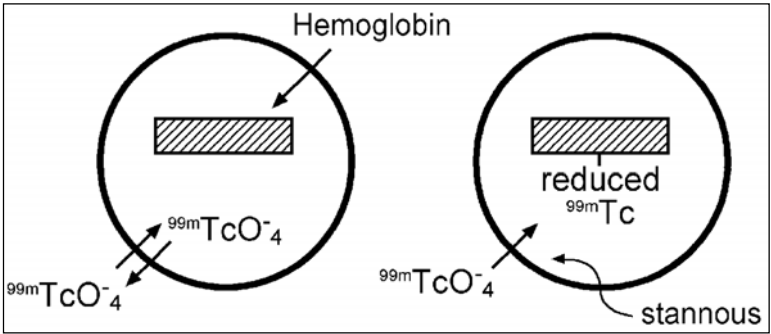
Figure 3. Radiochemistry of ^{99m}Tc-RBC labeling. ^{99m}Tc-pertechnetate diffuses both in and out of the red blood cell. A reducing agent, such as stannous ion, reduces the ^{99m}Tc allowing it to label hemoglobin.

projection is obtained by rotating the camera 30° clockwise from the best septal view.

Intravascular Agents

A tracer is needed that remains in the blood pool for sufficient time to allow for acquisition of the gated blood pool images. There are two approaches to achieve this: labeling of the patient's own red blood cells (RBCs) with technetium-99m or administering a technetium-99m labeled macromolecule such as ^{99m}Tc-HSA (human serum albumin). The latter technique is not commonly used since the residence time of ^{99m}Tc-HSA in the blood pool is less than that for ^{99m}Tc-RBCs. While we are not aware of any case in which hepatitis or HIV has been transmitted through the use of ^{99m}Tc-HSA, the use of autologous RBC labeling obviates this concern.

There are three methods available for labeling red blood cells:

(a) In Vivo: In this technique 10-20 μg/kg of stannous (Sn^{2+}) ions is injected. After 20-30 minutes, ^{99m}Tc-pertechnetate is administered. This sequence produces hemoglobin labeling with technetium-99m (Fig. 3). Labeling efficiency (ie. RBC/ Whole blood activity x 100%) with this technique ranges from 80-90%.

In Vitro: In this technique, several ml of blood are withdrawn from the patient labeled in a test tube (using Sn^{2+} and ^{99m}Tc-pertechnetate) and then reinjected. Labeling is reliable with typical labeling efficiencies in excess of 95%.

Modified in vivo (or in "vivitro"): In this technique, Sn^{2+} is injected in the same manner as for the in vivo technique. After 30 minutes, several ml of blood are withdrawn into a syringe containing ^{99m}Tc-pertechnetate. Several minutes are allowed for RBC labeling within the syringe after which the labeled RBCs are re-injected. Labeling efficiency is typically in the 90% range.

The in vitro technique provides the most reliable and highest quality labeling. However, the commercial kit used for in vitro labeling (Ultratag®) is not inexpensive. Moreover RBC labeling is performed on the "bench" removed from the patient. If multiple patients are being imaged, it is crucial that procedures are in place to pre-

vent the inadvertent mixing of blood samples. In our laboratory, we use the in vitro technique in patients in whom we have experienced (or anticipate) poor RBC labeling.

Ejection Fraction

The ejection fraction (EF) as the name implies is the percentage of blood in the left (or right) ventricle that is ejected during contraction of the heart. In echocardiography (and contrast ventriculography) the technologist traces the outline of the left ventricle at end-diastole and end-systole. On the assumption that the left ventricle has an ellipsoidal shape, end-diastolic and end-systolic volumes are calculated from which the ejection fraction is determined. If all ventricular walls contract equally this geometric assumption is accurate. It is less reliable if regional wall motion abnormalities are present. In ERNA, the left ventricular ejection fraction is determined without assumptions as to the shape of the heart; rather it is based on the principle that counts in the left ventricle are proportional to volume (Fig. 4). Using the best-septal view, outlines of the left ventricle at ED and ES are manually drawn or generated by an edge detection program (Fig. 5). Counts in the left ventricle can assumed to be proportional to volume. To correct for background activity in front and behind the heart and scatter from adjacent structures, a background region of interest is drawn adjacent to the heart and the EF calculated. Note that no geometric assumptions are made as to the shape of the heart. Normally the left ventricular EF is ≥50% while the right ventricular EF is >40-45%.

Parametric Images

In addition to analyzing the images in cine-mode for assessment of regional wall motion, it is possible to generate valuable information from parametric images. (A parametric image can be thought of as an image that condenses information from a series of images). Phase and amplitude images are two commonly generated parametric images. The phase image provides information as to the timing of contraction in various portions of the heart and the amplitude image on the degree of contraction (Fig. 6).

Clinical Applications

Various modalities are available to assess left ventricular function including ERNA, echocardiography, gated myocardial perfusion imaging (see Chapter 3) and contrast venticulography. The relative strengths and weaknesses of these procedures are listed in Table 1. The technique employed to evaluate ventricular function will depend on local expertise, test availability and the clinical scenario. For instance, in a patient with valvular disease, echocardiography can assess valve structure and function as well as ventricular function. On the other hand ERNA has proven to be an accurate and reproducible method of serially following the EF of patients being treated patients with cardiotoxic drugs such as doxorubicin.

Congestive Heart Failure

Congestive heart failure may be due to left ventricular systolic and/or diastolic dysfunction (Fig. 7). Systolic dysfunction is due to impaired contractility or afterload mismatch (increased wall tension due to an increase in intraventricular pressure or
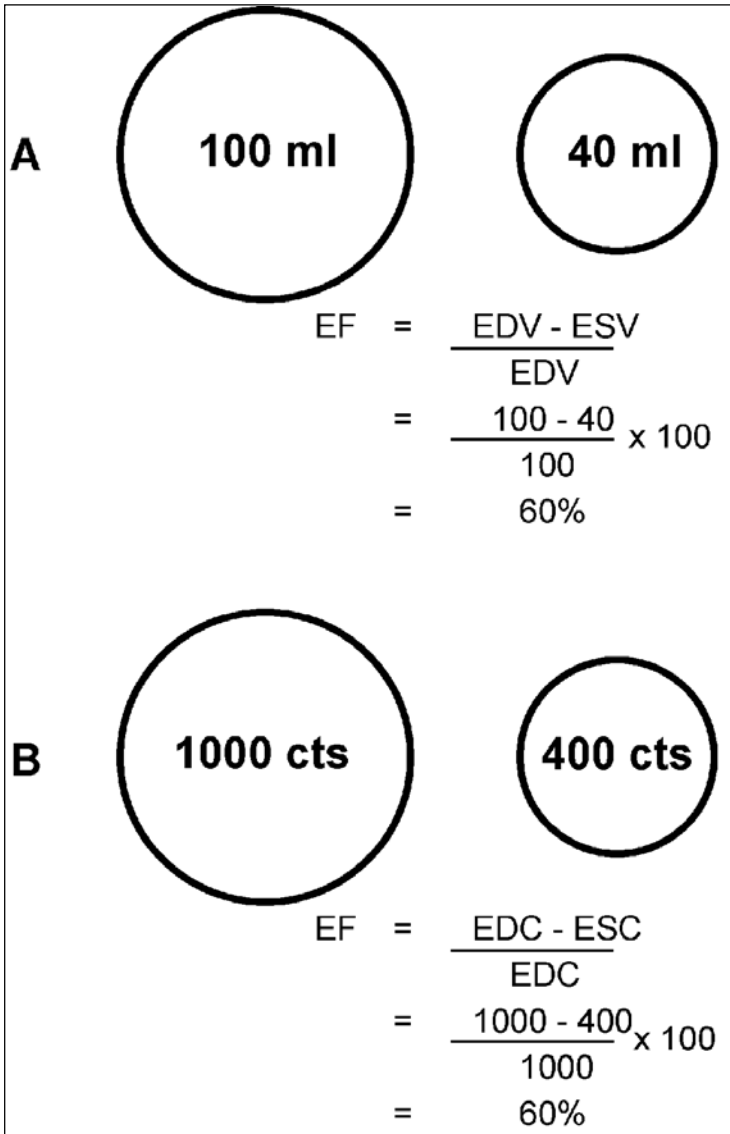
Figure 4. Count-based ejection fraction. The ejection fraction (EF) is the percentage of the end-diastolic volume (EDV) that is ejected during systolic contraction. In this example, EDV is 100 ml, end-systolic volume (ESV) is 40 ml and the EF is 60% (A). Assuming that the counts in the LV are proportional to volume the end-diastolic counts (EDC) and end-systolic counts (SC) can be used to calculate the EF (B).

4
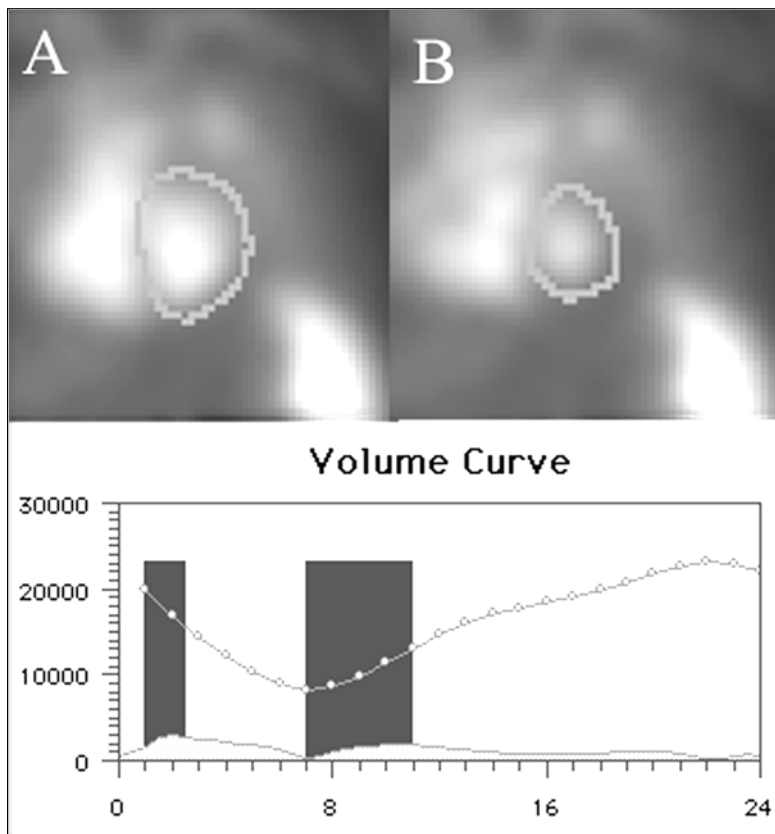
Figure 5. Left ventricular time-activity curve. Using the best septal view, regions of interest (ROIs) encompassing the left ventricle are either drawn manually or generated using an edge-detection program. Shown are computer-derived ROIs around the LV at end-diastole (A) and end-systole (B). ROIs are generated for all frames of the image set. After correcting for the contribution of background, a left ventricular time-activity curve is produced (C). Examining the curve, one can see that in the first frame (end-diastole) there are 20,000 counts in the left ventricle. The seventh frame has the fewest counts in the left ventricle (8,000) and is the end-systolic frame. The ejection frame is therefore 60%.

volume without adequate hypertrophy as can be seen in aortic regurgitation). This is characterized by a low ejection fraction with either a regional wall motion abnormality (CAD) or generalized reduction in systolic function (myocarditis, drug induced or idiopathic cardiomyopathy, aortic regurgitation). Heart failure may also occur because of increased resistance to ventricular filling referred to as diastolic dysfunction. This may be due to impaired relaxation (e.g., myocardial ischemia) or
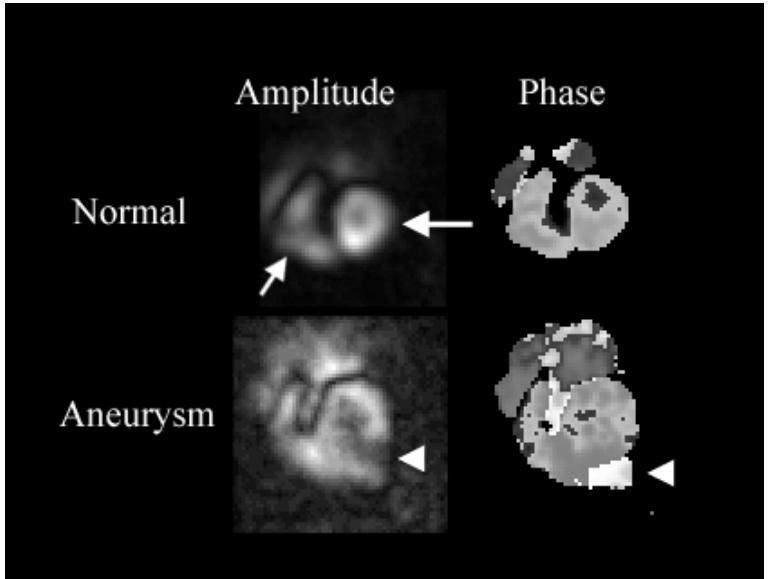
Figure 6. Phase and amplitude images. The series of ERNA images can be analyzed in such a way as to generate images depicting the degree of pixel change between end-diastole (ED) and end-systole (ES) as well as the timing of pixel change. The top row depicts a normal patient with the amplitude image showing a horseshoe area of activity (long arrow) in the left ventricle (since the peripherally located LV pixels show the greatest change between the ED and ES). Similarly, a crescentic area is seen for the RV (short arrow). The phase image shows a similar gray color for both the left and right ventricles indicating that they contract simultaneously. In the lower row there is a low amplitude area (i.e., little change between ED and ES) inferoapically which on the phase image is seen to be "out of pahse" with the remaining ventricular mass implying that it is dyskinetic (arrowhead).

decreased compliance (left ventricular hypertrophy, fibrosis, infiltrative cardiomyopathy). Commonly, patients with systolic dysfunction also manifest diastolic dysfunction.

Treatment of patients with systolic dysfunction with ACE inhibitors and beta-blockers increases survival. Patients with diastolic dysfunction will have treatment aimed at their underlying disease (e.g., ACE inhibitors in hypertensive patients) in addition to diuretics (to reduce preload) and drugs that slow the ventricular rate (to increase the diastolic filling period).

Table 1. Comparison of various modalities used in the evaluation of ventricular function

Modality	Strengths	Weaknesses
Contrast angiography/ venticulography	•Assesses anatomic CAD	•Invasive •Contrast reactions •Geometric assumptions in calculation of EF
Echocardiography	•Non-invasive •No radiation •Assesses valve structure and function •Assesses pericardial effusion +/- tamponade •Assesses wall thickening	•Requires acoustic window •Not optimal for RV assessment •Geometric assumptions in calculation of EF
Gated myocardial perfusion imaging (MPI)	•Non-invasive •Provides assessment of myocardial perfusion •Can assess wall thickening •No geometric assumptions	•Requires regular rhythm •May have difficulty tracking the myocardial wall with a severe defect
Equilibrium radionuclide angiocardiography (ERNA)	•Non-invasive •No geometric assumptions •Good RV assessment	•Requires good RBC labeling Need to modify technique (e.g., list mode) for arrythmias

Coronary Artery Disease

Resting Ejection Fraction

Myocardial Infarction

In the pre-thrombolytic era, the EF was the most important indicator of survival following infarction. Although the EF remains an important prognostic indicator, patients who receive thrombolytic treatment have a substantially lower mortality for any level of ejection fraction. Assessment of ventricular function within the first few days after myocardial infarction may be influenced by compensatory hyperkinesis of non-infarcted segments (increasing the EF) or by hypokinesis of "stunned" myocardium (lowering the EF). A more reliable estimate of ventricular function will, therefore, be obtained one to two weeks after the event.

Angina Pectoris

Prognosis of patients with chronic stable angina and multivessel coronary artery disease is also strongly influenced by left ventricular function. The Coronary Artery Surgery Study (CASS) demonstrated improved survival with coronary artery bypass
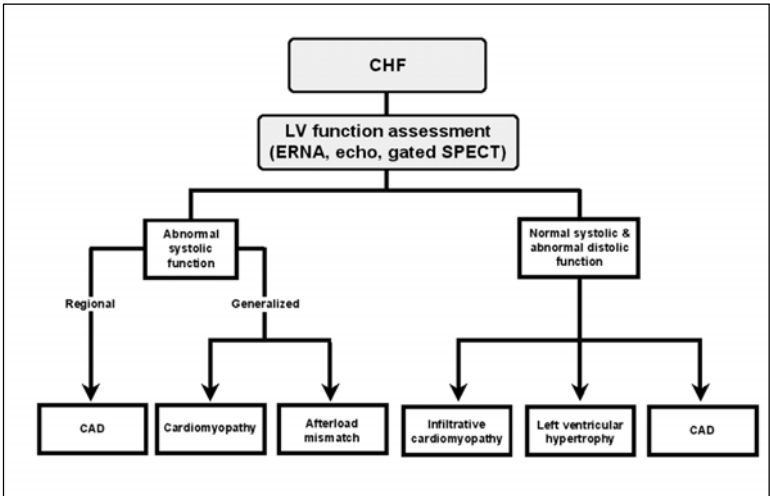
Figure 7. Left ventricular (LV) functional assessment in the evaluation of congestive heart failure (CHF).

grafting in patients with multivessel CAD and mild to moderate left ventricular dysfunction (EF 35-49%).

Exercise Ejection Fraction

In addition to determining the EF at rest, it is also possible to determine the EF during exercise (most commonly using supine bicycle exercise). The normal response to a progressive increase in workload is an increase in the EF of at least 5%. An abnormal response characterized by either failure of the EF to increase and/or the induction of a regional wall motion abnormality has a sensitivity of 80-90% for the detection of CAD. Sensitivity is higher in patients with more severe and extensive CAD. Sensitivity is reduced if patients are unable to achieve an adequate level of exercise i.e., cannot increase the product of their heart rate and systolic blood pressure to ≥25,000. Drugs such as nitroglycerine, calcium channel blockers and beta-blockers may prevent the development of myocardial ischemia during exercise and reduce test sensitivity. Because the specificity of exercise radionuclide angiography for CAD is only approximately 50% (factors limiting specificity of the test are listed in Table 2), most centers prefer myocardial perfusion imaging for the detection of CAD (see Chapter 3).

However, exercise ERNA can be helpful in determining prognosis. A low peak-exercise EF (representing the combined effect of previous infarction and reversible ischemia) and a decrease in EF from rest to exercise provide independent prognostic information in patients with coronary artery disease. Cardiac events (death and non-fatal MI) are increased when the EF at peak stress is less than 50% or if the EF falls by 5% or more from its resting value.

Table 2. Factors associated with failure of the ejection fraction to increase with exercise

Cause	Comment
Gender	Women increase their stroke volume with exercise mainly by an increase in end-diastolic volume (Frank-Starling mechanism) rather than by an increase in contractility
Hypertension	Patients with hypertension may have a fall in EF as a result of an exaggerated blood pressure response to exercise
Anti-anginal drugs	The negative inotropic action of beta-blockers and calcium channel blockers may blunt the normal increase in the ejection fraction with exercise
Age	Elderly patients may have an abnormal exercise response in the absence of coronary artery disease
Non-coronary disease	Myocardial contractility may be impaired in patients with a cardiomyopathy or valvular heart disease
Left bundle branch block	Patients with a LBBB may have an abnormal response to exercise in the absence of coronary artery disease

Doxorubicin Cardiotoxicity

Doxorubicin and other anthracyclines such as daunorubicin, epirubicin and mitoxantrone are commonly employed chemotherapeutic drugs which may be associated with significant cardiotoxicity. ERNA provides an accurate, reproducible and non-invasive method of serially monitoring left ventricular function. It has been recommended that ERNA be obtained prior to chemotherapy and if left ventricular function is normal (EF ≥50%) subsequent studies be obtained at a total doxorubicin dose of 250-300 mg/m^2, at 400-450 mg/m^2, and before each subsequent dose. Cardiotoxicity, defined by a decrease in the EF of ≥10% and an EF <50% is predictive of subsequent clinical cardiac failure if treatment is continued. If there is left ventricular dysfunction (EF <50%) on the pre-chemotherapy ERNA, additional studies should be obtained prior to each dose, with treatment discontinued if the EF falls by 10% or the EF decreases to 30% (Fig. 8).

Valvular Heart Disease

Echocardiography is preferred for the non-invasive assessment of patients with valvular heart disease since it provides information on valve structure in addition to assessing ventricular function. ERNA provides an alternative method of assessing ventricular function in patients with technically suboptimal echocardiographic studies or in patients with borderline left ventricular dysfunction for whom an independent assessment of left ventricular function may be helpful. Surgery is recommended when patients with valvular regurgitation develop symptoms or resting left ventricular dysfunction (EF <50% in aortic regurgitation and <60% in mitral regurgitation). Although the exercise ejection fraction response in asymptomatic patients with severe aortic regurgitation is an independent predictor of death, left ventricular dysfunction or the development of symptoms, there are no data to support aortic valve surgery based only on a fall in ejection fraction with exercise.
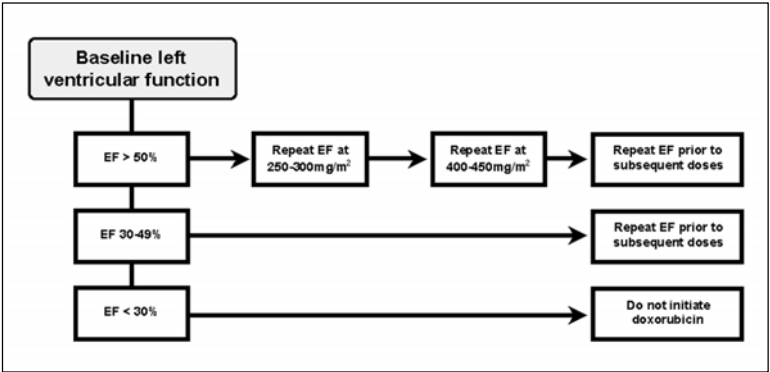
Figure 8. Flow chart outlining the use of ERNA in monitoring doxorubicin cardiotoxicity.
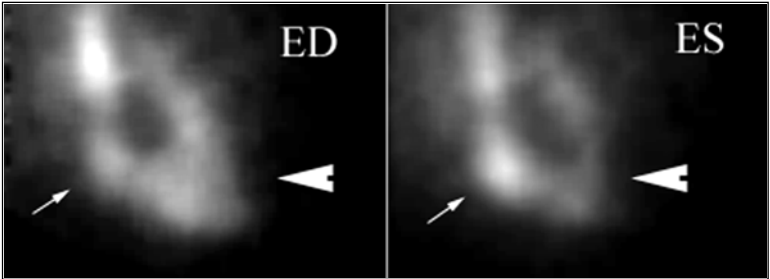
Figure 9. First pass study of right ventricle. Immediately after tracer injection into an antecubital vein, a gated study was acquired in the brief period that activity traversed the right heart but before arrival of tracer in the left heart. The study is typically acquired in an anterior or RAO projection to optimally separate right atrium (thin arrow) and right ventricle (arrowhead). With this technique, the right ventricular ejection fraction can be determined in the same manner as the left ventricular ejection fraction in an ERNA study.

Right Ventricle

Evaluation of right ventricular function is important in patients who are hemodynamically unstable following inferior infarction, patients with pulmonary hypertension and in patients suspected of having arrhythmogenic right ventricular dysplasia (fibro-fatty infiltration resulting in a dilated hypokinetic right ventricle). Right ventricular size and wall motion can be assessed on an ERNA study. Overlap of other cardiac structures (especially the right atrium) on the right ventricle limits the accuracy of a right ventricular EF determination. For this reason, a first pass study (see FAQs) is commonly used to assess the right ventricular EF (Fig. 9).
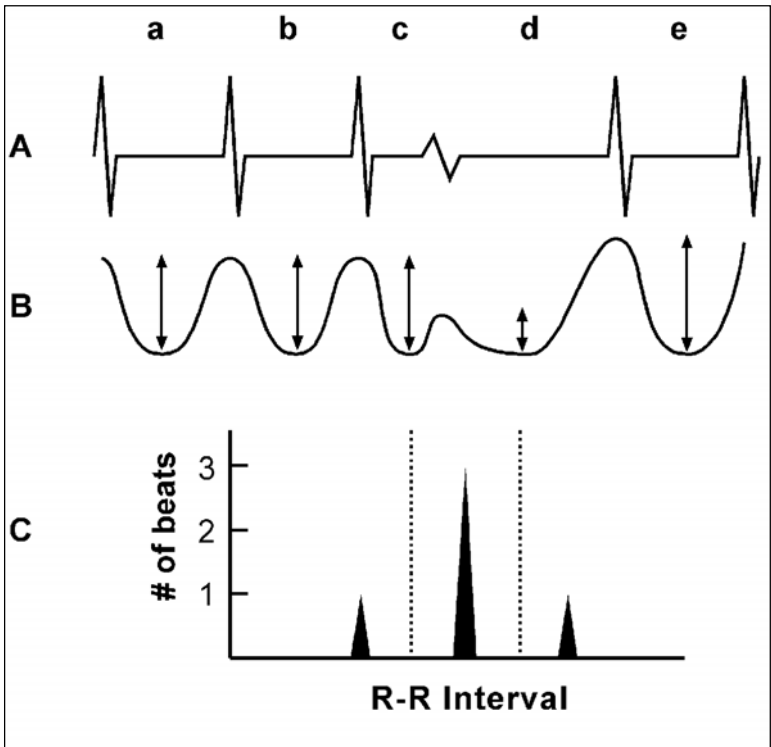
Figure 10. List mode acquisition. The rhythm shown in (A) is sinus (beats a, b, c and e) with a single ventricular premature beat (d). The volume curve (B) demonstrates the effect of the premature beat on the ejection frame (EF). Because of a longer diastole and greater ventricular filling following a ventricular premature beat (d), the EF of the next sinus beat (e) is increased. The premature beat itself has a decreased EF while the interrupted sinus beat (c) has a normal EF. With a list mode acquisition, an R-R histogram is generated (C) and only those beats with a normal R-R interval (between the dotted lines) are used to produce the series of ERNA images. As can be appreciated, this is not a perfect solution since sinus beat 'e' (with an elevated EF) will be included while the interrupted sinus beat 'c' (with normal EF) will be excluded from the acquisition.

Frequently Asked Questions (FAQ)s

What is meant by a "first pass study"?

In the body of the Chapter we discussed ERNA in the assessment of left ventricular function. It is also possible to assess left or right ventricular function by injecting a technetium-99m tracer and analyzing the first transit of this tracer through the heart (hence the term *first pass study*). Since only the first pass portion of the study is
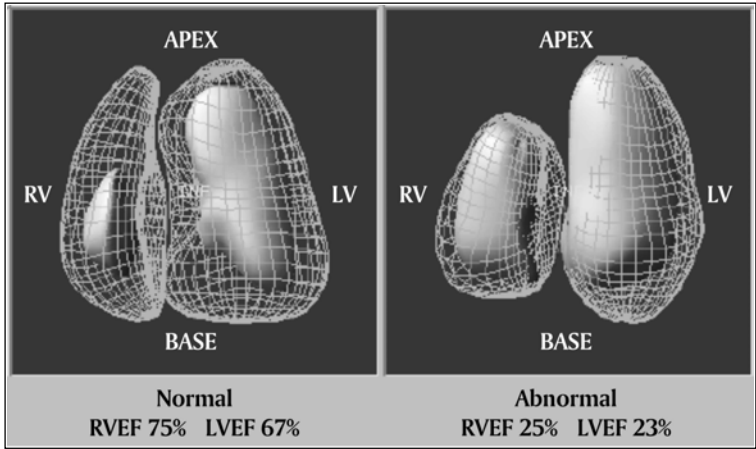
Figure 11. Normal SPECT ERNA in left panel and abnormal in right panel. The end-diastolic contours are shown in a cage display while the end-systolic contours are represented as solids. The number of voxels at end-diastole and end-systole are determined for both the right and left ventricles and from these the right ventricular ejection frame (RVEF) and left ventricular ejection frame (LVEF) are calculated. Note that this differs from the count-based approach used for planar ERNA studies. (Cases provided by ADAC Laboratories)

analyzed, one is not limited to tracers that remain in the intravascular blood pool (beyond the first pass through the heart). A variety of techniques can be used. These will not be discussed in detail. However, some factors to be considered are:

 • In a first pass study, separation of the right ventricle and left ventricle is achieved temporally (Fig. 9). While activity is in the right ventricle, right ventricular function can be assessed; after the activity leaves the right ventricle and reaches the left ventricle, left ventricular function is assessed.

 • An anterior or RAO projection is usually chosen to allow separation of right atrium from right ventricle and left atrium from left ventricle,

 • The study can be gated in the same way as an ERNA. Non-gated techniques are also available.

 • After injection, the bolus of activity spreads. This can be tolerated for assessment of right ventricular function but is a more severe problem with the assessment of left ventricular function. To maintain a tight bolus, a jugular injection is often required.

Does irregularity of the cardiac rhythm cause difficulties in interpreting an ERNA?

The ERNA technique generates a composite cardiac cycle based on several hundred heart beats. The data is then used to generate a time activity curve from which the ejection fraction is determined. Conceptually, one can consider several hundred individual time activity curves superimposed to form the composite time-activity

curve. Referring to Figure 10, it can be appreciated that if the data from ventricular premature beats is included, the evaluation of ventricular function during sinus rhythm will be distorted. Cardiac programs allow us to deal with this problem in two ways:

Many programs calculate the average R to R interval and reject data from beats with an R-R interval which are beyond a predetermined acceptance limit (e.g., beats with an R-R interval less than 80% or greater than 120% of the mean R-R interval).

Another approach is to collect the data serially in list mode. This data includes scintigraphic information, timing pulses and R wave pulse information. An R-R histogram is generated and the operator selects the appropriate R-R interval for reformatting the representative cardiac cycle (Fig. 10).

Gated SPECT studies are done for myocardial perfusion imaging. Can gated SPECT ERNA studies be performed as well?

Yes. Gated SPECT myocardial perfusion studies are now routine. The same technique can be applied to ERNA (Fig. 11). Indeed, any camera with the capability of acquiring gated SPECT myocardial perfusion images is also capable of acquiring gated SPECT ERNA. Potential advantages of this technique include: 1) absolute volumes can be calculated in addition to the EF, 2) no corrections is needed for background activity, 3) assessment of wall motion is not limited to those segments seen tangentially on the 3 routine views, 4) three-dimensional phase images can be generated. Once the software to generate volumes, ejection fractions and 3-D phase/amplitude images is readily available, this technique will probably supplant planar ERNA studies.

Additional Reading

1.   DePuey EG, Garcia EV. Updated imaging guidelines for nuclear cardiology procedures, Part 1. J Nucl Cardiol 2001; 8(1):G1-G58.
     An expert consensus on how to perform nuclear cardiology studies. Pages G17-29 deal with first pass and ERNA studies.
2.   Jain D. Cardiotoxicity of doxorubicin and other anthracycline derivatives. J Nucl Cardiol 2000; 7(1):53-62.
     Nicely written article dealing with mechanisms, diagnosis and prevention of cardiotoxicity.
3.   Lee K, Pryor DB, Pieper KS et al. Prognostic value of radionuclide angiography in medically treated patients with coronary artery disease: A comparison with clinical and catheterization variables. Circulation 1990; 82:1705-1717.
     A valuable report on the extensive experience with exercise ERNA at Duke University in risk stratifying patients with chronic coronary artery disease.
4.   Ritchie JL et al. ACC/AHA guidelines for clinical use of cardiac radionuclide imaging. J Am Coll Cardiol 1995; 25:521-547.
     Guidelines on the use of nuclear cardiology procedures published by the American College of Cardiology and the American Heart Association
5.   Ryan TJ et al. ACC/AHA guidelines for the management of patients with acute myocardial infarction. Circulation 1999; 100:1016-1030.
     Guidelines published by the American College of Cardiology and the American Heart Association on the investigation and treatment of patients with an acute MI.

Thromboembolic Disease

Daniel F. Worsley and Philip S. Wells

Introduction

Pulmonary embolism (PE) is a relatively common and potentially fatal disorder for which treatment is highly effective and improves patient survival. The diagnosis of acute PE requires an interdisciplinary team approach and may be difficult because of nonspecific clinical, laboratory and radiographic findings. The incidence of venous thromboembolism is approximately 1 in 1,000 per year. Approximately 10% of patients with PE die within one hour of the event. For those patients who survive beyond the first hour following PE, treatment with heparin or thrombolytic agents are both effective therapies. The mortality in patients with PE who are untreated has been reported to be as high as 30%. In contrast, the correct diagnosis and appropriate therapy significantly lowers mortality to between 2.5% and 8%. Although anticoagulant therapy is effective in treating PE and reducing mortality, it is not without some risk. The prevalence of major hemorrhagic complications has been reported to be as high as 10-15% among patients receiving anticoagulant therapy. Therefore, the accurate and prompt diagnosis of PE is not only essential to prevent excessive mortality but also to avoid complications related to unnecessary anticoagulant therapy.

Technical Considerations in Lung Scanning

Perfusion Lung Scanning

The agent of choice for perfusion imaging is ^{99m}Tc-labeled macroaggregated albumin (^{99m}Tc-MAA). Technetium-99m MAA particles range in size from 10-150 μm with over 90% of injected particles measuring between 10-90 μm. The injection of labeled particles should be performed with the patient in the supine position to limit the effect of gravity on regional pulmonary arterial blood flow. Following the intravenous administration of ^{99m}Tc-MAA, particles are mixed within the heart and then lodge within precapillary arterioles in the lungs. The usual administered activity is between 74-148 MBq (2-4 mCi) bound to 0.5-2.0 mg of human serum albumin. The distribution of particles within the lungs is proportional to regional pulmonary blood flow at the time of injection. Approximately 200,000-500,000 particles are injected during a routine clinical perfusion lung scan. The blockage of pulmonary precapillary arterioles by ^{99m}Tc-MAA is transient, and the biological half-life within the lung ranges between 2-6 hours. In pediatric patients, patients with right to left shunts, pulmonary hypertension or those who have undergone pneumonectomy or single lung transplantation, the number of particles injected should be reduced. A minimum of 60,000 particles is required to obtain an even distribution of activity

---
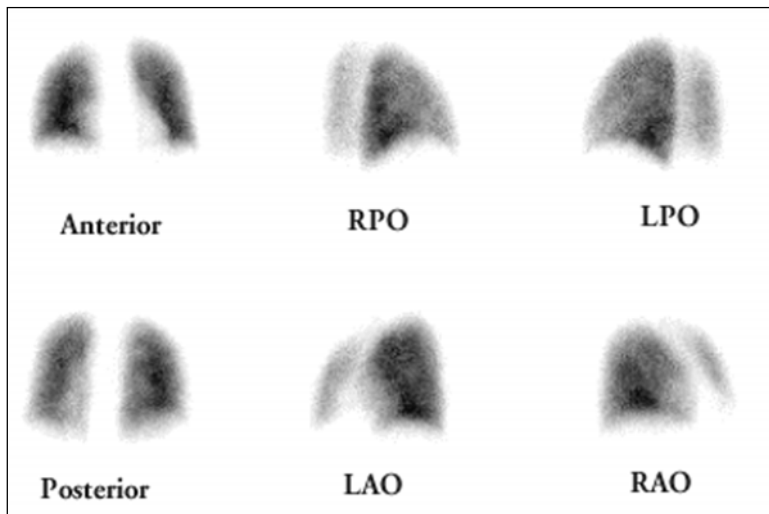
Figure 1. Normal ⁹⁹ᵐTc-MAA perfusion images. (RPO-right posterior oblique; LPO-left posterior oblique; RAO-right anterior oblique; LAO-left anterior oblique).

within the pulmonary arterial circulation and avoid potential false positive interpretations.

When performing perfusion scintigraphy, at least six views of the lungs should be obtained. These include anterior, posterior, right and left anterior oblique and posterior oblique views (Fig. 1). Additionally, right and left lateral views may be helpful in selected cases. Animal studies have demonstrated that perfusion imaging will detect greater than 95% of emboli which completely occlude pulmonary arterial vessels greater than 2 mm in diameter. In spite of this sensitivity, the perfusion scan may underestimate some perfusion abnormalities. For example, a perfusion defect limited to the medial basal segment of the right lower lobe is completely surrounded by normal lung; consequently a perfusion defect in this segment will not be detected on planar perfusion imaging.

Ventilation Lung Scanning

Perfusion scintigraphy is sensitive but not specific for diagnosing pulmonary diseases. Virtually all parenchymal lung diseases (including tumors, infections, chronic obstructive pulmonary disease [COPD] or asthma) can cause decreased pulmonary arterial blood flow within the affected lung zone. Ventilation imaging was combined with perfusion scintigraphy to improve the diagnostic specificity for PE based upon the principle that PE characteristically cause abnormal perfusion with preserved ventilation (mismatched defects) (Fig. 2). In contrast, parenchymal lung disease most often causes both ventilation and perfusion abnormalities in the same lung region (matched defects) (Fig. 3). Conditions in which the ventilation abnormality appears larger than the perfusion abnormality (reverse mismatch) include airway obstruction, mucous plug, airspace disease, atelectasis or pneumonia (Fig. 4). Patients
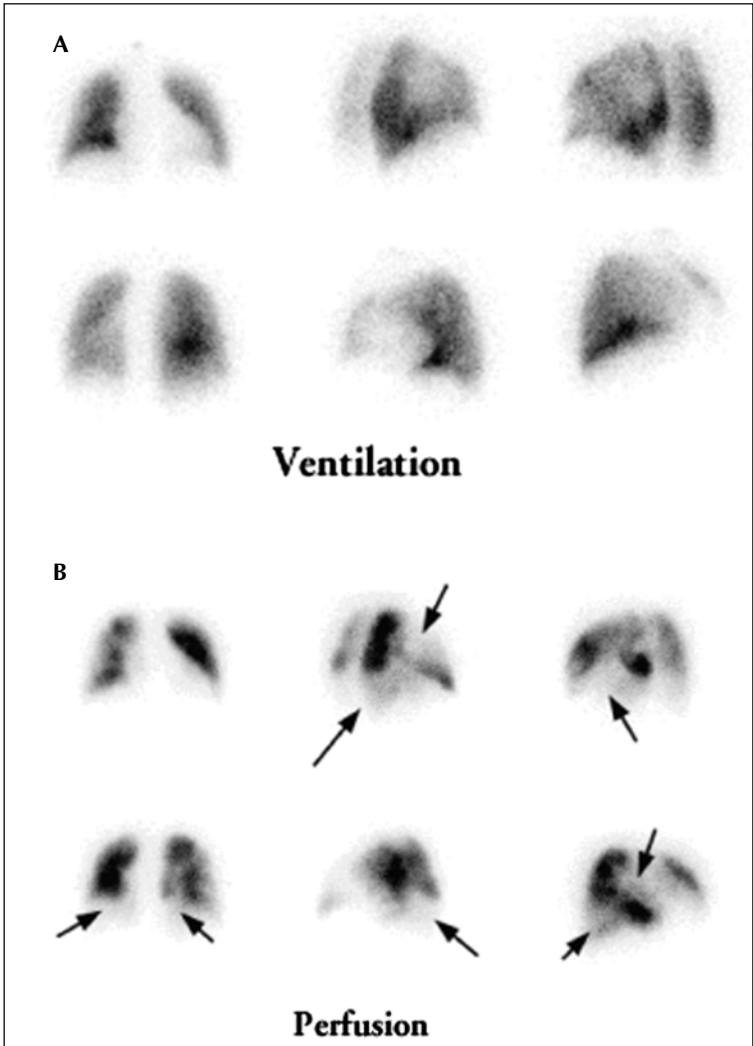
Figure 2. ^{99m}Tc-DPTA aerosol ventilation (A) and ^{99m}Tc-MAA perfusion (B) images demonstrate multiple segmental and subsegmental perfusion defects (arrows) in regions which are ventilated normally (V/Q mismatch). The findings indicate a high probability of acute pulmonary embolism. (Same image order as Fig. 1.)

with metabolic alkalosis, limited pulmonary vascular reserve or patients treated with inhaled bronchodilators may also have failure of hypoxic pulmonary vasoconstriction resulting in reverse mismatch.
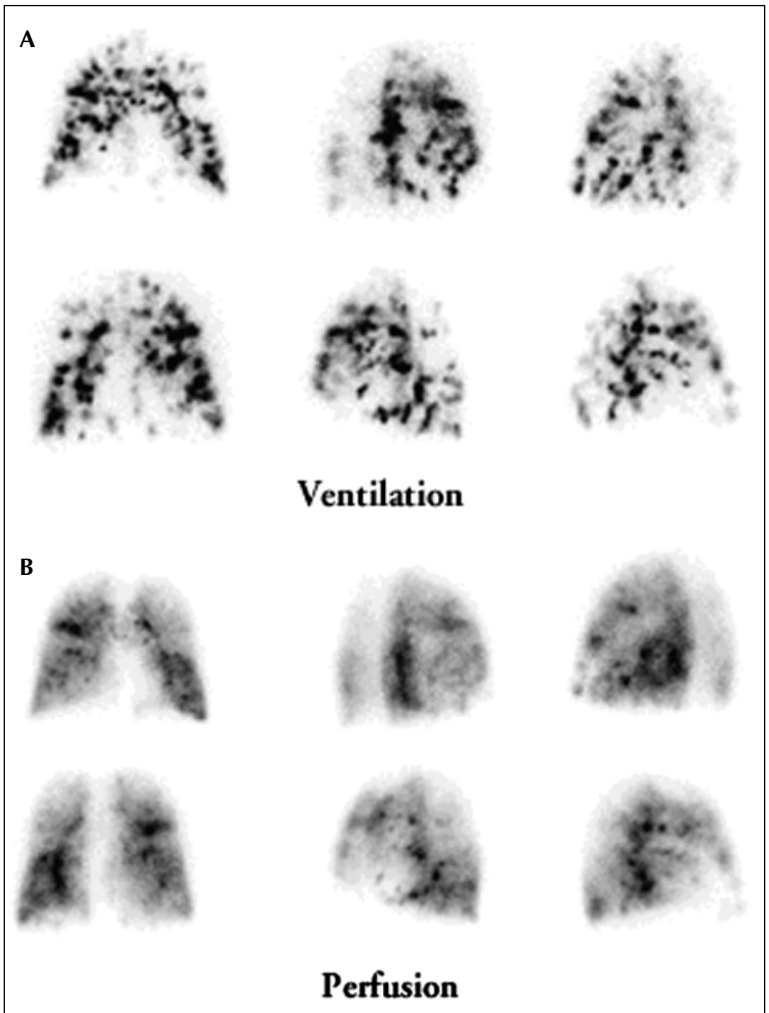
Figure 3. ^{99m}Tc-Aerosol ventilation (A) and ^{99m}Tc-MAA perfusion (B) images demonstrate an inhomogeneous distribution of activity within the lungs. Multiple matched regions of decreased ventilation and perfusion are present bilaterally typical of COPD. (The ventilation "hot spots" represent central airway deposition, some of which "shine through" on the subsequent perfusion scan.) (Same image order as Fig. 1.)
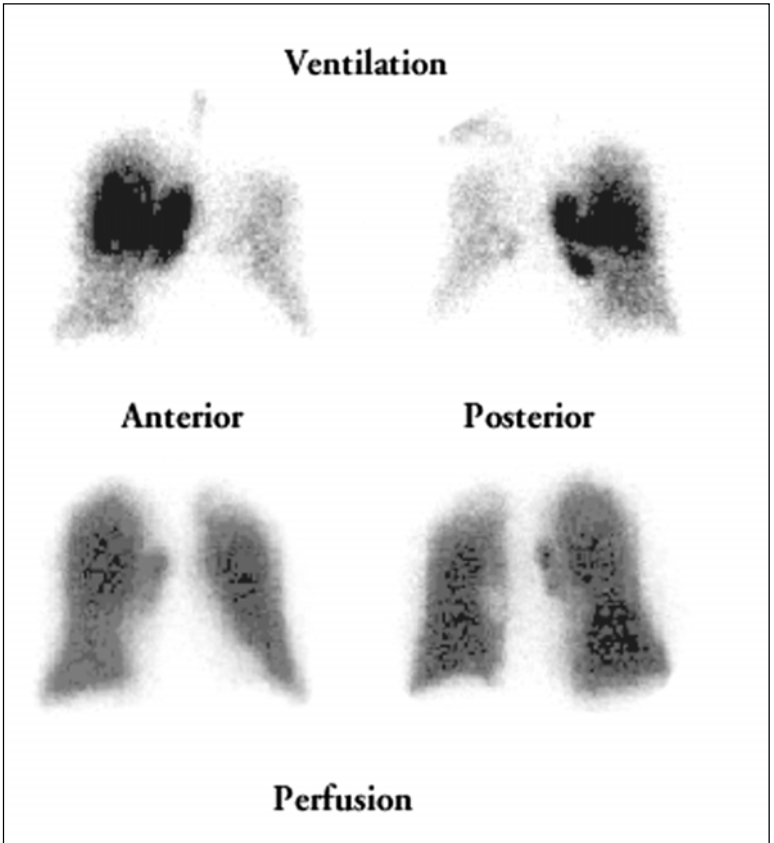
Figure 4. ^{99m}Tc-DTPA aerosol and ^{99m}Tc-MAA images in an intensive care unit patient with a low PaO$_2$ demonstrates generalized decreased ventilation within the entire left lung. The ventilation defects are more prominent then the perfusion defects (reverse mismatch) indicating partial airway obstruction within the left main bronchus. The patient subsequently underwent bronchoscopy which confimed mucous plugging of the left main bronchus.

Two groups of radiopharmaceuticals are used to assess lung ventilation. Xenon-133, the prototype for the radioactive noble gases, has been widely available for many years. More recently, a wide range of ^{99m}Tc-labeled aerosols have replaced ^{133}Xe in many facilities. Despite differences in physiology and technical procedure, overall diagnostic accuracy is similar with these agents. Alternative ventilation imaging techniques, which are less widely available include ^{127}Xe, ^{81m}Kr, ^{99m}Tc-Technegas and ^{99m}Tc-Pertechnegas.

Radioactive Gases for Ventilation Scanning

During inspiration, gas enters the various regions of the lung in proportion to ventilation. Conversely, during expiration clearance is faster from lung regions that have greater ventilation. This forms the basis for ventilation assessment with xenon-133: areas with reduced ventilation show reduced radioactivity during inspiration (defects) but greater radioactivity during expiration (trapping). To demonstrate this requires a dynamic imaging procedure consisting of three phases (Fig. 5):

Wash-in phase: An initial breath-hold image is obtained for 10-25 seconds immediately after the patient inhales the radioactive gas mixture and demonstrates regional lung ventilation.

Equilibrium phase: Images are obtained while the patient re-breathes the gas mixture, ideally for at least four minutes. Regions of the lung which appear as defects on the initial breath-hold image may normalize on the sequential equilibrium image because of collateral air drift.

Wash-out phase: The patient exhales the radioactive gas by breathing room air while sequential images are obtained. Regional air-trapping can be detected as focal areas of retained activity (Fig. 6).

Ventilation imaging with ^{133}Xe is usually performed as a single acquisition in the posterior position which limits the comparison with perfusion images which are obtained in multiple projections. The diagnostic performance of the V/Q lung scan is significantly better in patients who have ventilation studies performed in the erect position compared with the supine position. Because of its lower energy (81 kev) ventilation imaging with ^{133}Xe is generally obtained prior to perfusion imaging. Post-perfusion ventilation imaging with ^{133}Xe is difficult to perform but potential advantages are the ability to optimally position the patient to best demonstrate the perfusion abnormality and avoiding ventilation imaging when the perfusion lung scan appears normal.

The imaging technique with ^{127}Xe is similar to that of ^{133}Xe, but since ^{127}Xe has a higher energy than ^{99m}Tc, ventilation imaging with this agent may be performed following perfusion imaging. Xenon-127 does have several major disadvantages, namely it is more costly than ^{133}Xe and requires medium-energy collimation. Krypton-81m is another noble gas used to evaluate regional ventilation. This agent has a very short physical half-life (13 seconds) and, therefore, only wash-in or breath-hold images can be obtained. However, the short physical half-life of ^{81m}Kr enables one to obtain images in multiple projections. Krypton-81m is produced from a ^{81}Rb generator but the short half-life of the parent radionuclide (4.6 hours) limits the useful lifetime of the generator to a single day. Similar to ^{127}Xe, ventilation imaging with ^{81m}Kr is generally performed following perfusion imaging.

Radioaerosols for Ventilation Scanning

Currently, the most commonly used ventilation scanning agent is ^{99m}Tc-radiolabeled aerosol. Ventilation imaging with ^{99m}Tc-radiolabeled aerosols can be performed with several radiopharmaceuticals including ^{99m}Tc-DTPA, ^{99m}Tc-sulfur colloid, ^{99m}Tc-pyrophosphate, ^{99m}Tc-MDP or ^{99m}Tc-glucoheptonate. The most popular agent is ^{99m}Tc-DTPA, however, this agent has a relatively short residence time within the lung, especially in smokers, and in these patients ^{99m}Tc-sulfur colloid or ^{99m}Tc-pyrophosphate may be preferred. Technetium-99m-labeled radioaerosols
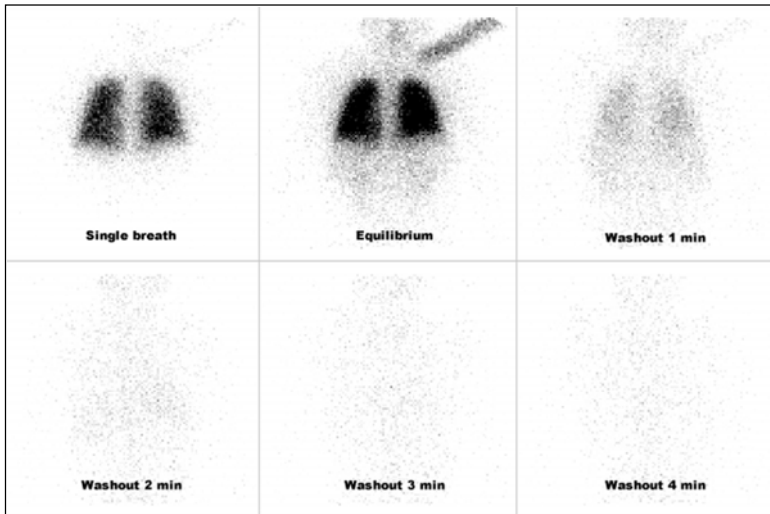
Figure 5. Normal xenon-133 ventilation study performed in the posterior projection. The study consists of single-breath (wash-in), equilibrium and wash-out phases.

are between 0.5-3 microns in size and are produced by adding the appropriate radiopharmaceutical to a commercially available nebulizer. For a routine ventilation study, 1.11 GBq (30 mCi) of ^{99m}Tc-DTPA in 3 ml of saline is placed within the nebulizer. Oxygen is then forced through the nebulizer at high pressure to produce aerosolized droplets which are inhaled by the patient through a mask or mouth piece. The patient generally breathes from the nebulizer for 3-5 minutes or until 37 MBq (1 mCi) of activity is deposited within the lungs. The distribution of activity within the lungs is proportional to regional ventilation. Multiple image projections can be obtained which correspond with those obtained during subsequent perfusion imaging. Ventilation studies with ^{99m}Tc-labeled radioaerosols require minimal patient cooperation, and portable studies or studies in patients on respirators can be performed relatively easily. In general, ventilation is performed prior to perfusion imaging but ventilation imaging with radiolabeled aerosols can also be effectively performed following perfusion imaging. Thus, in patients with a normal or near normal perfusion study, ventilation imaging can be omitted. Disadvantages of ^{99m}Tc-labeled radioaerosols relate primarily to central deposition of activity in patients with COPD or airway obstruction and the amount of activity which is wasted within the nebulizer.

Because of the problem with central deposition of ^{99m}Tc-labeled radioaerosol in patients with COPD, newer agents have been developed. These include ^{99m}Tc-Technegas and ^{99m}Tc-Pertechnegas. Both of these agents are formed by burning ^{99m}Tc-pertechnetate in a carbon crucible at very high temperatures which produces an ultrafine radiolabeled aerosol (particle size 0.02-0.2 microns). Pertechnegas is purged with 5% oxygen and 95% argon, compared with Technegas which is purged with 100% argon. This relatively minor difference causes profound changes in the
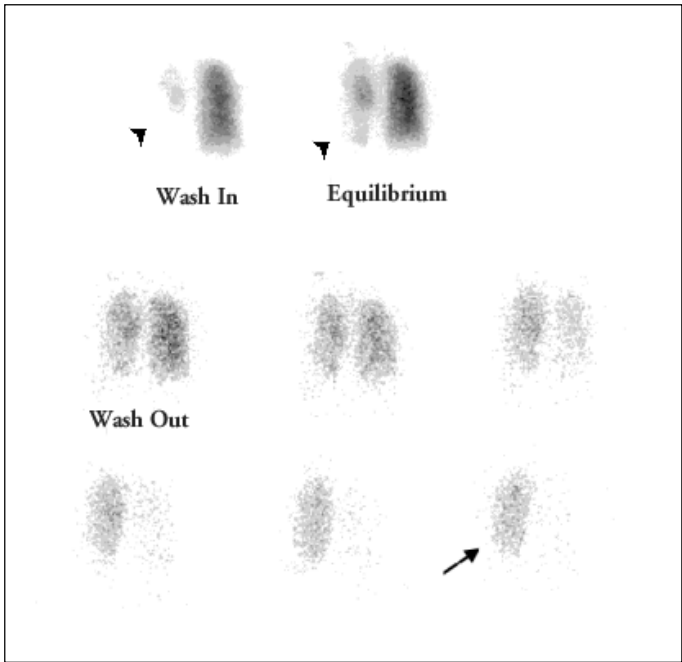
Figure 6. Xenon-133 ventilation study in the posterior projection demonstrating decreased ventilation within the left lung on wash-in and equilibrium images (arrowheads). On serial wash-out images diffuse air-trapping is present within the left lung (arrow).

biological distribution of activity. When inhaled, both agents distribute homogeneously within the lung proportional to regional lung ventilation and very little central deposition of activity is seen even in patients with COPD. Pertechnegas readily penetrates the alveolar epithelial membrane and the biological half-life in the lungs is quite short measuring approximately 6-10 minutes. On the other hand, there is very little transalveolar or mucociliary clearance of Technegas and the effective half-life approaches the physical half-life of the ^{99m}Tc label. Both agents require minimal patient cooperation and only 2-3 breaths are required to obtain sufficient counts in the lungs to perform ventilation imaging. In general, ventilation imaging with both Technegas and Pertechnegas is performed prior to perfusion imaging. Similar to ^{99m}Tc-radiolabeled aerosols, views of the lungs are obtained in multiple projections corresponding to the views obtained during perfusion imaging.

Thrombus Imaging

More recently, there has been considerable interest in radiolabeled antibody fragments and peptides directed against the GPIIb/IIIa receptor on activated platelets. The platelet aggregation process, which occurs in arterial and venous thrombosis,
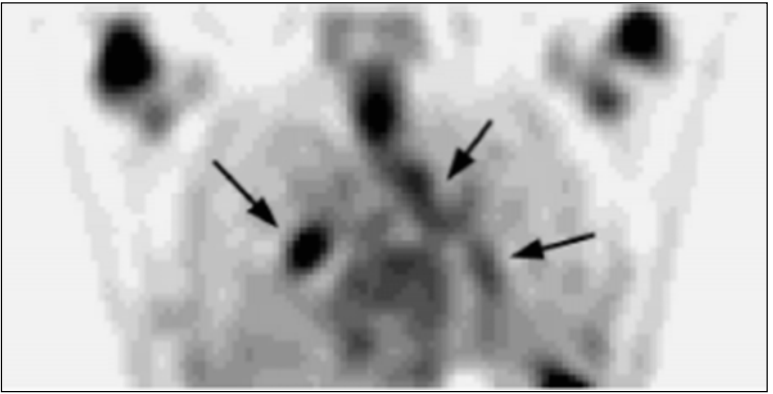
Figure 7. Single coronal SPECT image through the mid thorax demonstrates increased accumulation of ^{99m}Tc-DMP-444 (^{99m}Tc-GP IIb/IIIa antagonist) in a patient with documented PE within the right lower lobe, left main and left lower pulmonary arteries (arrows).

involves the cross-linking of fibrinogen and GPIIb/IIIa receptor on activated platelets. The Food and Drug Administration in the US has recently approved apcitide (AcuTect®), a ^{99m}Tc-labelled synthetic peptide which binds to the GPIIb/IIIa receptor, for evaluation of patients with suspected DVT. The main advantage of this agent is its ability to distinguish between acute and chronic DVT. Several ^{99m}Tc-labelled peptides directed against activated platelets are currently under investigation for the evaluation of patients with suspected PE (Fig. 7).

Diagnosis of Acute Pulmonary Embolism

Accuracy of Lung Scanning

In the Prospective Investigative Study of Acute Pulmonary embolism Diagnosis (PISA-PED), which utilized perfusion scanning alone in conjunction with the chest radiograph, the sensitivity and specificity of scintigraphy was 92% and 87%, respectively. By combining the clinical assessment of the likelihood of PE (very likely, possible or unlikely), the positive predictive value of a positive perfusion scan can be up to 99%. A perfusion scan without segmental defects combined with a low clinical likelihood of PE had a negative predictive value of 97%. It is particularly notable that these results were achieved without ventilation scanning.

To date the most comprehensive prospective study addressing the role of V/Q scanning in the diagnosis of PE has been the Prospective Investigation of Pulmonary embolism Diagnosis study (PIOPED), a multi-institutional study designed to evaluate the efficacy of various conventional methods for diagnosing acute PE. In particular, the study was designed to determine the sensitivity and specificity of V/Q lung scanning for diagnosing acute PE. In addition, the relative contributions of the clinical assessment, chest radiograph and other routine studies were assessed. The sensitivity, specificity and positive predictive value of a high probability V/Q scan interpretation for detecting acute PE were 41%, 97% and 87%, respectively. None

of the patients with a normal V/Q scan had PE. The overall diagnostic performance of the V/Q scan was similar in men and women, in patients of varying ages, and among patient with or without pre-existing cardiac or pulmonary disease.

Patients with suspected pulmonary embolism can be safely managed based on pretest probability and results of V/Q scanning. One prospective study in 1239 patients with suspected pulmonary embolism examined a clinical model used to categorize pretest probability of pulmonary embolism as low, moderate, or high (Wells, 1998). V/Q scanning and bilateral deep venous ultrasonography were performed. Only 3 of the 665 patients (0.5%) with low or moderate pretest probability and a non-high-probability scan had PE or DVT during the 90-day follow-up period.

Interpretation Pitfalls

False negative lung scan interpretations (low probability despite angiographic evidence of PE) do occur and patients who have a recent history of immobilization, surgery, trauma to the lower extremities and central venous instrumentation are a particularly high risk group. In patients with low or very low probability V/Q scan interpretations and no history of immobilization, recent surgery, trauma to the lower extremities or central venous instrumentation, the prevalence of PE is only 4.5%. In contrast, when patients with a low or very low probability V/Q lung scan interpretations have one of the above mentioned risk factors, the prevalence of PE is 12%; with more than one risk factors, the prevalence rises to 21% (Table 1). Patients with false negative lung scan interpretations tend to have non-occlusive and/or subsegmental thrombi with low pulmonary clot burden. In recent years, concern has been raised that a low probability lung scan interpretation may be misleading and result in unnecessary mortality as a sequela of PE. Nevertheless, the prognostic value of a low probability scan is excellent, particularly in patients with a low clinical pre-test likelihood of disease or negative ultrasound. In a recent series of 536 consecutive patients with this finding, there was no evidence that PE was a causative or contributing factor among patients who died within six months of imaging (Rajendran, 1999).

The most common cause of V/Q mismatch in patients who do not have acute PE are related to chronic or unresolved PE. Other causes of V/Q mismatch in the absence of PE (false positive interpretation) include extrinsic compression of the pulmonary vasculature (mass lesions, adenopathy, mediastinal fibrosis), vessel wall abnormalities (pulmonary artery tumors, vasculitis), intraluminal obstruction (tumor emboli, foreign body emboli) and congenital vascular abnormalities (pulmonary artery agenesis or hypoplasia). In patients with unilateral V/Q mismatch (hypoperfusion or absent perfusion) within an entire lung or multiple contiguous segments, and normal perfusion in the contralateral lung, extrinsic compression of the pulmonary vasculature, congenital abnormalities or proximal PE all need to be considered in the differential diagnosis. These patient will often require further imaging with CT or angiography.

Interpretation Criteria

Several diagnostic criteria have been developed for the interpretation of V/Q lung scans. The original PIOPED criteria had the highest likelihood ratio for predicting the presence of PE on pulmonary angiography. However, these also had

Table 1. Value of combining selected risk factors and the lung scan interpretation

	Prevalence of PE		
V/Q scan interpretation	0 Risk factors* (%)	1 Risk factor* (%)	≥2 Risk factors* (%)
High	82%	84%	97%
Intermediate	25%	37%	45%
Low/Very Low	4%	12%	21%
Normal	0%	0%	0%

*risk factors include immobilization for >3 days prior to presentation, recent surgery, trauma to lower extremeties or central venous instrumentation within 3 months of presentation

5

the highest proportion of V/Q scans interpreted as representing an intermediate probability of acute PE. Several subsequent revisions of the original PIOPED criteria have been made based on observations from the PIOPED study (Table 2). With these revisions it is possible to decrease the number of intermediate V/Q scan interpretations and correctly classify scans as low probability of acute PE. The use of the revised PIOPED criteria has been shown to provide a more accurate assessment of angiographically proven PE compared with the original criteria.

A single moderate-sized V/Q mismatch was classified as a low probability of PE using the original PIOPED criteria. However, 36% of patients with a moderate-sized V/Q mismatch had PE, therefore, this finding actually represents an intermediate probability for acute PE. In patients with single segmental V/Q mismatch and multiple risk factors, the prevalence of PE is higher and these patients should be considered to have PE until proven otherwise. In lung zones with matching V/Q defects and chest radiographic opacities (so-called "triple matches"), the overall prevalence of PE was 26%. Triple matches within the upper and middle lung zone had a lower prevalence of PE compared with triple matches in the lower lung zones. PE was present in 33% of lower lung zone defects demonstrating triple matches but in only 11-12% of upper and middle lung zone triple matches. Therefore, patients with matching V/Q defects and chest radiographic opacities isolated to the upper or middle lung zones can be considered to represent a low probability for acute PE. Similar findings within the lower lung zones suggest an intermediate probability for acute PE.

Among patients with no previous cardiopulmonary disease, no patient with PE had radiographic evidence of a pleural effusion which occupied more than one third of the hemithorax. Therefore, V/Q defects with large pleural effusions represent a low probability of acute PE. In contrast, the majority of patients with PE and pleural effusions had small effusions which caused only blunting of the costophrenic angles. The prevalence of PE within the lower lung zones in patients with small pleural effusions was 32% in the right hemithorax and 25% in the left hemithorax. Therefore, "triple matching" V/Q defects with a small effusion represent an intermediate probability of acute PE.

Table 2. Revised PIOPED criteria for ventilation/perfusion (V/Q) lung scan interpretation

High probability (>80%)
  ≥2 large (>75% of a segment) segmental perfusion defects without matching
              ventilation or CXR abnormalities
  1 large segmental perfusion defect and ≥2 moderate (25-75% of a segment)
              segmental perfusion defects without matching ventilation or
              CXR abnormalities
  ≥4 moderate segmental perfusion defects without matching ventilation or CXR
              abnormalities

Intermediate probability (20-79%)
  1 moderate to <2 large segmental perfusion defects without matching
              ventilation or CXR abnormalities
  Matching V/Q defects and CXR parenchymal opacity in lower lung zone
  Matching V/Q defects and small pleural effusion
  Single moderate matched V/Q defect with normal CXR findings
  Difficult to categorize as normal, low or high probability

Low probability (10-19%)
  Multiple matched V/Q defects, regardless of size, with normal CXR findings
  Matching V/Q defects and CXR parenchymal opacity in upper or middle lung
              zone
  Matching V/Q defects and large pleural effusion

Very low (<10%)
  Non-segmental perfusion defects (cardiomegaly, aortic impression, enlarged
              hila)
  Any perfusion defects with substantially larger CXR abnormality
  Single or multiple small (<25% of a segment) segmental perfusion defects with
              a normal CXR
  Defects surrounded by normally perfused lung (stripe sign)

Normal
  No perfusion defects

The "stripe sign" is defined as a rim of perfused lung tissue between the perfusion defect and the adjacent pleural surface. The presence of the sign excluded the diagnosis of PE within the affected zone in 93% of cases. Therefore, perfusion defects which demonstrate a stripe sign are unlikely to be due to PE and in the absence of perfusion defects elsewhere should be interpreted as representing a low probability for PE. Patients with partially resolving perfusion defects may have a similar appearance to the stripe sign, therefore this sign should be interpreted with caution in patients with more chronic symptoms.

Finally, the nuclear medicine physician's subjective estimate of the likelihood of PE (without using specific interpretation criteria) correlated well with the fraction of patients with angiographic evidence of PE. Thus, experienced readers (such as the PIOPED investigators) can provide an accurate estimate of the probability of PE based on radiographic and scintigraphic findings.
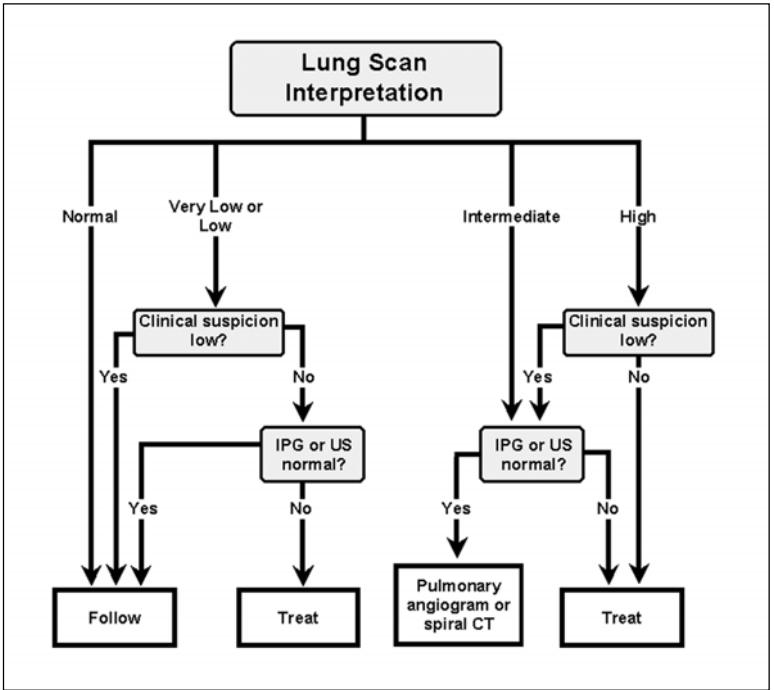
Figure 8. Diagnostic algorithm for suspected pulmonary embolism. (US = compression venous ultrasound, IPG = impedance plethysmography, CT = computed tomography.

Diagnostic Approach

Prospective and outcome-based studies permit the following conclusions in the diagnostic evaluation of patients with suspected PE (summarized in Fig. 8):

- A normal V/Q scan interpretation excludes the diagnosis of clinically significant PE.
- Patients with very low or low probability V/Q scan interpretation and low clinical likelihood of PE do not require angiography or anticoagulation.
- Patients with very low or low probability V/Q scan interpretation, intermediate or high clinical likelihood of PE, and negative serial noninvasive venous studies of the lower extremities do not require anticoagulation or angiography. If noninvasive venous studies of the lower extremities are positive, patients should be treated.
- Clinically stable patients with an intermediate probability V/Q scan interpretation require noninvasive venous studies of the legs and, if negative, require pulmonary angiography or CT angiography for a definite diagnosis.

- Clinically stable patient with a high probability V/Q scan interpretation and a high clinical likelihood of PE require treatment and need no further diagnostic tests to confirm the diagnosis.
- Clinically stable patients with a high probability V/Q scan interpretation and a low clinical likelihood of PE require noninvasive venous studies of the legs and if negative often require pulmonary angiography or CT angiography for a definitive diagnosis.

Evaluation of Pulmonary Hypertension

Chronic pulmonary thromboembolism is a serious and potentially surgically treatable cause of pulmonary hypertension (PHT). It has been estimated that between 0.5% and 4% of patients with acute pulmonary emboli will eventually develop chronic thromboembolic PHT. Unfortunately, the clinical features, laboratory investigations and other noninvasive investigations are often unreliable in distinguishing chronic thromboembolic PHT from primary and non-thromboembolic secondary PHT. Evaluation with pulmonary angiography is usually required to confirm the diagnosis and to determine whether surgical intervention is indicated. Although some authors have reported that pulmonary angiography can be performed safely in patients with severe PHT, others have documented a higher frequency of complications, including death. V/Q lung scanning provides a safe, noninvasive technique to select which patients with PHT require pulmonary angiography to confirm the diagnosis of chronic PE and determine eligibility for thromboendarterectomy. However, both V/Q lung scanning and pulmonary angiography may underestimate the severity of chronic thromboembolic material within the pulmonary vasculature as determined at surgery.

When performing a V/Q lung scan in patients with PHT it is important to avoid adverse hemodynamic effects by reducing the number of injected ^{99m}Tc-MAA particles. Previous studies have demonstrated that fewer than 60,000 particles cause an inhomogenous distribution of activity within the pulmonary vasculature. Consequently, we recommend that patients with PHT are injected with between 60,000 and 100,000 particles of ^{99m}Tc-MAA. Several studies have documented the safety of perfusion lung scanning in patients with PHT when the number of particles are reduced. In patients with chronic thromboembolic PHT, 96% have V/Q lung scans showing a high probability of pulmonary embolism and the remainder have intermediate probability scans. Therefore, pulmonary angiography is justified in patients with intermediate or high probability V/Q lung scan interpretations to confirm the diagnosis of chronic PE and determine surgical accessibility. Most patients with primary PHT and non-thromboembolic secondary PHT have low probability V/Q lung scan interpretations and demonstrate diffuse inhomogenous distribution of ^{99m}Tc-MAA within both lungs. Patients with thromboembolic PHT rarely (if ever) have normal or very low probability V/Q lung scan interpretations, and a low probability V/Q lung scan interpretation effectively excludes chronic thromboembolism as the cause of PHT.

Frequently Asked Questions (FAQs)

The following questions and answers were adapted from the ACCP Consensus Committee on Pulmonary embolism ("Opinions regarding the diagnosis and

management of venous thromboembolic disease" in Chest 1996; 109:233-37 and Chest 1998; 113:499-504).

Does a normal PaO$_2$ or normal alveolar-arterial oxygen difference exclude clinically significant PE?

A normal PaO$_2$ or a normal alveolar-arterial oxygen difference does not exclude PE. Although most patients with large PE have an abnormality of the PaO$_2$ or alveolar-arterial oxygen difference, these values may be normal in patients with clinical manifestations of acute PE.

Does a normal plasma D-dimer exclude PE with sufficient accuracy to eliminate the necessity of further diagnostic studies?

D-dimer is a degradation product of a cross-linked fibrin blood clot. Levels of D-dimer are typically elevated in patients with acute venous thromboembolism. D-dimer levels may also be increased in a variety of nonthrombotic disorders including recent major surgery, hemorrhage, trauma, malignancy or sepsis. Therefore, D-dimer assays are, in general, sensitive but non-specific markers for venous thromboembolism. The negative predictive value of the D-dimer increases proportionately depending upon the sensitivity of the assay and is inversely related to the prevalence of venous thromboembolism in the population under study. A normal plasma D-dimer, measured by enzyme-linked immunosorbent assay (ELISA), excluded all but 5 to 10% of patients with acute PE. A normal latex agglutination D-dimer was unreliable for excluding PE and should not be used. A whole blood agglutination assay (SimpliRED®) has the advantage that it is simple to perform, has a rapid turn around time and is inexpensive, however, the sensitivity of this assay is lower than several ELISA assays. Although investigations of the use of the D-dimer for the exclusion of acute PE have shown promising results, most believe that if there is a high clinical suspicion of acute PE, diagnostic tests should proceed in spite of a normal plasma D-dimer. If there is only a low level of clinical suspicion then a normal plasma D-dimer may strengthen the likelihood that no thromboembolic disease is present. At the present time, however, data on the use of the D-dimer are insufficient to allow complete reliance on this test.

What is the utility of the D-dimer in combination with V/Q scans?

The combination of a low D-dimer and low-probability V/Q scan has been shown to be diagnostically useful in assessing possible PE. Using the ELISA with the appropriate cutoff value, a negative D-dimer is strong evidence that the patient does not have a PE. That is, the ELISA for D-dimer has a high negative predictive value for PE. Until D-dimer testing is standardized and more widely validated in prospective outcome studies, however, widespread use of D-dimer measurement is not recommended.

If the combination of V/Q scan and clinical findings yields diagnostic uncertainty, should a noninvasive leg test be performed?

This would be a reasonable next diagnostic test.

If the V/Q scan indicates low or intermediate probability for acute PE, and a single noninvasive leg test is negative for DVT, would serial noninvasive leg tests be an acceptable approach?

Pulmonary angiography is warranted if noninvasive studies are inconclusive, particularly if there is a high clinical suspicion of PE. Serial noninvasive leg tests would be an appropriate approach to patients with nondiagnostic V/Q scans and a single negative leg test, providing there is good cardiopulmonary reserve. Serial leg testing originally used impedance plethysmography (IPG) on presentation (day 1) and repeated on days 2, 3, 5, 7, 10 and 14. Only 2-3% of tests become positive on serial testing. Venous compression ultrasound is more sensitive to nonocclusive thrombus and requires less frequent testing (days 1, 3 and 7).

Is there a role for echocardiography in excluding life threatening conditions that may simulate acute PE?

Echocardiography may be useful in hemodynamically unstable patients to exclude life threatening conditions such as ventricular septal rupture, aortic dissection, or cardiac tamponade. Right ventricular hypokinesis and dilatation, or direct visualization of right atrial or right ventricular thrombosis, increase the likelihood of PE.

If PE is suspected on the basis of clinical evaluation, should heparin be administered immediately, before diagnostic studies are completed?

The risk of recurrent untreated acute PE during the period of diagnostic tests usually exceeds the risks of bleeding from heparin. This is especially true for low molecular weight heparins. Therefore, the immediate administration of heparin is often recommended. Some reserve the immediate administration of heparin for those with poor cardiopulmonary reserve. The bleeding risk should be assessed, and if deemed excessive, evaluation for PE may need to proceed promptly prior to heparin therapy. Additional factors to consider are the speed with which diagnostic tests can be obtained, the level of suspicion for acute PE, the severity of the suspected acute PE and the patient's cardiopulmonary status.

Can a V/Q scan that improves over time be considered, retrospectively, to indicate that PE occurred?

A V/Q scan that improves over time does not necessarily indicate PE. Pneumonia, tuberculosis and other granulomatous diseases, asthma, chronic obstructive pulmonary disease (especially with transient mucous plugging) and collagen vascular diseases such as lupus erythematosus and sarcoidosis have the potential to improve with therapy or spontaneously. These diseases can cause mismatched perfusion defects. Consequently, an improving lung scan does not necessarily indicate acute PE.

Should follow-up diagnostic studies for acute PE include a repeat V/Q scan? If so, when should it be performed?

Some believe that a follow-up V/Q lung scan should be performed. The value of a repeat V/Q scan would be to seek an anatomic or pathologic explanation for failure of the patient to regain baseline performance or to serve as a new baseline to assess

new symptomatic episodes. Any resolution that occurs on the V/Q scan occurs within 3 months. A follow-up V/Q scan, therefore, is particularly useful at 3 months after the acute PE. If the patient is unable to return in 3 months, a V/Q scan at discharge may be useful if there is a prolonged hospitalization.

If the clinical circumstances indicate the necessity of an intervention to reduce clot burden in patients with suspected acute PE, and if thrombolytic therapy is the intervention of choice, is pulmonary angiography always necessary to confirm the diagnosis?

There is disagreement on this point. Some believe that the risk of serious and perhaps fatal bleeding with thrombolytic therapy is so great that a pulmonary angiogram must be obtained in all patients. Others believe that if there is a strong clinical suspicion of acute PE supported by a high probability V/Q scan (or in an extreme emergency, a noninvasive leg test showing DVT or an echocardiogram showing right ventricular dysfunction) then thrombolytic therapy may be administered on the basis of these noninvasive tests without a pulmonary angiogram. In the absence of a pulmonary angiogram, a high probability V/Q scan in the appropriate clinical setting offers the most useful information.

Does a ventilation scan need to be performed in all patients, or are there patients in whom the combination of a plain chest radiograph and perfusion scan are sufficient?

If V/Q scans are obtained with ^{99m}Tc-aerosols, a chest radiograph and a perfusion scan can be obtained initially and evaluated by the nuclear medicine physician. If a ventilation scan is deemed necessary, it can be performed by postperfusion techniques. If the perfusion scan is normal, no ventilation scan is needed. If the perfusion scan shows characteristic vascular defects in regions where the chest radiograph is normal, this would indicate a high probability for PE and a ventilation scan is unnecessary. In patients with prior cardiopulmonary disease, in whom matched perfusion and ventilation defects are likely to occur, both a ventilation and perfusion scan are often indicated.

What is the role of contrast-enhanced helical (spiral) CT?

This diagnostic modality is still under investigation and no firm general conclusions can be made without more extensive experience. It appears to be a useful addition to the panel of tests available for the diagnosis of PE, particularly in central arteries. In institutions where experience and skill with this modality are available, it can have value in diagnosing central PE in circumstances wherein established diagnostic tests are not immediately available. A normal contrast-enhanced CT scan does not exclude PE, particularly in subsegmental arteries. In patients with renal insufficiency, consideration should be given to the consequences of the load of

radiographic contrast material prior to choosing CT or conventional pulmonary angiography. Both contrast-enhanced CT and conventional pulmonary angiography require a substantial load of contrast material. If only a limited amount of contrast material can be given safely to a particular patient, it may be prudent to select the single most definitive test, conventional pulmonary angiography, rather than risk the requirement for a conventional pulmonary angiogram subsequent to a potentially nondiagnostic contrast-enhanced CT scan. Further studies are necessary to delineate the diagnostic role of contrast-enhanced helical CT in patients with suspected acute PE.

In patients with proven PE, particularly those with adequate cardiopulmonary reserve and no apparent source of deep venous thrombosis, is it ever proper to withhold therapy?

This issue needs clarification by means of prospective clinical trials. In the absence of further data, consensus opinion at this time is that any patient who has a proven diagnosis of PE needs to be treated unless there are extenuating circumstances such as terminal carcinoma. A few patients with mild PE who escaped treatment in PIOPED had a satisfactory outcome without treatment. Also, calculations from data reported in one trial suggest that some patients with serially normal results of noninvasive leg tests and nondiagnostic V/Q scans may have had PE, and did well without treatment. However, these data are insufficient to permit withholding treatment of PE at the present time. Contraindication to anticoagulants occurs in some situations but in these cases, unless death from end stage malignancy is imminent, inferior vena caval filters are indicated until anticoagulation can be safely administered.

Additional Reading

1. Bates SM, Ginsberg JS. Helical computed tomography and the diagnosis of pulmonary embolism. Ann Intern Med 2000; 132(3):240-242.
2. Carson JL, Kelley MA, Duff A et al. The clinical course of pulmonary embolism. N Engl J Med 1992; 326:1240-1245.
3. Miniati M, Pistolesi M, Marini C et al. Value of perfusion lung scan in the diagnosis of pulmonary embolism: Results of the prospective investigative study of acute pulmonary embolism diagnosis (PISA-PED). Am J Respir Crit Care Med 1996; 154:1387-1393.
4. PIOPED Investigators. Value of the ventilation/perfusion scan in acute pulmonary embolism. JAMA 1990; 263:2753-2759.
5. Rajendran JG, Jacobson AF. Review of 6-month mortality following low probability lung scans. Arch Int Med 1999; 159:49-52.
6. Rathbun SW, Raskob GE, Whitsett TL. Sensitivity and specificity of helical computed tomography in the diagnosis of pulmonary embolism: A systematic review. Ann Intern Med 2000; 132(3):227-232.
7. Wells PS, Ginsberg JS et al. Use of a clinical model for safe management of patients with suspected pulmonary embolism Ann Int Med 1998; 129:997-1005.
8. Wells PS, Anderson DR, Bormanis J, Guy F, Mitchell M, Lewandowski B. SimpliRED D-dimer can reduce the diagnostic tests in suspected deep vein thrombosis. Lancet 1998; 351:1405-1406.
9. Worsley DF, Palevsky HI, Alavi A. Clinical characteristic of patients with pulmonary embolism and low or very low probability lung scan interpretations. Arch Intern Med 1994; 154:2737-2741.

Bone Densitometry

William D. Leslie and Bruce E. Roe

Pathophysiology of Bone Loss and Osteoporotic Fractures

Pathophysiology of Bone Loss

Bone is a dynamic tissue consisting of cellular, organic and inorganic components with a complex internal structure (Fig. 1). It is much more than passive scaffolding for the rest of the body and undergoes considerable metabolic activity and remodeling. The mature skeleton consists of a mixture of cortical bone (85%) and trabecular bone (15%). The relative amounts of these vary widely between different anatomic sites (Fig. 2).

Bone tissue reacts to stress and injury through a well-orchestrated sequence for removing old bone and building new tissue. Bone remodeling is carried out by the basic multicellular unit (BMU), which consists of both osteoclasts and osteoblasts. The BMU typically takes 3-6 months to complete a cycle (Fig. 3). Bone remodeling affects 3-5% of cortical bone per year, but involves up to 25% of trabecular bone due in part to its greater relative surface area. The osteoclast, a multinucleated cell of monocyte origin, resorbs bone through the release of acid and enzymes such as cathepsin K from its ruffled border. Osteoblasts, derived from mesenchymal cells, enter the resorption pit and lay down organic matrix (osteoid). The osteoblast then dies or enters a dormant stage and is known as an osteocyte (if trapped within calcified tissue) or a lining cell (if found on the surface of calcified tissue). The osteoid is subsequently mineralized over a period lasting several months. There is close coupling of osteoclast and osteoblast activities, although the intercellular signaling involved is incompletely understood. It is clear, however, that processes which stimulate (or suppress) one cell type result in stimulation (or suppression) of the other. For example, after menopause, osteoblast activity increases in an attempt to compensate for increased osteoclastic resorption. On the other side of the equation, antiresorptive treatments targeted at suppressing osteoclast activity are only able to achieve a slight gain in bone mass as there is a parallel reduction in osteoblast activity (Fig. 4). The bone remodeling cycle is regulated by a myriad of factors, including growth factors and interleukins. A new molecule, osteoprotegerin ligand (OPGL), has recently been discovered and shown to be the primary regulator of osteoclast activity. Estrogen deficiency, glucocorticoid excess and vitamin D deficiency are common conditions where bone metabolism is altered.

Bone cell activity can be evaluated through the measurement of biochemical markers. Osteoblasts produce type I collagen (the primary collagen of bone tissue), non-collagenous proteins (such as osteocalcin) and enzymes (such as alkaline phosphatase). Many of these are measured in the serum as indices of bone formation.
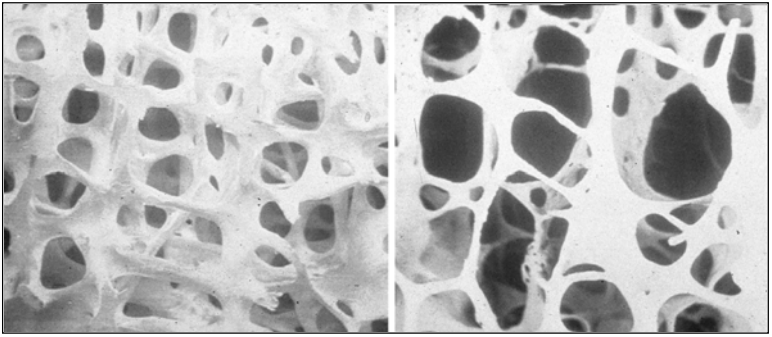
Figure 1. Scanning micrograph showing normal trabecular bone (left) and osteoporotic bone (right).

6
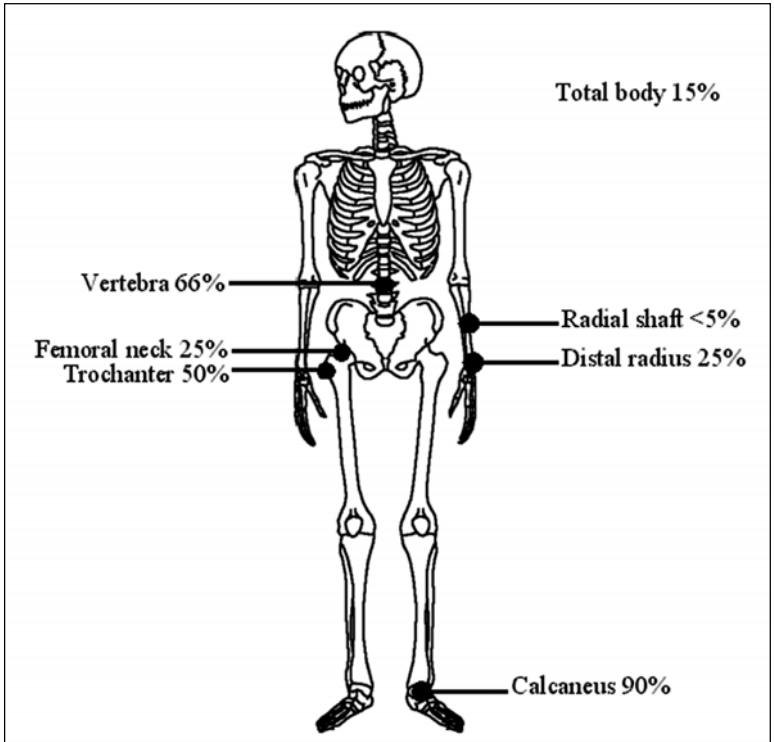
Figure 2. Percent of trabecular bone in skeletal sites commonly assessed with bone densitometry.
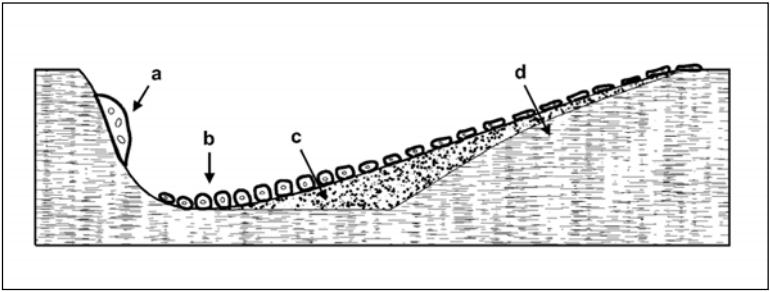
Figure 3. Bone remodelling cycle. Proceeding from left to right the sequence is (a) osteoclast resorption, (b) osteoblast proliferation, (c) osteoid matrix deposition and (d) mineralization.

6
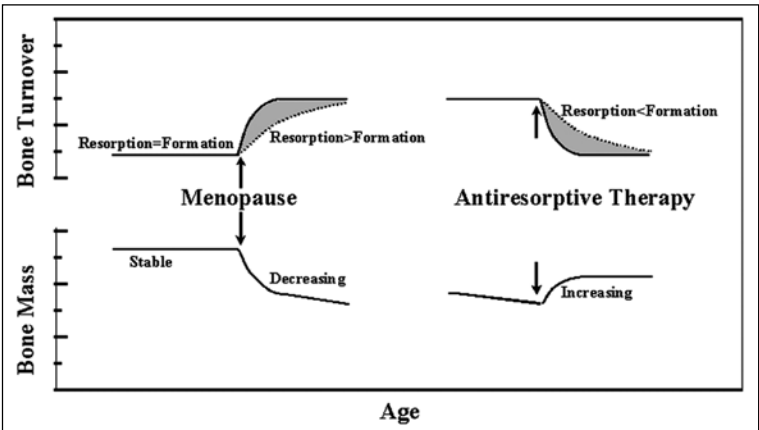
Figure 4. Bone turnover increases after menopause. Accelerated resorption (solid line) is the primary event that is soon followed by a secondary increase in bone formation (dotted line). Bone mass declines during the period of relative imbalance in bone resorption and formation (grey shading) and is followed by a slower progressive decrease. Antiresorptive therapy directly inhibits osteoclast action which is followed by an indirect suppression of osteoblast activity and a reciprocal increase in bone mass, though usually not to normal levels.

Collagen is a triple-helical molecule that undergoes extensive post-translational modifications including hydroxylation, glycosylation and covalent cross-linking. The degradation products of crosslinked collagen, which include C-telopeptide, N-telopeptide and deoxypyridinoline, may be measured in the urine as an index of osteoclast activity.

Skeletal mass accumulates rapidly during childhood, especially during the years of most rapid growth in early adolescence. Peak bone mass is achieved by age 20-25. Determinants of peak bone mass included genetics, physical activity and diet

---

Table 1. Secondary causes of bone loss

Genetic factors
>   Defects in collagen synthesis or structure
>   Idiopathic hypercalciuria

Nutritional
>   Low calcium intake
>   Vitamin D deficiency
>   Malabsorption

Drugs
>   Excess glucocorticosteroids
>   Anticonvulsants
>   Heparin

Lifestyle
>   Immobility
>   Smoking
>   Alcohol

Endocrine/Metabolic
>   Hypogonadism
>   Early menopause or prolonged hypoestrogenism
>   Glucocorticosteroid excess
>   Hyperparathyroidism
>   Hyperthyroidism
>   Diabetes mellitus
>   Renal insufficiency

Other
>   Myeloma
>   Malignancy

(especially calcium intake). The specific genes that influence peak bone mass have yet to be elucidated, but twin studies suggest that 80% of the variation in peak bone mass is determined by genetic factors. Ethnicity is also important. Blacks have higher average bone mass than Caucasians who in turn have higher average bone mass than Asians.

After early adulthood, both men and women start a slow, inexorable decline in bone mass that continues until death. Bone turnover accelerates in women at the time of menopause, especially in trabecular bone, and usually results in the loss of 5-15% of bone mass over the first 5 years after menopause. After early menopause, age-related bone loss continues at a rate of 0.5-1% per year. The pathogenesis of age-related bone loss is unclear, but may be related in part to changes in calcium absorption and vitamin D availability. Other factors which can increase bone loss are detailed in Table 1.

Pathophysiology of Osteoporotic Fractures

Osteoporosis is defined by the World Health Organization as "a systemic skeletal disease characterized by low bone mass and microarchitectural deterioration of bone tissue, with a consequent increase in bone fragility and susceptibility to fracture".

Bone mass is the primary determinant of bone strength, as studies of excised bone have demonstrated that 80-90% of bone strength is determined by the amount of bone. Measures of bone mass from different skeletal sites correlate moderately well, but site-to-site differences are not uncommon and may reflect genetic factors, hormonal influences and the individual's level and pattern of activity.

Microarchitectural deterioration also has an important effect on bone strength. Typical changes in trabecular bone include reduction in trabecular thickness and number, and perforation of trabeculae by deep resorption pits (Fig. 1). This results in loss of trabecular connectivity which is currently believed to be irreversible. These microarchitectural changes may not be reflected by reductions in bone density but still contribute to fracture susceptibility.

Although this discussion has focused on bone strength as a determinant of fracture risk, it is important not to overlook the many clinical factors that independently contribute to fracture risk assessment (see Section on Clinical Risk Factors to Predict Bone Density).

Technical Aspects of Bone densitometry

General Principles

All bone measurement techniques rely upon the ability of bone to block transmission of energy. In general, the more dense the bone the less energy is transmitted. The physical forms of energy used in clinical bone densitometry are x-rays (generated from an x-ray tube), gamma rays (released from decaying radionuclides) and sound (emitted from an ultrasonic transducer). Ideally, a bone density method would have high accuracy and precision (or reproducibility), and would be rapid, inexpensive, painless and safe (with little or no ionizing radiation). At the present time, no method completely satisfies all of these criteria.

Bone Density Technologies

Dual Energy X-ray Absorptiometry (DEXA)

DEXA grew out of dual photon absorptiometry (DPA) which used gadolinium-153 as the photon source. This method suffered from the need for radionuclide source changes, poor image resolution and reproducibility, and has been largely replaced by DEXA. DEXA uses an x-ray tube to generate two different x-ray energies. Bone blocks (or attenuates) x-rays to a greater degree than soft tissue, and lower x-ray energies are attenuated more than higher energies. An x-ray detector records the amount of attenuation for the two energies and can calculate both the amount of soft tissue and the amount of bone calcium in the path of the beam. The x-ray tube and detector scan over the area of interest, building up an image of bone mineral content (BMC) expressed in grams of calcium. The densitometer's software identifies the projected bone area using an edge-detection algorithm. Dividing BMC (grams of calcium) by the bone area (cm²) yields a real bone mineral density (BMD as grams/cm²). DEXA has the advantage of being rapid (particularly with newer scanners that use higher output x-ray tubes and a fan-beam configuration) and are able to scan the structures of greatest clinical interest such as spine, hip (Fig. 5), forearm and even total body. The radiation dose from a lumbar spine scan is much less than 10 µSv (1 mRem), a value similar to one day's normal background radiation and of

L2-L4 BMD (g/cm²)[1]	1.240 ± 0.01
L2-L4 T-Score[2]	0.33 ± 0.1
L2-L4 Z-Score[3]	2.22 ± 0.1
L2-L4 sBMD (mg/cm²)[7]	1181 ± 10

TOTAL BMD (g/cm²)[1]	1.075 ± 0.02
TOTAL T-Score[2]	0.62 ± 0.2
TOTAL Z-Score[3]	1.89 ± 0.2
TOTAL sBMD (mg/cm²)[7]	1021 ± 20
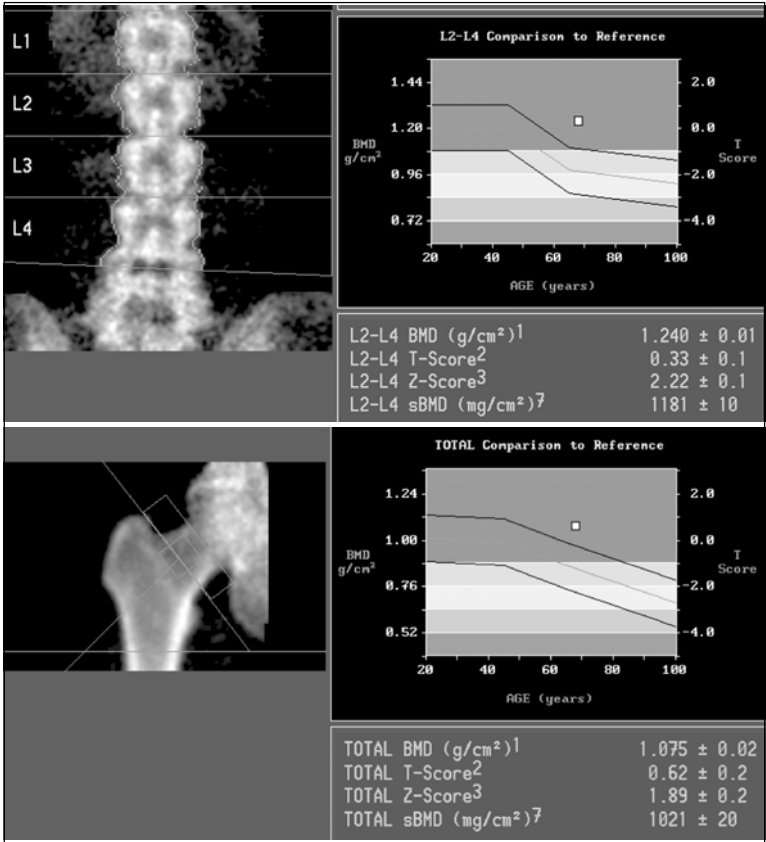
Figure 5. Normal DEXA scans of the spine (top) and hip (bottom). Results are plotted in the right panels in relation to the normal age- and gender-matched reference curves.

negligible risk. Radiation doses from scans of the hip, forearm and total body are even lower.

Peripheral X-Ray Absorptiometry

Conventional DEXA (also known as central DEXA) is able to measure all skeletal structures, including those in the thicker body regions such as lumbar spine and hip. Unfortunately, conventional DEXA equipment is expensive and heavy. Therefore, a variety of compact, portable devices have been developed for measuring bone density in the extremities such as the forearm and calcaneus. Single photon absorptiometry (SPA) used a radionuclide source (iodine-125) but required periodic source replacements and immersion of the body part in water. Peripheral DEXA (pDEXA)
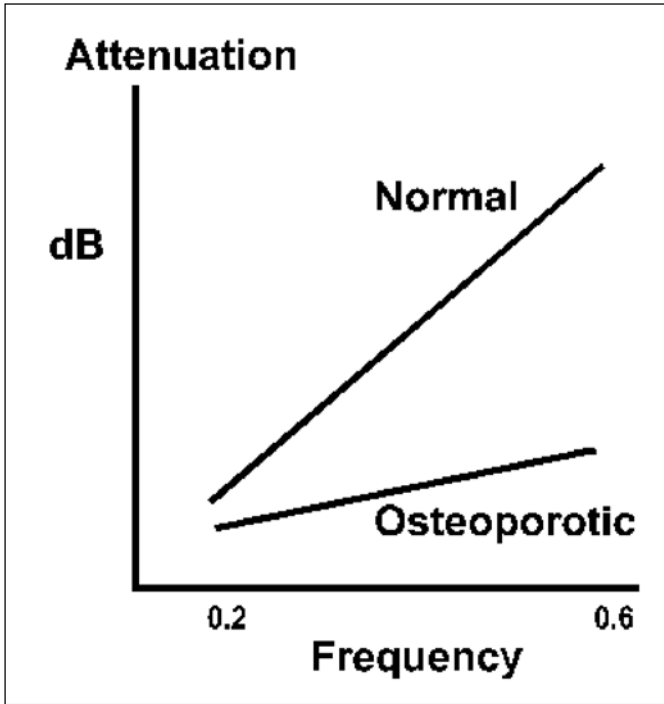
Figure 6. Broadbeam ultrasound attenuation (BUA) is defined as the slope of the relationship between sound frequency and loss in bone signal. Over the usual range of frequencies (0.2 to 0.6 MHz) higher frequencies are associated with greater signal loss (dB attenuation).

devices avoid these limitations and impart an exceedingly small radiation dose of less than 0.1 µSv (0.01 mRem).

Quantitative ultrasound

Ultrasound has recently emerged as another tool for characterizing bone strength and has the advantages of being radiation-free and using relatively inexpensive, portable devices. Ultrasound penetrates bone poorly, and higher frequencies are attenuated more than lower frequencies. Two measures are typically derived from quantitative ultrasound (QUS). One is the speed of sound (SOS), a measure of the speed with which sound travels from one transducer to the other through the bone (m/sec). The other is broadbeam ultrasound attenuation (BUA) which is the slope of the relationship between attenuation and frequency (dB/mHz) as shown in Figure 6. Due to ultrasound's difficulty in penetrating deep structures, most devices measure the more accessible bones such as the calcaneus, phalanges and tibia. While x-ray-based techniques are calibrated against calcium content, there is considerable

controversy over the physical properties measured by bone ultrasound. Whether QUS measures bone quality independent of bone density is currently an area of controversy.

Other X-Ray Based Techniques

CT scanners are capable of measuring bone density by using a calibrated phantom and specialized software. Such measurements are known as quantitative CT (QCT) and give bone density in terms of volume (mg/cm^3). Although QCT is expensive and has a relatively high radiation dose (100 μSv), it has the advantage of providing a true volumetric measure of bone density (rather than areal as with DEXA). This can be advantageous when skeletal size deviates markedly from average or when there are dense artifacts (such as heavily calcified aorta or osteophytosis of the lumbar spine) that preclude accurate DEXA measurements. Smaller CT devices have been developed for studying the distal radius and are referred to as peripheral QCT (pQCT).

Although conventional x-rays are not quantitative, they are still an important component in the assessment of osteoporosis since the presence of fragility fractures (such as vertebral compression fractures) indicates osteoporosis. Plain radiographs of the hand can also be used to measure cortical width in the fingers, but this is a relatively insensitive technique. With the introduction of aluminum calibration wedges, however, there is renewed interest in plain radiographs of the hands as an accessible and low-cost alternative to the methods previously listed.

Accuracy

Accuracy refers to how closely a measured result approximates the "true" value and is of critical importance when comparing an individual patient to a reference population. The accuracy of bone mineral measurements is determined by comparison with dry- or ash-weight of bone samples. DEXA is the predominant technology used for evaluating bone density, and has a measurement error of 5-7%. This error is small relative to the range of values in the population, enabling its use as a tool to diagnose osteoporosis and assess fracture risk. Bone density may be overestimated in anteroposterior measurements of the lumbar spine due to the presence of degenerative sclerosis or osteophytes (Fig. 7), compression fractures (Fig. 8), superimposed vascular calcification or other dense materials (eg,. barium, iodinated contrast or undissolved calcium tablets) (Fig. 9). Lateral spine DEXA measurements are less susceptible to these artifacts but this approach is limited by poorer precision. Discrepancies between spine measurements and other skeletal sites are more typically seen in older subjects (more than 60 years of age) and those with known spine disease. Hip or peripheral bone assessment can be of great value in these cases. Hip measurements are affected by patient positioning and the degree of hip rotation, which makes it critical for technologists to standardize their technique. Hip measurements are less susceptible to degenerative changes, but thickening of the medial cortex of the femoral neck (called "buttressing") will be reflected in bone density measurements. The trochanteric region appears to be relatively unaffected by these changes. Previous fracture, surgery or Paget's disease (Fig. 10) can affect hip results and the contralateral hip should be measured under such circumstances.

The accuracy of QUS is difficult to determine due to the wide range of instrument designs and the absence of an accepted calibration standard. Peripheral QUS values
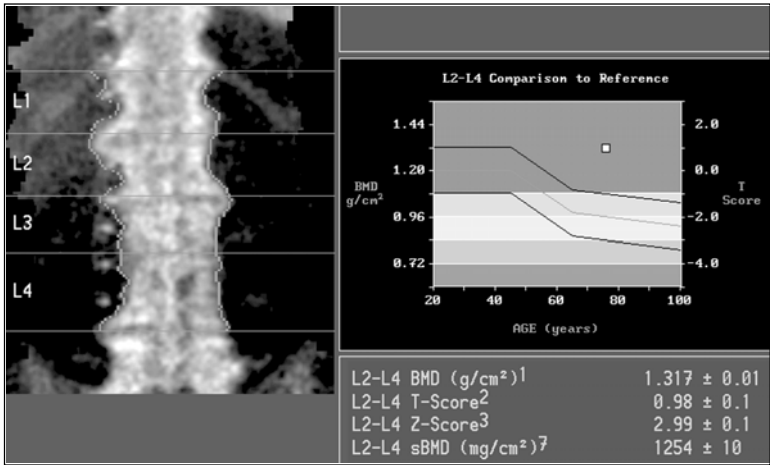
Figure 7. Spine spondylosis producing artifactually elevated spine bone density (1.317 g/cm², T-score+0.98). The hip measurement in this patient was normal (1.000 g/cm², T-score 0.00).

show only moderate correlation with bone density measured at proximal skeletal sites, though this is similar to the ability of peripheral x-ray-based measurements to predict central bone density. The accuracy of QUS can be indirectly validated through its ability to identify patients at risk of fracture. To date, this has only been reported for a small number of the available instruments, but available data show that fracture prediction with calcaneal QUS is comparable to that obtained with x-ray-based techniques.

Precision

Precision (also referred to as reproducibility) is the ability of a system to obtain the same results in repeated measurements of the same individual. A technique must have good precision if serial measurements are to be used in following an individual. Greater precision makes it possible to detect smaller changes in a subject. Current methodologies typically demonstrate precision errors that are larger than annual changes in bone density. Thus, in an individual patient, it may be difficult to determine whether a small change in the bone mass measurement reflects precision error or true change (Table 2).

DEXA reproducibility is influenced by instrument-, operator- and subject-dependent factors. These last two tend to be much more important than the instrument itself, and patient positioning is the single most important determinant. Reproducibility is optimized through a systemic process that includes careful quality control of the instrument, scanning technique and analysis (Table 3). Hip measurements are less reproducible than those of the spine, in large part due to the difficulty in obtaining consistent positioning. Reproducibility is further compromised when examining smaller regions of interest. Femoral neck precision is much worse

```
                     Bone  Results
                       DEXA Calibration
                       BMD        T         Z
          Region       g/cm²     Score     Score
          L1           0.512     -5.15     -4.70
          L2           0.422     -6.48     -6.03
          L3           0.449     -6.26     -5.80
          L4           0.500     -5.84     -5.38
          L1-L2        0.463     -5.73     -5.27
          L1-L3        0.458     -5.94     -5.48
          L1-L4        0.470     -5.92     -5.46
          L2-L3        0.436     -6.37     -5.91
          L2-L4        0.460     -6.17     -5.71
          L3-L4        0.476     -6.03     -5.57
```

```
                     Bone  Results
                       DEXA Calibration
                       BMD        T         Z
          Region       g/cm²     Score     Score
          L1           0.808     -2.68     -2.04
          L2           0.537     -5.53     -4.89
          L3           0.483     -5.98     -5.33
          L4           0.432     -6.40     -5.76
          L1-L2        0.675     -3.96     -3.31
          L1-L3        0.610     -4.66     -4.02
          L1-L4        0.550     -5.25     -4.61
          L2-L3        0.509     -5.76     -5.11
          L2-L4        0.476     -6.04     -5.39
          L3-L4        0.452     -6.23     -5.59
```

Figure 8. Spine compression fracture causing apparent improvement in bone density. The first scan (top) gives L1-L4 bone density 0.470 g/cm². The follow-up examination (bottom) shows an apparent increase in bone density to 0.550 g/cm². In fact, all of the change is confined to L1 (0.512 to 0.808 g/cm²) which is sclerotic on the image. After excluding L1 from the analysis, the L2-L4 spine shows stable bone density (0.460 to 0.476 g/cm²).

than the total hip region, and Ward's triangle (an area within the femoral neck that contains little trabecular bone) is so variable that it is of little clinical value.

Precision can be stated as either standard deviation (SD) or percent coefficient of variation (%CV, defined as 100 x SD/mean). Although precision error is commonly stated as a %CV, several reports indicate that error is independent of bone mass and will therefore be underestimated in the lower (osteoporotic) range. This suggests that it may be preferable to express precision error as the absolute SD. The smallest change that must be present before one can conclude (with 95% confidence) that the change is not related to measurement error is 2.8 x SD (or 2.8 x %CV).

The best sources of short-term precision data come from large multicentre studies that have used replicated patient measurements. Vendors frequently cite in vivo
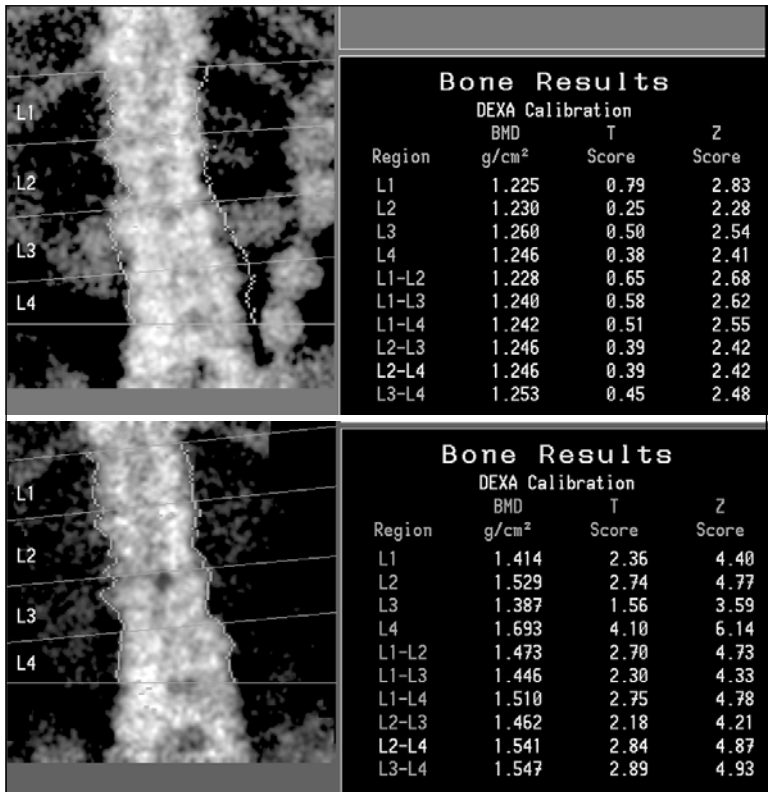
Figure 9. Spine artifact from a barium swallow performed one week earlier. Barium can be seen throughout the colon (upper) and had cleared out after a month (lower). Barium caused bone density to be underestimated (L2-L4 1.246 g/cm² with T-score +0.39) versus the repeat scan (1.541 g/cm² with T-score +2.84).

precision as $\approx 1.0\%$ for modern DEXA instruments. This probably underestimates the error seen in non-research, clinical populations. In routine clinical settings the following reproducibilities (%CV) have been reported: lumbar spine 1.8%, femoral neck 3.5%, total hip 2.5%.

Quality Control

A formal quality assurance program is an essential component of a bone density program. In the case of DEXA, this should minimally consist of a daily calibration check (usually with an anthropomorphic spine phantom) which is compared with predefined tolerance limits. The cumulative data is periodically analyzed to look for subtle changes or drifts in performance signaling the need for corrective action (Fig. 11). Calibration differences between otherwise identical machines are common. Such

	BMD	T-score	Z-score
Femoral Neck	1.314	+2.8	+4.5
Total Hip	1.435	+3.5	+5.1

	BMD	T-score	Z-score
Femoral Neck	0.634	-2.8	-1.1
Total Hip	0.678	-2.7	-1.1
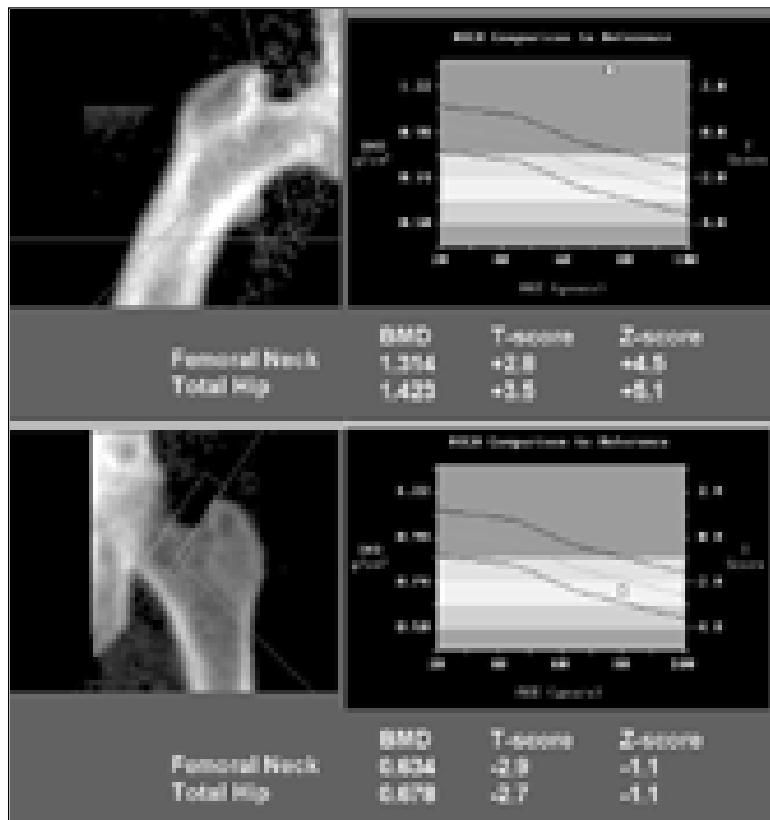
Figure 10. Paget's disease of the right hip. The bone expansion and sclerosis give a bone density measurement of the femoral neck that is well above normal (1.314 g/cm^2 with T-score +2.78) while the left hip is actually in the osteoporotic range (0.634 g/cm^2 with T-score -2.85).

differences are usually small (1-2%) but on occasion can be clinically significant (exceeding instrument reproducibility). Therefore, measurements from different machines are very difficult to compare, and whenever possible follow-up examinations should be performed on the same machine.

Clinical Role of Bone densitometry

T-Score and Z-Score

Absolute measurements of bone density are of little value since they are determined by the site of measurement, calibration used by the equipment manufacturer, and even the particular instrument. Since bone density follows a bell-shaped (Gaussian) distribution, measurements are conventionally described in terms of the number of

Table 2. Interval in years between two bone density measurements required to determine significant bone loss (P<0.05) in an individual patient

		0.5%	1%	2%	3%	5%
		Rate of bone loss (percent/year)				
Coefficient	1.0%	6	3	1.5	1	0.5
of variation	1.5%	8	4	2	1.5	1
(%CV) in	2.0%	11	6	3	2	1
bone density	2.5%	14	7	3.5	2.5	1.5
	3.0%	17	8	4	3	1.5

Table 3. Checklist when performing a bone density comparison

- Verify that the same vendor and instrument are being used.
- Verify that there has been consistent patient positioning.
- Verify that there has not been any dramatic change in the patient's weight.
- Verify that machine quality control is satisfactory (particularly if recent servicing).
- Verify that any change in bone density is reflected in the bone mineral content (BMC) measurement and not simply a change in area (edge-detection).
- Verify that changes are consistent between sites (considering site-responsiveness).
- Verify that changes are consistent with the patient's therapeutic regimen.

standard deviations (SD) that a value deviates from the population mean. Age-related changes in bone density, described earlier, must be taken into account. The *Z-score* refers to the number of SD above or below the mean for an age-matched population. The *T-score* refers to the number of SD above or below the mean for a young adult population. It is not enough for a bone density instrument to provide accurate and reproducible measurements. To interpret a patient value there must be valid normal data from a large reference population that is patient-appropriate (age, gender and ethnicity).

In interpreting an individual patient's test results, the following question is confronted: Should you compare the patient with someone of the same age or with a young adult? The former masks the increasing prevalence of osteoporosis with advancing age, while judging an 80-year-old against the same standard used in a 30-year-old seems unreasonable. In reality, both approaches have merit and are complementary (Fig. 12). An age-adjusted measurement indicates whether the individual is average for their age and, if not, how markedly they deviate from the expected value. On the other hand, bone strength depends upon bone mass and not the age of the subject, therefore predictions in terms of fracture risk are best based upon comparison with an absolute standard (young adult).

Diagnosis of Osteoporosis from Bone Density Measurements

The World Health Organization (WHO) formulated diagnostic ranges for osteoporosis based upon T-score. These ranges were originally intended to be used epidemiologically, but have subsequently been applied to individuals. The data reviewed for these recommendations was almost exclusively derived from post-
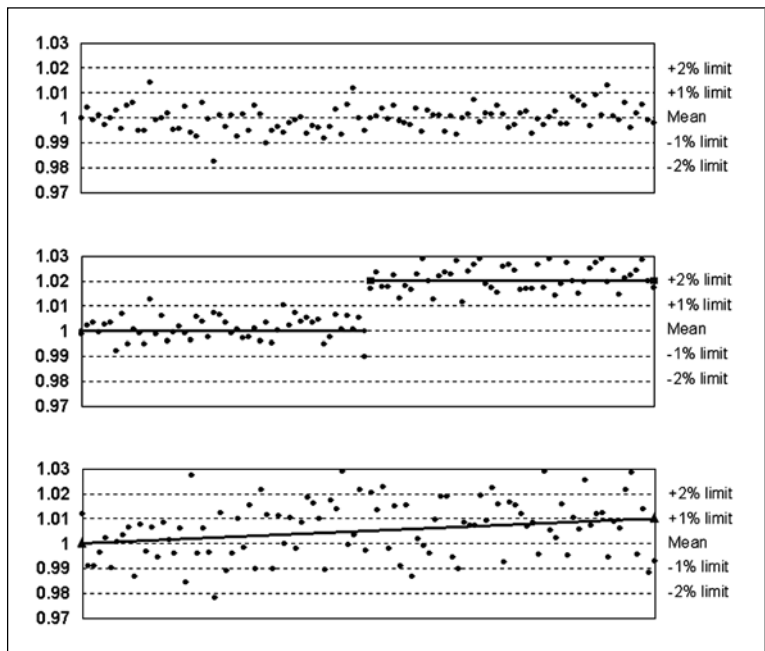
Figure 11. Quality assurance plots from three hypothetical systems with mean 1.000, standard deviation 0.005 (coefficient of variation 0.5%). The top plot indicates a stable machine, the middle plot indicates an abrupt shift in baseline (regression lines plotted to the data prior to and after the shift) and the bottom plot indicates a continuous drift in baseline (regression line plotted to all time points). The latter is particularly insidious and would be difficult to identify by visual inspection of the data alone.

menopausal Caucasian females, therefore caution must be exercised in extrapolating these to other groups (Table 4).

Predicting Fractures from Bone Density Measurements

As already noted, the mechanical strength of excised bone is strongly related to the amount of bone mineral. Many prospective studies have now shown that bone measurements will predict clinical fractures (Fig. 13). Although bone density is *on average* significantly lower in fracture patients than in non-fracture patients, there is considerable overlap between the two groups. Risk of fracture shows a continuous gradient relationship with bone density: there is no "fracture threshold". Results are usually stated in terms of relative risk (RR) of fracture per standard deviation (SD) change in bone density. It appears that any measured site provides fracture risk information about other sites, though the best measure for characterizing hip fracture risk is a measure of the proximal femur (with RR 2.6 per SD change in bone density). It will be recalled that a unit change in SD is the same as a unit change in the Z-score
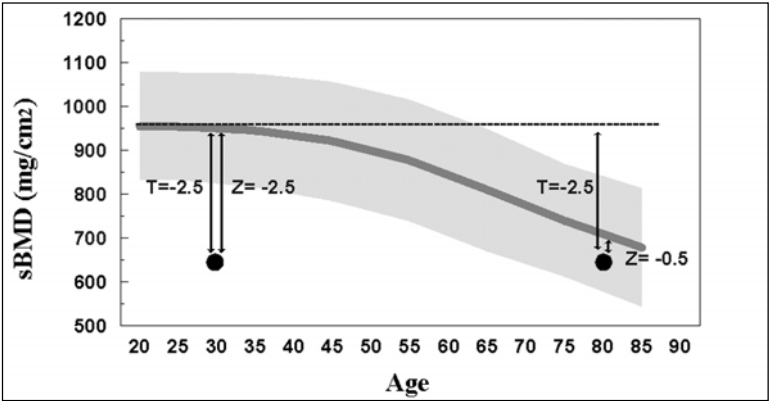
Figure 12. An 80-year-old woman with bone mineral density (BMD) of the hip that is average for her age (648 mg/cm²) will have a Z-score of -0.5 but a T-score of -2.5. A 30-year-old woman with exactly the same bone density measurement would have a T-score and a Z-score that are both -2.5.

(or T-score). The increase in fracture likelihood with decreasing bone density is exponential (not simply additive) (Fig. 14), and is given by the formula:

$$\text{Fracture Risk} = \text{Average Risk} \times RR^{-\text{Z-Score}}$$

An individual's risk of fracture is dependent upon (a) average risk for age, (b) the Z-score of the bone density measurement and (c) relative risk per SD change in bone density. The influence of age on fracture likelihood cannot be overstated as it occurs independent of any age-related decline in bone density as seen in Figure 15. This age-related fracture risk is in part secondary to an increased likelihood of falls in the elderly as well as microarchitectural changes in bone (such as increased bone turnover) that are not directly measurable with bone density.

Different technologies and skeletal sites show markedly different age-related changes in the T-score (Fig. 16). Lumbar spine QCT shows the earliest and most rapid change with the average woman crossing the osteoporotic threshold (T-Score -2.5) by age 61. In contrast, peripheral measurements are much less age-responsive and ultrasound of the calcaneus will not reach the same threshold until after age 100. T-scores cannot be used interchangeably between different sites and techniques.

Clinical Risk Factors to Predict Bone Density

There have been many previous attempts to use clinical risk factors to predict BMD and these have been largely unsatisfactory. The largest experience comes from the Study of Osteoporotic Fractures (SOF) which used a multivariate model based upon over 100 clinical risk factors to predict BMD in 7,963 ambulatory Caucasian women 65 years age or older. The best such model was only capable of predicting 21% of BMD variance, a level that is insufficient for clinical purposes.

Certain medical disorders can be important secondary causes of rapid bone loss (see Section on Clinical Management of Osteoperosis). Among healthy peri- and post-menopausal women is a subset that also loses bone at a rapid rate, appropriately

Table 4. World Health Organization (WHO) recommendations for patient classification based upon bone density T-score alone

Normal	T-score above -1
Osteopenia (low bone density)	T-score between -1 and -2.5
Osteoporosis	T-score below -2.5
Severe Osteoporosis	Fragility fractures and T-score below -2.5

termed "fast losers". Unfortunately, this group has few distinguishing features. There is some evidence that underweight women and those with higher initial bone density are at risk for more rapid bone loss. Such statements are of limited help in an individual patient due to the large degree of overlap.

Clinical Risk Factors to Predict Fractures

It may at first appear paradoxical that clinical risk factors can still be useful in predicting fracture risk given the poor correlation with bone density. Many of the factors important in the pathophysiology of fracture are not measurable with bone densitometry (Fig. 17). Several large studies have identified clinical markers for hip fracture that operate independent of bone density measurement (Table 5). Data from the Study of Osteoporotic Fractures (SOF) indicate that when there are few clinical risk factors, hip fracture rates are very low (1.1-2.6 hip fractures per 1000 women-years) (Fig. 18). In this study, women in the lowest bone density tertile with less than three clinical risk factors had a substantially lower fracture rate than those in the highest bone density tertile with at least five clinical risk factors (2.6 hip fractures per 1000 women-years vs 9.4 hip fractures per 1000 women-years).

The single most powerful predictor of future osteoporotic fracture is the presence of previous such fractures. A single vertebral fracture places that individual at higher risk of fracture than low bone density alone (Fig. 19). The combination of low bone density and previous fracture increases risk 25-fold and the presence of two vertebral fractures increases that risk 75-fold. Loss of height, a marker of asymptomatic vertebral deformities, is also a predictor of hip fractures (RR 1.7 if height loss >3 cm).

Falling is central to the pathophysiology of hip fracture and it is not surprising that studies have found that a history of fall in the preceding 12 months was a powerful (RR 1.6-2.4) predictor of hip fracture. An increased risk of falls is also seen with use of long-acting benzodiazepines and tricyclic antidepressant medications. Smoking has also emerged as an independent predictor of hip fracture (RR 2.0), likely due to direct effects on bone metabolism and indirect effects leading to low body weight and reduced overall health.

Evaluation of these clinical risk factors is valuable in determining the need for therapy.

Following Osteoporosis with Bone densitometry

Follow-up bone mass measurements in patients not receiving active treatment can help in the identification of individuals with rapid bone loss ("fast losers"). Repeat testing may also be useful in confirming a positive treatment response, although some evidence suggests that much of the anti-fracture effect of current antiresorptive therapies is mediated through mechanisms other than increasing bone mass.
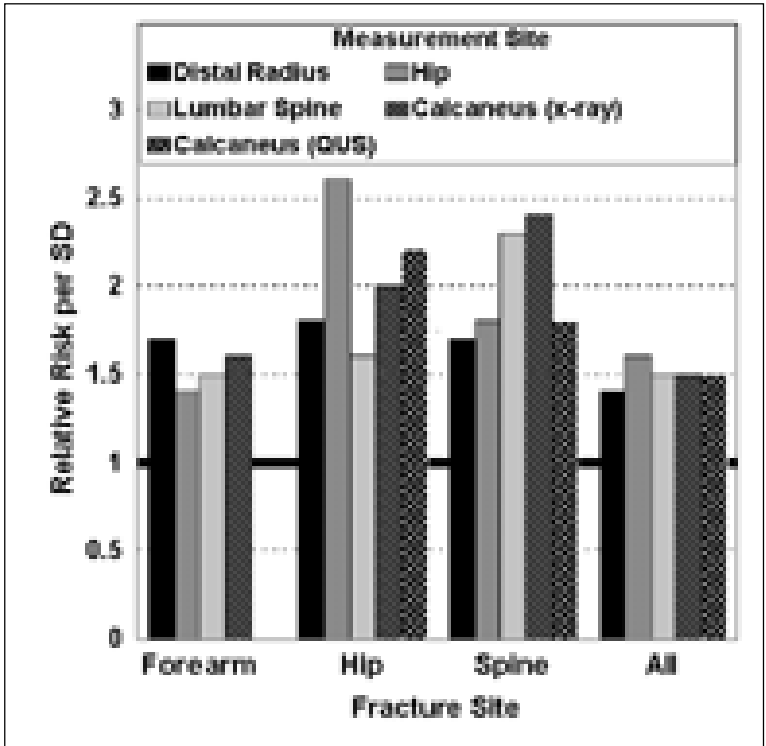
Figure 13. Meta-analysis of fracture prediction using different bne density measurement sites. (Adapted from Marshall D: BMJ 1996; 312:1254-1259)

Patient-related factors also need to be considered in the timing of repeat testing, including the average rate of expected bone loss and the maximum rate of loss that is likely to be encountered. The latter is critical since follow-up bone mass measurements should ideally identify patients who are failing treatment before substantial bone loss develops or fractures occur. Average rates of bone loss are greater in untreated early postmenopausal women (approximately 2% per year) than in older women (less than one percent per year). The site of most rapid bone loss also changes with age. Loss of trabecular bone from the spine exceeds that of the hip in early postmenopausal women. Similarly, increase in skeletal mass from antiresorptive treatment is usually most evident in the spine due to the relatively faster turnover of trabecular bone. For untreated older subjects the decline in the hip generally exceeds that of the spine due to the development of age-related degenerative artifacts in the spine. It should be emphasized that measurement imprecision makes it difficult to accurately assess loss rates in individuals. These have been stated to exceed 5% per year in some cases but the frequency of such rapid loss in the absence of major medical factors (such as high-dose steroid therapy) is unclear. It is likely that active
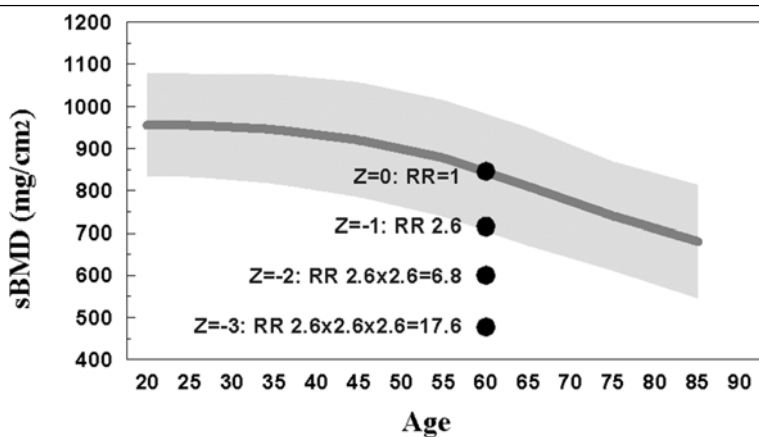
Figure 14. A 70-year-old woman has bone density measurements of the hip with T-score -4.2 and Z-score -3. Relative risk of hip fracture (compared with an average 70-year-old woman) increases with relative risk (RR) of 2.6 for each standard deviation (SD) below average. Therefore, relative risk of hip fracture is increased 18-fold (2.6³), placing the woman at markedly increased risk.

treatment induces a "shift to the right" of the bone loss distribution, decreasing the number of cases in which rapid loss occurs.

The optimal time interval for follow-up measurements is a function of machine precision and the expected rate of bone loss. For example, if a subject loses bone mass at a rate of 1% per year then it would take 3 years for this to exceed (with 95% confidence) the precision limits of a machine with "optimal" performance (CV 1%) and 6 years for a "typical" machine (CV 2%). To aid in ordering a repeat bone mass measurement, the relevant parameters are presented in Table 2 by relating test precision (%CV), maximum expected rate of bone loss (percent per year) and the minimum time interval between tests required to detect a change of this magnitude (with 95% statistical confidence). Thus, to exclude bone loss in the total hip (CV 2.5%) that is three times an average value of one percent, a follow-up interval of 2.5 years is appropriate. Finally, it should be remembered that minimum detectable bone loss is a statistical concept and needs to be distinguished from a clinically significant change in skeletal mass. The latter will be influenced by a history of symptomatic fractures, the severity of osteoporosis and use of active treatment.

Clinical Management of Osteoporosis

General Assessment

Although osteoporosis is most commonly seen in postmenopausal women and the elderly, a number of secondary causes of bone loss should be considered in the evaluation of an individual with low bone mass (Table 1). These factors may exist in isolation, or accelerate bone loss in postmenopausal osteoporosis. The clinical
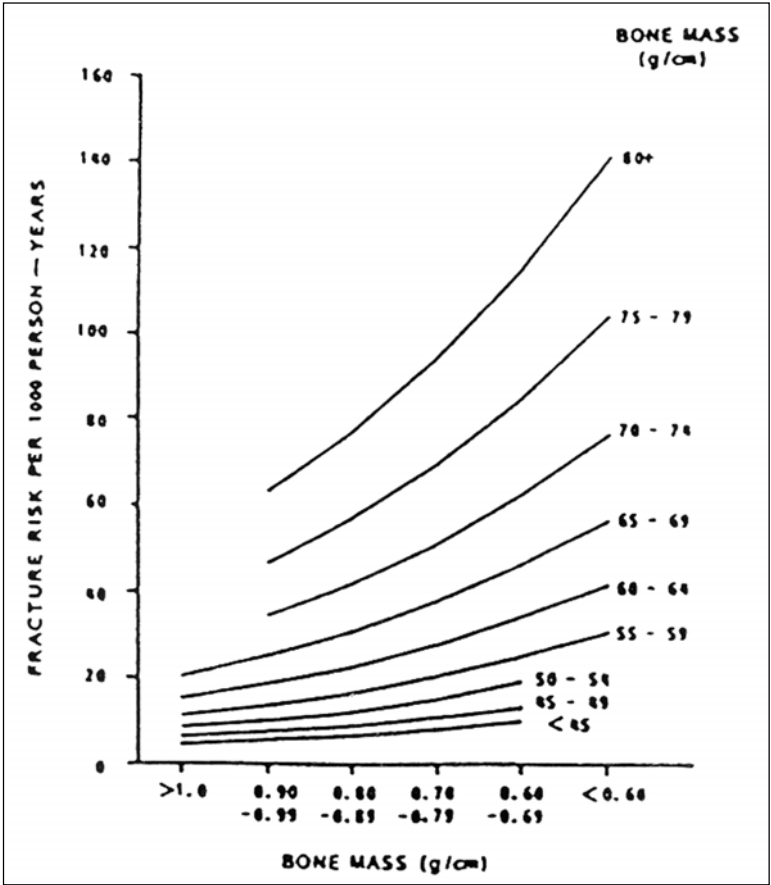
Figure 15. Estimated incidence of fracture as a function of age and bone mass. (From Hui SL et al. J Clin Invest 1988; 81:1804. Reproduced with permission of the American Society for Clinical Investigation, Inc.)

assessment should be directed towards elucidating these potential causes and any fracture history. Assessment of the risk factors for falls given in Table 5 is an important adjunct to measuring bone density. Laboratory testing can be limited to the measurement of serum calcium, alkaline phosphatase, creatinine and a complete blood count. In individuals with postmenopausal or age-related osteoporosis, all of these indices should be within the normal range. These investigations may be further expanded to include serum TSH, parathyroid hormone (PTH), serum 25-hydroxyvitamin D, protein electrophoresis, and 24 hour urinary calcium determination, as guided by clinical judgment. Although not routinely required, lateral x-rays of the thoracolumbar spine help to determine the number and type of

Figure 16. Age-related decline in mean Caucasian female T-scores for different BMD technologies based on manufacturer reference ranges. Total hip values (—◊—) are from the NHANES data implemented by all DEXA manufacturers. Also shown are L1-L4 PA spine (—□—), L2-L4 lateral spine (—◆—), "one-third" forearm (—●—) from the Hologic QDR-4500 DEXA; calcanus ultrasound (—▲—) from the Hologic Sahara, spinal QCT (—° —) from the Image 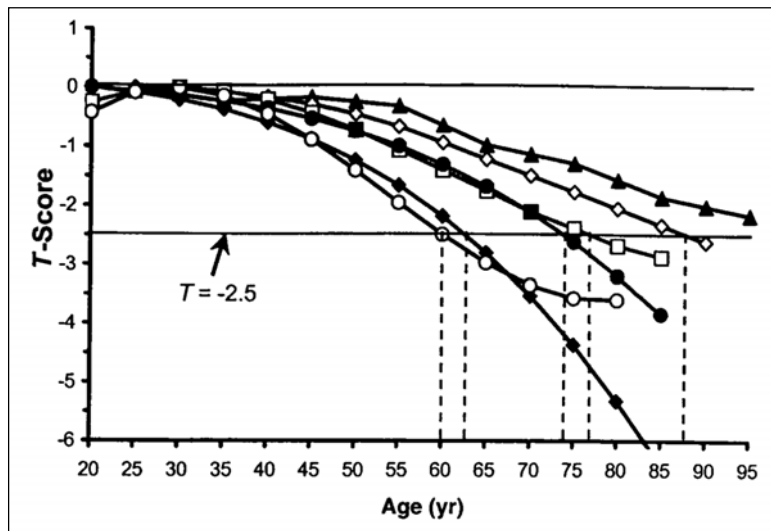Analysis system. (From Faulkner K et al. J Clin Densitometry 1999; 2:343-350. Reproduced with permission from Humana Press Inc.)

pre-existing vertebral fractures, and their presence indicates high risk for further fractures. Biochemical markers of bone metabolism may provide an indirect method to evaluate the rate of bone turnover. Osteocalcin, bone-specific alkaline phosphatase and procollagen I peptide can assess the level of bone formation while urinary excretion of collagen crosslinks (such as deoxypyridinoline and N-telopeptide) reflect the level of bone resorption. These markers have not been useful for diagnosing osteoporosis or for predicting bone loss, but some studies suggest that they independently predict fracture risk.

Non-Pharmacologic Therapy

General measures to reduce the risk of fractures should include assessment of hazards in the home environment, sedative use, muscle weakness, postural hypotension and uncorrected visual deficits. Exercise should also be encouraged in an attempt to preserve bone mass and to maintain or improve muscular conditioning.

Calcium supplementation is often necessary in postmenopausal and elderly women to reach recommended targets (1,200-1,500 mg per day). Calcium carbonate is the most commonly used supplement and is recommended for those who do not have achlorhydria (common in the very elderly and those on acid suppressing
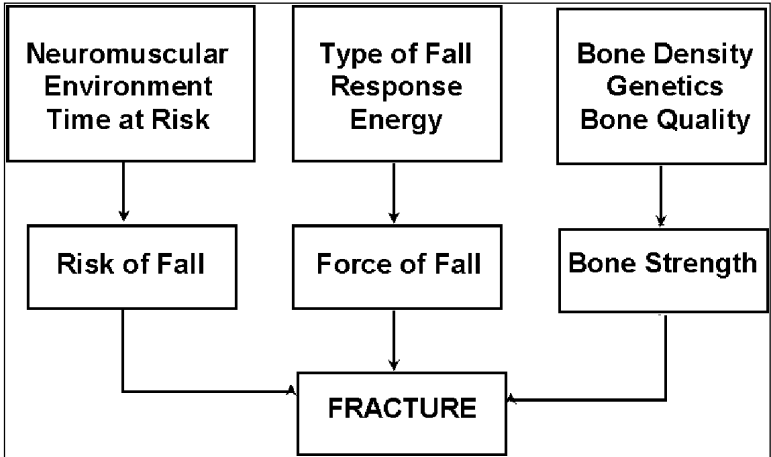
Figure 17. Factors leading to fracture.

medication). Vitamin D supplementation of 400-800 units daily is also advisable, even in those on antiresorptive therapy. The importance of calcium and vitamin D supplementation is even greater in the elderly as calcium absorption is impaired and sunlight exposure is reduced, especially in winter months.

Pharmacologic Therapy

There are expanding options for osteoporosis therapy in recent years. Estrogen replacement has been joined (but not replaced) by bisphosphonates, intranasal calcitonin and selective estrogen receptor modulators (SERMs). These agents, which are active for both the prevention and treatment of osteoporosis, act primarily through inhibition of osteoclast number and activity. They differ more in their associated risks and benefits than in their skeletal effects.

Estrogen

Hormone replacement therapy (HRT) is effective at preventing bone loss in postmenopausal women and is associated with a bone density increase of 4-6% in the first 2 years of therapy. In epidemiological studies HRT has been associated with a 50% reduction in fracture risk, but protection is lost with cessation of therapy. HRT is also associated with a 30% increase in the risk of breast cancer, increased risk for thromboembolism and must be taken with a progestin if the patient has not had a hysterectomy to avoid endometrial hyperplasia/carcinoma. The associated bleeding is unacceptable for some women, especially in older age groups. HRT is associated with a reduced incidence of cardiovascular events in cohort studies, but an increased early event rate seen with a secondary prevention trial underscores the need for data from prospective controlled trials of primary prevention such as the ongoing Women's Health Initiative.

Table 5. Risk factors for fracture with and without adjustment for history of previous fracture and calcaneal bone density. (Adapted from Cummings SR et al. N Eng J Med 1995; 332:767-773.)

Risk factor	Relative Risk (95% confidence interval) Base Model	Adjusted for fracture history and bone density
Age (per 5 years)	1.5 (1.3-1.7)	1.4 (1.2-1.6)
Maternal hip fracture	2.0 (1.4-2.9)	1.8 (1.2-2.7)
Weight increase since age 25 (per 20%)	0.6 (0.5-0.7)	0.8 (0.6-0.9)
Height at age 25 (per 6 cm)	1.2 (1,1-1.4)	1.3 (1.1-1.5)
Self-rated health (per 1-point decrease)	1.7 (1.3-2.2)	1.6 (1.2-2.1)
Previous hyperthyroidism	1.8 (1.2-2.6)	1.7 (1.2-2.5)
Current use of long-acting benzodiazepines	1.6 (1.1-2.4)	1.6 (1.1-2.4)
Current use of anticonvulsants	2.8 (1.2-6.3)	2.0 (0.8-4.9)
Current caffeine intake (per 190 mg/day)	1.3 (1.0-1.5)	1.2 (1.0-1.5)
Walking for exercise	0.7 (0.5-0.9)	0.7 (0.5-1.0)
On feet less than 4 h per day	1.7 (1.2-2.4)	1.7 (1.2-2.4)
Inability to rise from chair without using arms	2.1 (1.3-3.2)	1.7 (1.1-2.7)
Lowest quartile for visual depth perception	1.5 (1.1-2.0)	1.4 (1.0-1.5)
Lowest quartile for visual low-frequency contrast sensitivity	1.2 (1.0-1.5)	1.2 (1.0-1.5)
Resting pulse rate over 80 per min	1.8 (1.3-2.5)	1.7 (1.2-2.4)
Any fracture since age 50	-	1.5 (1.1-2.0)
Calcaneal bone density (per SD decrease)	-	1.6 (1.3-1.9)

6

SERMs

New agents have been developed that retain estrogen's positive effects on bone, while attempting to minimize the associated risks and side effects. This class of drugs is termed Selective estrogen receptor modulators (SERMs) and include raloxifene and tamoxifen. Raloxifene reduces the risk of vertebral fractures by approximately 40%, and produces increases in bone density of approximately 3% at the spine in its first three years. It also lowers total and LDL cholesterol, does not stimulate the endometrium, and probably reduces the risk of breast cancer.

Calcitonin

Salmon calcitonin has been used subcutaneously for many years. The recently released intranasal form is more acceptable for longterm use. Despite modest effects on bone density, vertebral fracture risk is reduced by approximately 40%. Intranasal calcitonin is well-tolerated and has minimal side-effects.
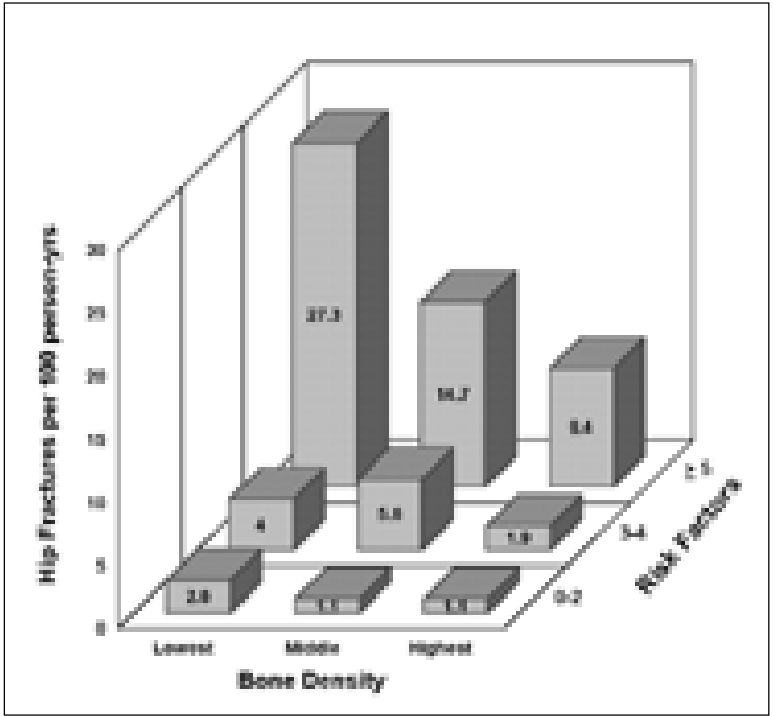
Figure 18. Independent interaction between clinical risk factors and bone mineral density. Risk factors were: age over 80, maternal history of hip fracture, any fracture since age 50, reduced self-rated health (fair or worse), previous hyperthyroidism, anticonvulsant therapy, current use of long-acting benzodiazepines, current weight less than at age 25, height at age 25 over 168 cm, caffeine intake more than the equivalent of two cups of coffee per day, on feet less than four hours per day, no walking for exercise, inability to rise from a chair without using arms, lowest quartile for visual depth perception, lowest quartile for visual contrast sensitivity, resting pulse rate greater than 80 beats per minute. (Adapted from Cummings SR et al. N Eng J Med 1995; 332:767-773.)

Bisphosphonates

This class of drugs inhibit osteoclast number and activity and have few extra-skeletal effects. Etidronate was the first available compound. It has low potency and inhibits bone mineralization when used continuously (though this is not seen with intermittent regimens). Alendronate is a potent aminobisphosphonate that is capable of increasing bone density at the lumbar spine by 8% over 3 years. More importantly, it has been proven to reduce hip and spine fractures by 50% in postmenopausal women with previous fractures. The main risk is erosive esophagitis, especially in patients with prior esophageal disease, gastroesophageal reflux or when directions are not carefully followed. Risedronate has also been demonstrated to produce similar
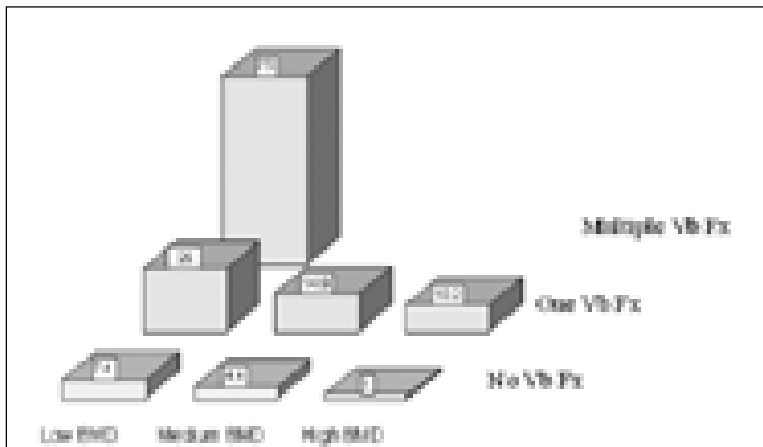
Figure 19. Risk for incident vertebral fractures (Vb Fx) based on current vertebral fracture status. (Adapted from Ross PD et al. Ann Intern Med 1991; 114:919.)

increases in bone density in postmenopausal osteoporosis and similar reductions in the incidence of vertebral and hip fractures.

Anabolic Agents

Strategies which directly stimulate osteoblast activity have the potential to produce larger increases in bone density and potentially larger effects on fracture prevention. One such strategy is the use of intermittent parathyroid hormone therapy which has been demonstrated to produce large increases in bone mineral density in various populations, and to reduce vertebral fractures by approximately 65% in postmenopausal women with previous fractures.

Who to treat?

General recommendations that apply to the entire population include ensuring adequate calcium and vitamin D intake, engaging in regular weight-bearing exercise, avoidance of smoking and limitation of alcohol use. Although whole population testing is not advocated, the National Osteoporosis Foundation (NOF) has defined guidelines for targeted screening(Fig. 20). In addition, the NOF has identified four clinical risk factors as being sufficiently common and predictive of osteoporosis in postmenopausal women to be useful in the clinical setting for guiding decisions on whether to recommend bone densitometry: (1) history of fracture after age 40; (2) history of hip, wrist or vertebral fracture in a first-degree relative; (3) being in the lowest quartile for body weight (less than 57.8 kg); and (4) current cigarette smoking.

The NOF established therapeutic cutpoints for antiresorptive therapy. According to these guidelines, therapy to reduce the risk of fracture should be initiated in the following groups: women with a T-score below -2; or women with a T-score -1.5 if any of the four risk factors given above are present. In addition, women over age 70
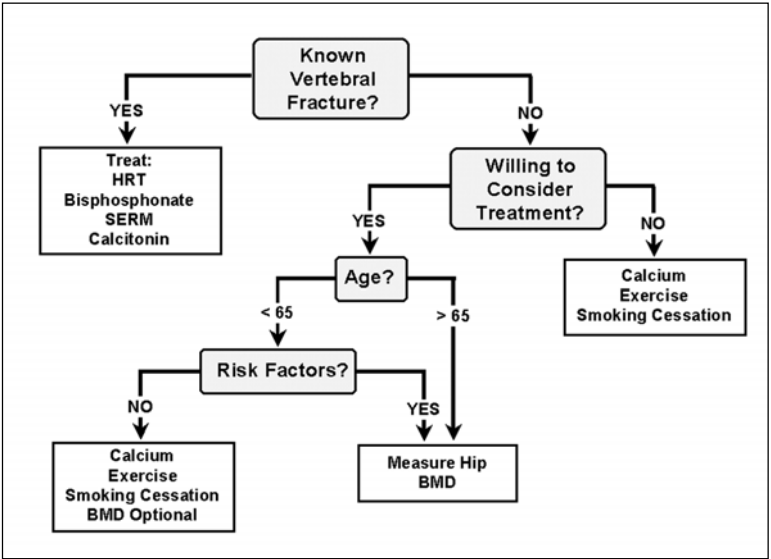
Figure 20. Guidelines for the targeted screening and treatment of osteoporosis. Major risk factors include (1) history of fracture over age 40; (2) history of hip, wrist or vertebral fracture in a first-degree relative; (3) being in the lowest quartile for body weight (less than 57.8 kg); and (4) current cigarette smoking. (Adapted from the National Osteoporosis Foundation's "Physician's Guide to Osteoporosis Prevention and Treatment".)

with multiple risk factors or previous vertebral fracture should receive therapy. The NOF cutpoints have not been universally accepted and do not take into account the low absolute risk of fracture of younger women who may have osteopenia. In these individuals, strategies to prevent bone loss should still be considered, such as HRT, low-dose bisphosphonates or raloxifene. Decisions to start therapy must clearly take into account the reversible and irreversible risk factors for fracture already described.

Frequently Asked Questions (FAQs)

Why don't all bone density instruments give the same readings?

Although DEXA instruments are ultimately calibrated against excised bone samples, methodologic differences in how this is performed have led to large discrepancies in patient measurements when performed on instruments from different vendors. Efforts to reconcile these differences have led to a consensus on converting DEXA measurements to standardized bone mineral density (sBMD). sBMD is expressed in mg/cm² to distinguish it from nonstandardized BMD which are in g/

cm². Use of sBMD should ensure that average patient values are similar on different instruments, but other methodologic differences exist and it should not be assumed that patient sBMD values will be identical on all instruments. Due to these limitations with current approaches to machine cross-calibration, small changes in bone density may not be appreciated. Therefore it is strongly recommended that follow-up measurements use the same instrument and scanning procedure.

Is it unusual to have a significant difference between a BMD measurement of the spine and hip? Which is a more reliable indicator of osteoporosis?"

Apparent discrepancies between hip and spine BMD measurements are common and emphasize the complexity of skeletal metabolism. As a "systemic skeletal disorder", osteoporosis affects all bones but the degree is modified by local determinants of bone metabolism which include bone composition (trabecular bone undergoes more rapid turnover and loss), mechanical loading (weight bearing enhances osteoblast activity) and age-related artifacts (usually elevate spine BMD). Accuracy errors for BMD measurements of the spine and hip are on the order of 5-7%. Together these factors help to explain why differences between spine and hip BMD measurements are so common.

The original World Health Organization (WHO) definition of osteoporosis based on BMD (more than 2.5 standard deviations below young adult mean value) does not specify a particular site. Although there is a tendency to use the lowest T-score in classifying a patient, fracture rates are known to increase in proportion to the number of osteoporotic sites. Therefore, all sites probably contribute independently to the global fracture risk. When it comes to assessing the risk of specific fractures, particularly hip fractures, a direct measurement of that site is preferred. The cost and morbidity of hip fractures coupled with the strength of their association with BMD has led to a recent proposal that the diagnosis of osteoporosis be reserved for BMD measurements of the hip. This does not negate the important fracture prediction information that can be obtained from other validated techniques and sites.

When evaluating fracture risk, it is the whole picture that counts rather than any single measurement viewed in isolation. An accurate assessment needs to consider information taken from both hip and spine, in addition to weighing non-BMD predictors of fracture such as age and falls.

How do you diagnose osteoporosis in groups other than postmenopausal Caucasian females?

The occurrence of fragility fractures, such as minimal trauma vertebral compression fractures, is sufficient for a diagnosis of osteoporosis in any group providing that other pathologic causes (such as tumour) have been excluded. The criteria for diagnosing osteoporosis from bone density alone are more controversial and caution is recommended before extrapolating the WHO recommendations. For example, men have higher average bone density than women but also have a lower fracture rate. The absolute likelihood of fracture in men seems to show the same relationship to absolute bone density as in women. This has led to uncertainty over whether the osteoporosis threshold in men should be based upon a male or female reference group. Similar concerns arise over comparison to non-Caucasian
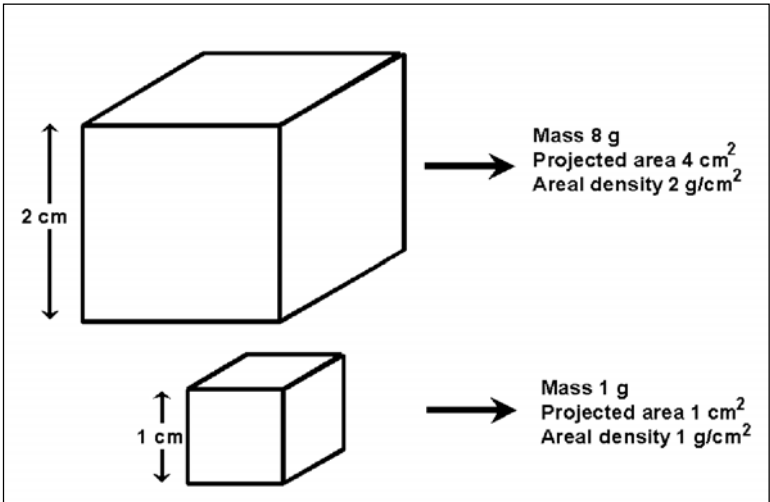
Figure 21. Bone volume strongly affects measured bone density using areal techniques such as dual energy x-ray absorptiometry (DEXA). Assume that two cubes are constructed from hydroxyapatite (1 gram/cm³). The larger cube will have twice the areal density of the smaller cube due to its greater depth since this is not measured in DEXA.

groups. Black subjects have significantly higher bone density and lower fracture rates than Caucasians, suggesting a similar relationship between absolute bone density and absolute fracture risk. In contrast, orientals have lower hip bone density than Caucasians but paradoxically have a much lower fracture likelihood. The reasons for this are still debated but probably include shorter stature, likelihood of falling, and possibly shorter femoral neck (also referred to as hip axis length). Normal children represent a dramatic example of where low bone density has a surprisingly low rate of fracture when one considers the frequency with which children are involved in falls and other trauma. It is inappropriate to generate T-scores or apply WHO diagnostic criteria to children since they have not yet achieved peak bone mass.

Many of the difficulties related to gender, ethnicity and children probably relate to the effect of bone size on areal bone density measurements. Since most bone density techniques give an areal measurement based upon a two-dimensional projection of bone (in grams/cm²), larger bones will have a higher apparent bone density than smaller bones due to the increased depth (Fig. 21). Although some techniques have been developed to try to address this (such as calculations of skeletal volume based upon modeling of the spine and femoral neck), only quantitative CT (QCT) provides a true volumetric measurement.

Additional Reading

1. Blake GM, Wahner HW, Fogelman I. The Evaluation of Osteoporosis: Dual Energy X-ray Absorptiometry and Ultrasound in Clinical Practice. London: Martin Dunitz Ltd, 1999.
    A detailed reference on the technology and clinical applications of bone density and ultrasound.

2. Cummings SR, Nevitt MC, Browner WS, Stone K, Fox KM, Ensrud KE et al. Risk factors for hip fracture in white women. New Engl J Med 1995; 332:767-773.
    A true "classic" that describes the contribution of non-densitometric clinical risk factors to hip fracture prediction in postmenopausal women.

3. Kanis JA. Glüer CC. The Committee of Scientific Advisors, International Osteoporosis Foundation. An update on the diagnosis and assessment of osteoporosis with densitometry. Osteoporos Int 2000; 11:192-202.
    A recent review of diagnostic criteria for osteoporosis from bone density measurements with recommendations for change.

4. Kong YY, Penninger JM. Molecular control of bone remodeling and osteoporosis.Exp Gerontol. 2000; 35(8):947-956.
    A review of exciting new developments in the regulation of bone metabolism through the osteoprotegerin system.

5. Marshall D, Johnell O, Wedel H. Meta-analysis of how well measures of bone mineral density predict occurrence of osteoporotic fractures. BMJ 1996; 312:1254-1259.
    A critical assessment of bone measurements and their ability to predict fractures.

6. National Osteoporosis Foundation. Physician's Guide to Prevention and Treatment of Osteoporosis.
    This clinical guideline is based upon a detailed report (Osteoporos Int 1998;8 Supplement 4) describing the evidence for the diagnosis, prevention, and treatment of osteoporosis in postmenopausal healthy white women. The guideline can be viewed on-line at www.nof.org/for_professionals/clinical/clinical.htm.

Skeletal Disorders

Leonard Rosenthall and Peter MacDonald

Introduction

The course of treatment for bone pain and skeletal abnormalities is effected by an accurate diagnosis of the problem. Nuclear medicine has a role to play in both the investigation of the problem and, in some cases, the treatment of bone and joint disorders.

Skeletal Anatomy and Physiology

In the long bones of adults, blood primarily enters the diaphyseal cortex by flowing outwards from the medulla rather than inwards from periosteal vessels. The nutrient artery divides in the medullary cavity and anastomoses with the epiphyseal and metaphyseal arteries which are direct branches of the regional systemic vessels and enter through the numerous foramina penetrating the bones near their ends. Blood flow from the epiphyseal and metaphyseal arteries is quantitatively greater than that of the nutrient artery supply to the diaphysis. Periosteal arteries are part of the network supplying the surrounding muscles. About two-thirds to three-fourths of the inner cortex is sustained by the medullary arterial network. An obstructed nutrient artery can result in a compensatory increase in centripetal periosteal flow to support the full thickness of the cortex through interconnecting channels. Flat bones, such as the cranium, and non-articular segments of short bones are supplied by numerous periosteal vessels which nourish the cortex, cancellous bone and medulla.

The three main cells in bone are osteoclasts, osteoblasts and osteocytes. Osteoblasts evolve from bone marrow-derived, pluripotent, stromal stem cells. Their role is to form and mineralize bone matrix, and to synthesize skeletal growth factors. The ultimate fate of the osteoblasts has not been clearly defined. Some are buried within the bone matrix as osteocytes, while others become lining cells which cover quiescent bone surfaces. Osteocytes are connected to each other and the lining cells through a canalicular network that contains the bone's extracellular fluid. They are believed to release chemical messengers in response to physical strains in order to initiate the appropriate modelling or remodelling response to mechanical stimuli. Osteoclasts are derived from the hematopoietic precursors of the monocyte-macrophage lineage and function in the bone resorption process. They are formed by the fusion of mononuclear cells and are characterized as large multinucleated cells with a ruffled border.

Technical Considerations

Radiopharmaceuticals

Bone imaging is achieved with ^{99m}Tc-labelled phosphate and diphosphonate complexes (collectively referred to as radiophosphate). The most commonly used

agent is ^{99m}Tc-labelled methylene diphosphonate (MDP). Uptake in bone is dependent on blood flow and extraction efficiency. As the vascularity increases, it is associated with an increase of the bone-seeking tracer in the extracellular fluid, which accumulates by passive diffusion. Tracer is then selectively concentrated by the reactive bone. The relationship between blood flow and tracer uptake is not linear. A point is reached when the uptake remains constant despite blood flow increase, indicating a diffusion-limited process.

The site of deposition of the radiophosphate complex has been fairly well established. Evidence from *in vivo* microautography indicates that ^{99m}Tc-phosphate is adsorbed preferentially onto the mineral phase of forming bone, and that this adsorption occurrs preferentially onto amorphous calcium phosphate before it matures into hydroxyapatite crystal. It has also been shown by chemical separation of mineral and matrix in a rat bone repair model that with the intravenous delivery of a double label, ^{99m}Tc-MD-^{32}P, there was preferential binding of ^{99m}Tc to the organic matrix while MD-^{32}P bound to the mineral phase. The deduction from these observations was that ^{99m}Tc-MDP is taken up by bone and then dissociates, allowing ^{99m}Tc to concentrate in newly formed matrix whereas the MDP moiety remains attached to the mineral phase. The preceding explains why uptake of bone tracer correlates with osteoblastic activity, since these areas are rich in unmineralized osteoid matrix and immature calcium phosphate.

Imaging Procedure

For imaging with ^{99m}Tc-MDP, a dose of about 740 MBq (20 mCi) is administered intravenously. Static scintigraphy is performed about 2-3 hours later, a time when normal urinary excretion has lowered the soft tissue background to acceptable levels. The procedure is modified for three-phase bone imaging i.e., sequential nuclear blood flow, blood pool and delayed static images. With the gamma camera head positioned over the area of interest, the radiotracer is injected as a bolus and immediately thereafter serial 3- or 5-second images are obtained for about 60 seconds to complete the blood flow phase. Within 5 minutes of the blood flow study a static blood pool image is taken. Three hours later, whole body or spot images, or both are obtained (Fig. 1).

In cellulitis, diffuse increased uptake occurs in the blood flow and blood pool phases, while it is normal or diffuse, but less intense because of a regional hyperemia, in the delayed phase. Acute osteomyelitis, for example, is characterized by a focal increased concentration in all three phases.

Trauma

Bone trauma can present as frank fractures, which are obvious by radiography, or occult fractures wherein plain radiography is not diagnostic. Fatigue (stress) fractures occur in normal bone, while insufficiency (fragility) fractures (Fig. 2) occur with osteoporosis. Other causes of bone injury are growth plate injuries, avulsion fractures, dislocations, shin splints, bone bruising and enthesopathy (where tendon attaches to bone).

The healing process in most fractures is triggered within hours of the insult. A procallus forms and at 24 hours buds of granulation tissue have already penetrated the hematoma at the fracture site. This leads to eventual lysis of the hematoma and
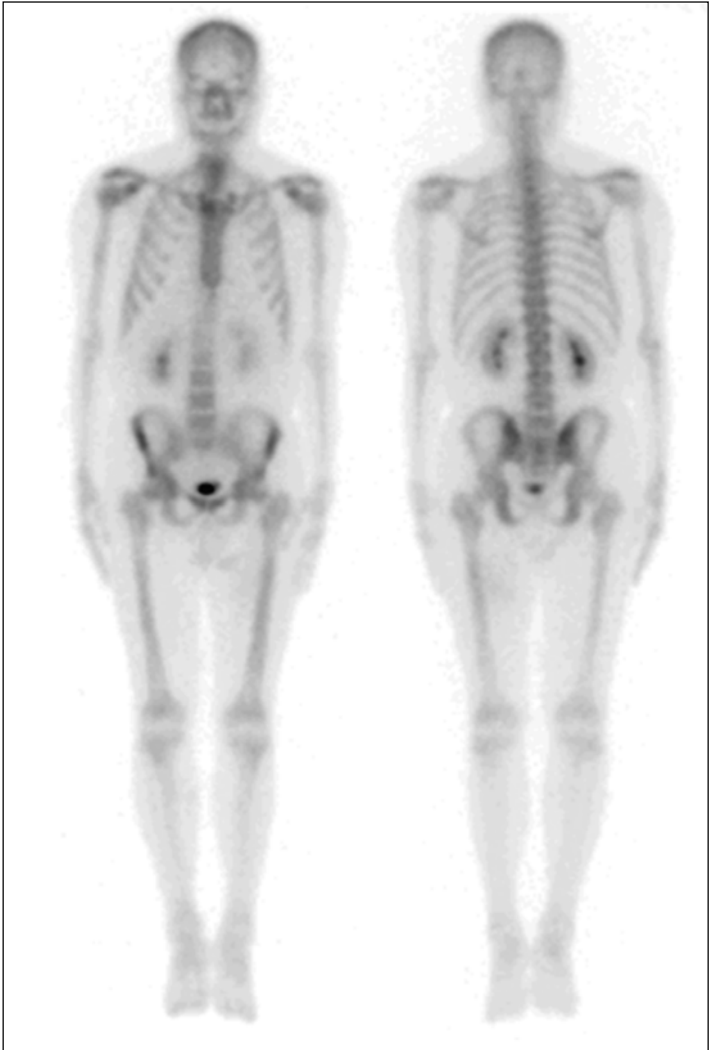
Figure 1. Normal whole body bone scan in the anterior (left) and posterior (right) projections. (Case provided by Dr. W.D. Leslie.)

replacement by dense fibrous tissue, some of which differentiates to form a connecting span of fibrocartilaginous callus to immobilize the fragments. At the end of the first week, as the resorption of hematoma and dead tissue is being completed, cartilage and endochondral bone formation takes place in the fracture gap, while the cellular and exudative inflammatory response subsides. Repair through ossification

Figure 2. Fractures through the sacrum and both sacroiliac joint regions in an 82 year old osteoporotic women who fell from a standing position. The configuration of the breaks is referred to as an "H" fracture.

simultaneously proceeds from the bony fracture surface, originating in the layers of viable endosteum and periosteum. The new bone migrates centrally from both ends and reinforces the ongoing ossification in the gap. The two processes form a solid bony bridge, and when it is completed the fracture is considered clinically healed. In the final phase of healing remodelling occurs as the woven bone of the callus is converted to more adult lamellar bone, the external callus is smoothed by osteoclasts and the medullary canal is reconstituted. Autoradiographic studies demonstrate that

Table 1. Stages of fracture healing

	Stage (duration)		
Findings on three-phase bone scan	Inflammatory (3 to 4 weeks)	Reparative (8 to 12 weeks)	Remodeling (variable)
Arterial flow phase	+	-	-
Blood pool phase	+	+	-
Delayed static phase	broad and diffuse area of hyperconcentration	focal and intense uptake at the fracture line	diminishing uptake with time as healing progresses

radiophosphate will deposit in the areas of new bone formation, with maximal uptake where this process is predominant.

Three stages have been attributed to normal fracture healing (Table 1). During the first 3 to 4 weeks after the break the site of trauma on the bone scan is characterized by a relatively broad and diffuse area of hyperconcentration. In the subsequent phase of 8 to 12 weeks duration the abnormal activity becomes more focal and intense about the fracture line as mineralization of the osseous defects takes place. Thereafter, the fracture exhibits a diminishing uptake with time as healing progresses. In the three-phase radiophosphate study, the angiographic first phase is positive for about the initial 3 weeks following the injury, whereas the blood pool phase can be positive up to 10 weeks.

Radiophosphate imaging can disclose the presence of a fracture within 24 hours of the injury in 95% of patients under the age of 65 years, but there may be a delay in the elderly and debilitated patient. It is recommended that patients over 75 years of age who have severe pain, but negative radiography and normal radiophosphate imaging soon after injury, should have the bone scan repeated 72 hours later. CT scan or plane tomograms may also aid in the diagnosis. The patient should be treated as a hip fracture and kept non-weight bearing or on a bed-to-chair restriction during this time. The negative predictive value for elderly patients suspected of hip fracture who are imaged 72 hours after an earlier negative scan varies between 96% and 99% (Fig. 3). The site of fracture is also a determinant of the degree of radiophosphate accumulation. Those close to joints show the highest rate of uptake, whereas the spine, pelvis and mid-shaft of the long bones have slower rates of uptake. This is probably related to the regional blood flow.

About 90% of closed fractures that do not require surgical reduction will portray normal radiophosphate uptake between 6 months and 2 years after injury. Intense focal accumulation may persist longer in geriatric patients and in the presence of compound and comminuted fractures. Orthopedic appliances can cause persistent increased uptake, but it is usually low grade in the absence of infection or hardware loosening. Persistent hardware uptake may be more common when plates and screws are used versus an intramedullary rod system (the latter is load sharing versus the former which is load bearing). Mechanical stresses at points of malalignment and
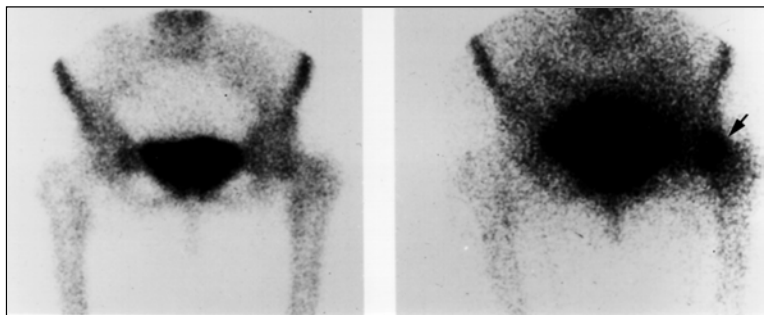
Figure 3. Left femoral neck fracture in a 92 year old woman who fell from a standing position. (*Left*): In the bone scan 1 day after the injury there was a moderately diffuse increased uptake in the hip region which could be attributed to regional hyperemia. (R*ight*): At day 4 there was definite evidence of a fracture (arrow).

angulation in weight bearing bones is another cause of prolonged enhanced radiophosphate uptake. Less than 50% of the latter group will return to complete quiescence within 3 years.

The bone scan can be helpful in dating vertebral fractures seen on the radiograph. Old compression fractures are inactive by radiophosphate imaging, except when complicated by degenerative disease, infection and tumor. Enhanced uptake in a collapsed centrum suggests an injury of at most 2 years duration, but if the uptake is intense the fracture probably occurred within a year.

Radiophosphate planar and SPECT imaging of the knee for the assessment of meniscal and cruciate tears has received considerable attention, but where MRI facilities exist there is little need for it today. Planar imaging can present a confusing picture in the acute phase of internal knee injuries, because the major site of injury is often hidden by diffuse uptake due to synovitis and generalized hyperemic reaction to the hemarthrosis, trauma and stress reactions at musculo-ligamentous insertions. SPECT imaging is able to unravel and define the various contributions to total uptake, and thereby enhance the diagnostic yield. For injury to the meniscus, SPECT sensitivity and specificity are reported to be 88% and 87%, respectively (Fig. 4). Focal accumulation of radiophosphate at the medial femoral condyle peripherally signals an avulsion of the medial collateral ligament, and pure anterior and posterior cruciate ligament tears depict foci on the anterior and posterior tibial joint surface, respectively. Cruciate tears may also be accompanied by focal intercondylar uptake.

Stress fractures

Repetitive episodes of inordinate minor stress in individuals engaged in unaccustomed exercise induce an accelerated remodelling phase in the bones affected by this strenuous activity. Bone remodelling consists of osteoclastic resorption which reaches a peak bone loss at about 3 weeks. This is followed by a slower osteoblastic filling of the osteoclastic cavities, reaching completion in about 90 days. As a consequence there is an interval of imbalance when the bone is weakened and
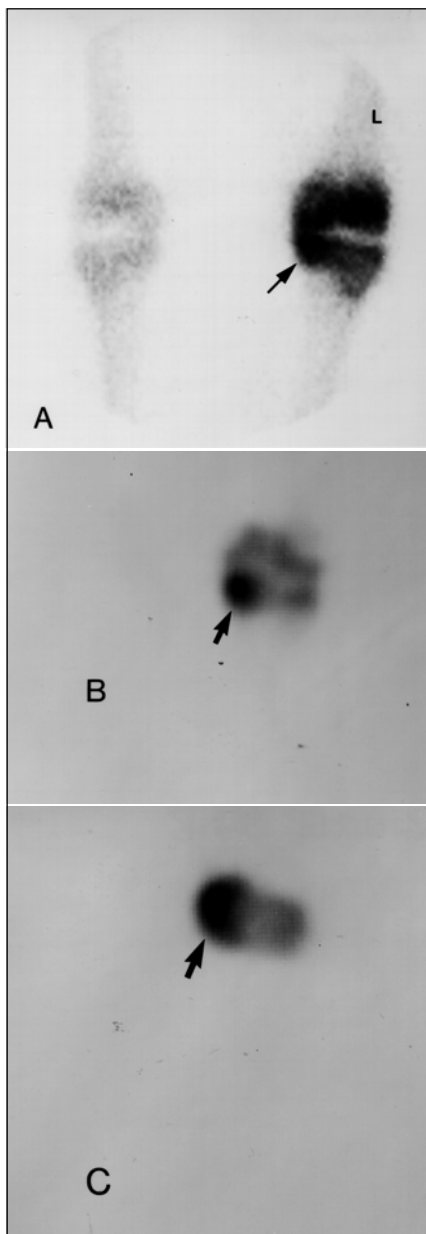
Figure 4. Left knee meniscal tear. (A): Anterior planar images of the knees exhibit a marked increase of radiophosphate uptake in the periarticular bone of the left knee. Arrow points to a subtle higher uptake in the medial tibial plateau. (B): Coronal SPECT clearly identifies this focal lesion (arrow). (C): There is increased uptake along the entire surface of the medial tibial plateau on the transverse SPECT image, consistent with a meniscal tear.

susceptible to microfracture. Periosteal and endosteal proliferation produce new bone in an attempt to buttress the structure. If the stressful activity is continued then a gross fracture may develop. Joggers, long-distance runners, ballet dancers, infantry recruits and weight lifters are candidates for this occult trauma. The radiophosphate portrayal at the onset of stress changes is that of a regional diffuse nondescript distribution. This represents the stage of resorption and remodelling and may be accompanied by pain if microfractures are present. The later stage of gross fracture, either incomplete or partial, is identified by an intense focal fusiform concentration. With curtailment of stressful activity the process subsides to normal. The radiographic signs indicating a stress fracture are periosteal reaction, endosteal thickening, a lucent transverse defect and linear sclerosis, but these are usually manifest after the radiophosphate images become positive. With early rest the radiograph may never become positive. Usually a negative scan in the presence of pain excludes the possibility of a stress fracture. Asymptomatic sites may be disclosed when imaging a symptomatic focus.

Shin splints

Shin splints are a common athletic disorder resulting from repetitive unaccustomed activity characterized by posteromedial tibial pain and tenderness. A periostitis develops near the origin of the flexor digitorum longus or soleus muscles, or both. The radiophosphate image exhibits a linear increase in uptake in the posteromedial cortex of the tibia, in contrast to the well defined fusiform uptake of a stress fracture (Fig. 5). The differential diagnosis includes exertional compartment syndrome, true stress fracture or tibialis posterior tendonitis. The manifestations of shin splints are similar to a number of other conditions due to injuries of muscle, tendon and ligamentous insertions to bone that can provoke a periostitis reaction on the scan. These include osteitis pubis, muscle insertion in the femur, trochanteric bursitis, achilles tendonitis, plantar fasciitis, patellar tendonitis and inflammation of the sesamoid bones.

Delayed and Nonunion

The time required for fracture healing varies according to the bone involved, the type of fracture, and the age of the patient. For example, a pediatric tibial fracture should heal within 4 to 6 weeks whereas an adult closed tibial fracture should heal within 16 weeks. A compound adult tibial fracture may take as long as 24 weeks to heal. Delayed union is an arbitrary term best applied to fractures that eventually heal, though at a slower pace than expected. Failure of solid fracture healing is called nonunion, and this is suspected clinically if motion between the fragments can still be elicited after the usual healing time for that particular fracture, or if serial radiography fails to display progressive healing. Interposition of soft tissue, infection and ischemic bone are local factors predisposing to delayed and nonunion, as well as systemic disorders such a osteomalacia and hyperparathyroidism. Routine static radiophosphate bone images have generally not been useful in distinguishing delayed from reactive nonunion, because both exhibit focal uptake at the fracture site. Atrophic nonunion is characterized by a failure of increased uptake of the scanning agent at the fracture ends and a photon deficiency representing the fracture gap. This lack of
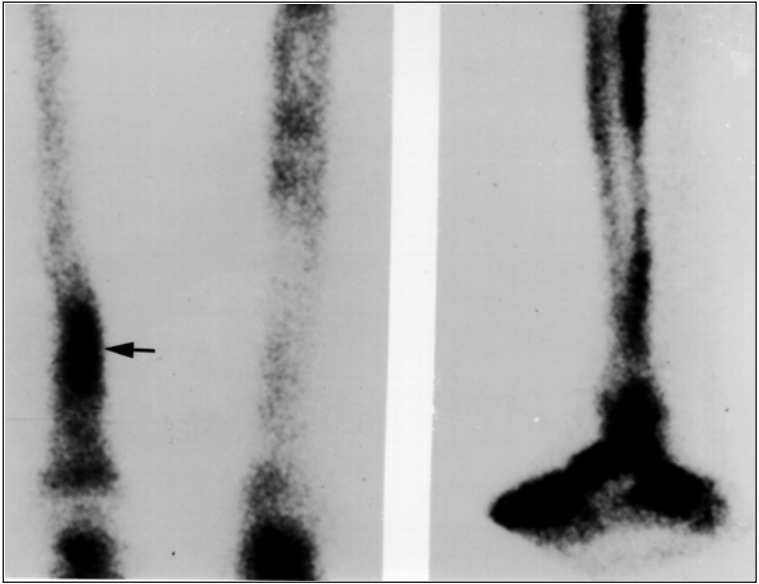
Figure 5. Shin splints and stress fracture in a young male athlete. (*Left*): Posterior bone scan showing a fusiform focus of increased activity in the left lower tibia suggesting a stress fracture (arrow). (*Right*): Lateral view of the right tibia depicting the linear increased cortical uptakes, more prominent posteriorly, which are characteristic for shin splints.

uptake implies an absence of bone remodelling and inability to heal without surgical intervention.

Pseudoarthrosis

Pseudoarthrosis is the formation of a false joint cavity in the dense scar tissue between the bone fragments. The hypertrophic type contains callus and a rich blood supply, whereas the atrophic type does not have these features. Hypertrophic pseudoarthroses show uptake of radiophosphate corresponding to the exuberant sclerosis that borders the false joint, compared to a lack of accumulation in the atrophic type. Difficulty may be encountered in discriminating between infected and noninfected pseudoarthroses, because both conditions may depict substantial uptake of ^{67}Ga-citrate (gallium).

Osteomyelitis

In suspected acute osteomyelitis plain radiography should be the initial diagnostic study. It usually takes 10 to 14 days after the onset of symptoms for the definitive changes to develop. Three-phase radiophosphate bone imaging can disclose uncomplicated acute osteomyelitis in adults within 3 days with a sensitivity and specificity of about 95%. Septic arthritis alone and septic arthritis with extension into adjacent bone can also be differentiated by three-phase radiophosphate

scintigraphy. Difficulties arise in the young pediatric group where the findings may be falsely normal or present with a photon deficient ("cold") defect. The latter finding should be highly suspicious for osteomyelitis. Three-phase imaging becomes less reliable when there is an underlying process that can induce enhanced bone remodelling, such as healing fracture, pseudoarthrosis, neuropathic osteoarthropathy and orthopedic appliances. ^{67}Ga-citrate and ^{111}In or ^{99m}Tc-labelled leukocytes are used to determine whether osteomyelitis is superimposed on these conditions with varying degrees of success.

Gallium localizes in infectious areas by granulocyte or bacterial uptake and binding to the lactoferrin that accumulates in the region. It is disadvantaged by its tendency for low to moderate concentration in non-infectious areas of enhanced bone remodelling, e.g., pseudoarthrosis. Reliance in the diagnosis of osteomyelitis is placed on an incongruence in the relative distributions of gallium and radiophosphate, or a concentration of gallium that approaches or exceeds that of radiophosphate. ^{111}In-leukocytes, when available, are significantly better for the diagnosis of osteomyelitis in the presence of complicating factors.

Chronic osteomyelitis is more difficult to diagnose because of its lower influx of leukocytes and the deposition of ^{111}In-leukocytes in areas of active marrow. Uptakes are generally low, and there is a debate as to whether all uptakes are abnormal or a threshold exists below which the accumulation is normal. In the central skeleton the normal active marrow uptake reduces the sensitivity for chronic osteomyelitis. Sensitivity and specificity are improved by combining ^{99m}Tc-colloid and ^{111}In-leukocytes. Any incongruity in bone marrow distribution of the two scanning agents is considered significant (Fig. 6).

Diabetic foot

Osteomyelitis is a common complication in diabetes, occurring most frequently in ischemic lower extremities. Its diagnosis can be impeded by an underlying neuropathy with its attendant aseptic inflammation, bone destruction, abundant periosteal and juxtaarticular bone proliferation and deformity. The radiographic portrayal of acute progressive osteomyelitis and the aseptic neurotrophic foot can be similar; both exhibit an avidity for radiophosphate, thereby confounding the diagnosis of a superimposed focal osteomyelitis. The radionuclide diagnosis of osteomyelitis in the diabetic foot requires a three-phase radiophosphate study followed by either a gallium or radiolabelled leukocyte scan (preferably the latter because increased uptake of gallium can occur in sterile inflammation and bone undergoing enhanced remodelling). Absence or very low uptake of gallium excludes acute infection with reasonable confidence, whether or not the radiophosphate bone scan is positive. If the intensity of gallium uptake approaches that of radiophosphate and is congruent with it in distribution, the presence of bone infection is suspected. A more widespread distribution beyond the radiophosphate deposition is suggestive of cellulitis, but it may mask an uptake of gallium in the infected bone, a condition that requires different management. Similar criteria apply for the labelled leukocyte scans, except that the degree of uptake in bone need not be as high as with gallium since it is not influenced by enhanced bone remodelling and degenerative or destructive bone disease, and considerably less by sterile inflammation. Deposition in soft tissues implies a cellulitis,
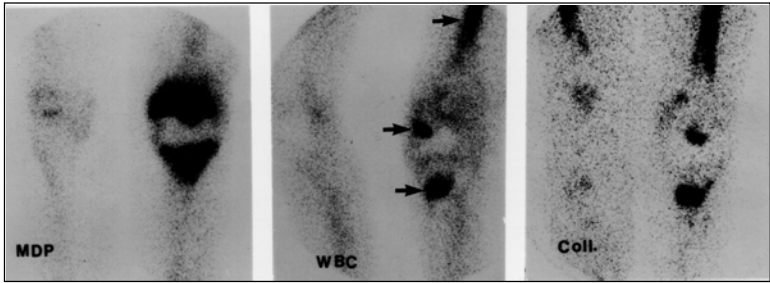
Figure 6. Left total knee arthroplasty. (*Left*): Radiophosphate image exhibits intense periarticular uptake. (*Middle*): There are three areas of ^{99m}Tc-white blood cell deposition (arrows). (*Right*): The ^{99m}Tc-colloid scan demonstrates uptake in the same areas as the ^{99m}Tc-white blood cells, indicating active marrow and weighing against infection.

but it may mask a co-existent osteomyelitis. Poor spatial resolution of ^{111}In contributes to the false negative and false positive scan interpretations.

In comparisons between combined three-phase bone and ^{111}In-leukocyte scanning versus MRI, the latter was more sensitive in disclosing osteomyelitis in the forefoot, but was less sensitive in the presence of a neuropathic (Charcot) joint. In a study of 24 diabetic patients with foot ulcers, 13 had proven osteomyelitis. Sensitivity for clinical evaluation was 54%, 38% for plain radiography, 77% for combined radiophosphate and ^{99m}Tc-leukocytes and 100% for MRI. Combined radionuclide and MRI studies registered an 82% specificity.

Vascular Disorders

There are multiple causes of avascular necrosis (AVN), both traumatic and nontraumatic. Fractures and dislocations can lead to AVN, the most common site being the femoral epiphysis following femoral neck fractures. Nontraumatic causes of epiphyseal AVN and intramedullary infarcts are thromboemboli to bone in disorders such as hemoglobinopathies, sickle cell disease (Fig. 7), sickle cell trait and sickle cell thalassemia. Decompression states (Caisson disease) that result from deep sea diving and high-altitude flying or ballooning can lead to AVN due to nitrogen emboli. Pancreatitis and alcoholism can be associated with fat necrosis and fat emboli that may lead to AVN. Systemic lupus erythematosis, polyarteritis nodosa and giant cell arteritis are connective tissue disorders involving small vessels which are consequently susceptible to occlusion and AVN of dependent tissue. Gaucher's disease, Cushing's disease and steroid therapy are associated with swollen fatty marrow cells which may compromise vascularity and cause AVN.

Spontaneous AVN commonly occurs in the medial condyle of the femur, but it may develop in the lateral condyle, tibial plateau and elsewhere. Its etiology is unknown and usually middle aged men and women are affected, in contrast to osteochondritis dissecans which is typically found in adolescent years. Other bones that can be afflicted with AVN are the humeral epiphysis, metacarpal and metatarsal
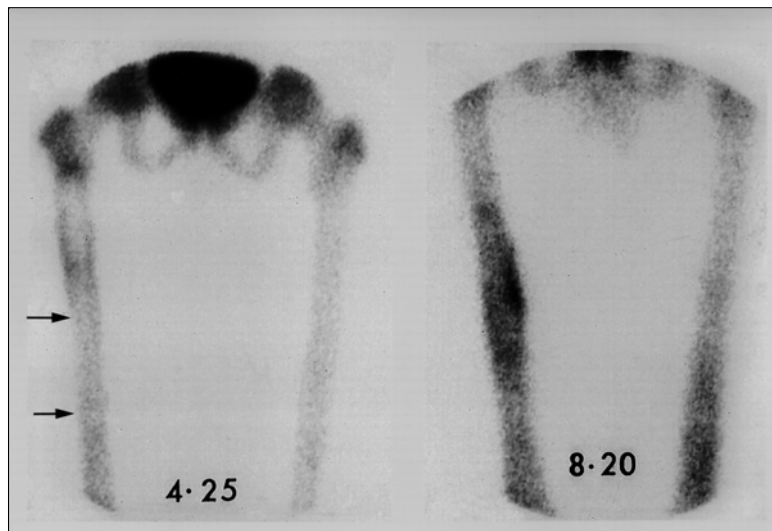
7

Figure 7. Bone infarct in a patient with sickle cell disease. Acute pain developed in the right thigh 2 days before the initial radiophosphate bone scan on April 25 (Left). It showed a segment of photopenia in the right femoral shaft relative to the activity in the bone above and below it (arrows). (Right) Four months later, August 20, there is increased radiophosphate deposition in the area reflecting bone repair.

heads, lunate, capitellum, tarsal navicular and the dome of the talus. Osteonecrosis can be a complication of frostbite (Fig. 8) and high voltage burns.

In AVN imaging with radiophosphate, a sequence of events are predicted, beginning with an initial photopenia that corresponds to the avascular focus and followed in time by an intense circumferential uptake of the reactive reparative phase. Upon completion of revascularization and healing, the uptake returns to normal. Because of the limitations of spatial resolution, the photopenia is not commonly seen in small bones, but may be detected in the femoral capital epiphyses and about the knees. To demonstrate this photopenia, which is characteristic of AVN, imaging must take place early in the evolution of bone necrosis with high resolution SPECT or pinhole collimation. In a comparison of imaging modalities, there were 14 patients with proven AVN but normal plain radiographs, in whom 54% had positive CT scans, 71% had characteristic radiophosphate bone scans and 86% had positive MRIs. In 55 patients with various stages of AVN, positive results were obtained in 78% of the plain radiographs, 87% of the radiophosphate scans, 96% of the CTs and 96% of the MRIs.

Where MRI is readily available it has largely replaced radiophosphate bone imaging in the initial work-up of suspected AVN or infarction because it is more sensitive and specific. AVN can be asymptomatic and be detected incidentally in bone scans ordered for other reasons. Some investigators suggest both MRI and
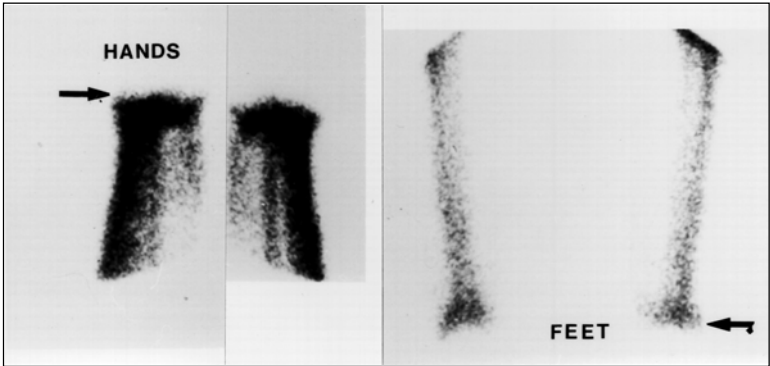
Figure 8. Frostbite. This patient sustained frostbite osteonecrosis of the hands and feet as a result of being stranded overnight in the mountains in sub-zero temperatures. Radiophosphate bone scans show complete absence of blood flow to the hands and feet, which were subsequently amputated. Arrows point to the demarcation between viable and nonviable bone at the wrist and ankle.

bone scanning should be performed because of the possible coexistence of asymptomatic AVN, as commonly occurs in organ transplant patients; radiophosphate imaging facilitates a total body search. Asymptomatic lesions are known to resolve without ever producing changes on the plain radiograph.

Reflex sympathetic dystrophy

There is a broad group of clinical conditions in which pain and autonomic dysfunction are closely related. Similarities between transient osteoporosis of the hip, regional migratory osteoporosis and reflex sympathetic dystrophy (RSD) attest to this observation, and they may represent different aspects of a single syndrome. RSD can follow trauma, surgical treatment, nonsurgical treatment or occur for no obvious reason. It is known under many descriptive names, reflecting the predominant signs, symptomatology and location as in causalgia, acute atrophy of bone, Sudeck's atrophy, peripheral acute trophoneurosis, posttraumatic angiospasm, posttraumatic edema, shoulder-hand syndrome, reflex algodystrophy and algoneurodystrophy. Signs and symptoms include pain, hyperesthesia, swelling, stiffness, hyperhidrosis and discoloration of the skin ranging from red to grayish blue, or a mixture of the two extremes. In the absence of remission, dermal atrophy and contractions may occur.

In adults, the three-phase radiophosphate portrayal in the acute stage is that of increased perfusion, blood pool activity, and uptake in the delayed static images, best appreciated in juxtaarticular bone. All three phases must be diffusely increased to all portions of the wrist and hand or the entire foot (Fig. 9). Plain radiographs depict mineral depletion, but its appearance is often antedated by the radionuclide abnormalities. With clinical remission, the enhanced perfusion and blood pool activity are the first to recede toward normal while uptake on the delayed image is the last to normalize. If the disorder proceeds to an atrophic fibrous stage, each of the phases
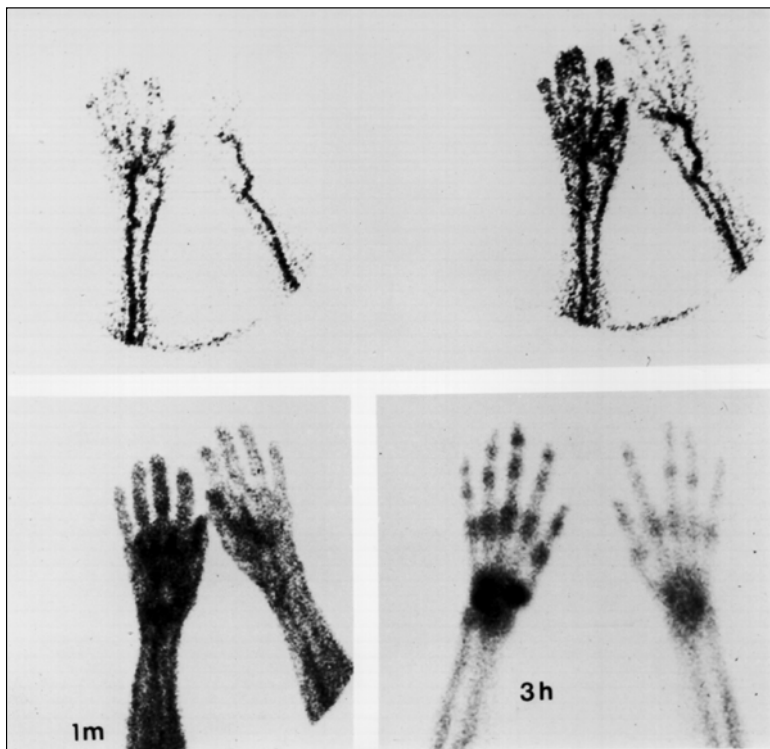
Figure 9. Acute reflex sympathetic dystrophy. Three-phase bone study showing perfusion, blood pool (1 minute) and delayed image (3 hours). There is increased activity in all phases on the right side.

will abate and may even exhibit activity levels below normal. In intermediate stages the diagnosis rests with the finding of increased uptake in the delayed images, and this has been found to be the most reliable sign for diagnosing and monitoring the disease. Sensitivity and specificity of the delayed images in the hand are 96% and 97%, respectively. In the foot sensitivity approaches 100%, but specificity is only 80% owing to complicating factors such as diabetes mellitus, infection, etc. Positive and negative predictive values are 54% and 100%, respectively. It has also been found that patients with higher uptakes in the delayed phase have, on average, a better response to therapy. The scan pattern in the pediatric age group may differ from adults in that all three phases may be decreased in RSD.

Joint Prostheses

Pain is the most common presenting symptom in disorders of prosthetic joints which include implant wear debris, component loosening, fractures of the component, bone fracture and infection. Imaging with a combination of radiophosphate, gallium, ^{111}In or ^{99m}Tc-labelled leukocytes, radiolabelled polyclonal antibodies or

antigranulocyte antibodies produces an acceptable sensitivity and specificity for these conditions.

Sterile Loosening

The diagnosis of loosening is based on the observation of increased radiophosphate uptake in the bone adjacent to the prosthesis, whether diffuse, focal or both. A confounding factor is the natural evolution of radiophosphate deposition which is high immediately after surgical implantation and subsides with time. One report reviewed 267 bone scans in 97 asymptomatic patients with cemented total hip arthroplasties of 1 to 3 years duration. In most implants the bone scan reverted to normal approximately one year after surgery. At the femoral tip 10% had enhanced uptake that persisted between 1 and 3 years. The greater trochanter showed higher uptake in 20% of the implants between 2 and 3 years, and the femoral shaft and lesser trochanter were virtually normal from 9 months onward. Moderate increases in acetabular activity were found between 2 and 3 years. The singular finding of a focal concentration at the stem tip after 1 year is more likely to be normal than a sign of loosening, and it is also possible for a combination of stem tip and greater trochanteric uptake to be normal. In a selected group of 20 patients who had revision surgery and prior bone scans, none had focal concentration limited solely to the femoral stem tip.

Design and composition of the prosthesis may influence the temporal changes in radiophosphate uptake in asymptomatic patients. A quantitative comparison was made between two cementless porous-coated hip implants, the S-ROMJ and the AMLJ. The S-ROMJ, a two component femoral device, was constructed from a titanium alloy, possessed a straight femoral stem with distal flutes for improved rotational control and a coronal slot to improve the tip-femur modulus mismatch. The stem fit into a variable sized metaphyseal sleeve that was circumferentially porous-coated with beads. In contrast, the AMLJ device consisted of a cobalt-chromium alloy, proximal porous-coating and a smooth stem. At 12 months after surgery significant differences in radiophosphate uptake were registered between the two implants. It was higher for the S-ROMJ at the stem and calcar/lesser trochanteric zones, and higher for the AMLJ at the femoral tip. In general, increased uptake for cementless prostheses may be the norm for the first year after implantation. Increased uptake in cementless prostheses on the femoral side may correlate with thigh pain which is usually a temporary symptom.

The natural history of radiophosphate accumulation in bone adjacent to a total knee prosthesis has also been studied. Most report that a persistent high uptake may be present beyond one year after surgery, particularly beneath the tibial component, thereby lessening the value of radiophosphate imaging to distinguish normal from abnormal uptake in a painful knee. Most total knees remain cemented in modern day orthopedic surgery.

Another technique for confirming the diagnosis of prosthetic loosening is radionuclide arthrography. It is performed in conjunction with radiographic contrast arthrography and entails the injection of a test agent, such as ^{99m}Tc-colloid, through the same needle used for the instillation of contrast into the joint cavity. After radiography is completed scintigraphy is performed any time up to 4 hours later. All of the studies comparing the efficacy of radiographic versus radionuclide arthrography
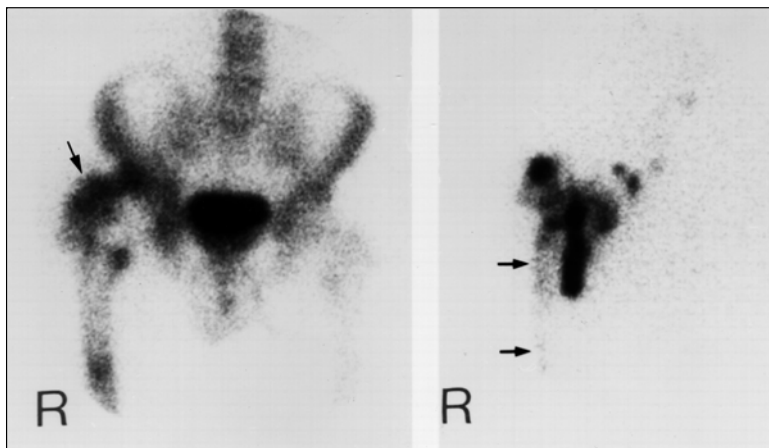
Figure 10. Radionuclide arthrography. (*Left*): Loose right cemented femoral hip prosthesis depicting increased focal uptake of radiophosphate at the stem tip and in the intertrochanteric area. The intense deposit superior to the prosthesis neck is due to heterotopic bone formation (arrow). (*Right*): Combined ^{99m}Tc-colloid and radiocontrast injection into the joint cavity for athrography. ^{99m}Tc scan shows radioactivity seeping into the space surrounding the femoral component indicative of loosening (arrows).

are related to the hip, and there is general acknowledgement that radionuclide arthrography is more sensitive for the femoral component but unreliable for the acetabular component (Fig. 10).

Infection

Three-phase bone imaging is very sensitive for the disclosure of infected arthroplasties but it is not specific. In a group of 98 patients presenting with painful arthroplasties and suspected of having an infection, a sensitivity of 100% and specificity of only 18% was confirmed by surgical documentation. A number of test agents can be used to increase the specificity. Gallium was the first to be introduced. If the distribution of gallium is incongruent with that of the radiophosphate, or if it is intense and congruent, the likelihood of infection is high. Low grade congruent uptakes are equivocal and since this is reported to occur in about half the cases, the use of gallium is limited.

The results of labelled leukocytes are better, but vary with the intensity of the inflammatory process. Normally the labelled leukocytes, unlike gallium, do not accumulate at sites of increased bone turnover in the absence of infection. Sensitivity was found to be poorest in chronic osteomyelitis, and this was attributed to the low leukocyte attraction to the site. Specificity was compromised in chronic osteomyelitis by the occasional low grade uptake from the aseptic inflammatory reaction associated with healing fractures or by uptake in active marrow adjacent to the hip and knee prostheses. With regard to the latter, it has been shown that in asymptomatic patients

with hip prostheses, ^{111}In-leukocyte activity was present in 48% of the femoral tips at 24 months, and 37% had significant uptakes in the region of the acetabular component. The addition of a ^{99m}Tc-colloid scan will aid in identifying these areas of disturbed marrow function adjacent to hip and knee implants so that their concentration of labelled leukocytes will not be misinterpreted as infection (Fig. 6). Results from using combined leukocyte/colloid marrow imaging are reported to vary in accuracy from 89% to 98%, with the improvement being largely due to increased specificity.

Radionuclide Synovectomy

Treatment of chronic synovitis by surgical synovectomy is not always successful as recurrences occur with regeneration of the synovium and there may be an associated prolonged rehabilitation due to joint stiffness and limitation of motion. In surgical management of hemophilic synovitis and hemarthrosis the problem of maintaining hemostasis can be daunting and expensive. Intraarticular injection of chemicals such as nitrogen mustard, thiotepa and osmic acid, although less invasive, were not consistently successful. Repeated intraarticular injections of corticosteroids pose a risk for systemic toxicity.

Although modern arthroscopic synovectomy has made radionuclide synovectomy less popular, it remains a valuable therapeutic option. When a beta emitting particulate radiopharmaceutical is injected into the inflamed joint, the synovium is exposed to a high radiation dose and atrophies. Desirable attributes for the agent include little or no leakage from the joint cavity, high affinity binding of the beta emitter, uniform distribution throughout the joint cavity, synovial uptake without initiating an inflammatory reaction and a biological half-life within the joint that should not be less than the physical half-life of the radionuclide. Leakage from the joint cavity via the lymphatics can lead to deposition in the regional inguinal nodes. Leakage has also been attributed to synovial inflammation and joint movement; therefore premedication with intraarticular glucocorticoids (to reduce the synovial hyperemia) and bed rest have been advocated to decrease the frequency and amount of radiocolloid deposition in the regional nodes. Many suitable radiopharmaceuticals have been developed (Table 2). The most frequently used are ^{32}P-chromic phosphate and ^{90}Y-citrate which have pure beta emission with energy for good tissue penetration, large particle sizes and are commercially available.

Ideally, the penetration of beta particles should be limited to the thickness of the synovium to avoid radionecrosis of the cartilage and bone, but this may only be a theoretical concern as cartilage is relatively resistant to radiation and no cases of necrosis have been reported. Chromosomal abnormalities have been seen, but in all the years of experience with intraarticular radiation synovectomy no instance of induced malignancy have been reported.

Treatment Procedure

For the knee, an injection of a local anesthetic is obtained under aseptic conditions, and through a lateral approach an 18 to 20 gauge needle is inserted into the joint cavity. Smaller joints such as the wrist and elbow, may require x-ray fluoroscopic control, perhaps with contrast injection to ensure absence of leakage and loculation. At the knee, the ease in aspiration usually ensures proper needle placement. The

7

Table 7.2 Physical data of radiocolloids used for synovectomy

Radiocolloid	Physical half-life In days	Emission	β Max MeV	β range in tissue (mm) Max.	Mean	Particle size (mμ)
(^{198}Au) Gold-198	2.7	β, γ	0.96	3.6	1.2	9-15
(^{32}P) Phosphorous-32 chromic phosphate	14	β	1.7	7.9	2.6	500-2000
(^{186}Re) Rhenium-186 sulfide	3.7	β, γ	0.98	3.6	1.2	5-10
(^{90}Y) Yttrium-90 citrate	2.7	β	2.2	11	3.6	100
(^{165}Dy) Dysprosium-165 ferric hydroxy macroaggrate	0.1	β, γ	1.29	5.7	1.8	3000-8000
(^{153}Sm) Samarium-153 hydroxyapatite	1.9	β, γ	0.8	3.2	0.8	5000-45000

dose of ^{90}Y-citrate instilled is 278 MBq (7.5 mCi) into the knee joint, 92.5 MBq (2.5 mCi) into elbow joint and 74 MBq (2 mCi) into the wrist. Hydrocortisone is generally instilled with the treatment dose to mollify a potential reactive radiation synovitis i.e., increased pain and effusion, which may occur between a few hours and 2 weeks after treatment. In order to assess placement and dispersion of the ^{90}Y-citrate, 37 to 74 MBq (1 to 2 mCi) of ^{99m}Tc-colloid is often included to permit scanning (Figs. 11 and 12). The joint is bandaged snugly and the patient is sent home with instructions to refrain from weight bearing and to rest the joint for 3 days and not undertake strenuous activities for at least 2 weeks to minimize leakage.

In rheumatoid joints, good results, seen as various degrees of pain relief, reduction in joint effusion and increased range of motion, were obtained in 50%-70% of the patients at 6 month to 12 month evaluations. This was independent of the radiopharmaceutical used. Hemophilic hemarthroses demonstrated a reduction in the frequency of hemorrhage in 80%-90% of the patients. Patients can be retreated if there is reactivation of symptoms.

Frequently Asked Questions (FAQs)

Can the bone scan differentiate septic arthritis from sterile synovitis (such as rheumatoid arthritis and gout)?

The application of radiophosphate and ^{67}Ga-citrate to differentiate septic and sterile rheumatoid synovitis has not been consistently successful. Joint-to-bone ratios of gallium uptake tend to be higher for septic joints but the overlap with sterile joints is quite large. Intense uptake suggests sepsis and a low concentration in an untreated joint favors sterility. The use of radiolabelled leukocytes has also been reported to yield false positive results for the presence of sepsis due to the variable amounts leukocytes in sterile rheumatoid and gouty effusions. Leukocytes are also present in the sterile effusions of osteoarthritis and may contribute to false positive
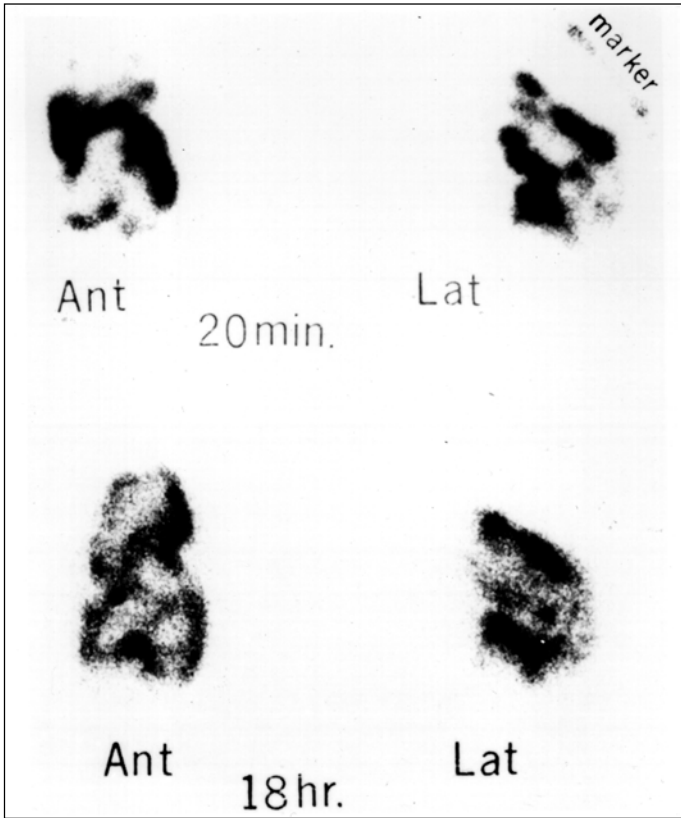
Figure 11. Radionuclide synovectomy. 148 MBq (4 mCi) ^{32}P-chromic phosphate and 37 MBq (1 mCi) ^{99m}Tc-colloid were instilled in the right knee cavity. ^{99m}Tc-colloid scans exhibit a good distribution without significant loculation at 20 minutes and a further small extension by 18 hours.

diagnoses. Radiolabelled leukocyte imaging is a sensitive method of assessing the inflammatory component for a synovitis irrespective of the cause.

Is the bone scan useful in confirming a cure of osteomyelitis following prolonged antimicrobial therapy?

The radionuclide features of acute osteomyelitis are increased uptake of ^{67}Ga-citrate, radiolabelled leukocytes and radiophosphate. At the end of the prescribed treatment course, a decrease in uptakes of the agent is objective evidence of a successful response (but they may not revert to normal at that time). Enhanced radiophosphate uptake will usually persist for some time thereafter due to reactive osteoblastic repair. This may be associated with low concentrations of gallium and radiolabelled
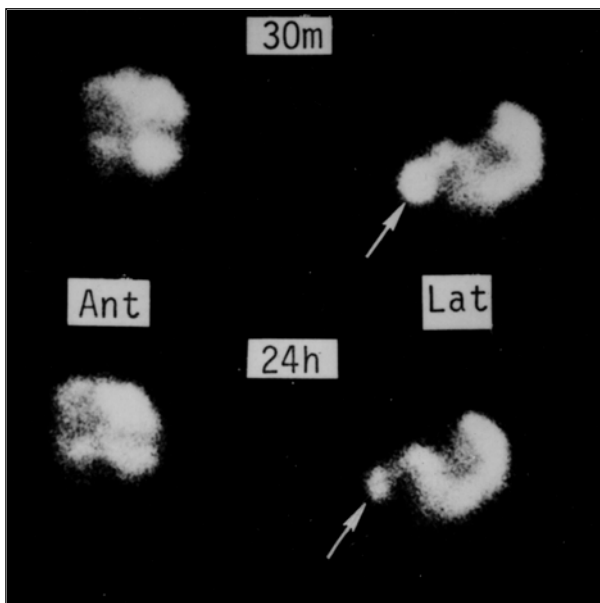
Figure 12. Radionuclide synovectomy. ^{99m}Tc-colloid scans of the knee following its intracavitary injection at the same time as ^{32}P-chromic phosphate for therapy. No evidence of loculation at 30 minutes and 24 hours, except for a small amount which entered a popliteal cyst (arrow).

leukocytes, a pattern that may also reflect chronic osteomyelitis. Predictably, a negative bone scan is highly predictive of a negative bacterial culture. The final arbiter of cure is the clinical evaluation.

Additional Reading

1. Holder LE (guest editor). Orthopedic Nuclear Medicine (Part 1). Seminars in Nuclear Medicine 1997; 27(4).
2. Holder LE (guest editor). Orthopedic Nuclear Medicine (Part 2). Seminars in Nuclear Medicine 1998; 28(1).
   A detailed review of the basic physiology, imaging techniques and clinical applications of nuclear medicine as applied to orthopedics.

Skeletal Oncology

Leonard Rosenthall and Ralph Wong

Introduction

Radioisotopes play an important role in the diagnosis of benign and malignant bone lesions. Bone scanning is commonly used to detect metastases from malignant tumors because it is more sensitive than x-rays and allows the whole body to be surveyed. The general principles of skeletal imaging are reviewed in Chapter 7. This Chapter will concentrate on aspects specific to bone tumors.

Primary Benign Bone tumors

Benign and malignant primary bone tumors can be quite difficult to distinguish with radiophosphate imaging. In general, benign lesions tend to have lower accretions than malignant lesions, but in the individual case it is neither reliable nor predictive of the histopathological outcome.

Adamantinoma

Adamantinoma is a rare tumor that occurs most commonly in the mid-diaphysis of the tibia. In rare cases it can behave like a malignant tumor with metastases to the lung. It appears as a large radiolucent lesion on the radiograph, and shows moderate uptake of radiophosphate.

Aneurysmal Bone Cyst

Aneurysmal bone cyst (ABC) is a distinctive non-neoplastic solitary lesion of bone consisting of a cystic cavity filled with nonendothelial-lined spaces containing blood. Radiographically, there is a striking "blow-out" distention of part of the contour of the affected bone, and it may simulate a malignant lesion. More than half of these lesions occur in the metaphyseal regions of the long bones or vertebrae, and up to one-third are linked to benign or malignant processes such as nonossifying fibroma, chondroblastoma and giant cell tumor of bone. Due to their location and potentially rapid, aggressive growth, they can be difficult to distinguish from a primary malignancy. Despite the presence of blood filled cavities, the perfusion segment of the three-phase radiophosphate bone study may be negative. More than half of the delayed images depict a doughnut pattern of uptake (central photopenia encompassed by a band of activity).

Bone island

A bone island is a common lesion that consists of a nest of compacted trabeculae of mature lamellar bone. It may enlarge after puberty, but it does not have malignant potential. Delayed bone scans are usually normal but may show a mild increased uptake (Fig. 1).
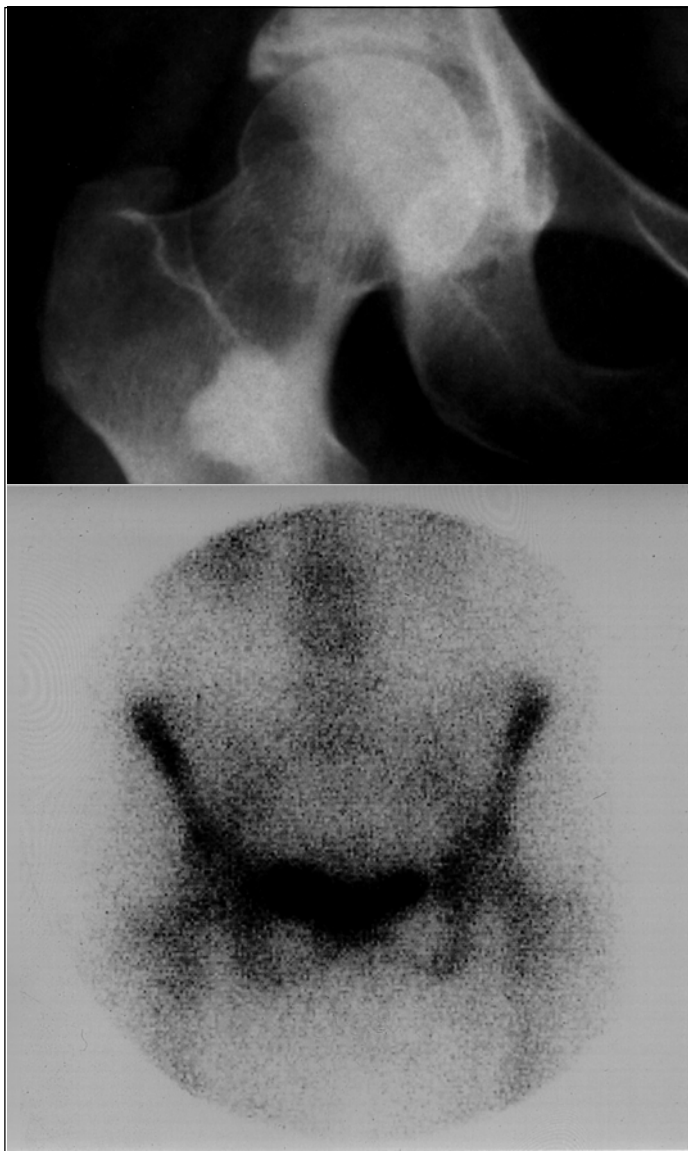
8

Figure 1. Bone island. *Upper*: Radiograph of a large sclerotic lesion in the intertrochanteric region. *Lower*: Radiophosphate bone scan shows no evidence of increased uptake. This confirms that the lesion is metabolically inactive.

Chondroblastoma

Chondroblastoma is an uncommon primary bone tumor of chondrogenic origin that is seen in younger individuals before epiphyseal closure. It usually has its origin from the region of the growth plate, most commonly in the proximal humerus, but it can arise in flat bones. They are composed of dense concentrations of rounded or polyhedral chondroblasts. Histological features are similar to chondromyxoid fibroma and the two may be related. Malignant transformation rarely can occur. Radiophosphate concentration in these lesions can be intense.

Desmoplastic Fibroma

Desmoplastic fibroma is an extremely rare benign intraosseous fibrous tumor occurring mostly in the long bones. Three quarters of the cases are seen below the age of 30 years, with peak incidence in the second decade of life. The tumor is usually located centrally in the metaphysis where it symmetrically expands the bone and thins the cortex. Radiographically it appears as an osteolytic lesion with well circumscribed margins. Nonspecific increased uptake of radiophosphate can be seen.

Enchondroma

Enchondroma is a common benign lesion that appears in the medullary portion of bone and is composed chiefly of mature hyaline cartilage. The solitary enchondroma has a predilection for the phalanges and metacarpals of the hand. It can also occur in large long and flat bones (pelvic and shoulder girdle) where they have a potential for malignant transformation, and may be difficult to distinguish from a low grade chondrosarcoma. The bone scan may demonstrate normal or mildly increased uptake of radiophosphate (Fig. 2). A lesion which changes from normal to high uptake over time, especially when associated with pain, is suspect for malignant conversion.

Multiple enchondromas, or enchondromatosis, is an anomaly usually disclosed in infancy. When one side of the body exhibits greater involvement than the other, the condition is called Ollier's disease. The combination of enchondromatosis and soft tissue hemangiomata is referred to as Maffucci's syndrome. About 8% of the cases of Maffucci's syndrome degenerate into chondrosarcomas.

Epidermoid Cyst

Epidermoid cysts are sharply delineated, squamous cell lined and filled with desquamated keratinized debris. They occur in the calvarium, but traumatic epidermoid cysts may develop in the phalanges. The scintigraphic presentation in the calvarium is usually normal, but if the lesion is large enough a photopenic focus may be appreciated.

Fibrous Defects

Fibrous defects are focal collections of nonspecific fibrous tissue located predominantly in the cortical bone, but they may also be found in cancellous bone. Sites of predilection are the long bones, primarily the femur and tibia. Several classifications have been proffered for these fibrous lesions, but a simplified version divides them into fibrous cortical defects and nonossifying fibromas. The former occurs in about 30% of children over 2 years of age, and radiographically it presents

8

Figure 2A. Benign enchondroma. Anterior (left) and lateral (right) radiographs of the left femur showing an area of mottled calcification in the distal femoral shaft with slight expansion of the cortex. Differential diagnosis includes benign enchondroma, central chondrosarcoma and infarct.
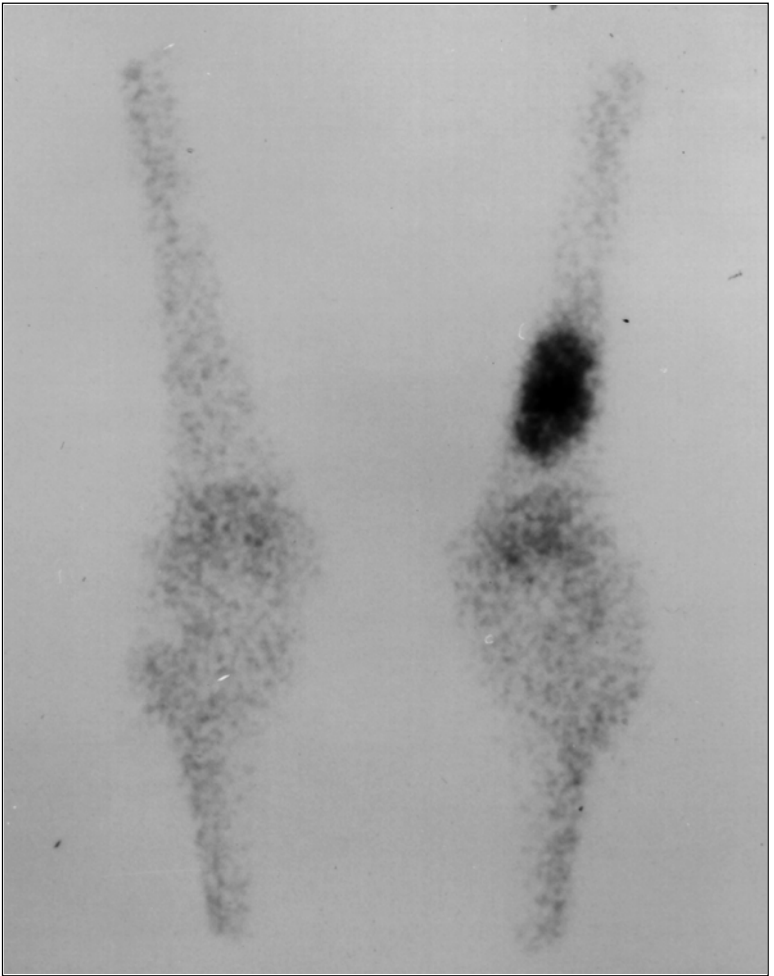
Figure 2B. Benign enchondroma. Radiophosphate bone image shows a nonspecific intense focus of uptake. A benign enchondroma was removed at surgery.

as a small lucent defect which is eccentrically located in the metaphyseal cortex of a long bone. It usually heals spontaneously and the bone scan is invariably normal, unless complicated by a fracture. Nonossifying fibromas are larger in size and may be located in the metaphysis or diaphysis of a long bone. Bone scans are usually normal, but low grade uptake has been reported.

Fibrous Dysplasia

Fibrous dysplasia is a benign tumor in which masses of fibroblasts and islands of cartilage replace cancellous bone in one or more locations. Less than 1% undergo

sarcomatous transformation. The lesions tend to stabilize at puberty. Of the solitary lesions, three-quarters are located in the ribs, femora, tibiae, skull and facial bones. The radionuclide manifestation is that of intense radiophosphate uptake in the lesion, indistinguishable from malignant tumors. About 10% to 15% of the lesions seen by radiography are reported to be negative by bone scan.

Giant Cell Tumor

Giant cell tumor appears to arise from non-bone forming supporting tissue, and histologically demonstrates a distinctive neoplasm composed of a vascularized network of spindle or ovoid stromal cells interspersed with multinucleated giant cells. Most frequently they occur in the third to fourth decades of life, but it has been described in the immature skeleton. It usually presents as an osteolytic process in the epiphyseal end of a long bone, particularly the distal femur and proximal tibia, in a skeletally mature patient. It comprises less than 5% of all primary tumors, and 90% of them are benign. Most giant cell tumors depict an avid uptake of radiophosphate. There is a 50%-60% recurrence rate following surgery, and about a 15% chance of converting to a malignant state. Many are hypervascular and are seen as such in the first segment of the three-phase bone scan (Fig. 3). This hyperemia may extend to the uninvolved bone adjacent to the joint, the so-called "extended" uptake.

Hemangioma

Hemangioma of bone is a benign, slowly growing tumor emanating from newly formed blood vessels. There are cavernous and capillary types. Cavernous hemangiomas are commonly located in the vertebrae and skull, whereas the capillary variety is more likely to be encountered in flat bones and the metaphyses of long bones. In the spine, the radiographic appearance of cavernous hemangiomas is that of exaggerated vertical trabeculae or collapse of the vertebral body. Radiophosphate scans are variable. The three-phase bone study may show increased perfusion coupled with photopenia on delayed views.

Osteoblastoma

Osteoblastoma is an uncommon, solitary lesion that is characterized by vascular osteoid and bone forming matrix rich in osteoblasts. It is closely related to osteoid osteoma, but differs in that it is larger (exceeding 2 cm) and reactive sclerosis is slight. Osteoblastomas constitute about 1% of all primary bone tumors and 3% of benign bone tumors, and affect patients between 10 and 30 years of age. About 50% are found in the vertebral column and skull, followed by the long bones, although they may be found at any site. The tumors do not regress spontaneously and may exhibit progressive growth. There are few reports of malignant transformation. Benign osteoblastomas avidly concentrate radiophosphate and are positive in both the blood pool and delayed phases.

Osteochondroma

Osteochondroma is a common tumor accounting for approximately half of all benign bone neoplasms and can be solitary or multiple. They arise in areas near the epiphyseal growth plates especially in the distal femur and proximal tibia. Radiographically, they appear as external nodular protuberances from or partially embedded in bone, and are characterized by an osseous stalk capped by hyaline
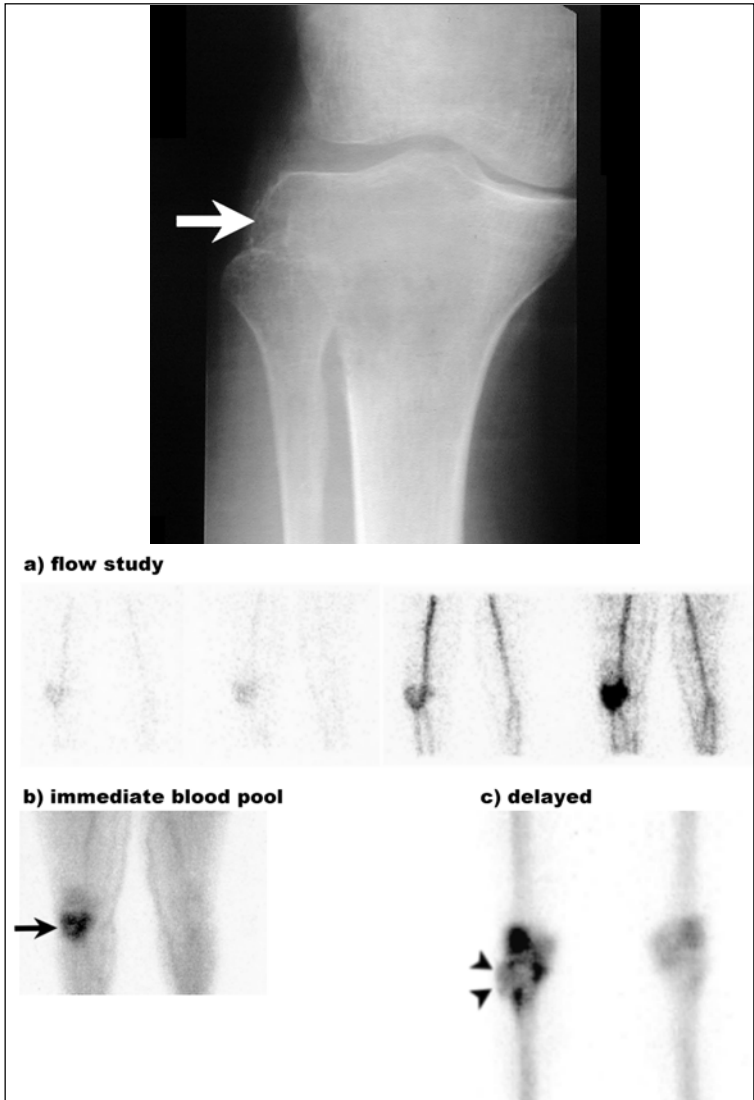
Figure 3. Giant cell tumor of bone. This 26 year old woman complained of increasing right knee pain following minor trauma associated with progressive swelling and inability to weight bear. Radiographs show a large lytic lesion in the lateral condyle of the tibia (white arrow). A three-phase bone scan shows marked hyperemia corresponding to the lytic lesion (black arrow) but reduced tracer accumulation centrally (arrowheads). This appearance is seen with hypervascular destructive bone tumors. (Case provided by Dr. W.D. Leslie.)

cartilage. MRI is the preferred modality to diagnose osteochondromas as it clearly demonstrates this cartilage cap. Growth is by enchondral ossification, and it ceases at the time of epiphyseal closure. Osteochondromas commonly present as a painless mass in patients between 10 and 20 years of age, or are found incidentally at all ages. In children, these tumors show an avid concentration of radiophosphate due to the ongoing enchondral ossification. Uptake wanes with fusion of the adjacent epiphysis. Reactivation or persistence of high abnormal uptake by the exostosis after skeletal maturation should be viewed as suspicious for malignant transformation. The frequency of transformation to chondrosarcoma is low in solitary exostosis (less than 1%) but is higher in hereditary multiple exostosis, exceeding 10% in some reports. Absent uptake of radiophosphate virtually excludes malignant change.

Osteoid Osteoma

Osteoid osteoma is a painful ("pain at site, worse at night") benign bone lesion which consists of a small core, or nidus, surrounded by a zone of sclerotic bone. The nidus is less than 1 cm in diameter and is made up of varying proportions of osteoid and spicules of newly formed osseous tissue in a bed of highly vascularized osteogenic connective tissue; it is surrounded by a margin of dense sclerotic bone. Over 50% of the lesions occur in the femur and tibia, about 10% in the vertebral column and the rest scattered between the ribs, carpals, tarsals, scapulae, patellae, calvarium and mandible.

The reactive sclerosis is most prominent in long-bone osteoid osteomas and, together with its lucent nidus, is readily appreciated by plain radiography. Lesions of the spine, intracapsular portions of the hip and small bones of the hands and feet often elude radiographic detection because of a paucity of reactive sclerosis and presence of overlying bony structures. It is at these sites where radiophosphate imaging is most useful (Fig. 4). SPECT can enhance detection of lesions in the spine (Fig. 5). Radiophosphate imaging can disclose the presence of osteoid osteoma with a sensitivity approaching 100%, and a normal bone scan virtually excludes the diagnosis. The bone scan has been used to guide surgical resection of the complete nidus, which is necessary to relieve the pain. When the lesion is located in the spine or hip scintigraphic guidance will limit the amount of bone required for removal. This is accomplished by injecting radiophosphate prior to surgery and scanning the resected bone intraoperatively to verify that it contains the nidus.

Radiography of the painful area should be performed first in the diagnostic workup as about two-thirds of the osteoid osteomas will be identified as such. The bone scan should be reserved for normal or equivocal radiographic findings. Some patients will present with referred pain and imaging should be continued above and below the painful site. For example, an osteoid osteoma in the intertrochanteric region could have pain referred to the knee.

Osteoma

The osteoma is a well-defined benign slow-growing tumor composed of osseous tissue and is found almost exclusively in the skull, paranasal sinuses and mandible. Histologically, it may be eburnated in type containing quiescent lamellae of bone, or spongy in type showing cellular, vascular connective tissue separating spicules of newly formed bone surrounded by rows of osteoblasts. They measure about 2 cm in diameter, are very dense on the radiograph and do not become malignant. The bone
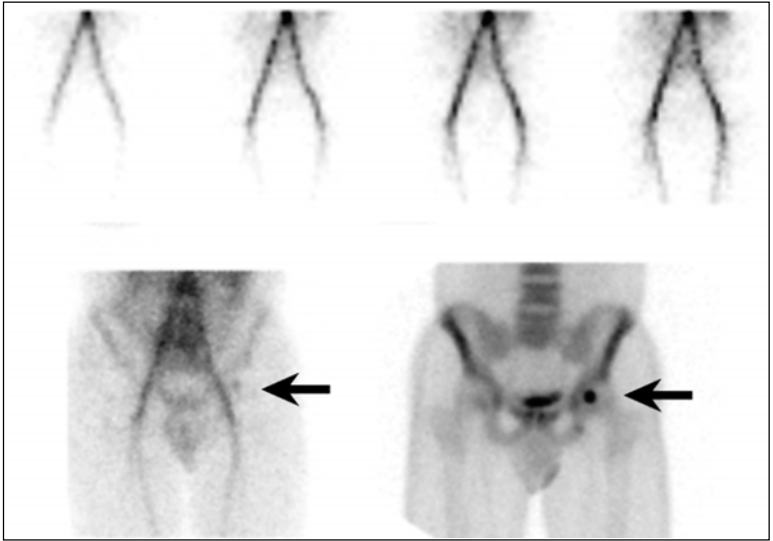
Figure 4 Osteoid osteoma. The arterial flow study is normal but there is focal hyperemia in the left femoral head on the immediate blood pool image and intense uptake on delayed images (arrows). (Case provided by Dr. W.D. Leslie.)

scan is usually normal, but there are isolated reports of increased uptake of radiophosphate.

Unicameral or Simple Bone Cyst

A bone cyst is an intramedullary cavity lined by fibrous tissue and is usually filled with a clear amber fluid, but it may be multi-chambered. The proximal metaphyseal ends of the humerus and femur are the most frequent sites of occurrence. The condition is seen in children and adolescents and thought to undergo involution as it is much less common in adults. Radiographically, the appearance is that of a large radiolucent lesion, broad at the metaphyseal end and narrow at the shaft end, and does not cross the epiphyseal plate. Lower extremity cysts are more likely to fracture than those in the upper extremity. Bone scans are usually negative, but a pattern of a slight increase in radiophosphate uptake at the margins of the cyst and photopenia in the center may be seen. A fracture will induce an avid concentration of the scanning agent.

Primary Malignant Bone tumors

Radiophosphate scanning is of limited use in the initial diagnosis of primary malignant bone tumors, as these lesions are detected by radiography when the patient first presents with local symptoms. Computed tomography (CT) and MRI are more accurate in defining the extent of the tumor, both in bone and soft tissue. There is a role for scintigraphy in the search for occult bone metastases, as may occur with osteosarcoma and Ewing's sarcoma.
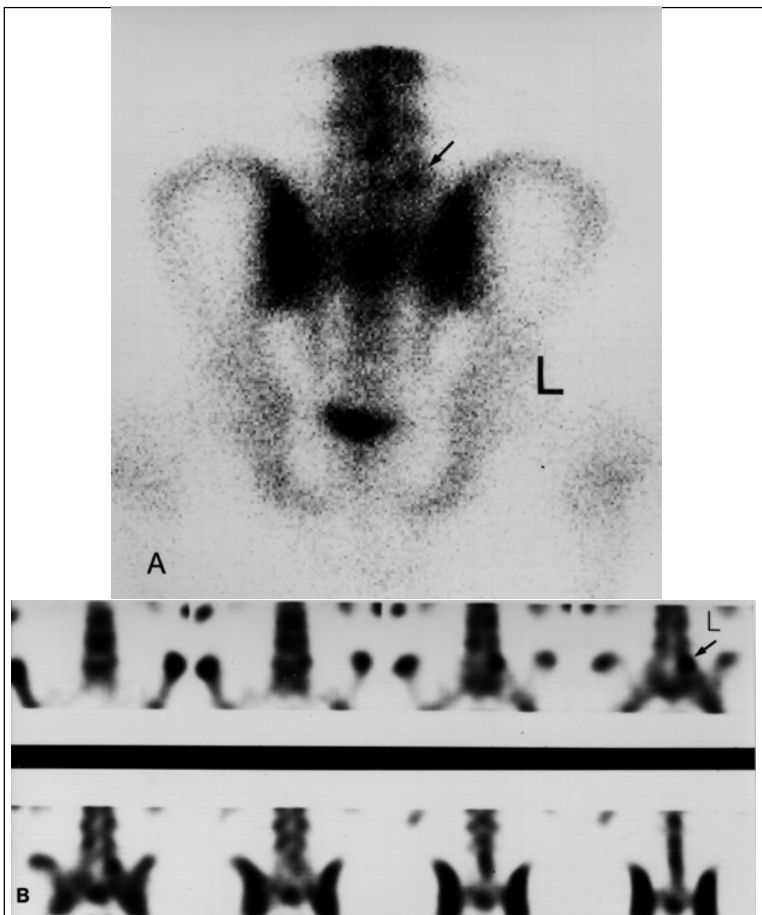
Figure 5. Osteoid osteoma. Posterior planar image of the lumbar spine depicts subtle increased uptake in the 5th lumbar vertebra (arrow). Coronal SPECT images clearly define and localize the lesion.

The radiophosphate manifestations of malignant tumors are dependent on the degree of adjacent reactive bone formation, regional hyperemia and the histological nature of the tumor itself. Tumor osteoid and bone are produced by the malignant connective tissue of osteosarcoma which facilitate an increased concentration of radiophosphate within the tumor itself. Chondrosarcomas feature cartilaginous tumor cells and a chondroid matrix which may undergo calcification and ossification that promote uptake of radiophosphate. "Pure" fibrosarcomas are less likely to exhibit tumor uptake because calcification and ossification are absent.

Osteosarcoma

Osteosarcoma is a high grade tumor that accounts for about 20% of all primary bone malignancies, and generally occurs during the second to third decades of life with another peak in the sixth decade. Those that arise later in life are associated with pre-existing conditions such as Paget's disease and previous bone irradiation. It is the most common primary malignant bone tumour with the exception of multiple myeloma. Most frequent sites of origin are the metaphyses of the long bones, and it is more common in males. Diseases that are predisposed to the development of osteosarcoma include osteochondromatosis (Ollier's disease), Maffucci's syndrome, multiple hereditary exostosis, osteogensis imperfecta and Paget's disease. The primary lesions have abnormally high uptake of radiophosphate, but are best characterized and defined by CT and MRI. Bone scintigraphy is a convenient modality for detecting osseous and soft tissue metastases and, thereby, aids in patient management.

Osteosarcoma arising in Paget's disease carries a poor prognosis. Typically the tumors present as large destructive unresectable lesions in the pelvis, proximal femur and humerus. They usually present as a relatively photopenic area surrounded by the high uptake of radiophosphate in the pagetic bone. In patients undergoing chemotherapy, the decrease of radiophosphate uptake in the tumor has been shown to parallel the degree of induced tumor necrosis. Thallium-201 and ^{99m}Tc-sestamibi are also reported to render a good assessment of tumor viability and response to chemotherapy.

Chondrosarcoma

Chondrosarcoma is the second most common primary malignant tumor of bone with a peak incidence during the fifth decade of life. Typically, it is located in the pelvis, femur and shoulder girdle. It is of cartilaginous origin and appears on the radiograph as a radiolucent expansile lesion. It may destroy the cortex and invade the adjacent soft tissue. It is best defined by CT and MRI. Avid uptake of radiophosphate can be seen in both the intramedullary and exostotic forms of the malignancy.

Ewing's Sarcoma

Ewing's sarcoma is the second most common primary malignant bone tumor of children and adolescents, and most occur between 10 and 20 years of age. It is thought to develop from a primary mesenchymal cell although the actual histogenesis has not been conclusively determined. It is commonly seen in the femur and pelvis. Unlike osteogenic sarcoma, it has a predilection for the flat bones. Plain radiography followed by MRI to define tumor extent are the main imaging modalities. The radiophosphate bone images can depict intense activity on all three phases of the study, but it is not specific or sufficiently detailed for management, and is therefore relegated mostly to the role of metastatic tumor search. Metastatic bone disease is present in 10% of patients on the initial clinical examination, and about 50% of patients eventually develop bone metastases. Some authors have recommended ^{99m}Tc-colloid marrow imaging to disclose marrow involvement, but it is unreliable after radiation and chemotherapy.

Multiple Myeloma

Multiple myeloma is a plasma cell dyscrasia of the bone marrow. It can be mistaken radiographically for metastatic bone disease because it presents with multiple osteolytic lesions or diffuse osteopenia. The other two elements of the "triad" are plasmacytosis of the bone marrow (>10%) and a monoclonal gammopathy (in serum and/or urine). Skeletal radiography is superior to bone scintigraphy in the evaluation of the presence and extent of the disease. On a site-by-site comparison radiography is reported to have a sensitivity of 82% relative to 42% by bone scanning. On a patient basis radiography and scintigraphy have sensitivities of 94% and 78%, respectively. Radiophosphate imaging often fails to demonstrate a hyperconcentration at sites of skeletal involvement by myeloma despite extensive disease by radiography. This occurs because reactive bone formation is not a feature of the disease; this might be due to release of an inactivation factor by the tumor. The bone scan may be helpful when there is focal pain and a negative radiograph.

Histiocytosis X or Langerhans' Cell Histiocytosis

Histiocytosis X comprises a spectrum of conditions from an isolated benign bone involvement (eosinophilic granuloma) to a benign dissemination (Hand-Schuller-Christian disease) to a highly malignant form (Letterer-Siwe disease). The disease can involve bone, soft tissue, or both. Bone scintigraphy is positive in many of the lesions (Fig. 6), but it is not reliable as a screening procedure. Plain radiography and CT are the recommended imaging methods for the initial assessment. Bone scintigraphy can be useful in searching for metastases or investigating pain in the context of a normal radiograph.

Diagnosis and Follow-Up of Skeletal Metastases

Radiophosphate bone scanning in metastatic disease is recognized for its high sensitivity and low specificity. As a consequence of parallel developments of competing diagnostic methods such as CT, MRI, ultrasonography and blood tests for tumor associated antigens, the role of bone scanning has changed. Initially it was recommended as a screening procedure for bone metastases in all newly diagnosed malignancies, but recent evaluations of its overall efficacy with different tumor types have qualified this routine use.

Pathophysiology of Skeletal Metastasis

The metastatic cascade begins with the release of a single cell, or a clump of cells, as a result of proteolysis induced by tumor enzymes. These cells enter the vascular or lymphatic systems where most are destroyed in transit by the cells of the immune system. Those few potent cells that escape the initial defense and reach a distant site require local conditions that promote implantation and growth. The cells adhere to receptors on the vascular endothelium or basement membrane, and then pass through the vessel wall to establish themselves in the organ. Local destruction is mediated by growth factors elaborated both by tumor cells and the invaded tissue. This provides space for tumor growth, and a concomitant stimulation of angiogenesis allows the tumor to meet its nutritional requirements. The majority of tumor deposits occur in the red marrow and this has been attributed to the slow transit through the marrow sinusoids. A requirement for tumor growth is local osteoclastic bone resorption. Tumor cell stimulation of osteoclastic activity is mediated by its release of such factors
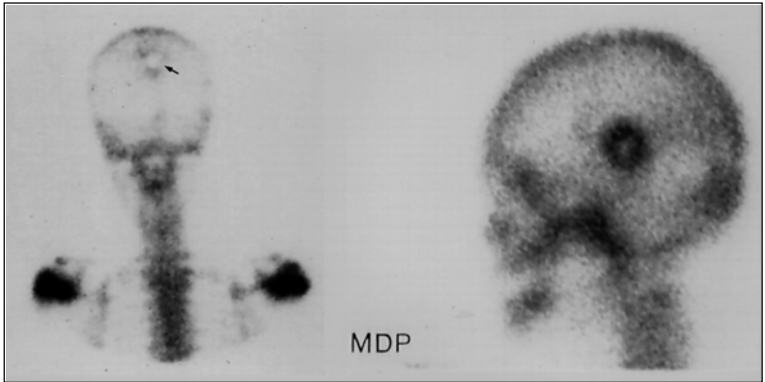
Figure 6. Eosinphilic granuloma of bone (histiocytosis X). Eosinophilic granulomas are found predominantly in flat bones such as the calvarium, mandible, pelvis and ribs. The radiophosphate bone scan can depict decreased, normal or increased uptake. Patient 1 (left): Posterior view of the skull showing an eosinophilic granuloma characterized by photopenia with a rim of minimal reactive radiophosphate uptake (arrow). Patient 2 (right): Lateral view of the skull demonstrating the "doughnut" sign, i.e., photopenia with a rim of marked reactive radiophosphate accretion.

8

as prostaglandin-E and procathepsin-D, or by inducing macrophages and other cells of the immune system to release tumor necrosis factor and interleukin-1. Increased osteoclastic activity at tumor sites may also be due to systemic factors such as parathyroid hormone-related protein and transforming growth factors alpha and beta. Not all the observed events related to the metastatic process have been fully explained at the molecular level and the subject is still under scientific investigation.

Interpretation of Bone Scans

When multiple foci of increased uptake are scattered randomly in the axial and proximal appendicular skeleton the diagnosis of metastatic disease is not difficult (Fig. 7). Given the low specificity of radiophosphate imaging and its sensitivity to increased bone remodeling from any cause, whether benign or malignant, the presence of one or just a few lesions renders the interpretation more difficult. An analysis of scans with one or two bone lesions in cancer patients without known metastases showed that 11% of single lesions were malignant, and 30% of the patients with two lesions proved to be malignant. About 10% of isolated rib uptakes reflect a metastasis. Location may help in the differentiation as benign lesions are more common at articular surfaces of joints in the vertebral column and extremities, suture lines of the skull, anterior rib ends and costovertebral joints. Metastases beyond the elbows and knees are infrequent. An increase in lesion uptake over time in serial studies favors a diagnosis of malignancy, particularly if new ones also appear; lesions that remain stable or wane in intensity are most likely benign.

The radiophosphate portrayal of a very high diffuse concentration in bone, low soft tissue activity and virtually undetected kidneys is referred to as a "super scan" (Fig. 8). This is encountered mostly in prostatic cancers. On close inspection, with
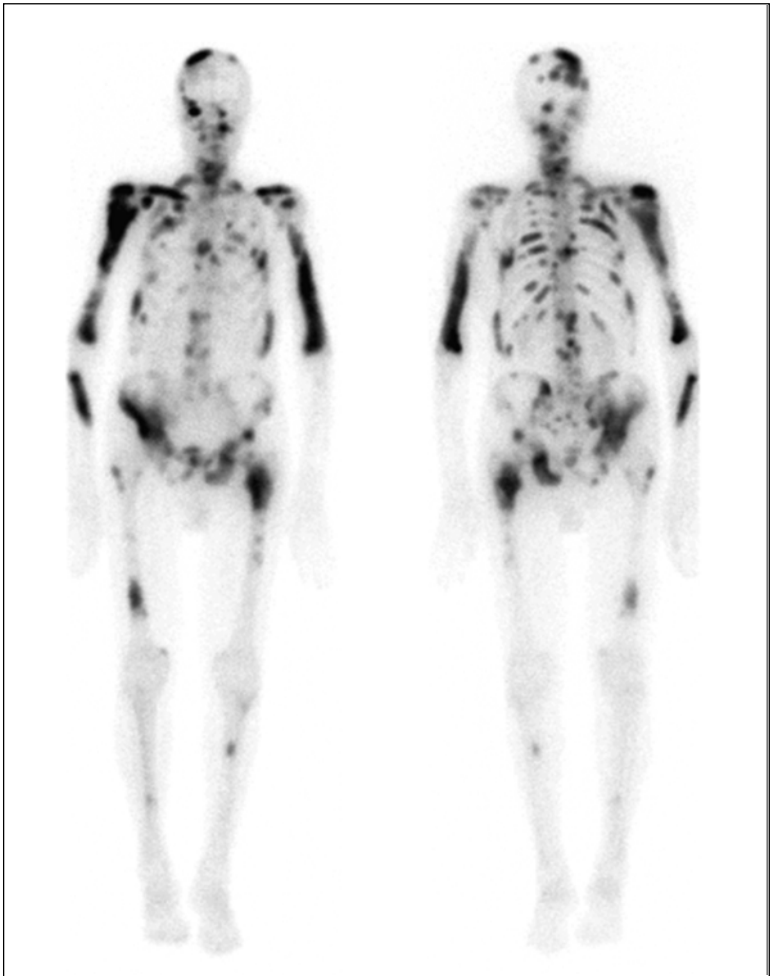
Figure 7. Skeletal metastases from prostatic carcinoma. Anterior and posterior total body scans show multiple focal sites of intense uptake involving both the axial and appendicular skeleton. (Case provided by Dr. W.D. Leslie.)

varying contrast settings, many will reveal a heterogenous rather than homogeneous distribution. With successful treatment the bone scan can revert to normal or a presentation of multiple focal abnormalities and the usual soft tissue background and visible kidneys.
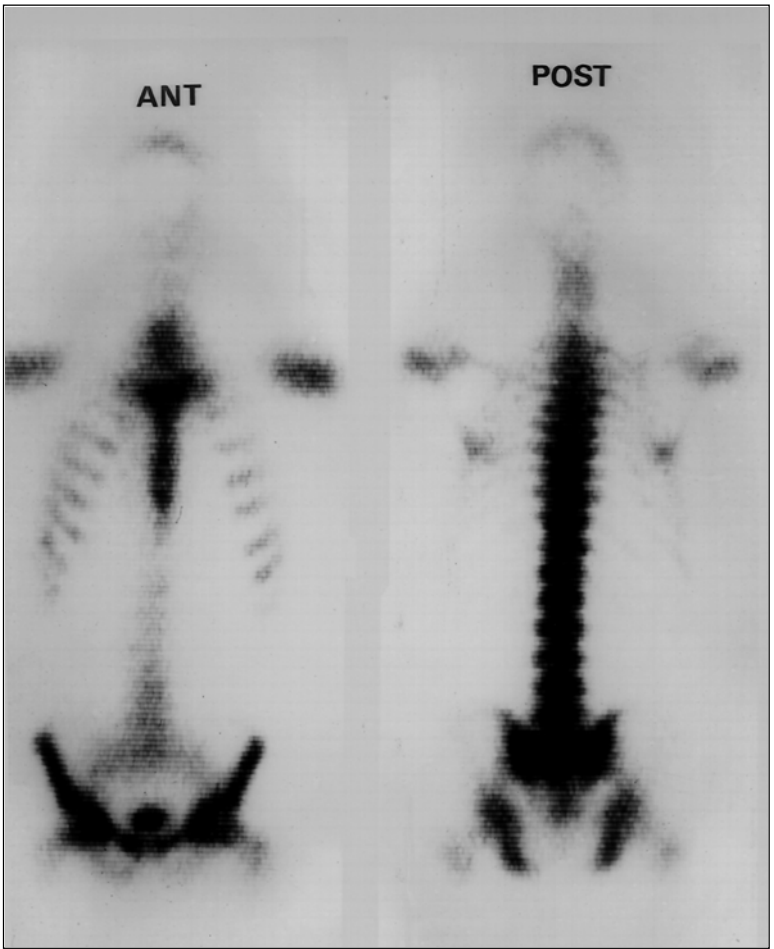
Figure 8. Diffuse prostatic metastases producing a "super scan". Anterior (left) and posterior (right) total body scans show intense uniform concentration in the vertebral column, pelvis and sternum. The usual soft tissue background and kidneys are not visible by comparison. Enhanced uptake in the skull and ribs is also present, but in this illustration is overwhelmed by the spine and pelvis.

Photopenic defects are an important sign of tumor presence and should be considered with the same gravity as focal increases in activity. They are probably due to vascular compromise as a result of tumor compression of the small marrow vessels.

Since photopenic or "cold" lesions are harder to resolve than the typical "hot" lesion, those "cold" lesions that are detected are relatively large (Fig. 9).
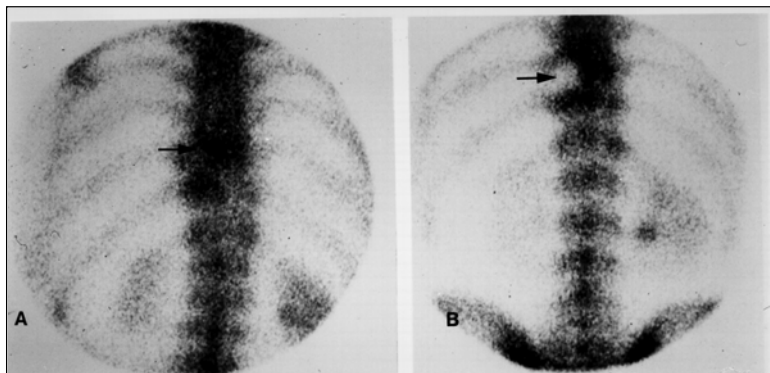
Figure 9. Photon deficient metastasis. This patient with carcinoma of the prostate had a solitary asymptomatic lesion (arrow) in the thoracic spine at staging. Six months later he developed upper back pain and the bone scan was normal except for a photopenic focus in a thoracic vertebra (arrow), which corresponded to the site of pain. A scan four months later revealed widespread metastatic disease.

8

Lung Carcinoma

Bone scans have been used to screen patients for metastases in newly diagnosed non-small cell lung cancer as part of the staging process. With the advent of CT and MRI, evidence of metastatic deposits in the hilar and mediastinal lymph nodes, liver and adrenals can be identified in order to establish non-resectability of the primary. The additional information gleaned from bone scan screening will not alter the staging or management even though it has been reported that the bone scan may be positive in about 40% of patients on initial presentation.

Most small cell lung carcinomas will have metastasized by the time the patient is first seen and these are readily revealed by physical examination, laboratory findings and radiographic techniques. Resectability is not an issue in this tumor category, and although it is reported that about 50% will show bone lesions by scintigraphy it has little influence on management in the initial phase.

Bone scanning is generally relegated to monitoring chemotherapy, assessing bone pain for possible local radiation therapy or orthopedic intervention to preclude fracture in the long bones or spinal cord compression, disclosing hypertrophic pulmonary osteoarthropathy as a cause of lower extremity pain (Fig. 10) or identifying nonmalignant causes of pain such as trauma, infection and osteonecrosis.

Breast Carcinoma

Present day evaluations of large clinical trials indicate that the frequency of bone metastases in stage I and stage II breast cancer patients is less than 10%. Most investigators are of the opinion that the use of bone scintigraphy for staging is unnecessary in stage I and most stage II individuals in view of the newer diagnostic radiographic methods that are available and the results of cost-effectiveness analyses. Bone scans have a role if the primary tumor is large or histologically aggressive, if
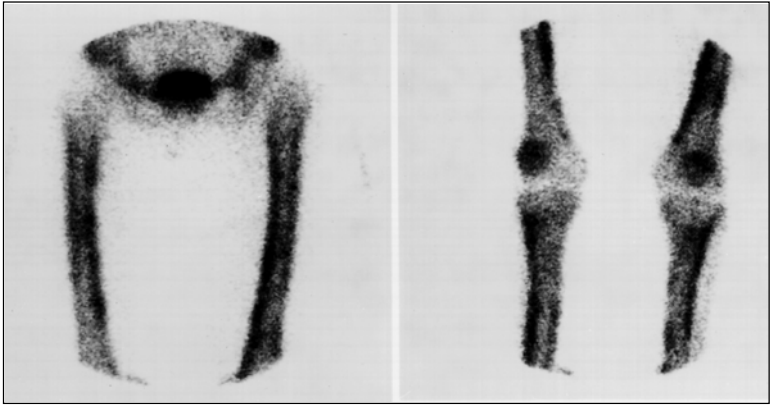
Figure 10. Hypertrophic pulmonary osteoartropathy. Radiophosphate bone scan in a patient with lung carcinoma. Note the extensive increased cortical activity in the femora and tibiae due to subperiosteal bone remodelling. Upper extremities were also involved.

8

there is bone pain or if conventional radiography is equivocal about the presence of metastases. The value of routine baseline scintigraphic bone surveys in all patients in order to better discriminate between preexisting benign and later newly acquired malignant lesions is also arguable and should be limited to selected patients who are known to have pre-existing benign disease. The current trend is to use bone scintigraphy only when it might influence management.

Genitourinary Tumors

Carcinoma of the prostate is the most common malignancy in men, and its incidence increases with age. The likelihood of positive bone scans varies with the clinical stage, histological score, and serum levels of prostate specific antigen (PSA) and prostatic acid phosphatase. Occurrence of positive bone scans at initial diagnosis in patients with PSA levels less than 20 ng/ml is under 1%. A staging bone scan is not recommended with PSAs less than 10 ng/ml, except if there are known preexisting conditions that could make later interpretations equivocal or if there are symptomatic or radiographic suspicions of malignancy. Staging bone scans are performed in patients with PSAs greater than 20 ng/ml. The prevalence of metastases increases as the PSA levels increase. Between 20 ng/ml and 100 ng/ml about half the patients will have one or more abnormalities on the baseline scan, and beyond 100 ng/ml most have extensive bone infiltration. Follow-up bone scans are not routine when the baseline bone scan is normal or even equivocal, but they can be helpful in the investigation of unexplained bone pain or a rising serum PSA. In established skeletal involvement serial bone scans can monitor the efficacy of therapy. Progressive extension of bone disease despite adequate treatment heralds a poor prognosis.

Staging scans in renal carcinoma are positive in less than 5% of the patients and are not recommended. Unlike prostate carcinoma which produces blastic metastatic lesions on the radiograph, renal metastases are usually lytic and the increased

radiophosphate uptake is due to the osteoblastic reaction in the surrounding bone. Large renal lesions may be seen as photopenic centrally, girded by a band of radiophosphate accretion.

The yield of the staging bone scan for urinary bladder, cervical, ovarian, endometrial and testicular malignancies is reported to be low. Bone scans are primarily directed at elucidating the source of pain or confirming questionable radiographic changes.

Thyroid Carcinoma

Thyroid metastases to bone are usually lytic by radiography but are seen as foci of increased radiophosphate uptake on bone images. If they are sufficiently large a central photopenic area may be resolved. ^{131}I in diagnostic doses of 74-185 MBq is the most commonly used agent to disclose metastases to bone and soft tissue, because increased uptake on the day 2 or 3 post-dose scan implies a potential for management with therapeutic doses of ^{131}I (3700 to 7400 MBq). This attribute is limited to papillary, follicular and mixed tumors which concentrate iodine and produce thyroglobulin. The diagnostic iodine-131 scans are often of poor quality as a result of low count rates and more information about the degree of skeletal involvement may accrue with supplemental radiophosphate imaging, particularly in the vertebral column. Medullary and the more undifferentiated thyroid tumors do not have an affinity for iodine, but their presence in bone is susceptible to radiophosphate detection. (A more detailed discussion of thyroid cancer is found in Chapters 13 and 14.)

Leukemia and Lymphoma

Leukemia and lymphoma can exhibit varying degrees of bone marrow infiltration and their radiophosphate portrayal is variable. In Hodgkin's disease, about 1% of unselected patients will have bone disease at the time of initial staging. Conservative estimates for non-Hodgkin's lymphoma bone involvement has been reported to be 7% for the diffusely infiltrating lymphomas and 1% for the nodular lymphomas at the time of diagnosis. In the appendicular skeleton, the radiophosphate pattern can be that of diffusely increased uptake or uniform periarticular increased uptake, particularly at the knees, which is suggestive of marrow expansion in response to central marrow compromise either by tumor or chemotherapy. A patchy inhomogeneous distribution may be seen, implying irregular marrow replacement by tumor, myelofibrosis, or both. The intensity of radiophosphate uptake in these manifestations can be subtle and images may require an appropriate number of counts to resolve the abnormalities. Impaction of the medullary cavity by tumor may lead to bone infarction in the long bones and vertebral column, thereby creating a photopenic focus. Depending on timing, size and resolution long bone infarction may demonstrate a progressive radiophosphate picture of initial photopenia, reparative circumferential and centripetal increased uptake, diffuse increased uptake within the infarcted area and finally a normal appearance with resolution.

Table 1. Differential diagnosis for a bone scan suggesting skeletal metastases

	Diagnostic Clues
Multiple fractures	History of trauma and plain radiographs usually suffice. Occasionally trauma may be minimal or absent (severe osteoporosis) in which case a follow-up scan should show resolution. In infants child abuse should be questioned.
Multiple benign tumors (e.g., enchondromatosis)	Childhood onset and lack of primary malignancy. Plain radiographs usually diagnostic.
Paget's disease (osteitis deformans)	Often asymptomatic despite dramatic scan findings. Typical appearance is diffuse involvement throughout the bone or uptake extending to the joint line; may show bowing. Radiographs often show enlargement of the bone and coarsened trabecular structure.
Hyperparathyroidism	Multiple "brown tumors" can be seen in severe disease. Hypercalcemia with inappropriately elevated serum PTH invariably present.
Multifocal osteomyelitis	Usually history of fever and/or bacteremia. Often immunocompromised host.
Degenerative joint disease	Periarticular distribution in commonly affected areas (shoulders, hips, knees, spine). Radiographs usually diagnostic.

8

Frequently Asked Questions (FAQs)

Are there any benign disorders that can give multiple areas of focal radiophosphate uptake on the bone scan and thereby simulate metastases?

It is always important to consider benign explanations before labelling a patient as having metastatic disease based upon scan appearance alone. Radiophosphate uptake accurately depicts the physiology of osteoblastic hyperactivity, but does not provide a specific pathologic diagnosis. Just as benign tumors, trauma, infection and a myriad of other causes can produce focally increased uptake, multiple occurrences of these lesions can incorrectly raise the specter of metastatic disease (Table 1). For example, Paget's disease of bone is often multifocal and can result in intense scan uptake, abnormal radiographs, elevated serum alkaline phosphatase and skeletal pain (Fig. 11).

Does bone scan worsening in a patient on treatment for skeletal Metastases indicate treatment failure?

Not necessarily. An increase in the number and intensity of metastatic lesions on follow-up bone scans in patients subjected to hormonal or chemotherapy treatment

Figure 11. Paget's disease of bone (osteitis deformans). Multifocal areas of increased uptake are scattered throughout the skeleton (arrows). Although some of these would be difficult to distinguish from metastatic lesions, the appearance of the tibia (diffuse involvement with bowing deformity) is characteristic for Paget's disease. The skull lesion shows peripheral uptake and central photpenia, a form of pagetic involvement known as osteoporosis circumscripta. (Case provided by Dr. W.D. Leslie.)

is usually a sign of disease progression. An exception is the "flare phenomenon" which occurs in 6% to 23% of treated patients with osseous deposits from prostate or breast cancer (Fig. 12). Even though the lesions are healing there is an initial increased intensity in the previously observed foci and it may also be associated with the appearance of new lesions, increased pain and hypercalcemia. This flare can last up to 6 months. During this interval the radiograph will show sclerotic changes, a
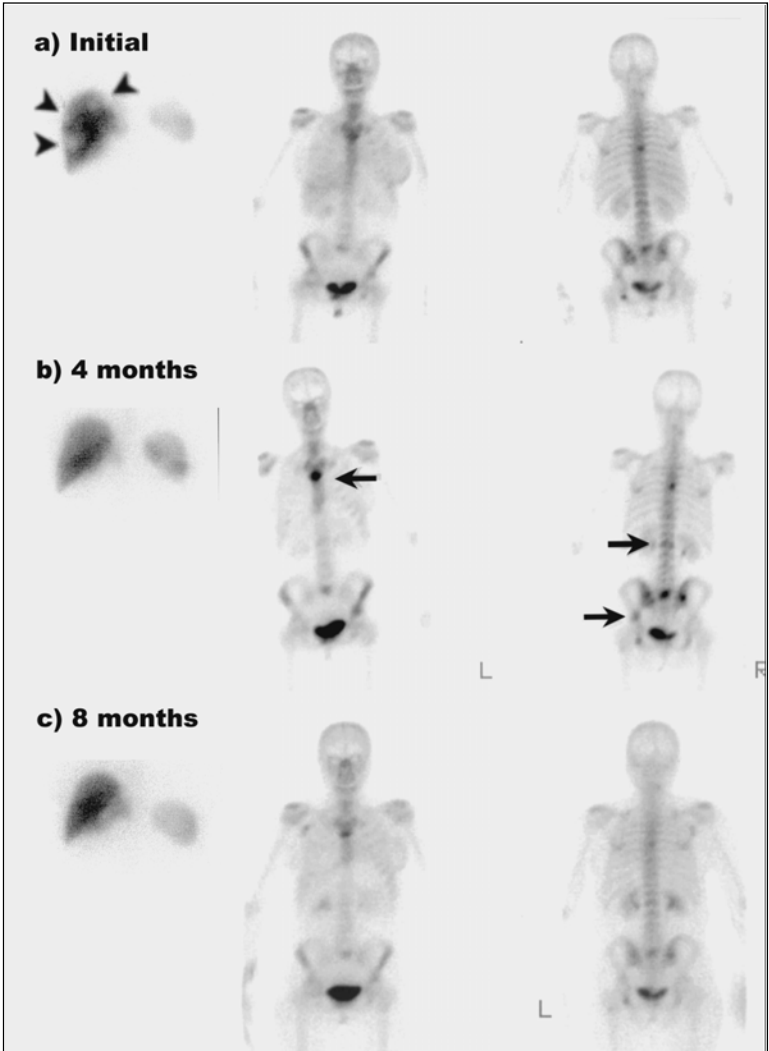
Figure 12. Metastatic flare reponse. (A) This 48 year old woman had breast cancer metastatic to liver (left) and bone (right). She was treated with a conventional doxorubicin-containing chemotherapeutic regimen and had follow-up bone/liver scans four (B) and eight months (C) later. There is dramatic improvement on both of the follow-up liver scans. In contrast, the bone scan shows transient worsening followed by later improvement. There had not been any alteration in the patient's therapy, and the improvement in the liver metastases shows that the tumor was sensitive to the chemotherapeutic regimen. (Case provided by Dr. W.D. Leslie.)

sign of tumor regression. Continued increase in the number and intensity of the lesions beyond 6 months after treatment indicates loss of control.

How long should you wait before repeating a bone scan?

That depends on the reason for the scan. Occasionally the diagnosis of skeletal metastases is still in doubt after a bone scan and conventional radiographs have been completed. If a follow-up examination shows worsening, then metastatic disease is very likely, whereas resolution (in the absence of anti-tumor treatment) confirms a benign process. Although some high-grade tumors can progress rapidly, usually 3-6 months are required to detect a change. On the other hand, if the scan is being used to evaluate response to treatment then at least 6 months should elapse to avoid confusion with the "flare phenomenon" (see previous question).

Additional Reading

1.   Jacobson AF. Primary and metastatic bone disease. In: Sandler MP, Coleman RE, Wackers FJT, Patton JA, Gottschalk A, Hoffer PB, eds. Diagnostic Nuclear Medicine. Baltimore: Williams & Wilkins, 1996:649-667.
2.   Charron M, Brown ML. Bone scanning in metastatic disease. In: Collier BD, Jr., Fogelman I, Rosenthall L, eds. Skeletal Nuclear Medicine. St. Louis: Mosby, 1996:87-123.

8

Kidney

Michael Hoskinson and Keevin Bernstein

Introduction

Nuclear medicine techniques for evaluating the kidney and urinary tract have evolved from pioneering studies with primitive radiopharmaceuticals and hand-held probe detectors to a sophisticated technology capable of providing important physiologic and anatomic information. The advent of the gamma camera placed emphasis on morphological evaluation of the kidneys. However, with recent advances in other anatomic imaging modalities, renal scintigraphy has rediscovered its roots in the evaluation of function. This can be appreciated in the discussion of radionuclide techniques that measure purely physiological processes such as glomerular filtration rate (GFR). Other sections deal with the important contributions of nuclear renal imaging in the evaluation of acute renal failure, renovascular hypertension, urinary tract obstruction and renal transplants.

Renal physiology

The renal parenchyma receives approximately 20% of cardiac output. In the normal person, 20% of renal plasma flow is filtered so that 180 litres of a protein-poor ultrafiltrate is produced each day. This occurs across highly permeable glomeruli which present a large surface area (1.6 m^2). The ultrafiltrate, which includes nitrogenous waste products and salts, traverses a complex tubular system where tubular secretion, reabsorption and metabolism of specific solutes occurs. The proximal nephron (proximal convoluted tubule) reabsorbs 55-70% of the salt and water presented to it. Fine-tuning of salt and water reabsorption occurs in the distal nephron (collecting tubules and ducts) so that less than 1% of the filtered load is ultimately excreted. Other solutes, such as potassium and hydrogen, undergo reabsorption and secretion at various sites along the nephron. The final urine constituents pass from the collecting ducts into the renal pelvis and calyces.

Under non-stressed physiologic situations, renal perfusion is autoregulated by smooth muscle in the afferent arteriole (myogenic reflex) to maintain a constant perfusion pressure and GFR over a wide range of systemic blood pressures. Under situations of compromised renal perfusion, there is balanced afferent and efferent arteriolar constriction mediated predominantly by sympathetic stimulation and angiotension II which helps to maintain glomerular filtration.

In the context of renal function, clearance can be conceptualized as the volume of plasma "cleared" of a material by the kidneys per unit time (usually per minute). If a substance is filtered at the glomerulus and neither secreted nor reabsorbed, its clearance is a measure of GFR. ^{99m}Tc-DTPA is one such material. In a normal adult patient, the GFR is approximately 120 ml/min. If a substance is completely cleared from the plasma as it passes through the kidney by any combination of filtration
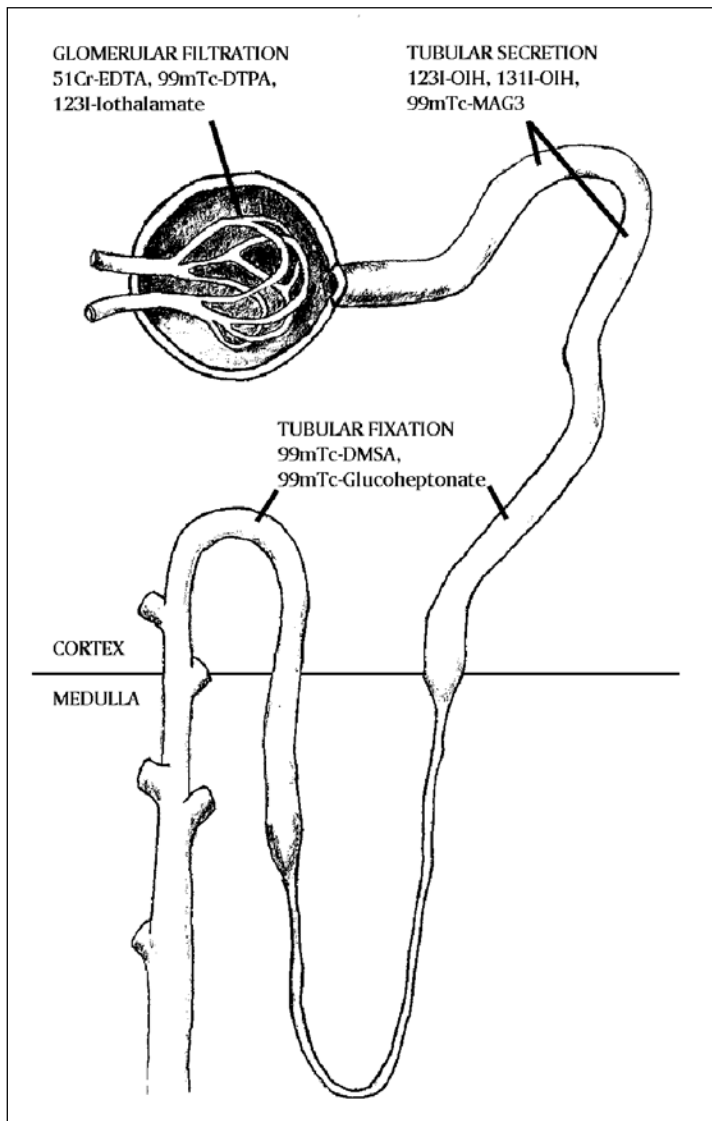
Figure 1. Diagram of the nephron showing GFR agents such as ^{99m}Tc-DTPA, ^{51}Cr-EDTA and ^{125}I-iothalamate filtered at the glomerular level. While ^{99m}Tc-MAG3 and ^{123}I- or ^{131}I-hippurate are filtered, their predominant method of renal excretion is by tubular secretion at the level of the proximal convoluted tubule. ^{99m}Tc-DMSA and ^{99m}Tc-glucoheptonate become fixed within the renal tubules. ^{99m}Tc-glucoheptonate is also filtered and secreted by the nephron. (Figure provided Ms. L.Ward.)

and secretion, its clearance is a measure of effective renal plasma flow (ERPF). ERPF is that plasma which flows through the kidney and is available for filtration and/or secretion, excluding capsular and interstitial perfusion.

Technical Considerations

Radiopharmaceuticals

Several tracers are available for renal imaging and functional assessment (Fig. 1). A brief description of some of the more common ones is presented below.

^{99m}Tc-Diethylenetriaminepentaacetic Acid (^{99m}Tc-DTPA)

This tracer is a nearly ideal agent for assessment of GFR. It is a small chelate with a molecular weight of 500, and its only mode of excretion is glomerular filtration. It is neither secreted nor reabsorbed by the kidneys. Its renal extraction reflects the filtration fraction of plasma (i.e., 20% first pass clearance). GFR determination using ^{99m}Tc-DTPA should take into account the possibility of binding of ^{99m}Tc-DTPA to plasma proteins. Protein binding is variable between different formulations of ^{99m}Tc-DTPA.

^{131}I- or ^{123}I-Orthoiodohippurate (^{131}I- or ^{123}I-OIH)

Hippurate is mainly excreted by tubular secretion (80%) and, to a lesser extent, by filtration (20%). Its first pass clearance is high (about 90%) and therefore it can be used to measure ERPF. ^{123}I-OIH is not available commercially in many areas (including North America), and ^{131}I-OIH can only be used in small amounts because of the high radiation dose that results from the iodine-131 label.

^{99m}Tc-Mercaptoacetyltriglycine (^{99m}Tc-MAG3)

This is a newer agent that is almost entirely excreted by tubular secretion. Although first pass extraction is only about 50%, it has much higher protein binding than OIH with more staying in plasma and available for uptake by the tubular cells. The appearance of the renogram with ^{99m}Tc-MAG3 is nearly identical to that of OIH. It is excreted faster than ^{99m}Tc-DTPA at all levels of renal function. Because of its ready availability and excellent imaging characteristics, it is the favored agent for diuretic renography. There is some liver excretion of ^{99m}Tc-MAG3, which complicates assessment for urine leaks on delayed views (2-3 hours or more after injection).

^{99m}Tc-Ethylenedicysteine (^{99m}Tc-EC)

This is another new agent with high extraction efficiency and excretion characteristics similar to ^{99m}Tc-MAG3. Its main advantage is easier preparation.

^{99m}Tc-Dimercaptosuccinic acid (^{99m}Tc-DMSA)

^{99m}Tc-DMSA is used for cortical imaging (Fig. 2) because about 50% of the injected dose is retained in the renal cortex, bound to sulfhydryl groups in the proximal convoluted tubules. Peak renal activity is seen at 4-6 hours after injection. It is the favored tracer for assessment of renal morphology and is used in the assessment of pyelonephritis and renal scarring. Its uptake is markedly reduced in conditions that result in acidification of the urine (e.g., renal tubular acidosis).
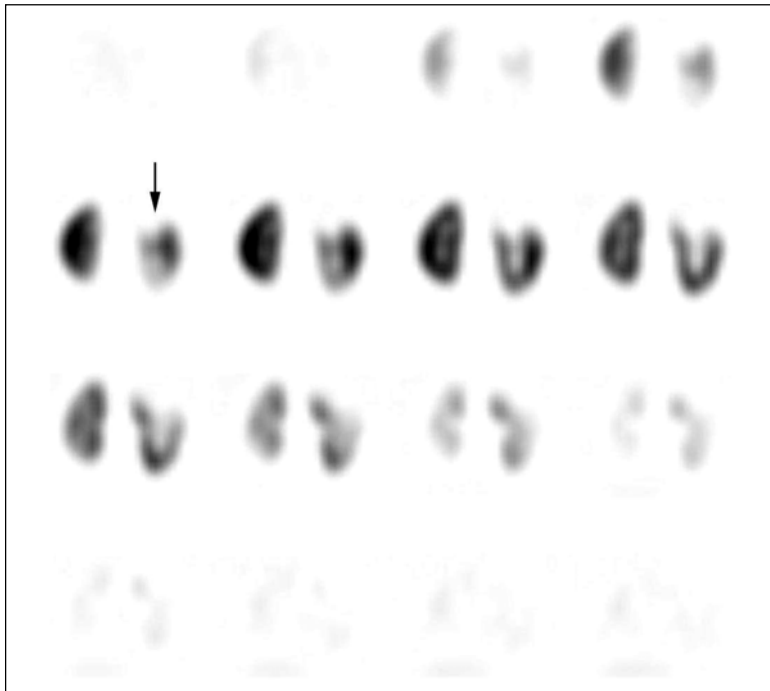
9

Figure 2. Coronal tomographic (SPECT) slices from a 99mTc-DMSA study. The slices go from posterior to anterior through the kidney. Note that the display orientation for SPECT is the same as for CT: the right side of the patient is on the left side of the image. The defect in the upper pole of the left kidney (arrow) is due to either acute pyelonephritis or a scar.

99mTc-Glucoheptonate (99mTc-GHA)

Glucoheptonate is a small carbohydrate that is partly filtered, partly secreted and partly (10-20%) retained in the proximal tubular cells. Its extraction efficiency is the same as that of 99mTc-DTPA. Delayed views at 2-4 hours show good images of the renal cortex, similar to 99mTc-DMSA. It is the preferred tracer for renal trauma assessment because of its ability to image perfusion, excretion and cortical integrity.

Non-Imaging Agents

125I-iothalamate is used as a tracer for GFR assessment. The energy of the photons emitted by iodine-125 is too low for imaging, and the 60 day half-life of this isotope requires a very small injected dose. GFR assessment involves plasma sampling and counting the radioactivity in a well counter.

51Cr-EDTA is a chelate similar to 99mTc-DTPA and is likewise filtered by the glomeruli. The compound is stable and the isotope long-lived. This agent is extensively used in Europe but has limited availability in North America.
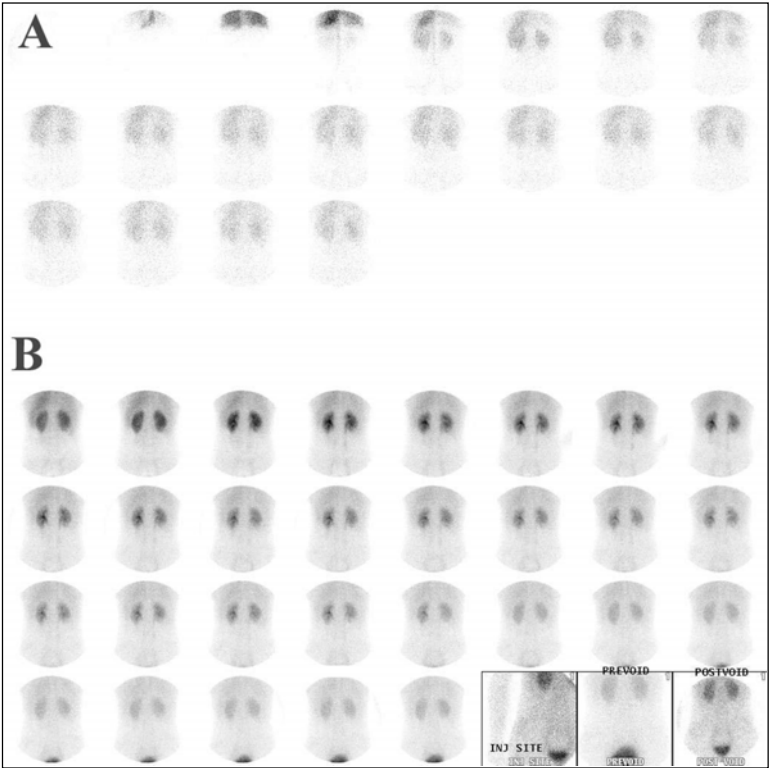
Figure 3. Normal ^{99m}Tc-DPTA scan. In the early part of the flow phase at 3 seconds per frame (A), the kidneys appear at the same time as the aorta. The left kidney is as intense or more intense than the spleen. In the 1 minute per frame dynamic images (B), activity is seen in the collecting systems and ureters by 2-3 minutes. Note that the bladder is not in the field of view in most of the dynamic images. Better positioning (bottom row on right: pre and post void images) allows visualization of the bladder. Note the image of the injection site (bottom row, third from right) showing no extravasation of tracer.

Procedure

The most important consideration in preparing a patient for renal scintigraphy is hydration (specifics are dealt with in the individual sections). For GFR quantification, it is suggested that the patient avoid eating a heavy meal for 4 hours prior to the study as a heavy protein load can increase GFR. It is also important to review the patient's recent medication use and hemodynamic status, particularly if pharmacological interventions (e.g., captopril stimulation) are anticipated.

Typically, the gamma camera is placed posterior to the patient. (Keep in mind that the images are displayed from the camera's perspective—in a posterior acquisition, the patient's right side is on the right side of the image, just as if the eyes of the
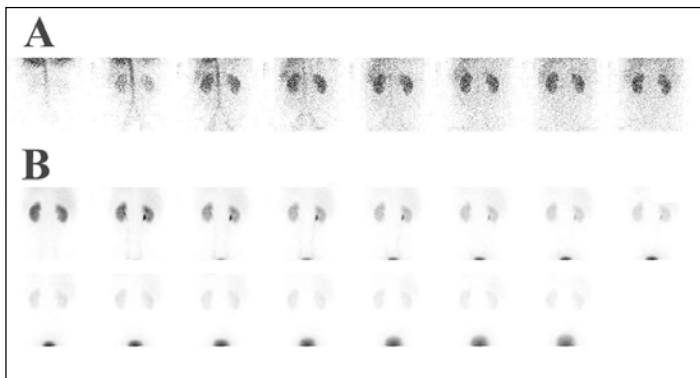
Figure 4. ^{99m}Tc-MAG3 flow (A) and sequential images (B). These show much better contrast between kidney and background than ^{99m}Tc-DTPA for two reasons: the higher first pass extraction efficiency of ^{99m}Tc-MAG3 and the fact that ^{99m}Tc-MAG3 is highly protein bound, so very little of it diffuses into the extravascular extracellular space, leaving a higher concentration available for excretion. Note that while the study was acquired at 1 minute per frame, the images are displayed as sequential 2 minute images. The time activity curves on the bottom reflect the normal rapid increase (uptake phase) and subsequent decrease (excretion phase) in renal tracer concentration seen with ^{99m}Tc-MAG3.

observer were behind the patient). Transplanted kidneys are more anterior than native kidneys, so the study is acquired with the camera anterior to the abdomen and pelvis.

As with any nuclear medicine procedure, renal scanning involves injecting a radioactive tracer and watching where it goes. Renal perfusion can be assessed with the various ^{99m}Tc-labeled tracers with the camera set to take rapid sequence images at a rate of 1-3 seconds per frame during the first minute of the acquisition. The remaining 20-30 minutes of the study is usually performed at a framing rate of 20-60 seconds to evaluate the uptake and excretion phases (Figs. 3 and 4). A 30-second image of the injection site is highly recommended at the end of the study. If a substantial portion of the injection is interstitial instead of intravenous, this can have a great effect on the renogram, with delayed excretion and a stretched-out curve. Interstitial injections invalidate efforts to quantify renal function.

Quantification of Renal Function

Computer Analysis of Renal Scans

By placing appropriate regions of interest (ROIs) over the kidneys, various parameters of renal function can be derived. These include differential renal function measurements, renogram curves generated from ROIs placed around the entire kidney (Fig. 5), renogram curves generated from ROIs placed over the cortex of the kidney (Fig. 6), and pelvic emptying curves (Fig. 7).
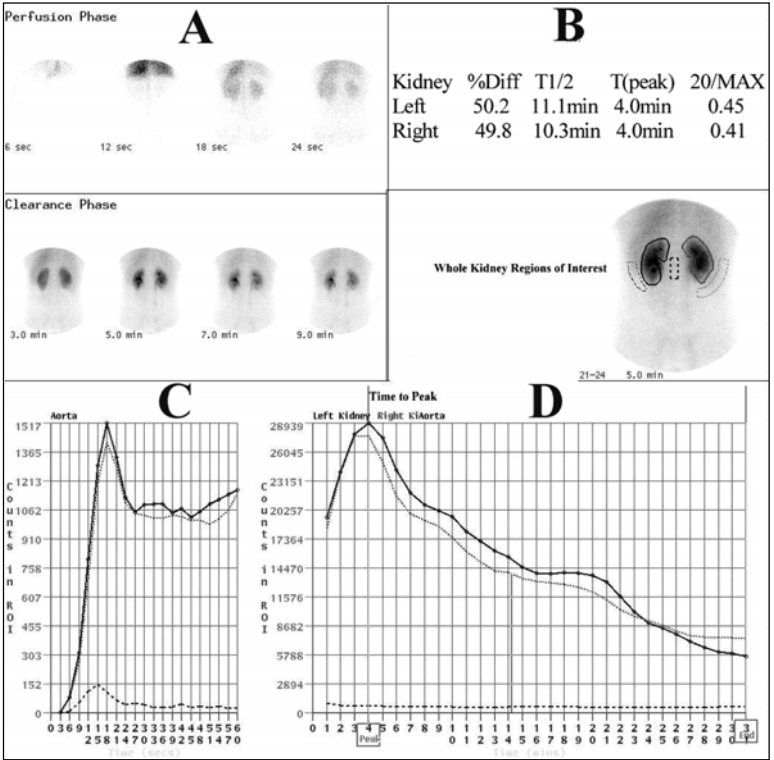
Figure 5. Renogram curves and differential renal function. Selected images from the flow and clearance phases are shown in (A). Five regions of interest have been drawn on an early image: left and right kidneys, "background" ROIs placed inferolateral to the two kidneys and an ROI placed over the aorta. These are used to derive a variety of quantitative measures (B) including each kidney's contribution to total renal function expressed as a percentage of the sum of the background corrected counts from the kidney ROIs. The calculation of differential renal function (%DIFF) is performed on data from one of the early images, before any activity has reached the collecting system. Flow (C) and renogram (D) curves are shown. The latter are time activity curves of the net counts within the previously drawn renal ROIs applied to the series of thirty 1 minute images and corrected for the background. (Correction for non-renal background activity is accomplished by subtracting [counts per pixel in background] x [number of pixels in kidney] from total counts in the kidney ROI.) The "time to peak" activity (Tpeak or Tmax) can be read off the graph (4 minutes in this example). This is the time when uptake in the kidney equals excretion. The rate of parenchymal clearance is expressed as the half-time (T 1/2) and the ratio of 20 minute to peak activity (20/MAX).
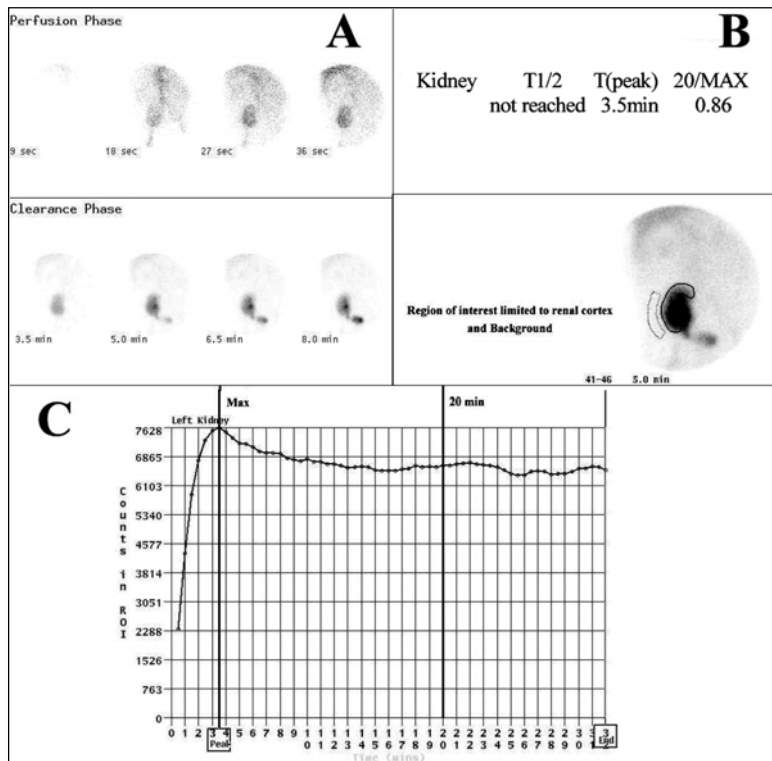
Figure 6. Cortical curve derived from a ^{99m}Tc-MAG3 renal transplant scan in a patient with acute tubular necrosis (ATN). Selected images from the anterior flow and clearance phases show the transplant in the right iliac fossa (A). The region of interest for the kidney includes cortex only, to avoid interference from the collecting system. The "20min/max" ratio can be used as an index of the rapidity of clearance from the renal cortex (B). The values for the maximum renal activity and the activity at 20 minutes can be read off the renogram curve. In this example the 20min/max ratio is high at 0.86. Note the relatively poor clearance from the renal cortex that can be appreciated visually and on the renogram curve (C).

Renal physiology Rate (GFR)

Non-imaging methods can be used to calculate the clearance of tracers. If ^{99m}Tc-DTPA is used, the GFR can be calculated. After injection, the tracer is assumed to mix rapidly in the blood leading to a uniform plasma concentration. The tracer then diffuses out of the plasma into the extracellular fluid (ECF) and eventually the intravascular and extracellular compartments reach equilibrium. The concentration of tracer in the plasma declines over time because of diffusion into the ECF and renal excretion. For example, Figure 8 is a plot of activity concentration over time on a semi-log graph after the injection of ^{99m}Tc-DTPA into a patient. The figure is
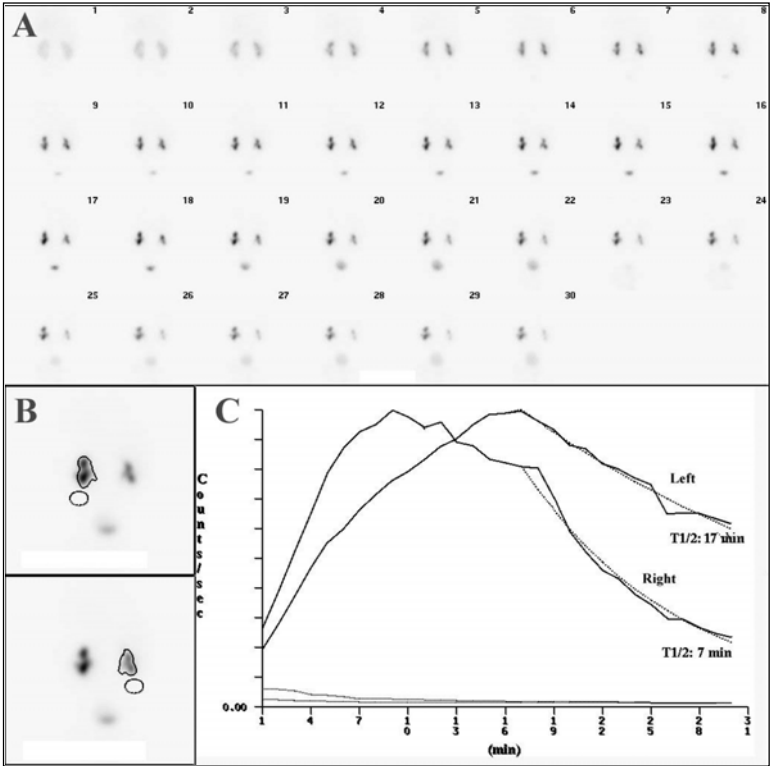
Figure 7. Calculation of pelvic emtying in response to diuretic. Sequential 1 minute images are shown in (A). Furosemide was injected at 12 minutes. Visually, the right renal pelvis is seen to empty while there is slower emptying from the left renal pelvis. Pelvic emptying in response to diuretic can be quantified by taking data from regions of interest drawn around the collecting systems (B). An exponential curve is fitted to the excretion portion of the curve and the half-time of excretion is determined (C). In this case, the right renal pelvis empties with a half-time of 7 minutes and the left with a half-time of 17 minutes. (A half-time of < 10 minutes is normal while > 20 minutes is associated with obstruction. A half-time of between 10 and 20 minutes is indeterminate and indicates the need for close follow-up.)

a computer-generated graph, similar to what would be obtained by taking multiple plasma samples over several hours. The rate of decline measured from these samples can be used to calculate GFR.

In clinical practice, it is not practical to take multiple plasma samples over 6-8 hours. One popular method of GFR calculation uses two plasma samples obtained one and three hours after ^{99m}Tc-DTPA injection, and fits the data into a regression equation derived from an eight sample 2-compartment model. An imaging approach
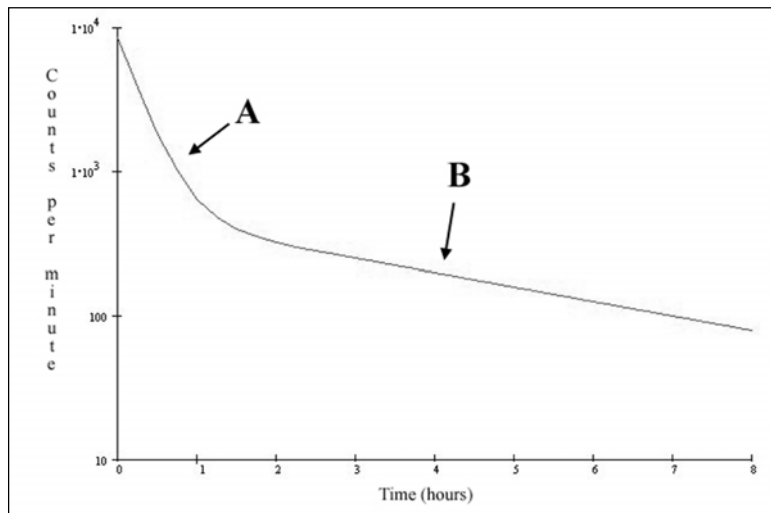
Figure 8. Computer-generated example of a plasma disappearance curve. The y-axis is logarithmic, i.e., the same as a graph on semi-log paper. The early steep part of the curve (A) represents a combination of renal excretion of tracer and tracer diffusing from the intravascular fluid compartment. The shallower portion of the curve (B) represents renal excretion of activity from the extracellular fluid. Analysis of the second portion of the curve allows for calculation of the clearance of the material (which in the case of ^{99m}Tc-DTPA is the GFR).

to measuring GFR (the "Gates" method) involves placing ROIs over both kidneys and calculating the uptake in the kidneys as a percentage of the injected dose (after correcting for scatter and soft tissue attenuation). A regression curve is used to relate this percentage to GFR.

Clinical Role in Acute Renal failure

Clinical

A large number of disorders (Table 1) can precipitate acute renal failure (ARF) and a detailed discussion is beyond the scope of this handbook. Pre-renal causes predominate, followed by renal and post-renal causes. A systematic approach to differential diagnosis and management is required since complete recovery is possible in many cases.

Usually the differential diagnosis can be narrowed following a thorough clinical assessment and the following limited investigations: urinary electrolytes (to calculate fractional excretion of sodium as a marker of pre-renal azotemia), urinalysis (to look for active sediment from glomerular or interstitial inflammation), and renal ultrasonography (to exclude obstructive hydronephrosis). Biopsy is reserved for patients in whom pre-renal and post-renal failure have been excluded and the cause of intrinsic renal azotemia is unclear. Renal biopsy is particularly useful when clinical

Table 1. Causes of acute renal failure

PRERENAL AZOTEMIA
I. Hypovolemia
  Hemorrhage, burns, dehydration, gastrointestinal fluid loss, sequestration in extravascular space
II. Low cardiac output
  Cardiac failure, arrhythmia, tamponade, massive pulmonary embolus
III. Altered renal-to-systemic vascular resistance ratio
  Systemic vasodilation: sepsis, antihypertensives, anaphylaxis
  Renal vasoconstriction: hypercalcemia, norepinephrine, epinephrine, cyclosporine, amphotericin B
  Hepatorenal syndrome
IV. Renal hypoperfusion with impairment of renal autoregulatory responses
  Cyclooxygenase inhibitors, angiotensin-converting enzyme inhibitors

INTRINSIC RENAL
I. Renovascular obstruction (bilateral or unilateral with one functioning kidney)
  Renal artery obstruction: thrombosis, embolism, dissection, vasculitis
  Renal vein obstruction: thrombosis, compression
II. Disease of glomeruli or renal microvasculature
  Glomerulonephritis and vasculitis
  Hemolytic uremic syndrome, thrombotic thrombocytopenic purpura, scleroderma
III. Acute tubular necrosis
  Ischemia (as for prerenal azotemia)
  Toxins: radiocontrast, cyclosporine, aminoglycosides, cisplatin, ethylene glycol, acetaminophen, endogenous (rhabdomyolysis, hemolysis, uric acid, oxalate)
IV. Interstitial nephritis
  Allergic: antibiotics, nonsteroidal anti-inflammatory agents, diuretics, captopril
  Infection: acute pyelonephritis, viral (e.g., CMV), fungal
  Infiltration: lymphoma, leukemia, sarcoidosis
  Idiopathic
V. Intratubular deposition and obstruction
  Myeloma proteins, uric acid, oxalate, acyclovir, methotrexate, sulphonamides

POSTRENAL (OBSTRUCTION)
I. Ureter
  Calculi, blood clot, sloughed papillae, cqncer, retroperitoneal fibrosis
II. Bladder neck
  Neurogenic bladder, prostatic hypertrophy, calculi, cancer, blood clot
III. Urethra
  Stricture, congenital valve, phimosis

9

assessment and laboratory investigations suggest diagnoses other than ischemic or nephrotoxic injury that may respond to disease-specific therapy. Examples include glomerulonephritis, vasculitis, and allergic interstitial nephritis.

   Definitive diagnosis of post-renal azotemia hinges on judicious use of radiologic investigations and rapid improvement in renal function following relief of obstruction. Anuria suggests complete urinary tract obstruction.

   Although nuclear imaging can measure whole and regional GFR precisely, this is of limited value in the assessment of the patient with obvious renal failure. A standard renal scan can tell if renal function is symmetric or asymmetric, can assess relative renal size and say something about ureteric obstruction. (Ultrasound, of course, is the first line investigation for renal size and obstruction.) The most important finding on a renal scan is preserved renal perfusion despite severely impaired function. This is the typical finding in acute tubular necrosis (ATN), and the preserved perfusion implies a good prognosis for return of function. If both perfusion and function are severely impaired, the prognosis is worse. Importantly, nuclear medicine can contribute to the diagnosis of two specific causes of renal failure: allergic interstitial nephritis and renal infarction.

Allergic Interstitial nephritis

   Renal failure associated with fever, arthralgias, and a pruritic erythematous rash following exposure to a new drug suggests allergic interstitial nephritis (AIN), even though systemic features of hypersensitivity are frequently absent. Eosinophiluria (>5 percent of urine leukocytes) is a common finding (90 percent) in antibiotic-induced AIN when studied using Hansel's stain; however, lymphocytes may predominate in AIN induced by nonsteroidal anti-inflammatory drugs. Eosinophiluria may also be seen in atheroembolic ARF. Treatment consists of identifying and discontinuing the offending agent and high-dose glucocorticoid therapy.

   ^{67}Ga-citrate can help support a clinical diagnosis of AIN which is distinguished from other forms of acute renal failure by intense renal uptake of gallium 48 hours or more after injection (Fig. 9). Non-inflammatory ATN typically shows little or no gallium accumulation. Unfortunately, gallium uptake is not a specific finding and is seen in a variety of inflammatory (lupus and pyelonephritis) and non-inflammatory states (proteinuric nephropathy and amyloidosis).

Renal infarction

   Autopsy studies suggest that embolic renal infarction is under-diagnosed antemortem. Flank pain may be a prominent symptom following occlusion of a renal artery or vein, but clinical and laboratory evidence of renal infarction may be completely lacking. Scintigraphy can help to differentiate renal infarction from renal parenchymal disease (Fig. 10).

Clinical Role in Hydronephrosis

Clinical

   Not all dilated renal collecting systems are obstructed (Fig. 11). The collecting system can remain dilated indefinitely after a previous episode of obstruction is relieved. Vesicoureteral reflux causes dilatation, and megaureter can be congenital. Relative obstruction can occur at high outflow states (Fig. 12). The term obstructive uropathy refers to dilatation of the renal pelvis and calyces caused by obstruction. Obstructive nephropathy refers to functional impairment of the kidneys caused by obstruction. Obstructive nephropathy can be as severe as absence of function in the
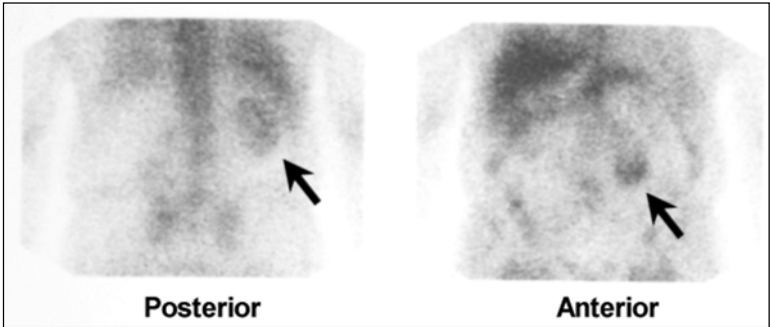
Figure 9. Acute allergic interstitial nephritis. Acute renal failure necessitating hemodialysis developed following a one week illness characterized by dyspnea, peripheral edema and low-grade fever. Renal ultrasound was essentially normal aside from a large left renal cyst displacing the left kidney anteriorly. A renal scan showed good perfusion with symmetrically reduced function. A diagnosis of acute tubular necrosis (ATN) was made initially based upon renal biopy though no significant antecedent illness was identified. Six weeks later the patient was still dialysis-dependent and the diagnosis was re-evaluated with a gallium scan. Moderate diffuse gallium uptake is seen in both kidneys (arrow on posterior image points to the right kidney, arrow on anterior image points to the left kidney). A repeat biopsy showed typical acute interstitial nephritis with eosinophil infiltration. The patient was treated with prednisone 60 mg daily and within one week his serum creatinine was normal and he was off dialysis. The first renal biopsy was reviewed and in retrospect was felt to show foot process fusion typical of minimal change nephropathy. The combination of minimal change nephropathy and interstitial nephritis has been reported with NSAID's; the patient was on ASA and this is the presumed (but unproven) cause. (Case provided by Dr. W.D. Leslie.)

involved kidney. Pediatric kidneys, in particular, have a remarkable propensity to recover function when obstruction is relieved (Fig. 13).

By provoking maximal urine flow with furosemide, the patency of the urinary outflow tract can be assessed with a technique known as diuretic renography. This is useful to determine the significance of a dilated pelvicalyceal system. Prompt washout of tracer from the collecting system and renal pelvis effectively rules out functionally significant obstruction.

Procedure

Adequate hydration of the patient is critical for diuretic renography. When the patient is dehydrated, excretion of tracer is impaired as is the response to furosemide. Adults and older children can be hydrated orally with water (5-10 ml/kg) before the study. Younger children should receive oral hydration ad libitum beginning two hours before the study, and intravenous hydration of 15 ml/kg over a 30-minute period beginning 15 minutes before tracer injection.

The patient should void before the study. A urine specific gravity greater than 1.015 indicates inadequate hydration. A full bladder can prevent proper drainage of
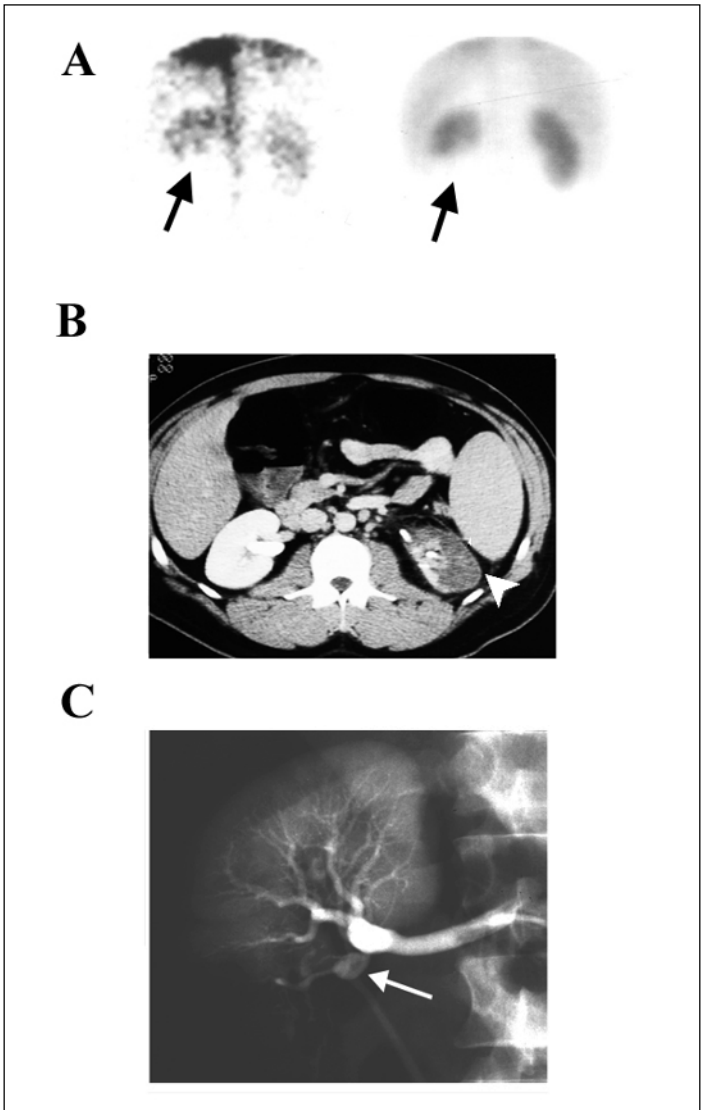
9

Figure 10. Renal infarct. 99mTc-DTPA flow and early static images (A) show absent flow and function in the lower pole of the left kidney (black arrows) in this patient with recent onset of flank pain. The CT scan (B) shows lack of contrast enhancement in the left kidney cortex (white arrowhead). A selective left renal angiogram (C, shown in the same orientation as the renal scan) shows an aneurysm arising from the left renal artery which is occluded distally (white arrow).
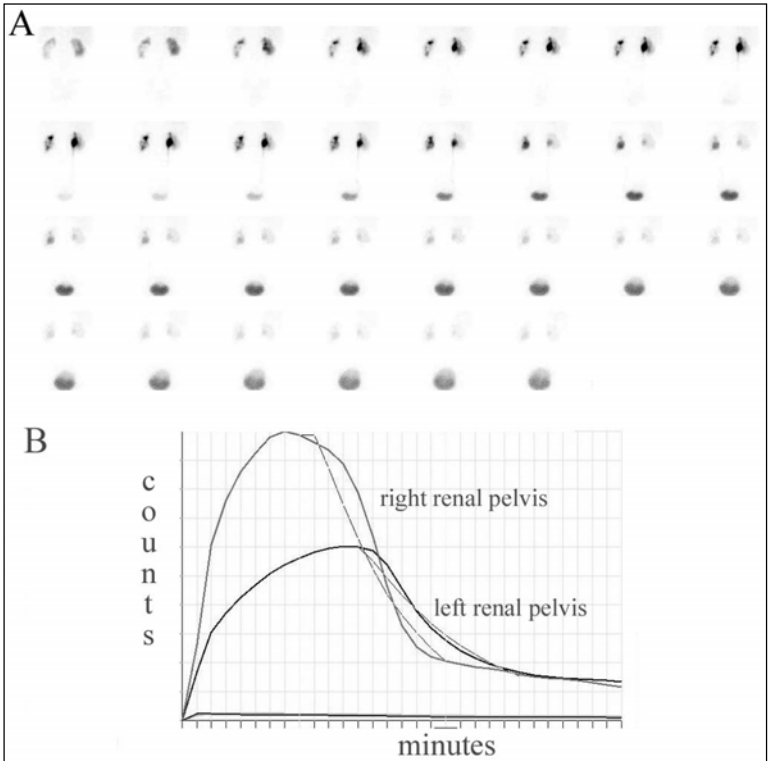
Figure 11. Non-obstructive hydronephrosis. Sequential 1 mintue images (A) show relatively diminished function on the left with hold-up of tracer in both renal collecting systems. Furosemide was given at 12 minutes with rapid emptying of the renal pelves. Time activity curves (B) were generated from regions of interest placed over the renal pelves and exponential curves fitted to the excretion portion of the curves. The half times are normal (<5 minutes) bilaterally.

the collecting systems by backpressure. Bladder emptying may need to be assured by catheterization, especially in cases of bladder dysfunction and known vesicoureteric reflux.

Because of its rapid excretion, ^{99m}Tc-MAG3 is preferred over ^{99m}Tc-DTPA. Activity in the renal pelvis and calyces will be greater before furosemide is given and will be washed out with urine of lesser activity, thus maximizing contrast between the pre and post diuretic images.

Furosemide is given intravenously at a dose of 40 mg for age > 16 years and 0.5-1 mg/kg for children. It is given if significant activity remains in the collecting system after a post-void view following a standard 20-minute renogram ("F+20" protocol). A further 15-20 minute study is then acquired.
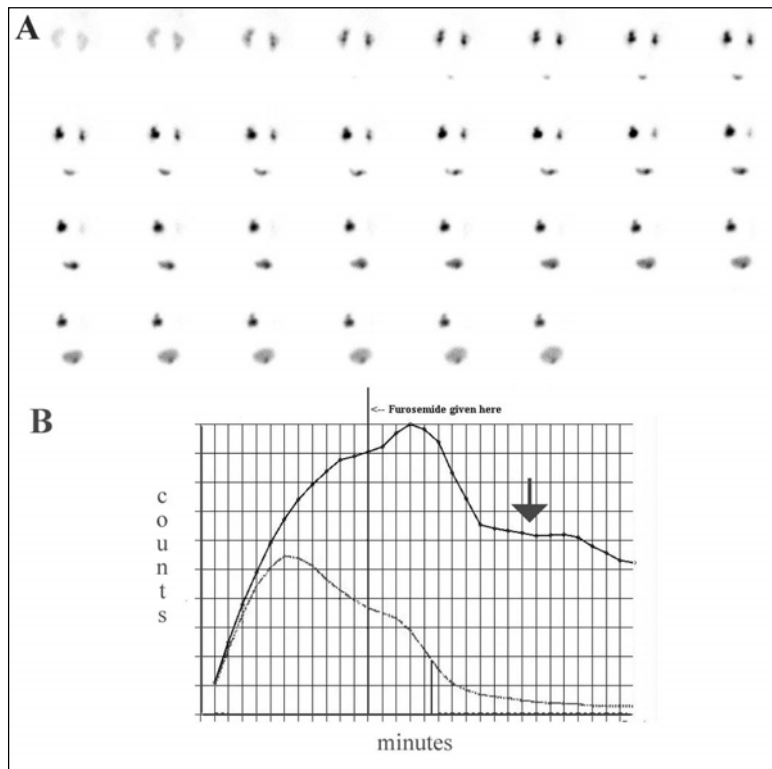
Figure 12. Flow-related obstruction. Sequential 1 minute images (A) and pelvic emptying curves (B) show rapid emptying from the right renal pelvis. On the left, there is an initial good response to furosemide but the clearance curve reaches a plateau (arrow) indicating flow-related obstruction (Homesy's sign).

The "F-15" protocol is an alternate protocol for furosemide administration that can be used in equivocal cases. The furosemide is given 15 minutes before tracer injection. The peak diuretic response to furosemide response is at 15-18 minutes after intravenous injection, so this approach allows maximum diuresis at the time of maximum tracer excretion. In intermittent hydronephrosis from extrinsic mechanical ureteropelvic junction obstruction, the urinary flow rate may not keep pace with increases in pelvic pressure. In some cases flow can actually decrease at high pressures because the ureteropelvic junction becomes self-obstructing ("kinked") as the pelvis enlarges (Fig. 12).

Processing and Interpretation
As described earlier, regions of interest are drawn around the renal collecting system and pelvis of each kidney and curves are generated from the post-diuretic
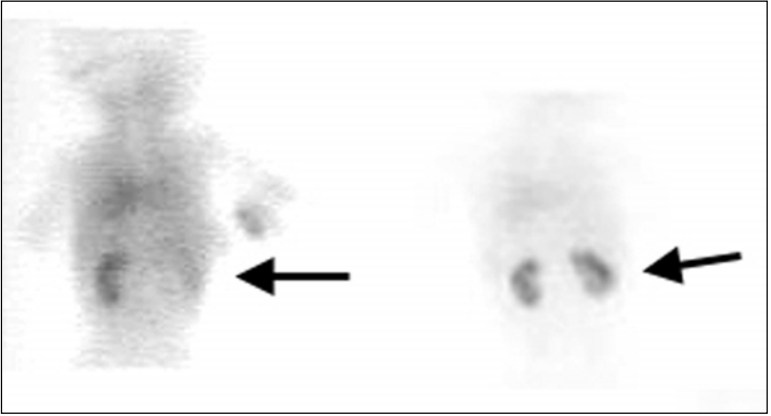
Figure 13. Recovery of renal function post pyeloplasty. Early ^{99m}Tc-MAG3 static images on a 6 month old infant before (A) and 10 months after a right pyeloplasty (B). There is minimal tracer accumulation in the kidney before the procedure and normal uptake following relief of obstruction.

study. The downslope of the curve from the moment of first action of furosemide to the end of the study is fitted to an exponential function from which is derived the excretion half-time. An unobstructed system will show rapid emptying and a sharp drop in the counts within the regions of interest (Fig. 11). The normal curve will have a concave slope, with a half-time of 10 minutes or less. An obstructed system will show a flat or even rising curve, or a half time of greater than 20 minutes (Fig. 14). In between these easy to recognize extremes are the intermediate curves that require further consideration.

Factors that make interpretation difficult are renal impairment (in which the kidney is incapable of increasing urine output sufficiently to wash out 'hot' urine from the renal collecting system) and large volume renal collecting systems (since the rate of washout will be inversely proportional to the volume). If function is preserved (single kidney GFR of 15 ml/min or greater) in the kidney with a suboptimal response, then an intermediate pattern likely indicates partial obstruction. If the single kidney GFR is less than 15 ml/min, then the study is truly indeterminate. With large volume collecting systems, the F-15 approach may be helpful in a repeat study. If the kidney has normal function, then even partial obstruction may not be functionally significant, and a conservative approach may be warranted.

Clinical Role in Renovascular hypertension

Clinical

Renovascular disease is an important correctable cause of secondary hypertension. While it accounts for less than 1% of mild hypertension, the incidence may be as high as 10-45% in patients with severe hypertension. It is also an increasingly recognized and potentially reversible cause of advanced renal failure. It may be
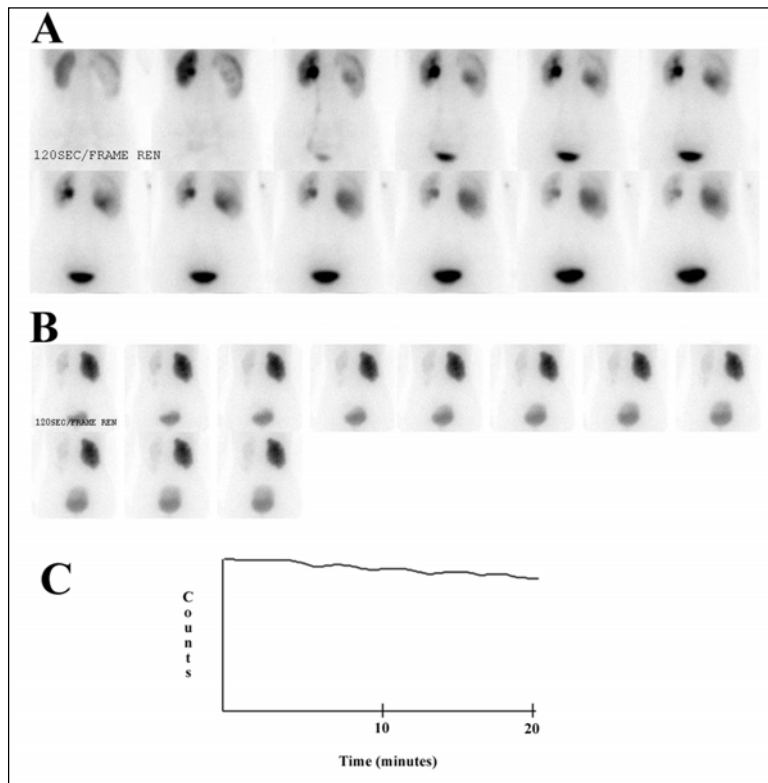
Figure 14. Obstructive hydronephrosis. The first phase (A) shows an enlarged right kidney (on the right hand side of the posterior image) with poor initial cortical uptake and slow filling of a dilated pelvis. The second phase (B) was then started with injection of furosemide 40 mg intravenously. Note that there is negligible clearance from the right renal pelvis visually and on the time activity curve (C). In contrast, the left renal pelvis shows normal drainage even before the diuretic injection.

Table 2. Indicators of renovascular disease

- Abrupt or severe hypertension
- Hypertension resistant to optimal medical therapy
- Onset of hypertension under age 30 or over age 55
- Bruits in the abdomen or flank
- Unexplained renal failure in an elderly hypertensive
- Worsening renal function during therapy with ACE inhibitors
- Hypertensive retinopathy (grade 3 or 4)
- Hypertension with asymmetric renal size, atherosclerotic heart or peripheral vascular disease
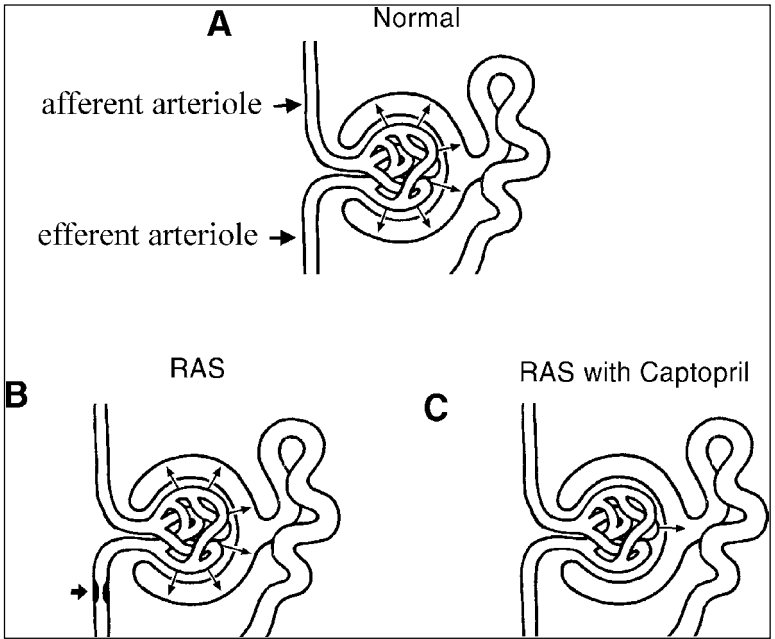

Figure 15. Principle of ACE inhibition (captopril) renography. In a normal patient (A), blood is delivered to the glomerulus via the afferent arteriole and leaves by the efferent arteriole. Normally, there is a sufficiently high glomerular pressure to allow for renal physiology (represented by arrows) across the capillary membrane and Bowman's capsule. In a patient with renal artery stenosis and renovascular hypertension (B), the initial drop in blood pressure in the glomerulus is counteracted with angiotensin II-mediated vasoconstriction of the efferent arteriole (arrow). Glomerular pressure and hence renal physiology is maintained. If captopril is administered (C), the efferent arteriole relaxes with a subsequent drop in glomerular pressure and filtration. This decrease in renal physiology can be detected with renal scanning. (Figure provided by Dr. I.D. Greenberg.)

secondary to atherosclerosis or, in the younger patient, fibromuscular dysplasia. Clinical indications to pursue renovascular hypertension are summarized in Table 2.

Renovascular disease is also the most difficult secondary cause of hypertension to detect non-invasively. The gold standard for diagnosing renal artery stenosis is the conventional renal angiogram. Renal artery stenosis can also be demonstrated by MRI and duplex ultrasonography. However, the demonstration of renal artery stenosis does not guarantee that the stenosis is causing renovascular hypertension. Furthermore angiography is associated with a risk of making renal failure worse secondary to iodinated radiographic contrast or cholesterol emboli.

Because of the low incidence of renovascular hypertension, a highly sensitive screening test is necessary. The captopril renal scan is the most useful test for detecting
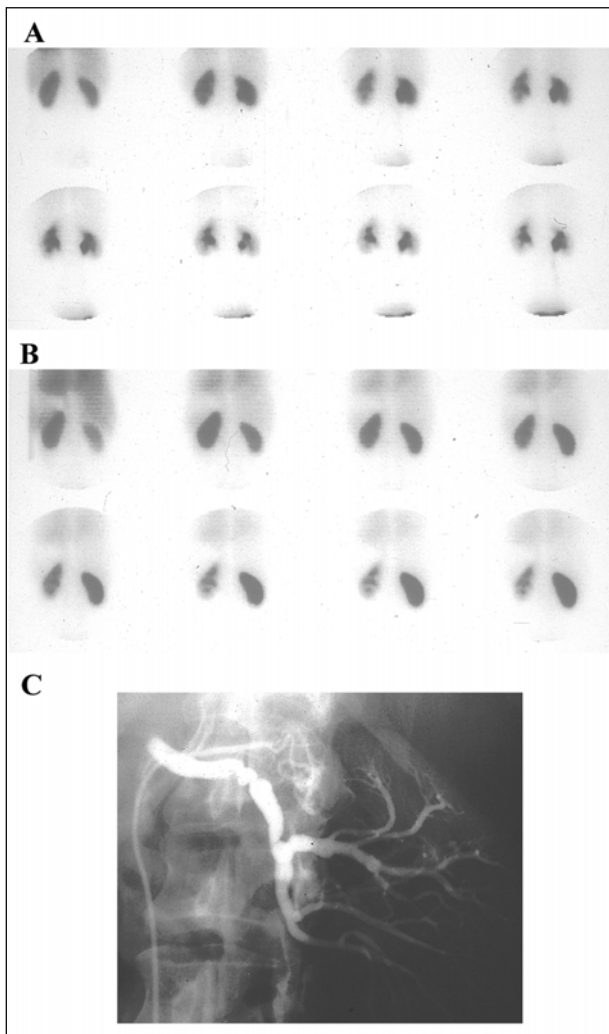
Figure 16. Renovascular hypertension secondary to fibromuscular hyperplasia in a young woman. The baseline ^{99m}Tc-DPTA study (A) shows mild asymmetry in initial renal uptake with quantitation (not shown) attributing 40% of renal function to the right kidney. There is normal clearance of tracer from the renal parenchyma. Following captopril (B), initial uptake on the right decreases with quantitation now attributing 30% of function to the right kidney. Clearance from the right kidney is slowed with marked parenchymal retention. A renal angiogram (C, inverted to correspond to the scan) shows fibromuscular hyperplasia.

Table 9.3 Change in tracer handling after angiotensin converting enzyme (ACE) inhibitor challenge for affected kidneys in renovascular hypertension

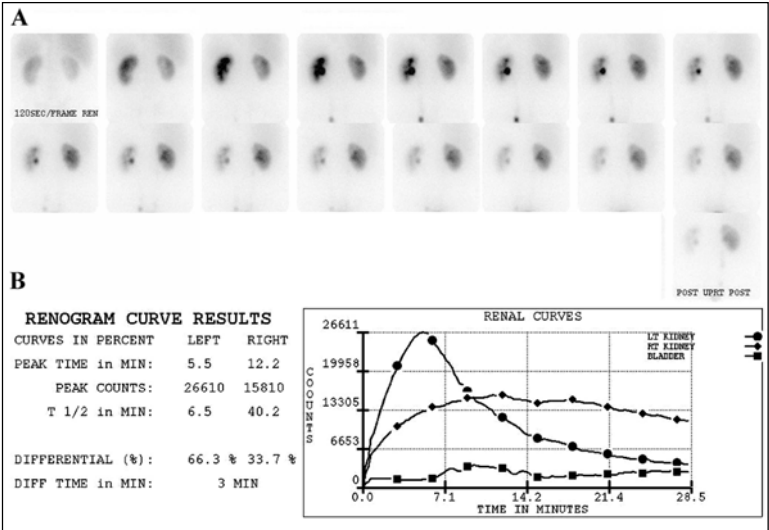|	Uptake	Transit
99mTc-DTPA	Decreased	Prolonged
99mTc-MAG3	No change	Prolonged

Figure 17. 99mTc-MAG3 scan in a patient with renovascular hypertension. (A) Sequential 2 mintue images show diminished initial uptake and slow clearance of tracer from the right kidney. Uptake and clearance on the left are normal. The same findings are evident on the renogram curves (B). The left kidney shows a normal renogram. The "time to peak" activity on the right is 12 minutes compared to 6 minutes on the left while the degree of parenchymal retention is considerably higher.

unilateral disease in patients with GFR > 30 ml/min. An unstimulated renal scan has a false negative rate of 20- 25%. The predictive value of scanning can be increased by performing a captopril-stimulated renal scan in the patient with normal or minimally impaired renal function (GFR > 30 ml/min) who is not on an ACE (angiotensin converting enzyme) inhibitor or AT1 (angiotensin type 1) receptor antagonist. In properly selected patients, the sensitivity and specificity of high probability findings approach 90%. A normal study will show symmetric uptake and prompt excretion on both the baseline and captopril studies and implies a low (<10%) probability of renovascular hypertension.
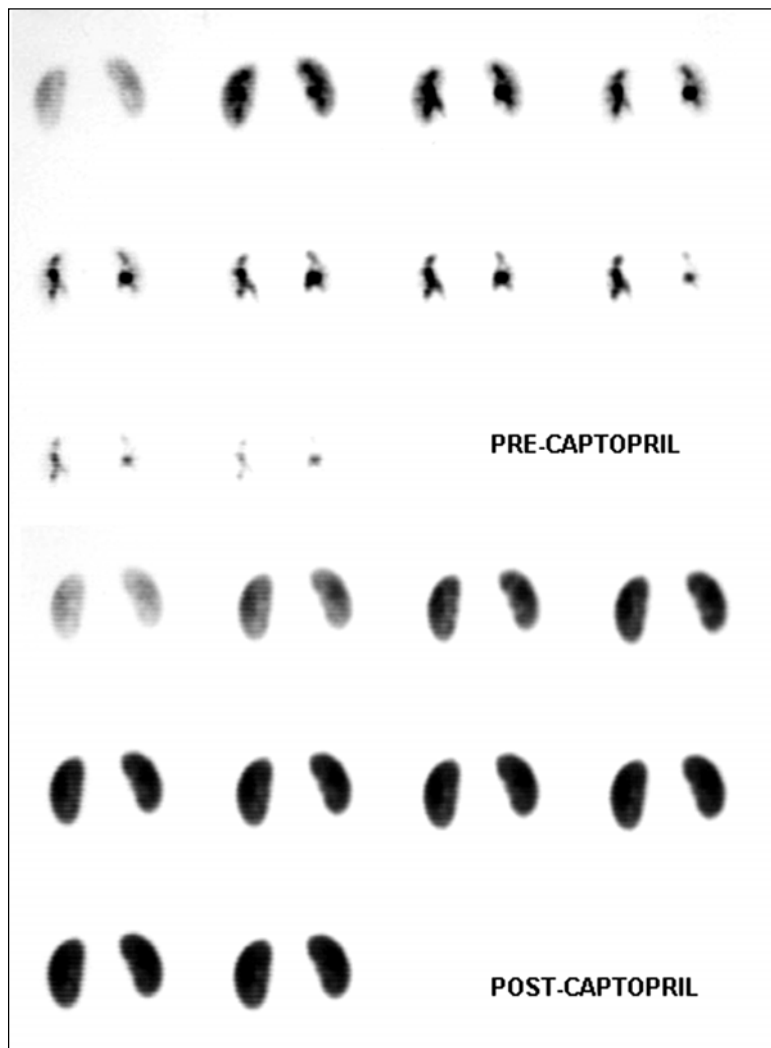
Figure 18. Bilateral symmetrical captopril induced changes. Testing was performed in this young woman with uncontrolled hypertension after interruption of ACE inhibitor therapy for 72 hours. The baseline ^{99m}Tc-MAG3 study (A) is normal. Following captopril (B), there is marked parenchymal retention symmetrically in the kidneys. This is a non-specific response that is attributed to a modest drop in the patient's blood pressure (from 150/90 to 135/75). (Case provided by Dr. W.D. Leslie.)
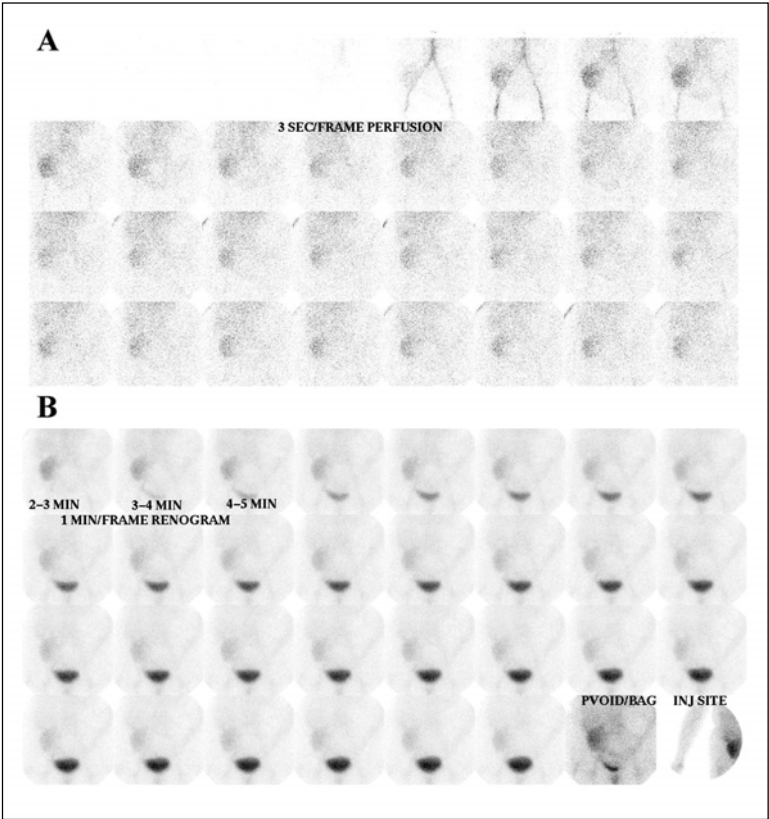
Figure 19. ^{99m}Tc-DPTA scan in a normal renal transplant. Both the flow (A) and 1 minute sequential images (B) are normal.

Pathophysiology

Renal artery stenosis causes a drop in pressure in the glomerulus. This would be expected to result in a loss of filtration were it not for compensatory mechanisms instigated by the juxtaglomerular apparatus (JGA). In response to inadequate pressure within the afferent arteriole of the glomerulus, the JGA produces renin which converts angiotensinogen to angiotensin I. Angiotensin I is subsequently converted to angiotensin II, a potent vasoconstrictor. Angiotensin II causes constriction of the efferent arteriole and results in increased pressure in the glomerulus and restoration of glomerular filtration. Angiotensin II also stimulates aldosterone which potentiates sodium retention and potassium secretion in the distal nephron. Both angiotensin II and aldosterone contribute to an elevated blood pressure. ACE inhibitors are pharmacologic agents which block the formation of angiotensin II, interrupting the compensatory mechanism of efferent arteriolar vasoconstriction thus lowering GFR in the affected kidney. This serves as the basis for ACE inhibition renography (Fig.
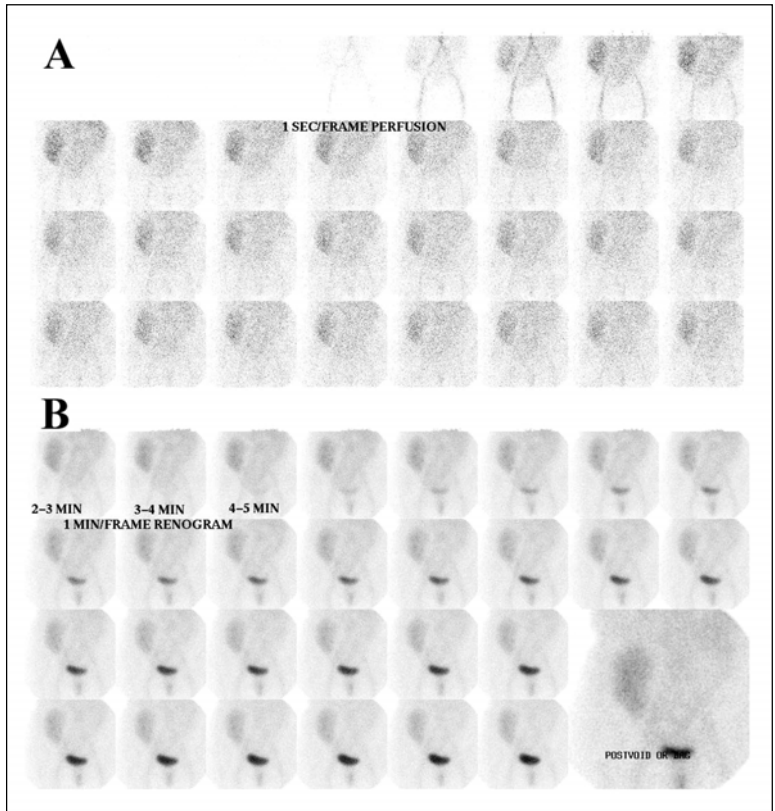
Figure 20. ^{99m}Tc-DTPA scan in a renal transplant with moderate acute tubular necrosis (ATN). Perfusion (A) is normal, but on the sequential images (B) uptake in the kidney is impaired and there is poor contrast between kidney and background.

15). Captopril is short acting, and is given orally for ACE inhibition renography. If a parenteral agent is required, enalaprilat can be used.

Procedure

Hydration is very important to proper performance of this study. Patients should be hydrated to the same extent as for diuretic renography. Captopril and especially enalaprilat can cause hypotension in dehydrated patients and, therefore, blood pressure should be monitored after administration of the ACE inhibitor. If hypotension occurs, the patient should be placed supine with legs elevated and rehydrated with an intravenous saline infusion. Patients for whom hypotension would be dangerous, such as those with a history of stroke, transient ischemic attacks, carotid stenosis or coronary artery disease, should have an intravenous line in place before the ACE inhibitor is given. The patient should not leave the department

until blood pressure has stabilized. There are some drugs which may reduce the sensitivity of ACE inhibitor renography. In our laboratory we discontinue (if possible) ACE inhibitors and AT1 receptor antagonists for 3 days prior to the examination.

Captopril is given orally and its absorption is reduced in the presence of food. Therefore, patients should not eat a solid meal for four hours before the study, though they should drink fluids freely. Captopril 25-50 mg is crushed to enhance absorption and is administered 60 minutes before the tracer. Alternatively, enalaprilat 40 µg/kg to a maximum of 2.5 mg is given intravenously over 3-5 minutes, 15 minutes before the tracer. The use of enalaprilat instead of captopril avoids potential problems with poor gastric absorption, but is associated with a higher incidence of hypotension.

Captopril renograms can often be performed without a baseline examination for comparison because a normal captopril challenge study is sufficient to rule out renovascular hypertension. A baseline study is useful in equivocal cases for detecting subtle captopril-induced transit abnormalities. The baseline and captopril studies can be performed on separate days or on the same day. In the latter situation, a larger dose is given for the captopril study e.g., 50 MBq of ^{99m}Tc-MAG3 for the baseline study and 250 MBq for the post captopril study. The same-day procedure should be considered for patients who have had to discontinue interfering medications, where a return visit would be difficult, and for in-patients since clinical and hydration status can change rapidly from one day to the next.

Processing and Interpretation

If the ACE inhibitor causes a drop in GFR of the involved kidney, the scan findings will depend on the tracer used (Table 3). Since GFR is reduced, ^{99m}Tc-DTPA uptake (a marker of GFR) will be reduced. Indeed, in severe cases, GFR may completely cease. In this case, blood pool activity will be seen in the affected kidney and, as tracer is excreted by the opposite kidney, the blood pool activity will decrease at the same rate as blood pool in other organs such as the liver and spleen. A reduced GFR leads to slowing in bulk urine flow through the kidney and any ^{99m}Tc-DTPA entering the nephron will likewise traverse it slowly i.e., transit through the kidney is prolonged (Fig. 16).

When ^{99m}Tc-MAG3 is used, its initial uptake is unchanged, because even if there is a substantial drop in filtration ^{99m}Tc-MAG3 is still delivered to the proximal convoluted tubule and excreted into the lumen. Because bulk urine flow is reduced, transit through the kidney is prolonged (as with ^{99m}Tc-DTPA). This can be assessed by visual inspection of the images or analyzing renogram curve parameters such as "time to peak" and 20 min/max ratio (Fig. 17). A normal time to peak with ^{99m}Tc-MAG3 is between 2 and 4 minutes. A prolongation of at least 2-3 minutes from the baseline to captopril study, or 40% of the baseline value, is considered significant. The normal 20 min/max ratio is less than 0.30. An increase in this ratio of 0.15 from the baseline study suggests a high likelihood of renovascular hypertension

Bilateral symmetrical changes are usually not due to renovascular hypertension (Fig. 18). Even if renal artery stenosis affects both kidneys, findings will be asymmetric in the vast majority of cases. Symmetrical changes are more likely to be caused by hypotension, dehydration or medications such as calcium channel blockers. A small poorly functioning kidney (< 30% uptake) may not show any change with ACE
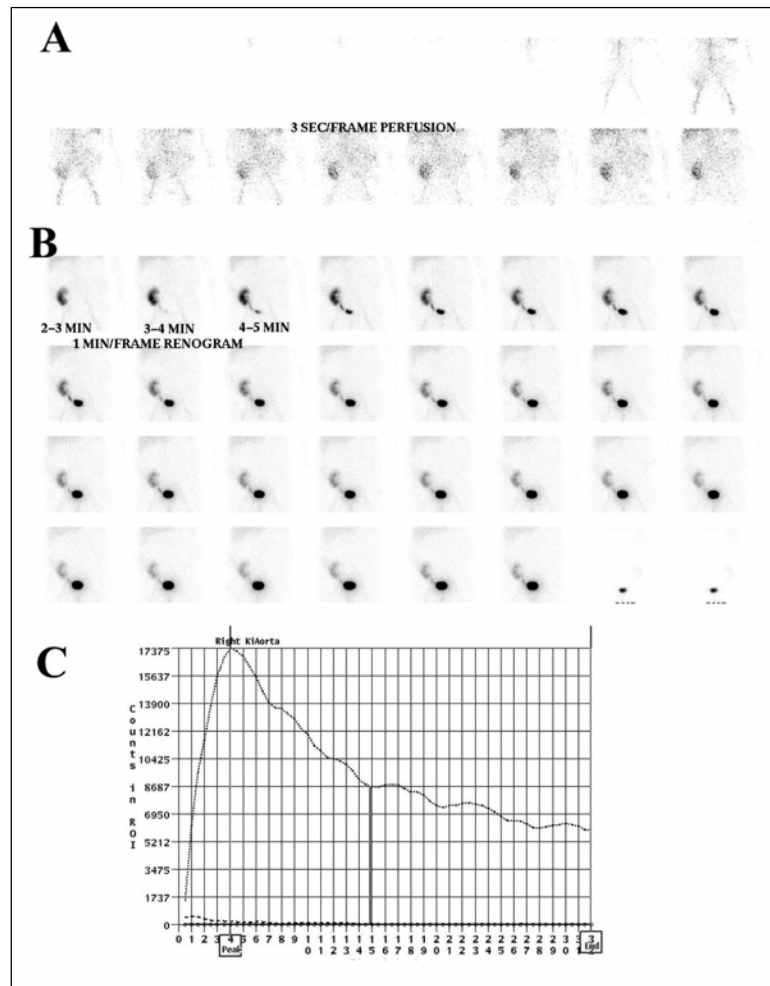
9

Figure 21. ^{99m}Tc-MAG3 scan in a normal renal transplant. Perfusion (A) is normal. There is excellent uptake and rapid excretion seen in both the sequential images (B) and the renogram curve (C).

inhibitor challenge. Such a finding should be interpreted as having an intermediate probability for renovascular hypertension.

Clinical Role in the Renal Transplant Patient

Clinical

Causes of renal failure in the renal transplant patient depend upon when they occur in relation to the transplant procedure. In the immediate post-operative period,
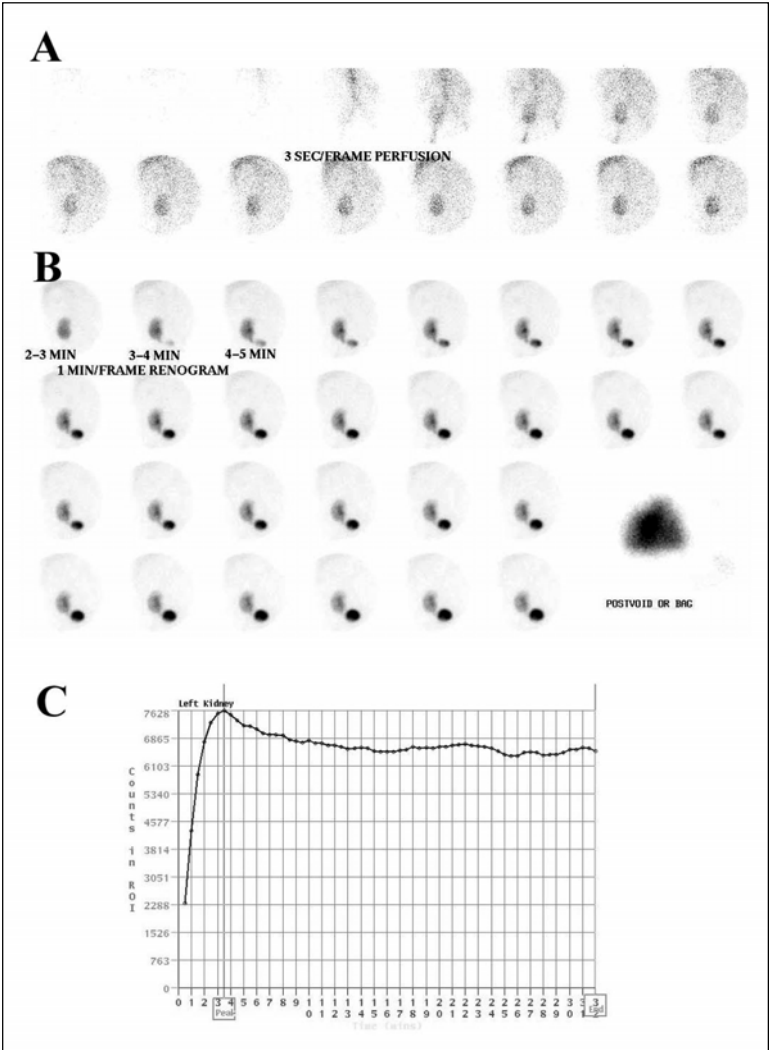
Figure 22. ^{99m}Tc-MAG3 scan in a renal transplant with moderate acute tubular necrosis (ATN). Perfusion (A) is normal. On the sequential images (B), initial uptake is good and there is excretion by 3-4 minutes. Parenchymal retention in the kidney is seen at the end of the study. The persistent activity can be appreciated on the renogram curve (C).
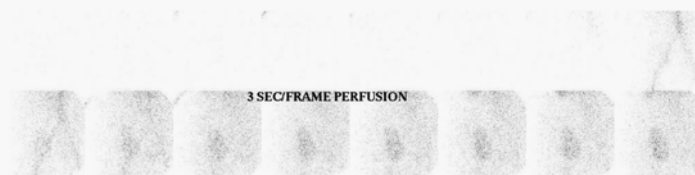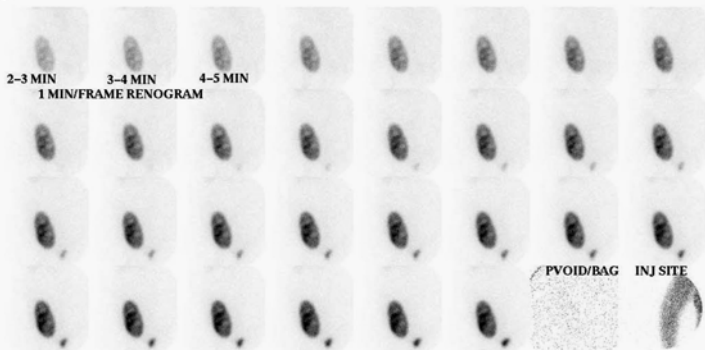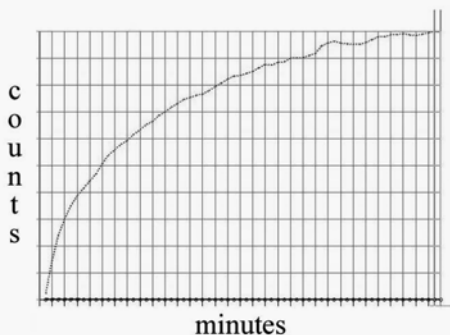
Figure 23. ^{99m}Tc-MAG3 scan in patient with severe acute tubular necrosis (ATN). Perfusion (A) is mildly imparied. The sequential images (B) show good uptake but excretion is greatly delayed and there is progressive accumulation of tracer in the kidney throughout the study. Ureteric obstruction is unlikely, because some activity does reach the bladder (though many transplant recipients have some residual function in their native kidneys which might be responsible for the bladder activity). If there is concern for obstruction, an ultrasound is usually helpful. The renogram curve (C) shows increasing activity in the transplant.

Figure 24. "Black hole sign". ^{99m}Tc-DTPA 1 minute sequential images of a left iliac fossa renal transplant 2 weeks post-op. This 44 year old woman initially had moderate acute tu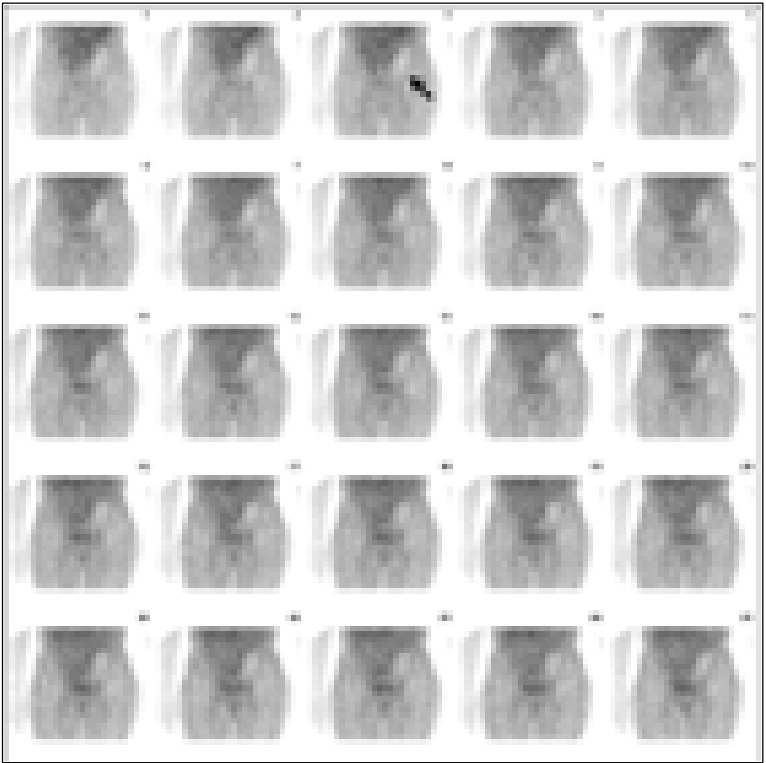bular necrosis (ATN) after a cadaveric transplant. She developed acute rejection 1 week post-op and despite therapy progressed to renal infarction. The black hole sign (arrow) is almost always indicative of a non-viable kidney.

differential diagnosis includes hyperacute vascular rejection, vascular injury, ATN, urinary leak, and obstruction. Late causes include acute or chronic rejection, drug nephrotoxicity (particularly cyclosporine), transplant renal artery stenosis, obstruction, and recurrent primary disease. The role of nuclear imaging in investigating patients is similar to the non-transplant situation. It can be particularly useful in the immediate post-operative period when the patient is oliguric or anuric to differentiate vascular problems from ATN, and to exclude a urinary leak.

Procedure

As noted earlier, the transplanted kidney is located anteriorily in the iliac fossa and therefore the study is performed with the camera in front of the patient. The standard renogram is performed, with a flow phase and a renogram phase (Fig. 19).
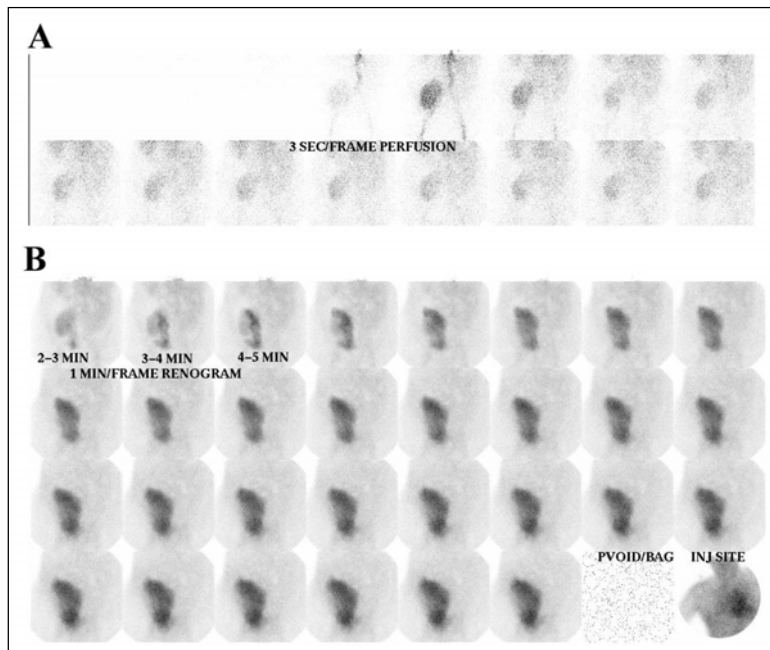
Figure 25. Urine leak post-transplant. Following injection of ^{99m}Tc-MAG3, excreted activity is first seen along the medial and inferior margins of the transplant; by the end of the study it surrounds the graft.

Patient preparation is the same as for any other renogram—hydration is a primary consideration.

Interpretation

Studies performed in the first few days post-op will show varying degrees of harvesting injury. Harvesting injury is very common in cadaveric renal transplants. Living related donor transplants usually fare much better, and renograms can be normal from the early post-operative period. The typical finding is that of ATN with well-preserved perfusion relative to the level of functional impairment. The scintigraphic findings will differ depending upon the tracer used. A ^{99m}Tc-DTPA study will show good perfusion but poor uptake, high background levels and little or no excretion (Fig. 20). In the most severe cases, there will be a noticeable impairment of perfusion. If the first study is done on the first post-op day, subsequent studies done 1-3 days later usually show a drop in perfusion in moderate to severe ATN, presumably because of edema in the kidney. The perfusion findings will be the same with ^{99m}Tc-MAG3. Since ^{99m}Tc-MAG3 uptake is usually much better than ^{99m}Tc-DTPA uptake, the functional impairment usually manifests as prolonged transit through the kidneys with a picture of progressive parenchymal accumulation of tracer throughout the study (Figs. 21, 22 and 23). Severe cases may not show any
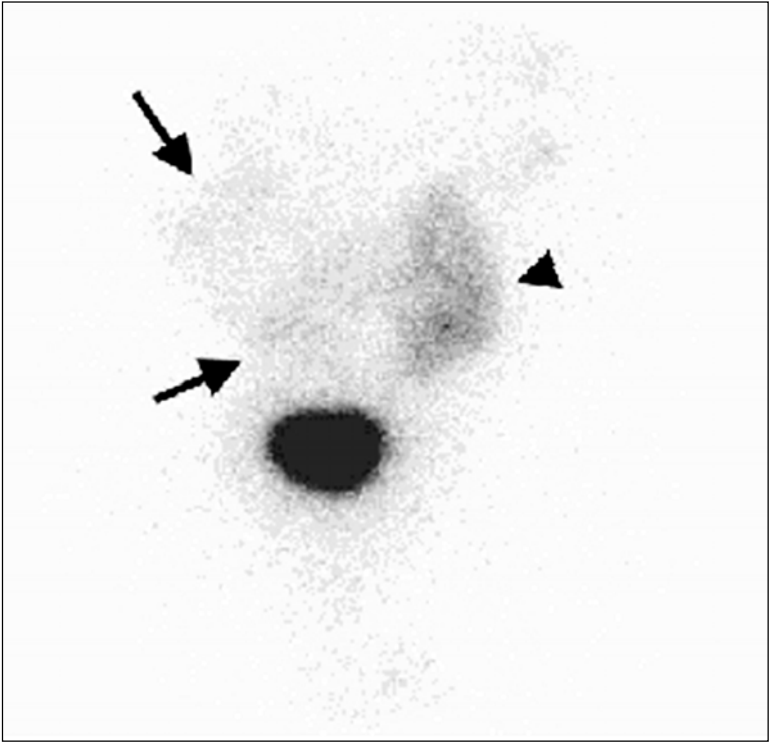
Figure 26. ⁹⁹ᵐTc-MAG3 scan obtained 4 hours post injection and showing gut activity. The transplant (arrowhead) is seen in the left iliac fossa. Irregular activity seen in the mid and lower abdomen on the right represents biliary excretion of the tracer into the gut and is usually present to some degree on delayed ⁹⁹ᵐTc-MAG3 views. Occasionally it can be so intense as to mimic a urine leak.

collecting system activity, and ultrasound must be relied upon to rule out ureteric obstruction. The most severe cases of harvesting injury may show poor perfusion, little uptake and high background levels even with ⁹⁹ᵐTc-MAG3.

Follow up studies in uncomplicated harvesting injury show progressive improvement over days to weeks. Beware of the case that shows improvement during the first week followed by a drop in perfusion or function. This may signal an additional complication such as rejection or cyclosporine nephrotoxicity.

Other complications in the early post-operative period include vascular catastrophe, hematoma, and urine leak. Renal artery or vein thrombosis presents as little or no perfusion or function, and may show the "black hole" sign, in which the transplant can be seen as a negative image with less activity than non-renal background (Fig. 24). This implies infarction of the graft. Hematoma presents as a photopenic area surrounding or adjacent to the graft. Hematoma can cause pressure on the kidney, impairing function directly or by causing ureteric obstruction. Urine leak
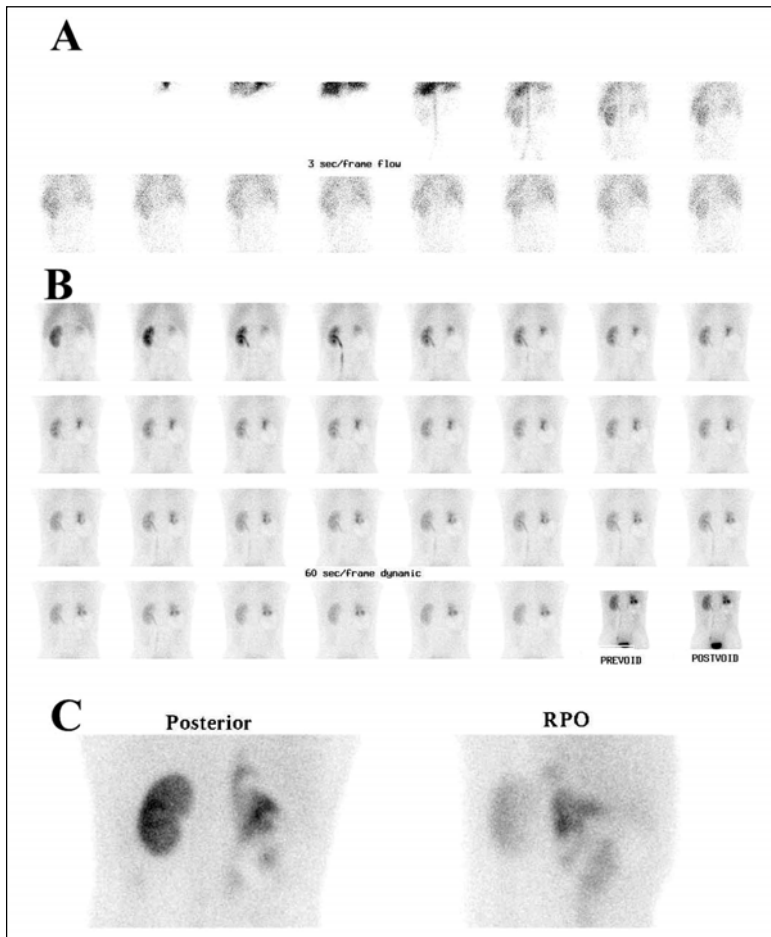
Figure 27. Renal trauma. ^{99m}Tc-glucoheptonate flow (A) and sequential images (B) on a young adult male injured in a car accident. There is very little flow and function in the right kidney. The large photopenic area inferior to the functioning upper pole represents infarcted kidney, hematoma and a small urinoma. The same patient was rescanned subsequently. Delayed images (C) show a normal left kidney, a right urine leak and a small amount of functioning right kidney.

often arises from necrosis of the ureter because of its tenuous blood supply. In the early post-op period, the patient is usually catheterized, so intense urine activity outside of the bladder is easy to detect (Fig. 25). If the patient is not catheterized, it is important to get an adequate post void view to assess for leak. Delayed views at 3-4 hours after injection can be helpful, but be aware that some ^{99m}Tc-MAG3 is excreted

by the liver, so that there is normally some activity in the gut on these delayed views (Fig. 26).

Frequently Asked Questions (FAQs)

Should renal scanning be used in the assessment of renal trauma?

The imaging investigation of choice for renal trauma is computed tomography (CT). CT allows investigation of the whole abdomen, whereas renography evaluates only the kidneys. If renography is required, it may be best done with ^{99m}Tc-glucoheptonate which allows assessment of renal perfusion, function, cortical integrity and urine leaks (Fig. 27). Hemorrhage can also be detected, especially during the blood flow phase of the study. Complete absence of activity, such as in the "black hole sign" mentioned above, indicates devascularization of the kidney.

Additional Reading

1. Conway JJ, Maizels M. The "well tempered" diuretic renogram: A standard method to examine the asymptomatic neonate with hydronephrosis or hydroureteronephrosis. J Nucl Med 1992; 33(11):2047-2051.
   A report from combined meetings of The Society for Fetal Urology and members of The Pediatric Nuclear Medicine Council, Society of Nuclear Medicine.
2. Dubovsky EV, Russel CD, Bischof-Delaloye A et al. Report of the radionuclides in nephrourology committee for evaluation of transplanted kidney (review of techniques). Semin Nucl Med 1999; 29:175-188.
   A review of the use of radionuclide techniques in the assessment of renal transplants.
3. Fine EJ. Interventions in renal scintirenography. Semin Nucl Med 1999; 29:128-145.
   This article, as evident from the title, concentrates on diuretic and ACE inhibitor renography and touches upon other possible interventions (aspirin, exercise).
4. Tayor A. Radionuclide renography: A personal approach. Semin Nucl Med 1999; 29:102-127.
   A nice review with emphasis on diuretic and ACE inhibitor renography.

9

Gastrointestinal

Peter Hollett and Ford Bursey

Introduction

A wide variety of nuclear medicine examinations are available for studying the function of the gastrointestinal tract. Tests include assessment of salivary gland function; motility studies of the esophagus, stomach, small and large bowel; measuring substrate absorption; localization of gastrointestinal bleeding; detection of Meckel's diverticulum (covered in Chapter 17) and tests for inflammatory bowel disease (covered in Chapter 12). This Chapter is not meant to be exhaustive but rather will concentrate on some of the more important and commonly requested tests.

Clinical Role in Esophageal Motility Disorders

The esophagus must transport swallowed material from the mouth to the stomach while minimizing reflux of stomach contents. Symptoms associated with impaired function are dysphagia, pain or regurgitation. Motility disorders can be primary or secondary (Table 1) and result from smooth muscle disorders (e.g., scleroderma) or disorganization of the intrinsic nervous system (e.g., achalasia, Chagas' disease, and diabetes). The identification of these disorders can be aided by nuclear esophageal motility studies though classification is still conventionally described in relation to esophageal manometry:

Normal: After a swallow, pressure in the upper esophageal sphincter (UES) and lower esophageal sphincter (LES) falls. A contraction wave starts in the pharynx and progresses down the esophagus.

Scleroderma: The lower part of the esophagus (smooth muscle) shows a reduced amplitude of contractions with hypotension of the LES.

Achalasia: The LES is usually hypertensive and fails to relax in response to a swallow. The body of the esophagus shows contractions that are reduced in amplitude and simultaneous in onset.

D*iffuse esophageal spasm (DES):* The lower part of the esophagus shows simultaneous-onset, large-amplitude, prolonged, repetitive contractions.

Hypercontractile esophagus ('nutcracker esophagus'): The major dysfunction is abnormal increase of contraction amplitude and normal propagation through the esophagus.

Non-specific motility disorder: Abnormalities that do not conform to any of the preceding patterns.

Technical Considerations

Most laboratories perform esophageal motility assessments with a liquid bolus, although some groups have claimed that semisolid materials are more sensitive. If

---

Table 1. Esophageal motility disorders

Primary motility disorders
        Achalasia
        Diffuse esophageal spasm
        Nutcracker esophagus
        Nonspecific motility disorder
        Presbyesophagus
Secondary motility disorders
        Collagen vascular disease (esp. scleroderma)
        Esophagitis (reflux, caustic, medication, infectious)
        Radiation injury
        Alcoholism
        Diabetes mellitus
        Thyroid disease
        Neuromuscular disorders

---

esophageal and stomach motility are to be evaluated together then a radiolabeled solid meal or resin is often used. To avoid any interference with material already within the stomach, patients are typically asked to fast for at least six hours prior to the procedure. Care should be taken to note medications that affect esophageal function. For example, some prokinetic drugs can increase pressure in the LES or increase the amplitude of the peristaltic waves in those with gastroesophageal reflux disease (GERD). Anticholinergic drugs, nitrates and calcium channel blockers may lessen the pressure in the LES and predispose to reflux. Otherwise, it is uncommon for medications to induce clinically significant disorders of esophageal motility.

Gravity aids the passage of material through the esophagus in the upright position. Therefore, most examinations are performed in the supine position to isolate the effect of esophageal peristalsis. The patient is placed either in the prone or supine position under a gamma camera. After a practice swallow, the test bolus (usually ^{99m}Tc-sulfur colloid 20 MBq) is introduced and dynamic imaging is commenced at a frame rate of 1 s/frame for 2 minutes. The patient is asked to "dry" swallow every 15 seconds.

There are two scintigraphic approaches to measuring esophageal motility (Fig. 1). In the first, regions of interest (ROIs) are placed over the upper, middle, and lower thirds of the esophagus as well as the entire esophagus and transit is measured through these segments after a single swallow. The second approach measures residual activity in the esophagus after several dry swallows. High residual activity implies abnormal esophageal motility. This approach has the advantage of averaging the emptying of the esophagus over several swallows and is therefore less influenced by the occasional aberrant swallow. For both techniques, it is essential to avoid including stomach in the ROI as this can lead to erroneous results. Visual review of the data set in a cine display is also helpful.

Clinical

Impaired swallowing, or dysphagia, may occur because of a wide variety of structural or functional conditions, including stroke, cancer, neurologic disease and GERD. An esophageal motility disorder should be considered in anyone who has dysphagia

10
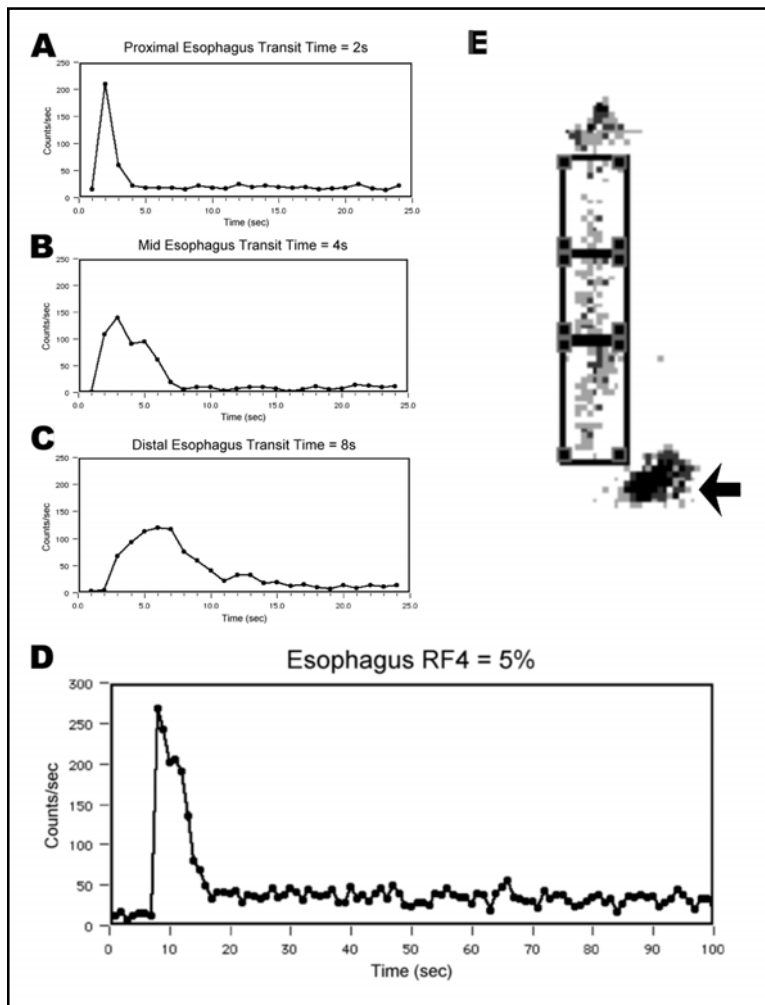
Figure 1. Normal esophageal study. To assess esophageal transit, ROIs are drawn over the proximal, middle and distal thirds of the esophagus avoiding the stomach (arrow) and hypopharynx (E). Time activity curves (TACs) are generated for the three esophageal segments. The transit or emptying times for the individual segments are calculated as the time from peak to 10% of peak (A,B,C). The RF4 is the residual fraction remaining in the esophagus after 4 swallows and is calculated from a TAC generated from a ROI placed around the entire esophagus (D).

for both liquids and solids. Often dysphagia is non-progressive and intermittent. Occasionally reflux induced esophageal spasm will present with dysphagia or atypical chest pain. Many patients may have non-specific disorders of motility related to unrecognized or untreated gastroesophageal reflux, though occasionally classic abnormalities such as achalasia and nutcracker esophagus are detected. Abnormal esophageal motility can also be seen with aging (presbyesophagus). Esophageal motility disorders are seen in many systemic diseases including systemic sclerosis (scleroderma), Parkinson's disease and diabetes.

Investigation of a patient with dysphagia begins with a careful history and physical examination. The physical examination should include an evaluation of the neck, mouth, oropharynx, larynx, and neurologic system. Supplementary testing with endoscopy and/or barium videoesophagography is usually required. The results from these investigations should indicate those with a mechanical or inflammatory etiology. Esophageal manometry should be arranged for those in whom no mechanical or inflammatory etiology is detected and in whom dysphagia persists despite therapy (e.g., dilatation and acid suppression for benign stricture from GERD).

Radionuclide transit studies are less sensitive and specific than manometry and cannot indicate which specific motility disorder is responsible for the abnormal transit. As a result the routine use of esophageal transit studies is not recommended in the initial investigation of dysphagia. Direct comparison of radionuclide transit measurements and videoesophagography indicates similar sensitivity (68-74%) and specificity (68-70%) for specific esophageal disorders, though both are less accurate than manometry in distinguishing nonspecific esophageal motility disorders from normal. Radionuclide transit measurement is a cheap, noninvasive and rapid supplementary examination which, when positive, can support further invasive studies of the esophagus in patients with unexplained chest pain.

Clinical Role in Gastric motility Disorders

Gastroparesis, defined as delayed gastric emptying because of abnormal gastric motility in the absence of mechanical outlet obstruction, is a common problem causing significant morbidity. Less commonly, accelerated gastric emptying can produce symptoms known as dumping syndrome. The current gold standard for quantifying gastric emptying is nuclear scintigraphy.

Physiology

The stomach has two distinct physiologic motor areas: the proximal stomach and the distal stomach. The proximal stomach, with its slow, sustained contractions, plays a key role in regulating intragastric pressure and emptying of liquids, while the distal stomach, with its peristaltic contractions, has a major role in mixing, grinding and emptying of solids. Gastric emptying is highly dependent on the meal's volume, caloric density, composition and concentration of fatty acids, carbohydrates and proteins. Receptors in the small bowel sense these elements and can release hormones or activate neural pathways that can greatly influence the rate of emptying.

The emptying of solid food from the stomach consists of three distinct phases. First, there is an initial lag phase during which little or no solid food is evacuated from the stomach into the duodenum as the meal is ground into small pieces (trituration), mixed and distributed by the muscular contractions of the stomach. During

the second phase there is a constant rate of emptying and then a much slower rate during the final third phase as the stomach approaches empty. Liquids do not need to be triturated and therefore emptying of liquids is more rapid than for solids and tends to follow an exponential rate of emptying. (Liquid phase studies are now rarely performed due to the wide variation in the normal handling of liquids within the stomach and lower sensitivity when compared to the solid phase examination.)

Technical Considerations

A wide variety of drugs can affect gastric emptying and therefore most medications should be discontinued, if possible, prior to a scintigraphic evaluation (Table 2). Evaluation is best done after a 12 hour fast. Diabetic patients should be studied in the morning 20-30 minutes after their normal insulin dosage. Smoking delays gastric emptying and should be avoided.

There are many variations on the testing procedure but the basic principles remain the same. Solid phase studies typically use ^{99m}Tc-sulfur colloid cooked with an egg preparation (though some centers use other protein sources). The prepared egg product is then administered orally, often with a small carbohydrate load (for example, with toasted bread as an egg sandwich). Image acquisition begins soon after the meal is eaten. The stomach lies obliquely within the abdomen and as food moves from the more posterior fundus to the more anterior antrum there is an apparent increase in anterior counts due to lesser depth (attenuation). For accurate quantitation, images in both the anterior and posterior projections are obtained with averaging (geometric mean). Recent work suggests that the use of a single LAO projection also minimizes geometric effects.

Data acquisition is performed for 60 to 120 minutes using either continuous or intermittent imaging. In cases where there is prolonged retention of material within the stomach even more delayed images up to 3 hours may be required. Continuous imaging permits complete visualization of the lag phase when food redistributes from fundus to pylorus. Imaging can be performed in the semi-upright, sitting or standing position. It is very important to establish normal ranges for the technique employed in each individual laboratory, as the results are highly dependent on the acquisition parameters and the test meal used.

The most commonly derived quantitative parameters for gastric emptying are the lag phase, fractional emptying and the emptying half time (Fig. 2).

Clinical

Gastroparesis can be seen as an idiopathic disorder or secondary to many conditions (Table 2). The autonomic neuropathy of long-standing diabetes mellitus is the most common identifiable cause and develops in about 20-30% of poorly controlled patients (Fig. 3). Neither the type of diabetes nor the age of onset been shown to predict the risk of developing diabetic gastroparesis.

Symptoms that evoke the possibility of gastroparesis include early satiety, postprandial fullness, halitosis and frequent belching. The sensitivity and specificity of these symptoms is poor as they also occur in the setting of non-ulcer dyspepsia and mechanical gastric outlet obstruction. It is important to rule out a mechanical cause, such as partial gastric outlet obstruction secondary to chronic peptic ulcer disease, with endoscopy or a barium contrast series.

Table 2. Common causes of altered gastric emptying

Delayed Gastric Emptying	Accelerated gastric emptying
Idiopathic gastroparesis	Endocrine
Endocrine	Hyperthyroidism
Diabetes mellitus (diabetes gastroparesis)	Zollinger-Ellison syndrome
Addison's disease	Acid-peptic disease
Hypothyroidism	Duodenal ulcer disease
Postgastric Surgery	Malabsorptive states
Vagotomy	Pancreatic exocrine
Antrectomy	insufficiency
Subtotal gastrectomy	Celiac sprue
Acid-peptic diseases	Postsurgical states
Gastroesophageal reflux disease	Gastroenterostomy
Gastric ulcer	Partial gastrectomy
Non-ulcer dyspepsia	Postvagotomy
Chronic gastritis	Prokinetics medications
Connective tissue diseases	Metoclopramide
Amyloidosis	Domperidone
Scleroderma	Erythromycin
Systemic lupus erythematosus	
Dermatomyositis	
Pseudo-obstruction	
Neuromuscular diseases	
Muscular dystrophies	
Polymyositis	
Poliomyelitis	
Malignancies	
Infiltrative (lymphoma)	
Paraneoplastic syndromes	
Brain tumors	
Medications	
Opiates	
Anticholinergics	
Tricyclic antidepressants	
Beta-adrenergic agonists	
Levodopa	
Calcium channel blockers	
Antacids (aluminum hydroxide)	
Progesterone	
Birth control pills	
Somatostatin	
Psychiatric disorders	
Anorexia nervosa	
Depression	

10

Rapid gastric emptying (dumping) may occur after gastric surgery as a result of altered vagal activity or in the Zollinger-Ellison syndrome as a result of acid hypersecretion. Hyperthyroidism may also increase the rapidity of gastric emptying.
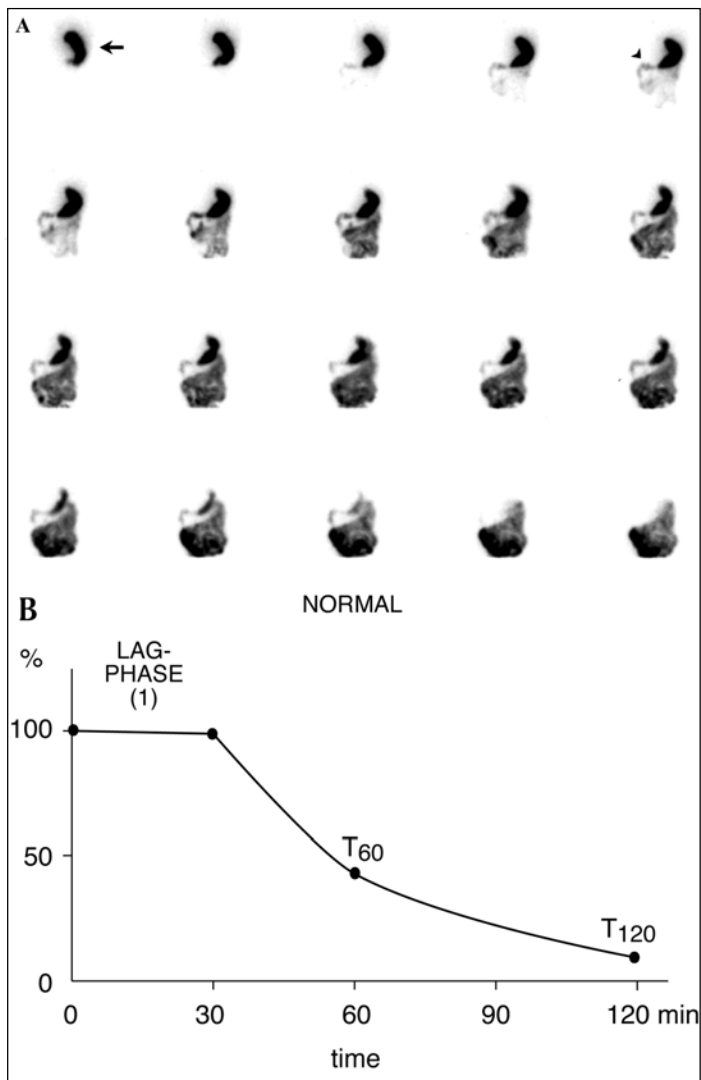
Figure 2. Normal gastric emptying in a 20 year old woman investigated for gastroparesis. (A) Sequential images displayed at 2 minutes/frame. On the initial images, activity is seen in the stomach (arrow) with rapid visualization of activity in the duodenum (arrowhead). By the end of the study only minimal activity remains in the stomach. (B) From a region of interest drawn over the stomach, the lag phase is the time for distribution of food from the fundus to the antrum and its end marks the beginning of gastric emptying into the duodenum. The percentage having left the stomach is generally assessed after a fixed time interval of 60 minutes and if required 120 minutes post eating. These are often recorded as T60 and T120.
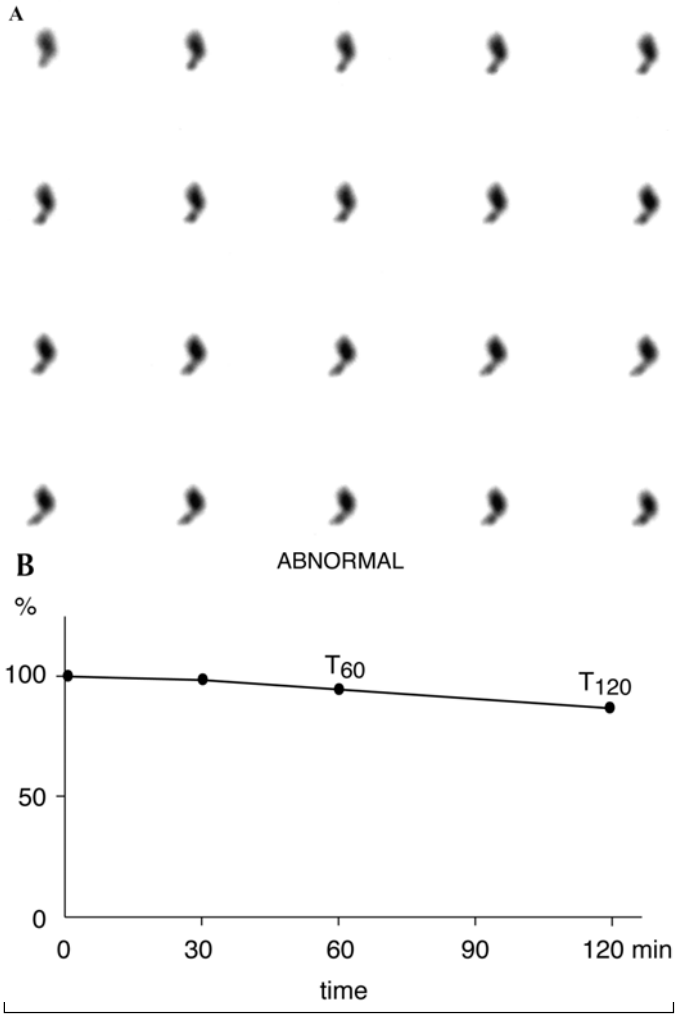
Figure 3. Abnormal gastric emptying study in a 43 year old woman with diabetes and suspected gastroparesis. (A) The bulk of activity remains in the stomach at the end of the study. (B) The amount having left the stomach by 60 minutes and 120 minutes is minimal.

Separating liquids in the diet from solids and ingesting the solids first may help to minimize symptoms.

Clinical Role in the Localization

of Gastrointestinal bleeding

The rapid localization of potentially life threatening GI hemorrhage is an urgent medical and surgical problem. The history and physical examination, while necessary, rarely reveal an exact cause of bleeding and further testing is usually required. Nuclear medicine scanning may help in the evaluation of both acute and chronic gastrointestinal bleeding.

Technical Considerations

Most centers use a labeled red blood cell technique for visualizing GI bleeds. A variety of red blood cell labeling technique techniques have been described (discussed in Chapter 4). It is critical that minimal free ^{99m}Tc-pertechnetate be present in the preparation since pertechnetate, which accumulates in the gastric wall and is secreted into the lumen, can cause a false positive examination. To minimize the amount of free pertechnetate, the in vitro labeling technique is preferred.

Dynamic imaging is performed for at least one hour or until a site of active GI bleeding is clearly identified. Many centers employ further delayed imaging if no active GI bleeding is encountered. One point cannot be overstated: it is essential to acquire dynamic images. GI transit can be rapid, particularly in the small bowel, and intermittent imaging can lead to erroneous localization of the bleeding. Review of the cine images greatly enhances detection of a bleeding site and following the direction of activity as it traverses the bowel further improves localization. For instance, a site of bleeding may be identified in the left upper quadrant of the abdomen. If activity descends along the left flank, the bleeding site is likely to be within the region of the splenic flexure. If activity moves inferiorly and to the right, the bleeding site is probably within the jejunum. Blood in the colon will generally move antegradely but occasionally it can move in a retrograde fashion *(*Fig. 4).

In patients who have had multiple negative diagnostic procedures, some centers use intravenous heparin to unmask the bleeding site. This should only be undertaken after less risky approaches have failed, when bleeding is recurrent and life threatening, and with preparation to administer blood products or perform other resuscitation as required.

Clinical

Gastrointestinal bleeding is a common clinical problem and a major cause of morbidity and mortality. An urgent assessment of hemodynamic stability is the foundation of the clinical approach to such patients. Obtaining venous access and ensuring that oxygenation and tissue perfusion is adequate are essential first steps. At the same time as supportive measures are taking place, an attempt should be made to determine the source of the bleeding and whether the bleeding is ongoing. A complete blood count and coagulation profile should be checked and blood cross-matched in the event that transfusion is required.

In most patients it is clinically apparent if the bleeding is originating from the upper or lower gastrointestinal tract, though occasionally this presents a diagnostic challenge. Endoscopy will determine the source of bleeding in almost all who present with hematemesis and most who present with melena. Passage of a nasogastric tube may help in the evaluation of GI bleeding but a negative gastric aspirate does not exclude an upper GI source. Acid peptic disorders account for up to 70 percent of
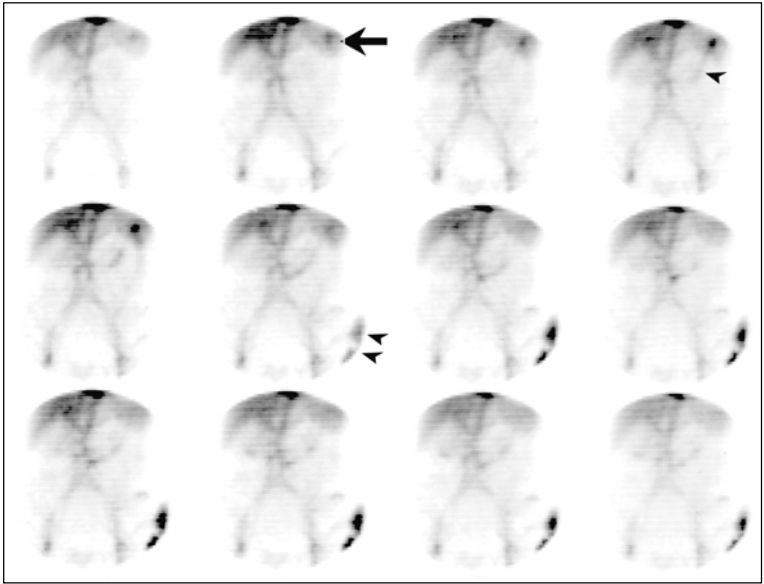
Figure 4. ^{99m}Tc-RBC study showing a bleeding site in the colon. This 82 year old woman with a history of a recent sigmoid resection for carcinoma of the colon presented with three bouts of dark red bleeding into the colostomy bag. Sequential images displayed at 3 minutes/frame show active bleeding originating from the transverse colon near the splenic flexure (arrow) with activity moving in retrograde fashion into the transverse colon (arrowhead) and in antegrade direction into the colostomy bag (dual arrowhead). Surgery confirmed a bleeding diverticulum within the splenic flexure.

causes of upper gastrointestinal bleeding. Other frequent causes of upper GI bleeding include esophageal varices, trauma to the lower esophagus (Mallory-Weiss tear) and neoplasia. In most cases a specific cause will be determined. Therapeutic endoscopy has resulted in a significant reduction in the likelihood of rebleeding, and the need for transfusion, surgery and prolonged hospitalization.

The timing of colonoscopy for suspected lower GI bleeding is less urgent as most causes of lower GI bleeding will cease spontaneously. Common causes of lower GI bleeding include angiodysplasia (particularly from the right side of the colon), diverticular disease, carcinoma, inflammation and, in children, Meckel's diverticulum of the small bowel. The success of determining the cause is enhanced when adequate bowel preparation has taken place.

Despite careful endoscopic examination, the cause of bleeding will not be determined in a small percentage of cases. It is in this select group of patients that nuclear medicine scanning is most useful. The overall accuracy may be as low as 45%, however, as bleeding is intermittent. This scenario occurs more commonly in the setting
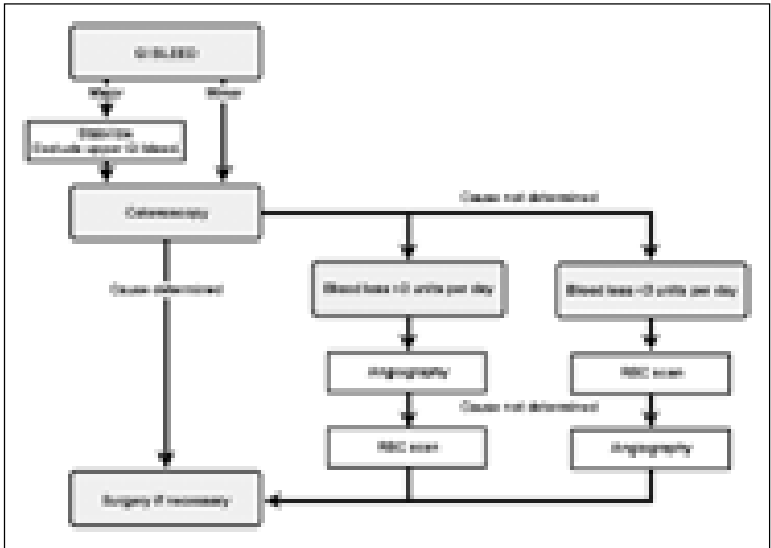
Figure 5. An approach to the investigation of lower GI bleeding.

of suspected lower GI bleeding. Nuclear medicine scanning can detect smaller rates of bleeding than angiography, is less invasive and may help to focus the efforts of the angiographer. As angiography offers the potential of therapeutic intervention, the decision as to whether a GI bleeding scan is performed in conjunction with angiography or not is dictated by the urgency of the clinical situation (Fig. 5).

Clinical Role of Urea breath testing

The discovery of the causal relationship between the gram-negative spiral rod, *Helicobacter pylori*, and peptic ulcer disease (PUD) has dramatically changed the investigation and approach to therapy. While only a small number of patients that harbor *H. pylori* develop PUD, most patients with PUD are infected with *H. pylori*. Although the diagnosis of *H. pylori* infection can be established by histological examination of gastric biopsy specimens, urea breath testing is non-invasive, inexpensive and highly accurate (over 95% sensitivity and specificity).

Technical Considerations

Urea breath testing relies upon the fact that the urease enzyme is not present in mammalian cells and *H. pylori* is the only bacteria commonly found in the stomach that contains the enzyme. Following an overnight fast the patient swallows a small amount of ^{14}C-urea. Gastric *H. pylori* cleaves the urea into ammonium and ^{14}C-bicarbonate which is absorbed into the bloodstream (Fig. 6). Under the action of carbonic anhydrase, bicarbonate is transformed into ^{14}C-carbon dioxide, which is exhaled in the breath. Carbon-14 activity in the breath is therefore an indicator of *H. pylori* urease activity.
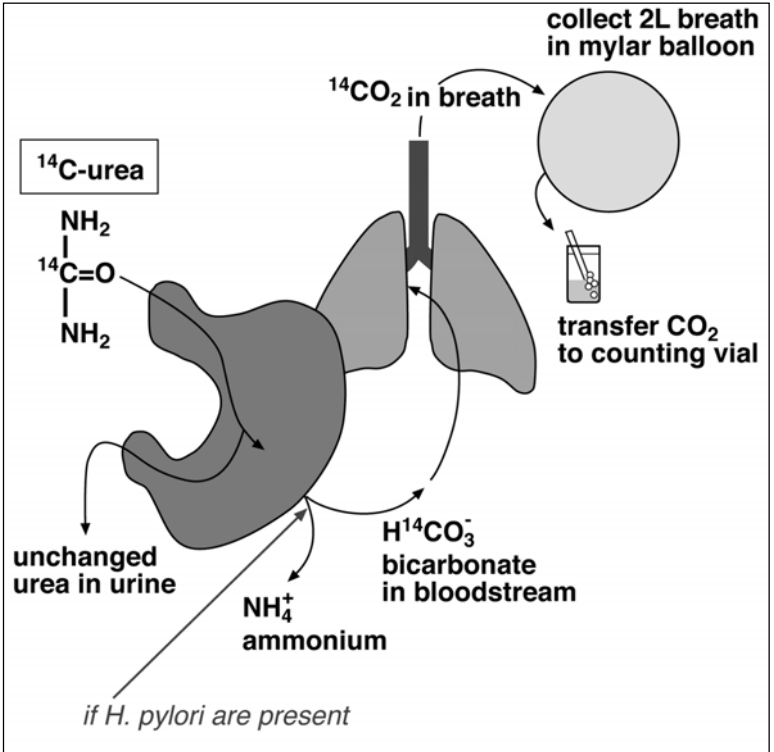
Figure 6. Schematic showing rationale for carbon-14 urea breath testing.

Peak radioactivity in the breath is reached in approximately 10–20 minutes. The breath sample is captured in a non-diffusible balloon or trapping solution. The sample is then counted by liquid scintillation and reported as carbon-14 activity per mmole of CO_2 in the breath. Results can usually be classified as definitely positive or definitely negative. A small number of cases show detectable radioactivity that falls below the abnormal threshold and are considered indeterminate.

A number of medications can interfere with the examination. Treatment with antibiotics or bismuth-containing preparations in the previous month can give a false negative result related to suppression of *H. pylori* growth. Proton pump inhibitors suppress *H. pylori* growth and may interfere with the diffusion of carbon dioxide across the gastric mucosal surface. This results in a false negative test in over one third of patients and therefore the agent should be discontinued for at least 7-14 days prior to performing the examination. Sucralfate can also suppress active *H. pylori* for up to one week. Antacids and H2 antagonists are usually stopped as well, though they probably have little effect on test results. Gastric surgery can cause a false negative result if the isotope empties too rapidly from the stomach. False posi-

tive results are rare, but occasionally bacterial overgrowth from species other than *H. pylori* will metabolize the labeled urea.

Techniques are now available for using urea labeled with non-radioactive carbon-13, though the radioactive format is still the most widely available. The non-radioactive method requires a standardized meal, a larger dose of urea and more specialized equipment (mass spectrometer or laser spectroscope).

Clinical

The accuracy of diagnosing PUD from history is poor. The diagnosis is confirmed in only 50% of those in whom it is suspected. After excluding ulcers related to nonsteroidal antiiflammatory drugs (NSAIDs), the vast majority of duodenal and gastric ulcers are caused by chronic infection with *H. pylori.* With standard treatment regimens such as a one-month treatment with an H2 receptor antagonist or a proton pump inhibitor, there is a high rate of ulcer relapse (50 to 90%) after acute ulcer healing. Eradication of the organism dramatically alters the natural history of PUD with a marked decrease in ulcer recurrence. Highly effective (>90%) eradication of *H. pylori* is achieved with 7-10 days of a triple drug regimen (bismuth or a proton pump inhibitor and two antibiotics—clarithromycin and either metronidazole or amoxicillin). Adherence to such complex regimens is variable and side effects are not infrequent.

The traditional approach to the diagnosis of PUD has included either an upper GI series or endoscopy to document an ulcer. Determination of *H. pylori* status followed by eradication therapy of patients found to be *H. pylori* positive may be a rational and cost-effective approach to the investigation and management of patients with suspected PUD *(*Fig. 7). With a "test and treat" approach, a positive *H. pylori* breath test removes the need for endoscopy if no "alarm" features (anemia, evidence of bleeding, weight loss or early satiety) are present. Due to the increased risk of malignancy in older patients, this approach should be confined to those less than 50 years of age. A small number (20-30%) of patients with *H. pylori* infection and non-ulcer dyspepsia also appear to benefit from eradication therapy, though this remains controversial.

H. pylori has been associated with a two- to threefold increase in risk for gastric cancer. Studies are in progress to determine if *H. pylori* eradication will alter the risk of malignancy. Gastric maltoma, a lymphoproliferative disorder of gastric mucosal associated lymphoid tissue (MALT), is related to infection with *H. pylori*. Eradication of *H. pylori* in early stages of this low-grade tumor may lead to complete remission. Surgical resection and chemotherapy are also effective treatment modalities. If a non-operative approach to management is chosen then these patients need to be followed very closely.

If peptic ulcer disease is uncomplicated, i.e., no evidence of bleeding, perforation or obstruction, then documentation that eradication has been successful is felt to be unnecessary. The success of eradication should be confirmed in all those with complications, taking care to avoid medications that can give a false negative examination.
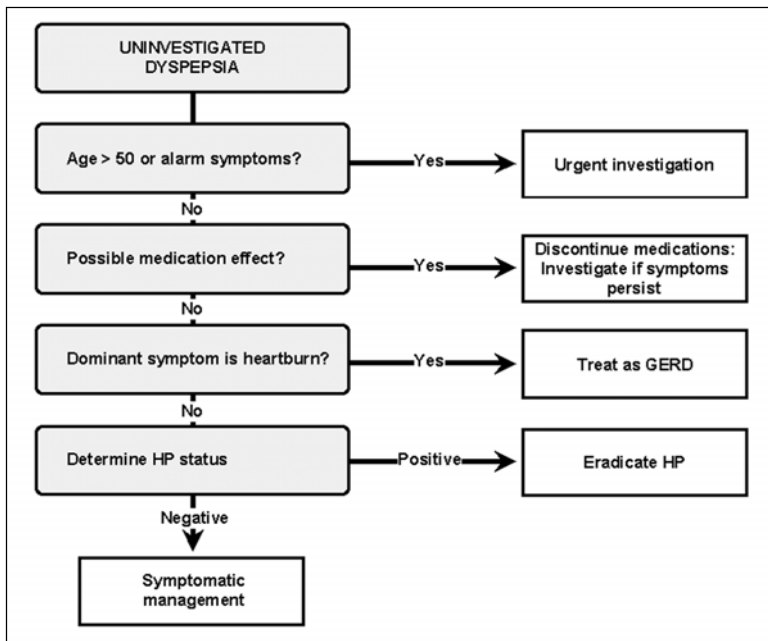
Figure 7. Flowchart outlining the evaluation of uninvestigated dyspepsia.

10

Frequently Asked Questions (FAQs)

Are Nuclear Medicine techniques used in diagnosing gastroesophageal reflux disease (GERD)?

Nuclear Medicine has a definite clinical role in the evaluation of infants with excessive spitting up or possible pulmonary aspiration (discussed in Chapter 17). Its place in adult GERD is more questionable. Radionuclide testing attempts to demonstrate abnormal entry of stomach contents into the esophagus. The test is performed after a six to eight hour fast. Medications known to affect function of the LES, such as caffeine, alcohol and smoking, are avoided prior to testing. Orange juice 150 ml containing ^{99m}Tc-sulfur colloid is ingested in the erect position to completely clear the esophagus, after which the patient is positioned supine under the gamma camera. Dynamic images are obtained at 30 seconds per frame. Some centers perform provocative maneuvers to increase intra-abdominal pressure, such as having the patient perform a Valsalva maneuver or the application of an abdominal binder (slowly inflated to a maximum of 100 mm Hg).

A clinical diagnosis of GERD can be made if the predominant symptom is regurgitation or an epigastric burning sensation that radiates towards the throat. If there are other complaints, the diagnostic accuracy lessens. In those patients without "alarm symptoms" such as dysphagia, anemia, weight loss or bleeding, it is rea-

sonable to proceed with a clinical trial of medication (H2 receptor antagonist or proton pump inhibitor). Investigation of those who have heartburn or reflux in relation to occasional dietary indiscretion is unnecessary. Endoscopy and 24-hour pH studies are reserved for atypical cases. Given the proven clinical utility of these, radionuclide studies are now rarely used in the evaluation of patients with suspected GERD.

How useful are serologic tests for **H. pylori***?*

While serologic testing for *H. pylori* may provide useful information, the operating characteristics are such that the results are not interchangeable with the results from a breath test. For instance, in populations with a low prevalence of infection, such as Canadians under 50 years of age, a positive serologic test may not truly identify a patient currently infected with *H. pylori*. The positive predictive value may only be 70% in such a population, i.e., the false positive rate can be as high as 30%. This obviously could lead to the inappropriate selection of patients for a course of therapy.

Serologic testing to determine whether eradication has occurred is inappropriate. Antibodies may remain detectable for more than one year after successful eradication of *H. pylori*. If a patient has persistent dyspepsia after treatment for *H. pylori* one must consider the possibility that it is due to non-ulcer dyspepsia, gastroesophageal reflux disease or persistent infection. Only a properly conducted breath test or mucosal biopsy can accurately determine whether a persistent infection exists.

Additional Reading

1. Kim CK, Worsley DF, Machac J. Interventions in gastrointestinal nuclear medicine. In: Freeman, LM, ed. Nuclear Medicine Annual 1996. Philadelphia: Lippincott Williams and Wilkins, 1996:213-258.
    A well-rounded collection of tidbits for imaging and helpful hints for interpretation of examinations.
2. Klein HA and Wald A. Esophageal transit scintigraphy. In: Freeman, LM, Weissman HS, eds. Nuclear Medicine Annual 1988. Philadelphia: Lippincott Williams and Wilkins, 1988:79-124.
    An older but still excellent discussion of scintigraphic approaches to measuring esophageal motility.
3. Malmud LS, Fisher RS, Knight LC, Rock E. Scintigraphic evaluation of gastric emptying. Semin Nuc Med 1982; 12(2):116-125.
    While an older reference, it is still relevant and written by one of the founders of this field.
4. Thomson ABR, Shaffer EA eds. First Principles of Gastroenterology: The Basis of Disease and an Approach to Management. Fourth edition. Mississauga: Astra Zeneca Canada.
    An excellent resource for students or busy clinicians. This book was published as a result of an unrestricted educational grant from Astra Zeneca Canada Inc. which is listed as the publisher. The book is endorsed by The Canadian Association of Gastroenterology and the Canadian Association for the Study of the Liver.
5. Van Santen S, Flook N, Chiba N, Armstrong D et al. An evidence-based approach to the management of uninvestigated dyspepsia in the era of *Helicobacter pylori*. Can Med Assoc Journal 2000; 162 (12 Suppl):S3-23.
    A thorough review of dyspepsia and its management. Discusses the role of a 'test and treat' approach to dyspepsia.

10

Hepatobiliary Imaging

Reinhard Kloiber and Gary R. May

Introduction

Historically, liver imaging using radionuclides focused on the detection of liver masses. More recently, anatomic imaging modalities including ultrasound, CT and MRI have replaced colloid imaging because of their greater sensitivity and ability to distinguish cystic from solid lesions. Solid masses may nevertheless have a nonspecific appearance on anatomic imaging requiring the use of radiopharmaceuticals that identify certain cell lines, metabolic properties or surface characteristics of specific lesions. The modern technetium-99m labeled hepatobiliary agents retain a pivotal role in studying biliary flow and dynamics.

Radiopharmaceuticals

IDA Analogues

Analogues of technetium-99m labeled iminodiacetic acid (^{99m}Tc-IDA) first became available for clinical use in the 1970s and remain the most widely used radiopharmaceuticals for hepatobiliary imaging (Fig. 1). After intravenous injection, these organic anions are taken up by hepatocytes in a manner similar to bilirubin. They are secreted into bile without conjugation. ^{99m}Tc-IDA uniformly mixes with bile, thereby becoming a marker of bile flow to the gallbladder and bowel. No significant intestinal reabsorption or enterohepatic cycling occurs. Ideal agents exhibit high extraction efficiency by liver (even in the presence of liver dysfunction), rapid transit, and high concentration in bile. Commercially available ^{99m}Tc-disofenin (Hepatolite®) and ^{99m}Tc-mebrofenin (Choletec®) meet these criteria.

Colloids

^{99m}Tc-sulfur colloid and a variety of other colloids are phagocytosed from the blood stream by Kupffer cells in the liver and other reticuloendothelial cells. Under normal circumstances, 85% of the dose accumulates in liver, 10% in the spleen and the remainder in bone marrow (Fig. 2). Metastases, cysts and abscesses all displace normal Kupffer cells and appear as "cold" defects. Some benign focal liver lesions contain Kupffer cells and the benign nature of the mass can be confirmed by showing colloid uptake within it.

Red Blood Cells

Red blood cells can be labelled with technetium-99m (^{99m}Tc-RBC) and are used to identify cavernous hemangiomas within the liver. These consist of large blood filled spaces. Blood flow is generally low in relation to the volume of blood present and filling after intravenous injection of a substance may require a significant period of time. Radiographic contrast material leaks rapidly from the intravascular space
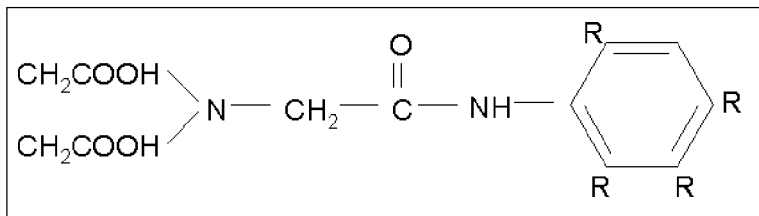
Figure 1. Structure of iminodiacetic acid. The groups on the benzene ring labelled R can be hydrogen or short organic chains. They determine the specific attributes of the analogue such as avidity of uptake by the liver and rates of excretion.

into the extracellular fluid space. Late enhancement of a mass on CT therefore does not prove that the lesion is filled with blood but can also be seen in malignant masses with an expanded extracellular fluid space. ^{99m}Tc-RBCs remain confined to the circulation and even hemangiomas that require hours to equilibrate can be correctly diagnosed. (For more on the technique of labelling RBCs, refer to Chapter 4.)

Other tracers

Antibodies
Antibodies directed at characteristic surface antigens selectively expressed by specific neoplasms, such as prostate specific antigen (PSA) or carcinoembryonic antigen (CEA), appear in theory to be the ideal agents. Unfortunately, all antibodies or fragments are metabolized in liver yielding a high background. Mapping of normal tissue with ^{99m}Tc-sulfur colloid and subtraction from the antibody images to highlight areas of abnormal binding can improve detectability. Antibody imaging of liver lesions holds theoretical promise but, after years of investigation, is still of limited clinical utility.

Receptor-Specific Agents
The indium-111 labelled pentapeptide analogue of somatostatin (^{111}In-pentetreotide or octreoscan® binds to receptor-positive carcinoids and a variety of pancreatic islet cell and neuroendocrine tumours. Lesion to liver ratios are often sufficiently high to confirm the nature of metastases (Fig. 3). Extrahepatic sites are demonstrated with even greater sensitivity. The technique is complementary to CT.

Gallium Citrate
Certain neoplasms, including lymphomas, carcinoma of the lung, sarcomas and hepatomas, may exhibit avid uptake of gallium-67 citrate (^{67}Ga). Gallium acts as an iron analogue. It binds to transferrin after intravenous injection and is stored in liver and bone marrow. Small quantities are excreted in bile. Normal liver therefore contains moderately high background activity. Many adenocarcinomas originating in the gastrointestinal and genitourinary tracts show only low grade uptake and metastases appear as photopenic defects relative to normal liver. Imaging characteristics of ^{67}Ga are poor compared with ^{99m}Tc and the masses must be substantial in size to be
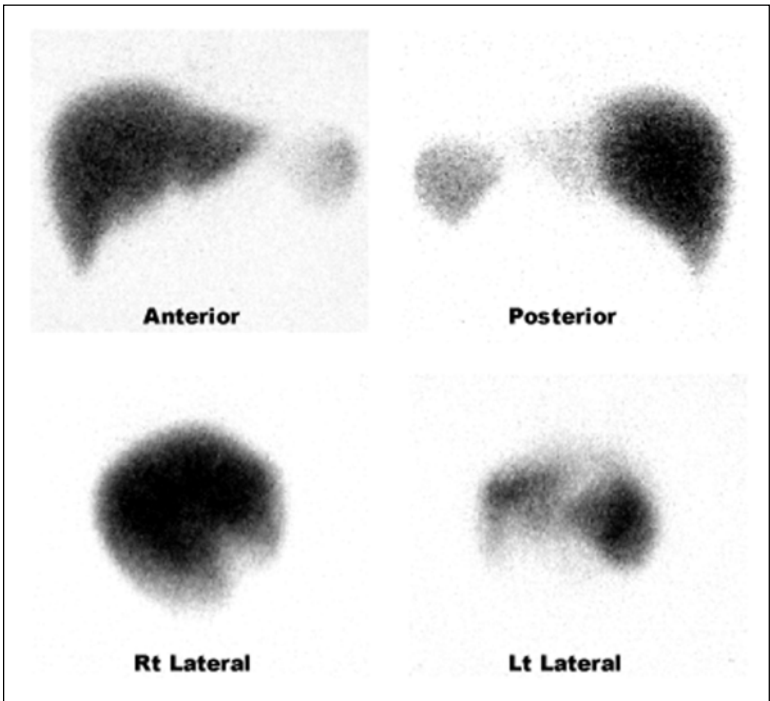
Figure 2. Normal planar ^{99m}Tc-sulfur colloid liver spleen imaging. Activity throughout the liver and spleen are uniform. Splenic activity is less than liver activity. The bone marrow is only faintly seen.

evaluated. Simultaneous mapping of normal tissue with ^{99m}Tc-sulfur colloid adds sensitivity. Gallium accumulation in an area of absent ^{99m}Tc-sulfur colloid uptake in a liver distorted by advanced cirrhosis is highly suggestive of a hepatoma (Fig. 4). In less well defined clinical situations, gallium uptake is nonspecific and may be present in focal infection or inflammation and a wide variety of neoplasms.

Fluorodeoxyglucose

Fluorine-18 labelled fluorodeoxyglucose (^{18}F-FDG) is a glucose analogue taken up by cells through the same transport system as glucose. Following cellular uptake, FDG is phosphorylated. Since FDG-phosphate cannot be metabolized further, it is effectively "trapped" in the cell and can be used as a marker of glucose metabolism. As with gallium, uptake is nonspecific. Because of the high sensitivity of anatomic imaging modalities in detecting liver masses, the greatest utility of FDG imaging is in the detection of extrahepatic sites for tumour staging (see Chapter 15). Availability of positron emitting radioisotopes, including ^{18}F, has been limited to date but is improving.
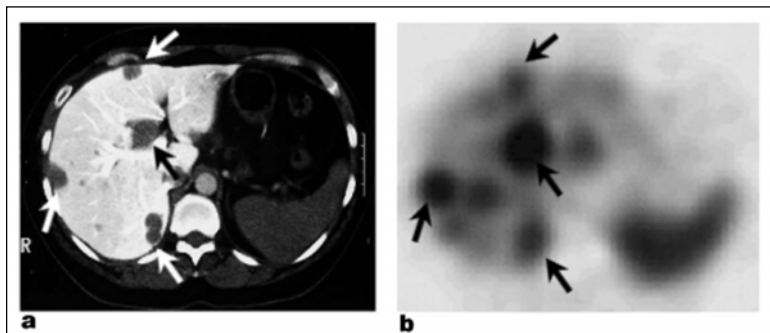
Figure 3. Metastases from malignant carcinoid. A 46 year old woman with past resection of a small bowel carcinoid presents with carcinoid syndrome. A CT image during CT arterial portography (a) shows multiple hypodense masses (arrows). The corresponding ^{111}In-pentetreotide SPECT transaxial image (b) confirms that these are somatostatin receptor positive metastases (arrows).

Clinical Role in the Evaluation of the Biliary Tree

Following bolus injection of ^{99m}Tc-IDA agents, initial images show blood pool and uniform hepatic activity which, in the absence of hepatocellular disease or cholestasis, clears rapidly. Bile duct activity appears within 10 to 15 minutes of injection.

In healthy fasting patients, the gallbladder is usually visualized within 15 to 30 minutes after injection of the ^{99m}Tc-IDA, and almost always within 60 minutes (Fig. 5). Confirmation of the anterior location of the activity on lateral or oblique views is recommended to avoid mistaking duodenal activity for the gallbladder. All excreted bile may enter the gallbladder if the sphincter of Oddi is closed (a not uncommon finding in the fasting patient) or variable portions may drain to the duodenum. The greatest utility of the filling phase is to confirm patency of the cystic duct.

As long as no additional bile enters the gallbladder, externally detected activity is proportional to relative volume and is independent of gallbladder shape or geometry. Contraction of the gallbladder may be stimulated by infusion of a synthetic active octapeptide of cholecystokinin (CCK-8 or sincalide, Kinevac®) or endogenously released CCK after a meal. CCK-8 infusion is easier to control and is the preferred method.

The most commonly used single quantitative measurement that reflects emptying is the ejection fraction (EF), which represents the percentage of initial volume or activity evacuated with contraction. It is calculated from the following formula:

$$EF = \frac{\left(A - Bg_a\right) - \left(B - Bg_b\right)}{\left(A - Bg_a\right)} \times 100\%$$
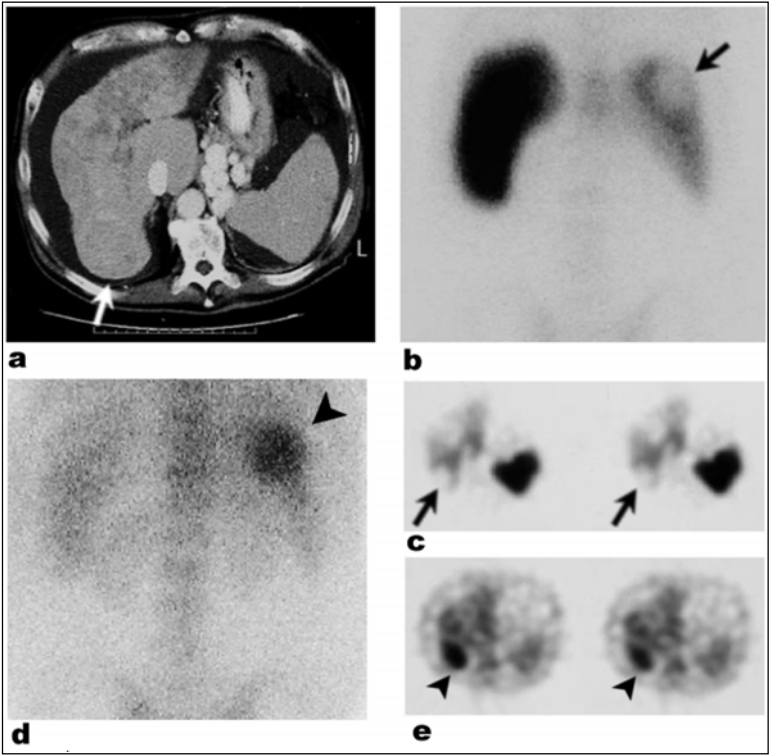
Figure 4. Hepatocellular carcinoma (HCC) in a cirrhotic liver. A 75 year old man with alcoholic cirrhosis presents with worsening liver failure. The enhanced CT image (a) shows the small cirrhotic liver with cavernous transformation of the portal vein and surrounding ascites. The posterior aspect of the right lobe of the liver shows a bulbous projection suggesting a mass (white arrow). The planar (b) and transaxial SPECT (c) ^{99m}Tc-sulfur colloid images show the mass to be devoid of Kupffer cells indicating that it is not regenerating liver tissue (black arrows). A more anterior defect on ^{99m}Tc-sulfur colloid SPECT images represents scarring. ^{67}Ga activity within the mass on planar (d) and transaxial SPECT images (e) is consistent with HCC (black arrowheads).

Where:	EF	=	Ejection fraction
	A	=	Initial gallbladder activity
	Bg_a	=	Initial background activity
	B	=	Post contraction gallbladder activity
	Bg_b	=	Post contraction background activity

All activity measurements are derived from regions of interest placed on digitized images. Background activity is normalized to the area of the gallbladder region and
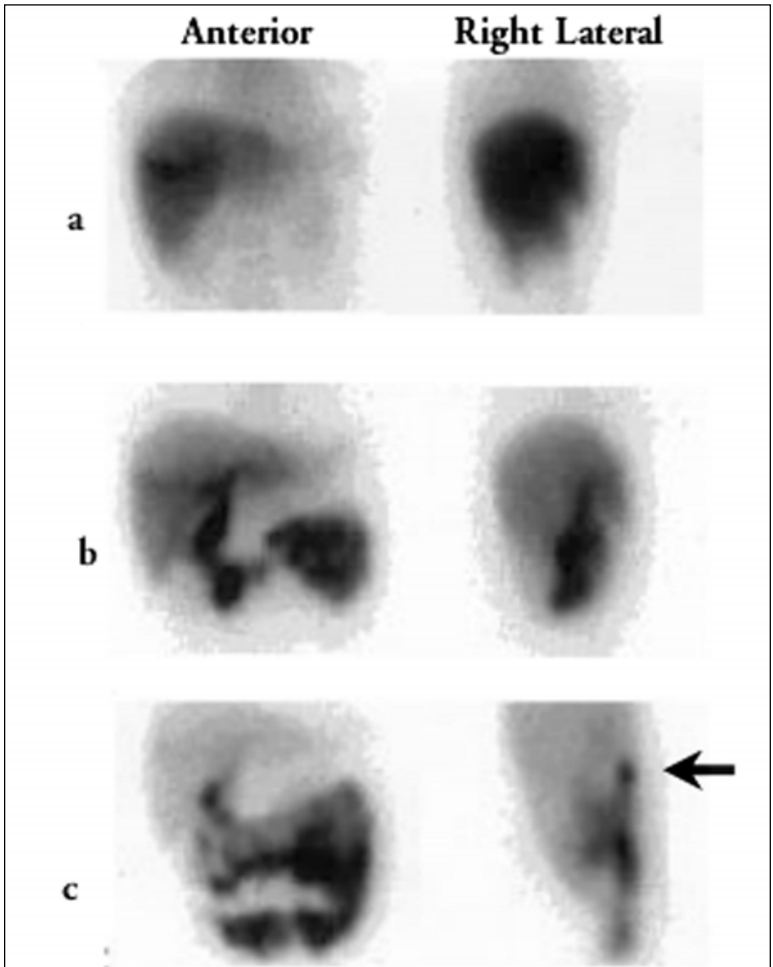
Figure 5. Normal ^{99m}Tc-IDA study. Anterior and right lateral images immediately after injection (a) show uniform activity throughout the liver. Activity in the heart is low-grade with normal liver function. By 30 minutes (b) the biliary tree and bowel are seen. The normal gallbladder (arrow) is seen within one hour (c). A right lateral view is important to prevent potential confusion between activity in the gallbladder (anteriorly placed) and duodenum (posteriorly placed) on the anterior view alone.

post contraction activity is corrected for decay. The method assumes complete mixing of the radiotracer with bile. The EF can be overestimated if abundant stones or sludge are present because only the portion of the gallbladder volume filled with radiolabelled bile would be measured. The EF may have a role in evaluating patients
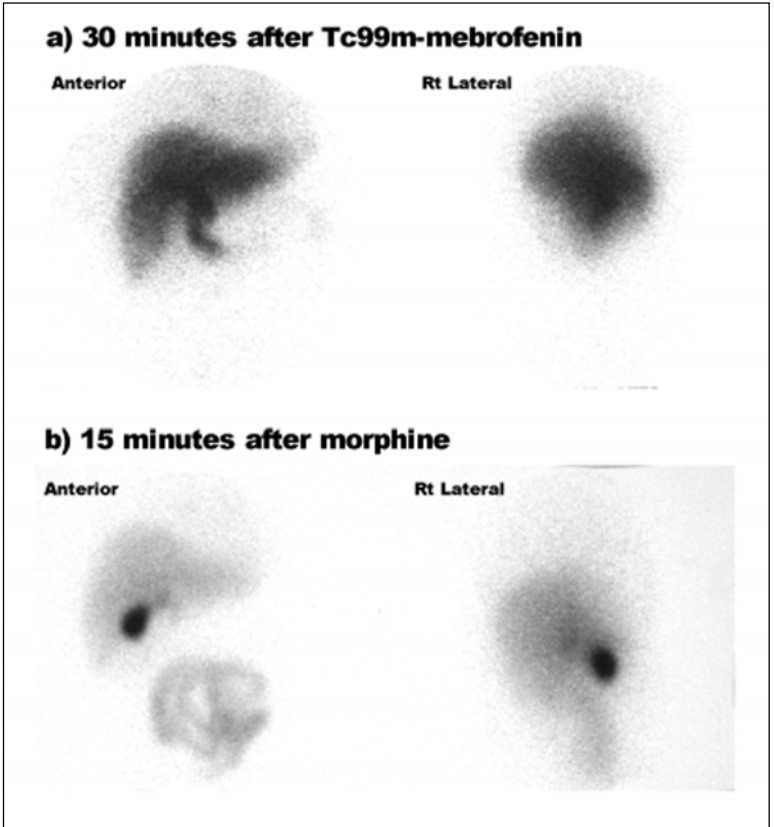
Figure 6. Gallbladder visualization after morphine. Images at 30 minutes in a 53 year old woman with unexplained acute right upper quadrant pain fail to show the gallbladder (a). It is well seen 15 mintues after morphine injection (b) excluding cystic duct obstruction and acute calculous cholecystitis.

with acute or chronic biliary type pain in the absence of demonstrable calculi (see section on Biliary-Type Pain in the Absence of Calculi). Emptying rates and patterns of emptying have not been sufficiently studied to determine their relevance.

Time activity curves generated from regions over the heart, liver, and bile ducts offer no advantage over biochemical indices in assessing liver function but may be of value in partial obstruction or sphincter of Oddi dysfunction (see section on Postcholecystectomy Pain).

Acute Calculous Cholecystitis: The Emergency Room Setting

The vast majority of outpatients presenting with symptoms of acute cholecystitis have cystic duct obstruction by calculi. Ultrasound is typically the initial imaging
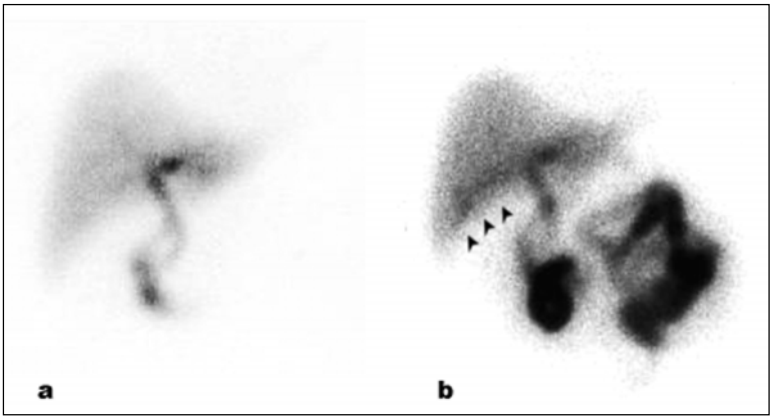
Figure 7. Rim sign in acute cholecystitis. 15 minute (a) and 15 minute post morphine (b) images fail to demonstrate any filling of the gallbladder indicating cystic duct obstruction in this 42 year old man with acute right upper quadrant pain. The inflamed liver adjacent to the gallbladder fossa shows delayed excretion compared with the remainder of the liver (arrowheads). This finding adds specificity to the diagnosis of acute cholecystitis.

procedure. It is usually readily available in the emergency room setting, can assess multiple abdominal organs and yields results quickly. It is the procedure of choice to detect calculi in the gallbladder with a sensitivity approaching 98%. In the presence of acute inflammation it can show thickening of the gallbladder wall, pericholecystic fluid, and elicit localized tenderness (the sonographic Murphy's sign). Unfortunately, calculi are a common problem and unless they are located in the gallbladder neck or cystic duct, they imply acute cholecystitis in only 50 to 70% of cases. Gallbladder wall thickening and fluid are infrequent findings and are also nonspecific, being found with ascites and other edematous states. CT has similar advantages and disadvantages. It is better at demonstrating the distal portion of the common bile duct, which may be obscured by gas on US, but clearly cannot be used to assess tenderness over the gallbladder.

In this setting, nonvisualization of the gallbladder within 60 minutes on scintigraphy has a sensitivity for acute cholecystitis approaching 100%. The finding is unreliable if biliary excretion is reduced as a result of hepatocellular disease or cholestasis. Of patients with proven chronic cholecystitis, 80% will show normal gallbladder filling and the remainder will have delayed visualisation (after 1 hour) or persistent nonvisualization. The latter results in an unavoidable number of false positive studies. The proportion depends on the prevalence of chronic cholecystitis in the population studied.

Infusion of morphine at a dose of 0.04 to 0.10 mg/kg is used to accelerate filling of the gallbladder by causing spasm of the sphincter of Oddi and increasing intrabiliary pressure. Morphine-induced gallbladder visualization usually occurs within 30 minutes and imaging beyond that time is unnecessary unless there is delayed excretion.
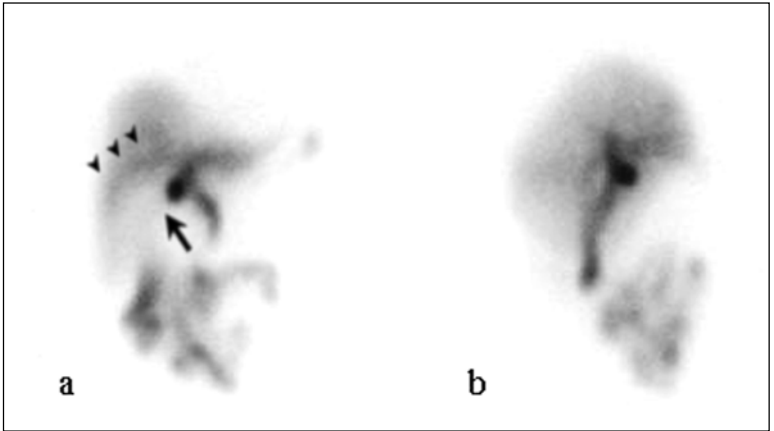
Figure 8. Partial filling of the gallbladder with obstruction distal to Hartmann's pouch (cystic duct sign). Anterior (a) and right lateral (b) images 30 minutes after ^{99m}Tc-IDA injection show a small focal collection of radiotracer in the gallbladder fossa. The inflamed gallbladder was enlarged on ultrasound (US) and is only partially filled by the radiotracer (arrow). A faint rim sign is also present (arrowheads).

Morphine should not be given if there is no significant excretion or if there is a history of hypersensitivity. Hyperamylasemia is a relative contraindication as pancreatitis may be exacerbated. Naloxone should be available in the event of side effects, but these are rare with the low doses used. In patients that experience an acute exacerbation of pain following morphine, CCK-8 can also be used to relieve the sphincter of Oddi spasm.

Sensitivity and specificity with the morphine augmented protocol are 90-100% and 85-95%, respectively (Fig. 6).

Ancillary signs of acute cholecystitis are hyperperfusion in the gallbladder fossa on a flow study and the "rim" sign on later images (Fig. 7). The latter reflects extension of the inflammatory reaction into adjacent liver tissue with impaired excretion and prolonged retention resulting in a rim of relative increased activity around the gallbladder fossa after normal liver tissue has cleared. The sign is associated with an increased incidence of gangrenous wall perforation. On occasion a dilated cystic duct or gallbladder neck is visualized (cystic duct sign) with obstruction of the distal portion of the gallbladder (Fig. 8). Comparison of gallbladder size on US is helpful in avoiding a false negative diagnosis.

Although many episodes of acute cholecystitis may resolve with supportive care, the ease and low rate of complications from laparoscopic cholecystectomy have favored a more aggressive approach to treatment of patients who have a typical clinical presentation. US or CT tend to be the initial imaging procedures. Anatomic imaging can guide percutaneous drainage of pericholecystic fluid collections and cholecystostomy in patients at high operative risk. Cholecscintigraphy has been shown

11

to significantly increase diagnostic confidence and improve therapeutic decision making, but is usually reserved for complex cases or for patients with an atypical presentation.

Acute Acalculous Cholecystitis: The ICU Setting

Acute cholecystitis in patients in the intensive care setting with prolonged fasting, total parenteral nutrition, and severe intercurrent illness may occur in the absence of calculi in up to 50% of cases. Stasis of bile from fasting for greater than 24 hours may prevent filling of a normal gallbladder. Many departments use a short infusion of CCK-8 to partially empty the gallbladder and prepare it for filling prior to injection of the radiotracer.

The incidence of gallbladder necrosis and spontaneous rupture is high in patients with acute acalculous cholecystitis and morphine-induced increased biliary pressure has, on rare occasions, been suspected of causing rupture. The risk is, however, low and morphine infusion is still an acceptable intervention for patients whose gallbladder does not fill spontaneously within 30 minutes.

Some patients with acute acalculous cholecystitis will have cystic duct obstruction secondary to edema, but many others will have functional obstruction due to stasis alone. Theoretically, morphine induced elevated biliary pressure may overcome the relative cystic duct obstruction in the latter group resulting in false negative gallbladder visualization.

Because the severely inflamed gallbladder is unlikely to be able to contract, demonstration of a response to a CCK-8 infusion (although not necessarily a normal EF) in cases where the gallbladder fills only after morphine increases confidence that gallbladder filling represents a true negative finding. The precise impact of these confounding factors on the accuracy of cholescintigraphy in the ICU setting has not been adequately studied.

Many of these patients have a septic presentation and whole body imaging with radiolabelled white blood cells or other inflammation-specific radiopharmaceuticals may help to confirm acute gallbladder disease and identify additional occult sources of infection.

Biliary-Type Pain in the Absence of Calculi

Most patients with chronic cholecystitis have calculi demonstrable by ultrasound. However, a subset of patients with typical biliary type pain does not. Abnormal gallbladder emptying (a reduced EF) may be a marker for those patients who will improve after cholecystectomy, though definitive proof of this has been difficult to obtain.

The majority of gallbladders from patients with a satisfactory clinical response to surgery fail to show histologic evidence of cholecystitis and pain is presumed to be on the basis of a motility disorder. Clinical remission of pain after cholecystectomy is the most appropriate endpoint. Several retrospective studies have shown a rate of pain remission of 69 to 100% following cholecystectomy (comparable to the response rate in surgery for calculous cholecystitis) in patients with gallbladder EF of less than 35 to 40%. Unfortunately, no prospective studies where patients were randomized to cholecystectomy and nonsurgical treatment after gallbladder EF measurement have been performed, nor are they likely to be performed in the future.

Considering the vagaries of clinical assessment, selection biases (likely skewed towards those cases with the most significant pain), and the small number and proportion of patients who have surgery, it is impossible to calculate meaningful sensitivity and specificity.

Careful patient selection and meticulous technique are essential to avoid a falsely reduced gallbladder EF:

• Use of a meal to stimulate gallbladder contraction is unreliable. CCK is released from the duodenal mucosa in response to the presence of nutrients in the duodenal lumen, particularly fats and proteins. The composition of the meal will affect the rate of delivery to the duodenum because of the effect on gastric emptying. Delayed gastric emptying resulting from diseases such as diabetes or renal failure will impair CCK release. Release of CCK is also dependent on normal pancreatic exocrine function and an intact duodenal mucosa which may be affected by conditions such as celiac disease or enteritis.

• Infusion of CCK-8 is the optimum method to stimulate gallbladder emptying. Maximal and reproducible gallbladder contraction is achieved by a physiologic infusion at a rate of 0.020 µg/kg per hour over a one hour period. Rapid infusion or bolus injection may result in submaximal contraction and nonspecific cramping abdominal pain. Pain reproduction is a poor indicator of disease and should not be used as a criterion.

• Gallbladder contraction is also dependent on cholinergic innervation, calcium ion concentration and pressure within the biliary tree. A wide variety of medications including those with cholinomimetic or inhibitory action, calcium channel blockers, opiates, and possibly H2 receptor antagonists and progestins may alter the normal response to CCK-8. Vagotomy, advanced neuropathy of diabetes and generalized smooth muscle abnormalities as may be seen with pseudo-obstruction syndromes can lead to reduced contractility (Table 1). The effect of body habitus, phase of menstrual cycle, oral contraceptives remain uncertain.

Reduced gallbladder contraction provides supporting evidence of a biliary cause for pain and for potential benefit from cholecystectomy. Scintigraphy should be reserved for patients thought to have biliary type pain by an experienced clinician. The patients must be free of serious concurrent illness and should not be taking medications which may impair gallbladder contractility. The use of scintigraphy as a screening procedure in patients with nonspecific upper abdominal pain is not recommended.

Assessment of the nature of the pain by an experienced clinician is probably the key criterion. Reduced gallbladder contractility in a patient with typical biliary type pain may provide confirmatory evidence of gallbladder dysfunction.

Post-Cholecystectomy Pain

Cholecystectomy results in remission or improvement in biliary type pain in most patients with calculi and pathologic findings of chronic cholecystitis. Ten to 40 % of patients may continue to experience symptoms. Most of these can be traced to nonbiliary causes such as pseudo-obstruction syndrome, gastroesophageal reflux, pancreatitis, and other unrelated conditions. Others have anatomic abnormalities of the biliary tree such as retained calculi, strictures or neoplasms which are best diagnosed by anatomic studies such as magnetic resonance cholangiopancreatography

---

Table 1. Factors contributing to a falsely low gallbladder ejection fraction

Too rapid or high dose CCK-8 infusion
Concurrent medications
                Drugs with cholinergic or anticholinergic action
                Calcium channel blockers
                Opiates
                H2 receptor antagonists
                Progestins
Autonomic neuropathy (diabetes)
Vagotomy
Pseudo-obstruction syndromes
Advanced liver disease
Pancreatitis
Any acute abdominal disease

(MRCP), CT or US. Endoscopic retrograde cholangiopancreatography (ERCP) is indicated for patients with normal anatomic imaging (apart from nonspecific CBD dilatation).

Symptoms in a small residual group without anatomic abnormality remain unexplained and may be on the basis of a functional disorder termed sphincter of Oddi dysfunction (SOD). Patients with typical biliary pain, a transient rise of liver enzymes after an episode of pain, and a dilated CBD (>12mm) or delayed drainage of ERCP contrast material from the CBD (>45 min) have been categorized as type 1 sphincter of Oddi dysfunction and should have an endoscopic sphincterotomy (ES). ES in this situation has been shown to stop attacks of pain in the majority of patients. Patients who have typical biliary pain but only some (type 2 SOD) or none (type 3 SOD) of the other findings are more problematic. Types 2 and 3 SOD patients with abnormal sphincter of Oddi pressures on manometry may respond to ES but abnormal sphincter of Oddi manometry is only seen in approximately 60% of these patients. Moreover manometry is not widely available, is technically difficult to perform and in this population has a high risk of complications (pancreatitis in 10-25%). Noninvasive testing with scintigraphy can be of value (Fig. 9).

Because these patients have intermittent or low grade obstruction, visual inspection of cholescintigrams lacks sensitivity. In the presence of a functioning gallbladder, bile may flow to the bowel or gallbladder depending on the sphincter of Oddi tone. After cholecystectomy, the biliary tree becomes a single outlet system. Bile flow from the canaliculi through small and large ducts to the duodenum follows a predictable temporal sequence that lends itself to quantification. A dilated biliary tree from prior obsruction can cause prolongation of transit, even in the absence of obstruction, because of the increased time it takes for a bolus to traverse a large volume duct compared with a normal calibre duct. Nevertheless, time to peak and 50% of peak activity in liver and bile ducts has proven useful to a number of investigators in identifying patients with SOD (Fig. 10). Combining the quantitative indices with semi-quantitative observations such as time of appearance of bile duct and bowel activity and degree of prominence of the bile ducts may be more accurate.
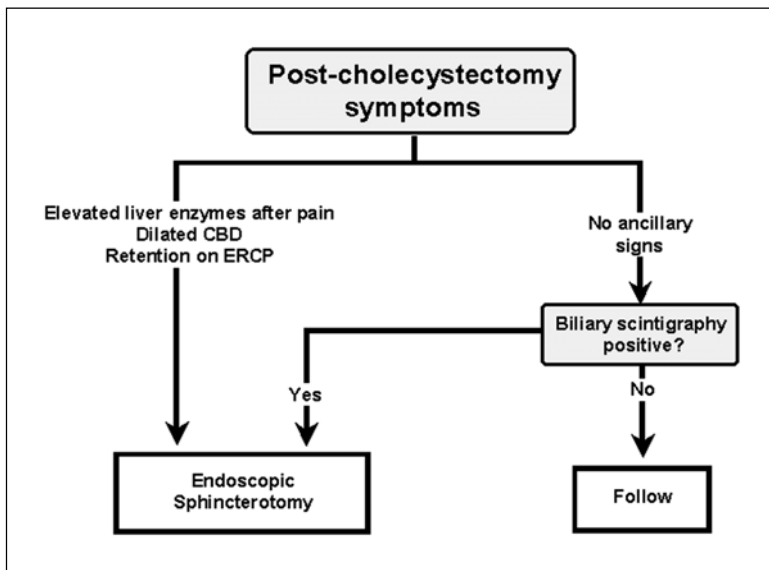
Figure 9. Flowchart for the investigation of post-cholecystectomy pain.

Obstruction in some patients may result from paradoxical contraction of the sphincter of Oddi in response to CCK and may only be apparent on CCK-8 augmented scintigraphy. Since CCK-8 enhances bile formation, signs of obstruction will be more apparent during high flow bile states compared with the low rates of production in the interdigestive phase—analogous to the use of diuretic renography to diagnose urinary tract obstruction. CCK-8 may also reduce the intermittent emptying seen during fasting. A prolonged physiologic infusion of CCK-8 should yield the best results.

Biliary obstruction

High grade biliary obstruction results in elevated intrabiliary pressure which reduces bile formation by opposing secretion from the liver and, over time, results in dilatation of the biliary tree. Bile duct dilatation is the hallmark of obstruction on anatomic imaging studies. US can easily detect dilatation of the CBD but may have difficulty visualizing its distal portion because of interference by bowel gas. CT and MRI are less affected by bowel gas and may be able to identify the cause. Scintigraphy shows abnormal retention of radiotracer in the biliary tree, or if intrabiliary pressure exceeds secretion pressure of the liver, will show hepatic uptake with prolonged retention. The findings are independent of biliary dilatation and a diagnosis can be made during the first hours or days before the diagnosis can be made by anatomic imaging. Scintigraphy, however, can seldom demonstrate the precise cause and anatomic imaging is the initial procedure of choice regardless of the time of suspected onset of biliary obstruction.
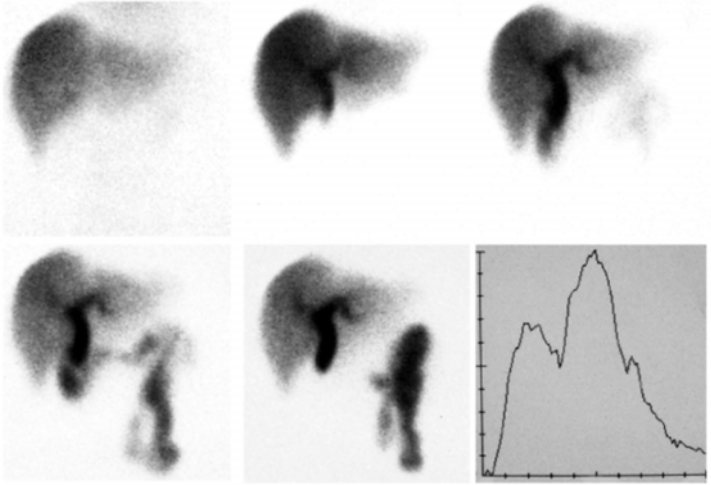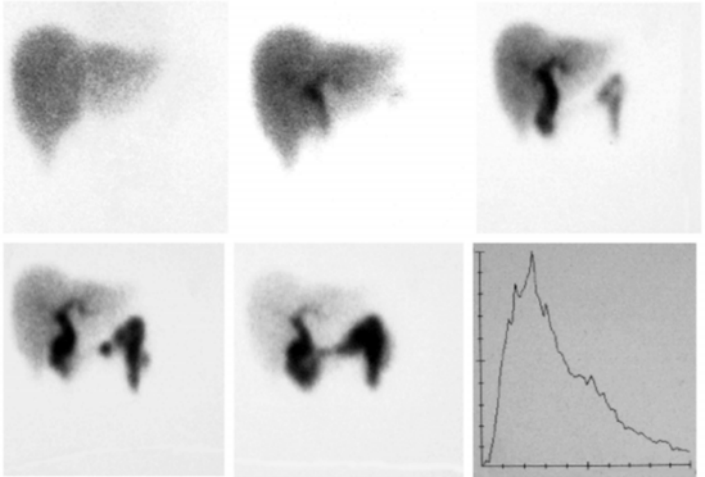
Figure 10. Postcholecystectomy sphincter of Oddi dysfunction (SOD) responding to endoscopic sphincterotomy. This 37 year old woman complained of recurrent right upper quadrant pain one year after cholecystectomy. Ultrasound was normal. ^{99m}Tc-IDA imaging shows prolonged retention in the biliary tree and a protracted bile duct curve (a). Symptoms resolved after endoscopic sphincterotomy and bile duct emptying also returned to normal (b).

Scintigraphy is an elegant way to visualize biliary-enteric diversions and was frequently used to assess anastomoses which were not accessible endoscopically. ERCP is still the preferred approach because it can reveal the cause of obstruction and provide an avenue for treatment. More recent surgical anastomoses include a fistula for endoscopic access. Moreover the greater use of endobiliary stents have significantly reduced the need for surgical diversion.

Post Traumatic or Post Surgical Bile leaks

The presence and location of fluid collections are best demonstrated by anatomic imaging studies. However these are seldom able to determine its makeup. Filling of the collection with radiolabelled bile confirms a bile leak. Tamponade from increased pressure within the collection may delay or even prevent further filling, interfering with diagnosis. Delayed imaging is essential in this instancce. Extraluminal surgical drains should not be clamped if the objective is to detect a bile leak but biliary drains should be clamped. Multiple views or SPECT can allow better localization and correlation with anatomic imaging.

Scintigraphy is particularly helpful following laparoscopic cholecystectomy because of the acute nature of the complications. Obstruction from retained calculi or a misplaced clip, or bile leaks from injury to the CBD or loss of cystic duct closure, are readily detected (Fig. 11). Complications are not infrequent after initial introduction of the procedure but as the endoscopic surgeons gain experience, the rates fall significantly.

Clinical Role in the Characterization of Liver Masses

The anatomic imaging modalities of CT and MRI are the procedures of choice for detection of focal liver masses. US is less sensitive but may reveal a liver mass as an incidental finding during a search for other suspected disease. The typical appearance of the masses, their enhancement characteristics on dynamic infused helical CT, or findings on different pulse sequences using MRI are often sufficient to provide a confident diagnosis. Masses of atypical or nonspecific appearance, particularly if the findings are at variance with the clinical presentation, may require further investigation. Nuclear medicine, because of its ability to differentiate cell types based on their antigenic coating or surface receptors, overall metabolic activity, or tissue specific metabolic function, is in a unique position to further characterize nonspecific masses independent of their anatomic appearance (Table 2).

Most liver masses displace the normal Kupffer cells and do not contain phagocytic cells of their own. These masses appear as photopenic defects if they are large enough to be resolved. Even using multidetector SPECT with high resolution collimation, the defects must be close to 2 cm at the surface of the liver and 3 cm deep within it in order to be visualized. Smaller masses cannot be confirmed to contain Kupffer cells unless uptake is greater than normal liver. Detectability for "hot" lesions relates to both size and relative intensity of uptake.

All masses (or pseudomasses) seen on CT, MRI, or US which take up ^{99m}Tc-sulfur colloid contain Kupffer cells and are benign. These include regenerative nodules, unusual lobulations of the liver, focal fatty sparing or infiltration, and focal nodular hyperplasia (FNH). Masses devoid of ^{99m}Tc-sulfur colloid uptake can be benign or malignant.
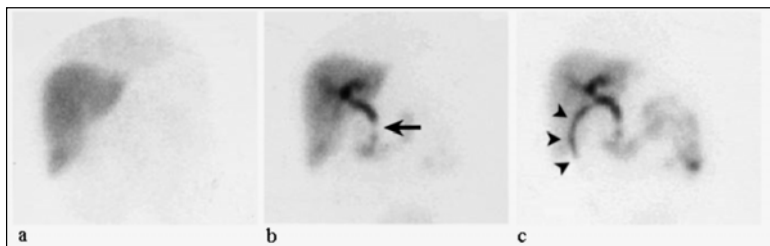
Figure 11. Bile leak after endoscopic cholecystectomy. A 73 year old man suffered increasing pain two days after endoscopic cholecystectomy. The immediate image (a) shows normal liver activity. Retention of radiotracer is seen in the biliary tree at 30 minutes (b). A defect in the distal CBD (arrow) is a retained calculus. Bile extravasation surrounding a biloma in the gallbladder fossa (arrowheads) is seen at 60 minutes (c).

^{99m}Tc-IDA is a marker for hepatocytes. Masses containing hepatocytes such as FNH, adenoma or hepatoma do not contain bile ducts connected to the biliary tree. Images performed shortly after injection may or may not demonstrate the mass. If visible, it may appear more or less intense than normal liver depending on the relative uptake. As normal liver excretes the tracer, the masses become relatively more intense than normal liver. The technique is most useful in localizing the masses on delayed SPECT images as the precise location may be difficult to determine from US examinations where images can be obtained in any orientation. Unfortunately, benign and malignant masses cannot be separated with complete confidence as well-differentiated hepatomas will also accumulate ^{99m}Tc-IDA.

Cavernous Hemangioma

Cavernous hemagiomas are single or multiple well-circumscribed clusters of large blood filled sinuses (Figs. 12 and 13). They occur predominantly in women. Most are asymptomatic and are discovered as incidental findings during CT, MRI or ultrasound performed for other reasons. Rarely pain may result from hemorrhage or thrombosis.

On US most cavernous hemagiomas are well-defined and hyperechoic because of reflections from multiple internal septa and vessel walls. Mixed echogenicity can result from thrombosis, hemorrhage, necrosis and scarring. Findings are nonspecific and hemangiomas cannot be confidently distinguished from vascular metastases, FNH, adenoma, or hepatoma.

On CT hemangiomas are hypodense without contrast enhancement. After contrast injection there is initial peripheral or globular enhancement ("puddling") which progresses toward the center. Small lesions may enhance rapidly and may be indistinguishable from other vascular masses. Large hemangiomas may not enhance completely or fill only later when most of the contrast is in the extracellular fluid space.

On MRI most hemangiomas are well defined and hyperintense on T-2 weighted images. Large lesions and those with hemorrhage, thrombosis or scarring tend to

Table 2. Characterization of liver masses

	RBC	SC	IDA	Ga	Technique	Sensitivity %	Specificity %
Cavernous hemangioma	++	-	-	-	RBC	80	100
Focal nodular hyperplasia (FNH)	N	++	++	N	SC/IDA	80	> 90
Hepatic adenoma (HA)	N	-	+	N	SC/IDA	80	> 90
Hepatocellular carcinoma (HCC)	-	-	+/-	++	Ga/SC	80	> 90
Focal fatty infiltration	N	N	N	N	SC	N/A	> 90
Focal fatty sparing	N	N	N	N	SC	N/A	> 90

RBC = ^{99m}Tc-red blood cells, SC = ^{99m}Tc-sulfur colloid, IDA = ^{99m}Tc-iminodiacetic acid (biliary), Ga = ^{67}Ga-gallium citrate, N/A = not applicable.
Key: ++ = much greater than normal liver, + = greater than normal liver, N = equal to normal liver, - = less than normal liver.

have atypical appearance. Differentiation from other vascular masses may be difficult.

The classic appearance on ^{99m}Tc-RBC imaging is an area of reduced perfusion on a flow study and reduced activity on immediate planar or SPECT because blood flow is low in relation to blood volume in the hemangioma. After 1 to 2 hours the radiolabelled cells have equilibrated and hemangiomas become uniformly intense and similar in intensity to the heart and major vessels. With this pattern, specificity approaches 100% making ^{99m}Tc-RBC imaging the procedure of choice. Hemangiomas as small as 1 cm can be visualized. When they are 1.5 cm or more, the sensitivity for detection exceeds 80%. Hemangiomas with extensive hemorrhage, necrosis, or scarring may not have the typical pattern, and small lesions adjacent to major vessels can be missed. Small suspected hemangiomas that are deep within the liver or adjacent to the heart are best studied with MRI.

Focal nodular hyperplasia

Focal nodular hyperplasia (FNH) is a hamartoma containing cords of hepatocytes and Kupffer cells separated by sinusoids and arranged into nodules. The nodules are separated by fibrous septa which radiate from a central scar and contain rudimentary bile ducts. The arterial supply originates at the center and radiates outward from the
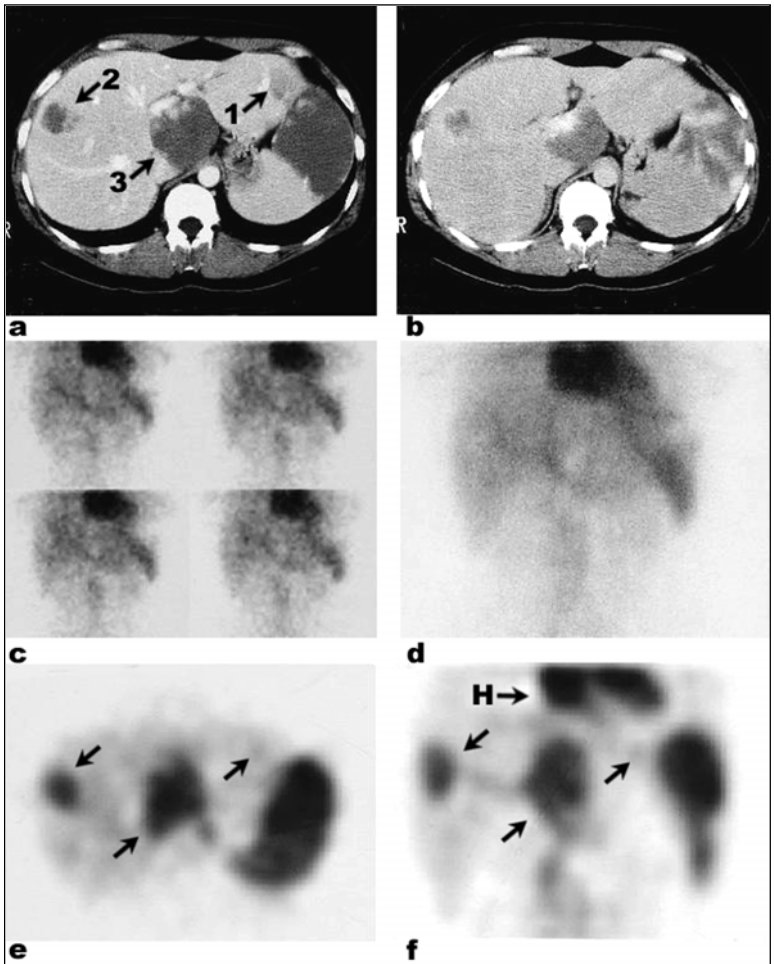
Figure 12. Multiple cavernous hemangiomas. Utrasound performed for pain in this 41 year old woman showed multiple large liver masses. Early and late images from an infused CT (a and b) show progressive centripetal (lesion 1), globular (lesion 2) and inhomogeneous (lesion 3) enhancement. The larger lesions are incompletely opacified. The masses are hypovascular on the flow and immediate images (c and d) and uniformly filled with ^{99m}Tc-RBC on transaxial (e) and coronal (f) delayed SPECT images. Activity in the hemangiomas is equivalent to the cardiac chambers (H).

outward from the center through the septa, unlike the peripheral origin and centripetal flow seen with adenomas and metastases.
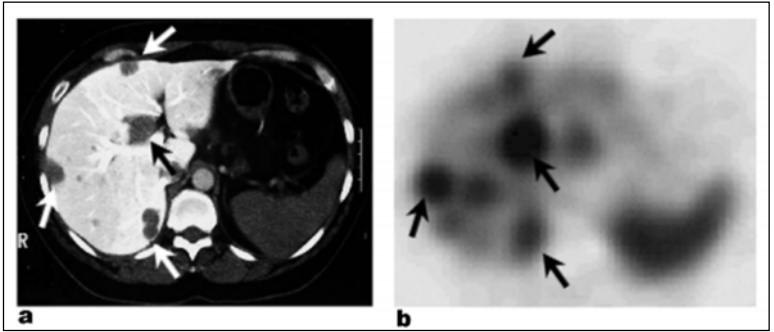
Figure 13. Multiple hemangiomas. The infused CT (a) done for staging of lung cancer in this 70 year old man shows non-specific small peripherally enhancing lesions in the liver (white arrows) with a larger lesion centrally (black arrow). ^{99m}Tc-RBC activity is equivalent to that in major vessels on the transaxial (b) delayed SPECT image (arrows).

On anatomic imaging the appearance is often nonspecific. On US, FNH tends to be well defined and isoechoic or hyperechoic. Doppler may show increased flow but this is also seen with other masses including metastases and hepatoma. On CT, FNH is usually isodense or hypointense and become hyperintense during bolus infusion of contrast. The central scar with radiating septa is characteristic but inconsistently seen.

^{99m}Tc-sulfur colloid imaging (Fig 14) shows intense uptake in 10%, a finding that is diagnostic for FNH. Twenty to 30% show no demonstrable activity or are too small to assess confidently. In the remainder, there is variable activity confirming the benign nature of the mass. A more specific diagnosis can be made by also demonstrating ^{99m}Tc-IDA uptake in the lesion.

Hepatocellular adenoma

Heptatocellular adenoma (HA) is a rare neoplasm that occurs almost exclusively in young women or those receiving ovarian hormone replacement therapy. Unlike FNH, HA has a high risk of hemorrhage, necrosis, infarction and even rupture with significant morbidity and mortality. HA consists of normal appearing hepatocytes. Arterial supply is from the periphery. The appearance on anatomic imaging is nonspecific.

Kupffer cells may be present but not in sufficient quantities for the masses to demonstrate ^{99m}Tc-sulfur colloid uptake. The pattern on ^{99m}Tc-IDA imaging is similar to FNH. In the absence of ^{99m}Tc-sulfur colloid uptake, this appearance is nonspecific and can also be seen with well-differentiated hepatomas.

Hepatocellular Carcinoma

Hepatocellular carcinoma (HCC) in North America typically occurs in the presence of cirrhosis making diagnosis difficult using the standard anatomic imaging modalities. Patients exposed to aflatoxins or anabolic steroids, or those with the
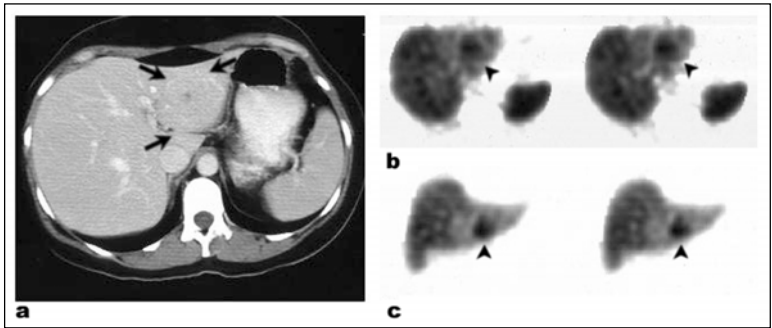
Figure 14. Focal nodular hyperplasia (FNH). The infused CT (a) performed for abdominal trauma in this 32 year old woman shows an isodense mass in the lateral segment of the left lobe of the liver (arrows). A central hypodense area suggests the central scar of FNH. Transverse (b) and coronal (c) ^{99m}Tc-sulfur colloid SPECT images show greater activity in the lesion (arrowheads) compared with normal liver confirming the diagnosis of FNH.

fibrolamellar variant of HCC, may have an otherwise normal liver. In that situation HCC often presents as a nonspecific vascular mass. A high proportion of advanced tumours will have portal vein thrombosis in the absence of portal vein compression.

^{99m}Tc-sulfur colloid imaging is useful in evaluation of a liver distorted by cirrhosis. Mass like areas that accumulate colloid represent localized areas of hypertrophy or regenerating nodules. Areas of absent colloid activity that accumulate gallium or some other marker of metabolic activity likely represent hepatoma (Fig. 4). Since close to 90% of all hepatomas accumulate gallium to some degree, simultaneous ^{99m}Tc-sulfur colloid subtraction yields the greatest sensitivity. In the absence of cirrhosis, the technique is less specific and other gallium-avid tumours cannot be differentiated.

On ^{99m}Tc-IDA imaging, the level of uptake by the HCC reflects the level of differentiation and greater accumulation carries a better prognosis. Well-differentiated HCC however cannot be differentiated from HA with confidence. Elevated alpha-fetoprotein supports a diagnosis of HCC.

Focal Fatty infiltration and Sparing

Fatty infiltration of the liver is seen with alcohol abuse, obesity, diabetes mellitus and other disorders of metabolism. Increased fat content results in hyperechogenicity on US and decreased density on CT. In some cases the fat deposition is nonuniform with areas of focal fatty infiltration or focal fatty sparing. The focally altered echogenicity on US or density on CT may be difficult to distinguish from metastases.
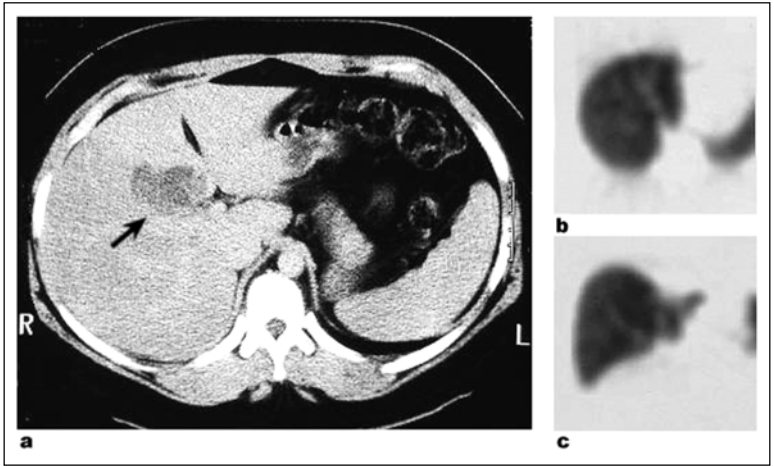
Figure 15. Focal fatty infiltration. Ultrasound performed for abdominal pain in this 27 year old woman showed a 4 x 5 cm. echogenic focus in the liver. A noninfused CT (a) shows a localized area of hypodensity in the medial segment of the left lobe of the liver (arrow). A traversing vessel appeared undisplaced suggesting focal fatty infiltration rather than a mass, but the appearance was not definitive. Transaxial (b) and coronal (c) ^{99m}Tc-sulfur colloid images show uniform activity confirming a benign process.

Lack of displacement of vessels and the characteristics of fat on MRI are helpful in the diagnosis in both situations. Kupffer cells are unaffected and the liver appears homogeneous on ^{99m}Tc-sulfur colloid imaging (Fig 15).

Frequently Asked Questions (FAQs)

Can scintigraphy predict whether or not a patient's atypical chronic symptoms are related to the presence of known gallstones?

No. Gallstones are common and do not necessarily result in symptoms. Delayed visualization or nonvisualization of the gallbladder or abnormal emptying can certainly be seen in asymptomatic patients. The value of these scintigraphic findings in predicting who will have a favorable response to cholecystectomy is unknown. Clinical assessment as to the nature of the pain is the most reliable predictor.

Does nonvisualization of the gallbladder in a patient with acute RUQ pain confirm the presence of acute cholecystitis?

No. Visualization of the gallbladder effectively excludes acute calculous cholecystitis. Cystic duct obstruction in the absence of acute inflammation, a contracted gallbladder filled with stones, inadequate fasting, impaired liver function, and other acute intra-abdominal disease can also result in nonvisualization. Focal

in the gallbladder fossa or a "rim" sign add specificity to the diagnosis of acute cholecystitis but are relatively uncommon findings.

Are all masses that accumulate ⁹⁹ᵐTc-sulfur colloid benign?

Yes. Anatomic variations in the shape of the liver, regenerating tissue, focal fatty infiltration or sparing and FNH all contain Kupffer cell populations. If one of the above named conditions is suspected, ⁹⁹ᵐTc-sulfur colloid imaging is the initial procedure of choice. The only caveat is that the "mass" must be large enough to be resolved as a photopenic area in the absence of ⁹⁹ᵐTc-sulfur colloid uptake.

Are all masses that accumulate ⁹⁹ᵐTc-IDA benign?

No. Although the level of uptake reflects the degree of differentiation of hepatocytes in the mass, well-differentiated HCC will show activity comparable to some cases of HA and FNH. ⁹⁹ᵐTc-IDA imaging is an ancillary procedure to localize a mass or to make a specific diagnosis of FNH in a mass already proven to be benign by ⁹⁹ᵐTc-sulfur colloid uptake.

Does failure to visualize a hemangioma suspected on US or CT using ⁹⁹ᵐTc-RBC indicate a malignant mass instead?

No. Hemangiomas may not be visible because of their small size or proximity to the heart or larger vessels deep within the liver. MRI may be useful in that situation. Hemorrhage, thrombosis, or fibrosis may obliterate the blood filled spaces. Serial anatomic imaging, to ensure stability in size, or biopsy may be necessary.

Additional Reading

1. Heiken P. The liver. In: Lee J, Segal S, Stanley R, Heiken J, eds. Computed Body Tomography with MRI Correlation. 3rd ed. Philadelphia: Lippincott-Raven, 1998:701-778.
   A detailed review of the role of CT and MRI in the diagnosis of liver masses.
2. Kinnard M, Alavi A, Rubin RA, Lichtenstein GR. Nuclear imaging of solid hepatic masses. Seminars in Roentgenology 1995; 30:375-395.
   A detailed description of the role of scintigraphy in characterization of liver masses.
3. Katsuyoshi I, Kazumitsu H, Takeshi F et al. Liver neoplasms: Diagnostic pitfalls in cross-sectional imaging. Radiographics 1996; 16:273-293.
   A pictorial overview of problems in diagnosis of liver lesions with CT and MRI.

11

Inflammatory Disorders

William D. Leslie and Pierre Plourde

Pathophysiology of Inflammation

Inflammation is the organized reaction of the microcirculation to tissue injury. Tissue injury sets in motion a carefully orchestrated complex cascade of events in an attempt to eliminate the offending agent and repair any damage. Acute inflammation is typically brief (lasting minutes to days) and features the neutrophil as the dominant cell. In contrast, chronic inflammation persists much longer (from weeks to months) and the cellular response is dominated by tissue macrophages and lymphocytes. It is important to recognize that there is a continuum in these two processes, and most inflammatory responses consist of a measure of both.

Acute inflammation leads to three basic tissue responses: (a) vasodilation and increased blood flow (hyperemia) with slowing of the microcirculation (stasis), (b) loss of endothelial integrity with leakage of fluid and plasma components, and (c) emigration of leukocytes into the extravascular tissue. The clinical counterparts of these pathologic events are local hyperemia, swelling and pain. Acute inflammation is mediated by plasma-derived and cellular components (Fig. 1). The importance of adhesion molecules has recently been recognized. These are membrane glycoproteins found on the surface of activated endothelial cells, leukocytes and platelets. The complementary expression of these molecules on leukocyte and endothelial surfaces induces an interaction characterized initially by rolling, subsequent adhesion and finally transmigration of the leukocyte between adjacent endothelial cells.

Granulocytes combat invading microorganisms in several ways. If possible, the organisms are phagocytosed and then destroyed with powerful oxidants such as superoxide and hydrogen peroxide generated through a "respiratory burst". Other microorganisms are rendered susceptible to phagocytosis through opsonization with immunoglobulins or activated complement. Lactoferrin is discharged from the granulocytes' secondary granules and binds iron, an essential growth factor for many bacteria and fungi. Neutrophils predominate in the inflammatory infiltrate during the initial 6-24 hours but have a short life span. They spend a brief period of time in the circulation (half-life about 6 hours) and, having migrated out of the vascular space, are then unable to reenter it. In the extracellular space neutrophils undergo programmed cell death (apoptosis) after only 24-48 hours.

In some situations *chronic inflammation* evolves from an acute inflammatory process, but in other scenarios (including viral, parasitic, autoimmune, foreign body, and malignant inflammatory processes) it represents the primary immune response. The chronic tissue response is often characterized by fibrosis, cellular proliferation and granulation tissue formation. The activated T-lymphocyte is responsible for the production of chemotactic and growth factors which act to recruit monocytes and induce tissue proliferation of macrophages. Activated tissue macrophages may fuse
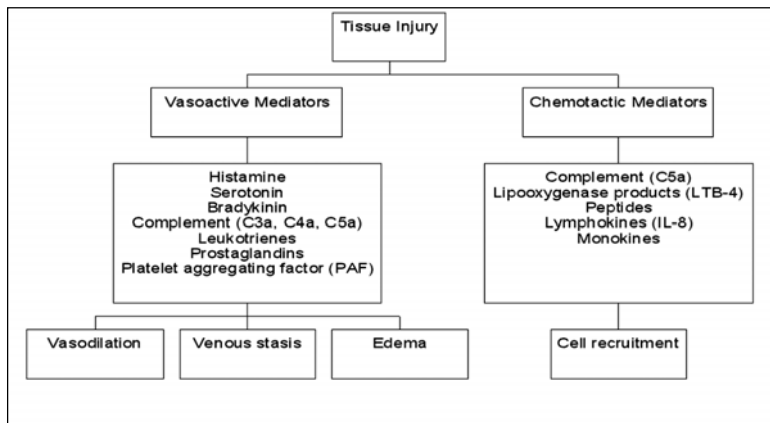
Figure 1. Mediators of the inflammatory response can be divided into vasoactive and chemotactic factors.

to form the multinucleated giant cells found in granulomata. *Granulomatous inflammation* is often used for dealing with indigestible materials, and is the form of chronic inflammation typically seen in fungal infections, tuberculosis, foreign body reactions and sarcoidosis.

Technical Considerations

From the foregoing discussion it can be seen that several points in the inflammatory cascade are potential targets for nuclear medicine scanning techniques. There are two primary mechanisms that cause tracers to localize at sites of inflammation: *active migration* and *passive diffusion* (Fig. 2). Active migration exploits chemotaxin-directed motility of leukocytes that have been labeled ex vivo or after injection of anti-granulocyte antibodies. In contrast, passive diffusion occurs when the agent—usually a large metal-protein chelate—leaks through inflamed permeable capillary walls and is the primary mechanism of accumulation for gallium, polyclonal immunoglobulins and nanocolloids.

111In-Leukocytes

Indium is a heavy metal that shares many of the chemical properties of iron and gallium. The ^{111}In radioisotope is linked to host leukocytes which are actively recruited to sites of inflammation. Following reinjection, ^{111}In-leukocytes rapidly leave the intravascular space to enter the liver (10- 20%), spleen (20-40%) and hematopoietic bone marrow (30-60%) (Fig. 3). By 24 hours, there is minimal residual intravascular activity, although some blood pool may persist if excessive numbers of labeled erythrocytes are present. Identification of inflammatory foci in the liver or spleen is therefore very difficult due to the normal levels of accumulation. Inflammatory lesions in areas of hematopoietic marrow, such as the spine, may also be hard to detect. The absence of appreciable leukocyte accumulation in most soft tissue areas is a considerable advantage, however, as inflammatory lesions are usually very striking against the low background.
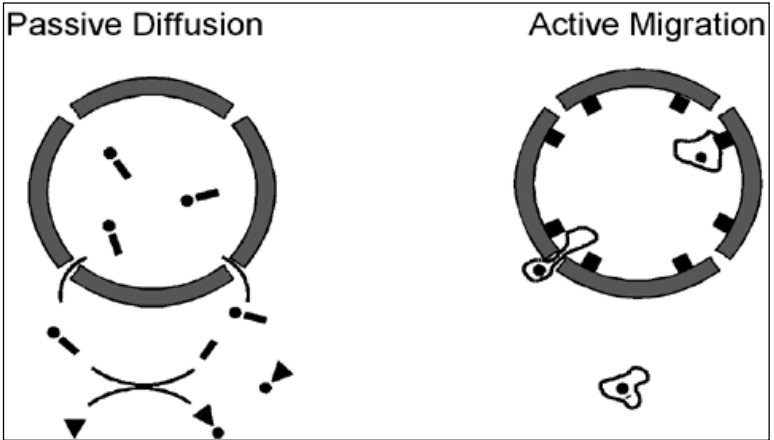
Figure 2. Mechanisms of radiopharmaceutical accumulation at sites of inflammation. In passive diffusion (left), a metal radionuclide (circle) bound to a circulating plasma carrier protein (rectangle) extravasates through permeable capillary endothelium. A leukocyte-derived protein (triangle) may bind the radionuclide in the interstitium. In active migration (right), leukocytes labelled with a metal radionuclide (circle) are induced to adhere and transmigrate by the presence of endothelial adhesion molecules (rectangles).

Preparation

In order to cross the leukocyte's cell membrane, indium must be chelated to a lipophilic carrier molecule such as oxine or tropolone. The labeling protocol is outlined in Table 1. Not all departments have the ability to perform cell labeling as this requires experienced personnel, laminar flow hoods and impeccable quality control to ensure a safe and satisfactory product. Although there is no specific patient preparation for the test, it is important to ensure that the patient has an adequate number of circulating leukocytes (at least $3x10^9$/L). A large quantity of anticoagulated blood (40-50 ml) must be withdrawn from the patient to obtain sufficient numbers of leukocytes. Autologous leukocyte scanning is not feasible in infants due to the large volume of blood required. Similarly, neutropenic patients are unsuitable subjects. In rare circumstances, donor leukocytes can be used.

Leukocytes must be handled gently to avoid activation as this compromises their viability and ability to migrate to sites of inflammation. In general, the period of time during which leukocytes remain ex vivo should be as short as possible and ideally less than 2 hours.

Imaging Considerations

Imaging typically involves both early and late scans. Early imaging is performed between one and four hours post-injection and the delayed images are performed at 24 hours. Due to the long half-life of ^{111}In (approximately 3 days), further images up to 48 hours are also possible. With inflammatory bowel disease leukocyte
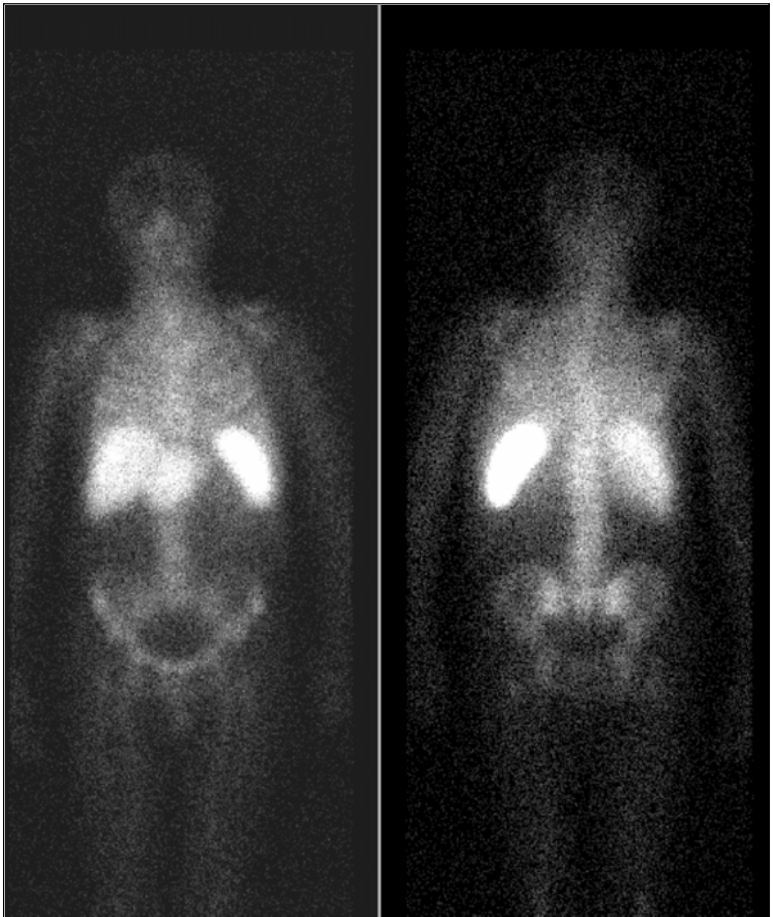
Figure 3. Normal ¹¹¹In-leukocyte scan. Note the normal accumulation within bone marrow, liver and spleen. As in this patient, the spleen typically shows the most intense accumulation of ¹¹¹In-leukocytes.

accumulation in the inflamed mucosa is typically extremely rapid but peristalsis of leukocytes shed into the bowel lumen can lead to distal migration with inaccurate localization unless very early (1 hour) images are obtained. Low grade inflammation may not be apparent on the early images and sensitivity is much better at 24 hours. Occasionally non-inflammatory hyperemia can be misinterpreted as inflammation if only one set of images is acquired. Comparing early and delayed images is particularly helpful in this regard, since true inflammation should show a progressive increase in leukocyte activity.

Table 1. Generic procedure for ^{111}In-leukocyte cell labeling

1. Blood (40-50ml) is drawn into an anticoagulated syringe.
2. The syringe is placed upright for one hour to allow erythrocyte sedimentation, a process that is accelerated by the addition of hydroxyethyl starch.
3. The leukocyte-rich plasma is transferred to a sterile tube where it undergoes centrifugation. Platelets remain suspended in the plasma and a leukocyte pellet forms at the bottom of the tube.
4. The cells are resuspended and incubated with the lipophilic ^{111}In-chelate.
5. ^{111}In-leukocytes are slowly reinjected intravenously into the patient with a typical dose of 18.5 MBq (500 µCi).
6. Extreme care must be taken in the labeling of the blood sample at each stage and in its handling to avoid any possibility of mix up with other blood samples. The label and the patient's identity must be carefully verified before re-injection.

Due to the low injected activities, imaging is prolonged (10-20 minutes per static view) and the low counts result in limited image detail. This can make it difficult to localize a focus of uptake, particularly in the peripheral extremities which normally lack hematopoietic marrow and where leukocyte uptake can appear as an isolated "point in space". The gamma camera is able to distinguish isotopes photon energies (^{111}In energies 247 and 173 keV versus ^{99m}Tc 140 keV). This makes it possible to scan two different tracers simultaneously: the ^{111}In- leukocytes detect inflammation and a ^{99m}Tc-labeled tracer is used for localization and diagnostic correlation. Examples of dual-isotope strategies are as follows: ^{99m}Tc-bone tracers for localization and simultaneous assessment of suspected osteomyelitis (Fig. 4); ^{99m}Tc-colloid to map marrow in suspected infection of an orthopedic prosthesis; and ^{99m}Tc-erythrocytes in identifying vascular graft or shunt anatomy (see section on Clinical Role in Vascular graft infection).

^{99m}Tc-Leukocytes

The general principles of ^{111}In-leukocyte preparation also apply to ^{99m}Tc-leukocytes. ^{99m}Tc- HMPAO (hexamethylpropyleneamine oxime) is a lipophilic chelate that readily crosses the cell membrane of the leukocyte and then undergoes conversion to a secondary complex through a glutathione-dependent process. Technetium-99m activity becomes bound to intracellular organelles and is "trapped". The advantage of using the ^{99m}Tc label is its ready availability in any nuclear medicine laboratory. The short half-life of ^{99m}Tc means that a much higher dose (550 MBq or 15 mCi) is injected resulting in much higher image counts, improved image quality and the possibility of performing tomographic SPECT imaging. Labeling can be performed in plasma which minimizes deleterious effects on cell viability, function and lung sequestration.

^{99m}Tc-leukocytes share the same distribution as the indium-111 analog with intense spleen, moderate liver and hematopoietic marrow accumulation. In contrast to ^{111}In-leukocytes, however, there is also significant gastrointestinal and urinary tract activity (Fig. 5). This probably occurs through elution of technetium-99m activity from labeled leukocytes which is subsequently excreted through hepatobiliary and renal mechanisms. Biliary tract activity can be seen within one hour of injection but gut activity is usually absent prior to three hours. The more soluble nature of
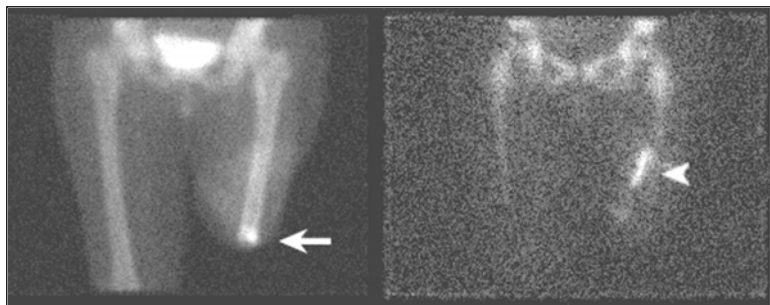
Figure 4. Soft tissue infection of a left above-knee amputation stump imaged simultaneously with a dual-isotope method. A conventional bone scan with 99mTc-MDP (left) shows normal reaction at the surgical amputation site (arrow). The 111In-leukocyte scan (right) shows focal accumulation more proximally that tracks along the medial femoral cortex (arrowhead).

technetium-99m also leads to greater elution of the label from the WBC and therefore the fractional uptake at 18-24 hours is usually less than with 111In-leukocytes. Nonetheless, in direct comparisons the improved image quality seen with 99mTc-leukocytes offsets any reduced retention such that the two agents are equivalent in terms of their ability to detect inflammatory lesions.

Imaging Considerations

As with 111In-leukocytes, early and delayed imaging should be performed. Due to the shorter half life, however, this is usually performed one and four hours post-injection. Images can also be performed at 24 hours, although isotope decay and normal bowel activity limit image quality.

Gallium

Gallium is a heavy metal that is handled by the body in a manner very similar to iron. It is injected in the form of 67Ga-gallium citrate, the gallium component of which then binds avidly to transferrin. The circulating metal-protein complex is thought to localize at sites of inflammation through the following mechanisms: increased delivery due to hyperemia, increased pooling due to vasodilation, passive diffusion into the interstitium through "leaky" capillaries, and binding of gallium to other iron-avid proteins such as granulocyte-derived lactoferrin or bacterial siderophores. Lactoferrin is also responsible for the normal visualization of lactoferrin-secreting glands such as the lacrimal glands and breasts. It is currently believed that the most important factor is diffusion across inflamed capillaries with retention within the interstitial space. There is negligible binding of gallium to viable granulocytes and localization can occur in the absence of leukocytes. Gallium has therefore proven to be an effective agent in immunosuppressed and leukopenic patients.

Gallium normally concentrates in sites of iron storage (liver, erythropoetic bone marrow and to a lesser degree spleen), in secretory organs that produce lactoferrin

Figure 5. Normal ^{99m}Tc-leukocyte scan. Imaging performed 4 hours post-injection shows late appearance of non-specific bowel activity in the right abdomen and urinary bladder activity.

(lacrimal glands, salivary glands, breast) and in the skeleton (Fig. 6). In normal persons, gallium is taken up by the liver (5%), spleen (1%), kidneys (2%), bone marrow (5%), and skeleton (13%). During the initial 24 hours the urine accounts for a small amount of gallium excretion (25%), and subsequent clearance proceeds
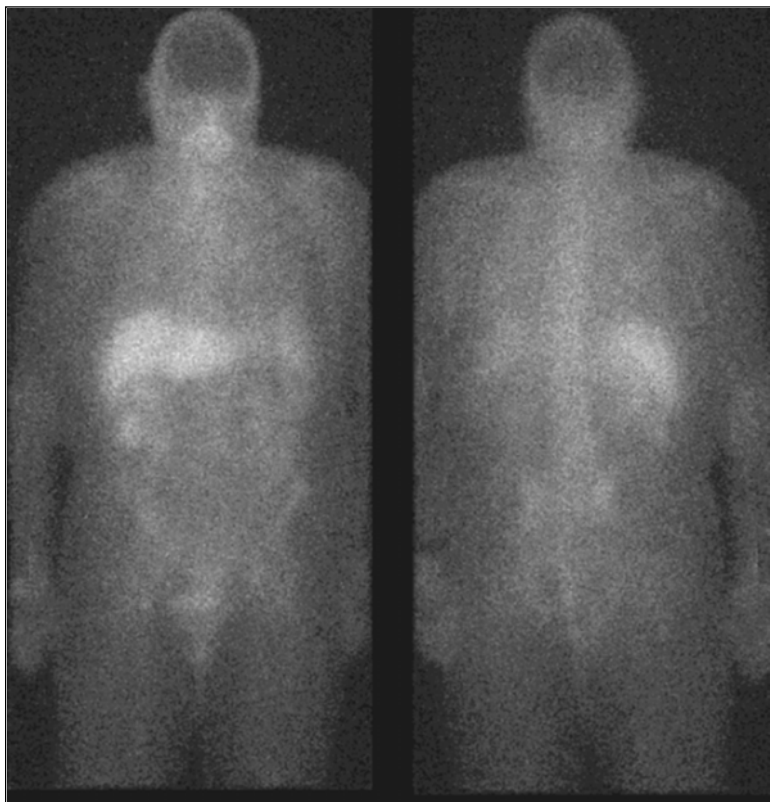
Figure 6. Normal ^{67}Ga-gallium citrate whole body scan (left anterior, right posterior). There is normal accumulation in the liver, bone marrow and soft tissues. Uptake in the right upper quadrant of the abdomen reflects normal gut excretion.

very slowly (at 7 days post-injection the decay-corrected whole body retention is still 65%). Variable uptake in the nasopharyngeal lymphoid tissue, lacrimal glands and salivary glands can also be a normal finding. Posterior images of the abdomen may reveal faint renal uptake up to 24 hours post-injection. Thymus and spleen uptake may be prominent, particularly in children or following chemotherapy.

Abnormal patterns of gallium accumulation can be seen when the plasma carrier protein, transferrin, becomes saturated e.g., following chemotherapy, blood transfusion, hemochromatosis or iron therapy. The scan pattern tends to resemble a bone scan, with prominent skeletal uptake, little soft tissue uptake, and increased renal and bladder activity. If this is suspected then measuring serum iron and transferrin should reveal the nature of the problem.

Figure 7. Normal ⁹⁹ᵐTc-antigranulocyte antibody scan (LeukoScan®).Imaging performed 1 hour (left) and 4 hours (right) post-injection show late appearance of nonspecific bowel activity. (Courtesy of ImmunoMedics Inc., Morris Plains, NJ).

12

Imaging Considerations

The usual dose of ^{67}Ga-gallium citrate is 111-185 MBq (3-5 mCi) injected intravenously. Higher doses up to 370 MBq (10 mCi) are used if tomographic SPECT imaging is planned. Gallium localizes relatively slowly and images are usually first obtained at 24-48 hours which is a disadvantage in acutely ill patients in whom a rapid diagnosis is required. There is variable gallium excretion by the gastrointestinal tract. Many groups routinely use cathartic bowel preparations to clear gastrointestinal activity. In most situations, performing delayed views (up to one week post-injection) will clarify if abdominal activity is physiologic excretion (which typically clears over time) or inflammatory in nature (which usually stays "fixed").

Monoclonal Antibodies

Monoclonal antibodies have long held the promise of increased diagnostic specificity. In theory, such agents could be directed at antigens expressed on immunologically competent host cells or at epitopes on infectious organisms. The greatest experience has been with mouse-derived (murine) antigranulocyte antibodies directed at cell surface antigens. Granulocytes in the circulation, as well as those already localized at the inflammatory site, become labeled by isotope bound to the injected monoclonal antibody. Some contribution from passive diffusion is probably present though this has not been quantified. The use of monoclonal antibodies directed towards leukocyte cell membrane antigens thus has the potential of combining the "best of both worlds". In addition to the excellent inflammatory targeting of leukocytes, these agents can be administered through simple intravenous injection. This avoids the inconvenience and risk of cell handling, cell activation and reinjection of a blood product.

Soon after injection the tracer is confined to the vascular spaces, but then gradually accumulates in liver, spleen and bone marrow (Fig. 7). As with ^{99m}Tc-leukocytes, some of the ^{99m}Tc label separates from the antibody and can appear in the bowel after 3 hours. Antibody fragments are nearly completely eliminated by the kidneys and accumulate in renal tubular cells, which limit its use for evaluating the urinary tract.

Preparation

Several antibody preparations and radionuclide labels have been investigated, including ^{111}In, ^{99m}Tc and ^{123}I. A convenient ^{99m}Tc-based kit formulation of Fab' fragments, known as sulesomab (LeukoScan®), is currently approved in some countries and undergoing clinical trials in others. A ^{99m}Tc-labeled intact IgG antibody is available in Europe for (Granulozint®). Both products target antigens shared by carcinoembryonic antigen (CEA) and granulocytic normal cross-reacting antigens (NCA-90 and NCA-95, respectively). Early clinical trials with ^{99m}Tc-anti-CD15 (LeuTech®) also appear promising.

Although doses of antibody exceeding 10% antigen saturation can lead to cell activation, this can be avoided by keeping the administered dose less than 1 mg. Lower doses and the use of antibody fragments deficient in the Fc-terminal also avoids the induction of human anti-mouse antibody (HAMA), an important consideration since HAMA leads to accelerated immunoglobulin clearance and may preclude additional administrations. Monoclonal antibodies are used in a variety of laboratory tests such as serum CEA, a tumor marker, and results may be affected (usually falsely low).

Imaging Considerations

Imaging is similar to labeled leukocytes. In general, Fab' fragments are much smaller than intact antibodies (50 kD in comparison to 180 kD) leading to more rapid clearance from the circulation and earlier diagnosis. Images as early as one hour can show diagnostic findings and delayed images up to 24 hours can also be performed. These agents appear to be comparable to [111]In- leukocyte imaging for identifying acute inflammation with sensitivity and specificity in the range of 77-91% and 67-75%, respectively (Fig. 8).

Polyclonal Immunoglobulins

The ability of polyclonal human immunoglobulin IgG (HIG) to detect inflammatory foci was a serendipitous discovery. Passive diffusion is probably the primary mechanism of uptake with retention in the interstitium due to the large molecular size (169 kD). HIG can be labeled with either ^{99m}Tc or [111]In. However, interest in radiolabeled immunoglobulins has waned considerably after reports that viral infections (most notably hepatitis C) have been transmitted with therapeutic doses.

Nanocolloids

Nanocolloid refers to a human albumin colloid (Nanocoll TN®). The ^{99m}Tc-labeled particles (mean particle size of 30 nm and virtually no particles larger than 80 nm) are small enough to extravasate through leaky inflamed capillaries. Plasma clearance by the reticuloendothelial system (RES) is extremely rapid which permits imaging between 30 minutes and 2 hours post-injection. Normal uptake by liver, spleen and hematopoetic tissue limits assessments of the abdomen, spine and areas with surgically disturbed marrow. Good results have been reported in peripheral bone and joint inflammation but sensitivity for soft tissue infections is only 59% (compared to 97% for labeled leukocytes in the same series).

Newer Agents

A variety of newer radiopharmaceutical agents are being developed, and many of these have already undergone clinical trials. Promising results have been reported with a two-step streptavidin-biotin approach. The unlabeled streptavidin is injected and allowed to localize through passive diffusion. Subsequently, the patient is injected with radiolabeled ^{111}In-biotin, which is much smaller and has high binding affinity for streptavidin. Streptavidin-biotin imaging appears to be clinically useful for orthopedic and vascular graft infections. Advances in the understanding of the pathophysiologic mechanisms of diseases and the associated molecular biology may lead to exciting developments in radiotracers that target endothelial selectin receptors expressed in response to local inflammatory stimuli. In areas where positron emission tomography (PET) is available, ^{18}F-fluoro-deoxyglucose (FDG) appears to be a sensitive technique.

All of the previous radiolabeling techniques fail to distinguish between bacterial-mediated infection and non-bacterial inflammation. Recently, ^{99m}Tc-Infecton, a novel ciprofloxacin based imaging agent, has been proposed to be specific for bacterial infection. In preliminary reports this agent has shown a sensitivity of 70% and a specificity of over 90% for detecting infective foci, with better imaging results than even radiolabeled leucocytes. False negative results were attributed to previous or current antibiotic treatment and/or infection with organisms that do not take up
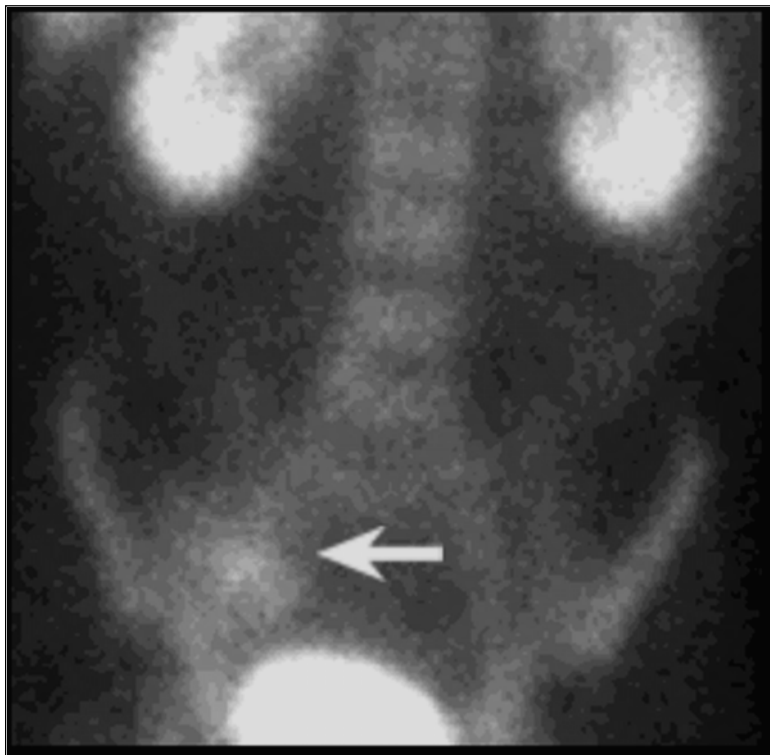
12

Figure 8. Abnormal ^{99m}Tc-antigranulocyte antibody scan (Leukoscan®). Imaging performed 1 hour post-injection shows focal accumulation in the right lower quadrant (arrow) subsequently surgically proven to represent acute appendicitis with an atypical clinical presentation. (Courtesy of ImmunoMedics Inc., Morris Plains, NJ.)

Infecton. If this agent lives up to the initial promise then Infecton will have major advantages over current imaging techniques, including radiolabeled leucocytes, and may prove to be a superior method for localizing bacterial infections.

Clinical Role: General Principles

Inflammation reflects a pathophysiologic process whereas the gross anatomic changes may lag far behind. Conventional imaging typically provides information on only one part of the body, and detects disturbance to the normal anatomy. In contrast, nuclear medicine can scan the whole body and localize occult disease processes. In many cases, anatomy may be severely distorted by previous disease, surgery or prosthetic materials with the result that conventional imaging is severely degraded. For these reasons, nuclear medicine occupies an important niche in diagnosing and localizing inflammation when conventional imaging is unsuccessful.

Nuclear medicine is particularly helpful in the following situations: (1) when an inflammatory process is suspected but there are no localizing features clinically (2) when there is clinical localization but conventional imaging is not diagnostic or is uninterpretable.

As part of the patient preparation it is important to identify any recent surgical interventions, wounds, drains, tubes or ostomy sites since these can be a cause of tracer accumulation.

The two most commonly used agents for the detection and localization of inflammatory foci are ^{111}In-leukocytes and ^{67}Ga-gallium citrate. These agents are not interchangeable; each has its own strengths, weaknesses and applications. For example, false-negative studies with labeled leukocytes tend to occur in infections that are more than two weeks old, the reverse of gallium which appears to be better for chronic granulomatous non-pyogenic infections. Thus the two agents should be seen as complementary.

There have been very few clinical studies comparing the various inflammatory nuclear medicine agents. In animal models of abscess formation, the abscess/blood or abscess/soft tissue ratio seen with ^{111}In-leukocytes is approximately an order of magnitude greater than with passive diffusion agents (Fig. 9). ^{99m}Tc-leukocyte uptake in experimental infections is also less than with ^{111}In-leukocytes due to release of the technetium-99m from leukocytes.

The sensitivity of leukocyte scanning for identifying sites of pyogenic infection is 80-88%; specificity is close to 97%. Noninfectious causes of uptake can be seen with ^{111}In-leukocytes and with all of the other agents discussed in this Chapter (Table 2). Bilateral diffuse pulmonary uptake is a non-specific finding that can be seen with unsatisfactory labeling (from cell activation), severe sepsis, congestive heart failure, radiation pneumonitis, adult respiratory distress syndrome and pulmonary vasculitis (Fig. 10). More focal pulmonary uptake suggests the presence of pneumonia, abscess, empyema, septic embolus or infected bronchiectasis. The incidence of leukocyte uptake by neoplasms is 2-34%, but is usually quite low grade.

Most studies of chronic musculoskeletal infections, such as infected orthopedic prostheses, report that leukocyte scintigraphy is still highly accurate. This may reflect the fact that most laboratories use a mixed leukocyte population that contains a significant fraction of lymphocytes. Soft tissue infections often produce dramatic uptake (Fig. 11). It has been questioned whether antibiotics modify the inflammatory response but studies show little effect from short-term treatment. Antibiotics may sterilize bacteria but once the inflammatory cascade has been set in motion it is maintained by the inflammatory effects of cellular debris and bacterial cell membranes.

[99m]Tc-leukocytes can be used in many of the same situations as ^{111}In-leukocytes. In general, they may be preferred in acute sepsis when earlier imaging permits a more rapid diagnosis or when tomographic SPECT imaging is necessary. An advantage in inflammatory bowel disease is the ability to perform dynamic imaging which may improve localization. Proctitis may be masked by urinary activity in the bladder, however.

Gallium is of limited usefulness in the abdomen and pelvis due to normal excretion into the gut. Noninflammatory gallium uptake can occur with fractures, myositis ossificans, heterotopic bone and hematomas. Soft tissue infections are usually well seen due to low levels of uptake in the adjacent tissue (Fig. 12). Since the lungs are

Table 2.   Causes of noninfectious leukocyte accumulation leading to false positive scan interpretation

Noninflammatory	Inflammatory
Accessory spleen	Sterile infarction
Gastrointestinal bleeding	Sterile arthritis
Swallowed respiratory tract activity (pulmonary, sinus) simulating abdominal disease	Adult respiratory distress syndrome
	Sarcoidosis
Focal vascular activity (aneurysm)	Inflammatory bowel disease
Cell clumping (pulmonary)	Pancreatitis
Tumors	Drugs (pneumonitis, interstitial nephritis)
Fractures	
Ostomy sites	
Hematomas	
Organ transplants	
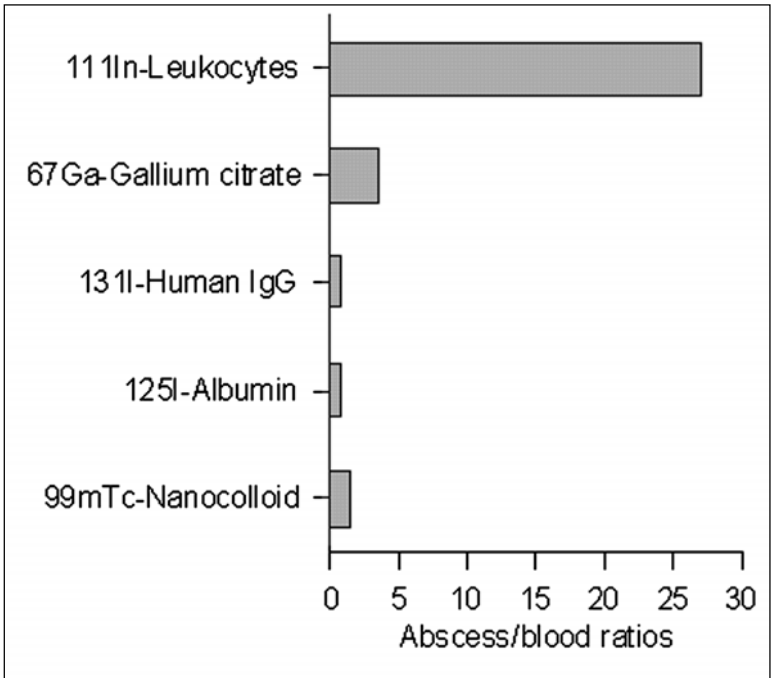
Figure 9. Abscess/blood ratios for several inflammation radiopharmaceuticals. Leukocytes lead to much higher accumulation ratios than passive diffusion agents. (Adapted from data in McAfee J et al, J Nucl Med 1991; 32:2126-2131.)
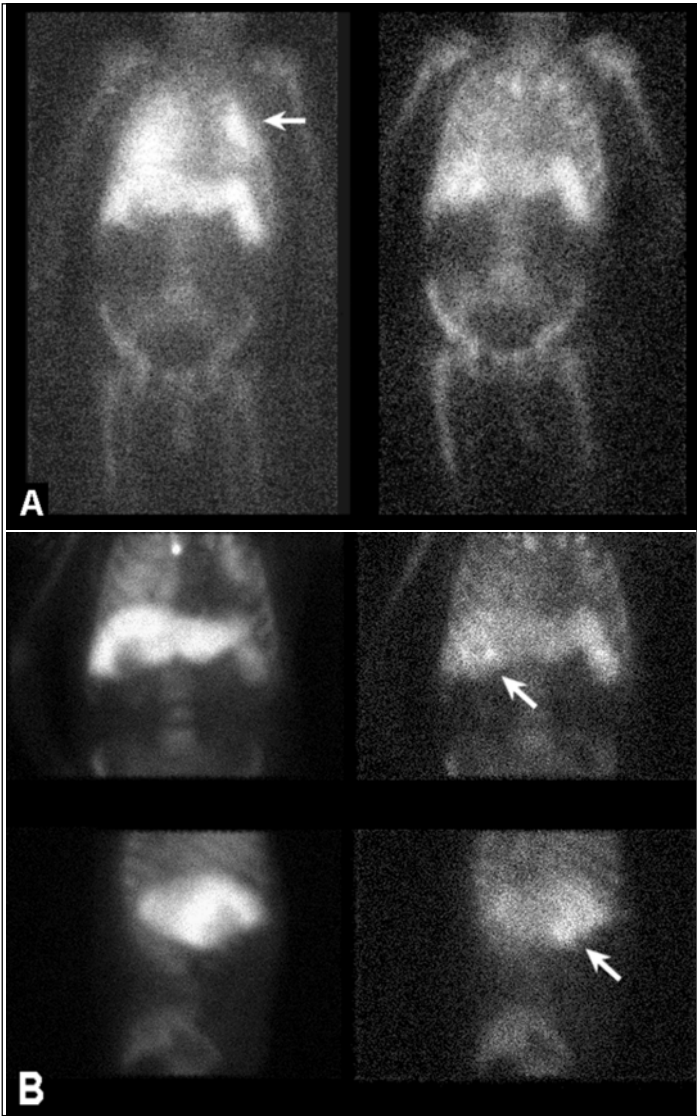
Figure 10. ¹¹¹In-leukocyte scan with transient nonspecific lung accumulation in a patient suffering from "sepsis syndrome". (A) Diffuse lung accumulation (arrow) is seen 4 hours post-injection (left) that clears by 24 hours (right). (B) The source was subsequently localized to a liver abscess (diagonal arrows) localized by dual isotope ⁹⁹mTc-sulfur colloid liver (left) and ¹¹¹In-leukocyte imaging (lower right). Images in the upper half of the panel are anterior views of the liver and in the lower half right lateral views.
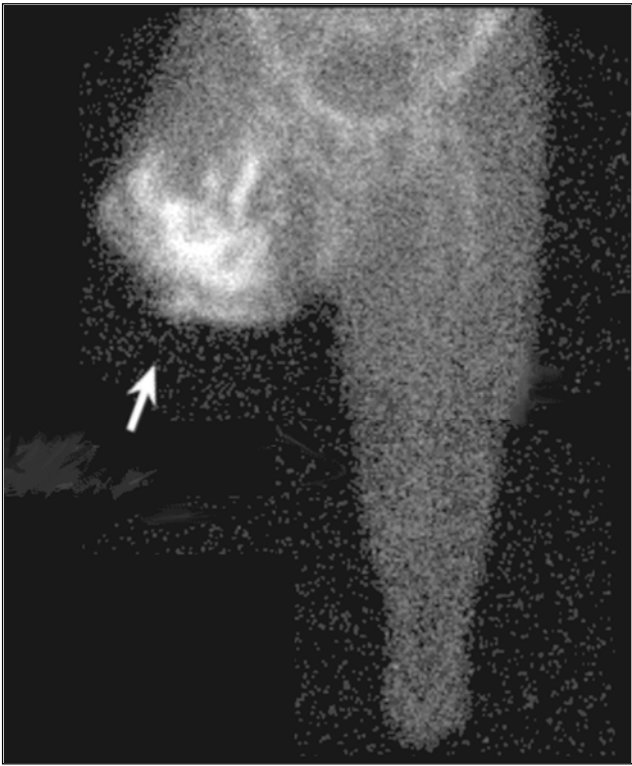
Figure 11. Infected above-knee amputation stump imaged with ^{111}In-leukocytes. A 63 year old diabetic man on dialysis for end-stage renal disease developed severe peripheral vascular disese with gangrene of the left great toe resulting in a left below-knee amputation. His right foot became ischemic with gangrene of the great toe necessitating right below-knee amputation. To salvage the remainder of the limb the patient simultaneously underwent a right femoral-popliteal bypass. His post-operative course was complicated by ongoing stump infections with breakdown and acute rupture of an infected right femoral artery pseudoaneurysm. Unfortunately, the stump infection could not be managed medically and the patient eventually underwent a right above-knee amputation. Once again there was evidence of post-operative sepsis with low-grade fever and rising leukocyte count (up to 30.6x10^9/L). The patient complained of considerable pain and tenderness in the right above-knee amputation stump but clinically the wound was described by numerous consultants as clean and not the source of the patient's complaints. An ^{111}In-leukocyte scan was requested to exclude other occult sources of infections such as intra-abdominal abscess or graft infection, and revealed striking and clinically unsuspected accumulation in the right thigh stump (arrow). (Note that the left below-knee amputation stump does not show any evidence of active inflammation or infection.) Ten days later the patient went for surgical debridement and multiple pockets of pus were found in the stump.

largely devoid of gallium uptake, pulmonary processes are well depicted with gallium. The sensitivity is high for acute bacterial pneumonia (91%), pulmonary fungal infection or tuberculosis (97%) and sarcoidosis (75%). Certain patterns of uptake strongly suggest the diagnosis of sarcoidosis; these are known as the "panda sign" (symmetrical uptake in the lacrimal and salivary glands suggesting the face of a panda) and "lambda" pattern (bilateral symmetrical uptake in the paratracheal, mediastinal and bronchopulmonary lymph nodes in the shape of the Greek letter). As would be predicted from the lymphocytic nature of sarcoidosis, labeled leukocytes are much less sensitive than gallium. Labeled leukocytes also show low sensitivity for chronic pneumonias (30%) and pulmonary fibrosis (30-50%), where gallium is again the preferred inflammatory imaging agent. Diffuse bilateral pulmonary uptake can be a striking and unexpected finding (Fig. 13). The most common causes include sarcoidosis, opportunistic infections such as *Pneumocystis carinii*, and drug-induced pneumonitis. The most common drugs implicated are bleomycin, busulphan, nitroureas, amiodarone, cyclophosphamide, methotrexate and nitrofurantoin. The chest radiograph is frequently normal in these cases.

Normal gastrointestinal activity does not usually obscure renal abnormalities. Focal renal gallium uptake can be seen with tumors such as hypernephroma or lymphoma. Renal abscess or acute focal bacterial nephritis can also be responsible. Sensitivity of gallium imaging for renal infection is 75% with a specificity of 87%. As with pulmonary uptake, diffuse bilateral renal uptake of gallium can reflect bilateral pyelonephritis, collagen vascular disease producing glomerulonephritis, and certain forms of renal failure. Among the latter, allergic interstitial nephritis tends to show more intense renal uptake than other causes. Many drugs have been implicated, and it is important to establish the diagnosis as the renal failure is potentially reversible if the drug is withdrawn and the patient treated with systemic steroids. Since gallium is frequently used as a tumor tracer, it has reduced specificity in patients with underlying malignancies.

Clinical Role in Fever of unknown origin (FUO)

Clinical Information

Not infrequently, patients will experience prolonged or recurrent febrile episodes that defy diagnosis despite careful clinical assessment and conventional imaging. In choosing a nuclear medicine technique, it is important to distinguish two broad groups: those with a suspected acute pyogenic process (typically developing in hospitalized patients or when there has been recent surgery) and a chronic process (usually developing in a nonhospitalized patient). In the former, a pyogenic bacterial cause is likely whereas in the latter the differential is much broader and includes non-infectious etiologies such as lymphoma, solid tumors and sarcoidosis.

Classical FUO refers to persistent fever (at least 2-3 weeks) of 38.3° C or higher in generally healthy adults that eludes diagnosis after at least three days of hospital investigation (or three out-patient visits). Under this strict definition, an infectious etiology is actually infrequent. This contrasts with persistent fever in hospitalized (nosocomial) or neutropenic (fewer than 500 neutrophils/mm³) patients in whom bacterial and fungal infections are the dominant cause. Persistent fever in an individual with confirmed HIV infection is intimidating due to the extensive differential that includes common infections (bacterial, viral, mycobacterial, fungal), non- infectious
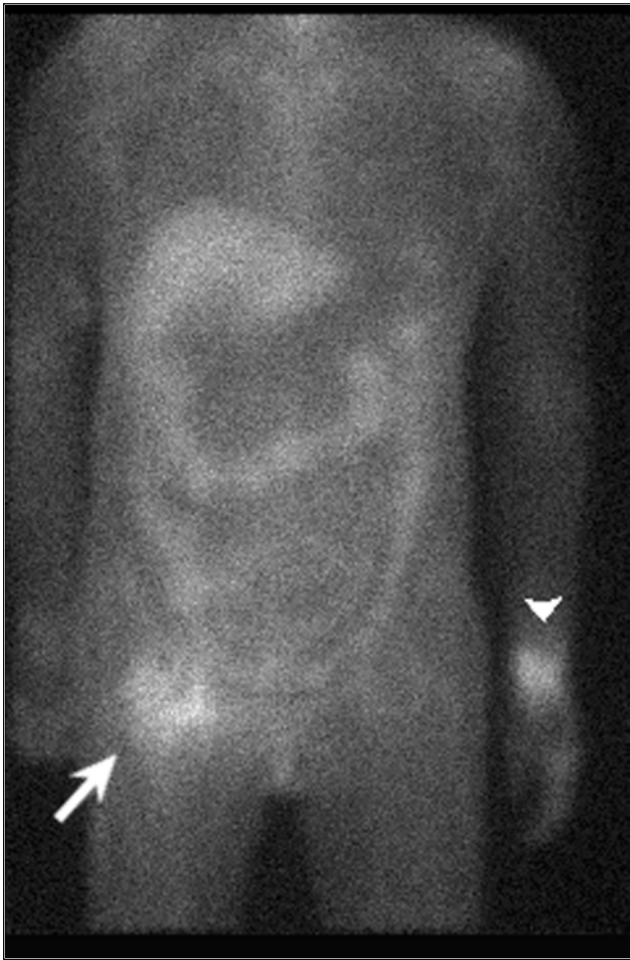
Figure 12. ^{67}Ga-gallium citrate scan showing multifocal septic arthritis in a hemodialysis patient with *S. aureus* bacteremia. Scan shows focal gallium uptake in the right hip (arrow) and left wrist (arrowhead) which were symptomatic but did not show diagnostic abnormalities on x-ray, bone scan or initial aspiration.

causes (neoplastic, drugs) and many unusual disorders (*Pneumocystis carinii*, cytomegalovirus, microsporidiosis, Kaposi's sarcoma).

A few general rules should be remembered:

(1) A systematic approach must be followed to avoid random investigation which is frequently fruitless, costly and potentially dangerous.
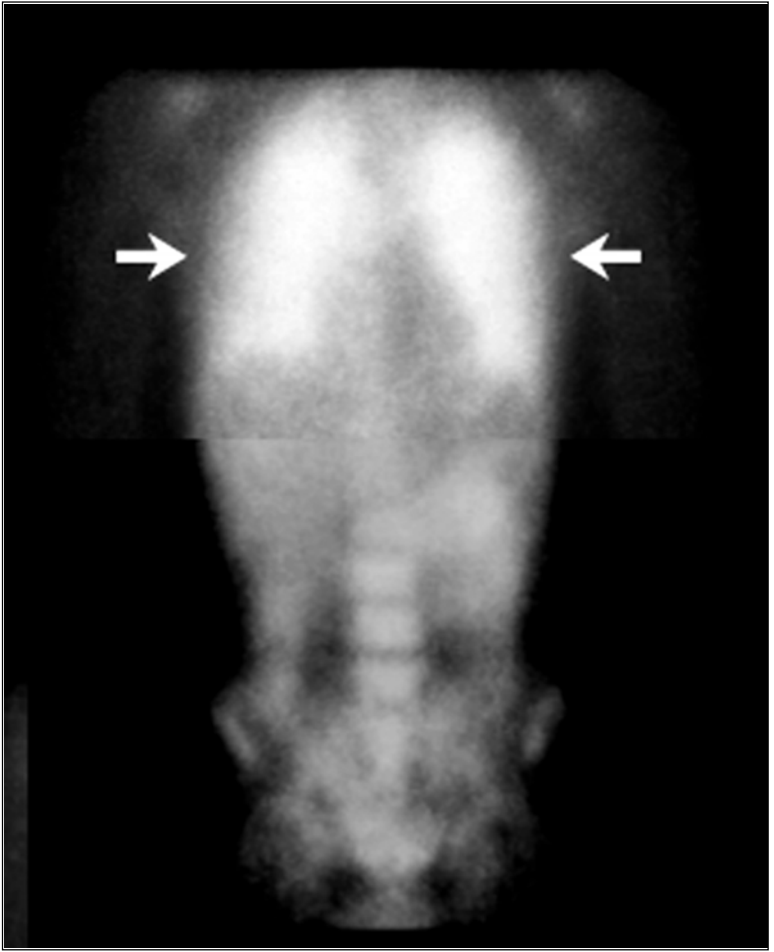
Figure 13. ^{67}Ga-gallium citrate scan showing drug-induced pneumonitis. This 34 year old man was undergoing chemotherapy for Hodgkin's lymphoma (alternating courses of MOPP and ABVD). He developed dyspnea and fever but had a normal chest x-ray and thoracic CT scan. A gallium scan was performed to assess the status of his lymphoma and to exclude an occult focus of infection. The intense diffuse lung uptake (arrows) was attributed to bleomycin and resolved with supportive therapy.

(2) As the duration of fever increases, the likelihood of an infectious cause decreases.

(3) Infection, neoplasm and collagen-vascular disease account for over 70% of classic FUO cases.

General Diagnostic Testing

Having the patient maintain a fever diary where time and temperature are recorded at least twice daily (morning and evening) serves to confirm the presence of significant febrile episodes. Occasionally, an exaggerated circadian temperature rhythm can be misinterpreted as pathologic fever.

A comprehensive system review is required. Easily overlooked are transient skin rashes, travel history or animal exposure. Insect bites or travel through areas endemic for tick-transmitted diseases, coccidiodomycosis, histoplasmosis and blastomycosis are important to elicit. A complete physical examination may be required several times during the course of FUO investigation as many of the findings can be subtle or transient.

Besides performing a complete blood count, biochemical panel which includes assessment of renal and liver function, and urine examination, the blood smear needs to be carefully inspected for toxic changes, hematologic malignancy or intra-erythrocytic infection. Multiple blood cultures (at least three) should be collected to exclude endocarditis or transient bacteremia. Culture of other body fluids should be performed as indicated by these investigations. Elevated levels of acute phase reactants lead to an increase in the erythrocyte sedimentation rate (ESR) and C-reactive protein(CRP), non-specific findings that can occasionally suggest the diagnosis of temporal (giant cell) arteritis-polymyalgia rheumatica. A chest x-ray should always be obtained to rule out chronic pneumonia, empyema and mass lesions which may give few clinical clues. An abdominal CT scan is indicated at this stage for excluding liver abscess and other mass lesions.

Radionuclide Testing

When an acute pyogenic process is suspected, labeled leukocytes are preferred. However, the ability of gallium to identify tumors and nonpyogenic inflammation makes this the agent of choice for classical FUO. Occult osteomyelitis can cause FUO, particularly when there has been a previous bacteremic episode and skeletal scintigraphy can be valuable in this setting. Radionuclide techniques can evaluate the entire body in a single study, a considerable advantage when there are no clinical features to aid in the localization of FUO (Fig. 14).

Clinical Role in Vascular graft infection

Clinical Information

The accurate diagnosis and treatment of vascular graft infections is important due to the potential for limb and life threatening complications. Early vascular graft infections usually present with obvious clinical findings of redness, fluctuance, fever or a draining fistula. However, the clinical manifestations of late infections are frequently subtle or absent. Delayed diagnosis is quite common and demands a high index of clinical suspicion supplemented with appropriate imaging. The incidence of vascular graft infection ranges from 0.5% to 5%, with higher rates occurring when there is a groin incision, preoperative infection, a post-operative wound infection or with underlying disorders such as diabetes mellitus. Once established, infection is associated with a mortality rate up to 75%. Infection can develop from direct contamination at the time of surgery, through contiguous extension from an adjacent

site of infection, or through bacteremic seeding from a distant site of sepsis. *Staphylococcus aureus* and *S. epidermidis* account for 33% and 12% of all infections, respectively. The remainder consist of Streptococci (11%) and a variety of gram-negative aerobic bacilli (31%). Infections are polymicrobial in 37% of cases, usually in the setting of abdominal or groin infections. Resistance to bacteremic seeding increases with the duration of time since surgery as graft material is incorporated into host tissues and covered by a connective tissue and fibrinous pseudointima, though true endothelialization is actually quite rare. It is important to consider this early inflammatory reaction since it can affect imaging studies producing false-positive radionuclide results.

Approximately two-thirds of infections involving the extremities develop within two months of surgery, but intraabdominal graft infections usually present more than one year after surgery. Clinical findings in the extremities include localized inflammation, abscess or sinus drainage. False aneurysm formation is suggested by a rapidly enlarging, pulsatile swelling and is a surgical emergency. Similarly, arterial thrombosis or distal arterial embolization can threaten limb viability. Intraabdominal graft infections are usually more subtle in their presentation, with fever and bacteremia being the most common findings. Occasionally the diagnosis will be suggested by findings of a false aneurysm, graft thrombosis or septic emboli. One of the most dramatic and dangerous situations is when an aortic graft forms a fistulous communication with the bowel, clasically between the proximal anastomosis and the third part of the duodenum. Massive uncontrollable bleeding can develop, and therefore any upper gastrointestinal bleeding in a patient with an aortic graft should be considered a possible "sentinel" bleed.

Treatment almost always requires a combination of surgery and antibiotic therapy. Rarely it is possible to eradicate the infection with débridement and antibiotics alone, but most cases require removal of the entire graft as well. If immediate revascularization is required to maintain viability of distal structures, this should be performed to avoid the infected field. Antibiotics are usually continued for at least four weeks after removal of the prosthetic material. Prophylactic antibiotics are known to significantly reduce the rate of post-operative wound and graft infections.

General Diagnostic Testing

The diagnostic approach begins with careful physical examination since many cases of peripheral graft infection can be strongly suspected from the clinical findings. The presence of a persistent bacteremia also supports the presence of an intravascular infection. The approach to diagnostic imaging must be considered in relation to the time since surgery, as fluid collections and graft inflammation can lead to false-positive investigations. Fluid collections can be visualized with ultrasound, CT or MRI. Fluid collections from sterile perigraft reaction can be seen for 6-8 weeks after surgery, but their presence after this evokes the possibility of infection. Gas should never be present after the immediate post-operative period and is virtually pathognomonic for infection. More invasive investigation with arteriography can establish the integrity of the suture line or presence of intraarterial thrombus. Occasionally, CT-guided diagnostic aspiration can be performed for suspected graft infection. In some cases only surgical exploration and intraoperative cultures can adequately confirm or exclude the presence of infection.
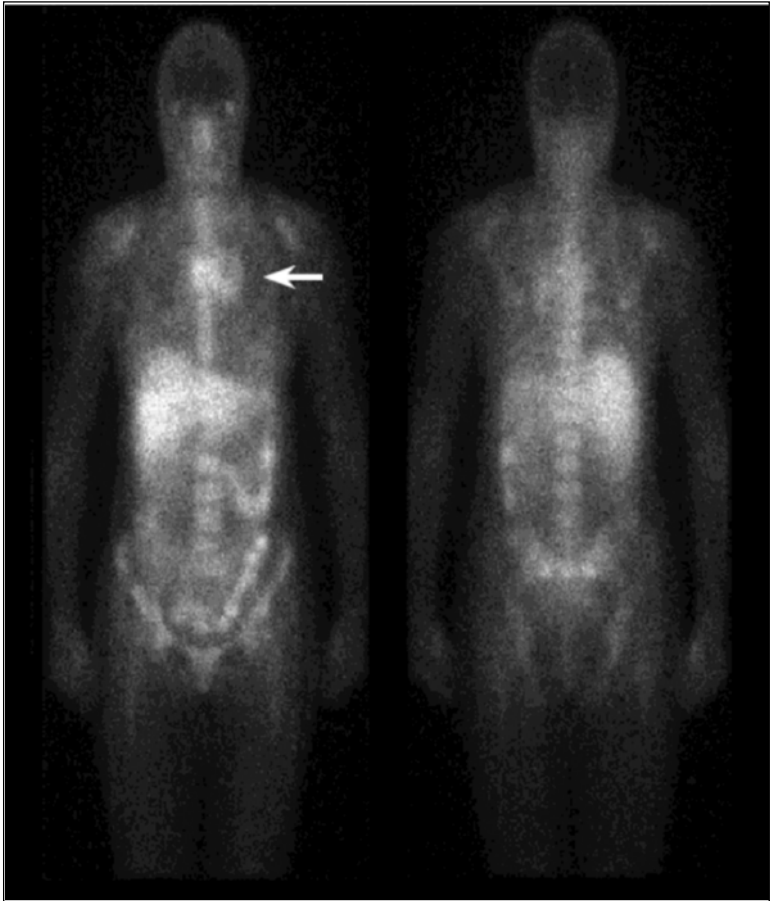
Figure 14. Small cell lung cancer presenting as fever of unknown origin (FUO). An 81 year old woman had a past history of smoking and remote breast carcinoma treated with mastectomy and post-operative radiotherapy. She fell at home and began experiencing back and left chest pain, weakness, dyspnea and a ten pound weight loss. Examination was unremarkable except for persistent fever and reduced air entry in the right hemothorax. Extensive investigations in hospital (hematology, biochemistry, blood cultures, abdominal ultrasound, echocardiogram) were normal. The chest x-ray revelaed left upper lobe fibrosis from the previous radiotherapy. X-rays of the lumbar spine and bone scan showed compression fractures of T11 and L1. The possibility of lumbar osteomyelitis was entertained based upon the fever, back pain, x-rays and bone scan. A gallium scan (left: anterior view, right: posterior view), performed to confirm focal spine inflammation, showed minimal gallium vertebral accumulation but marked mediastinal and left perihilar uptake (arrow). A chest CT scan confirmed extensive mediastinal and perihilar adenopathy. Subsequently scalene and supraclavicular nodes appeared and biopsy demonstrated metastatic small cell carcinoma of the lung.

Radionuclide Testing

Leukocyte scintigraphy is the preferred study for the investigation of possible graft infection, particularly within the abdomen. The finding of focally intense accumulation strongly suggests infection (Fig . 15) whereas low-grade diffuse uptake by the graft is more in keeping with non-specific adherence to the pseudointima. The diagnostic sensitivity with leukocyte scintigraphy is high, and specificity can be improved by assessing the pattern of accumulation. The sensitivity of labeled leukocytes consistently exceeds 90%, whereas the comparative sensitivity of CT scan is 37-50%. The specificity of labeled leukocytes is more variable, ranging from 53% to 100%. Causes of false-positive graft uptake include perigraft hematoma, graft thrombosis, pseudoaneurysm and wound infections that do not involve the graft directly. Nonspecific platelet adherence may persist for many weeks (or even months) following surgery. The inadvertent labeling of platelets may contribute to nonspecific graft uptake, and some groups routinely extract a platelet-depleted leukocyte population using a gradient sedimentation method. Other agents, such as gallium, polyclonal human immunoglobulin and nanocolloids, have not been as successful as leukocytes.

Dialysis Fistulas

Dialysis fistulas are also prone to infection, particularly if they include implanted prosthetic material, while native vessel arteriovenous fistulas are relatively resistant to infection. *Staphylococcus aureus* accounts for 60-90% of access site infections, suggesting direct contamination from skin at the time of access. As with other graft infections, clinical findings can be extremely subtle and are completely absent in approximately one-third of cases.

When an infectious process is limited to a small area away from the suture line antimicrobial therapy and débridement may be sufficient to eradicate the infection. Unfortunately, in many cases this is insufficient and the arteriovenous fistula must be completely removed.

Nuclear imaging of a dialysis fistula can be difficult to perform and challenging to interpret. Frontal and profile views of the fistula are required, but it can be difficult to control for the degree of forearm pronation. Furthermore, some camera designs are cumbersome to position for areas close to the antecubital fossa. The large amount of blood contained within the fistula can often be seen as low-grade activity, especially on early images or when significant erythrocyte cross-labeling has occurred. Occasionally, normal bone marrow can be a source of confusion and highlights the importance of mapping any uptake to the fistula itself. Clinical assessment of the patient while still under the gamma camera is an essential step. With these precautions nuclear imaging can be highly accurate in the diagnosis of an infected fistula (Fig. 16).

Frequently Asked Questions (FAQ's)

How do I determine which nuclear medicine technique to use?

Knowledge of the normal biodistribution and excretion patterns of the tracers described above can lead to a rational approach to selecting one method over another (Table 3). Soft tissue infections are usually bacterial and generate an acute pyogenic inflammatory response. Labeled leukocytes are preferred due to their high levels of
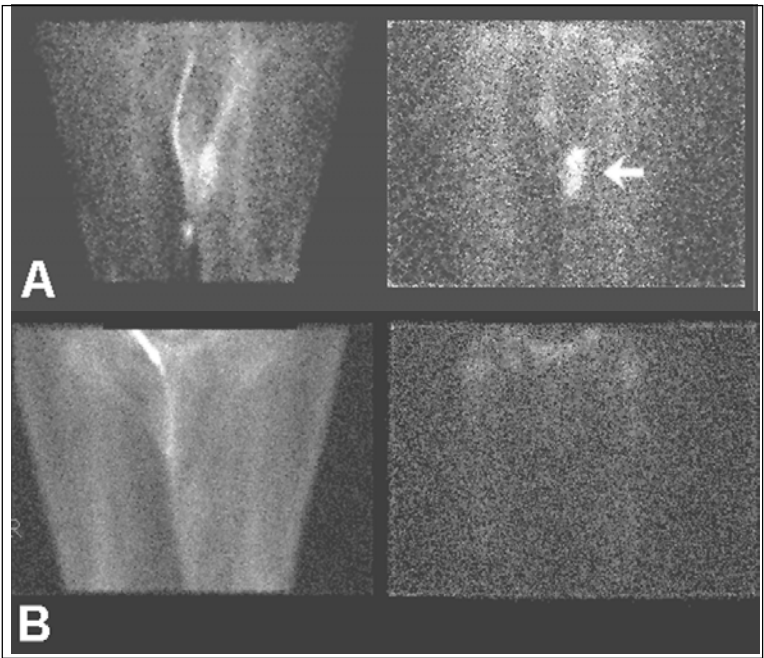
Figure 15. Infected left femoral-popliteal graft before and after prolonged antibiotic therapy. An 81 year old man with severe vascular insufficiency and gangrene of the great toe underwent a distal left femoral-dorsalis pedis bypass graft using a segment of saphenous vein. The left great toe was quite necrotic, with ulceration extending to bone and purulent discharge. The thigh wound showed continued serous drainage and with accumulation of a lymphocele which required exploration and drainage three weeks after the original surgery. Throughout this time the patient had been on antibiotics as draining fluid grew multiple organisms, although the patient remained afebrile with only very slight local erythema. (A) The graft was clearly localized on the ^{99m}Tc-erythrocyte blood pool image (left) and the striking ^{111}In-leukocyte (right) accumulation in the left mid-thigh medially corresponded to infection in the proximal graft anastomosis (arrow). Note how localization is enhanced through simultaneous dual-isotope blood pool imaging. The patient was managed aggressively with intravenous antibiotics (pipericillin/tazobactam) for three weeks followed by an additional four weeks of oral antibiotics. (B) The repeat scan showed complete resolution on the ^{99m}Tc-erythrocyte (left) and ^{111}In-leukocyte (right) images.

uptake, but passive diffusion agents can also be valuable. Assessment of the abdomen requires delayed imaging and is best achieved with agents which do not show physiologic bowel excretion. Overall, ^{111}In- leukocytes are ideally suited to this function (Fig. 17). Neither ^{111}In- leukocytes nor ^{67}Gallium show appreciable urinary tract excretion. These agents can be valuable for confirming pyelonephritis or
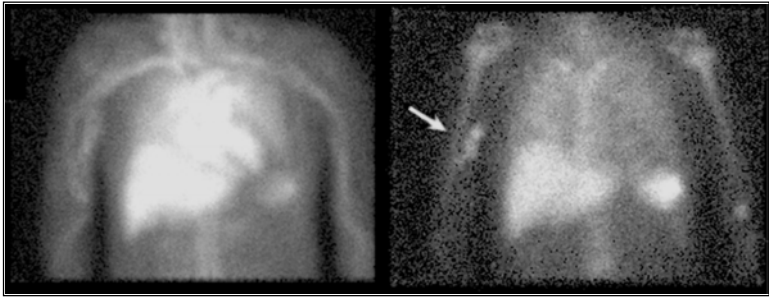
Figure 16. Infected right brachial-axillary graft. A 61 year old woman with end stage renal disease due to diabetic nephropathy and hypertension was receiving hemodialysis through a right brachial-axillary graft. She developed acute onset of fever (up to 40.1° C) associated with non-specific abdominal and low back pain. Blood cultures were positive for two different gram positive cocci: *Staphylococcus aureus* and alpha-hemolytic *Streptococcus*. Clinical examination was unhelpful as were many investigations (chest x-ray, chest/abdominal CT scan, echocardiogram and lumbar spine CT) and consultations conducted in an attempt to determine the cause of the fever. Dual-isotope scaning with ^{99m}Tc-erythrocytes (left) localized the fistula while the ^{111}In-leukocyte scan (right) demonstrated intense leukocyte accumulation in the right brachial-axillary graft from a graft infection (arrow).

perinephric abscess. Gallium is preferred for chronic or granulomatous disorders, and when an occult tumor is a significant consideration.

When should a nuclear medicine technique be the first line investigation and when should conventional imaging with ultrasound or CT be the first line?

When clinical findings and x-ray examinations lead to specific localization of suspected anatomical disturbances, conventional imaging with ultrasound and CT may provide the most useful information. Nuclear medicine may therefore serve as a first line investigation when an inflammatory process is suspected but there are no localizing clinical features, or when there is clinical localization but conventional imaging is either not diagnostic or is uninterpretable.

Which agent is most helpful for suspected vertebral and paravertebral infections?

Although radiolabeled leukocytes show excellent sensitivity for most bacterial infections, vertebral osteomyelitis is a definite exception. This relates to normal levels of marrow visualization "masking" the abnormality. Increased uptake occurs in only a minority of patients with vertebral infection (17% to 39%), although its presence almost always indicates bacterial spondylitis (specificity 98%). More often, there is reduced vertebral activity but this finding has low sensitivity (54%) and specificity (52%). Reduced uptake has also been reported in vertebral osteomyelitis imaged with antigranulocyte monoclonal antibodies and probably occurs with ^{99m}Tc-nanocolloid as well. Reduced uptake can be seen with many sterile bone processes

Table 3. Relative usefulness of various radiopharmaceuticals in the diagnosis and localization of inflammatory disease.

	^{111}In-Leukocytes	^{99m}Tc-Leukocytes	^{67}Ga-Gallium citrate
"Classic" FUO	++	++	+++
Nosocomial FUO	+++	+++	++
Soft tissue	++	+++	++
Intra-abdominal	+++	++	++
Inflammatory bowel disease	+++	+++	+
Urinary tract	+++	+	+++
Vascular grafts	+++	++	++

+=least useful, ++=moderately useful, +++=most useful

such as compression fracture, tumor and Pagets disease. Prior antibiotic therapy may be correlated with a higher incidence of false-negative scans and photon-deficient uptake. Of patients with clinically resolved infection, many who initially present with increased activity will show decreased vertebral activity on follow up studies.

In contrast to the poor imaging performance of ^{111}In-leukocytes, ^{67}Ga-gallium citrate usually shows markedly increased uptake and is the preferred agent for suspected vertebral osteomyelitis and/or discitis, frequently revealing a "butterfly" pattern from paravertebral spread. Fungal and tuberculous vertebral infections can also be detected with gallium. Gallium can be diagnostic where radiographic abnormalities are originally lacking, and confirm a current and/or ongoing septic process at sites where vertebral destruction is already present on x-ray.

Although the bone scan is also very sensitive for skeletal infection, in the spine and sacroiliac joints it may lag behind the gallium scan for several days. Therefore, if infectious spondylitis-diskitis is strongly suspected on clinical grounds, a normal bone scan should still be followed by a gallium scan.

Can nuclear medicine methods determine when it is safe to stop antibiotic therapy?

Since nuclear medicine methods are designed to identify sites of active inflammation, whether acute or chronic, absence of inflammation can be a very useful tool in determining when antimicrobial therapy should be discontinued. For example, it is often difficult to know when to stop treating chronic diabetic osteomyelitis or a prosthetic joint infection that has been managed with several weeks or months of antibiotics. Some markers that can be used to monitor progress include acute phase reactants such as erythrocyte sedimentation rate and repeat radiographs to look for improvement in anatomical defects. However, nuclear medicine methods can add a level of reassurance by confirming the absence of inflammatory activity, thus aiding in the decision to discontinue antibiotic therapy.
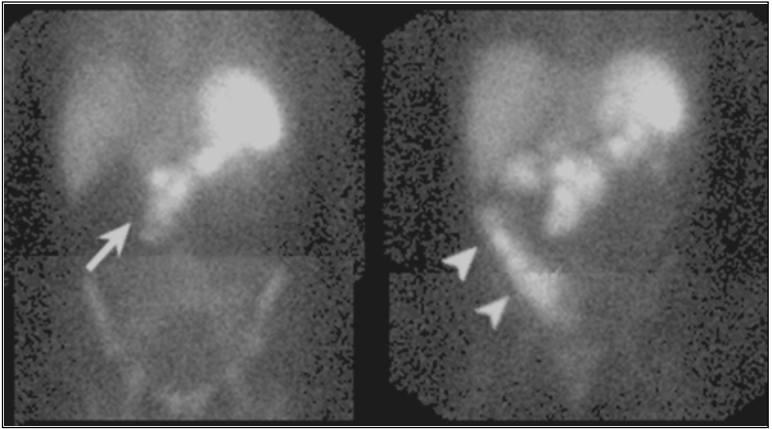
Figure 17. Infected pancreatitis with fistulous internal communication to the gut imaged with ^{111}In-leukocytes. The early images (left) show intense accumulation in the pancreas (arrow). By 24 hours (right), activity now is clearly evident in the cecum and ascending colon (arrowheads).

Additional Reading

1. Becker W. The contribution of nuclear medicine to the patient with infection. Eur J Nuclear Medicine 1995; 22(10):1195-1211.
   Reviews the basic pathophysiology of inflammatory imaging.
2. Datz FL. Abdominal abscess detection: Gallium, [111]In-, and ^{99m}Tc-labeled leukocytes, and polyclonal and monoclonal antibodies. Seminars in Nuclear Medicine 1996; Vol XXVI, No. 1:51-64.
   Reviews abdominal imaging, including mechanisms of uptake, labeling procedures, normal patterns and artifacts.
3. Datz FL. Infection imaging. Seminars in Nuclear Medicine 1994; Vol XXIV, No. 2.
   This volume covers the full range of nuclear techniques, including mechanisms of uptake, labeling procedures, normal patterns and artifacts. There are individual articles on [111]In- leukocytes, ^{99m}Tc-leukocytes, gallium, antibodies and chemotactic peptides.
4. Mandell GL, Bennett JE, Dolin R. Principles and practice of infectious diseases, Fifth Ed. Philadelphia: Churchill Livingstone, 2000.
   One of the "classics" on infectious diseases and well worth the trouble of consulting for both common and exotic disorders. Detailed discussion on the clinical approach to undiagnosed fever.
5. Peters AM. Localising the cause of an undiagnosed fever. Eur J Nucl Med 1996; 23(3):239-242.
   An excellent discussion of the differences between out-patient and nosocomial fever and how these influence differential diagnosis and testing.
6. Rennen HJ, Boerman OC, Oyen WJ, Corstens FH. Imaging infection/ inflammation in the new millennium. Eur J Nucl Med 2001; 28(2):241-252.
   A survey of different nuclear medicine approaches to the imaging of inflammatory diseases: past, present and future.

12

Thyroid Disorders

Albert A. Driedger and Thomas J. McDonald

Thyroid Anatomy and Physiology

Embryology and Anatomy

The normal thyroid gland begins as a primitive diverticulum at the base of the tongue in the third week of gestation and grows caudally toward its ultimate position anterior to the thyroid cartilage. In the adult it forms a butterfly-shaped structure weighing about 20 grams. Some thyroid tissue may remain along the thyroglossal duct to form a pyramidal lobe or a thyroglossal thyroid remnant in post-natal life. In rare cases the thyroid fails to descend and forms at the base of the tongue (lingual thyroid) where it may present as a mass. The thyroid originates near the formation site of the aortic sac, and for this reason accessory thyroid tissue may be found in the mediastinum.

The normal thyroid is made up predominantly of follicular cells whose function is the production, storage and secretion of thyroid hormone. These cells are able to trap iodine and produce thyroxine by about the 11th week of gestation. The follicular cells, possibly under the influence of TSH, arrange themselves to form follicles into which they secrete thyroglobulin. A second population of cells, known as parafollicular or C cells, is derived from the neural crest. These appear about midgestation and are responsible for the secretion of calcitonin. The C cells do not form follicles and their secretory polarity is oriented toward the capillaries.

There are relatively few lymphatics in the thyroid compared to capillaries and these are concentrated in the pericapsular areas. Thyroidal lymphatics drain to nodes on the thyroid, trachea, larynx and in the tracheo-esophageal groove as well as to the deep cervical nodes along the internal jugular vein. Drainage to nodes in the upper mediastinum is also common (Fig. 1).

Normal Physiology and Metabolism

The follicular cells reversibly take up iodide ions from the bloodstream against a 30-fold concentration gradient and irreversibly convert them to an organic form, which is secreted into the follicles (Fig. 2). The steps of uptake and organification are stimulated by thyroid stimulating hormone (TSH). Uptake is competitively inhibited by large anions such as thiocyanate and perchlorate. Organification is blocked by the thyroid-blocking drugs, propylthiouracil (PTU) and methimazole. Oxidized iodine is secreted into the colloid where synthesis of mono- and diiodotyrosines occurs, going on to the production of thyroxine (T4) and tri-iodothyronine (T3). These steps are also blocked by anti-thyroid drugs. Within the follicle, thyroid hormones are bound to thyroglobulin (Tg). The storage capacity of the thyroid as an endocrine gland is exceptional: an average gland contains about 3
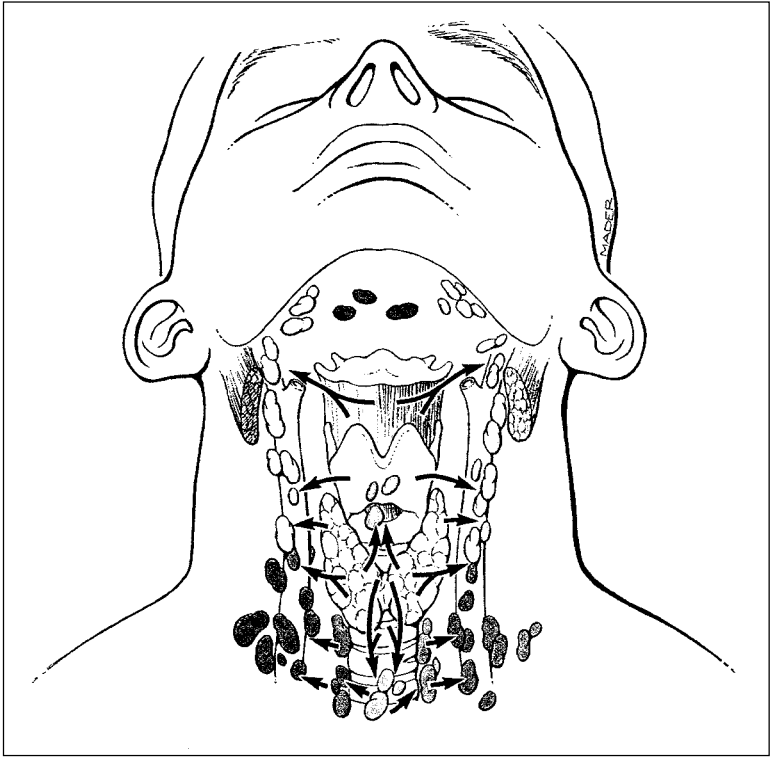
Figure 1. Anatomic distribution of lymph nodes that drain the thyroid gland. (From Agur AMR. Grant's Atlas of Anatomy, 9th Ed., 1991. Reproduced with permission from Williams & Wilkins.)

13

months supply of hormone. The amount of iodine contained in a normal gland, subject to an adequate iodine intake, is about 7-10mg. Release of hormone from the follicle is stimulated by TSH and inhibited by iodide and lithium.

Tg is a large protein (660kd) that serves as the matrix for thyroid hormone synthesis in the follicles and also as the storage vehicle. Tg synthesis is stimulated by TSH via the cyclic AMP mechanism. Of the 134 tyrosine residues in the molecule, no more than 15-17 are usually iodinated, including no more than 2-4 molecules of T4 and T3. The release of the hormone seems to result in the destruction of the Tg molecule, seemingly an inefficient process when the energy costs of synthesizing such a large molecule are considered. Normally, Tg is largely retained within the follicles, but it may be released into the blood stream in disease states. Tg is often produced by neoplasms derived from follicular cells and is a useful marker for recurrence of tumor.

Production of thyroid hormone is regulated by the pituitary gland through the secretion of TSH, which in turn is regulated by hypothalamic production of
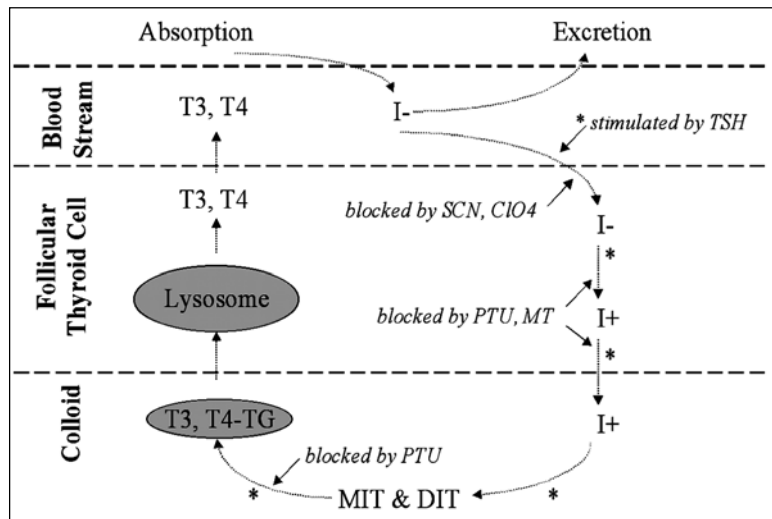
Figure 2. A schematic representation of iodine metabolism in the thyroid gland.
SCN-thiocyanate; ClO4-perchlorate; PTU-propylthiouracil; MT-methimazole;
MIT&DIT-mono- and di-iodo-tyrosine; Tg-thyroglobulin; *-sites stimulated by TSH.

thyrotropin-releasing hormone (TRH). TRH is a tripeptide that may be transported
to the pituitary along direct neuronal interconnections. Circulating levels of thyroid
hormone, especially T3, provide the negative feedback required to regulate the level
of TRH and TSH.

Circulating thyroid hormone is protein-bound. Thyroxine-binding proteins are
present in the fetal blood stream by mid-gestation, an important consideration in
Nuclear Medicine as maternal exposure to iodine isotopes will be associated with
fetal uptake and retention through this mechanism.

Calcitonin, the secretory product of the C cells, is a polypeptide of 32 amino
acids, whose major effect is to inhibit osteoclastic bone resorption. In humans the
physiological importance of calcitonin remains unclear. Thyroidectomized patients
with normal parathyroid gland function do not exhibit any apparent abnormality of
bone metabolism.

Technical Aspects of Thyroid Scintigraphy

Radiopharmaceuticals for the Assessment of Thyroid Function

Much of modern Nuclear Medicine began with the challenges presented by the
thyroid gland. It was known prior to the era of radioactive isotopes that the thyroid
gland concentrated iodine. For instance, Dr. Plummer's introduction of Lugol's iodine
to block release of thyroid hormone in preparation of thyrotoxic patients for surgery
at the Mayo Clinic in the early 1920s reduced the post-surgical mortality from 11%
to <1% within a year. When, in the late 1930s, it became possible to produce
radioactive isotopes of iodine with cyclotrons, they were first used to study the

metabolism of iodine administered in blocking doses. Thus, the potential of iodine isotopes for physiological investigations and diagnostic work has been established for more than 60 years. Radiation doses for those radiopharmaceuticals commonly used in thyroid imaging are listed in Appendix 2.

In addition to the stable form (iodine-127), 32 radioactive isotopes of iodine have been identified. Only two of these have suitable half lives and radioactive emissions for diagnostic work: iodine-123 and iodine-131. Iodine-125 is useful for laboratory work as it is a relatively long-lived (59 days) nuclide emitting an Auger electron.

Iodine-123

[123]I has a half-life of 13.2 hours and a 159 kev gamma emission which, for external imaging purposes, is nearly ideal. The radiation dose to the patient is low and the emission is well suited for gamma camera detection. However, ^{123}I is not available everywhere and it is more expensive than alternatives such as ^{131}I or ^{99m}Tc-petechnetate.

Iodine-131

[131]I has a half-life of 8 days. It has a complex spectrum of both beta and gamma emissions with a dominant gamma at 364 kev, a high energy requiring thick collimation to exclude scatter and thick scintillation crystals for efficient detection. The beta emissions contribute heavily to the thyroidal radiation dose, which may be in the range of 0.5-1Gy from a diagnostic imaging study. The advantage of ^{131}I is that it is inexpensive and its half-life is long enough to permit keeping it in inventory for use at short notice. One practical solution to the dose-price quandary is to perform a radioactive iodine uptake (RAIU) with a small dose of ^{131}I and use ^{99m}Tc-petechnetate for thyroid imaging.

[99m]Tc-Pertechnetate

[99m]Tc-pertechnetate is a universally available and inexpensive radiopharmaceutical whose half-life of 6 hours and monoenergetic gamma emission of 140 kev provide high quality images with a low radiation dose. Pertechnetate follows iodide uptake by follicular cells, but is not organified, and the uptake remains reversible.

Follicular Tumor Imaging

[201]Tl-thallium chloride and ^{99m}Tc-sestamibi may be useful in rare situations where needle biopsy has not provided a definitive diagnosis of a thyroid nodule and where evidence is needed to support a decision for surgical excision. Thallium uptake and washout has been characterized recently and is claimed to have better sensitivity and specificity than fine needle aspiration. ^{99m}Tc-sestamibi is concentrated by many neoplasms, not only those originating from the thyroid. This agent is better suited for imaging than thallium: it is useful to image the post-surgical neck for evidence of recurrent malignancy and as an adjunct to ^{131}I imaging in the follow-up of treated thyroid cancer patients.

[18]F-fluorodeoxyglucose (FDG) is assuming increasing importance for the imaging of suspected malignancies and for pre-operative staging. In relation to thyroid cancers, FDG is concentrated by many tumors that do not concentrate [131]I. The usefulness

13

of FDG lies in follow-up of patients with elevated serum thyroglobulin and negative ^{131}I scans.

Many follicular-derived cancers have somatostatin receptors on their cell surfaces and can be imaged with radiolabelled somatostatin analogues such as ^{111}In-pentetreotide (octreotide, Octreoscan®).

Parafollicular Tumor Imaging

Medullary thyroid cancer requires a different approach as follicular cell imaging will, at best, only identify that a cold lesion exists within the thyroid gland. Possibly the preferred radiopharmaceutical at this time is ^{111}In-octreotide, which has affinity for somatostatin receptors on tumor cell surfaces. This agent has a reported sensitivity of about 65% for the detection of medullary carcinoma.

[99m]Tc(V)-dimercaptosuccinic acid (DMSA) is reported to detect primary and recurrent medullary carcinomas with sensitivities of 50-80%. The method of production and the isomeric composition of the product seem critical to its performance.

[131]I-*meta*-iodobenzyl guanidine (MIBG) and ^{123}I-MIBG are concentrated by some medullary carcinomas. For diagnostic purposes, the sensitivity of 30% is too low to be very useful, but some symptomatic patients with MIBG uptake may be treatable with ^{131}I-MIBG. ^{201}Tl-thallium and ^{99m}Tc-sestamibi are non-specific tumor agents and, as with follicular tumors, may be helpful when other approaches have proven unsuccessful.

Scanning of the Thyroid

Radionuclide imaging of the thyroid is a direct extension of the clinical examination. It is important for the nuclear physician to be familiar with the setting in which the examination is being requested. Patients may be self-medicating with vitamins, kelp or other substances containing iodine and it is recommended to defer the examination for several weeks after discontinuation of these substances (Table 1). Clinical examination of the patient while under the camera allows correlation of palpable features with those of the scan. This ought always to be done by the physician who will report the examination and who should be aware of the presenting complaint, the relevant clinical history and laboratory data. A positive family history will increase the pre-test likelihood for multinodular goitre and Graves's disease. A complaint of pain predisposes toward thyroiditis. A history of radiation exposure with a symptomatic mass increases the probability of a malignancy.

Thyroid imaging is best performed on a camera fitted with a pinhole collimator in order to achieve the highest possible spatial resolution. The disadvantages of pinhole collimation are those of image distortion in depth caused by parallax and of the low sensitivity. Parallax increases as one moves from the center of the field to the periphery and will distort an off-centered image. Externally placed anatomical markers may seem misplaced on account of parallax.

The uptake probe is a nonimaging device that has high sensitivity for counting radiation and is routinely used to measure RAIU by the thyroid. The uptake measurement requires calibration of the probe with the patient dose. When the uptake has stabilized (about 24 hours later) the patient's neck is counted and the percent uptake is calculated with a correction for decay during the interval. In North

Table 1. Iodine-containing materials that interfere with nuclear procedures

Substance	Time to clear
Thyroxine preparations	3-6 weeks
Multivitamin preparations	2 weeks
Amiodarone	6-12 months
Radiographic contrast	2-4 weeks
Restaurant-cooked meals	2-3 weeks
Betadine-containing hygiene products	2-4 weeks
Occupational exposures:	
Dairy farmers	2-3 weeks
Restaurant employees	2-3 weeks

America, a normal iodine uptake is usually below 25%. In iodine-deficient populations the normal uptake is reported to be as high as 60%.

Thyrotoxicosis

Thyrotoxicosis is a clinical syndrome with manifestations of a hypermetabolic state in the presence of elevated serum free thyroxine (T4) and/or free triiodothyronine (T3) levels. If thyrotoxicosis results from increased biosynthesis and secretion of thyroid hormones from the thyroid gland, the condition can be called correctly hyperthyroidism. However, not all cases of thyrotoxicosis result from increased thyroid hormone biosynthesis; for example, the ingestion of excessive T4 or T3 can result in a thyrotoxic state but, via normal feedback suppression of pituitary TSH secretion from resulting elevated serum levels, thyroid function will decrease. Hence, the various causes of thyrotoxic states can be separated into thyrotoxic states resulting from hyperthyroidism and thyrotoxic states without hyperthyroidism.

Although the diagnosis of thyrotoxicosis is established by clinical and biochemical means, radioiodine uptake and thyroid scans are very useful in the differential diagnosis of the various causes of thyrotoxic states. RAIU and scans in thyrotoxic patients may be obtained at 4 to 24 hours post administration of iodine-123, but iodine-131 uptake together with ^{99m}Tc-pertechnetate scanning is also effective and less costly. Table 2 outlines the conditions to be considered in the differential diagnosis of thyrotoxicosis and identifies the radionuclide patterns produced by specific disease entities. The treatment of the hyperthyroid disorders is discussed in Chapter 14.

Thyrotoxicosis with Elevated RAIU

Graves' Disease

Graves' disease is a common form of thyrotoxicosis which results from the production, for unknown reasons, of antibodies which react with and activate the TSH receptor on the thyroid follicular cell membrane. These autoimmune TSH receptor antibodies activate adenylate cyclase in thyroid follicular cells, increasing synthesis and secretion of thyroid hormones. Also similar to the stimulatory effect of TSH, growth of the thyroid gland may occur. Although a clear familial aggregation occurs with Graves' disease, suggesting an inherited tendency to develop the problem, unknown environmental factors are necessary to trigger development of the condition.

13

Table 2. Differential diagnosis of thyrotoxicosis

	RAIU Elevated	RAIU Reduced
Common	Graves' disease Toxic multinodular goitre Toxic adenoma	Subacute thyroiditis Silent thyroiditis
Uncommon	TSH-secreting pituitary adenoma Thyroid hormone resistance (partial) Trophoblastic tumors	Exogenous thyroxine (factitious) Iodine-induced (Jod- Basedow effect) Struma ovarii syndrome Thyroid cancer metastases

Graves' disease may appear at any age but occurs most often in females aged 20-50 years. The presenting signs and symptoms are secondary to: an increased metabolic rate, increased adrenergic activity and manifestations of infiltrative dermopathy and ophthalmopathy. Patients may present with complaints of heat intolerance, weight loss in spite of an increased appetite, loose stools, tachycardia, tremor, emotional lability, fatigue and insomnia. Children may present with hyperactivity. In contrast, elderly patients may appear depressed and apathetic, having withdrawn from customary activities.

On examination, untreated patients may appear nervous and hyperactive or fatigued and listless. With Graves' disease, there is commonly mild to severe diffuse thyroid enlargement of the gland which has been described as having a "beefy" consistency. Bruits may be audible over the gland, the skin is warm and moist. There may be tremor of the outstretched hands and tachycardia is commonly observed. Thyrotoxic stare, lid retraction and lid lag may be present. Clinical signs of infiltrative ophthalmopathy are seen in fewer than one-half of patients on presentation. Pretibial myxedema and thyroid acropachy are relatively rare findings. Treatment with beta blocking drugs may abolish the signs of adrenergic overactivity (eg. tremor, tachycardia, stare and lid lag). The use of beta blockers does not compromise diagnostic testing with radionuclides.

In Figure 3 the ^{99m}Tc-pertechnetate thyroid scans of common thyroid disorders, including a typical patient with Graves' disease, are displayed. On occasion, patients with other forms of chronic thyroid disease may develop TSH receptor antibodies producing a thyrotoxic state. The distinction is not very important except that the latter may be at lower risk of developing eye complications. In these cases, the radionuclide pattern may be somewhat patchy rather than the diffuse homogenous pattern of uptake seen with Graves' disease.

Toxic Multinodular Goitre

Toxic multinodular goitre, also known as Plummer's disease, is primarily a disease of older people who may have had a longstanding nodular goitre. The clinical onset is often insidious and, in the elderly age group, may be superimposed on other chronic pathologies. Congestive heart failure, atrial fibrillation or other arrhythmias, weight loss or an apparent psychiatric illness may be seen. The appearance of an
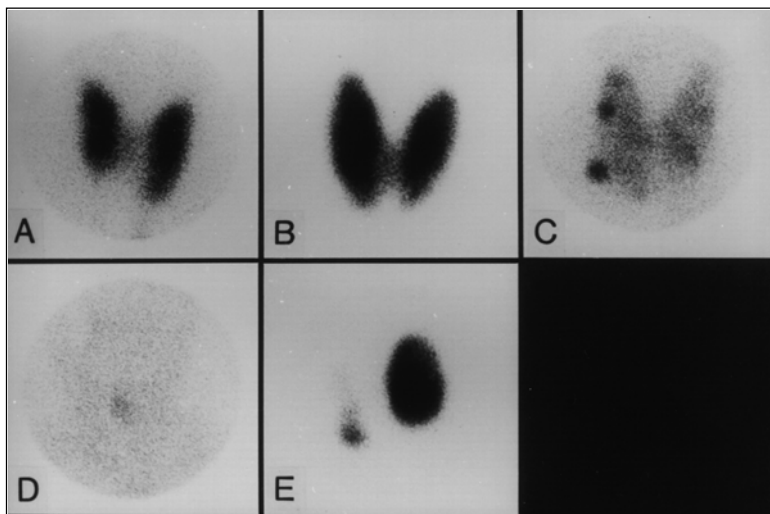
Figure 3. ⁹⁹ᵐTc-pertechnetate scans of representative patients: A. a normal thyroid gland. The gland is normal to palpation and the activity is uniformly distributed on the scan; B. a patient with Graves's disease. The gland is enlarged to palpation with "beefy" uniform consistency and the uptake is increased uniformly; C. a multinodular toxic gland. The nodules are palpable and firm while the uptake is irregularly distributed into the active nodules; D. silent thyroiditis. The uptake is near background and the gland may be tender to palpation and; E. a dominant toxic nodule in a multinodular gland.

unexpected illness together with the presence of a goitre requires the exclusion of thyrotoxicosis.

The thyroid scan in a toxic multinodular goitre has an irregular distribution of "hot" and "cold" regions and the RAIU may be normal or only mildly elevated. In patients who have iodine-induced thyrotoxicosis, the uptake may be low initially but will increase on serial uptakes once the source of iodine is eliminated. With sufficient uptake, radioiodine therapy provides an effective treatment mode.

Toxic Adenoma

Autonomously functioning nodules are benign adenomas, which operate independently of the thyroid-pituitary feedback control mechanisms. Recent evidence suggests that a number of these adenomas may result from somatic mutations occurring in the TSH receptor, resulting in constitutive activation of the receptor and autonomous cellular function. Thyrotoxicosis results when the output of thyroid hormone from such a nodule exceeds the body's requirements. As the symptoms of thyrotoxicosis are often mild, an initial work up may, in certain cases, begin with the exclusion of malignancy by a fine needle aspiration biopsy of a clinically detected nodule. The finding of a low serum TSH level in association with elevated thyroid hormone levels should be followed by an ¹²³I or ⁹⁹ᵐTc-pertechnetate scan to confirm increased uptake occurring in the nodule. In this setting, a preference for radioiodine

scans has been expressed by some authors because of the observation that some malignancies concentrate pertechnetate but fail to concentrate iodine. In our view, an aspiration biopsy, and not a radionuclide scan, is the better arbiter of the presence or absence of malignancy; hence, there is little need to prefer one radionuclide over the other for imaging.

Elevated beta-HCG Levels and Inappropriate TSH Secretion Syndrome

Occasionally beta-HCG levels may be sufficiently elevated to react with the TSH receptor and result in elevated free T4 and free T3 levels. This situation can be seen in an otherwise uncomplicated pregnancy, in hyperemesis gravidarum, in hydatidiform moles and in choriocarcinomas. In these conditions, the radionuclide scan demonstrates a diffuse homogenous uptake, similar to that seen with Graves' disease. The thyrotoxic state usually is not severe. Thyrotoxicosis in association with greatly elevated beta-HCG levels in the appropriate clinical situation establishes the diagnosis.

The syndrome of inappropriate secretion of TSH is rare. The finding of a normal or elevated TSH level together with unequivocally elevated thyroid hormone levels should direct diagnostic attention from the thyroid towards the pituitary gland. Such patients may have either a TSH-secreting pituitary adenoma or resistance of the pituitary (and peripheral tissues in some cases) to the inhibitory effect of circulating thyroid hormone. It is important to recognize secondary hyperthyroidism for what it is and not to ablate the gland with [131]I.

Thyrotoxicosis with Low RAIU

Disease states characterized by thyrotoxicosis without hyperthyroidism are important to identify as the appropriate treatment is quite different from those states characterized by hyperthyroidism. In these cases (see Table 2), the clinical features of thyrotoxicosis and the biochemical findings of elevated thyroid hormone levels occur in association with a low RAIU.

Subacute Thyroiditis

Subacute thyroiditis (or de Quervain's disease) is a relatively uncommon form of thyroiditis characterized pathologically by the presence of extensive follicular cell destruction, extravasation of colloid and aggregation of histiocytes around colloid, coalescing into giant cells. There is strong but indirect evidence that this pathology may result as a reaction to a preceding viral infection, but immune mechanisms may also play a role. Patients often present with cervical pain, tenderness of the thyroid (at times exquisite), symptoms of thyrotoxicosis and in some cases, systemic symptoms of an inflammatory illness. Thyrotoxicosis results from an unregulated release of preformed thyroid hormone from an inflamed gland. As the thyroid gland is depleted of preformed hormone and the thyroiditis subsides, the serum T4 and T3 concentrations fall to normal and in some cases to subnormal levels, before recovery of the gland with normalization of function. The entire course of the illness may last as long as 6-9 months, at times longer.

Silent Thyroiditis

This form of thyroiditis is dominated by the pathological picture of a prominent lymphocytic infiltration of the gland. The evidence to date suggests that silent thyroiditis is a variant of lymphocytic thyroiditis. Both have a predilection to occur in the post-partum period but are also common in the non-pregnant state. In contrast to subacute thyroiditis, the clinical features are usually (but not invariably) milder. There is usually less or no pain in the cervical region and less or no thyroid tenderness, despite, at times, acute enlargement of the thyroid. There are minimal if any systemic symptoms and the thyrotoxic symptoms, if present, may be quite mild. The subsequent evolution in the thyroid biochemical abnormalities has a similar clinical course to that of subacute thyroiditis. However, in contrast to subacute thyroiditis, patients with silent thyroiditis often have recurrences and up to one-half of the patients may develop permanent hypothyroidism in the future.

Factitious Hyperthyroidism

The clinical history is usually sufficient for the diagnosis of excessive exogenous thyroid hormone ingestion. Occasionally this may be deliberate and surreptitious.

Iodine-Induced Hyperthyroidism, Struma Ovarii, Thyroid Metastases

These disorders share in common increased thyroid hormone synthesis in the face of a low RAIU. Iodine-induced production of a hyperthyroid state is also known as the Jod-Basedow effect. Excessive iodine intake results from ingestion of iodine-rich foods, from over-the-counter pharmaceutical or health food store preparations, from radiological contrast media or from prescribed pharmaceuticals. Of particular note, amiodarone used for the treatment of cardiac arrhythmias, has complex effects on thyroid function producing a thyrotoxic state by overloading the patient with iodine (Jod-Basedow effect) or via stimulation of the immune system to produce a so-called silent thyroiditis state or even Graves' disease. The rare struma ovarii syndrome is characterized by uptake of radioiodine into a pelvic mass. Similarly, rare cases of thyrotoxicosis produced by massive thyroid cancer metastases, usually in bone, are characterized by an abnormal site of radioiodine uptake and these may be suspected from the past medical history.

Hypothyroidism

The diagnosis of hypothyroidism is achieved by clinical and biochemical laboratory means. RAIU no longer plays a role in documenting hypothyroidism. The high level of iodine intake through diet and nutritional supplements in North America has reduced the normal range of RAIU such that there is now substantial overlap between the normal and hypothyroid ranges. Both congenital and acquired organification defects can result in situations in which the trapping function is preserved despite little or no production of organified iodine. Under the stimulation of elevated TSH, this can result in an elevated RAIU, often to very high values, in the face of profound hypothyroidism. Organification defects can be demonstrated by use of the perchlorate release test.

Thyroid Nodules

Goitres occur both endemically in regions characterized by iodine deficiency as well as sporadically in all populations. Common to all goitrogenic processes is an increase in the number of follicles. A number of factors, of which TSH is a major contributor, can stimulate growth of new follicles. Many patients with nontoxic goitres have thyroid-stimulating antibodies similar to those seen in Graves' disease. It is possible that at the outset of goitrogenesis the process is always, or nearly always, diffuse. The newly generated follicular cells may display heterogeneous growth potential and nodules develop from the most rapidly growing clones. The process is usually slow, requiring years or decades. The properties of the original cells, which give rise to nodules, tend to be maintained in their daughter cells: thus, individual nodules in a multinodular goitre will display distinct behaviours. It is this morphological heterogeneity that gives rise to the presence of hot, warm and cold nodules coexisting in the same goitrous gland. Secondary events, such as central necrosis in a rapidly growing nodule or loss of functional capacity over time, may also contribute to the conversion of functioning adenomas into cold nodules.

The incidence of goitre increases with age and the reported rate of increase is a function of how the gland is examined. Thyroid enlargement most often comes to light through direct observation or palpation. The use of ultrasound imaging has greatly facilitated the characterization of goitres and its use permits a confident determination of whether the gland is diffusely enlarged or contains one or more nodules. RAIU and imaging can play a useful supplementary role to determine the functional status of goitres and of palpable nodules. However, nuclear studies no longer play the major role in goitre evaluation that they did prior to the availability of high-resolution ultrasound imaging.

Nodules that are large and that are enlarging rapidly, or that have other suspicious features such as fine calcification, must be evaluated to exclude the possibility of malignancy. The primary means of doing this is with needle aspiration biopsy, preferably ultrasound-guided. In the event that several repeated needle biopsy attempts are non-diagnostic, radionuclide imaging should be used to determine the functional status of suspicious nodules. Nodules that concentrate iodine or pertechnetate are very rarely malignant and can be safely followed while cold nodules that are suspicious of malignancy should be resected. The approach to the investigation of a thyroid nodule is given in Figure 4.

Thyroid Cancer

Although thyroid cancer accounts for less than 1% of all clinical cancers, it is the commonest form of endocrine malignancy and accounts for more deaths than all other endocrine cancers combined, excluding cancers of the reproductive tract. Thyroid neoplasms may arise from either the follicular endothelium or from the C cells (Table 3). The parafollicular C cells give rise to medullary carcinomas. Rarely, the thyroid may be the site of origin of a lymphoma or sarcoma. Primary tumors of kidney, breast, lung and melanomas can metastasize to the thyroid gland.

Follicular-Derived Thyroid Cancers

In North America the incidence of differentiated thyroid cancers has been increasing throughout much of the 20th century, certainly since the 1930s. However,
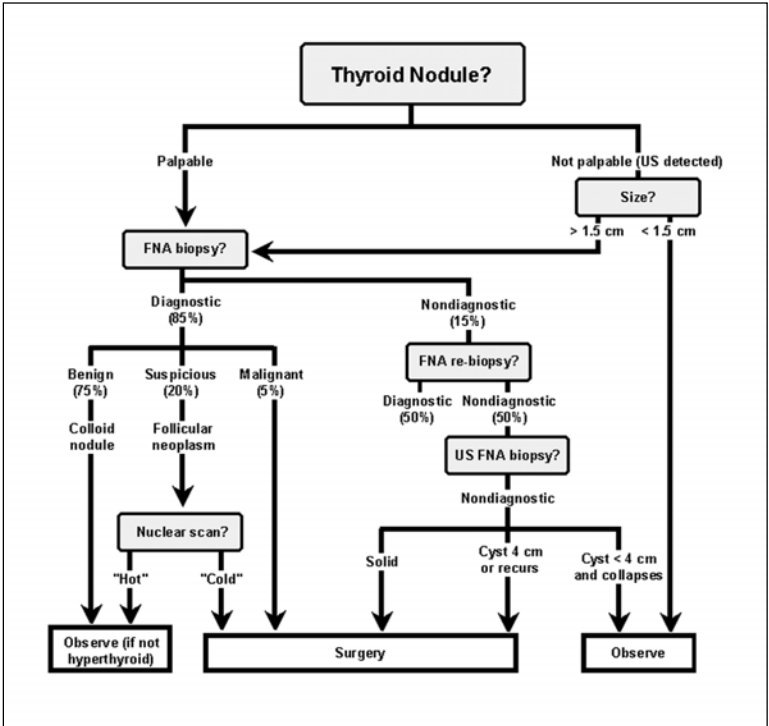
Figure 4. Approach to the investigation of a thyroid nodule. (Adapted from Gharib H. Thyroid Today 1997; 201:1.)

the mortality rate from thyroid cancers has remained stable, a reflection of improved therapies. Women are affected about three times more often than men. Unlike medullary carcinomas, which may be sporadic or occur in families, the follicular-derived neoplasms are said to occur mainly sporadically. Nonetheless, familial groupings of papillary cancer do occur with greater than chance frequency. There is a familial predisposition to thyroid cancer in Gardner's syndrome (multiple colonic and rectal polyposis) and in Cowden's disease (multiple hamartoma syndrome).

The only environmental factor known to increase the incidence of thyroid cancers is exposure to ionizing radiation. In the early part of the 20th century, x-rays were used to treat facial and neck hemangiomas of infants and lymphoid hyperplasia (tonsils, adenoids and thymus) of young children. In the following decades there was an increased number of thyroid cancers in these patients, which began to appear about a decade after the exposure, reached a peak incidence at about 25 years and continued to appear at greater than the sporadic population incidence throughout the lives of these people. In the post WWII years, the state of Israel used x-irradiation to treat immigrant children for scalp ringworm. These children developed an excess number of thyroid cancers in adult life. The experience of radioactive fallout, with a

Table 3. Classification of thyroid cancer

	Percentage
Follicular-cell derived:	
differentiated carcinoma	
. papillary and papillary-follicular	60-80%
. follicular	20-25%
. Hurthle cell (oncocytic)	5-10%
poorly differentiated carcinoma	5%
undifferentiated (anaplastic) carcinoma	10%
Parafollicular-cell derived	
medullary carcinoma of the thyroid	5-10%
Nonepithelial tumors:	
Lymphoma	<1%
Sarcoma	
Epidermoid carcinoma	
Metastatic	<1%

Adapted from: Biddinger P and Nikiforov YE. Pathologic features of thyroid tumors. In: Thyroid Cancer. Fagin JA (ed.); Kluwer Academic Publishers. 1998.

large component of radioiodine isotopes, in the Marshall Islands following atmospheric nuclear weapons testing was that exposed persons developed thyroid nodules and an increased incidence of cancers after several decades. It was anticipated at the time of the Chernobyl nuclear reactor accident, which also released a large amount of iodine isotopes, that there would be an increase in the number of thyroid cancers but the rising incidence within only five years was surprising at the time. In retrospect, this early appearance was predictable as it merely reflects the progressive broadening of the Gaussian distribution of risk on account of the very large exposed population to that event. In the 15 years since the Chernobyl accident, it appears that the population at highest risk of developing thyroid cancers is the group that ranged from the second trimester in utero to about five years in age at the time of exposure and that the annual incidence of new cases may now have peaked.

In the United States, the National Cancer Institute estimated that radiation exposure of Americans from weapons testing fallout may have been responsible for 7,000-70,000 thyroid cancers. This estimation assumes that the linear, no threshold hypothesis holds at the doses and dose rates in question. The question then arises whether the diagnostic use of x-rays and isotopes also contributes to the incidence of thyroid cancers. It appears, from the Swedish Cancer Registry, that patients who underwent ^{131}I imaging in the past do not have an increased incidence of malignancy compared to those who had similar radiation exposures from x-rays. The difference has been attributed to difference in dose rates.

Iodine deficiency is a possible carcinogenic factor, acting through chronic TSH stimulation. It has been argued that differentiated cancers occurring in iodine-deficient regions behave more aggressively.

Pre-existing nodules and goitre have been identified with an increased incidence of cancer but the significance of this is difficult to ascertain. The relationship may reflect only an ascertainment bias secondary to increased observation of these patients.

The diagnostic algorithm of suspected thyroid cancer is that of the suspicious nodule. Aspiration needle biopsy is the primary diagnostic tool. Ultrasound imaging may be required to define those nodules that are difficult to palpate and ultrasound-guided biopsy may be necessary to ensure satisfactory sampling. Suspicion of malignancy on fine needle aspiration biopsy should direct the patient to surgery for a near-total thyroidectomy. A good quality biopsy with a benign diagnosis should direct the patient to long term follow up and ultrasound is also useful to follow these nodules. In current practice, radionuclide imaging should be reserved for evaluation of nodules with a non-diagnostic biopsy and cold nodules thus identified should be surgically removed. This protocol has been shown to maximize the yield of malignancies while reducing the number of operations. Post-surgical imaging and follow-up of thyroid cancer is covered in Chapter 14.

Medullary Carcinoma

Medullary thyroid carcinoma (MTC) accounts for 5-10% of all thyroid cancers. The majority are sporadic cases occurring in elderly people. About one-quarter of the cases are familial with an autosomal dominant expression and present as one of three distinct clinical syndromes: multiple endocrine neoplasia (MEN) 2A, MEN 2B and familial medullary thyroid cancer (FMTC). MEN 2A is associated with pheochromocytomas and hyperparathyroidism. The 2B form is associated with pheochromocytomas and mucosal and gastrointestinal neuromas, while non-MEN FMTC has none of these associations.

The diagnostic hallmark of MTC is an elevation of the serum calcitonin level. The low incidence of the disease, relative to the incidence of nodules, makes it impractical to perform the assay on every patient presenting with a thyroid mass. The assay ought to be performed when malignancy is suspected and FNA has not indicated a follicular-derived lesion.

Mutations of the *Ret* proto-oncogene, a single trans-membrane growth factor-like receptor, result in the familial disorders multiple endocrine neoplasia Types 2A and 2B and FMTC: each of these conditions features the development of MTC. Genetic screening of potentially affected patients for the presence of these germ line mutations is now readily available and has proven more effective than screening via serial challenges with pentagastrin/calcium to detect abnormal calcitonin responses. Testing with pentagastrin/calcium was often performed in follow up of patients previously treated for medullary carcinoma but pentagastrin is no longer being commercially produced.

For patients with the familial forms of medullary carcinoma, the preoperative workup must address not only the thyroid mass but also the possibility of associated endocrinopathies. If pheochromocytomas are suspected, 24-hour urinary metanephrines should be measured. CT or MRI may be used to determine whether there are adrenal mass lesions but neither modality is able to determine the functional
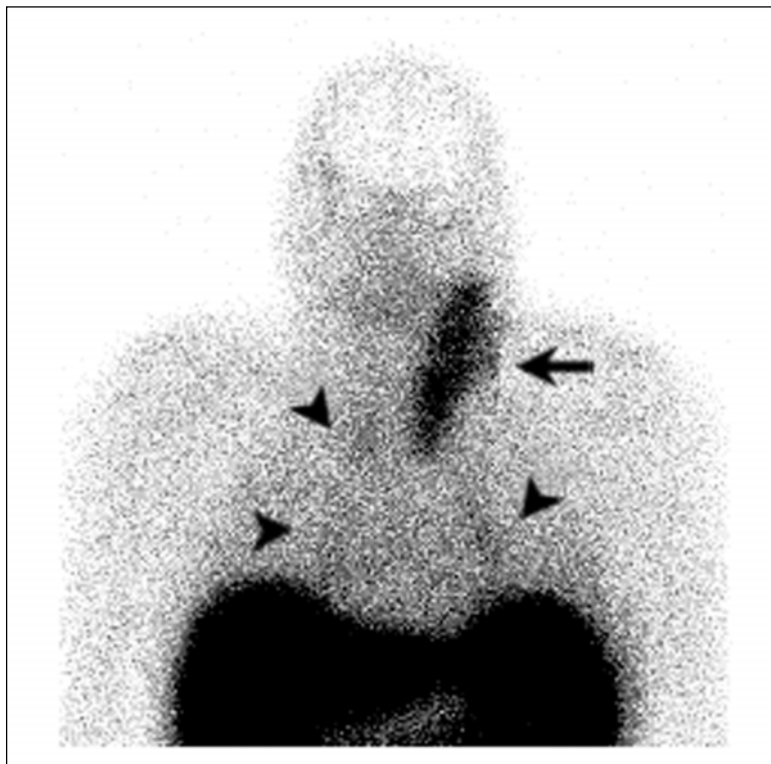
13

Figure 5. ^{111}In-Pentetreotide scan of recurrent medullary thyroid cancer with metastases to the neck (arrow) and pericardium (arrowheads). The patient subsequently achieved a partial remission with ^{111}In-octreotide therapy.

13

nature of the masses and, therefore, imaging with ^{131}I-MIBG or ^{111}In-pentetreotide is often required.

When MTC presents as clinically palpable disease, surgical cure is rare despite regional lymph node dissection. The persistence or recurrence of disease is detected through serial calcitonin and carcinoembryonic antigen (CEA) assays. When these assays are elevated, the localization of residual or recurrent disease becomes important as 30% of these patients may be rendered eucalcitonemic by further surgery. The best way of localizing disease remains unclear, but there are many approaches that work sometimes. Selective venous catheterization is technically demanding. CT and MRI are excellent for anatomic definition but inferior to radionuclide imaging for this purpose.

Either ^{201}Tl-chloride or ^{99m}Tc-sestamibi can image the neoplasm if calcitonin levels are elevated above 1000 mg/L. These agents are less sensitive if calcitonin elevations are only slightly increased. ^{99m}Tc-labelled pentavalent dimercapto-succinic acid (DMSA) will concentrate in tumors where there is active calcification, but the specificity is low as DMSA is also concentrated in amyloid deposits. Some 40-50%

of MTC will take up MIBG, though uptake is highly specific for tumors with an active amine uptake mechanism. This radiopharmaceutical may serve a dual purpose as about 85-90% of associated pheochromocytomas will also take up MIBG. Many MTC have somatostatin receptors and can be imaged with ^{111}In-octreotide or other somatostatin radiopharmaceutical analogs (Fig. 5). Metastases in or near the liver, spleen or kidneys may sometimes be difficult to image on account of the normal high concentration of somatostatin receptors in these organs.

Frequently Asked Questions (FAQs)

Can the thyroid scan be used to follow the size of a goitre or nodule?

That would not be the best use of the technology: ultrasound is better. The size of nodules is possibly less important than their cytology. If you need to know what a nodule is about, biopsy it.

Does everybody with thyrotoxicosis need a thyroid scan and RAIU?

Not if you already know what you are dealing with or if RAI treatment is out of the question. For instance, a pregnant thyrotoxic woman would be managed without recourse to these tests. These tests serve to distinguish among the forms of hyperthyroxinemia and, in thyrotoxic patients, to select the therapy dose.

Why isn't the thyroid scan a first-line test for thyroid nodules any longer?

The thyroid scan is able to determine the functional status of nodules that are larger than about 1.5 cm. It lacks the ability to exclude malignancy in cold nodules. A fine needle aspiration biopsy does that.

Additional Reading

1. Cases JA, Jurks MI. The changing role of scintigraphy in the evaluation of thyroid nodules. Seminars in Nuclear Medicine 2000; 30:81-87.
   This review article develops the current algorithms for the investigation of thyroid nodules. The roles of the laboratory, biopsy, radionuclide and ultrasound scanning and surgery are reviewed.
2. Mazzaferri E. Management of a solitary nodule. New Engl J Med 1993; 328:553-559.
   This short review article illustrates an efficient approach to the characterization of thyroid nodules.
3. Berne RM, Levy MN, eds. The thyroid gland. In: Physiology. Mosby Year Book, 1993:932-948.
   This is a very readable account of thyroid gland physiology.
4. Tuttle RM, Becker DV. The Chernobyl accident and its consequences: Update at the millenium. Seminars in Nuclear Medicine 2000; 30:133-140.
   This is a review of the state of knowledge concerning radiation-induced thyroid cancers and, especially, of what we learned from the Chernobyl accident.
5. Braverman LE, Utiger RD, eds. The Thyroid. Eighth ed. Philadelphia: Lippincott Williams & Wilkins, 2000.
   A comprehensive, heavily referenced work concerning thyroid diseases.

13

Radionuclide therapy of Thyroid Disorders

Albert A. Driedger and Thomas J. McDonald

Introduction

Of the diseases discussed in Chapter 13, some are treatable with radioactive iodine (RAI). In diagnostic applications it is optimal that as little energy as possible be deposited in tissue so that the signal deposited in the detector can be maximized. That is why diagnostic imaging utilizes gamma-emitting isotopes. However, in therapy the intent is to deposit as much energy as possible in a target tissue in order to kill those cells. For this application, nuclides whose emissions have a short path length in tissue are essential. Historically, these have been beta emitters with path lengths of a few mm in soft tissue. The most frequently used therapeutic nuclide of this class is ^{131}I even though its associated gamma emissions give rise to problems in radiation protection. In future it is likely that Auger electron and alpha-emitting nuclides will also find applications in therapy. With these emissions the energy of the decay will be largely concentrated in the individual cells that concentrated the isotope.

Benign Thyroid Disorders

Indications for Radioiodine therapy

Graves' Disease

All treatments for Graves' disease disable or destroy the thyroid by one means or another as we have no means to repair the intrinsic immunologic abnormality leading to thyrotoxicosis. The three therapeutic modalities are partial thyroidectomy, long term antithyroid drugs or RAI.

Surgery is rarely used in western practice but may be the preferred treatment in a few instances such as:

1. thyrotoxicosis during pregnancy or amiodarone-induced thyrotoxicosis where there is intolerance of antithyroid medications
2. serious adverse reaction to antithyroid medications in patients who refuse RAI
3. concern about a co-existing malignancy.

Antithyroid medications, such as propylthiouracil or methimazole, will achieve remission in some patients and are the preferred treatments during pregnancy. It is the view of some endocrinologists, especially in Europe, that all patients ought to have a trial on antithyroid drugs and that RAI should be reserved for those who do not respond or who develop side effects. These drugs are associated with adverse effects, which may range from skin rashes to reversible agranulocytosis and hepatitis.

Elderly patients with cardiovascular disease are best treated with a course of antithyroid medications to deplete the gland of thyroid hormone prior to receiving RAI. Without this precaution there is a possiblity of an abrupt symptom exacerbation as hormone is released from the damaged follicles. Rarely thyrotoxic patients are treated long term with antithyroid medications alone.

In the western world, RAI is a common treatment of choice, even in the young and in those with small goitres, although there are differences of opinion about the goals of therapy. Many endocrinologists prefer ablation of the thyroid while some attempt to minimize the likelihood of ensuing hypothyroidism by use of smaller ^{131}I doses. The attempt to avoid hypothyroidism may be futile, since immune thyroiditis to some degree is a component of every case of Graves' disease. The immunologic assault on the thyroid will continue despite RAI therapy and may ultimately lead to hypothyroidism when the residual follicles cease to function. Euthyroidism, if it is achieved, is unlikely to be permanent. It is a commonly held view that, for most patients, ablation is the proper endpoint of RAI therapy.

The only absolute contra-indication to RAI therapy is pregnancy as it may ablate the fetal thyroid gland and could contribute to mental retardation if given during the first trimester when cortical cell migration in the fetal brain is very sensitive to radiation. RAI should also be deferred in a breast-feeding patient, as iodine is secreted into breast milk. In all other patients RAI can be considered. The only proven long term risk is that of permanent hypothyroidism. There is no increased risk of cancer or leukemia following RAI therapy nor is there any risk demonstrable to children of subsequent conceptions. It is usually recommended that conception be delayed for 6-12 months post-therapy by which time a stable euthyroid state ought to have been achieved. There is no absolute contraindication to the treatment of thyrotoxic adolescents and children with RAI.

In the short term, ^{131}I administration may result in a large release of thyroid hormone and, rarely, may produce thyroid storm unless precautions are taken. The precautions can be achieved either through pre-treatment for a few weeks with antithyroid drugs or by the concommittant use of beta blockers. Patients who have thyrotoxic ophthalmopathy may experience transient worsening of their eye problems in the weeks following treatment and this can be avoided by administration of a short course of high dose steroids.

Multi-Nodular Toxic Goitres

Patients with multi-nodular toxic goitres are typically older than those with Graves' disease and are more likely to have co-existing cardio-pulmonary, hypertensive and other co-morbid disease.

Multi-nodular goitres are usually benign but rapid enlargement, lymphadenopathy or hoarseness should signal the possibility of a concurrent malignancy. Suspicious areas, usually enlarging cold nodules, are best biopsied by fine needle aspiration prior to RAI treatment.

It is less likely than in the case of Graves' disease that patients with multi-nodular toxic goitres will be rendered hypothyroid by a single treatment. The least abnormal tissues are likely to be suppressed by hormone output from the more autonomous nodules and the survivors will resume function after the currently toxic nodules have been destroyed. The delivered radiation dose from any one treatment will vary

from nodule to nodule secondary to the variable uptake. The under-treated nodules tend to become more autonomous over time, with possible recurrence of the toxic state. These patients should be made aware that treatment may need to be repeated. Treatment with larger doses of ¹³¹I will help to minimize the risk of recurrence.

Autonomous Nodules

Autonomous single nodules may occur in young adults but do so more commonly in older people. Definitive treatment is achieved with either surgery or RAI. With RAI therapy there is little risk of ensuing hypothyroidism as the function of normal tissue is suppressed at the time of treatment and it will recover when the thyroid stimulating hormone (TSH) levels subsequently normalize. There is no direct evidence, but an argument can be made for a theoretical risk of carcinogenesis from RAI therapy in this setting as the normal tissue adjacent to the nodule will receive a significant, but non-lethal, radiation dose. Thus, it is common practice to resect these nodules from younger people and to reserve RAI for older patients in whom surgery carries a greater risk.

Non-Toxic Goitres

Non-toxic goitres with compressive symptoms are, in the main, best treated by surgery. However, in circumstances where surgery is risky, reduction of goitre size can be achieved with RAI. In the past it was thought that RAI treatment might be dangerous if the goitre was compressing the trachea as the induction of swelling by the action of radiation might compromise the airway. However, evidence has emerged that significant airway compression does not occur and that RAI therapy is safe even if the pretherapy CT scan demonstrates up to 50% narrowing of the trachea.

The clinical assessments of large goitres systematically underestimate their size and this is a factor responsible for failure of RAI therapy. An ultrasound examination defines the gland size better than palpation. If there is a large intrathoracic goitre then CT may be the preferred way to determine gland size. The doses of ¹³¹I often need to be quite large, up to the range of doses used in cancer therapy, as the RAI uptake tends to be low. Pretreatment of the patients with a low-iodine diet for 10-14 days tends to increase the uptake and permit reduction of the dose. The former practice of restricting outpatient doses to 1.11 GBq (30 mCi) or less may have promoted a practice of under-treating large goitres of this type if there were no hospital beds available for isolation purposes. In these circumstances, it was common practice to administer the maximum outpatient dose without regard for the fact that this might not achieve a cytocidal concentration in any part of a very large goitre.

Preparing the Patient for Therapy

As with all other therapies, it is critical that the patient be informed and able to consent to the proposed administration of RAI. The prevailing high public level of negativity about nuclear technology, combined with the difficulty that thyrotoxic people may have in focusing their thoughts, can make it difficult to obtain an informed consent. In such cases it may be best to institute a short course of antithyroid medication to provide a hesitant patient some time to consider the treatment options. At a minimum, patients need to understand the nature of their illness, its natural course, the proposed treatment and its probable consequences. They also need to

understand that although RAI treatment is safe for them, there will be a period during which they must take care to avoid radiation exposure of their closest family, social and workplace contacts. Women of childbearing age and who are sexually active need beta-HCG documentation to ensure that one does not treat a pregnant woman.

Methimazole and propylthiouracil should be discontinued for 3-4 days prior to administration of [131]I. If they are not discontinued beforehand, the treatment will be less effective as the radioiodine will not be organified and will be rapidly excreted. Most often these drugs need not be reinstituted. If required to control symptoms then they should be withheld for 5-7 days. They may exert an unwanted radioprotective effect on the thyroid since the thionamide drugs are free radical scavengers. PTU given prior to therapy has a radioprotective effect on the gland that may last up to a month. Thyrotoxic recurrences are more common in PTU pre-treated people and one way to minimize recurrences is to increase the ^{131}I dose by 10-15%.

It is important to provide all patients, but thyrotoxic ones in particular, with written instructions about radiation safety and the protection of their families and close associates in the days or weeks following treatment (Table 1). The International Commission on Radiological Protection (ICRP) has recommended that members of the public should receive no more than 1mSv of ionizing radiation exposure per year from man-made sources, including incidental contact with recently treated patients. The ICRP has also declared that non-pregnant adult family members and close associates of the patient who are involved in provision of care and comfort may be allowed a larger exposure, provided that they are informed and do so "knowingly and willingly". In order to advise the patient and family appropriately, it is necessary to answer the questions posed in Table 2.

In the main, outpatient treatment of thyroid diseases with RAI is safe. Patient and family must understand the restriction on intimate social behaviours in the days following treatment. The physician can most efficiently provide them with behavioral advice while describing the risks and benefits of treatment and can thereby alleviate everyone's anxiety about the significance of low dose radiation exposure. There are several software products that can be used to model the likely exposure of others from RAI and other radionuclides. (Once such program is available without charge from rajc@flinders.edu.au.) They do not take the possibility of contamination into account but this is of little consequence as about 99% of the dose to others will be gamma radiation. These software programs take dose, uptake and the projected proximity of contact into account and can be used to support the instructions given to patients.

There are circumstances in which the assurance of radiation protection may be challenging, such as in the cases of very active young children, mothers with responsibility for the care of young children, intellectually challenged adults or the frail elderly. In these complex situations, management requires coordination of a multidisciplinary team whose skills include technical expertise as well as a variable range of social resources. It is essential for nuclear physicians to educate families, nurses, social workers and others about the salient aspects of radiation safety when such situations arise. It should always be possible to provide all the care that the

---

Table 1.   Patient instructions following low-dose radiation therapy

Instructions for Patients Following Treatment with a Radioactive Material

Date____/____/_____ For_____(Patient Name)

The radioactive medicine that you have received will expose others to radiation and a small part of the radioactive medicine can potentially be transferred to other people through close contact. The radiation dose to them will be low but, by observing the following precautions, you can reduce it still further.

General Instructions for the next 3 days:
- keeping your distance from others helps to greatly reduce their radiation exposure
- reducing your time spent with others helps to reduce their radiation exposure
- drink plenty of liquids.
- avoid mouth to mouth or other close personal contact.
- do not share items that contact the mouth (e.g., eating utensils, toothbrushes).
- use separate eating utensils and wash them separately.
- wash hands frequently and especially after using the toilet.
- whenever possible allow others to prepare food that is not for your own consumption.
- shower daily.
- tissues used to blow nose or hold fluid extracted from mouth should be flushed down toilet.

Observe the following for the days listed:
- use a separate bathroom for _____ days. Flush the toilet twice after each use. Men should sit to urinate. Keep your towels and washcloths for only your use.
- sleep in a separate bed (at least 2 meters separation) for _____days.
- limit close contact with children and pregnant women to 30 minutes per day for _____ days.
- maintain a distance of at least 1 meter from other people for ____days.
- do not travel in a car with others for more than 2 hours within 2 days of treatment.
- delay return to work for ____days.

At the end of ____ days you should:
- wash your bedclothes and dayclothes worn since treatment and thoroughly clean your bathroom before returning it to use by others.

If questions arise after you have gone home, call Dr _____ at _____.

Treatment provided by Dr _____ on _____20__

In the event of an emergency contact the Nuclear Medicine Physician on call _____.

Table 2. **Basic home assessment questionnaire for considering out-patient radioiodine therapy**

- Who lives in the home?
- Does the patient have responsibilites for the care of others, especially infants and children?
- Can someone other than the patient prepare meals for the first two days?
- Can the patient's bed be adequately separated from others?
- Is it possible to designate one bathroom exclusively for the patient's use during the designated period?
- Does the patient experience stress incontinence?
- Are there circumstances in the workplace where others might receive an exposure of >1mSv from the patient?

---

patient needs without undue exposure of the staff if attention is paid to the time-distance rule and to the minimization of contamination.

The administration of a large therapy dose is not in itself an indication for admission to hospital. In-hospital therapy may be necessary for a patient who requires concurrent medical care, comes from a long distance by public transportation or is unable to comply with instructions. The patient must be admitted to a single room with a non-absorbent floor covering and equipped with a private shower and toilet. If the facility is not designed for radiopharmaceutical therapy, then care must be taken to avoid exposure of patients in adjacent rooms. Adult visitors should be restricted to brief visits (15-30 minutes). It is important that patients not be made to feel that they are "locked up": the door to the room may be open, the room should be cleaned as needed and staff should not feel so pressed to leave the room as to have no time for social interaction with the patient.

Discharge may occur when the patient no longer needs concurrent medical care and when it can be reasonably assumed that no member of the public will receive a dose in excess of the public limit from the patient.

In many countries there are national advisory committees that have developed useful documents to promote quality assurance and safety in radionuclide therapies. These are often up to date and should be consulted in the preparation of a local therapy protocol.

Dosimetry

The dose of ^{131}I is derived from consideration of the gland size, the iodine uptake and the intrathyroidal transit time. This is easier to do with diffuse Graves' disease than with nodular glands whose uptake is irregular. Gland size is usually estimated by palpation, although when a retrosternal goitre is suspected, ultrasound or CT examination may be required. Iodine uptake is measured with ^{131}I or ^{123}I. The intrathyroidal transit time is not routinely measured but may be assumed to be about 4 days. In some thyrotoxics the transit time may be much shorter and this will result in underdosing of those patients unless there is appropriate dose compensation. To achieve thyroid ablation requires administration of a radiation dose of 70-100 Gy to the gland. Thus, in principle, the ^{131}I dose may be calculated as:

14

Administered dose (MBq) = $\dfrac{\text{Desired dose (MBq/g) x Gland weight x 100}}{\text{Radioiodine uptake at 24 h (\%)}}$

A typical dose of ^{131}I is in the range of 3-5 MBq/g, which for an average size gland and uptake, results in a dose of 250-400 MBq. Patients treated at the lower end of the dose range will have a 10-15% recurrence rate. The circumstances in which the dose should be increased include rapid thyroidal transit, recurrence of hyperthyroidism following previous therapy, large goitres and a history of recent treatment with anti-thyroid drugs.

Considering the substantial errors that are inherent in the inputs to the dose calculation, some centers prefer to treat with a standard dose according to whether the gland is mildly, moderately or greatly enlarged. For purposes of quality management it is helpful if all practitioners at a center can agree on the approach to be taken to dosing.

Multinodular glands should be treated at the higher end of the recommended dose range. Usually the uptake is somewhat lower than is the case with Graves' disease. Based on considerations of uptake, gland size and heterogeneity of uptake, a typical treatment dose will roughly fall between 1 and 4 GBq. A low iodine diet for 1-2 weeks before treatment will often allow a modest dose reduction (Table 3).

Follow-Up of the Treated Patient
Systematic follow up of the RAI-treated patient is important.
Short term follow up should identify:
- frail patients who may need to be supported with antithyroid drugs or beta blockers for several weeks until the gland ceases to release thyroid hormone
- in the case of Graves' disease with ophthalmopathy, the need to treat exacerbations of thyrotoxic exophthalmos with steroids
- in the case of large dose treatments, radiation thyroiditis and its treatment with a short course of steroids.

Long term follow up primarily aims to:
- document that hyperthyroidism has been eradicated
- detect and treat hypothyroidism when it occurs in the months or years following therapy.

The patient may need supplemental hormone by about 3 months. A stable level of function may not be achieved until 5-6 months.

Follicular Cell-Derived Thyroid Cancers
The discussion of thyroid cancer RAI therapy must be grounded in the risk factors for recurrence of disease presented by the diagnosis. There are many clinical schemes for evaluating risk, such as AMES, where:

A means age at diagnosis

M means presence/ absence of metastases

E means local extent of disease

S means size of the primary lesion.

Such a scheme is helpful in evaluating the post-surgical risk of thyroid cancer recurrence and essential in guiding discussions with the patient concerning post-surgical treatments or ongoing surveillance. Other risk assessment protocols exist,

---

Table 3. **Simplified low-iodine diet typically used for 10-14 days prior to radioiodine scanning or therapy for thyroid cancer**

These are high iodine foods and should be avoided.

Table salt or sea salt (do NOT use salt in food preparation or at the table)
All fish, sea food and shellfish
Potato chips, pizza, salted nuts and other heavily salted foods
Tea and instant coffee
Canned soups, canned vegetables/fruits and canned vegetable juices (unless unsalted)
Milk and other dairy products (see below)
Eggs (maximum one per day) (see below)
Foods or beverages containing red food coloring, chocolate or molasses
Some medicines (multiple vitamins, Buckley's mixture, cod liver oil, amiodarone)

Restaurant preparation techniques and ingredients are usually unknown, and should probably be avoided as well.

No other foods need to be restricted.

Foods that contain small amounts of eggs or milk can be used
Unsalted meats, fresh fruits and vegetables, breads, cereals, pasts and unsalted french fries can also be used

---

such as AGES (Age, Grade, Metastasis and Size) and TNM (Tumor, Node, Metastasis). There is no universal agreement about which scheme is preferable. Clinical validation for the AMES variables has come from follow up of large series, with recurrence rates ranging from 6.8% in stage I to 50% in stage IV (Mazzaferri criteria). For purposes of illustration, the AMES criteria will be discussed here.

A Adults older than 45 years of age tend to have disease with more aggressive behaviour. Older patients should all be considered to be at increased risk of recurrence, regardless of tumor characteristics.

M The most common sites of metastases from papillary carcinoma are the regional lymph nodes and the lungs. The presence of lymph node involvement of itself has little effect on the prognosis as these are usually easy to treat by resection and RAI. However, bilateral neck or mediastinal lymph node disease may adversely affect the prognosis. Lung metastases signal a high risk for disease persistence/recurrence. Hematogenous dissemination occurs rarely, typically to bone and brain, and is associated with a grim prognosis. Follicular carcinoma, on the other hand, tends to metastasize via the hematogenous route with involvement of bones, lungs, brain and other viscera, yet metastatic disease may be compatible with prolonged survival.

Accurate preoperative detection of distant metastases is typically not possible with these cancers underscoring the importance of RAI imaging to detect extent of metastatic disease and the difficulty inherent in imaging them while the thyroid gland is in place. Thus, the definitive discussion of prognosis must often await ablation of remnants with RAI and post-therapy scanning.

E The local extent of disease includes consideration of extrathyroidal extension of tumor into adjacent tissues, vascular invasion, the finding of tumor at the resection

margin and lymph node involvement. In the case of papillary carcinoma, multifocality ought to be included as a risk factor, especially if the gland resection has been incomplete.

S The probability of disease recurrence rises with increasing size of the primary tumor and may reach 40% for lesions greater than 4 cm. Small subcentimetre lesions discovered incidental to other surgery probably do not require ablation, but there is still a small risk of metastatic disease arising even from 2-3mm primary tumors. Multicentricity, a history of exposure to ionizing radiation (e.g., treatment for Hodgkin's disease) or aggressive-appearing histology may be risk factors that would justify total thyroidectomy and RAI ablation, even with a small primary lesion.

Patients who are negative on all parameters of the AMES assessment can be considered as being at low risk (~5%) for future recurrence. In contrast, those who have major risk factors can have up to a 50% recurrence rate. Regardless of the grading, all patients with previous thyroid cancer should have lifelong follow up as recurrences may occur even decades after the initial diagnosis.

Indications for RAI Therapy

RAI treatment may be considered under two indications:
1. ablation of thyroid remnants and
2. treatment of iodine-avid metastases.

Prerequisites for RAI treatment are that all necessary surgery has been completed and there are no urgent clinical issues that mandate immediate intervention (e.g., airway obstruction, spinal cord compression or symptomatic brain metastases). It is in the interest of patients that there be a smooth working relationship between surgeons, endocrinologists and nuclear physicians to ensure that all clinical issues are addressed in an efficient manner.

Indications for Ablation

Post-surgical ablation of remnant thyroid tissue is justified in most cases. The goals of ablation are debated but the outcomes are clear: the incidence of recurrence is thereby reduced. At a minimum, the administration of ^{131}I destroys normal remnants remaining after surgery, remnants that might contain additional foci of disease or a propensity to form new carcinomas. Additionally, occult foci of metastatic disease in lymph nodes may be destroyed. In other cases, ablation of the remnant makes it easier to detect early recurrences. An exception might be made for those patients with incidentally discovered primary microcarcinomas (<10mm) as these do very well with surgery alone. One cannot always know at the time of ablation, until the post-therapy scan, whether the patient has metastatic disease (Fig. 1).

Indications for Treatment of Iodine-Avid Metastases

About 75% of all differentiated thyroid cancer metastases will concentrate RAI and thus all patients merit an attempt at treatment. The only way to be certain that the tumor does not concentrate iodine is to administer a therapeutic dose and to perform a post-therapy scan 5-7 days later. Unless there is a clinical emergency, such as a spinal cord or airway compression, RAI should be considered as the primary radiation modality for treatment of these cancers. Depending upon the iodine avidity of the tumor, the radiation dose administered to the tumor may approach 8-10 times that which can be administered by external beam irradiation. When one is
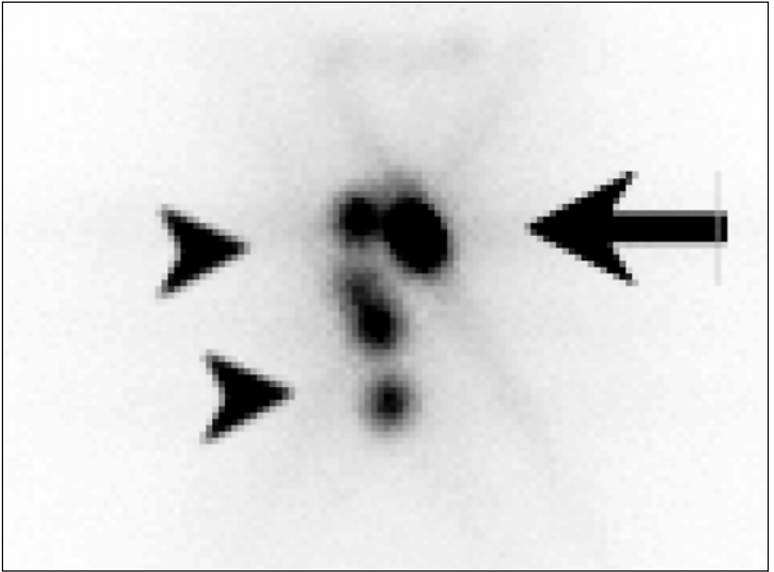
Figure 1. A post-surgical patient with papillary carcinoma and no nodes detected at surgery. Post-therapy imaging (anterior projection) reveals an unexpected chain of nodal involvement in the right neck. This scan was obtained 5 days after treatment with 3.7 GBq of iodine-131. The dark spot is in the thyroid bed (arrow) and the linear array represents the right anterior cervical chain of nodes (arrowheads). A follow-up scan subsequently confirmed that all the activity in the nodes had been obliterated.

confronted by a life-threatening lesion, external beam radiation therapy may be required in order to obtain early benefit. However, iodine avidity is often seen, even after high dose radiation.

Patient Preparation for RAI Therapy

After near-total thyroidectomy the patient may suffer from temporary or permanent hoarseness or hypocalcemia. Hoarseness can result from accidental surgical trauma to the recurrent laryngeal nerve or from deliberate sacrifice as part of the tumor resection. The loss of one recurrent laryngeal nerve results in hoarseness and in loss of an effective cough. Over time, there may be recovery through adaptation of the contralateral cord. Bilateral paralysis results in stridor and requires a tracheostomy to protect the airway. Hypocalcemia may be transient or permanent, depending upon the surgeon's success in salvaging the parathyroid glands. Hypoparathyroidism usually manifests within hours of surgery and is treated with supplemental calcium. Often parathyroid function recovers within a few weeks. If the disease extent required resection of all parathyroid glands then the deficiency is permanent. Such patients need management with large doses of supplemental calcium and vitamin D.

14

The nuclear physician should ideally meet the patient after surgery but prior to discharge from hospital to discuss the purpose of radioiodine therapy and to prepare the patient for the ensuing temporary hypothyroid symptoms. A timing of about 5-6 weeks post-surgery works out well in most cases. There are several reasons for not proceeding more quickly to ablation:

- it allows time for patient recovery from surgery prior to RAI treatment
- endogenous levels of iodine will be high for several weeks after surgery as a result of transcutaneous absorption of iodine from the pre-operative skin preparation
- it will take up to 5 weeks to elevate TSH levels adequately (greater than 30 mU/L) as the circulating half-time of thyroxine is about one week
- a low iodine diet for the last 10-14 days will help to maximize the iodine uptake when the treatment is given (Table 3).

Not all patients will become symptomatically hypothyroid on this protocol as they will be supported to variable degrees by the remnants of normal thyroid, which nearly always remain as a result of the surgeons' attempts to spare the parathyroid glands. If the patient has a large remnant with a high uptake, it may prevent an adequate rise of TSH and obscure the presence of metastases in the post-ablation scan. At the other extreme are some patients for whom hypothyroidism may be intolerable by virtue of their frail medical state. There have been many attempts to minimize the symptoms of hypothyroidism by shortening the hypothyroid interval as much as possible. While the most common protocol is to withhold all forms of thyroid hormone for 5-6 weeks, some centers replace the patient with short-acting liothyronine (T3, Cytomel®) for three weeks followed by 2-3 weeks off all thyroid hormone. This protocol may not always elevate TSH to the same degree as complete withdrawal and liothyronine may not be readily available in some countries.

In some cases, it may be unwise to make frail patients hypothyroid. In addition, rare patients may have diminished pituitary function and be unable to raise their TSH levels in response to hypothyroidism. With recombinant human TSH (Thyrogen®) it is possible to treat such patients while on full dose thyroid hormone replacement following several daily intramuscular injections of rh-TSH (Fig. 2). (At the time of this writing Thyrogen is only approved for diagnostic scanning but can be obtained for treatment on a case by case basis from Genzyme Corporation.)

A diagnostic scan prior to therapy is helpful in several ways, provided that therapy will follow soon after so as to minimize the potential for stunning (see section on Dosimetry). The uptake at 48 hours is useful to estimate the retention of the treatment dose and to support discussions with the patient about the duration of precautions when outpatient treatment is given. If the pathology is that of a single small lesion without aggressive characteristics and limited to one lobe in a young person along with an undetectable thyroglobulin (Tg) and the uptake is nil, then ablation arguably may be abandoned and the patient placed on long term follow up. Those with an elevated Tg and a negative scan need a therapy dose and post-therapy imaging.

One of the most important indicators of residual cancer is the Tg level and this is most sensitive if performed when the patient is hypothyroid. It is important to also measure antithyroglobulin antibodies at the same time as their presence may suppress the Tg value. Further, in follow up, a rise in anti-Tg titre may indicate disease recurrence.
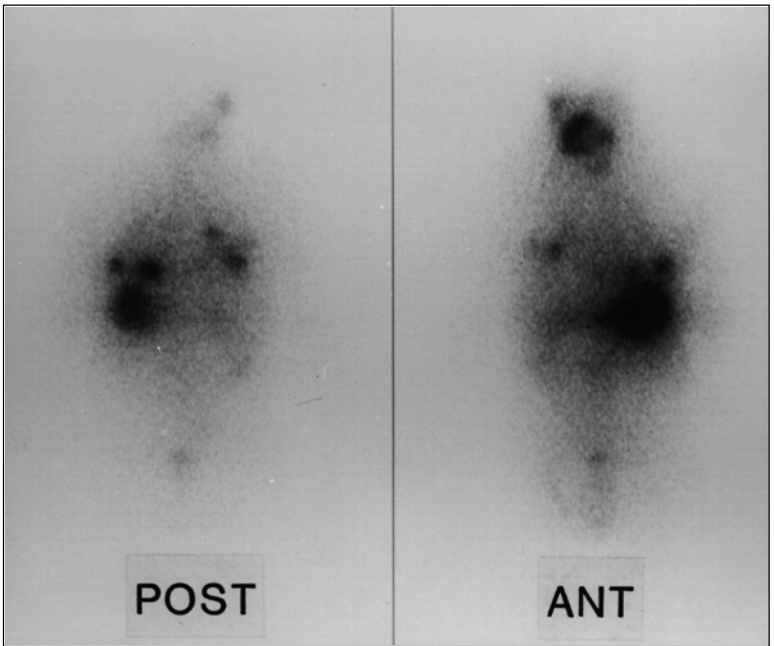
Figure 2. A frail elderly man with congestive heart failure and metastatic papillary carcinoma who became paraplegic during thyroid hormone withdrawal. He recovered on thyroid hormone. Subsequently, while on thyroid hormone replacement he was given recombinant thyroid stimulating hormone (rh-TSH) prior to ^{131}I administration. His post-therapy scan performed a week after treatment with 3.7 GBq of ^{131}I demonstrates uptake into multiple pulmonary metastases.

For those patients with recurrent but iodine-negative cancer and for those with metastatic medullary carcinoma, there is an emerging prospect of new therapies using somatostatin receptor-avid agents, such as ^{90}Y-octreotide or ^{90}Y-lanreotide. These therapies are experimental at this time.

Dosimetry

In recent years there has been concern expressed over the possibility of thyroid "stunning" by diagnostic doses resulting in less ^{131}I uptake from the treatment dose than was anticipated on the diagnostic scan. This phenomenon is attributed to sublethal radiation damage by the diagnostic dose, which could prejudice the outcome of subsequent therapy. To avoid stunning, some centers have abandoned pretherapy scanning, choosing to base the decision to treat on other criteria and proceed directly to administration of the therapy dose. On closer examination, it seems that the stunning is observed when there is a prolonged interval (up to several weeks) between the diagnostic and therapeutic administrations. In centers where the interval between the two procedures is minimized, stunning is not observed. With coordination, it is

possible to complete any desired RAI imaging and to proceed to therapy within 48-72 hours. For patients presenting for initial ablation, the imaging and uptake measurements of the remnants can be done with 50-70 MBq of ^{131}I. If the patient is presenting for consideration of retreatment of known metastases, then higher scanning doses up to 350 MBq may be used without prejudicing an immediately following therapy. Metastases typically have much lower ^{131}I uptake per gram than normal remnants.

Unlike external beam therapy, where administered doses can be accurately calculated, radionuclide therapies do not lend themselves to similar dosimetric precision. The goal of therapy is to ablate normal thyroid tissue and tumor while avoiding toxicity to the bone marrow and lung. There are two possible approaches to dosing:

- use of a standard dose or
- pretreatment dosimetry study with a low ^{131}I dose to approximate target organ and remnant or tumor radiation doses.

The outcomes are similar between the two approaches, although there are circumstances, such as concurrent renal failure, in which accurate dosimetry is necessary to avoid toxicity within the customary range of doses.

The objectives of RAI ablation remain a vexing source of controversy. If the objective is only to reduce the volume of normal tissue then ablation is possible with a low dose of ^{131}I e.g., 1.1 GBq. However, if one wishes to truly ablate the remnants with a single administration of RAI, then a mean dose of about 3 GBq seems to be required. If one also intends to destroy malignant cells then a still higher dose in the range of 3.5-5.5 GBq administered to a hypothyroid patient may be necessary. Typically, one cannot know which situation applies until the post-therapy scan (at the earliest). The Tg level may help one to decide the range of dose that is warranted. In order to avoid missing the opportunity to destroy tumor, most practitioners opt for a larger ^{131}I dose. Single doses of 1.1 GBq (30 mCi) do not reliably achieve remnant ablation and patients so treated tend to be lost to follow up, possibly as a result of becoming disaffected by serial bouts of hypothyroidism needed to complete the ablation. In our view, the goal should be to achieve ablation with a single treatment and this justifies doses of 3-4 GBq. If the goal is to also treat known residual tumor then the initial dose will be higher. If the Tg is elevated, a follow up scan is required in 6-12 months with retreatment if tumor persists.

Patients who have previously been ablated may require retreatment of metastatic disease. In these cases there is an advantage to the dosimetric method, which will allow administration of the largest non-toxic dose. If standard, non-dosimetric approaches are used, the administered dose should be in the range of 5.5-7.5 GBq and sometimes higher, provided that the blood counts and renal function are normal. If multiple treatments are required, they may follow at intervals of 6-12 months depending upon the clinical urgency (Fig. 3).

External beam radiotherapy of the neck has little place in the management of iodine-avid thyroid cancer. The dosage that can be delivered to tumor is generally lower than with RAI, except in those that are not iodine-avid. External beam therapy should be reserved for treatment of non-iodine-avid disease and for management of emergencies when RAI cannot be mobilized quickly enough.
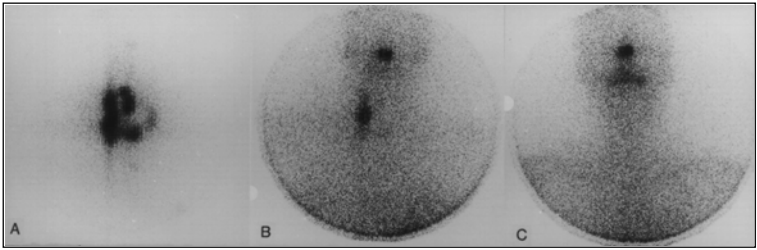
Figure 3. A 20 year old female who presented with locally invasive and surgically unresectable papillary carcinoma. Each image was obtained 48 hours after administration of 70-370 MBq of ^{131}I. In (a) the pretreatment image shows intense uptake into thyroid tissue; (b) partial response following first treatment with a persisting focus of disease in the right neck and (c) ablation of all iodine-avid tissue. She has now been disease-free for a decade.

Lung metastases are generally treatable with RAI, especially if they are larger than 1-2 mm in size. Microscopic metastases may not be treatable because the mean path length of the beta particle is then much larger than the tumor diameter (Fig. 4). Most of the radiation dose is then deposited in normal lung and may cause pulmonary fibrosis. Consideration has been given to the use of ^{125}I whose low-energy Auger electrons have a much shorter path length (less than 72 microns) and would deposit more energy within the small dimensions of the tumor but this approach is still investigational.

Bone metastases from papillary carcinoma are very resistant to treatment and they tend to progress even if they concentrate RAI. In such cases, treatment with RAI should be followed with external beam radiotherapy to the metastatic site. For a suspected solitary site, surgical excision might be attempted, but most cases are associated with other sites of blood-borne metastases. Bone metastases from follicular carcinoma may respond well to RAI alone as their uptake tends to be greater (Fig. 5).

The historical model for radiation safety concerning RAI treatment considered the patient as an iodine point source and modeled the radiation safety protocol accordingly. In fact, the patient is an attenuated, distributed source, which greatly reduces the gamma dose to others. Nor did the historical model take into account the concept of the effective dose equivalent (see Chapter 2). These three factors, taken together, reduce the risk posed by the patient by a factor of about 20 relative to the model. The historical modeling also did not take account of the ability of patients and families to follow instructions to further reduce exposures from the patient and the possibility of individualizing instructions to the patient. It was from this historical model that a fixed limit of 1.1 GBq (30 mCi) for out-patient therapy was determined.

The assumptions inherent in this model came to be questioned as a result of recommendations to reduce public exposures from 5 to 1 mSv/year. Mere intensification of past practices would have greatly increased the need for hospitalization for both malignant and benign therapies. The re-evaluation has served to justify modification of the approach to these treatments. In many countries,
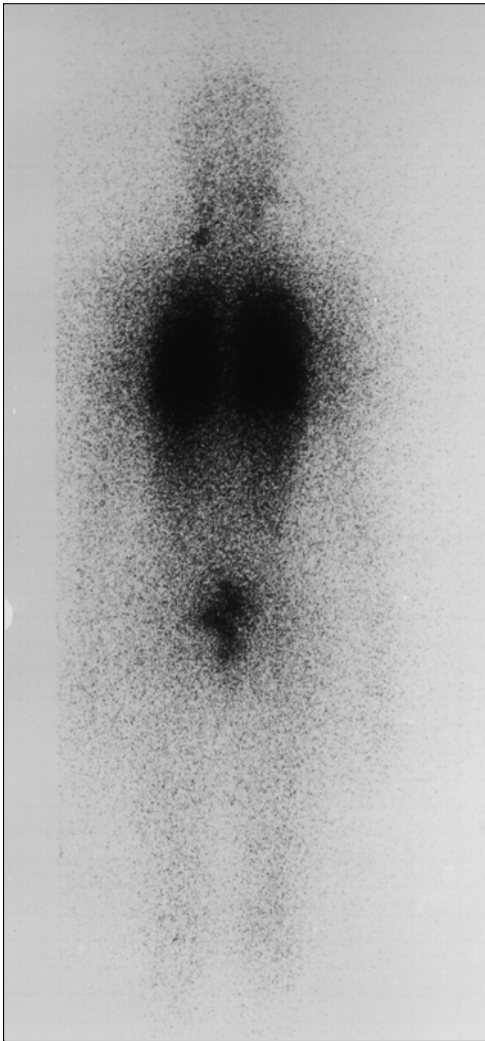
Figure 4. A 12 year old girl who presented with papillary carcinoma with lymph node and diffuse pulmonary metastases. Her presenting pO2 was 50. Several RAI treatments were given along with steroids to minimize pulmonary fibrosis. This ablated the lymph node but did not change the lung uptake. She died of cardiopulmonary failure 10 years later.

including the United States and Canada, there is no longer a rigid requirement to admit patients for large dose therapies.

Most thyroid cancer patients do not require supportive hospital care. If they are admitted, it is because they do not have the domestic facilities necessary for self-sequestration at home, that they have come for treatment from a distance or with public transportation, or that they are considered to be unlikely to follow instructions. If these patients were treated as out-patients, they would constitute a source of radiation exposure to members of the public or to juvenile or pregnant family members. Thus, some patients are still best treated in hospital. For others, out-
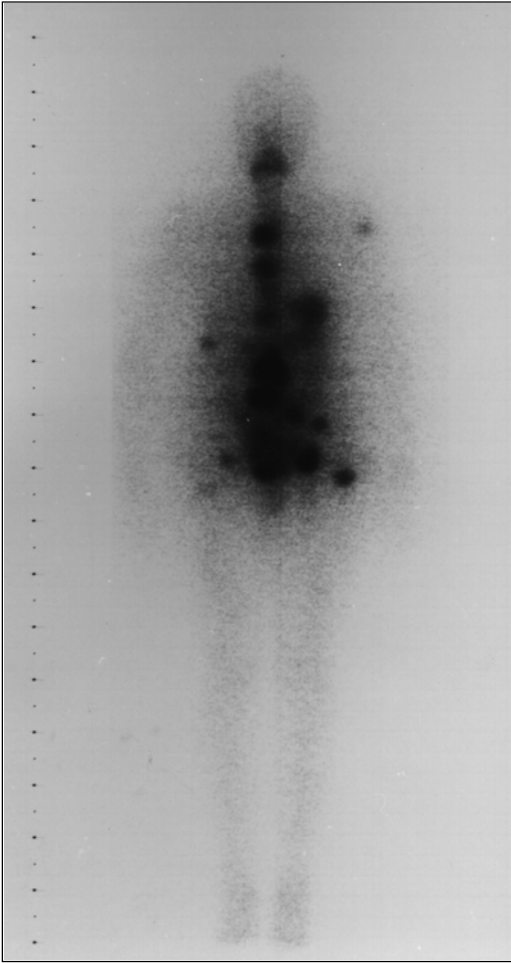
Figure 5. A 62 year old woman who presented with a pathological fracture secondary to metastatic follicular carcinoma. Her hemoglobin was 80g/L and platelets <100x10^9/L. With RAI therapy her disease regressed and bone marrow function normalized but the bone metastases were never ablated. She remained active for most of the next 14 years, requiring repeated RAI treatments and occasional external beam treatments when she developed non-iodine-avid metastases.

14

patient treatment is both safe and preferable in terms of availability of the emotional support from families. The requirement for safe home treatment is that family and other close associates of the patient do not receive more dosage than is permitted by the local nuclear safety regulations.

The instructions for at home behaviour will be similar to those given to patients treated for benign disease except that they will take account of the small to absent organified component. As a result, iodine is much more rapidly eliminated from the body. Patients who are totally athyrotic and have no tumor uptake may be nearly clear of radioactivity by 2-3 days. Those with remnants and a significant uptake will need to remain isolated for a longer time. The patient can be given a behavioural

Figure 6. A 26 year old woman with papillary carcinoma of thyroid. Her tumor does not secrete Tg. The first post-surgical scan showed bilateral positive nodes in her neck and the follow-up scan showed clearing after one RAI treatment. She then developed recurrent neck node disease. After a bilateral neck dissection she had a negative post-therapy RAI scan. However the FDG PET scan showed multiple nodes in the upper mediastinum, a finding confirmed by a subsequent CT scan. The image is a coronal section. The margins of the neck are defined by FDG uptake into the sternocleidomastoid muscles and the positive nodes are located centrally.
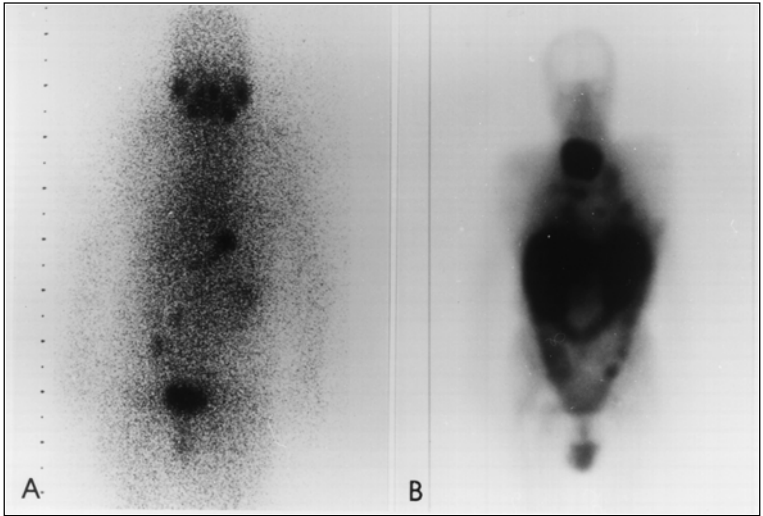
Figure 7. A woman in her 60s who has pulmonary and neck metastases from a papillary carcinoma that does not take up iodine as in (a). The tumor avidly concentrates ^{111}In-pentetreotide (b). Note the intense focus in the anterior neck and the multiple lung lesions. The neck mass corresponds to palpable disease.

prescription concerning contacts with family and other close associates based on measurements of dose retention from the diagnostic uptake.

Post-Therapy Imaging and Follow-Up

The sensitivity of radioiodine imaging increases asymptotically toward a maximum with increasing administered dose up to the therapeutic range. Thus, the best possible opportunity for accurate staging is by whole body scanning 5-7 days following administration of a therapy dose. Several scenarios will emerge:

- If the scan reveals only a small remnant within the thyroid bed and no metastases and the Tg is normal, then the prognosis is excellent. These patients may be reassured and scheduled for long term follow up.
- If the scan reveals only thyroid bed remnants and the Tg is slightly elevated, the latter may have originated from the stimulated normal tissue. These patients may be guardedly reassured but should be rescanned in 6-12 months to ensure that ablation was complete and that the Tg has normalized.
- If the scan reveals metastatic disease, the patient will need a further scan and possible retreatment in 6-12 months.
- If the scan reveals no metastases and the Tg is high, then iodine-negative metastases must be suspected. These patients need supplementary imaging, including ultrasound of the neck and CT of the neck and chest. Positron

14
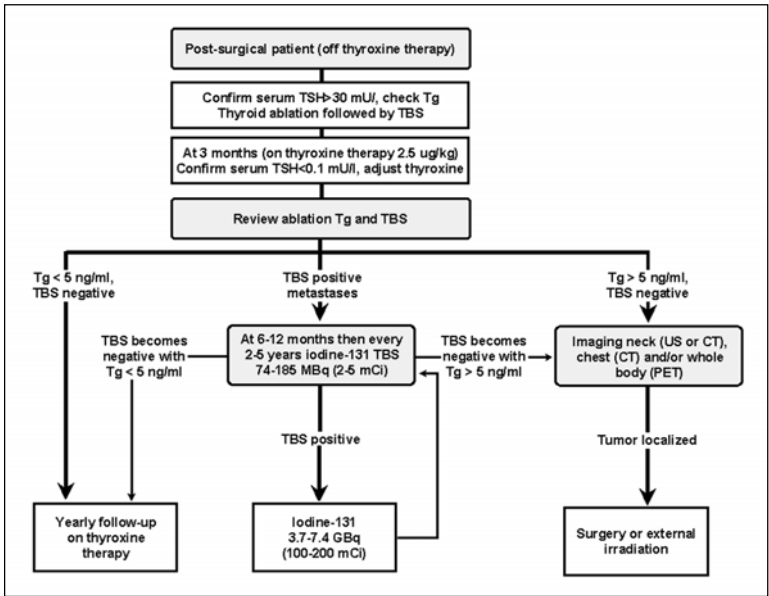
Figure 8. Recommended follow-up of patients after total thyroid ablation, on the basis of serum thyrotropin (TSH) and thyroglobulin (Tg) measurements and iodine-131 total-body scanning (TBS). The decision whether to perform iodine-131 scanning depends on the assay used to measure serum thyroglobulin; with a given assay, it depends on the tumor stage and the clinical likelihood of recurrent or persistent disease.

emission tomography (PET) with ^{18}F-FDG is becoming a useful examination for iodine-negative metastases (Fig. 6). ^{111}In-pentetreotide can also be useful to image disease that is not iodine-avid (Fig. 7).

Imaging with ^{99m}Tc-sestamibi is a useful screening tool that can be used while the patient is on thyroid hormone replacement. However, RAI imaging remains the reference standard and is necessary to predict response to RAI treatment.

All patients should be placed on TSH-suppressive doses of thyroxine within 24-48 hours of receiving RAI and returned to normal diet. Systematic follow-up is necessary to detect evidence of recurrence in the higher risk patients and to ensure that TSH suppression is maintained (Fig. 8). A T4 level above normal is acceptable so long as the free T3 level remains within normal limits.

Frequently Asked Questions (FAQs)

What is the role of RAI in Graves' disease with severe ophthalmopathy?

Patients with ophthalmopathy must be warned that the long-term response of the eyes to ^{131}I treatment is unpredictable. Some will improve, but not all. Many will

have an acute worsening in the 6-8 weeks following treatment and treatment with prednisone during this interval should be given. Ophthalmopathy may first occur years after the hyperthyroid state has been fully treated.

Can you predict if metastatic disease is likely or unlikely to be iodine-avid before treatment?

No. We do not designate the disease as non-iodine-avid unless the post-therapy scan is negative in the presence of other evidence of disease i.e., an elevated Tg or a positive biopsy.

How do you alter your approach for Hurthle cell, tall cell or insular cell carcinomas?

The initial ablation approach is identical. The Tg level with the patient off thyroid replacement is very important. Occasionally Hurthle cell tumors and other poorly-differentiated papillary cancer variants do take up ^{131}I. Tall cell and insular variants often take up ^{131}I quite avidly. If the post-therapy scan is negative and disease is suspected, then a PET FDG scan is obtained. Imaging with ^{111}In-octreotide can also be helpful in such cases.

What treatments are available for non-iodine avid metastases?

Surgery should be considered. If the lesion cannot be excised then external beam radiotherapy should be considered. If the lesion is thought to have a high risk of further recurrence then both modalities may be used. Lesions that bear somatostatin receptors, and that are not readily treated by more established means, may be treatable with ^{111}In or ^{90}Y-octreotide. Chemotherapy has not been very successful with differentiated thyroid cancers but occasionally anthracyclines may achieve a remission.

Additional Reading

1. Atay-Rosenthal S. Controversies on treatment of well-differentiated thyroid carcinoma and factors influencing prognosis. Nuc Med Ann 1999:303-334.
    A comprehensive review of long term outcomes of thyroid cancer treatment of a large population in Turkey.
2. Fatourechi V, Hay ID. Treating the patient with differentiated thyroid cancer with thyroglobulin-positive iodine-131 diagnostic scan-negative metastases: Including comments on the role of serum thyroglobulin monitoring in tumor surveillance. Sem Nucl Med 2000; 30:107-114.
    The title says it all.
3. Freitas JE. Therapeutic options in the management of toxic and non-toxic goiter. Sem Nucl Med 2000; 30:88-97.
    This article reviews therapeutic options in a more extensive fashion than space allowed in this Chapter.
4. Freitas JE. Therapy of differentiated thyroid cancer. Nucl Med Ann 1998:83-108.
    A comprehensive recent review of thyroid cancer from the perspective of the nuclear medicine specialist.
5. Garcia M, Bvaskin HJ, Feld S et al. AACE Clinical Practice Guidelines for Evaluation and Treatment of Hyperthyroidism and Hypothyroidism. 1996. http://www.aace.com/clin/guides/thyroid_guide.html.
    Another formally developed guideline.
6. Ladenson PW. Recombinant thyrotropin versus thyroid hormone withdrawl in

14

evaluating patients with thyroid carcinoma. Sem Nucl Med 2000; 30:98-106.
Although it deals only with the currently approved diagnostic uses of rh-TSH, this article will support the reader who wishes to know more about this exciting new drug.

7.   Shapiro B, Rufini V, Jarwan A et al. Artifacts, anatomic and physiological variants and unrelated diseases that might cause false positive whole-body I-131 scans in patients with thyroid cancer. Sem Nucl Med 2000; 30:115-132.
This is an excellent reference for the resident who must become familiar with pitfalls and traps in scan reading and thyroid cancer care.

8.   Singer P A, Cooper DS, Levy EG et al. Treatment guidelines for patients with hyperthyroidism and hypothyroidism. JAMA 1995;273:8098-8112.
One of several formally sanctioned clinical guidelines on treatment of thyroid dysfunction.

9.   Singer PA, Cooper DS, Daniels GH et al. Treatment guidelines for patients with thyroid nodules and well-differentiated thyroid cancer. Arch Int Med 1996; 156:2165-2172.
Formal clinical guidelines on the treatment of thyroid cancer.

10. Schlumberger MJ. Papillary and follicular thyroid carcinoma. N Engl J Med 1998; 338(5):297-306.
A compact review of the state of knowledge concerning thyroid cancer.

11. Utiger RD. Follow-up of patients with thyroid carcinoma. New Engl J Med 1997; 337:928-930.
A brief discussion of standards of care for follow-up of thyroid cancer.

12. Braverman LE, Utiger RD, eds. The Thyroid. Eighth ed. Philadelphia: Lippincott Williams & Wilkins, 2000.
A comprehensive, heavily referenced work concerning thyroid diseases.

14

Tumor Imaging

A.J.B. McEwan

Introduction

The role of nuclear medicine in the management of patients with cancer has changed significantly over the past 10 years. Improved anatomical visualization through the introduction of multi-slice CT and MRI sequences for chest and abdominal imaging has returned the role of radionuclide imaging to the functional assessment of primary and metastatic cancer.

The ability to target a biochemical, metabolic or pathologic process with a specific radiopharmaceutical provides nuclear medicine with a unique ability to contribute to patient management by the functional assessment of tumor status or the demonstration of functional abnormalities at sites too small to be identified as abnormal with anatomical imaging techniques.

An understanding of the choice of radiopharmaceuticals is key to the appropriate use of nuclear medicine in patient management, while the ability to define a metabolic target against which a radiopharmaceutical can be developed offers a unique perspective on tumor imaging. Techniques such as positron emission tomography, peptide receptor imaging and other methods of assessment of functional status such as hypoxia imaging also allow the use of nuclear medicine as predictive assays of treatment response, confirmation of tumor presence, definition of tumor type and whole body assessment of metastatic spread.

The goals of cancer imaging with nuclear medicine techniques are slowly being redefined (Table 1). Most of the indications listed as "under investigation" are still considered developmental and have not progressed beyond Phase I or Phase II trials. However, convincing data now exist for at least the first three indications in this group (predictive assay of treatment response, assessment of treatment efficacy, and assessment of multi-drug resistance) and for specific tumors these may be considered routine indications.

Mechanisms of Radiopharmaceutocal Uptake

The radiopharmaceuticals most commonly used in imaging in oncology are reviewed below and are summarized in Table 2. Most of these radiopharmaceuticals rely on pathophysiological or biochemical differences between neoplastic and normal cells to provide a target to background ratio which is suitable for imaging.

The development of cancer is characterized by the development in the cell of key characteristics such as the loss of local contact inhibition, the ability to divide without control, transmissibility of these changes, angioneogenesis and the ability to metastasize. The resulting abnormal mass will invade surrounding tissues and cells may be shed to migrate via lymphatic or vascular channels to form distant metastases.

Table 1. General indications for radionuclide tumor imaging

Established	Under Investigation
1. Staging or definition of residual disease	1. Predictive assay of treatment response
2. Confirmation of recurrence	2. Assessment of treatment efficacy
3. Assessment of disease burden at relapse	3. Assessment of multi-drug resistance
4. Monitoring treatment response	4. Assessment of nucleoside or protein synthesis
5. Differentiation of viable tumor from other causes of anatomically defined masses	5. Determination pre-therapy of tumor "aggressiveness"
6. Differentiation of benign from malignant lesions	6. Assessment of viable tumor burden
	7. Assessment of gene transfection

These changes derive from mutations or altered activation of specific classes of genes which control the cell cycle. The genes that control or contribute to malignant transformation are divided into proto-oncogenes and suppressor genes.

Proto-oncogenes are regulators in the process of growth and division of normal cells; mutation results in uncontrolled growth by interruption of normal growth regulation signaling pathways. Proto-oncogenes that have mutated are called oncogenes; mechanisms that lead to activation of this mutation pathway include local alterations in DNA structure, translocation, gene amplification, and DNA or RNA containing retroviruses. Genes that normally restrain growth are called tumor suppressors and unregulated cell growth arises if their function is lost.

Characteristics of neoplastic transformation include:

- Enhanced growth due to lack of normal growth control mechanisms (leading to increased protein synthesis);
- Increase in mitoses associated with increased growth rate which leads to accumulation of cells in S-phase and increased nucleoside synthesis;
- Increased tumor perfusion from angioneogenesis of chaotic and non-innervated neovasculature;
- Development of central hypoxia associated with abnormal neovasculature;
- Abnormalities in receptor density and receptor function;
- Altered glucose metabolism associated with overexpression of glucose transporters;
- Altered or aberrant antigen expression;
- Altered or abnormal membrane transport functions;
- Increased utilization of metabolic precursors for protein synthesis, norepinephrine or DNA.

Alterations of cellular metabolism associated with neoplastic transformation have led to the development of a number of radiopharmaceuticals which can non-specifically or specifically target a cancer associated abnormality.

15

Table 2. Imaging radiopharmaceuticals physical characteristics

Radiopharmaceutical Time Post Injection	Route of Administration Procedure	Half-Life	Imaging Dose (MBq)	Imaging Life	Length of Time Post Injection
^{18}F-FDG	IV	110 min	120-370	2-3 hrs	1-2 hrs
^{67}Ga-Gallium citrate	IV	3.3 days	370	2-6 d	2-3 hrs
^{123}I-mIBG	IV	13 hrs	200	4 - 48 hrs	2-4 hrs
^{111}In-Pentetreotide	IV	2.8 days	200	4 + 24 hrs	2-4 hrs
^{99m}Tc-Sestamibi/ Tetrofosmin	IV	6 hrs	740	0 + 2-3 hrs	1-2 hrs
^{99m}Tc-Sulfur colloid	SC	6 hrs	20-40	0-60 min	1-2 hrs
^{201}Tl-Thallium chloride	IV	3.1 days	80	0 + 1 hr	1-2 hrs

Radiopharmaceuticals Used in Cancer Management

^{18}F-Fluorodeoxyglucose (FDG)

Mechanism of Uptake

Positron emission tomography (PET) is a nuclear medicine imaging technique which uses radiopharmaceuticals labelled with positron emitting radionuclides to derive functional and biological information about tumor status. These radionuclides are characterized by a short half life (fluorine-18 = 110 minutes; carbon-11 = 20 minutes; nitrogen-13 = 10 minutes; oxygen-15 = 2 minutes). The only radiopharmaceutical currently used in routine practice is ^{18}F-FDG. This radiopharmaceutical is a glucose analogue which is transported into the cell by an active transport mechanism (to date seven transporter proteins have been described) and metabolized through the glycolytic pathway. ^{18}F-FDG is phosphorylated by hexokinase to ^{18}F-FDG-6-phosphate; however the structural differences between FDG and glucose mean that the next metabolic step, mediated by glucose-6-isomerase, does not occur and the FDG-6-phosphate remains trapped in the cell and available for delayed imaging.

There is now unequivocal evidence of increased FDG uptake in many human cancers. Preferential accumulation of FDG in cancer cells is probably related to a number of factors, including:

1. upregulation of glucose transporters;
2. increased metabolic activity in viable tumor cells;
3. increased angioneogenesis and inflammatory response;
4. increased glycolytic rate.

Normal Distribution

Following intravenous injection, activity is seen in the brain and the heart; cardiac activity can be decreased by fasting. Excretion is by the renal route; kidneys are faintly visualized and the bladder may be a confounding element in pelvic imaging. The liver is also faintly seen throughout the period of the study. Muscle activity, including talking around the time of injection, will result in accumulation within the corresponding muscle group. Figure 1 shows the normal biodistribution of FDG.

15

Figure 1. Anterior view of normal ^{18}F-FDG distribution. Note uptake in myocardium, bladder, kidneys and bone marrow. GI activity is seen in the right lower quadrant. (Courtesy of ADAC Labs and Dr. D. Froehling, Karlsruhe, Germany.)

Note the visualization of the brain, heart and bladder; the kidneys, bone marrow and GI tract are faintly seen. Patient preparation is key to successful FDG imaging. False positive uptake may be seen in sites of inflammation and granuloma.

Imaging Parameters

Patients should fast for 4-6 hours prior to FDG imaging. Lorazepam (Ativan®) or diazepam (Valium®) are commonly administered to reduce muscle activity. Following intravenous administration, patients should lie quietly for 1-2 hours prior to imaging. Imaging is performed on a PET scanner as a series of 6-8 tomographic images which are reconstructed to display a whole body image as well as transverse, coronal and sagittal slices. Lesion resolution down to 0.5 cm has been reported.

67Ga-Gallium citrate

Mechanism of Uptake

This radiopharmacuetical is a radiometal that binds in vivo to iron binding proteins such as transferrin, lactoferrin and ferritin. The mechanism of uptake into the cell is associated with the intravascular gallium-transferrin complex binding to transferrin receptors on the tumor cell surface; this binding is followed by endocytosis and binding to intracellular proteins such as lactoferrin. Transferrin receptor and lactoferrin concentrations may be increased in malignancy. Secondary mechanisms of uptake include increased diffusion from the intravascular into the interstitial space.

Normal Distribution

Following intravenous injection, normal uptake is seen in salivary and lacrimal glands, liver, spleen, skeleton, bladder and large bowel. Uptake will also be seen in the lactating breast and in sites of inflammation such as infection, granulomata and post surgical sites.

Imaging Parameters

Patients are usually imaged 48-72 hours after injection, by which time optimal visualization of neoplastic processes will be seen. SPECT imaging will enhance visualization of small lesions. Delayed imaging at 5 or 6 days may occasionally be needed to allow for gut clearance and improved visualization of the abdomen and pelvis.

123I or 131I-metaiodobenzylguanidine (mIBG)

Mechanism of Uptake

mIBG is a guanethidine derivative and functional analogue of norepinephrine. It enters the cell by the amine uptake 1, sodium dependent pump, following the same pathway as noradrenaline. Once within the cell, it accumulates in the intracellular storage granules found in cells of the sympathetic nervous system. The patient must be screened to ensure that no medications are present that could affect the uptake mechanism. This includes sympathomimetics (found in some over-the-counter decongestants and inhaled bronchodilators), tricyclic and "atypical" antidepressants, antipsychotics, antihypertensives (reserpine, calcium channel blockers, labetolol) and cocaine. Excretion is primarily by the renal route. Uptake has been reported in benign and malignant pheochromocytoma, carcinoid, neuroblastoma and medullary thyroid cancer.

Normal Distribution

Following intravenous injection, uptake of mIBG is seen in salivary glands, heart, lungs (early), liver and bladder. Late splanchnic activity is seen in about 20% of patients and with an 123I label, the normal adrenals may be visualized, particularly with SPECT imaging.

Imaging Parameters

Imaging may be performed with mIBG labeled with either 123I or 131I. 123I-mIBG is the imaging agent of choice with far superior imaging characteristics. Planar and SPECT images are routinely performed 24 and often 48 hours after

15

injection. The presence of a neuroendocrine tumor is confirmed by uptake of the radiopharmaceutical with a tumor to background ratio that increases over time.

^{111}In-Pentetreotide (Octreoscan®)

Mechanism of Uptake

Somatostatin is a 14 amino acid peptide which is widely distributed in the central and peripheral nervous systems and in cells of neuroectodermal origin. It functions as a neurotransmitter, neuromodulator or neurohormone, acting primarily as a down-regulator of function. Some of these functions in the gut, for example, include a reduction in mesenteric blood flow, reduction in gastric and gallbladder emptying and a decrease in intestinal absorption of nutrients. It also inhibits immunoglobulin synthesis and is reported to have antiproliferative effects. Five somatostatin receptors have been cloned (SSTR 1-5) which bind somatostatin with high affinity and selectivity.

Octreotide is a synthetic octapeptide which was introduced as a subcutaneous therapy to block the effects of hormone secretion in patients with carcinoid and reduce symptoms such as diarrhea and flushing. Pentetreotide (Octreoscan®) is a commercially available octreotide analogue which is labeled with indium-111. It has proven to be an effective agent for imaging the presence of somatostatin receptors. Octreotide binds to SSTR2 primarily and also to SSTR3 and 5. In addition to demonstrating the presence of receptors on tumors of neuroectodermal origin, binding of ^{111}In-pentetreotide has also been demonstrated in some prostate and colonic adenocarcinomata, in non-small cell lung cancer (NSCLC) and in some patients with breast cancer. Somatostatin receptors also appear to be common in many patients with lymphoma.

Normal Distribution

Normally, ^{111}In-pentetreotide accumulates in liver, spleen, kidneys and bladder. The gallbladder may be visualized at both imaging time points (4 and 24 hours) and should not be confused with hepatic metastases. At 24 hours, bowel activity is almost always seen. The normal pituitary is seen in 20-40% of patients.

Activated lymphocytes also show binding of octreotide and therefore false positive uptake may be seen in sites of granulomata, acute inflammation, recent surgical scars, radiation fields and arthropathies.

Imaging Parameters

Patients are usually imaged 4 and 24 hours after the injection of the radiopharmaceutical. SPECT imaging, performed optimally at 4-6 hours, is essential to the accurate interpretation of these images, particularly in the evaluation of residual disease and in the examination of the neck and mediastinum in patients with medullary thyroid cancer.

^{99m}Tc-Sestamibi and ^{99m}Tc-Tetrofosmin

Mechanism of Uptake

Like thallium, these two radiopharmaceuticals were introduced as myocardial perfusion agents. Both agents have relatively high lipophilicity with rapid transit

across the cell membrane. Binding within the cell occurs to mitochondrial proteins, a process that appears to be energy dependent. Transport out of the cell is mediated by P-glycoprotein.

Mutations of the *p53* suppressor gene and *p21-ras* oncogenes are associated with increased expression of the multi-drug resistance gene (*MDR-1*). Amplification of this gene increases expression of P-glycoprotein which leads to increased outflow of ^{99m}Tc-sestamibi, ^{99m}Tc-tetrofosmin and many chemotherapeutic agents. This finding has led to the postulate that absent uptake of either radiopharmaceutical by a tumor may predict failure of chemotherapy.

Normal Distribution

Following intravenous injection uptake is seen rapidly in salivary glands, thyroid, heart, liver, bowel, kidneys and bladder. Washout over 1-2 hours is seen in normal tissue. Delayed washout from tumor provides a tumor to background ratio that can be seen as focal uptake in the tumor at 2-3 hours post injection. Skeletal muscle is commonly seen and exercise increases this uptake.

Imaging Parameters

Because of gut excretion, ^{99m}Tc-sestamibi and ^{99m}Tc-tetrofosmin are most effective when imaging tumors in the brain and above the diaphragm, and have been reported as effective in imaging thyroid, lung and breast cancer. Following intravenous injection, planar images are obtained at 15 and 120-180 minutes. SPECT imaging will improve the diagnostic yield for small lesions.

^{99m}Tc-Sulfur colloid

Mechanism of Uptake

Although colloids are not accumulated by tumors, they are useful for sentinel node mapping which is an increasingly important part of the modern management of patients with melanoma and breast cancer. Lymphatic spread is a common route of dissemination of these tumors—if there is metastatic involvement of the regional nodes then the drainage basin also needs appropriate treatment. The assumption that lymphatic drainage is an orderly and sequential flow from the primary site has led to the concept of the sentinel node—the first nodal group that receives drainage from the tumor site. This drainage route is not predicted accurately from standard anatomical models and trunk lesions often have more than one drainage route. If this nodal group can be defined and biopsied then the presence or absence of metastatic spread can be confirmed and appropriate treatment instituted.

^{99m}Tc-sulfur colloid injected intradermally or peri-tumorally will be removed from the injection site by lymphatic channels and will be retained first in the sentinel lymph node. This can then be identified by imaging or by probe to guide the surgeon to the biopsy site.

Normal Distribution

Following peritumor intradermal injection, the lymphatic channels may be visualized and the draining nodes will typically be seen. In most cases this occurs rapidly after injection so imaging should commence as soon after injection as is feasible. Node visualization is slower following a subcutaneous injection. The 6 hour half life

15

of ^{99m}Tc allows identification of the sentinel node with a surgical probe. The technique is well described in the surgical literature.

Imaging Protocol

^{99m}Tc-sulfur colloid is injected in a small volume (0.25 ml) in 4 quadrants around the tumor. The patient is then placed under a gamma camera and sequential images obtained until the sentinel node is visualized.

Optionally, the site is then marked with indelible dye on the skin (some centres report the successful use of a radio-opaque needle for node localization). The patient can then be transferred to the surgical suite for probe guided open biopsy.

^{201}Tl-Thallium chloride

Mechanism of Uptake

Thallium is a physiological analogue of potassium; uptake into the cell is by the ATP-ase dependent Na$^+$/K$^+$ pump. Initially ^{201}Tl was introduced as a myocardial perfusion agent and it is believed that uptake by tumor cells is associated with the increased perfusion seen in angioneogenesis; there is also evidence of delayed washout. Thallium uptake requires the presence of a vascular supply and the presence of viable cells.

Normal Distribution

Following intravenous injection, uptake is seen rapidly in salivary glands, thyroid, heart, liver, bowel, skeletal muscle, kidneys and bladder. Washout over 1-2 hours is seen in normal tissue; delayed washout from tumor provides a tumor to background ratio that can be perceived on delayed images.

Imaging Parameters

Thallium is most effective when imaging tumors in the brain and above the diaphragm, such as thyroid cancer. Following intravenous injection, planar images are obtained at 15 and 60 minutes; SPECT imaging at 60 minutes may improve the diagnostic yield for small lesions.

Monoclonal Antibodies

Mechanism of Uptake

One of the differentiating features of cancer cells compared to normal cells is the overexpression of cell surface antigens or the expression of cancer associated antigens. Monoclonal antibodies (MAbs) may be produced against these antigens, radiolabelled with technetium-99m, indium-111 or iodine-123, and used to image patients with cancer. For example, ^{111}In-satumomab pendetide (OncoScint®) is a MAb directed against TAG72, a tumor associated glycoprotein. After intravenous injection the MAb binds to tissues overexpressing the antigen and clears from normal tissue to provide a high target to background ratio.

In addition to complete antibodies, MAb fragments such as ^{111}In-capromab pendetide (Prostascint®), directed against prostate specific antigen, and ^{99m}Tc-arcitumomab (CEAscan®), directed against carcinoembryonic antigen have entered clinical use. These fragments are characterized by rapid clearance from the background and more rapid penetration into tumor masses.

Normal Distribution

Following intravenous injection, the whole body image initially shows a blood pool distribution. Thereafter clearance is by the urinary and GI routes; bladder, liver, and GI tract will always be seen. In MAbs labelled with radiometals, kidney and splenic visualization is normal.

Imaging Parameters

For MAb fragments immediate and delayed images at 4-6 and 24 hours are usually obtained to compare blood pool activity with late tumor binding. Some authors recommend obtaining a blood pool image and using subtraction techniques to improve diagnostic yield. Intact MAbs clear much more slowly and are usually labeled with ^{111}In or ^{131}I with imaging up to 7 days.

Images are not easy to interpret and a learning curve is required to appreciate the significance of the subtle scintigraphic findings. MAb imaging has been used to define the functional nature of a mass and to evaluate residual disease.

Contributions of Nuclear Medicine to Cancer Imaging

The clinical indications for nuclear imaging with the radiopharmaceuticals discussed in the preceding section are summarized in Table 3 and are discussed in more detail below.

Brain tumors

MRI remains the primary diagnostic imaging modality for the diagnosis of patients with primary and metastatic brain tumors, both at presentation and at time of recurrence. However, the differentiation of scar tissue or radiation necrosis from viable tumor and perhaps the in vivo assessment of grade of malignancy may be most appropriately achieved using molecular imaging techniques. Thallium-201 may be used for SPECT imaging and ^{18}F-FDG for PET imaging. Radiopharmaceutical accumulation confirms the presence of viable tumor (Fig. 2). Sensitivity for both techniques is high, and although numbers of patients are small this is an important indication for nuclear medicine imaging. The presence of abnormal radiopharmaceutical uptake at a morphologically abnormal site may be confirmed by the use of fusion imaging whereby the functional and anatomical images are overlaid.

Some data show that survival in patients with high grade gliomas is inversely proportional to FDG uptake; this finding may lead to the development of the technique as a predictive assay of treatment response.

Abnormal ^{111}In-pentetreotide uptake has been reported in meningioma, pituitary adenoma and astrocytoma. Although sensitivity is moderate to high for these lesions, there is little indication for routine use. Some authors, however, do suggest a possible role for in vivo differential diagnosis in highly selected patients.

Breast cancer

Two techniques have been described that contribute to the staging of patients with breast cancer and to their re-evaluation at time of recurrence.

Axillary lymph node status is one of the most important criteria in assessing prognosis of patients at presentation. Patients with histological evidence of tumor in axillary nodes have a significantly lower overall survival and disease free interval;

15

Table 3. Imaging radiopharmaceuticals clinical indications

	Staging	Metastatic	Suspected Burden	Tumor vs Scar Recurrence/ Restaging	Monitor Response
Brain tumors					Thallium
		+	+		
FDG			+	+	?
Octreotide	±				
Breast cancer					
Sentinel Node	+		+		
MIBI	±	±	+	+	
FDG	+	++	++	+	+
GI Cancer					
FDG	±	+	++	++	±
MAb	+	±	±	+	
Lung					
FDG	++	++	+	++	+
Lymphoma					
Gallium	±	+	+	+	+
FDG	±	++	++	++	+
Melanoma					
Sentinel Node	++		+		
FDG	+	++	++	+	±
Gallium	±	++	+	±	
Octreotide	++	?			
Neuroendocrine tumors					
mIBG	**++**	**++**	**++**	**++**	**+**
Octreotide	++	++	+	±	

++=very useful, += useful, ±=sometimes useful

those with more than 3 nodes involved do less well than those with 1-3 nodes involved. The current standard management of patients with breast cancer includes axillary dissection—to acquire prognostic information, to effectively treat the axilla if disease is present, to possibly improve long term survival and to treat locally advanced disease. However, axillary dissection is associated with significant morbidity in up to 30% of patients. Symptoms include pain, lymphedema and loss of range of movement. Internal mammary node involvement is less common and more difficult to diagnose than axillary involvement but may be more frequent when the primary tumor lies in the inner quadrants. The prognostic implications of internal mammary node involvement are comparable to those of axillary involvement. Most radionuclide imaging techniques have been developed with the hope that they can contribute to improved staging and assessment of internal mammary and axillary node status.

Lymphoscintigraphy and Sentinel Node Imaging

The goal of sentinel node imaging is to identify the node(s) closest to the primary tumor site. After peritumor injection of ^{99m}Tc- sulfur colloid, imaging of the anterior
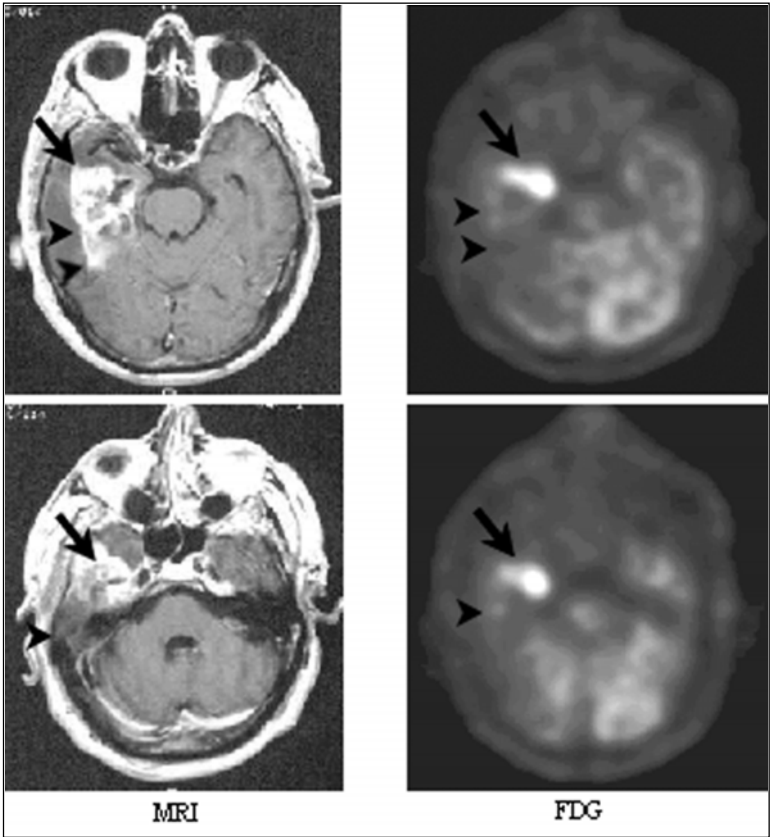
Figure 2. MRI and ^{18}F-FDG transaxial images in a patient with recurrent glioblastoma multiforme. The MRI shows an extensive area of abnormal signal in the right temporal lobe (arrow) in a patient with a suspected recurrent glioblastoma. The ^{18}F-FDG image shows recurrent tumor only anteriorly (arrow). The lower part of the abnormality seen on the MRI scan is therefore scar (arrowheads). (Courtesy of ADAC Labs and Dr. Carreras, Clinical PET Institute, Madrid, Spain.)

15

chest and axilla will usually show focal uptake in the sentinel nodes of the axilla and internal mammary chain within 30 minutes (Fig. 3). The site of the sentinel node can then be marked on the skin and subsequently identified at dissection using a gamma probe. In this way a limited number of axillary lymph nodes are removed, sparing the patient a complete axillary lymph node dissection.

In one series, lymphatic nodal mapping had an accuracy rate of about 40% for the radioactive technique; 2 false negatives were identified at surgery and at axillary lymph node dissection, 4 patients had false positive images associated with histologically negative nodes. However, in other series the success rate in identifying
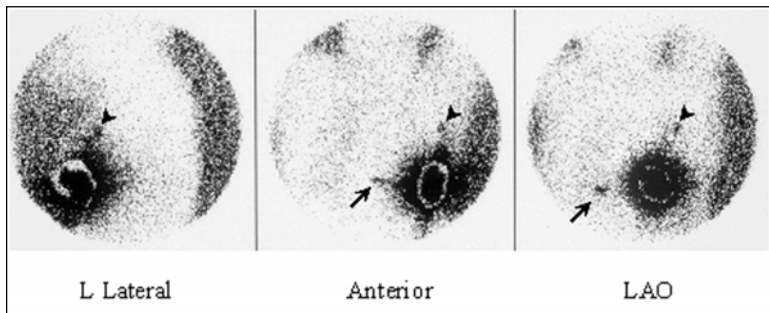
Figure 3. Sentinel node imaging in a patient with breast cancer. The peritumoral injection site of ^{99m}Tc-sulfur colloid is seen as an area of intense activity. Sentinel nodes are seen in the internal mammary chain (arrow) and axilla (arrowhead). (Courtesy of Dr. R. Kloiber, Foothills Hospital, Calgary, Canada.)

sentinel nodes has been as high as 90% (up to 100% in one series of 34 patients). Experience appears to be important to successful imaging.

The technique is now becoming standard of care in many breast centers allowing a decrease in the axillary node dissection rate; the effectiveness of this technique in improving survival or disease free interval is not established.

FDG Imaging

Although the role of FDG imaging in breast cancer is still being defined, indications will probably include detection of recurrence and monitoring treatment response. It may also have a role in the initial staging. Although sensitivities as high as 80-100% have been reported in the visualization of primary breast cancer, the effectiveness of morphological techniques, scintimammography and fine needle aspiration mean that PET is less likely to have a major role in this setting.

Staging

For staging, PET imaging offers the ability to detect involvement of both the axillary and internal mammary chains. While axillary node dissection—perhaps in conjunction with sentinel node imaging—remains the standard for staging the axilla, there are no effective tests for evaluating the internal mammary chains. Sensitivities of 85-100% have been reported in most large series for detecting nodal metastases (Fig. 4); specificity is somewhat lower, typically 65-90%. Although some authors have suggested that a negative PET scan of the axilla can be used to exclude axillary lymph node dissection, microscopic disease and lesions less than 7-10 mm will be missed. Distant metastases in the small percentage of patients who present with Stage IV disease will be accurately demonstrated.

Recurrence

Several studies have shown PET to be more accurate than CT or MRI in detecting local recurrence, locoregional lymph node metastases and distant metastases; a high sensitivity in detecting osteolytic metastases has also been claimed. In a patient with
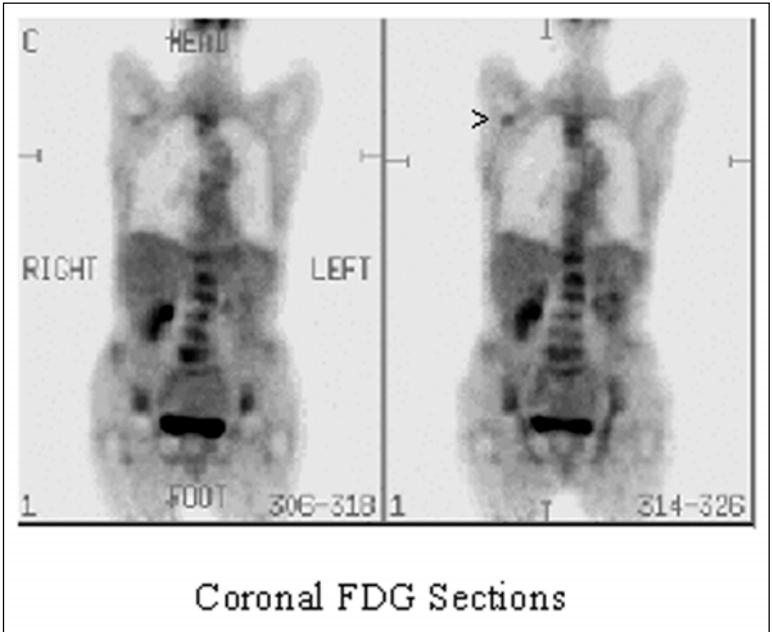
Figure 4. Coronal sections from an ^{18}F-FDG scan in a patient with metastatic breast cancer. Abnormal accumulation of ^{18}F-FDG in a lymph node metastasis in the right axilla is indicated by the arrowhead. (Myocardial activity is seen in the mediastinum.) (Courtesy of ADAC Labs and Dr. J.-F. Gaillard, HIA Val de Grace, Paris, France.)

suspected recurrence it is probable that PET imaging will become the primary investigation in assessing degree of spread.

Monitoring Response

It is well known that a significant number of patients will fail first line chemotherapy. Data are now available from several centres suggesting that if FDG uptake by the tumor fails to decrease significantly after the first 2 cycles of chemotherapy, the patient is likely to be a non-responder. Absent FDG uptake after 2 cycles appears to predict a good response. If this is confirmed in additional clinical trials, then monitoring of response will probably become a routine measurement in PET imaging.

Scintimammography

Recent years have seen a significant increase in disease free survival in patients with breast cancer, in part due to earlier diagnosis. A key tool in early diagnosis is the widespread use of screening mammography. Up to 8% of screening mammograms show abnormalities considered to be suspicious for malignancy. Patients are then usually referred for additional investigations, including diagnostic mammography,

Anterior   Left lateral
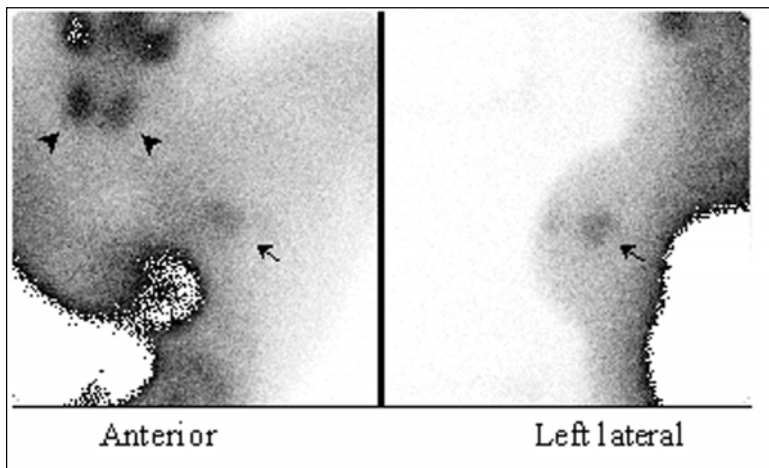
Figure 5. Scintimammogram with ^{99m}Tc-sestamibi in a patient with a primary breast cancer in the left breast (arrow) measuring 2 cm. Note normal thyroid activity (arrowheads) on the anterior view; the heart and liver activity is saturated out. A small amount of activity is seen in the nipple

ultrasound and MRI. Even if these additional studies show probable cancer, biopsy confirms the diagnosis in only about 30% of patients. Therefore, while mammography has a high negative predictive value, it has low specificity, even in conjunction with additional conventional imaging. The specificity of mammography, ultrasound and MRI is particularly poor in patients with dense breasts, previous breast conserving surgery and implants.

It has been postulated that scintimammography with ^{99m}Tc-sestamibi has a role in the management of this latter population of patients (Fig. 5). In several large series, high sensitivity (80-92%) and high specificity (80-100%) have been demonstrated; negative predictive values of up to 96% have been reported. However, these data are for lesions >1 cm in diameter and diagnostic accuracy is lower for smaller lesions.

Scintimammography is not a screening tool, but as a supplementary examination to mammography and ultrasound it may have a role in evaluating specific populations of patients as defined above and in evaluating inconclusive morphological images. The technique is likely to become routine for the evaluation of the dense breast and the assessment of recurrence in patients who have had previous surgery. The advantages of functional imaging become clear in these settings.

Gastrointestinal Tract

CT and ultrasound are the primary investigations for staging and assessing recurrence of these tumors. Nuclear medicine techniques may contribute to management of some cases of esophageal and colorectal cancers.

FDG Coronal Images
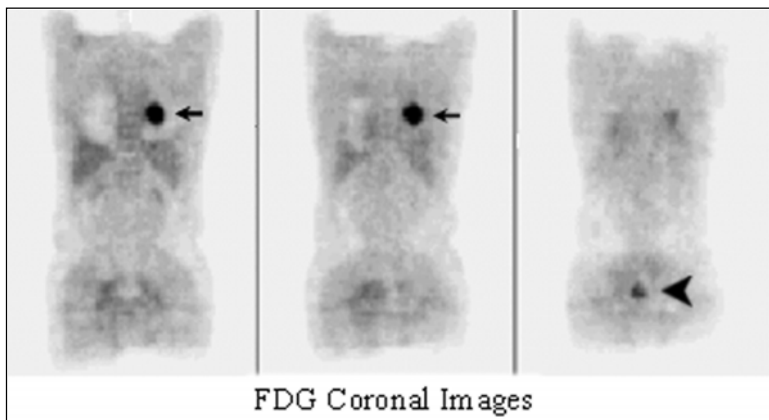
Figure 6. Coronal PET images of a patient with a large metastatic colorectal lesion in the left lung (arrow) and a local recurrence in the pelvis (arrowhead). (Courtesy of ADAC Labs and Dr. J.-F. Gaillard, HIA Val de Grace, Paris, France.)

Esophageal Cancer

The incidence of esophageal cancer in the United States is 3.5/100,000, although it is considerably higher in parts of China and is more common in France, Singapore, Iceland and Switzerland. Initial presenting symptoms include dysphagia and weight loss. Two year survival is only 20%.

Early data have suggested that FDG imaging may be an important tool in staging this population of patients. FDG images were more accurate than CT in demonstrating spread to mediastinal lymph nodes and were considered to have altered staging and management in approximately one-third of the patients. As surgical and radiotherapeutic morbidity are high, accurate staging of these patients will not only improve management but should also contribute to improved quality of life.

Colorectal Cancer

Colorectal cancer affects approximately 1 in 20 people in the United States and in most developed countries. If diagnosed early, it is curable by surgery. Spread is initially through the muscularis mucosa and into the submucosa. With penetration of the bowel wall, it spreads by local invasion; nodal metastases occur in approximately 20% of patients in whom the cancer is localized to the bowel wall. Nodal spread is usually through the lymphatic network along the major vessels. The liver is the commonest site of distant metastasis. Treatment of advanced disease is by chemotherapy with surgery only if required for control of symptoms.

FDG has no role in the initial staging of this population. However, in patients with locally advanced disease, FDG has been shown to be an effective management tool for identifying distant metastases (Fig. 6). The most important role of FDG imaging is in discriminating between residual tumor and scar in patients with prior therapy and in identifying the presence of local recurrence (Fig. 7). For both indications FDG has demonstrated sensitivities of the order of 90-95% compared

15
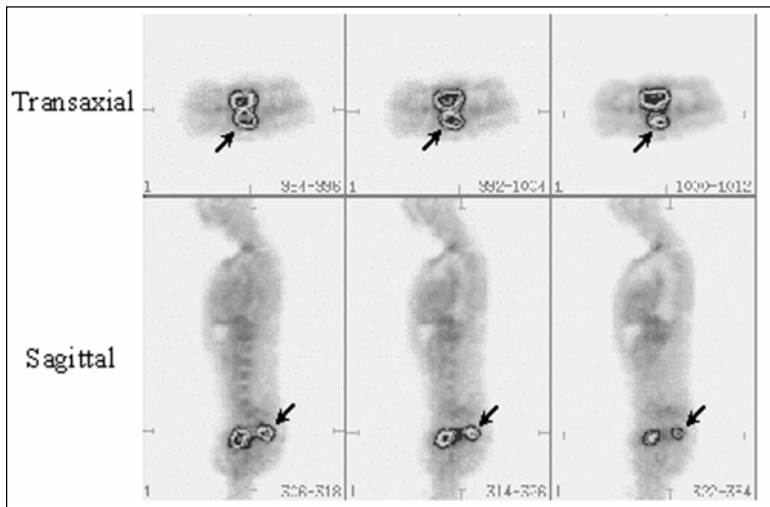
Figure 7. Transaxial and saggital sections of an ¹⁸F-FDG image showing normal bladder activity anteriorly and recurrent rectal carcinoma posteriorly (arrow). (Courtesy of ADAC Labs and Dr. J.F. Gaillard, HIA Val de Grace, Paris, France.)

with CT sensitivity of 65-75%; FDG specificity is also high. FDG imaging alters the management of colorectal cancer in about 30% of patients. Some data suggest that FDG imaging might monitor response to therapy. A fall in FDG uptake after 1 cycle of chemotherapy appears to predict a good response whilst no change or an increase in uptake suggests treatment failure and progression.

MAbs have also been reported as being effective in evaluating patients with colorectal cancer. Mabs such as arcitumomab (CEAscan®) and satumomab pendetide (OncoScint®) may either be used in conjunction with an intraoperative gamma probe or by conventional imaging techniques. Arcitumomab (CEAscan®) has been demonstrated to increase the clinical accuracy of CT when used in conjunction with CT: it improved the correct prediction of resectability by 40% and the correct prediction of unresectability by 100% when compared with CT alone. Using the same MAb, radioimmunoguided surgery has been shown to increase the number of tumor sites in a locoregional distribution; although long term follow-up has not been reported, the study argues for the inclusion of radioimmunoguided surgery in the management of patients with locoregional extension.

MAb imaging is technically more difficult than many nuclear medicine procedures and there is a steep learning curve to image interpretation; routine imaging with MAbs should only be performed in departments with experience in the technique and training courses are available for the use of radioimmunoguided surgery. If available, ¹⁸F-FDG imaging is probably a more sensitive and routinely interpretable investigation.

15

Coronal FDG Images
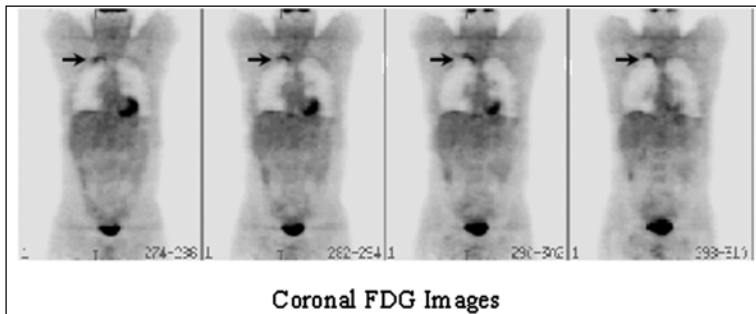
Figure 8. ^{18}F-FDG scan in a patient with a primary lung cancer involving the right apex (arrow). The mediastinum is normal and the patient is a surgical candidate. (Courtesy of ADAC Labs and Dr. J.-F. Gaillard, HIA Val de Grace, Paris, France.)

Lung cancer

Lung cancer is now the most common single cause of cancer related death in both sexes, having recently overtaken breast cancer in women. In the United States there are in excess of 160,000 new cases annually and survival at 5 years is approximately 15%.

The most important contributions of nuclear medicine to the management of patients with lung cancer are in the evaluation of solitary pulmonary nodules and in staging of confirmed disease using PET imaging with ^{18}F-FDG; both indications can often be performed with a single examination.

Most series have shown the sensitivity of PET to be of the order of 95% in diagnosing cancer in a solitary pulmonary nodule; quantitative assessment with the standardized uptake value (SUV) > 2.5 has a specificity greater than 90%. (The SUV is an index of lesion uptake and is calculated as decay-corrected lesion activity divided by the injected activity/body weight).

Once the presence of non-small cell lung cancer (NSCLC) has been confirmed, an evaluation of the mediastinum for locoregional metastatic involvement is required to plan therapy. CT has a sensitivity of 60-70% and specificity of 65-75% in defining mediastinal involvement, and mediastinoscopy an accuracy of 89%. Metastatic involvement has been shown to be present in 13% of nodes <1 cm on CT and in only 36% in nodes >2 cm, so current staging techniques have significant limitations.

FDG imaging can improve patient management. Sensitivity and specificity in detecting mediastinal disease has been reported as 90-95% and up to 95%, respectively. The commonest cause of false positive uptake is granulomatous disease. Prospective comparisons of conventional staging (CT, ultrasonography, bone scanning, and, when indicated, needle biopsies) with FDG PET have shown that PET improves the rate of detection of local and distant metastases in patients with NSCLC. In jurisdictions where PET is readily available, it has become the investigation of choice (Fig. 8). In addition to evaluating mediastinal involvement the ability of PET to provide whole body images will define that group of patients who present with Stage IV disease (Fig. 9).

Using these criteria for staging patients with NSCLC, several groups have shown changes in management based on the PET images; one recent study has shown
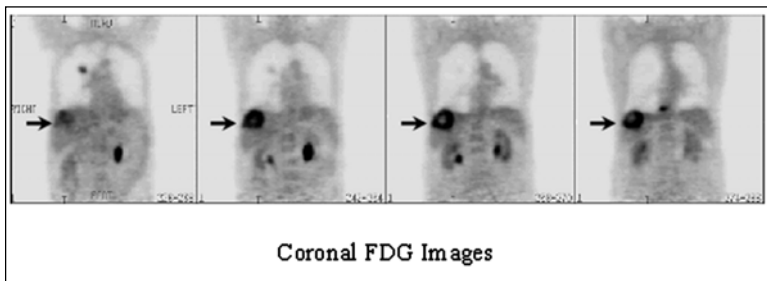
Coronal FDG Images

Figure 9. Coronal ^{18}F-FDG images in a patient with squamous carcinoma of the lung metastatic to the liver. The large hepatic metastasis (arrow) has a photopenic center suggesting a central area of necrosis. (Courtesy of ADAC Labs and Dr. A. Alavi, University of Pennsylvania, Philadelphia, USA.)

management changes in 67% of patients based on the PET scan. In addition there are good data suggesting that the appropriate use of PET imaging in patients with NSCLC can produce significant savings to the healthcare system by avoiding unnecessary—and unhelpful—interventions.

FDG imaging should be the standard of care in the management of patients with NSCLC at presentation and probably for assessment of possible relapse.

Lymphoma

Lymphomas make up 8% of all malignancies. Hodgkin's disease (HD) is characterized by the presence of Reed-Sternberg cells. Four histologic subtypes have been described: nodular sclerosing (40-60%), lymphocyte predominant (2-10%), mixed cellularity (20-40%) and lymphocyte depleted (2-15%). Spread is characteristically sequential from nodal group to nodal group and intrathoracic disease is common. Non-Hodgkin's lymphoma (NHL) is a more heterogeneous group of tumors, defined as high, intermediate or low grade by the Modified Working Classification. High grade tumors are aggressive with a short median survival if untreated. Low grade tumors are more indolent with a longer median survival.

Staging for both HD and NHL uses the Ann Arbor system. The presence of systemic symptoms (fever, night sweats, weight loss > 10% body weight) or pruritus are considered poor prognostic indicators. Treatment, according to stage and classification, is by chemotherapy and/or radiation therapy. Peripheral stem cell or autologous bone marrow transplantation have proven effective salvage therapy options and antibody therapies are now completing Phase III trials. To date one agent, ^{99}Y-ibritumomab tiuxetan (Zevalin®) has received FDA approval for treatment of low-grade CD20+ β-cell NHL.

Lymphoma is, therefore, a treatable cancer for which accurate staging, demonstration of therapeutic effectiveness and early detection of recurrence are key elements of successful management strategies. Imaging with gallium has conventionally been the nuclear medicine investigation used in the management of this patient population; however, the Centers for Medicaid Services (CMS, formerly
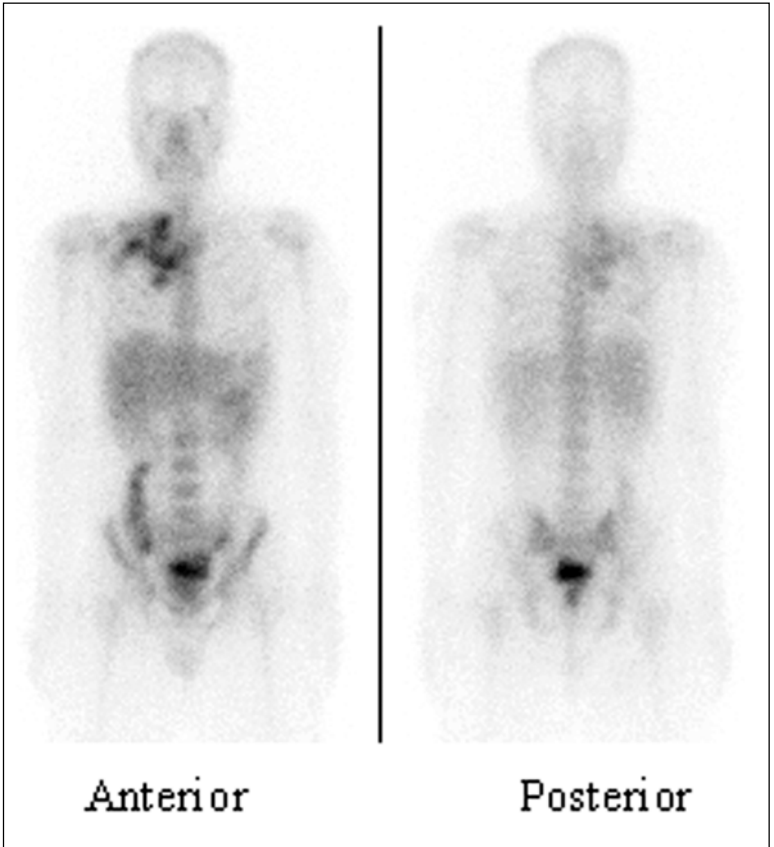
Figure 10. Anterior and posterior views of a gallium scan in a patient with extensive lymphoma in the right supraclavicular fossa extending into the mediastinum. Note normal distribution in liver, bone marrow, large bowel and bladder.

HCFA) in the United States has recently approved the use of FDG in settings where gallium would previously have been used. ^{111}In-pentetreotide has also been shown to have uptake in a percentage of lymphomas, but the role of the radiopharmaceutical in this patient population has not yet been defined.

Staging

Currently, the two most important investigations in the management of lymphoma are CT scanning above and below the diaphragm and biopsy for tumor characterization. Gallium imaging has a limited role—in the identification of lymph nodes or other abnormalities felt to be equivocal on CT and, less usefully, as a whole body screening tool in the assessment of patients with Stages III and IV disease.
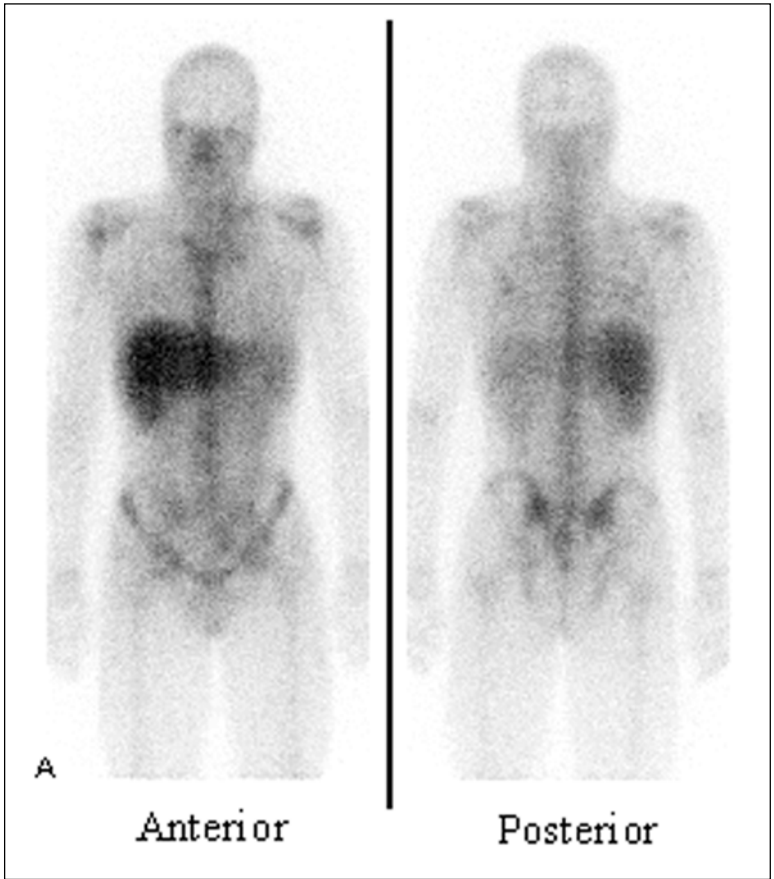
Figure 11A. Anterior and posterior gallium scans in a patient with non-Hodgkin's lymphoma (NHL) in the left supraclavicular fossa. Although asymmetry is seen between the 2 supraclavicular fossae, the disease extent is not well perceived.

15

While planar imaging may be diagnostic (Fig. 10), in other cases SPECT is a necessary tool in determining the presence and extent of disease (Fig. 11).

If the radiopharmaceutical is to be used to monitor treatment response or detect relapse, it is also important to have a pre-treatment gallium scan to confirm that the tumor is gallium-avid. About 95% of patients with HD and between 70-80% of patients with NHL have positive uptake. Gallium imaging can be used to exclude distant metastases (Fig. 12). Recent chemotherapy and in particular G-CSF can cause significant alterations in gallium biodistribution (Fig. 13).

^{18}F-FDG has higher sensitivity and specificity than gallium imaging and if PET is available should be the investigation of choice (Fig. 14). PET is more sensitive

B

Coronal SPECT images
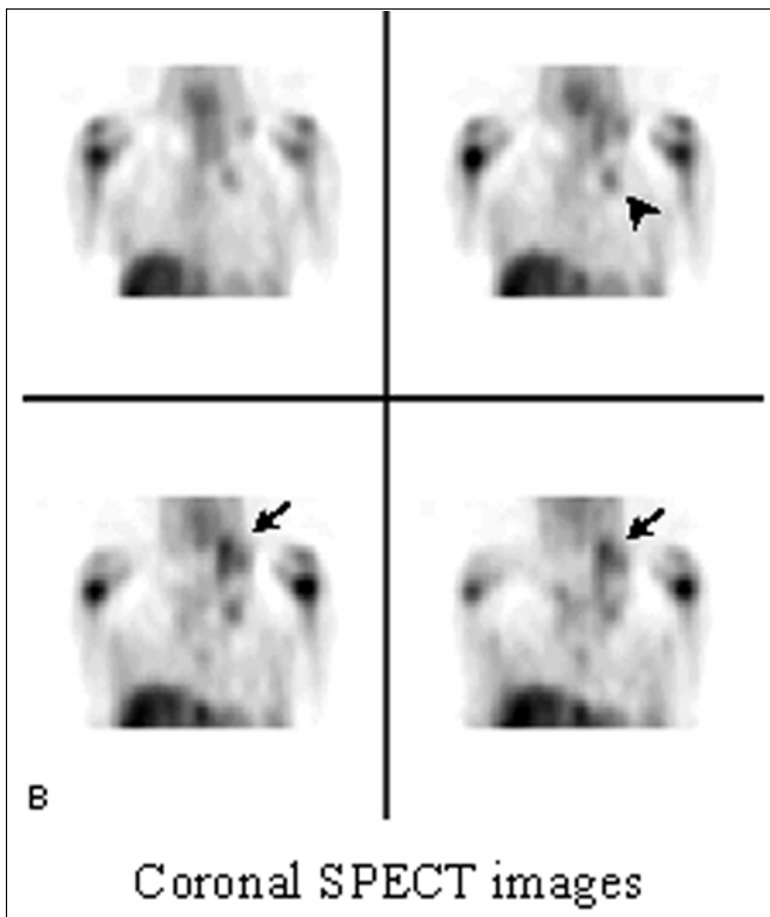
Figure 11B. Coronal SPECT slices. Note how the disease extent can be readily seen (arrow), in contrast to the planar images. Extension into the mediastinum is now obvious (arrowhead).

than CT scanning in evaluating tumor burden at presentation, although anatomical localization remains important for treatment planning. The data supporting the routine use of FDG at presentation are more persuasive than they are for gallium and most centres which have PET available as a routine tool will use FDG imaging as part of their staging protocol.

Monitoring Response to Therapy

Anatomic imaging will often demonstrate residual tumor masses after therapy—often for years after completion of therapy. The exclusion of viable disease at these
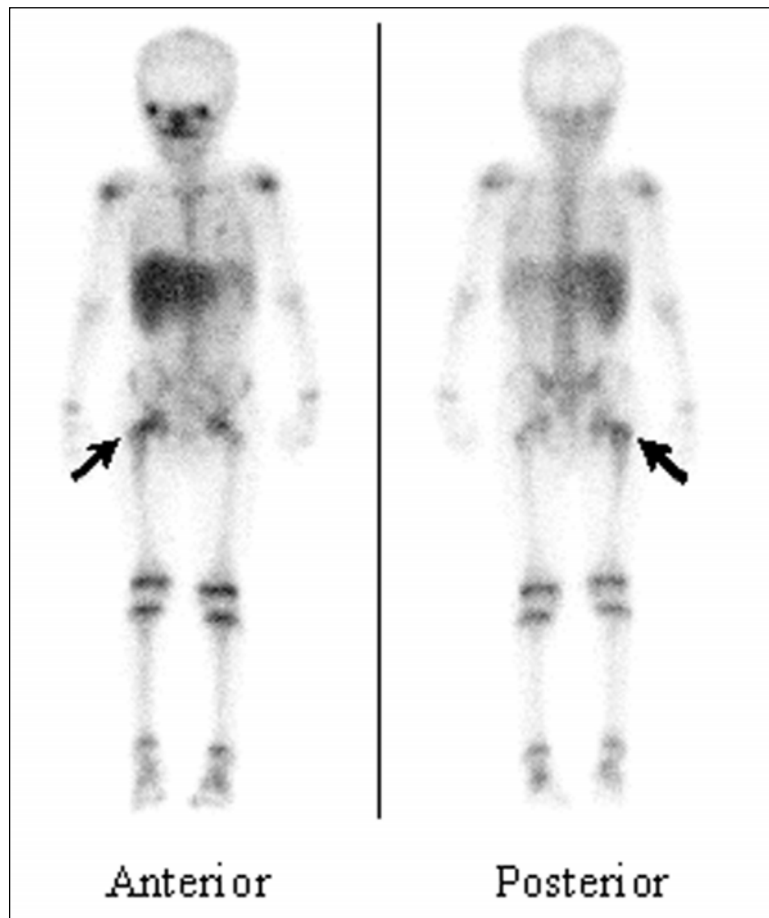
Figure 12. Anterior and posterior gallium scans in a 10 year old boy with Burkitt's lymphoma affecting the right proximal femur (arrows). No additional lesions are seen.

15

sites is fundamental to the definition of response—most series suggest that 50-60% of those patients do not have viable disease. Both gallium and FDG have high sensitivity and specificity in defining the presence of active tumor and are the investigations of choice.

Repeating the gallium imaging after 2 cycles of chemotherapy may predict treatment failure if gallium uptake persists. Positive gallium uptake at the end of treatment also appears to predict reduced survival and reduced disease free interval. The same parameters for predicting treatment failure can probably be applied to PET. In children a confounding feature is uptake within a hyperplastic thymus; this
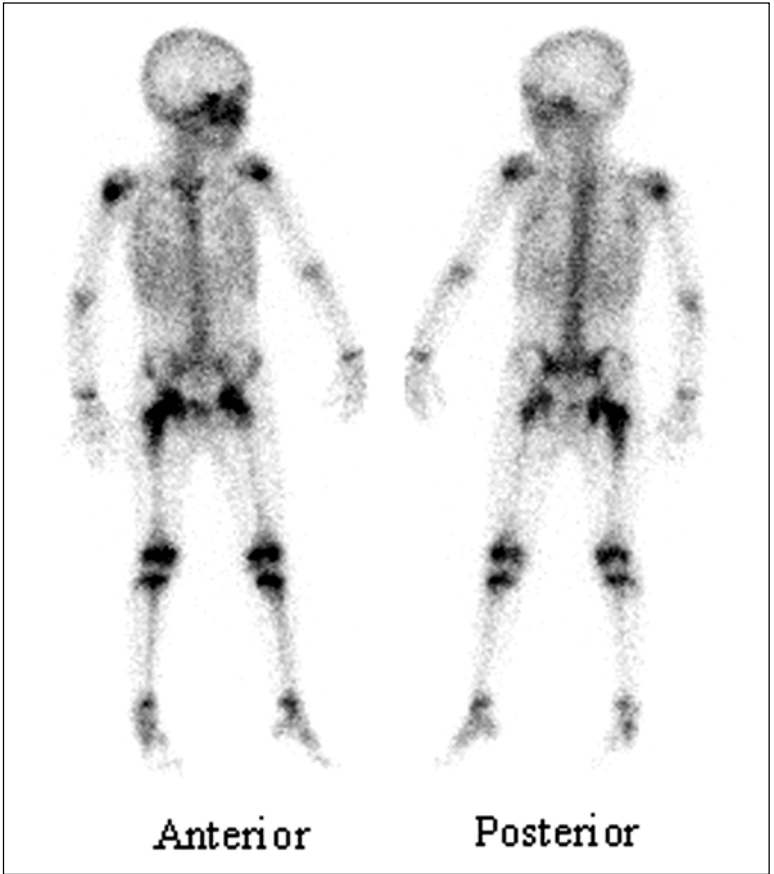
Figure 13. Gallium scan after G-CSF. There is altered biodistribution of the radiopharmaceutical. Almost all activity is seen in the skeleton, with non-visualization of the liver. (Same patient as Figure 12.)

15

may be differentiated by tomographic imaging where a characteristic "H" pattern of uptake is seen on coronal sections.

Evaluating Relapse and Restaging

With more aggressive—and successful—salvage protocols, early detection of recurrence has become important in the management of these patients. Gallium and FDG have very high clinical accuracy in confirming the presence of active tumor and defining the extent of disease burden. Both radiopharmaceuticals are useful in evaluating a residual mass on CT, functionally defining a CT abnormality, and whole
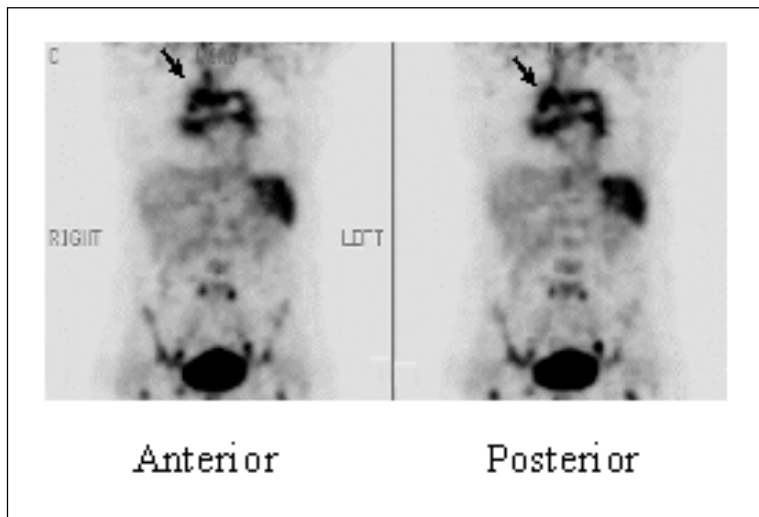
Figure 14. Anterior ^{18}F-FDG scan of a patient with extensive mediastinal lymphoma (arrows). Metastases to pelvic lymph nodes are also present (arrowheads). (Courtesy of ADAC Labs and Dr. A. Alavi, University of Pennsylvania, Philadelphia, USA).

body screening in high risk patients or those with palpable nodes. Standard of care in this patient population should include imaging with either gallium or FDG.

As PET imaging becomes routinely available, FDG will almost certainly replace gallium as the investigation of choice. If the preliminary data supporting its role as a predictive assay of response are confirmed, it will be routinely performed prior to treatment, after 1 or 2 cycles of therapy, and during follow-up.

Melanoma

Melanoma is increasing in incidence in most of the developed world, and in countries such as Australia the incidence is doubling every ten years. At presentation the most important prognostic indicator is tumor thickness as described by the Breslow classification.

Five year survival in patients with Stage IIB (tumor thickness ≥ 4.00mm) or worse is poor—chances of curative therapy depend entirely on the accuracy of staging and the completeness of radical dissection. Locoregional recurrence is high and restaging at recurrence carries the same requirements as at presentation. Interferon alpha-2a (IFN alpha-2a) is efficacious as adjuvant therapy in stage IIB and III melanoma, but is toxic and expensive. Accurate staging is therefore required before embarking on a course of therapy.

Lymphoscintigraphy

Lymphoscintigraphy with sentinel node mapping has revolutionized the staging of patients with melanoma, providing the surgeon with an accurate localization of sentinel nodes. Orderly and sequential drainage to the sentinel node and then to the
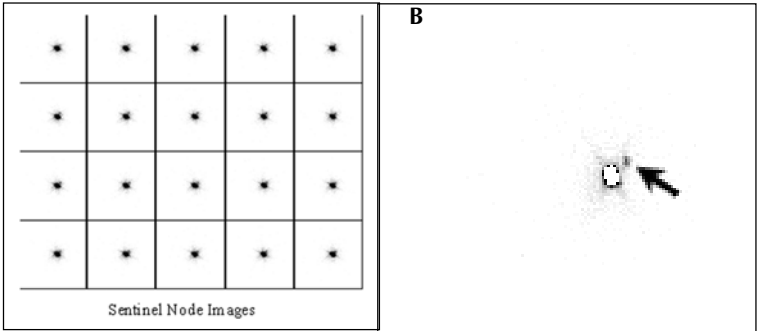
FIgure 15. A) Sentinel node imaging showing 1 mintue sequential frames after intradermal injection of ^{99m}Tc-sulfur colloid. The sentinel node is seen as a small focus of activity at about 2 o'clock superior to the injection site. B) Summed view of the sequential images. The injections site has been shielded and there is improved visualization of the sentinel node (arrow).

regional nodal basin is typical of melanoma, with less than 1% of patients presenting with "skip" lesions. The histological evaluation of the sentinel node, therefore, is an important prognostic indicator and one which directs appropriate wide field dissection. Five year survival in patients with tumor negative sentinel lymph nodes is 90% following selective dissection and 93% following complete lymph node dissection. Surgical intervention therefore can, with confidence, be limited in patients with negative sentinel lymph nodes.

Imaging after peritumoral intradermal injection usually shows the lymphatic channels within 20 minutes of administration and the sentinel node(s) should be seen by 30 minutes (Fig. 15). Whilst one nodal basin is usually seen for lesions on the limbs, up to three geographically disparate nodal basins may be demonstrated after injection around a melanoma site on the trunk or head and neck region and up to 40% of patients will show unexpected drainage patterns. A skin marker is placed over the node(s) and the patient moved to the operating room for sentinel node excision. A hand held gamma probe is an important adjunct to the localization of the marked node at surgery.

In this population of patients, sentinel node imaging has been shown to be effective in identifying the sentinel nodes in 90-95% of patients in most series and should now be regarded as standard of care in the management of this rapidly expanding patient group.

FDG Imaging

Most authors believe that PET imaging with FDG is the most effective way of identifying locoregional and distant metastases. PET imaging methods show a sensitivity and specificity of over 90% in patients with medium to high pre-test probabilities. Tumor deposits as small as 5 mm have consistently been identified, and sensitivity is significantly higher than for either CT or MRI. However, because of high background activity in the liver and brain, small lesions in these sites will be more effectively diagnosed with morphological imaging techniques. False positive
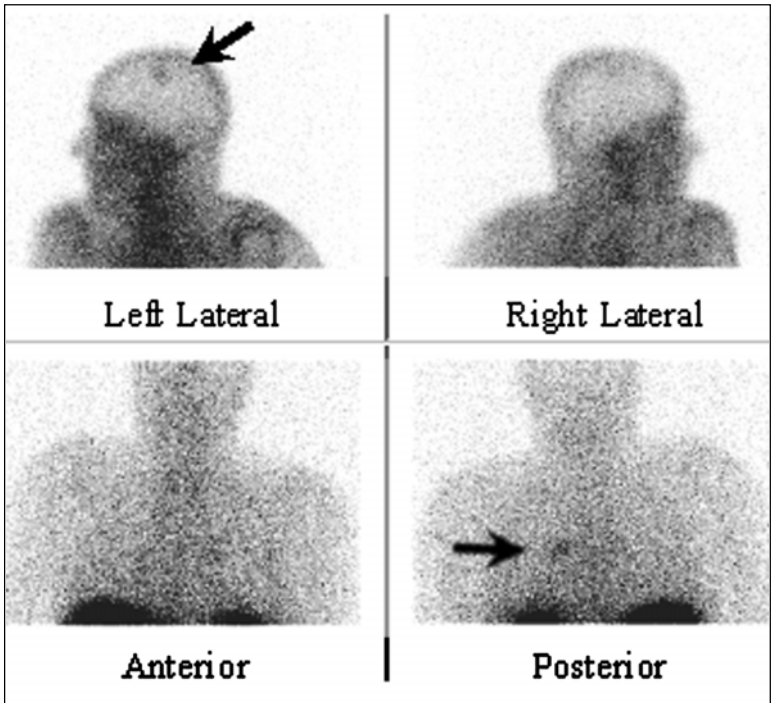
Figure 16. ^{111}In-Pentetreotide image in a patient with melanoma showing a metastasis in the left frontal lobe and in the left hilium (arrows).

studies will occur in patients with infection and recent surgery; these factors should be considered when requesting the examination.

At present FDG imaging in patients with melanoma is most effectively used in staging patients with a high likelihood of distant metastases (i.e., Stage IIB or III) and in evaluating patients at high risk of recurrence.

Gallium Imaging

Gallium shows high sensitivity for melanoma (80-85% with high dose administrations), but specificity has been lower (typically 60-75%) and imaging of the lungs and brain is ineffective.

However, if PET is not available, then there will be a small group of patients in whom CT or MRI is equivocal and biopsy is difficult and in whom gallium imaging with SPECT may make a contribution to management.

[111]In-Pentetreotide

Several groups have now reported sensitivities of up to 75% in patients with melanoma. No attempt has yet been made to test the contribution to patient management, though some preliminary data suggest that uptake may be a predictor
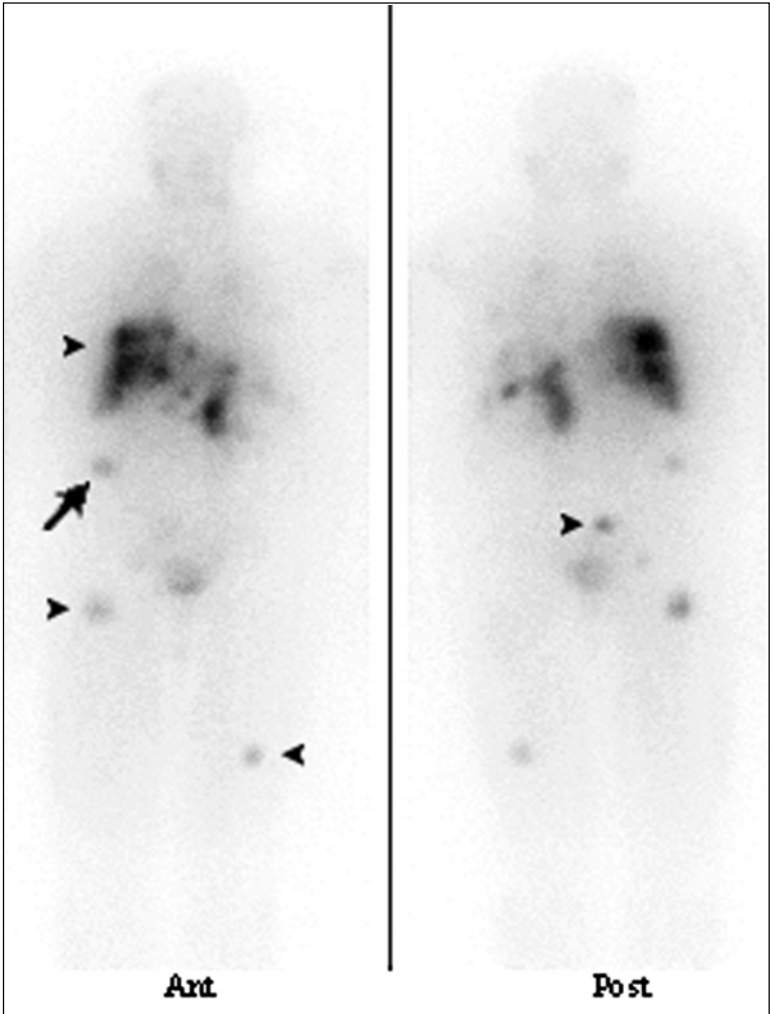
Figure 17. Anterior and posterior ^{123}I-mIBG images in a patient with very advanced metastatic carcinoid from an ileocecal primary seen in the right lower quadrant (arrow). Note extensive metastatic involvement of the liver and bones (arrowheads).

of treatment response. Specificity is likely to be a problem in this population of patients and high kidney uptake will mean that abdominal SPECT is technically difficult to interpret. It may be an effective agent for imaging metastases in the brain, however (Fig. 16).

Neuroendocrine tumors

Carcinoid Tumors

Carcinoid tumors arise from enterochromaffin cells and are the most common neuroendocrine tumors of the GI tract. The commonest sites of primary presentation are the appendix and small bowel. Tumors arise, rarely, in the bronchus, thymus and pancreas. Primary treatment is surgical; spread to the liver is not uncommon and in a minority of patients causes the carcinoid syndrome, characterized by flushing, diarrhea and asthma.

The role of nuclear medicine imaging is to confirm the neuroendocrine nature of masses visualized on CT or ultrasound, to assess disease extent and to plan for therapy. ^{123}I-mIBG is highly accurate (80% in most series) in detecting metastases from mid and hind gut carcinoid. Primary lesions will occasionally be seen (Fig. 17). The overall accuracy of ^{111}In-pentetreotide (Fig. 18) is somewhat higher than ^{123}I-mIBG, probably in the order of 80-85%. Many patients appear to have 2 clones of cells, those which take up mIBG and those which have somatostatin receptors and bind octreotide. Both radiopharmaceuticals may be used to determine metastatic burden, although ^{111}In-pentetreotide should be the agent of choice if it is available.

Symptoms of carcinoid syndrome may be effectively controlled with subcutaneous octreotide (Sandostatin®). In the absence of ^{111}In-pentetreotide uptake by hepatic metastases, it is improbable that this will be an effective treatment. We perform ^{111}In-pentetreotide scanning in all patients with metastatic carcinoid prior to commencing octreotide therapy and exclude those patients who show no uptake.

Islet cell tumors

These neuroendocrine tumors arise in the pancreas and comprise a group of tumors characterized by the expression of characteristic functional neuropeptides. Classically the group comprises insulinomas (about 60% of all islet cell tumors) and gastrinomas; other neuroendocrine tumors of the pancreas such as glucagonomas, somatostatinomas, VIPomas and nonfunctioning islet cell tumors are also often included in this broad group of neoplasms. Table 4 characterizes the tumors, their hormone products and associated symptoms.

Because of the hormones that they release, the initial diagnosis is often clinical. Direct assay of secreted hormones will often characterize the tumor. Between 10 and 40% are malignant; insulinomas and gastrinomas are often small (< 3 cm) at diagnosis and difficult to localize. The other tumors may be large and easily seen on morphological imaging.

Morphological imaging techniques such as CT, ultrasound and angiography are now being supplemented by ^{111}In-pentetreotide imaging to increase the accuracy and sensitivity of detection of smaller lesions, to characterize larger or metastatic lesions, and to select patients for subcutaneous octreotide treatment (Fig. 19). The radiopharmaceutical may also be used to monitor chemotherapy or biotherapy in patients with metastatic involvement (Fig. 20) and to evaluate the success of surgical extirpation.

[111]In-pentetreotide imaging should be considered standard of care in patients with evidence of these tumors. mIBG has no role.
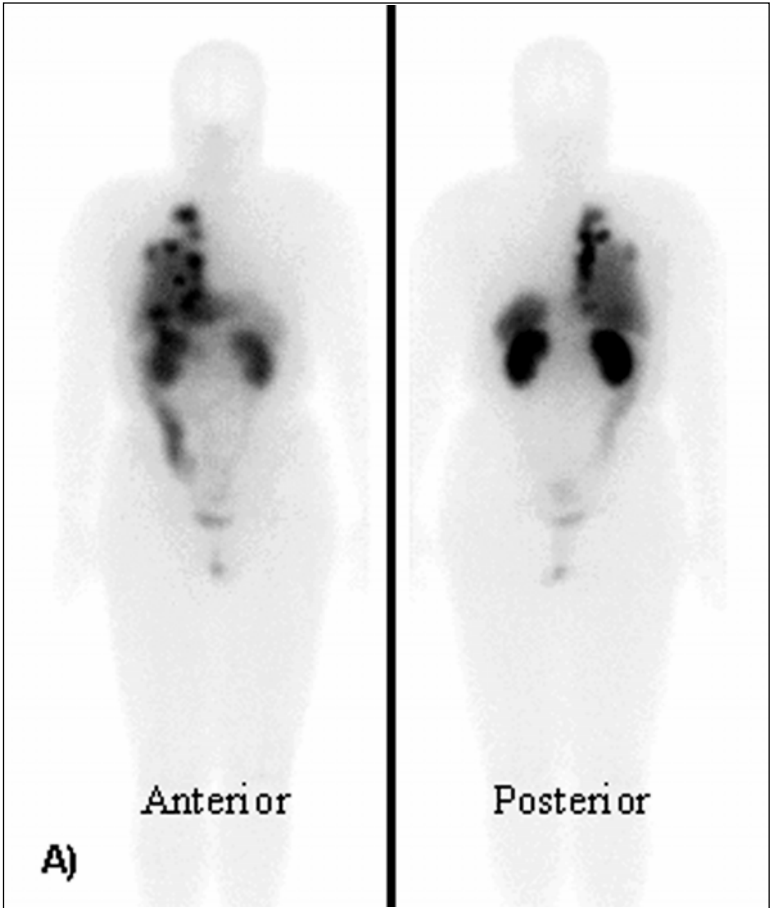
Figure 18A. Anterior and posterior ¹²In-Pentetreotide images in a patient with extensive mediastinal carcinoid. Multiple sites of abnormal uptake are identified in the mediastinum and right lung. The patient has had a left pneumonectomy.

Medullary thyroid cancer (MTC)

MTC arises from the neuroendocrine parafollicular cells in the thyroid gland and is associated with increased secretion of calcitonin. It is usually sporadic (75-80%) but may occur as an inherited autosomal dominant disorder (MEN syndromes 2A and 2B, or isolated familial MTC). In this latter population, early genetic screening (*Ret* oncogene) is an important part of detection; however, in patients with sporadic disease the patient is likely to present with thyroid swelling. Metastatic spread is to locoregional and mediastinal nodes, and metastasis to lung and bone is not uncommon. Primary treatment is surgical.

15
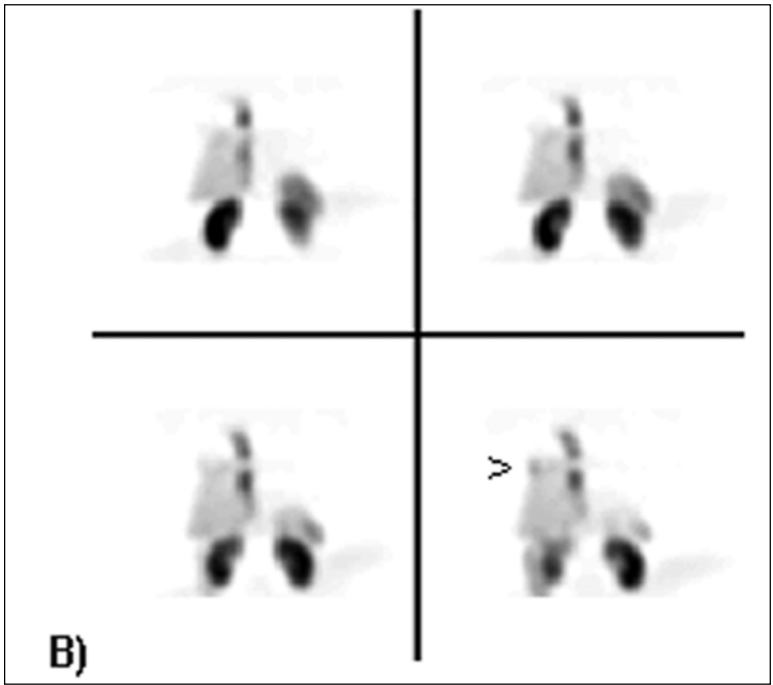
Figure 18B. Coronal SPECT images showing the ability of SPECT to better delineate the distribution of tumor within the mediastinum. The arrowhead indicates an apical pulmonary metastasis.

Although several radiopharmaceuticals have been described which show uptake by MTC, ^{111}In-pentetreotide (Octreoscan®) remains the mainstay of nuclear medicine imaging. The role of mIBG is uncertain; although it has very high specificity, sensitivity is reported as 35-50% in most series. Our practice is to use mIBG only for treatment stratification.

[111]In-pentetreotide has a reported sensitivity of between 50-80% in small series. If SPECT is performed using higher doses of indium-111 then accuracy is around 70-75%, especially for detecting mediastinal recurrence or residual tumor in the neck.

[111]In-pentetreotide imaging is a valuable addition to anatomic imaging techniques (which have relatively low sensitivity) in patients with a rising calcitonin or CEA, as a post operative evaluation or in patients with symptoms.

Neuroblastoma

Neuroblastoma is the commonest solid tumor of childhood and the fourth commonest pediatric neoplasm. Its incidence is approximately 10 per million. Despite aggressive combination chemotherapy regimes, the outlook remains bleak for those presenting with Stage IV disease. Approximately 50% of younger children and 75% of older children present at this advanced stage.

Table 4.   Islet cell tumors

Tumor	Primary Site	Incidence of Malignancy	Symptoms
Gastrinoma	Pancreas	30 – 40% Stomach Duodenum Jejunum	Peptic ulcer disease Zollinger-Ellison syndrome Diarrhea Hypercalcemia
Insulinoma	Pancreas 10% multiple	10 – 15%	Neuropsychiatric Hypoglycemia Blurred vision Palpitations/ diaphoresis
Glucagonoma	Pancreatic body Pancreatic tail	70%	Necrolytic migratory erythema Diabetes/weight loss Glossitis/stomatitis DVT Depression
VIPoma (vasoactive interstinal polypeptide)	Pancreatic tail (75%) Pancreas (20%) Autonomic chain (pediatric)	50%	Secretory diarrhea Hypokalemia Hypochlorhydria Acidosis
Somatostatinoma	Pancreas (70%) Duodenum (20%) Ampulla of Vater (5%) Small bowel (5%)	75%	Diabetes Gallstones Steatorrhea Epigastric pain Diarrhea/weight loss
PPoma (pancreatic polypeptide)	Pancreatic head	?	Rash Diarrhea Pain Weight loss Jaundice
Non-functioning	Pancreatic head (60%) Pancreatic body (20%) Pancreatic tail (20%)	80 - 100%	Pain Jaundice Weight loss Hepatomegaly

Reprinted with permission from Oxford Medical Publications: Thyroid Cancer and Endocrine Tumors. In: *The Management of Advanced Cancer.* Eds: N. Cherny, et al, In Press.

15

Anterior   Posterior
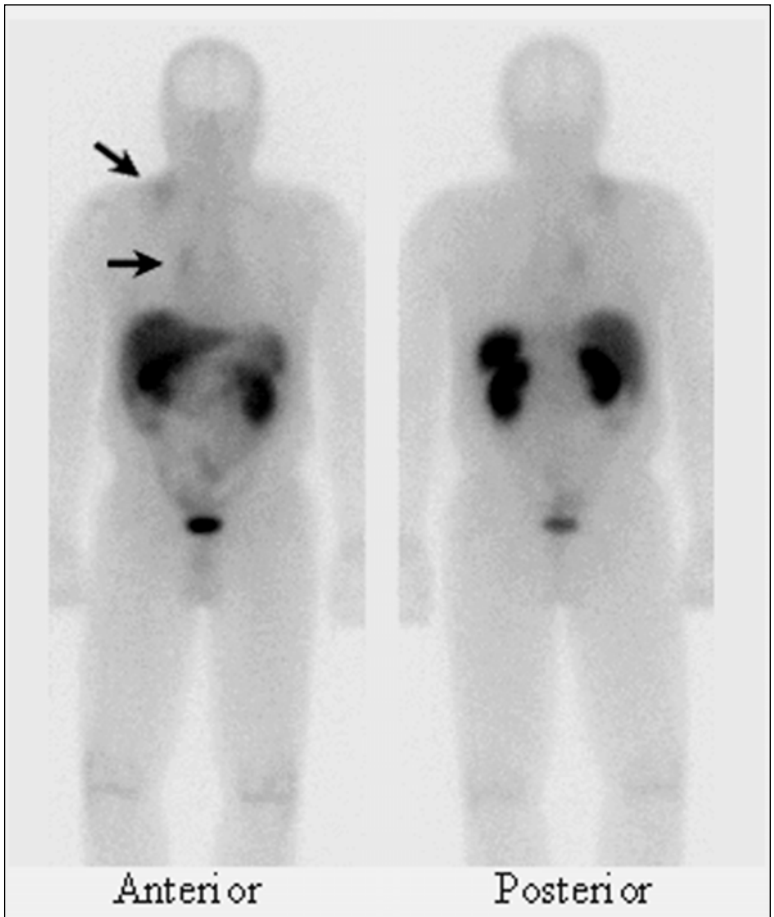
Figure 19. Anterior and posterior ^{111}In-pentetreotide images of a patient with a non-functioning neuroendocrine tumor with an unknown primary. Metastases are seen in the right supraclavicular fossa and the mediastinum (arrows).

[123]I-mIBG is the investigation of choice for initial staging, restaging after treatment, assessment of post surgical residual disease (Fig. 21), monitoring treatment response and for the early detection of recurrence on routine follow-up. The sensitivity and specificity of the technique in these settings are in excess of 94% and 95%, respectively. It may be the only indicator of bone marrow involvement where a pattern of diffuse uptake in long bones is characteristically seen (Fig. 22). mIBG uptake in an abdominal mass in a small child is pathognomonic of neuroblastoma and can often speed diagnosis and progress to treatment.
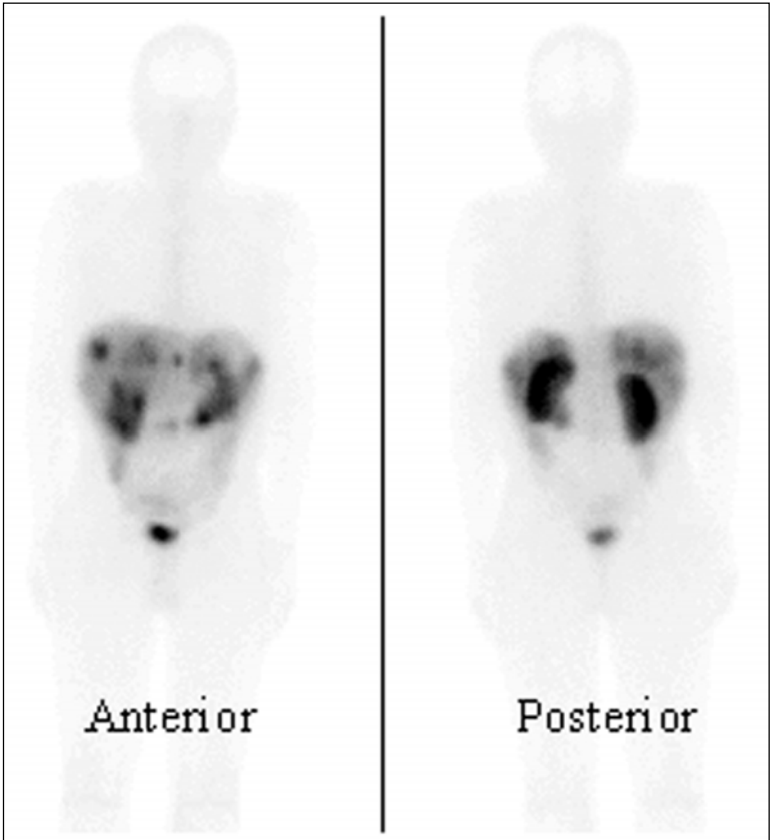
Figure 20. Anterior and posterior ^{111}In-pentetreotide images in a patient with an insulinoma. This post-treatment scan shows persistent extensive hepatic metastases.

^{131}I-mIBG may be used to evaluate these patients but clinical accuracy is reduced because of technical factors, and small or subtle lesions will be missed; it is not recommended if ^{123}I-mIBG is available.

Pheochromocytoma

Pheochromocytoma is a rare tumor of the sympathetic nervous system which produces characteristic symptoms of headache, sweating, diaphoresis and palpitations caused by catecholamine overproduction. Usually they present as unilateral intra-adrenal tumors, but bilateral tumors, extra-adrenal or pediatric presentations and metastatic spread occur in about 10% of patients. The diagnostic screening tool is measurement of urinary catecholamines or metanephrines while CT or ultrasound will define the presence of a mass.

15
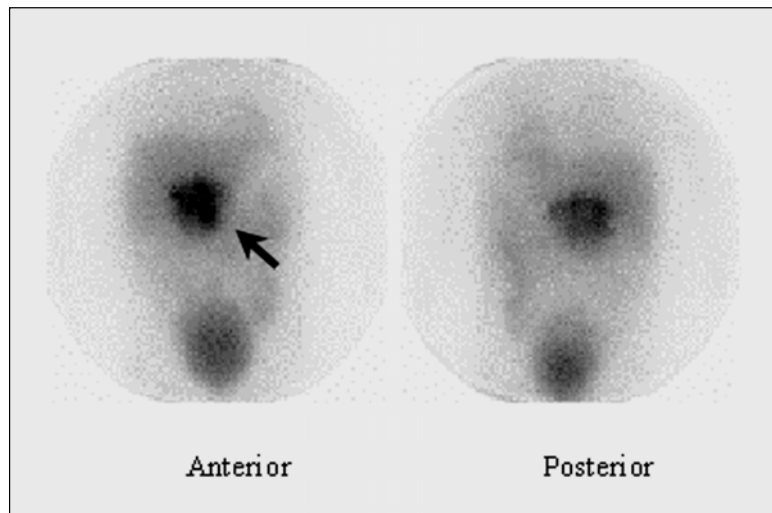
Figure 21. ^{123}I-mIBG scan of a child with residual abdominal neuroblastoma seen as activity distributed on both sides of the midline (arrow).

Imaging with ^{123}I-mIBG is indicated to confirm the functional diagnosis prior to surgery and to exclude metastatic or multifocal sites. Uptake is seen in over 90% of pheochromocytomas and is pathognomonic (Fig. 23).

Patients with extra-adrenal and pediatric presentations have a high likelihood of developing malignant pheochromocytoma in the future and should be followed for life with catecholamine estimations, which if abnormal or equivocal, should be supplemented with ^{123}I-mIBG scintigraphy. Metastatic involvement may be extensive and involve bone and soft tissue (Fig. 24)

^{111}In-pentetreotide also has a sensitivity of 80-90% for pheochromocytoma and should be used if ^{123}I-mIBG is not available or if it is negative in the presence of high clinical suspicion.

Parathyroid adenoma

Primary hyperparathyroidism is characterized by excess secretion of parathyroid hormone (PTH) which manifests clinically as hypercalcemia and hypophosphatemia. It occurs in 0.02% of women over age 40 and in 0.005% of men, and is caused either by adenoma (80% single and 5% multiple), hyperplasia (10-20%) or carcinoma (very rare). Secondary and tertiary hyperparathyroidism are not indications for radionuclide imaging and will not be discussed further. Treatment is usually surgical removal of the affected gland(s). Medical therapy with bisphosphonates and/or estrogen can be considered in cases of mild hypercalcemia (serum calcium <3 mmol/L) without symptoms or complications, or when there are medical contraindications to surgery.

Radionuclide imaging has been reported to be effective in the following indications: (i) urgent or difficult diagnostic questions such as hypercalcemic crisis, equivocal calcium measurements, or where parathyroid carcinoma is suspected; (ii)

15
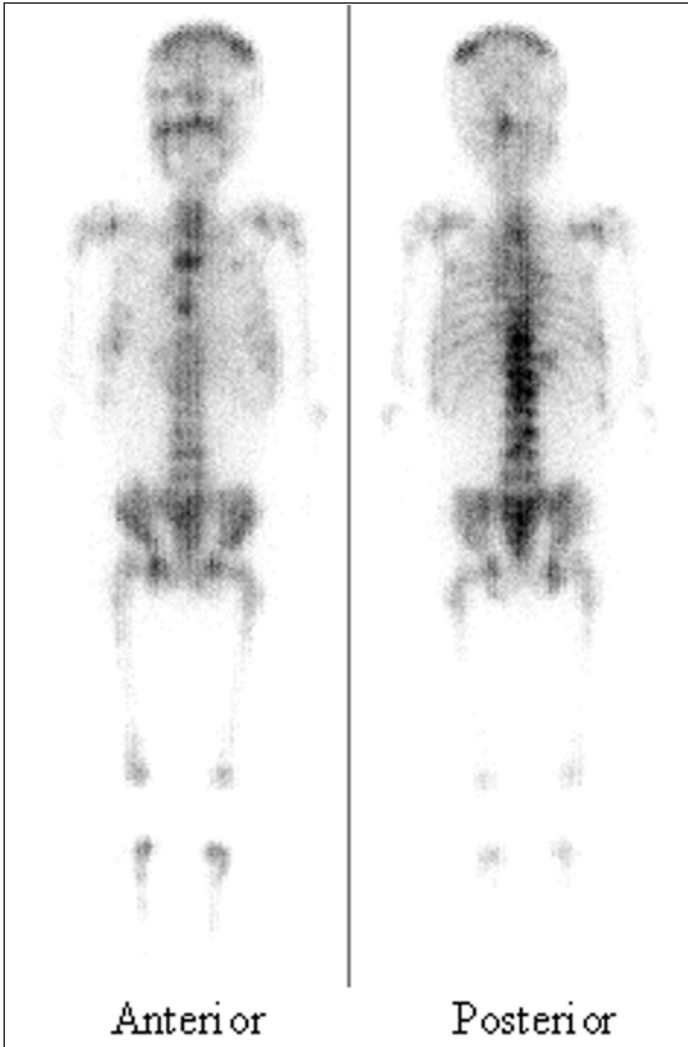
Figure 22. ^{123}I-mIBG scan in a five year old child with extensive skeletal metastatic involvement with neuroblastoma. There is diffuse abnormal activity throughout the skeleton resulting in an ^{123}I-mIBG scan which looks like a bone scan.

possible technical difficulties such as prior neck surgery; (iii) patients in whom surgery is high risk; or (iv) equivocal ultrasound or CT (sensitivities of 50-75%).

Although thallium imaging with ^{99m}Tc-pertechnetate thyroid subtraction was performed in the past, most centers now use ^{99m}Tc-sestamibi, either with ^{99m}Tc-pertechnetate or alone. ^{99m}Tc-sestamibi has high sensitivity and specificity (85-95%),

15

Anterior   Posterior
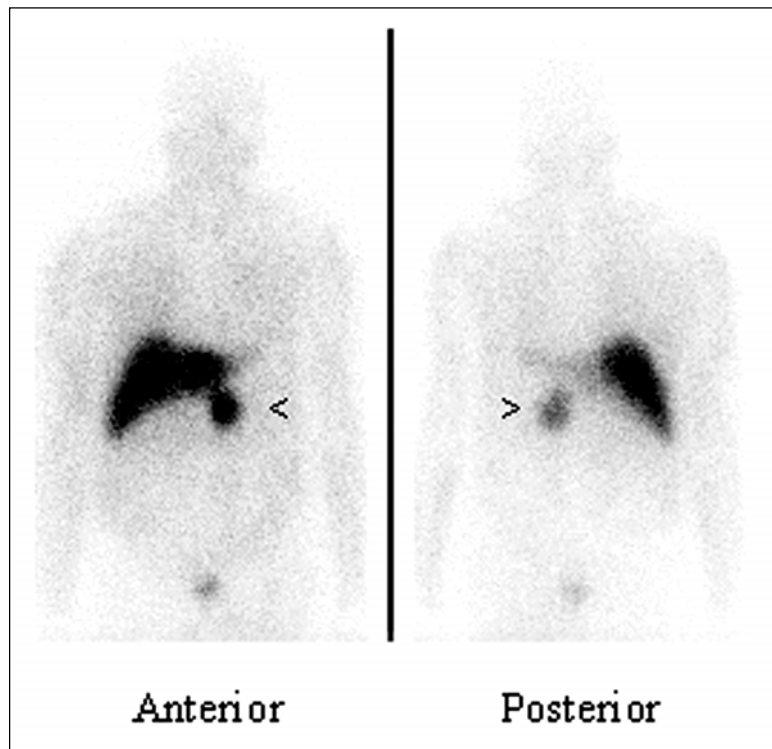
Figure 23. Anterior and posterior ^{123}I-mIBG scan in a patient with a left adrenal pheochromocytoma (arrowheads).

is technically easy to perform, and has become the investigation of choice. Images are obtained immediately after ^{99m}Tc-sestamibi injection and at about 2-3 hours by which time washout from normal thyroid tissue will have occurred and activity will be retained in the parathyroid adenoma (Fig. 25). ^{99m}Tc-pertechnetate or ^{123}I imaging may be useful in defining the functional anatomy of the thyroid gland for comparison with ^{99m}Tc-sestamibi abnormalities.

Prostate cancer

The most frequent nuclear medicine examination performed in patients with prostate cancer is the bone scan which is discussed elsewhere in this handbook. More recently, there has been interest in the use of a radiolabelled monoclonal antibody, capromab pendetide (Prostascint®), in evaluating patients with: (i) a new diagnosis of prostate cancer, (ii) those with a high risk of recurrence, or (iii) a rising PSA with negative bone scan and CT. Several groups have reported a management benefit when antibody imaging is used as an adjunct to CT, particularly in the first 2 indications. There is a steep learning curve to the interpretation of these images,
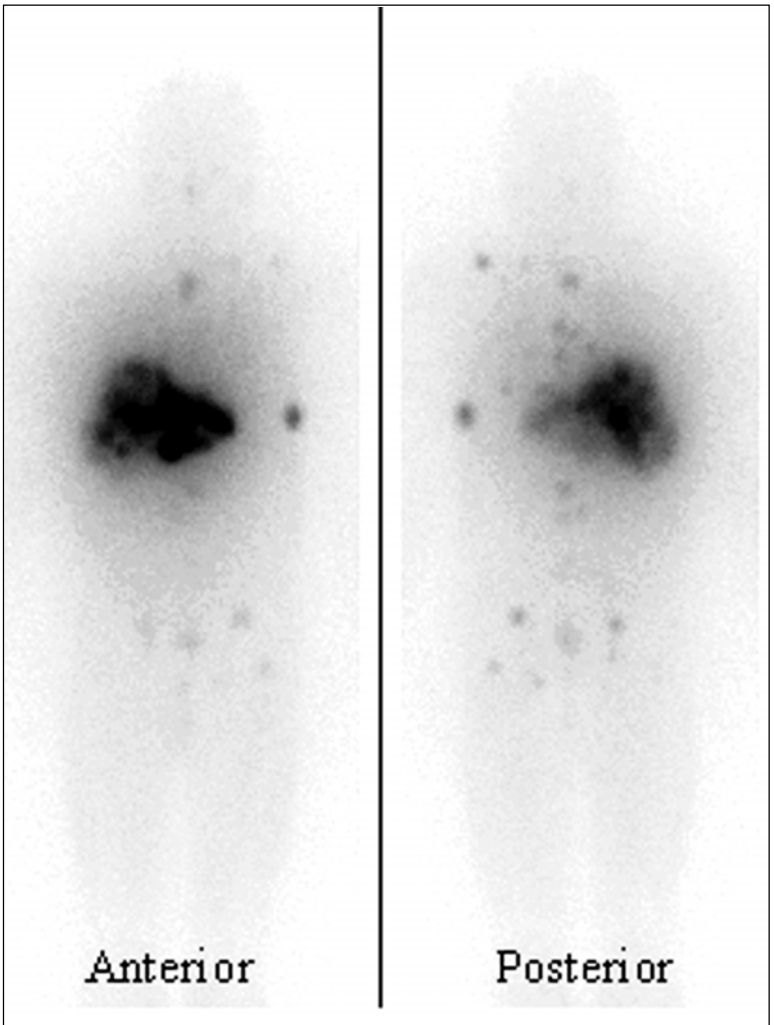
Figure 24. Anterior and posterior ^{123}I-mIBG images in a patient with advanced metastatic pheochromocytoma. Note abnormal distribution of activity involving adrenal, liver, bone, lungs, mediastinum and abdominal lymph nodes.

but in experienced hands the technique can improve patient management (sensitivity and specificity of 50-75%).

Radioisotope Therapy

The ability of nuclear medicine to design radiolabelled molecules that will target specific cancers for diagnostic use raises the intriguing possibility that the same

Anterior
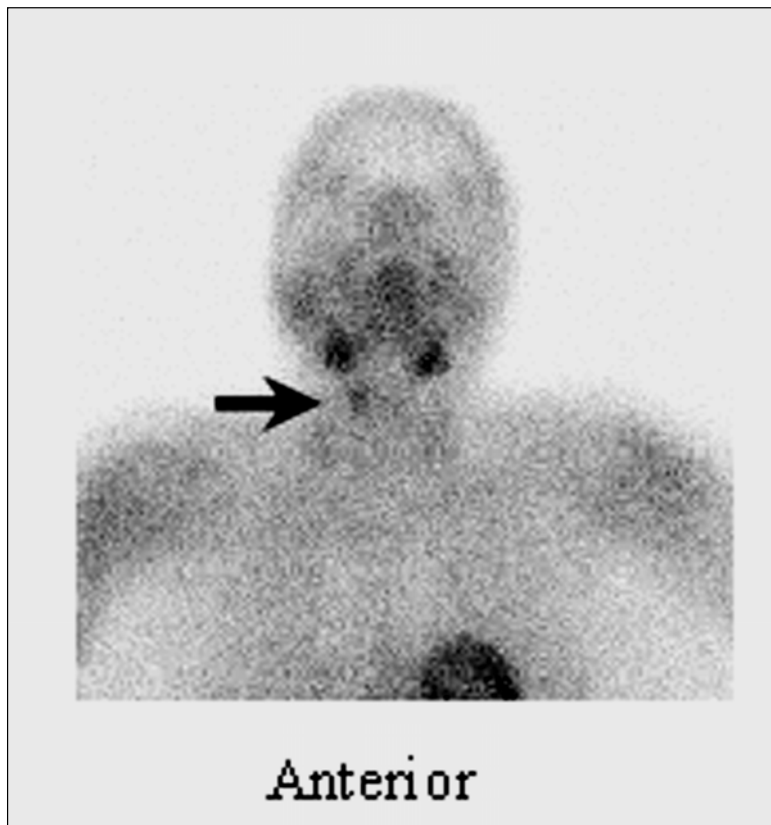
Figure 25. Delayed ^{99m}Tc-sestamibi images showing uptake in a parathyroid adenoma involving the right superior gland (arrow).

targeting strategy can be used to systemically deliver therapeutic doses of radioisotopes to patients with metastatic cancer. The archetypal radioisotope therapy is iodine-131 for the treatment of benign and malignant thyroid disease (discussed in Chapter 14). Table 5 outlines those radiopharmaceuticals that are currently in routine clinical use or which are in late Phase III trials.

^{131}I-mIBG is used extensively in Europe to treat neuroblastoma, pheochromocytoma and carcinoid. Characteristically, most radioisotope therapies are systemically administered, will treat all metastatic lesions, may be given on multiple occasions, have low toxicity and are probably underutilized. Another common application of radioisotope therapy is the use of bone seeking radiopharmaceuticals for pain palliation.

Table 5. Therapy radiopharmaceuticals

Radiopharmaceutical	Half-Life	Particle	Maximum	Indication Range in Tissue (mm)
^{131}I-Sodium iodide	8 d	β	3	Thyroid cancer
^{131}I-mIBG	8 d	β	3	Neuro-endocrine tumors
^{32}P-Phosphate	14.3 d	β	8	Polycythemia rubra vera
^{89}Sr-Strontium chloride	50.5 d	β	6.7	Pain palliation
^{153}Sm-EDTMP	2 d	β	3.4	Pain palliation
^{90}Y-Ibritumomab	2.6 d	β	11	Non-Hodgkins lymphoma
^{111}In/^{90}Y-Octreotide (experimental)	2.6 d	b	11	Neuro-endocrine tumors

Pain palliation

In patients with metastatic cancers of the prostate, lung and breast, bone metastases are seen in over 85%. In most of these, pain will become a dominant management problem. This pain is often severe and progressive, requiring escalating doses of narcotic analgesics to achieve palliation. Associated symptoms such as depression, anxiety and fear can also erode patients' quality of life. It has been estimated that up to 50% of patients with cancer metastatic to bone have inadequate control of their symptoms. Table 6 outlines strategies that may be used to achieve symptom control.

In patients with multiple sites of pain, recurrent pain in a radiation field or with progressive symptoms, palliation may be achieved by the administration of bone seeking radiopharmaceuticals, of which strontium-89 (Metastron®) is the most commonly used (Table 5). Strontium-89 is a pure β emitter with a half life of 50.5 days. Biologically strontium is metabolized by the same pathway as calcium; it is incorporated into the inorganic matrix and the degree of uptake is proportional to osteoblastic activity. There is increased retention of strontium-89 in metastases which show increased uptake of activity on a bone scan—typically there is a ratio of about 10:1 between metastatic lesions and normal bone.

Prerequisites for the use of strontium-89 have been extensively discussed in the literature and are summarized in Table 7. Appropriate patient selection is important to the effectiveness of the treatment. Contraindications to the use of this treatment for pain palliation have been established (Table 8).

Most efficacy data have been published for patients with prostate and breast cancer metastatic to bone, although the therapy has been reported as effective in most primary cancers which have metastases with positive bone scans. Overall response rate is about 75-80% and approximately one-third of these patients become pain free. Responses typically take 7-10 days to develop and are sustained, on average,

15

Table 6. Interventions in pain palliation

- Non-narcotic analgesics
- Adjuvant analgesics (antidepressant and antiepileptic drugs)
- Non-steroidal anti-inflammatory drugs
- Narcotic analgesics
- Hormone therapy
- Chemotherapy
- Local field external beam radiotherapy
- Wide field radiotherapy
- Unsealed source therapy with bone seeking radiopharmaceuticals
- Interventional anesthetic techniques
- Bisphosphonates

Reprinted with permission from Mary Ann Liebert, Inc.: Cancer Biotherapy & Radiopharmaceuticals, 1998; 13(6):413-426

Table 7. Prerequisites for palliative therapy with bone seeking radiopharmaceuticals

Karnofsky performance score $\geq$ 60
Patient has cancer metastatic to bone
Positive bone scan (irrespective of x-ray appearance)
Pain (one of the following)
    Recurrent pain in radiation therapy field
    Multiple sites of pain
    Multiple transient pains
    Diffuse bone pain
    Pain requiring opiate analgesics
    Pain requiring RT to a single site with multiple bone scan abnormalities.

Modified with permission from Mary Ann Liebert, Inc.: Cancer Biotherapy & Radiopharmaceuticals, 1998; 13(6):413-426

---

from 3-6 months. Retreatment is possible and is usually effective if the initial treatment was successful.

Toxicity is limited to thrombocytopenia which should not be severe if the patient is appropriately selected. In patients with advanced prostate cancer disseminated intravascular coagulation (DIC) should be excluded.

Frequently Asked Questions

What nuclear medicine approach can be taken to diagnose adrenocortical tumors?

The radiopharmaceutical most commonly used is norcholesterol labeled with ^{131}I (NP-59). When NP-59 is injected intravenously it is incorporated into low-density lipoprotein (LDL). Cellular uptake is mediated by LDL receptors. Cholesterol is the normal substrate for adrenal steroid hormone synthesis and the radiolabelled analogues are esterified, stored in the intracellular lipid pool, but not further

---

Table 8. Contraindications to unsealed source therapy in patients with cancer metastatic to bone

Karnofsky performance score < 60
Platelet count < 100,000 (relative contraindication)
Platelet count < 60,000 (absolute contraindication)
White count < 2.5 x 10⁶/Litre
Rapidly falling blood counts
Evidence of disseminated intravascular coagulopathy
Impending pathological fracture
Impending cord compression
Less than two months projected survival
Prior to myelosuppressive chemotherapy
Extensive soft tissue metastases

Modified with permission from W.B. Saunders Company: Semin Nucl Med, 1997; 27(2):165-182.

---

metabolized. It therefore provides a model for imaging either increased cellular mass, increased receptor mediated transport or intracellular storage. This uptake and retention within the cell is controlled by action of the hypothlmic-pituitary-adrenal axis (Cushing's disease) or of the renin-angiotesin-aldosterone axis (hyperaldosteronism).

By 2-3 days the normal adrenals may be faintly and symmetrically visualized. Uptake may be quantified by standard nuclear medicine techniques and normal ranges have been published. Abnormal uptake is seen as intense and progressive uptake within the adrenal which quantitatively lies outside the established normal range. Anterior and posterior images of the abdomen are obtained 5 and 7 days after intravenous injection of the radiopharmaceutical. Images may be acquired after dexamethasone suppression which suppresses uptake in the normal adrenal but not in an autonomously functioning gland or adenoma. In this way the detection of mineralocorticoid and androgen secreting tumors is enhanced.

The demonstration of adrenal masses by abdominal CT is a not uncommon finding in routine imaging studies. While these might require follow-up for patient management decisions, radionuclide imaging is most clearly indicated when there is evidence of adrenocortical hypersecretion based on clinical diagnosis and appropriate hormonal measurements. Whilst several groups have reported on adrenocortical scintigraphy in this group of patients with "incidentalomas", there is no evidence that there is a routine clinical role for the technique.

The three clinical syndromes for which adrenocortical scintigraphy may be used are Cushing's syndrome, hyperaldosteronism and hyperandrogenism. The imaging techniques and interpretation for these latter 2 syndromes are identical to that used in Cushing's syndrome but require dexamethasone suppression.

The results of imaging are reported both on the basis of qualitative and quantitative uptake; the abnormal patterns of uptake seen are shown in Table 9. Figure 26 shows bilateral adrenal hyperplasia in a patient with Cushing's syndrome. Whilst this technique is not commonly performed, it can provide invaluable data to the surgeon in planning his surgical approach.

15

Table 9.   Imaging patterns in adrenal cortical imaging

Non-Visualization Symmetrical Uptake	Bilateral Asymmetrical Uptake	Bilateral	Unilateral Uptake
Carcinoma	Normal adrenals (late)	ACTH independent nodular hyperplasia	Adenoma
Hypercholestero-lemia	ACTH dependent bilateral hyperplasia Ectopic AcTH Secondary hyperaldosteronism Dexamethasone suppressible aldosteronism	Remnants Cushing's syndrome	Conn's syndrome
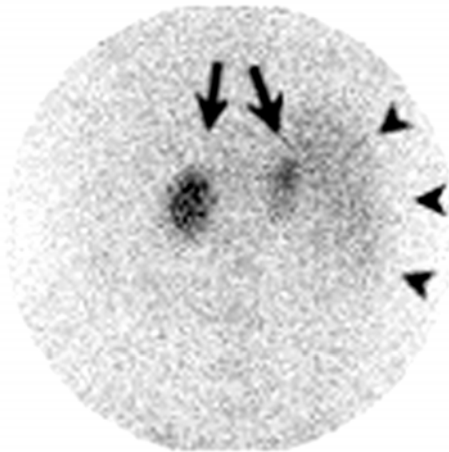
Figure 26. 131I-norcholesterol scan obtained 10 days post-injection. Bilateral adrenal uptake (arrows) is demonstrated, more so on the left in this patient with bilateral adrenal hyperplasia. Faint activity is seen in the liver (arrowheads).

Additional Reading

1.   Aktolun, Tauxe WN, eds. Nuclear Oncology. Berlin: C. Springer-Verlag, 1999.
     *Major textbook of the role of nuclear medicine in oncology. Provides most of the key
     references required for further reading and expands the scope of discussion on individual
     areas.*
2.   Berman CG, Choi J, Hersh MR, Clark RA. Melanoma lymphoscintigraphy and
     lymphatic mapping. Semin Nucl Med 2000; 30:49-55.
     *Background reading of the theory of the technique, clinical overview of the state of trials
     and current indications for use.*
3.   Hoefnagel CA. Radionuclide cancer therapy. Ann Nucl Med 1998; 12(2):61-70.
     *General overview of radioisotope therapy with background on most radiopharmaceuticals
     in use or in trials.*
4.   Maisey MM, Wahl RL, Barrington SF. Atlas of Clinical Positron emission
     tomography. Arnold Publishing Group, 1999.
     The definitive textbook on clinical applications of PET.
5.   McEwan AJ. Use of radionuclides for the palliation of bone metastases. Semin
     Radiat Oncol 2000; 10:103-114.
     *Overview of indications for palliative treatment of bone metastases with
     radiopharmaceuticals. Review of the agents available, indications and contraindications
     and departmental requirements for use.*
6.   Pauwels EKJ, McCready VR, Stoot JHMB, van Deurzen DFP. The mechanism of
     accumulation of tumour-localising radiopharmaceuticals. Eur J Nucl Med 1998;
     25:277-305.
     *The definitive paper of radiopharmaceuticals used in nuclear oncology. Extensive reference
     list and background information on all current radiopharmaceuticals and many currently
     being evaluated.*
7.   Phelps ME. PET: The merging of biology and imaging into molecular imaging. J
     Nucl Med 2000; 41:661-681.
     *Past, present and future of PET and molecular imaging with particular reference to
     cancer.*
8.   Pieterman RM, van Putten JW, Meuzelaar JJ, Mooyaart EL, Vaalburg W, Koeter
     GH et al. Preoperative staging of non-small-cell lung cancer with positron-emission
     tomography. N Engl J Med 2000; 343(4):254-261.
     *A recent prospective comparison of conventional staging with FDG PET showing that
     PET improves the rate of detection of local and distant metastases in patients with non-
     small-cell lung cancer.*

15

Neuropsychiatric Disorders

Jean-Paul Soucy, Denis Lacroix and Catherine Kissel

Introduction

Nuclear medicine has a lengthy and distinguished reputation in the fields of neurology and psychiatry as a powerful research and clinical tool. Noninvasive in vivo demonstration of brain lesions was initially performed more than forty years ago with agents which accumulated nonspecifically. Since then we have witnessed an important evolution in the techniques used for the diagnosis of neuropsychiatric disorders. The "traditional" brain scan, based on agents sensitive to blood-brain barrier (BBB) disruption (Fig. 1), has been replaced by anatomically superior approaches such as x-ray transmission computed tomography (CT) and magnetic resonance imaging (MRI) for the study of most focal lesions.

More recently, the demonstration by nuclear medicine techniques of disturbances in regional perfusion patterns, energy consumption and neurotransmission in the brains of psychiatric patients has made a major contribution to the recognition that mental diseases (including drug addictions) are organically-based metabolic alterations, in every way comparable to diseases found in other systems. Presently, the most frequently performed clinical nuclear medicine test in neuropsychiatric disorders is SPECT evaluation of cerebral perfusion. These perfusion maps provide a snapshot of "brain activity" and are altered in a variety of neurological and psychiatric conditions even when anatomic imaging is normal.

Until recently in vivo study of neurotransmission was only possible with positron emission tomography (PET), but new SPECT agents have made this much more widely available. PET itself is undergoing a major increase in availability through technological developments that are making it a far less complicated and costly technique. Neurology and psychiatry can only benefit from this transformation.

Regional Cerebral Perfusion

Non-invasive measurements of regional cerebral blood flow (rCBF) were initially performed with freely diffusible tracers such as xenon-133 (imaged in planar or SPECT mode) or ^{15}O-water and ^{11}C-butanol (imaged with PET). Unfortunately, those techniques had limited availability due to complexity and the high cost of the required equipment. The development of iodine-123-labelled compounds (^{123}I-IMP, ^{123}I-HIPDM) which have a blood-flow related distribution in the brain afforded an easy means of evaluating rCBF, not through absolute quantification but through the description of its relative distribution. Subsequent development in the field of radiochemistry led to the synthesis of the currently used radiopharmaceuticals, ^{99m}Tc-HMPAO (Hexa Methyl Propylene Amine Oxime, Ceretec®) and ^{99m}Tc-ECD
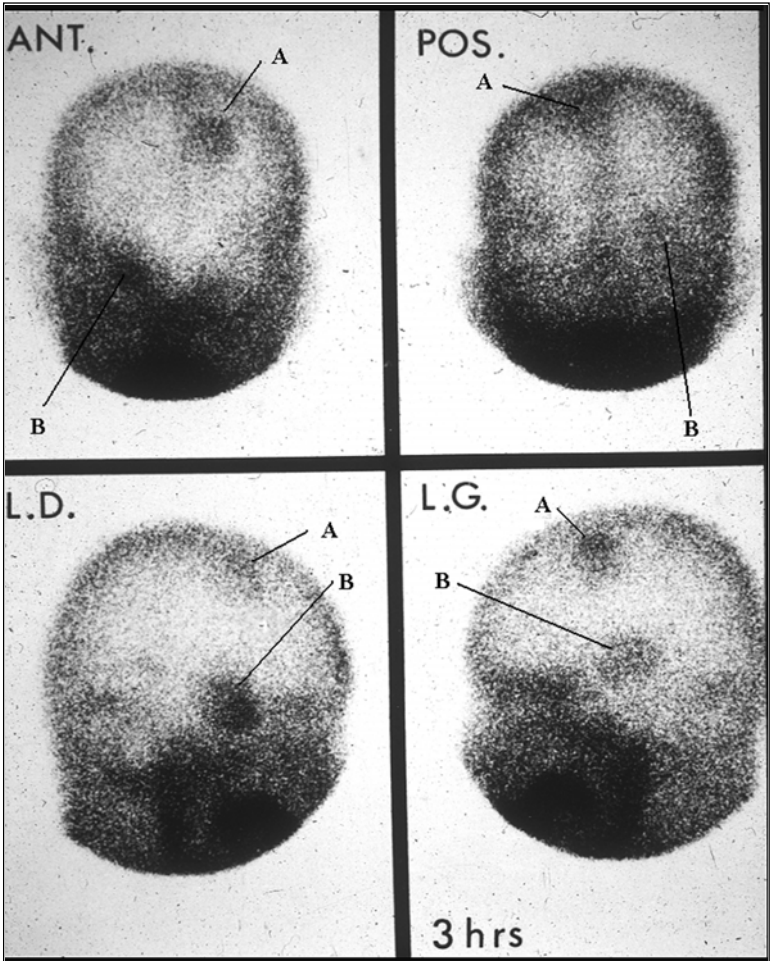
Figure 1. Disrupted blood-brain barrier (BBB). Two metastases (left posterior frontal, A, and right temporal, B) from a lung carcinoma: the tumors are devoid of normal astrocytes and therefore of an intact blood-brain barrier. This allows passage of ^{99m}Tc-glucoheptonate, normally excluded from the cerebral parenchyma, into the lesions.

(Ethylene Cysteinate Dimer, Neurolite®). The following discussion will focus on these two agents.

Principles of rCBF Imaging

^{99m}Tc-HMPAO and ^{99m}Tc-ECD (Fig. 2) the two most commonly used agents for imaging rCBF, are injected into a peripheral vein which allows uniform mixing
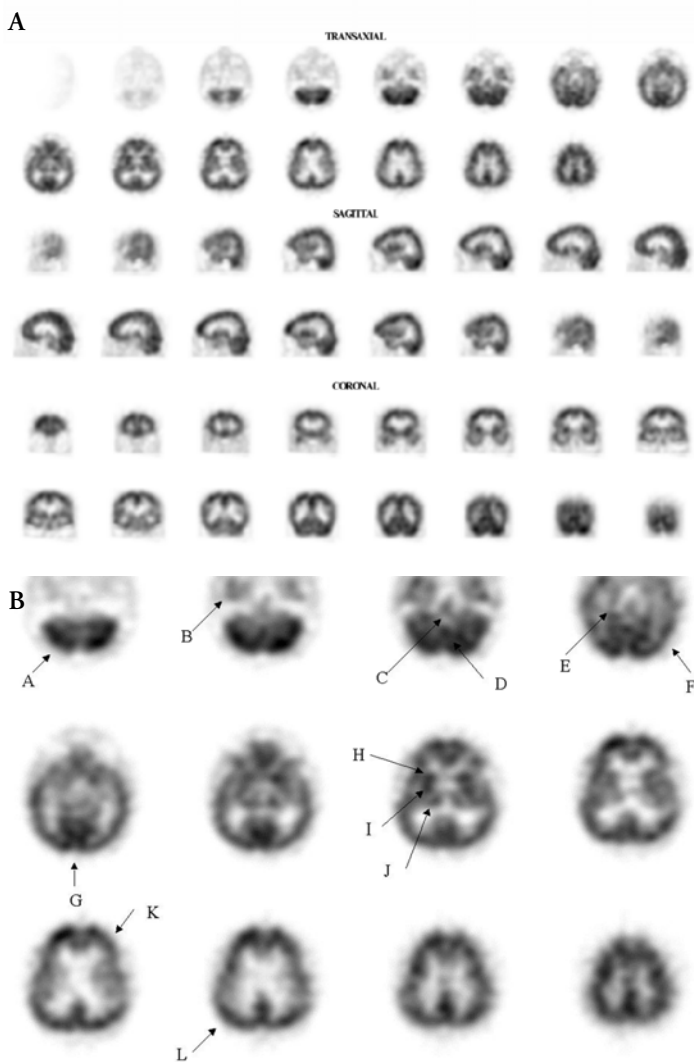
Figure 2. Normal brain perfusion. (A) Transaxial, sagittal and coronal slices of a normal rCBF SPECT study with ^{99m}Tc-ECD. Notice preferential perfusion to cortical and sub-cortical grey matter. (B) Some of the structures which should be routinely depicted on a state of the art rCBF SPECT study are A: cerebellar hemisphere. B: temporal lobe. C: brain stem. D: vermis. E: hippocampal region. F: lateral temporal cortex. G: occipital cortex (calcarine region). H: head of the caudate. I: putamen. J: thalamus. K: frontal lobe. L: parietal lobe.

of the molecules in the blood before they reach the brain. The more blood that flows through a given brain region, the more tracer it receives. Both agents are highly lipophilic and easily cross the BBB. Once in the brain, they undergo conversion to polar compounds that cannot diffuse back into the blood. The precise mechanisms involved are still disputed: in the case of ^{99m}Tc-HMPAO a significant part of the transformation is through reaction of the native molecule with reduced glutathione in astrocytes, whereas for ^{99m}Tc-ECD most of the transformation is through the action of esterases located both extra- and intra-cellularly.

Four principles must be kept in mind when interpreting SPECT studies:

- After first pass uptake, tracer trapped within brain tissue remains essentially stable over time. One can therefore consider that the SPECT images produced are a "snapshot" of the distribution of rCBF at the time of injection of the tracer.

- Although these tracers are highly lipophilic, they are diffusion limited at high flow rates. Overall, high flow regions accumulate more radioactivity than low flow ones, but the relationship is not linear: as flow increases, the relative accumulation decreases. Techniques that correct for this effect are either cumbersome or inexact. Practically speaking, underestimation of high blood flow is of limited clinical importance as precise determination of rCBF is not generally required.

- Since ^{99m}Tc-HMPAO and ^{99m}Tc-ECD do not undergo the same chemical transformations, it is not surprising that their exact distributions differ slightly. This is most important for the diagnosis of sub-acute cerebral infarctions. During the luxury perfusion phase these lesions can show significant uptake of ^{99m}Tc-HMPAO, sometimes to levels that overestimate actual perfusion, perhaps due to locally increased glutathione concentrations. In contrast, ^{99m}Tc-ECD uptake is decreased in these cases, probably because the maintenance of the esterase activity which allows trapping of the tracer is energy dependent.

- SPECT rCBF studies represent a technically simple method for assessing complex neurophysiological events. Whereas it might be "simple" to interpret the very focal cortical activation associated with a strong sensory stimulation (strobe light in the eyes, vibrating ball in the hand) or a convulsive episode, evaluation of the more elaborate operations involved in the performance of tasks of greater complexity, cognitive function or emotion is more daunting. The emerging view of "brain function" is that the completion of even simple tasks relies on the activation of large distributed networks which interact extensively, are shared by a variety of different tasks, and can be efficiently replaced by secondary centres. In that context, highly specific associations between a given clinical state and a brain perfusion pattern are the exception rather than the norm.

Decreased rCBF arises through two mechanisms:

- Decreased vascular supply: Occlusive vascular disease directly interferes with nutritive blood flow. SPECT imaging can help to determine the hemodynamic effect of a vascular lesion.

16

- Decreased energy demand: Under most circumstances, brain energy utilisation and blood flow are tightly coupled (probably through nitric oxide [NO] release from specialized neurons). This allows small resistive vessels of the brain to dilate or constrict as energy consumption increases or falls. Since energy consumption in the brain is mostly devoted to sustaining glutamatergic (excitatory) transmission, rCBF mapping is essentially an indirect indicator of excitatory neurotransmission. SPECT imaging can thus depict the distribution of brain activity in neurologic disorders (such as primary degenerative processes) and psychiatric diseases that directly affect neurotranmission.

Techniques to separate these two processes rely on the fact that, under normal circumstances, cerebral perfusion increases or decreases according to local energy requirements by dilating or constricting resistance vessels. If a feeding vessel is stenotic then downstream vessels will dilate and the total blood volume will increase. Flow is thus maintained at a constant value at the expense of reducing "vasodilatory reserve". Cerebrovascular vasodilators, such as carbon dioxide (CO_2) and acetazolamide, will increase flow to the normally supplied brain. Because of the decreased vasodilatory reserve in the area subtended by the stenotic vessel, flow will increase less than in areas with normal circulation. If, however, energy demand is decreased then decreased perfusion is adaptive and the vessels will respond normally to direct carbon dioxide (CO_2) and acetazolamide. Both agents have been frequently used in the study of cerebrovascular diseases, but the highly variable results of those studies cast serious doubts on the clinical usefulness of such techniques.

Technical Considerations in rCBF Imaging

Both ^{99m}Tc-HMPAO and ^{99m}Tc-ECD are available in kits that allow easy labelling of the precursor molecule. Once labelled, ^{99m}Tc-ECD is stable for at least 6 hours. Unmodified ^{99m}Tc-HMPAO is stable for only 30 minutes, though a stabilized preparation is also available. Injection is made through a pre-installed IV catheter in a quiet environment (usual dose 750 MBq). For some applications, the injection is timed to coincide with a specific event (e.g., seizure onset).

Scan acquisition usually starts 30 to 60 minutes after injection. ^{99m}Tc-HMPAO has slower blood clearance than ^{99m}Tc-ECD and background activity usually takes longer to decrease. Some ^{99m}Tc-HMPAO defects become more obvious with time after injection (probably attributable to local ischemia with secondary vasodilatation and increased blood volume), and in this setting up to 2 hours should elapse before imaging.

Technical parameters for rCBF SPECT acquisition should attempt to maximize counts and optimize resolution. Reconstruction techniques and image display play a crucial role and must be standardized: the same projection dataset can give rise to vastly different results depending on the reconstruction algorithm, choice of filter, attenuation correction, scatter correction and choice of display (film, computer screen, colour scale and contrast/background settings).

Deciding whether a study is normal or abnormal can be easy, as in cases with massive perfusion defects, but for milder abnormalities interpretation is more complicated. Most clinicians rely on a subjective visual interpretation where "normal" denotes symmetrical activity largely confined to grey matter in the cerebral cortex,

cerebellum, basal ganglia and thalamus (white matter shows little uptake due to relatively low levels of blood flow).

More complex approaches for quantification are used in research and in some clinical settings. These methods often require spatial registration, resizing and warping of the images in an effort to superimpose different scans from the same patient (either of the same or different modalities obtained at different times) or from different patients (fused in order to compare groups of subjects). Most analytical tools were developed for PET or fMRI studies which have spatial resolution and temporal sampling capacities quite different from SPECT. Although the same techniques are applicable to SPECT, they have not been optimised for it and therefore have to be utilised with a good understanding of their characteristics and limitations.

Clinical Applications of SPECT rCBF Imaging

To date nuclear neuroimaging has been used more for research than for clinical problem-solving. The clinical usefulness of SPECT rCBF imaging was carefully reviewed by an expert panel of the American Academy of Neurology. Based upon quality and strength of evidence they rated various clinical applications (Table 1). The indications designated as "established" are few and have not been expanded since the publication of this report in 1996. Although many other applications are "promising" and may eventually be accepted, *for the moment* caution is recommended before using rCBF SPECT studies on a systematic clinical basis in these conditions. Many of these conditions have not been evaluated in sufficient numbers and in adequately controlled prospective studies to allow firm, evidence-based conclusions to be drawn on the *general* usefulness of this application. This should not be construed to mean that it is useless to perform such studies on patients affected with these conditions, since many *may* benefit from the information provided. In some cases, the perfusion study will be useful in simply confirming an observable organic basis to symptoms and signs otherwise not linked to recognisable abnormalities on conventional imaging (CT or MRI). One such application is in the field of head trauma, where the very nature of some brain lesions (shearing at the microscopic level) can produce persistent memory and concentration problems despite normal CT and MRI examinations. Such lesions are expected to alter perfusion, and the demonstration of cerebral perfusion abnormalities helps to support claims for compensation or disability payments. An even more direct application is in the evaluation of vascular spasm following subarachnoid haemorrhage (SAH) where the cause of a deterioration in the neurological status of a patient with a known SAH is an alteration in blood flow (Fig 3). The results from SPECT rCBF studies seem to correlate very well with those of angiography but SPECT is a much less invasive technique for recognizing this serious complication and evaluating response to therapy. Other neurological conditions (such as AIDS dementia complex and viral encephalitis) have been reported to show altered patterns of brain perfusion, but the available evidence remains insufficient at this time to gauge the overall performance of SPECT perfusion studies in such cases.

The same remarks can be made for psychiatric illnesses, which are also associated with a variety of abnormal brain perfusion patterns. The observation of these patterns has been useful in helping to understand the pathophysiology of these afflictions, but to date they do not allow the use of SPECT rCBF studies as clinical tools for diagnosis or follow-up. For instance, the reported observations of activation in the

Table 1 Effectiveness of clinical applications of brain SPECT rCBF studies

Disorder	Application	Rating
Stroke	Detection of acute ischemia	Established
	Determination of stroke subtypes	Promising
	Vasospasm following SAH	Promising
	Prognosis/recovery from stroke	Investigational
	Monitoring therapies	Investigational
	Diagnosis of TIA	Investigational
	Prognosis of TIA	Investigational
Neoplasm	Grading of gliomas	Investigational
	Differentiating radiation necrosis from tumor recurrence	Investigational
HIV encephalopathy		Investigational
Head trauma		Investigational
Epilepsy	Presurgical ictal detection of seizure focus	Established
	Localization of seizure focus	Promising
	Differential diagnosis of ictus	Investigational
	Interictal detection of seizure focus	Investigational
	Determination of seizure subtypes	Investigational
	Receptor studies (not rCBF)	Investigational
	Monitoring therapy	Doubtful
Alzheimer's disease	To support clinical diagnosis	Established
Huntington's chorea		Investigational
Persistent vegetative state		Investigational
Brain death		Promising

Adapted from: Assessment of brain SPECT—Report of the Therapeutics and Technology Assessment Subcommittee of the American Academy of Neurology. Neurology 1996; 46:278-285.

auditory cortex during auditory hallucinations, or the modification of cerebral perfusion in a predictable way during the course of anti-depressant therapy (improved perfusion to the left dorsal pre-frontal cortex) shed light on the regions involved but have no impact on patient classification or management.

The three "established" clinical indications will be discussed in some detail.

Presurgical Localization of a Seizure Focus

Patients with medically uncontrollable epilepsy are potential candidates for surgical removal of the focus from which the attacks originate. This represents a substantial number of patients, since it is generally accepted that 15-25% of patients with epilepsy are sub-optimally to poorly controlled with medication alone. Conventional imaging
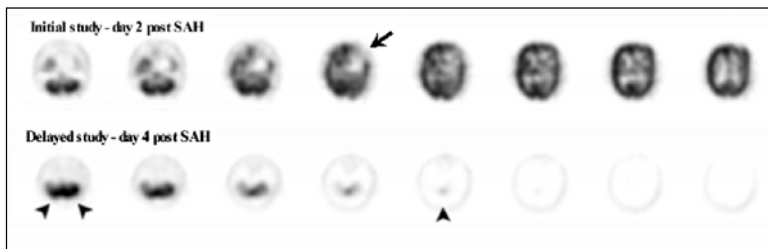
Figure 3. Vasospasm post subarachnoid hemorrhage (SAH). Brain SPECT ECD scans were performed 2 and 4 days post-SAH. Only the transaxial images are shown. The initial study shows decreased left frontal perfusion secondary to intraparenchymal bleeding (arrow). The delayed study performed after the patient showed severe clinical deterioration reveals perfusion limited to the cerebellum and the lower brain stem (arrowheads), indicating bilateral cerebral hemispheric infarction with no possibility of regaining normal cerebral function.

(CT or MRI) relies on the detection of an anatomical lesion which may or may not be the actual ictal focus. A recent meta-analysis has confirmed the value of ictal SPECT (and PET) rCBF studies: focally increased perfusion has a sensitivity of 97% and a specificity of at least 98.5% for temporal lobe epilepsy localisation (Fig. 4). Although the most useful part of a SPECT evaluation is the ictal study, an interictal one (obtained if possible with EEG monitoring to exclude subclinical ictal activity at the time of injection) is warranted in order to facilitate interpretation of the ictal scan. Unlike the ictal scan, the one obtained interictally demonstrates decreased perfusion of the epileptogenic focus. Simple visual inspection of the two studies can be supplemented with statistical analysis that looks for regions of significantly increased perfusion in the ictal phase. The interictal study alone, however, cannot be relied upon to localise epileptic foci (sensitivity only 50% for temporal lobe epilepsy with false localisation rate of 10%).

For ictal studies, injection must be performed immediately after seizure onset, as rapid modification in the distribution of brain activation and perfusion can occur. For extra-temporal epilepsy, generalisation can be extremely rapid. Frontal lobe epilepsy requires an injection delay of no more than 10 seconds after clinical initiation of the seizure before epileptic activity spreads to other parts of the brain. In temporal lobe epilepsy the optimal interval for injection is during the first 30 seconds, although acceptable studies can be obtained for up to 60 seconds. If a first try is negative then repeat examinations must be obtained: the importance of precisely determining which area of the brain to remove can hardly be overemphasized. Its non-invasiveness, relatively low-cost, and remarkable performance amply justify the use of rCBF SPECT in the preoperative assessment of epilepsy.

To Support a Clinical Diagnosis of Alzheimer's Disease

Dementia can be defined as a deterioration in cognitive abilities that impairs the previously successful performance of activities of daily living. Ten percent of persons over age 70 and 20 to 40 percent of individuals over age 85 have clinically significant memory loss. Although there are many causes (Table 2), four types of dementia—

| | AXIAL | CONONAL | SAGITTAL |

INTERICTAL

ICTAL

MRI REGISTERED
Mean + 2 SD
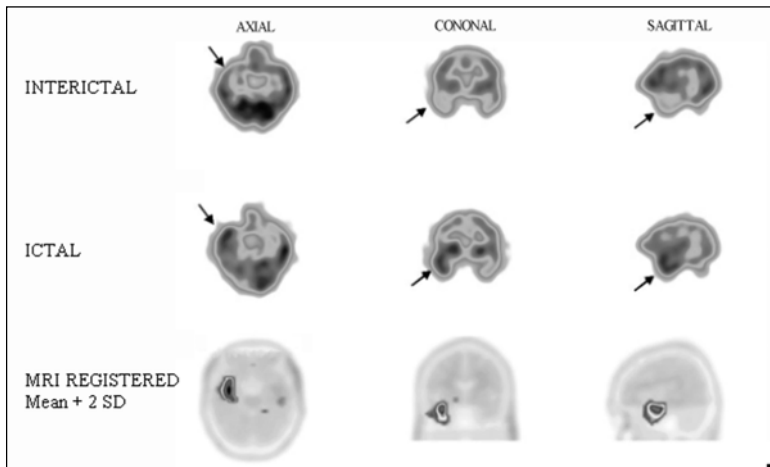
Figure 4. Epilepsy. Interictal and ictal transaxial, coronal and sagittal slices showing right temporal focus of decreased interictal perfusion and ictal hyperfusion. These images are 3D co-registered, allowing for precise subtraction (Ictal-Interictal) and superimposition over an MRI atlas of voxels with a subtraction value of more than 2 SD over the mean.

Alzheimer's disease, diffuse Lewy body dementia, frontotemporal dementia and vascular dementia—account for 90% of all cases.

SPECT rCBF imaging can be a valuable adjunct to clinical evaluation and conventional neuroimaging (CT and MRI) in patients with dementia. Certain scan patterns increase the likelihood of specific sub-types of dementia (Fig. 5), information that is valuable in establishing prognosis. This may also help in targeting drug therapies, a potentially useful application now that several medications have been approved for the treatment of Alzheimer's disease with additional agents undergoing clinical trials. However, SPECT interpretation must be integrated with all other information on the patient: on its own it can neither be used to prove nor disprove the presence of dementia, nor to establish a specific diagnosis of a sub-type of dementia, as patients with no clinical signs of dementia can have perfusion studies with a pattern suggestive of Alzheimer's disease (bilaterally decreased parietotemporal perfusion), and conversely some patients with documented dementia can retain a normal perfusion pattern. Special reconstruction techniques along the hippocampal long axis can reveal severe hypoperfusion of these structures. Some investigators believe that SPECT can help to differentiate nondementing illnesses (e.g., late-onset depression) from organic dementia, though others have questioned this.

Detection of Acute Ischemia

MRI and CT are both usually normal for several hours after interruption of flow to the brain as the tissue properties measured by these modalities take time to become abnormal. SPECT imaging of rCBF is a highly effective means for detecting acute

Table 2. SPECT patterns according to dementia subtype

	Percentage of All Dementias	Most Common Pattern of SPECT rCBF Reductions
Alzheimer's disease	50-70	Bilateral parietotemporal (relative sparing of sensorimotor cortex, basal ganglia and cerebellum).
Diffuse Lewy body dementia	10-20	Like Alzheimer's disease
Vascular dementia (multi-infarct)	10	Multiple asymmetric cortical and subcortical in a vascular distrubution
Frontotemporal dementia (including Pick's disease)	5-10	Bilateral anterior frontal lobes and inferior temporal lobes
Normal pressure hydrocephalus	6	Global with an enlarged subcortical low-flow region
Cortical basal degeneration	<5	Unilateral cortex, basal ganglia and thalamus (contralateral to the affected limb)
Parkinson's disease	<5	Like Alzheimer's disease
Chronic drug intoxication	3	Normal
Cerebral trauma	2	Prefrontal and temporal poles (occasionally occipital *contre-coup* defects)
Huntington's disease	2	Caudate nuclei
HIV encephalopathy		Global with superimposed cortical and subcortical heterogenity
Progressive supranuclear palsy (Steel-Richardson syndrome)	Rare	Global but most pronounced in frontal areas and basal ganglia
Normal aging (benign Forgetfulness of the elderly)	—	Normal

Table summarizes data from multiple studies, usually small case series.

16

stroke. Since reduced blood flow is the primary event, SPECT rCBF studies become abnormal immediately and are only limited by the size and location of the affected area.

The clinical usefulness of SPECT rCBF to demonstrate early interruption in blood flow to the brain is still unclear as no obvious impact in terms of prognostic information or patient management has emerged. This situation may change if it can be shown to help guide patient selection for therapies such as thrombolysis. Successful lysis of blood clots obstructing cerebral blood vessels can dramatically improve post-stroke functional status if it is achieved in the first few hours. This benefit is partially offset by a significant risk of intracranial hemorrhage. This complication might be predicted by SPECT rCBF studies: the presence of large areas of profoundly decreased perfusion reveals tissue that has been submitted to severe ischemia, and in which vascular cells may have been irreversibly damaged. Reflow into such vessels is prone to intraparenchymal bleeding with a high rate of complications related to acutely increased intracranial pressure. Inclusion of SPECT rCBF studies in stroke protocols to evaluate suitability for thrombolysis will depend on clinical confirmation that it reliably predicts which patients are at increased risk of bleeding (Fig. 6). In theory, it should be easy to detect the large, severe decrease in tracer uptake that would portend a poor outcome.

Energy Metabolism and Neurotransmission Studies

Although still largely limited to research applications, direct measurement of energy metabolism and of specific binding of radioligands to a variety of molecular targets in the brain are emerging as potential clinical applications in neuropsychiatric nuclear medicine. As more agents aimed at specific molecular targets become available, nuclear medicine will be able to characterise brain metabolism and neurotransmission with ever greater precision, thereby shedding light not only on the mechanisms underlying the diseases studied but also contributing to the development of new therapies and allowing disease diagnosis through molecular characterisation.

Energy Metabolism Studies

Glucose Consumption

Cerebral metabolism is mainly assessed with the most frequently used radiopharmaceutical in PET, ^{18}F- fluorodeoxyglucose (FDG). This glucose analogue is transferred across the BBB and taken up by cellular glucose transporters (largely on the cell membranes of astrocytes). Once inside the cell, ^{18}F-FDG is phosphorylated to ^{18}F-FDG-6-PO_4 but cannot be further metabolised by the enzymes involved in glycolysis. As there is also very little phosphatase activity in the brain, the ^{18}F-FDG-6-PO_4 compound is "trapped" where it was initially taken up. Mathematical modeling of the combined imaging and arterial blood measurements allows calculation of the regional cerebral metabolic rate for glucose (rCMRGlu).

As with blood flow, ^{18}F-FDG uptake most closely parallels the distribution of glutamatergic transmission. ^{18}F-FDG PET studies also benefit from the much greater spatial resolution and quantitative capacities of PET as compared to SPECT. On the other hand, ^{18}F-FDG PET studies have low temporal resolution, since accumulation of the tracer in brain tissue must proceed for up to 45 minutes before acquisition can begin: the resulting data reflect the integrated activity of the brain over that period of time. This is not a problem when studying a disease or a
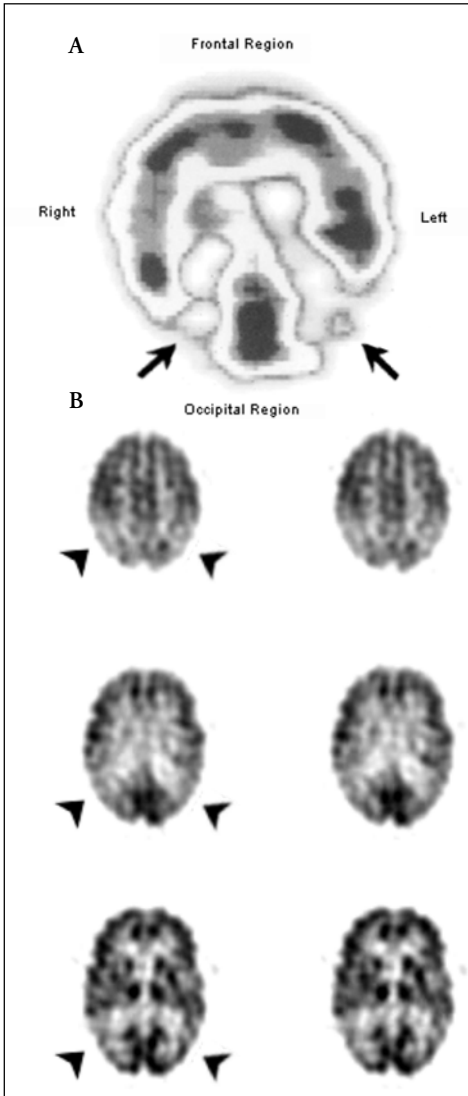
Figure 5. Alzheimer's disease. (A) SPECT brain perfusion in a patient presenting with dementia and moderate diffuse atrophy on CT scan. This single transaxial slice shows marked hypoperfusion bilaterally at the level of the parieto-occipital junctions (arrows). (B) ^{18}F-FDG PET study (transaxial images) showing marked symmetrical glucose hypometabolism in the posterior parieto-temporal cortex (arrowheads). (Case provided by Dr. D. Worsely.) These scan patterns are typical of Alzheimer's disease.
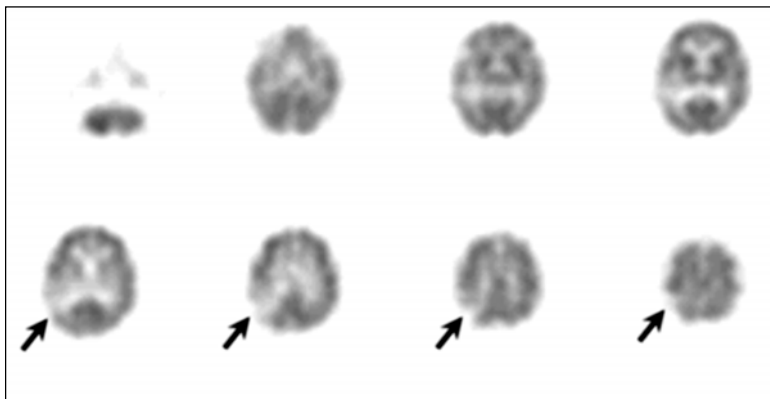
Figure 6. Thrombolysis assessment. Transaxial slice from patient with acute non-hemorrhagic infarction and a limited perfusion defect (arrows). Thrombolysis with tPA should be considered within 3 hours of symptom onset when the CT scan is normal. Large or multiple lesions are probably contraindications to thrombolysis due to an unacceptably high risk of hemorrhagic transformation. (Case provided by Dr. W.D. Leslie.)

phenomenon which is stable over such a time frame, but is obviously a drawback for activation studies where it is often difficult to perform a given task for such a long time.

Oxygen Consumption

Cerebral energy metabolism can also be assessed through measurements of molecular oxygen (O_2) consumption. Oxygen (as ^{15}O-O_2) is administered by inhalation and measurement of its accumulation is used to determine the regional cerebral metabolic rate for oxygen ($rCMRO_2$). This can aid in determining whether decreased rCBF results from a primary vascular problem (obstruction) or decreased metabolic demands (parenchymal dysfunction). By simultaneously measuring rCBF and $rCMRO_2$ it is possible to obtain an oxygen extraction fraction (OEF). A normal OEF signals a match between needs and supply, and implies parenchymal hypoactivity; an increase indicates abnormally decreased perfusion with neural tissue attempting to extract more oxygen from a decreased supply. One day this approach may help select patients for a cerebral revascularisation procedure.

Amino Acid Metabolism

Other metabolic studies can be performed with analogues of amino acids labelled with iodine-123 (SPECT), carbon-11 (PET) and fluorine-18 (PET). Most frequently these are derivatives of tyrosine, methionine and leucine. Usually used as markers of tumoral activity, these agents can also evaluate protein and neurotransmitter synthesis.

Clinical Applications

Excellent results have been obtained in studying epilepsy and the dementias (where results are even better than with SPECT perfusion studies) with ^{18}F-FDG PET imaging. It also can help guide biopsies, establish prognosis, evaluate recurrence of brain neoplasms, and differentiate residual masses from other conditions such as radiation necrosis (see section on Intracranial Mass Lesions). The high levels of cortical glycolysis normally observed can mask detection of low-grade brain tumors.

Studies of Neurotransmission

Nuclear medicine is still the *only* means for studying neurotransmission directly and non-invasively in vivo. A broad array of SPECT and PET tracers are available, including neuroreceptor ligands (generally antagonists), neurotransmitter metabolic precursors, ligands of plasma membrane and synaptic vesicle transporters, substrates of neurotransmitter catabolising enzymes and components of intracellular transduction chains (Fig. 7). PET has long dominated this landscape, but over the past ten years progress in the field of radiopharmacy has contributed many SPECT tracers.

Mathematical modeling of dynamic PET or SPECT acquisitions permits estimation of physiologically relevant parameters such as neuroreceptor densities for a large variety of chemically defined transmission systems, synthetic and catabolic enzymatic activities within those systems, numbers of neuronal terminals of a given nature, neurotransmitter concentrations in the synaptic cleft and even second messenger generation. Data acquired in these domains has revolutionised our understanding of neurologic and psychiatric diseases.

Clinical Applications

While very few clinical applications are presently established for neurotransmitter studies, their potential for growth is probably the greatest in all of neuropsychiatric nuclear medicine. One suggested use is in the monitoring of therapy for psychoses. "Classical" neuroleptics, such as the phenothiazines, block the D2-subtype of the dopamine receptors. These receptors exist in high concentration in the striatum and are intimately involved in regulation of motor activity. Excessive blockade (beyond 80-85%) of striatal D2 dopamine receptors has been associated with an increased risk of developing long term side effects such as tardive dyskinesia. The level of D2 blockade can be measured with both PET and SPECT ligands, and patients found to have excessive blockade may benefit from a lower dose of medication or from an atypical neuroleptic with minimal affinity for D2 receptors.

Predicting response to dopaminergic therapy in patients with a parkinsonian syndrome might also be possible. The striatal complement of D2 dopamine receptors is normal (or even increased through receptor up-regulation) in Parkinson's disease since the lesion resides in the nigro-striatal fibres (Fig. 8). In diseases such as progressive supranuclear palsy or syndromes producing primary striatal degeneration the D2 dopamine receptor concentration is reduced. The latter are not responsive to dopaminergic therapy since the defect is on the "receiving end" of the dopaminergic transmission process. This could be quite useful since even in specialised centres Parkinson's disease and parkinsonian syndromes are confused in up to 20% of patients.
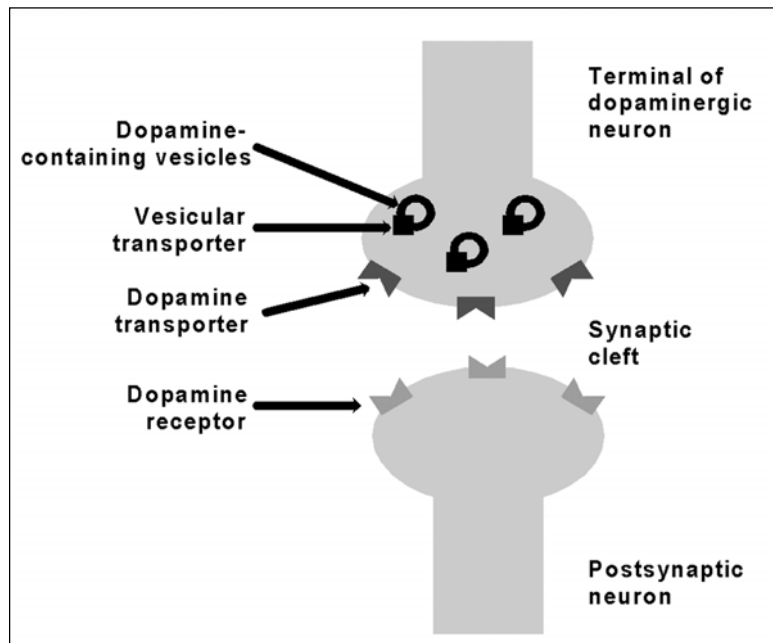
Figure 7. Simplified dopaminergic synapse. Dopamine (DA) is synthesized in the axon terminal, stored (via the vesicular transporter VMAT2) in secretory vesicles and released when an action potential depolarizes the terminal. Released DA diffuses toward the postsynaptic membrane where it can bind to a variety of DA receptors (5 subtypes have been cloned). DA can also bind to receptors on the presynaptic membrane (not illustrated), which modulate its synthesis and release. Some DA also diffuses out of the synapse and can act on non-synaptic DA receptors. Termination of DA action on receptors is brought about mostly by reputake into the axon terminal through the DA transporter for "repackaging" into secretory vesicles. Some DA undergoes enzymatic catabolism by MAO (intracellular) or COMT (synapse).

Cerebrospinal Fluid Assessment

Physiology

The ventriculo-subarachnoid system consists of two fluid compartments: the intracranial component occupies 140 ml (about 25 ml of which is intraventricular) and the spine is bathed with an additional 75 ml. Daily production of CSF reaches 500 ml, 90% of which is produced by the choroid plexi. The remainder comes from exudation through intraparenchymal vessels, reaching the subarachnoid space by diffusion along the spaces of Virchow-Robbins, and from extracellular fluid reaching the ventricular system across the highly permeable ependyma. Production is largely
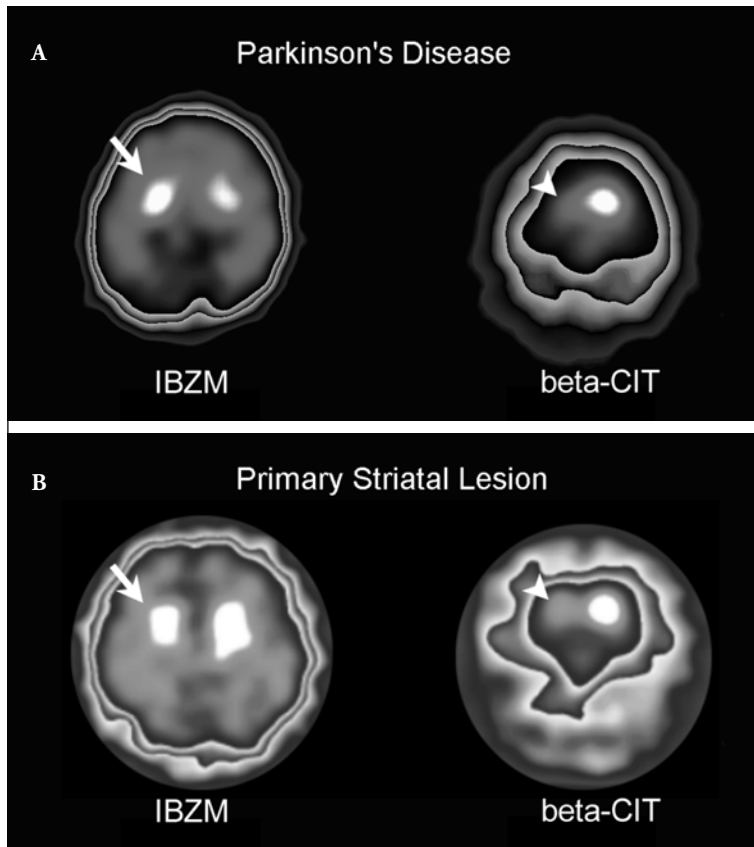
Figure 8. Abnormal dopamine neurotransmission in (A) idiopathic Parkinson's disease and (B) primary striatal lesion causing parkinsonism. Note the comparative uptake of tracers that bind to the dopamine D2 receptor (^{123}I-IBZM, left) and the dopamine transporter (^{123}I-beta-CIT, right). Both disorders demonstrate reduced dopamine transporter function by the right basal ganglion (arrowhead). In idiopathic Parkinson's disease there is increased uptake of IBZM (arrow) due to a combination of decreased dopamine release and D2 receptor up-regulation reflecting normal neostratum with loss of dopaminergic (nigro-striatal) input. In contrast, with a primary striatal lesion there is slightly decreased IBZM uptake (arrow).

independent of the pressure found within the ventriculo-subarachnoid space. Normally, CSF produced by the choroid plexi flows through the ventricular system to the fourth ventricle, where it exits the intracerebral spaces through the foramina of Luschka and Magendie. From there, some CSF descends into the perispinal subarachnoid spaces while the remainder enters the cisternae at the base of the brain and the cerebellum. Most of the CSF flows around and between the hemispheres, converging towards the superior sagittal sinus where it re-enters the circulation

through arachnoidal invaginations into the lumen of the sinus (called Paccionian granulations). A small portion of the CSF is reabsorbed across the arachnoid into blood vessels along the neuraxis. Progression of the CSF along these different paths is ensured by a pressure gradient between the production and resorption sites, vascular pulsations, and intracranial and intraspinal pressure waves of multifactorial origin.

Nuclear Cisternography

The circulation of the CSF can be studied with nuclear cisternography in which an inert radiotracer (usually ^{99m}Tc- or ^{111}In-DTPA) is injected into the lumbar subarachnoid space. Sequential scintigrams of the spine and head are obtained for 24-72 hours. A normal study shows rapid progression of radioactivity from the injection site towards the head, with intracranial activity noted anywhere between 1 and 3 hours post-administration. Activity progressively permeates all of the intracranial subarachnoid space without significant penetration into the ventricular system (though transient but minimal ventricular penetration is not unusual). By 24 hours, most of the activity should have been transferred to the superior sagittal sinus and excreted through the kidneys with most remaining intracranial activity superior to the cerebral convexities (Fig. 9).

Clinical Applications

Hydrocephalus

Since an increase in CSF pressure does not block its formation, CSF can accumulate intracranially with symptoms that vary depending on the speed at which the build-up occurs. For instance, malformations, hemorrhages or tumors in the posterior fossa can obstruct the egress of CSF from the ventricular system, giving rise to a condition known as non-communicating hydrocephalus (i.e., no communication between the ventricular system and subarachnoid space). More commonly, scinticisternography is performed for suspicion of communicating hydrocephalus. After such events as meningitis, subarachnoid hemorrhage or intracranial surgery, the subarachnoid space may become obstructed, impeding the normal flow of CSF. This situation can give rise to normal pressure hydrocephalus (NPH). The term NPH is a misnomer: by the time the disease comes to clinical attention spinal opening pressure may be normal because compensatory mechanisms have come into play to reduce intracranial pressure. Before this stage is reached, CSF pressure is probably periodically increased, resulting in ventricular dilatation. The "classic" clinical triad of NPH is dementia, gait disturbance and incontinence. The dementia is potentially reversible, and in a small number of carefully selected individuals there is a dramatic response to CSF shunting.

The major compensatory mechanism to NPH is a marked increase in transependymal passage of CSF into brain parenchyma. This is accompanied by an *inverted* flow of CSF from the subarachnoid space into the ventricles. This phenomenon is well depicted by scinticisternography, where marked ventricular activity will accumulate and persist for a sustained period of time. This pattern is considered confirmatory of the clinical diagnosis of NPH. Most neurologists do not recommend performing this test on a routine basis, reserving it for atypical cases that do not manifest the "classic" clinical presentation. It has been suggested that reflux of radioactivity into the ventricles that lasts for more than 24 hours indicates
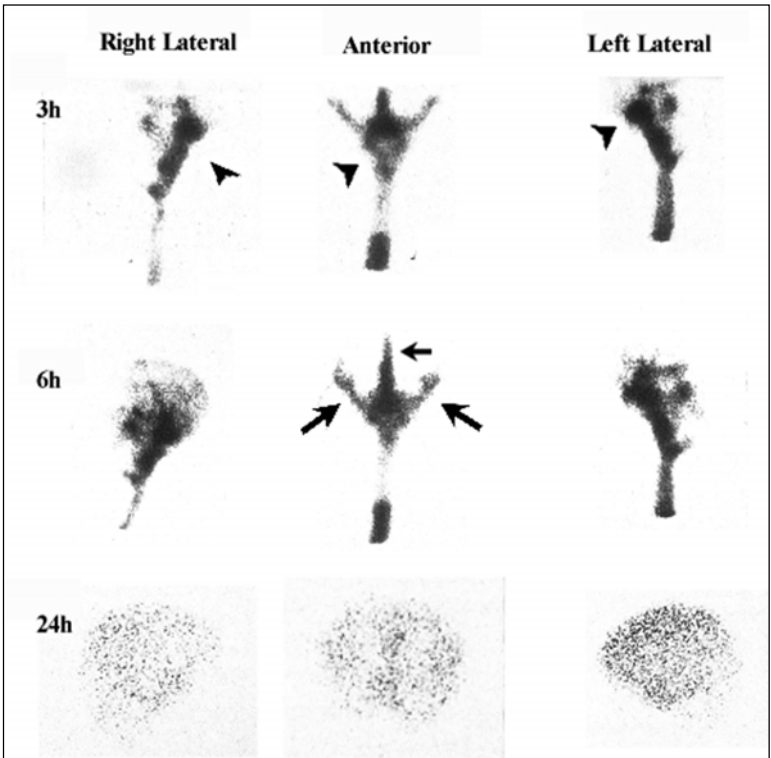
Figure 9. Normal radionuclide cisternography. ^{111}In-DTPA was injected into the lumbar subarachnoid space. Note initial activity within the extracerebral subarachnoid spaces and basal cisterns (arrowheads) which progresses to the Sylvian and interhemispheric fissures by 6 hours (arrows). By 24 hours resorption is almost complete. Normally the ventricular system is not visualized.

that compensatory reabsorption is not well established and that deterioration is likely (Fig. 10). This may indicate a better response to ventriculo-peritoneal shunting than when only transient reflux is observed, since the latter suggests a stabilised condition with established, nonreversible damage to the periventricular brain tissue. In fact, no test (including scinticisternography) is particularly successful at predicting the response to surgery, emphasizing the importance of recognizing the "typical" clinical presentation.

CSF Leaks

The second major indication for scinticisternography is in the identification of a CSF leak. Such leaks can occur after skull fractures, destructive infections or neoplasms, surgical interventions, and radiation therapy. This can lead to repeated
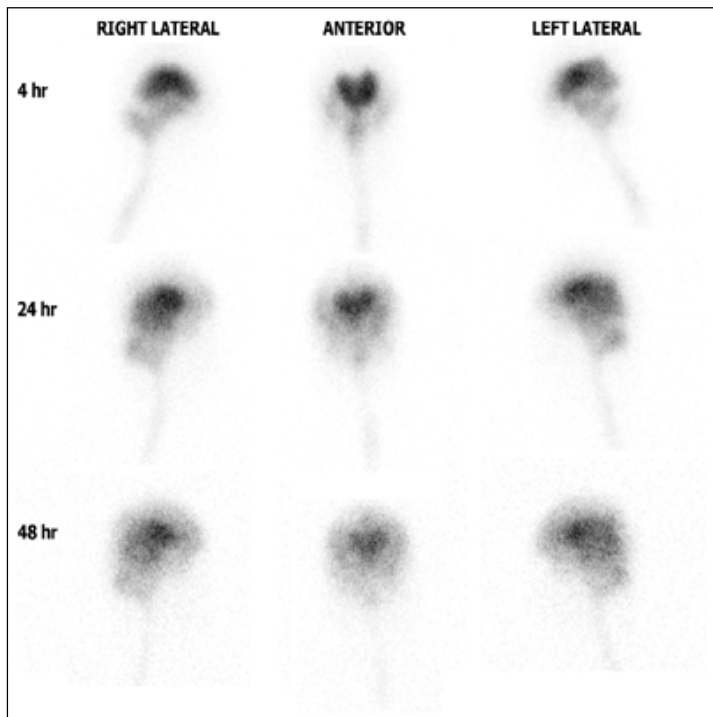
Figure 10. Normal pressure hydrocephalus (NPH). Radionuclide cisternography shows early, persistent ventricular penetration with absence of progression along the convexities indicating an obstructed sub-arachnoid space. (Case provided by Dr. W.D. Leslie.)

episodes of meningitis and requires surgical closure of the defect. Scinticisternography can confirm CSF leak by finding high levels of radioactivity in fluid draining from a craniofacial orifice (rhinorrhea or otorrhea). Identifying the anatomical origin often requires multiple projections and positioning of the head to increase the flow.

Intracranial Mass Lesions

The high sensitivity and superb anatomic resolution of conventional neuroimaging (CT and especially MRI) has relegated nuclear medicine methods to a secondary role in the evaluation of intracranial masses. Nuclear medicine's contribution is in characterizing the nature of a known mass lesion, and in well-defined conditions can narrow the differential diagnosis. Numerous reports have suggested that agents such as ^{18}F-FDG, thallium-201, ^{99m}Tc-sestamibi, ^{99m}Tc-tetrofosmin and pentavalent ^{99m}Tc-DMSA can detect primary intra-cranial tumours with sensitivities and specificities that are over 80%. Among these agents, ^{99m}Tc-labelled radiopharmaceuticals offer better spatial definition than thallium-201 and have some
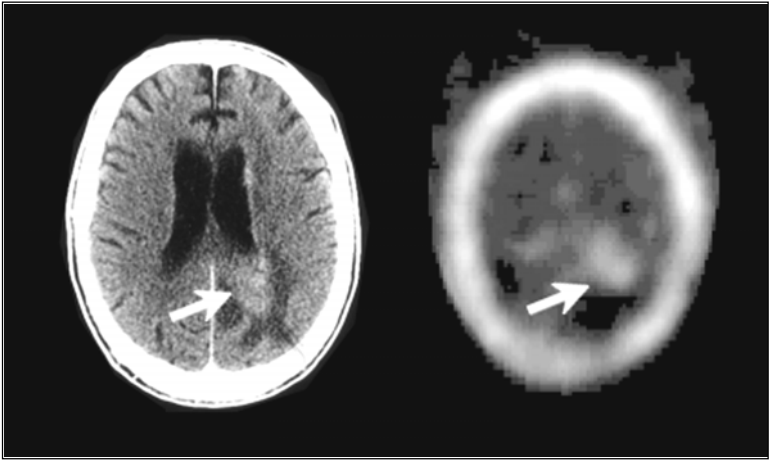
Figure 11. Brain mass lesion with ^{99m}Tc-sestamibi uptake. This 39 year old HIV positive man was admitted to hospital with dyspnea and fever in association with *Staphylococcus aureus* bacteremia and then developed new-onset seizures. A CT scan (left) showed an enhancing mass lesion in the periventricular white matter of the left parietal-occipital lobe (arrow) measuring approximately 3 cm in diameter with peritumoral edema. The radiologic fetaures were most consistent with CNS lymphoma, with toxoplasmosis considered a less likely alternative. SPECT sestamibi brain scanning (right) confirmed increased uptake in the lesion (arrow) further supporting a diagnosis of lymphoma which is almost uniformly sestamibi-avid while toxoplasmosis is usually negative. (Case provided by Dr. W.D. Leslie.)

differences in their distribution (for example, ^{99m}Tc-sestamibi normally shows intense pituitary and choroid plexus uptake).

Mass Lesions in AIDS

One established indication is in the differential diagnosis of infectious and neoplastic lesions in immunosupressed subjects with AIDS. Most neoplastic lesions will take up the agents listed above (Fig. 11), while most infectious causes such as toxoplasmosis will not (Fig. 12). The CT and MRI appearance of primary CNS lymphoma and toxoplasmosis can be indistinguishable, but therapy is radically different.

Radiation Necrosis

These radiopharmaceuticals can also distinguish radiation necrosis and tumour persistence or recurrence in areas shown to be abnormal by CT or MRI. Usually radiation necrosis shows little or no tracer uptake, though rare cases have been described with elevated uptake.

16
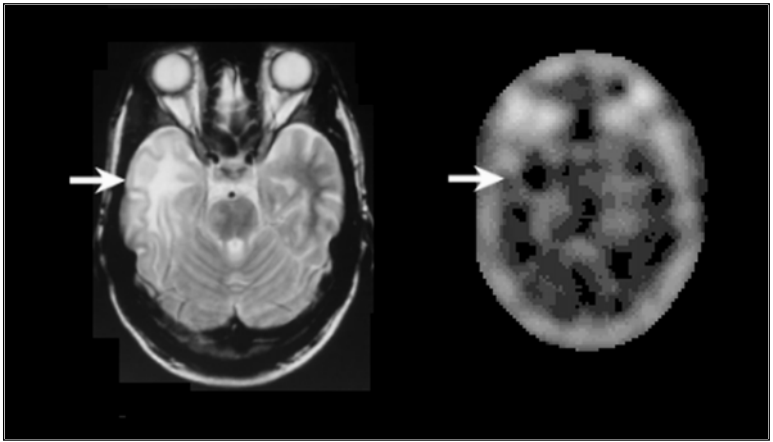
Figure 12. Brain mass lesion without ^{99m}Tc-sestamibi uptake. This 28 year old man with HIV (CD4 count only 6) presented to hospital with a two week history of gradually progressive left-sided weakness (arm worse than leg) and left homonymous hemianopsia. The patient had declined anti-retroviral therapy, with the result that he had numerous infectious complications from HIV. A CT scan showed decreased attenuation in the right temporal lobe white matter without contrast enhancement, hemorrhage or significant mass effect. An MRI scan (left) showed extensive white matter changes in the right temporal lobe extendng into the right internal and external capsule, the right frontal lobe, the right midbrain and the right cerebellar peduncle. There was no evidence of gadolinium enhancement or mass effect. Differential diagnosis was felt to be most likely progressive multi-focal leukoencepholopathy or non-enhancing lymphoma. Brain SPECT (right) was performed with ^{99m}Tc-sestamibi and failed to show any uptake (arrow). This is strong evidence against CNS lymphoma which is typically strongly avid for flow tracers such as sestamibi and thallium. PML is more variable in its appearance, since it can show absent or increased uptake, but is strongly supported by the absence of uptake in this case. The patient's clinical condition deteriorated and he died with a tentative diagnosis of PML without a post-mortem examination. (Case provided by Dr. W.D. Leslie.)

Tumor Grading

PET and SPECT imaging with ^{18}F-FDG, thallium-201, ^{99m}Tc-sestamibi or ^{99m}Tc-tetrofosmin also seem to offer prognostic information on the behaviour of brain tumours Those with the highest uptake tend to have a higher grade and more aggressive behavior. Early imaging after the initiation of therapy has been reported to be a good predictor of the final therapeutic response, and PET/SPECT is superior to CT or MRI for this purpose.

Somatostatin Receptors

Finally, ^{111}In- or ^{99m}Tc-pentetreotide, somatostatin analogues used essentially for the diagnosis of neuroendocrine tumours, can be taken up by the somatostatin receptors found on the cells of gliomas, glioblastomas, meningiomas and possibly schwannomas. These agent cannot cross the intact BBB and will not detect lesions
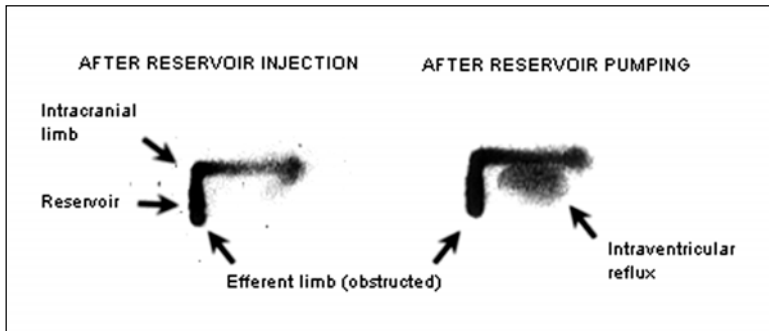
Figure 13. Ventriculo-peritoneal shuntogram. ⁹⁹ᵐTc-MAA was injected into the subcutaneous reservoir. Immeditae passage into the intracanial tube is observed with reflux of activity into the ventricles after pumping of the reservoir. No activity is seen in the efferent limb immediately inferior to the reservoir indicating distal obstruction at the level of the reservoir valve.

with somatostatin receptors that do not disturb the BBB, such as low-grade gliomas. Tumours which are outside of the BBB, such as meningiomas, consistently concentrate the tracer.

Conclusions

The full scope of nuclear medicine's role in the clinical evaluation of brain disorders is still evolving. Some applications have emerged as clearly useful, but others must be used in a prudent manner until there is additional documentation of their efficacy. Research in psychiatry, neurology and nuclear imaging should help us to characterise diseases affecting the human brain at their most fundamental, molecular level. Nuclear medicine imaging techniques are uniquely suited to the *in vivo*, non invasive measurement of such parameters. Neuropsychiatric nuclear medicine is probably at the threshold of an explosion in its clinical use.

Frequently Asked Questions (FAQs)

What is a "shuntogram"?

A "shuntogram" is a nuclear medicine procedure used in patients who have previously had a ventriculo-peritoneal or venticulo-atrial shunt inserted. The tubing may become obstructed at different levels (intracranial segment, extracranial subcutaneous tubing, reservoir, reservoir exit valve, or subcutaneous tubing to the peritoneal cavity or left atrium). It is simple to inject radioactive tracer directly into the reservoir and then follow its migration. Depending upon shunt design, the reservoir may optionally be "pumped" to facilitate CSF movement. The pattern of CSF flow can be used to deduce the site of obstruction, if any (Fig. 13).

How is a "brain death" study done and what is its accuracy?

The development and evolution of the concept of brain death has been necessary due to our technologic advances in medical care and organ transplantation. The
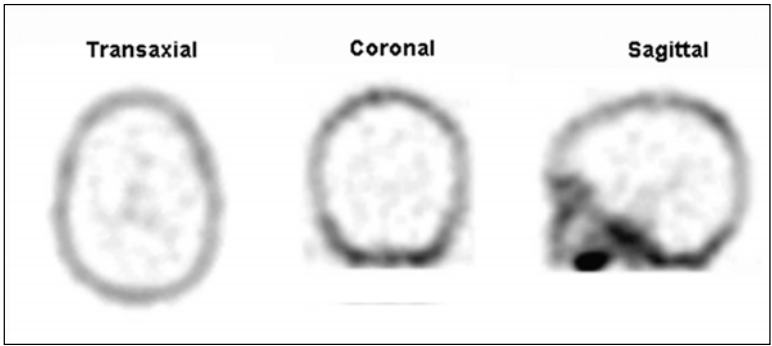
Figure 14. Brain death. This young woman sustained anoxic brain injury while recovering from emeregency surgical replacement of a mitral valve prosthesis infected with *Staphylococcus aureus*. Cardiorespiratory arrest led to 18 minutes of anoxia before circulation could be restored and she remained in a comatose state. Neurological assessment of brain stem function strongly suggested brain death, but a confirmatory test was requested before discontinuation of support. The patient was injected with 99mTc-ECD in the intensive care unit and scanned in Nuclear Medicine shortly thereafter. The scan demonstrates only scalp and facial flow with an "empty skull". There is absent perfusion of the cerebral cortex and brain stem. (Case provided by Dr. W.D. Leslie.)

current definition of brain death describes the clinical state of totally absent central nervous system function in a hemodynamically stable, normothermic, nonintoxicated patient, which is followed inevitably by cardiovascular collapse. Diagnosis is based on coma, absent brain stem reflexes, and apnea (despite a documented pCO2 of > 60 mm Hg), with selective use of confirmatory testing. Under normal conditions, the presence of an electrocerebrally inactive EEG is a valid indicator of brain death. However, in some situations (such as in the presence of high doses of sedative/hypnotic medications), the EEG can be unreliable. Complete cessation of cerebral perfusion as demonstrated by brain scintigraphy, transcranial Doppler sonography, or cerebral pananangiography is also evidence of brain death. Contrast angiography is least desirable since it is invasive and the contrast exposure can threaten subsequent organ harvesting. Numerous studies confirm the reliability of brain scintigraphy in the diagnosis of brain death. The great majority of patients (98.5% in one large series) judged to be brain dead by other criteria show absent brain blood flow ("empty skull") on "conventional" radionuclide angiography or rCBF imaging (Fig. 14). Even if an initial examination shows some preserved blood flow, a repeat study 72 hours later is usually diagnostic. There are no reported cases of neurological recovery following a definite scintigraphic diagnosis of brain death.

Can rCBF studies be used in brain activation studies?

Activation studies involve having the patient use the function being studied while changes in rCBF are measured as a marker of the structures being activated or inhibited. The design of such protocols is a highly specialised field calling for close collaboration between imaging specialists, statisticians, and clinical scientists from
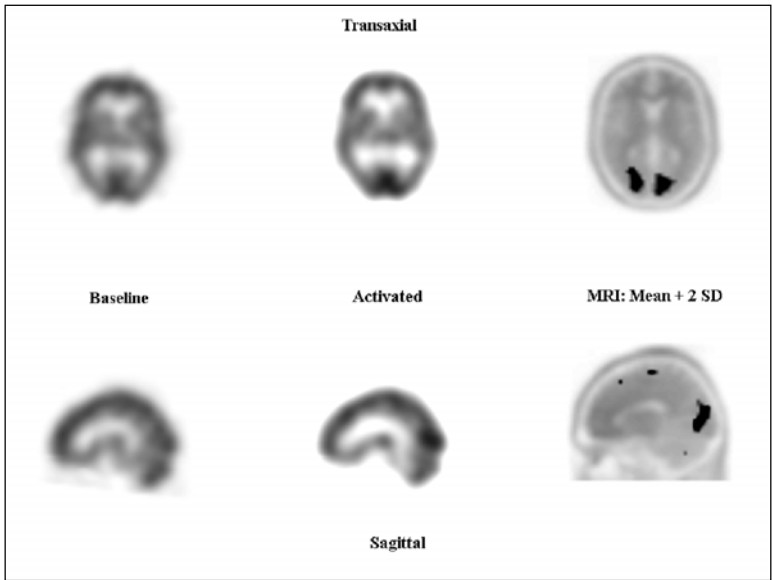
Figure 15. Activation study. Baseline 99mTc-ECD SPECT scans were obtained at rest with eyes closed. The patient was then exposed to bright, colored, rapidly moving geometric shapes for 10 seconds prior to and for 3 minutes after a second injection of 99mTc-ECD. Statistical maps were obtained after spatially coregistering the studies, subtracting the baseline from the activation study and superimposing activated voxels (subtraction value more than 2 SD over the mean) on an MRI atlas. Note intense activation of calcarine visual cortex regions.

neurology, psychiatry and psychology. Presently, fMRI, by virtue of its high temporal and spatial resolutions, is considered by many to be the tool of choice for such studies, and in large measure has displaced PET for this purpose. However, SPECT with either 99mTc-HMPAO or 99mTc-ECD, has an advantage over both of these methods: as these radiopharmaceuticals "capture" the distribution of cerebral blood flow at the time of injection and allow for delayed imaging, the patient can undergo complex activation protocols using instrumentation that either cannot be brought close to the powerful magnetic field of a fMRI scanner or that cannot be physically accommodated by PET or fMRI systems. In SPECT, the subject can be prepared with a simple intravenous line and then submitted to the activation protocols during which she/he is injected with the radiopharmaceutical at the moment of maximal stimulation of the structures involved in the task (Fig. 15). Later, after completion of other measurements, the patient can be brought to the imaging laboratory for the acquisition phase of the study. SPECT rCBF is the only non-invasive approach capable of this type of intervention.

Additional Reading

1. Talbot PR, Lloyd JJ, Snowden JS, Neary D, Testa HJ. A clinical role for [99mTc]-HMPAO SPECT in the investigation of dementia ? J Neurol Neurosurg Psychiatry 1998; 64:306-313.
    A well written paper proposing a framework within which rCBF studies could be used in the evaluation of dementia.

2. Assessment of brain SPECT—Report of the Therapeutics and Technology Assessment Subcommittee of the American Academy of Neurology. Neurology 1996; 46:278-285.
    A "must read" reference despite its publication date: it covers all of the present and foreseeable indications of rCBF studies.

3. Alexandrov AV, Masdeu JC, Devous MD, Black SE, Grotta JC. Brain single-photon emission CT with HMPAO and safety of thrombolytic therapy in acute ischemic stroke. Stroke 1997; 28:1830-1834.
    This paper describes what could possibly be one of the most important indications for rCBF studies in the coming years, and provides a good basis for standardizing interpretation.

4. Sperling RA, Sandson TA, Johnson KA. Functional imaging in Alzheimer's disease. In: Scinto LFM, Daffner KR, eds. Early Diagnosis of Alzheimer's Disease. Totowa: Humana Press, Inc., 2000.
    A very up-to-date review of the field.

5. Juni JE, Waxman AD, Devous MD, Sr., Tikofsky RS, Ichise M, Van Heertum RL et al. Procedure guideline for brain perfusion SPECT using technetium-99m radiopharmaceuticals. J Nucl Med 1998; 39:923-926.
    The "official" basic technique. A useful introduction but like every recipe, variations based upon experience will enrich it.

6. Devous MD, Thisted RA, Morgan GF, Leroy RF, Rowe CC. SPECT brain imaging in epilepsy: A meta-analysis. J Nucl Med 1998; 39:285-293.
    A very strong paper that makes it clear why the previous paper endorsed rCBF studies for epileptic focus localization.

16

Pediatric Nuclear Medicine

David Gilday

Introduction

Nuclear medicine studies have an important role to play in the diagnosis, treatment and follow-up of several pediatric conditions and the use of radiopharmaceuticals for diagnostic testing in children is increasing. Although general imaging principles are reviewed in the related "adult" chapters, special technical challenges and a very different spectrum of disorders warrant a separate discussion for children. This chapters highlights selected clinical problems in pediatric nuclear medicine.

Technical Considerations

Environment

When examining children, consideration must be given to patient motion, fear, and parental involvement. The study and approach to the exam must be tailored to the child's problem.

Children are much more aware than is generally appreciated—and thus the goal should be to provide a quiet and friendly environment. The staff should behave in a calm, relaxed manner with a kind, confident and sympathetic approach towards the child. Each study done should be designed to minimize the length of time the child must lie still. Therefore, long dynamic studies such as gastric emptying and transit studies are modified to sequential static images allowing the child to move between images.

All children old enough to comprehend (usually about age three) should have their procedure explained to them in simple words appropriate to their level of understanding. It is also important to gain the parent's cooperation as the parent's attitude can positively or negatively influence their child. Positive aspects of the study should be emphasized, negative aspects minimized. However, it is crucial never to mislead the child about what is about to happen. A child's trust in the staff may be difficult to obtain; once gained it is easily jeopardized. The most valuable distracter is a television, a VCR and a good video. Soothers and sticker awards for being injected all help to make it easier to get a first class result.

Parents should be present unless the procedure requires a sterile field. It has been our experience that with well-trained staff and cooperative parental involvement, it is rare that there is a problem with the study. Occasionally, a child may be a disciplinary problem and is more uncooperative when a parent is present. In these circumstances we ask that the parent stay in the waiting room.

Careful restraint is frequently necessary in the younger patient but should be used in moderation. The goal is to prevent motion as well as an accidental fall from

an imaging stretcher or couch. Children are best immobilized with restrainers strapped around the stretcher top using Velcro straps.

Sedation

If moderate restraint is not successful then sedation is required for a technically satisfactory study. This is especially true for lengthy procedures such as SPECT or whole body imaging. Sedation is recommended in overly anxious patients who refuse to cooperate, very young or hyperactive patients who are unable to remain still, and retarded patients who lack the mental capacity to follow simple instructions.

Sedation may take several forms. In the correct setting, sedation with intravenous pentobarbital sodium (Nembutal®) is very effective. Using a dose of 5 mg kg^{-1} (to a maximum of 100 mg), we administer half the volume rapidly, wait 60 seconds and then administer a quarter of the dose. This usually puts the child to sleep in about two to three minutes. If not, the remaining quarter dose is given. The child remains asleep for about 45-60 minutes. The advantages of this technique are that the child falls asleep very quickly, the effect is more reliable than with intramuscular injection, and the child recovers faster. As with all sedatives, cardiac and respiratory status must be closely monitored by appropriately trained individuals. We currently use an automated pulse oximeter.

Pentobarbital is contraindicated in neonates less than 2 months of age. This group lacks adequate levels of the liver enzymes required to metabolize pentobarbital. In place of pentobarbital we use an elixir of promethazine (Phenergan®) and chloral hydrate administered 30-45 minutes before scanning. While the effect is less pronounced than with pentobarbital, it is usually adequate and the patient arouses readily. Midazolam (Versed®) orally is useful in some cases.

Diazepam (Valium®) and pentobarbital suppositories have all been found to be inadequate. None produces the deep sleep required to perform nuclear medicine procedures on the patient.

Injection Techniques

Radiopharmaceutical injection in small children presents several minor difficulties, all of which are easily overcome by modifying adult techniques. Children may be completely covered by the head of a large field of view camera. This increases the child's anxiety and makes injection difficult. This is resolved by placing the child supine on the gantry or stretcher top and having the camera underneath. In smaller children, for head, feet or hand imaging, holding the child directly on the camera collimator is a very good technique.

Finding a suitable vein for intravenous injections is rarely a problem. Although the antecubital fossa frequently has the largest vein, the elbow is less easily immobilized than the hand or foot which are the preferred injection sites. With procedures requiring repeated blood samplings (e.g., GFR determination), the insertion of an intravenous catheter is the best approach.

Radiopharmaceutical Dosage

The amount of radioactivity administered can be readily calculated by referring to a chart, using body surface area estimated from the patient's weight and height. The percentage of the standard adult dose is then determined according to the patient's

body surface area. This dose calculation is preferred to using weight alone since it results in equal tracer concentration per unit area of planar organ imaging.

It is very important to establish a minimum dose for each radiopharmaceutical. To get an adequate study, especially a dynamic one, there have to be enough photons detected to adequately assess the patient's problem. It is better to accept a slightly higher delivered radiation dose than to have an uninterpretable study. This is especially true in children where one wants the imaging time to be as short as possible in order to avoid motion. The risk of the higher radiation dose is negligible, especially if we have contributed to an accurate diagnosis.

Image Evaluation

It is mandatory to view all images on the imaging workstation using its windowing capability. In musculoskeletal imaging, it is very important to see the physes (growth plates) clearly as well as the diaphyseal long bones which can only be properly performed with multiple window level settings. Reviewing a dynamic study on the workstation is valuable. For example, in voiding cystography a "whiff" of reflux not apparent on hard copy is easily appreciated on the monitor display.

Clinical Role in the Assessment of Childhood Musculoskeletal Disorders

In benign bone diseases the two major indications for nuclear imaging are pain and fever/infection. Plain film examination should be carried out first. Frequently, CT is done to detect and characterize a lesion. The usual bone scanning technique is to acquire blood pool images and static or SPECT images of the areas of clinical interest. The highest resolution system available is used to obtain the best quality images in small children and infants. Magnification with converging or pinhole collimation is frequently used.

Osteomyelitis

The child with osteomyelitis may present with joint pain or tenderness, limited range of motion, soft tissue swelling, erythema, fever or bacteremia. Differentiation of osteomyelitis from cellulitis or septic arthritis may be difficult clinically, and unfortunately, the plain film examination is often non-diagnostic. Frank radiographic bone changes of osteomyelitis are rarely seen due to early diagnosis and treatment. The combined use of blood pool and bone scintigraphy makes it possible to differentiate osteomyelitis from cellulitis.

The typical appearance of osteomyelitis is a well-defined focus of increased bone metabolism associated with an identical area of hyperemia in the blood pool images (Fig. 1). This is most often located in the metaphysis of a long bone. Occasionally other bones are involved, especially if a puncture wound has occurred. This appearance is specific for osteomyelitis and is readily differentiated from the patterns of cellulitis and septic arthritis. However there is some evidence that the technique has less sensitivity in infants of less than 44 weeks gestational age.

The hyperemia involving the metaphysis of the long bone is usually seen between 24 and 36 hours after the onset of symptoms, whereas bone scintigraphy usually becomes positive between 36 and 72 hours. If the findings are not typical of osteomyelitis then gallium imaging is used to determine whether or not infection is present (Fig. 2).

17
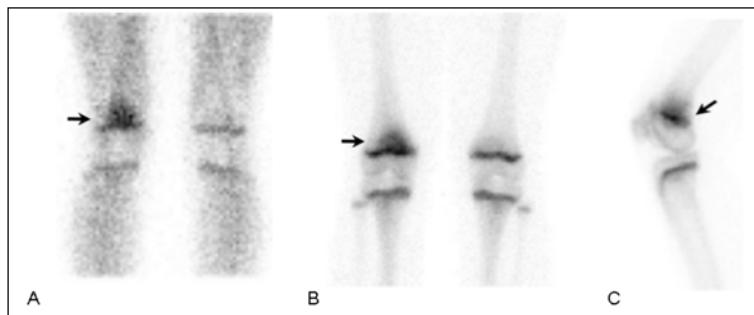
Figure 1. Acute osteomyelitis. (A) Anterior blood pool of the knees, (B) delayed anterior bone scan of the knees and (C) delayed medial bone scan of the right knee following injection with ^{99m}Tc-MDP. There is increased blood pool activity and delayed uptake in the metaphysis of the right femur (arrows). Note the loss of demarcation of the physis and the metaphysis. The location and appearance of the abnormality are typical of acute osteomyelitis.

Cellulitis

Cellulitis has a distinctive appearance, which is a diffuse increase in radioactivity involving both the soft tissues and the bone. This is more readily apparent in the blood pool images than in the bone images. The appearance is due to a diffuse soft tissue hyperemia and is readily distinguished from the appearance described above for osteomyelitis (Fig. 3).

Septic Arthritis

Septic arthritis has a similar appearance to that described for cellulitis but the hyperemia involves both sides of the joint. Subchondral bone on either side of the affected joint has marked increased metabolism. These investigations are usually carried out in conjunction with ultrasound which is very sensitive for detecting the effusions associated with septic arthritis. The two studies should be interpreted together.

Legg-Perthes' Disease

Avascular necrosis of the femoral head (i.e.., Legg-Perthes' disease) is usually detected radiologically. In those patients where the radiographs are normal or show mild capsular distention, the use of MRI has become the main means of evaluating the hip. Bone scintigraphy can be used either as an adjunct to determine degree of viability or to detect avascular necrosis in the presence of an inconclusive MRI study. Bone scintigraphy, especially when using pinhole magnification, remains an excellent technique for detecting avascularity of the femoral capital epiphysis (Fig. 4).

Non-Accidental Trauma

Our socio-medico-legal system has developed an enlightened sensitivity to child abuse. The estimated incidence of reported child abuse has increased from 30/1000 in 1985 to 45/1000 in 1992. The incidence of skeletal injury in these children is approximately 20% and is more common among those under 1 year of age. Fractures
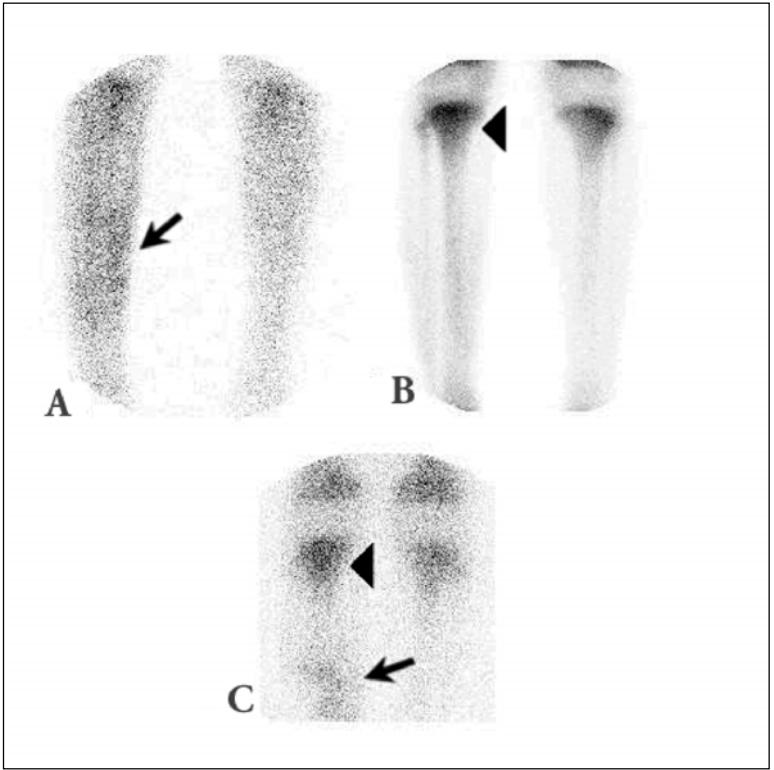
Figure 2. Cellulitis and early osteomyelitis. (A) Blood pool image, (B) delayed bone scan image and (C) gallium image. There is increased blood pool activity and increased gallium uptake (arrows) in the right mid-leg. While on the delayed bone scan image, mild diffusely increased activity is present in the right mid-tibia related to the adjacent soft tissue inflammation, there is a focal abnormality suggestive of osteomyelitis in the right proximal tibial metaphysis that also has increased gallium accumulation (arrowheads). Osteomyelitis was confirmed by aspiration.

are usually multiple, involving the long bones, skull, vertebrae, ribs, and facial bones, and usually show different stages of healing. In most pediatric hospitals, the approach is to radiograph the clinically affected body parts. If the suspicion of child abuse arises then a total body radiographic examination is done. After this a total body bone scan is performed to locate any unsuspected bony injuries. Metaphyseal-epiphyseal injury is common. Careful positioning and correct window-level settings are important to avoid the pitfall of "blooming" in the image, which may obscure a mild abnormality. Accurate interpretation will depend on assessment of the intensity and shape of the abnormality. Prime sites of investigation are the ribs, costovertebral junctions, spine, and diaphyses of long bones (Fig. 5). If the bone scan is normal 3 days or more after injury, then the probability of bony injury is very low. Disadvantages
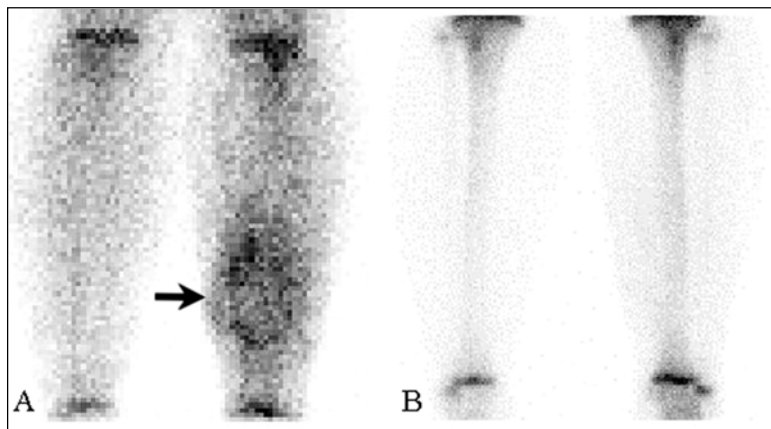
Figure 3. Pneumococcal cellulitis after trauma from a hockey puck. (A) Blood pool image and (B) delayed bone scan of the lower legs. Increased blood pool activity is seen (arrow). While there is mild diffusely increased uptake in the left tibia, no focal area of increased uptake is seen.

of the bone scan include: inability to determine the type, extent, and age of each injury; poor bone accumulation of the ^{99m}Tc-MDP in cases of severe malnutrition; and inability to differentiate systemic and metabolic disorders associated with trauma from trauma alone.

If one or more areas are found to be abnormal then high detail, multiple view radiography is performed to confirm the abnormality and to help date it. With greater recognition of this problem, more studies are being performed. Skull radiography is best performed to detect trauma to the calvarium, as the detection of fractures of the flat bones of the skull by bone scan is very poor.

Clinical Role in Childhood Malignancies

Osteogenic Sarcoma

Osteogenic sarcomas usually occur in the metaphyses of long bones, a common site being the distal femur or proximal tibia. The common age range is from 10 to 17 years. Occasionally, several sites may be involved at the time of presentation. The plain film always is abnormal but the appearance can mimic other diseases such as chronic osteomyelitis.

Untreated osteogenic sarcoma has a typical bone scan appearance. It demonstrates an uneven intensely increased distribution of tracer in the metaphysis. The blood pool image shows increased blood volume within the tumor. The flow study however has a markedly increased blood flow when compared to what would be expected from the blood pool image. This is due to the presence of arteriovenous connections with direct arteriovenous shunting (Fig. 6).

17
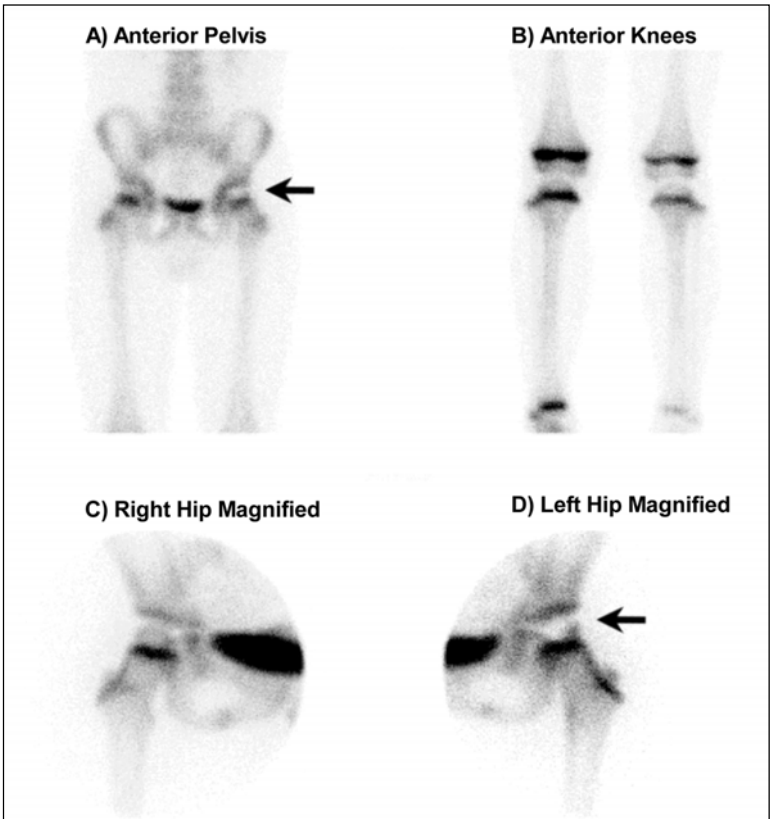
Figure 4. Legg-Perthes' disease. The left femoral capital epiphysis is photopenic centrally with revitalizing evidence laterally (arrows). This is the classical appearance of recovering Legg-Perthes' disease. Note the dramatic decrease in activity of the rest of the left leg due to disuse atrophy. X-rays done two months later showed a small dense femoral capital epiphysis typical of Legg-Perthes' disease.

The use of bone scanning in the follow-up of the primary tumor is limited since the scan remains positive because of ongoing bone remodeling. There is a good correlation however between the initial uptake of thallium-201 or ^{99m}Tc-sestamibi and the histological response to treatment. A reduction in thallium or sestamibi uptake after treatment indicates a response to chemotherapy.

Recently, there have been attempts to predict the response to chemotherapy by measuring the washout of ^{99m}Tc-sestamibi from the tumour. P-glycoprotein is present in cell membranes and protects cells from a variety of chemotherapeutic drugs by facilitating their washout from the cell. Those tumor cells with a high level of P-glycoprotein will be protected from the accumulation of chemotherapeutic agents.
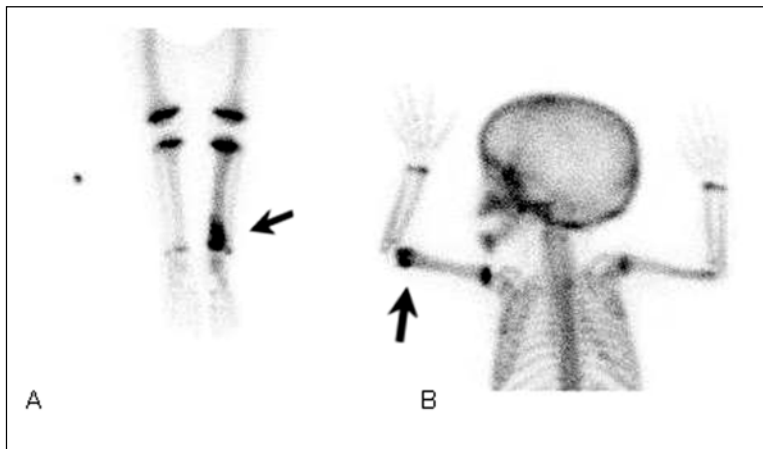
Figure 5. Non-accidental trauma. (A) Anterior bone scan of the legs with (B) posterior view of the upper body. The child refused to move the left leg. Intense uptake related to a fracture of the distal left tibia is readily seen (A, arrow). An unexpected fractue of the distal left humerus was also detected (B, arrow).

$99m$Tc-sestamibi washout is also facilitated by P-glycoprotein and hence the measurement of $99m$Tc-sestamibi washout during the three hours after injection can provide an index of P-glycoprotein levels and the likelihood of multiple drug resistance.

Lymphoma

Gallium scanning has replaced bone scanning in the evaluation of children with lymphomas (Fig. 7). Bone scanning has no place in the evaluation of childhood lymphoma unless it is being used to evaluate an orthopedic problem. Hodgkin's lymphoma, non-Hodgkin's lymphoma and Burkitt's lymphoma are all quite gallium-avid in children. Both the presenting sites, as well as metastases, are readily identified. A 72 hour scan, performed after laxatives to clear normally excreted bowel activity, usually shows any involvement of abdominal nodes. SPECT can be added to better depict lesions in the abdomen when colonic activity is present.

Neuroblastoma

Neuroblastoma is the commonest non-CNS tumor in childhood and frequently metastasizes to bone. Bone scans are more sensitive than radiographic skeletal surveys and, therefore, should be the primary investigation. Multiple foci of increased activity in the metaphyses of long bones are commonly seen, and involvement of the skull, vertebrae, ribs, pelvis, and long bones may also occur. Symmetric metaphyseal involvement is a frequent but subtle abnormality, especially around the knees and involving both femora and tibiae (Fig. 8). The physis is normally slightly elliptical in infants under 18 months of age and is plate-like in older children. The metaphyseal border is always well demarcated. When the physeal activity is wedge-shaped or
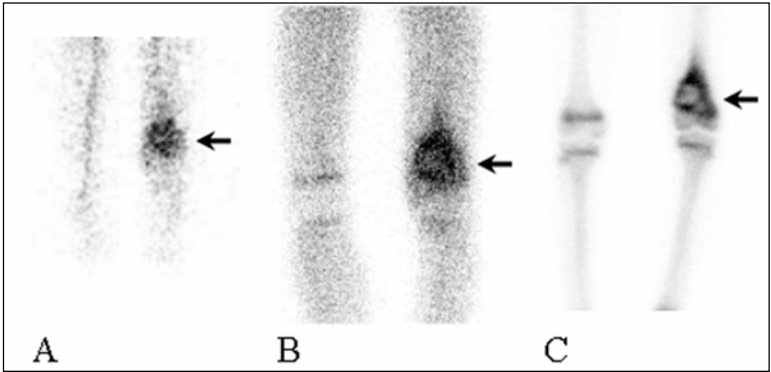
Figure 6. Osteogenic sarcoma. (A) Anterior flow image, (B) anterior blood pool image and (C) anterior delayed bone scan of the knees. Arrows show site of involvement in left distal femur. The blood pool and bone scan images both have decreased activity centrally at the site of the increased flow on the frame from the radionuclide angiogram. This indicates arteriovenous shunting in the core of the rapidly growing sarcoma which is typical of osteogenic sarcoma. The blood pool image does not capture the shunting but does reflect the bone repair in response to the tumor.

globular, or if there is blurring of the metaphyseal border, metastasis should be suspected even if the involvement is symmetric.

The primary tumor accumulates bone scanning materials such as ^{99m}Tc-MDP in 50%-70% of cases (Fig. 9). When the primary tumor is intra-abdominal, renal abnormalities such as nonfunction, obstruction, or inferior and/or lateral displacement are commonly seen. Blood pool and sequential renal scans should be performed during the first 15 minutes after ^{99m}Tc-MDP injection in any child suspected of having neuroblastoma or abdominal tumor.

Metaiodobenzylguanidine (MIBG) is an analog of guanethidine and is taken up by a variety of tumors of neural crest origin including neuroblastoma. ^{131}I-MIBG was first introduced in 1983, but has subsequently been replaced by ^{123}I-MIBG because of the better imaging characteristics of iodine-123. ^{123}I-MIBG is effective in detecting soft tissue or marrow neuroblastoma lesions (Fig. 8). MIBG will also detect most but not all bony lesions. In view of the inability of ^{123}I-MIBG scanning to detect all bony metastases, children with a diagnosis of neuroblastoma must have both ^{123}I-MIBG and bone scanning to stage and monitor their disease.

Clinical Role in Neonatal jaundice

One of the more difficult but rewarding investigations in pediatrics is the evaluation of neonatal jaundice. The problem of differentiating neonatal hepatitis from biliary atresia is extremely difficult to achieve with complete reliability. In neonates with biliary atresia, there is good tracer extraction in the first 60 minutes (extraction fraction usually in excess of 85%) but none is excreted into the duodenum. At twenty-four hours no radiotracer is seen in the bowel (Fig. 10). However, with

17

Figure 7. Lymphoma. Anterior (left) and posterior (right) whole body gallium scans showing abnormal uptake in both hila (arrowheads). There is normal accumulation in the skeleton, liver and lacrimal glands.

neonatal hepatitis there is typically reduced hepatic extraction and delayed clearance with radiotracer appearing in the bowel within 24 hours. We have found that although no neonate with biliary atresia will excrete the radiotracer, a significant number of babies with neonatal hepatitis will also show no excretion. Therefore, while the
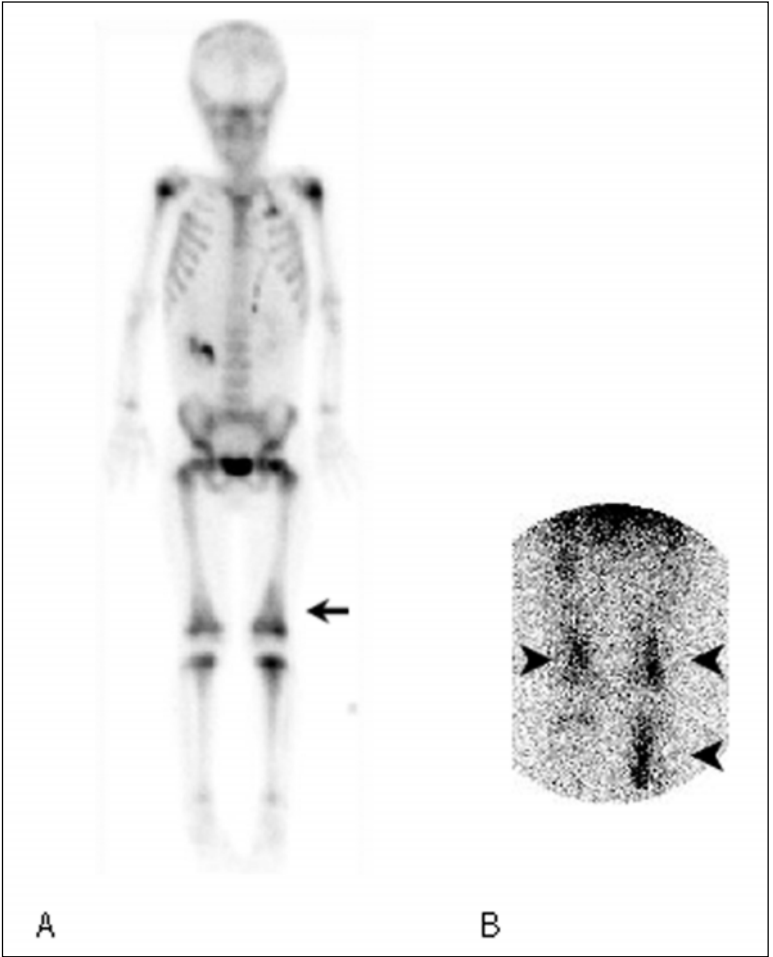
Figure 8. Neuroblastoma. (A) 99mTc-MDP whole body bone scan and (B) 123I-MIBG images of the knees. On the bone scan, abnormal uptake is particularly evident in the long bones where increased metaphyeal uptake (arrow) causes loss of definition of the physis. While the bone scan reflects the response of normal bone to tumor infiltration, the 123I-MIBG scan shows tumor uptake in the left distal femur, left tibia and right femur (arrowheads).

presence of tracer in the bowel eliminates the possibility of biliary atresia, the converse is not true as neonatal hepatitis, bile duct paucity syndrome and total parenteral nutrition (TPN) can cause absent excretion of the radiotracer into the bowel. It is important to premedicate the patient for five days with phenobarbital (2.5 mg kg1
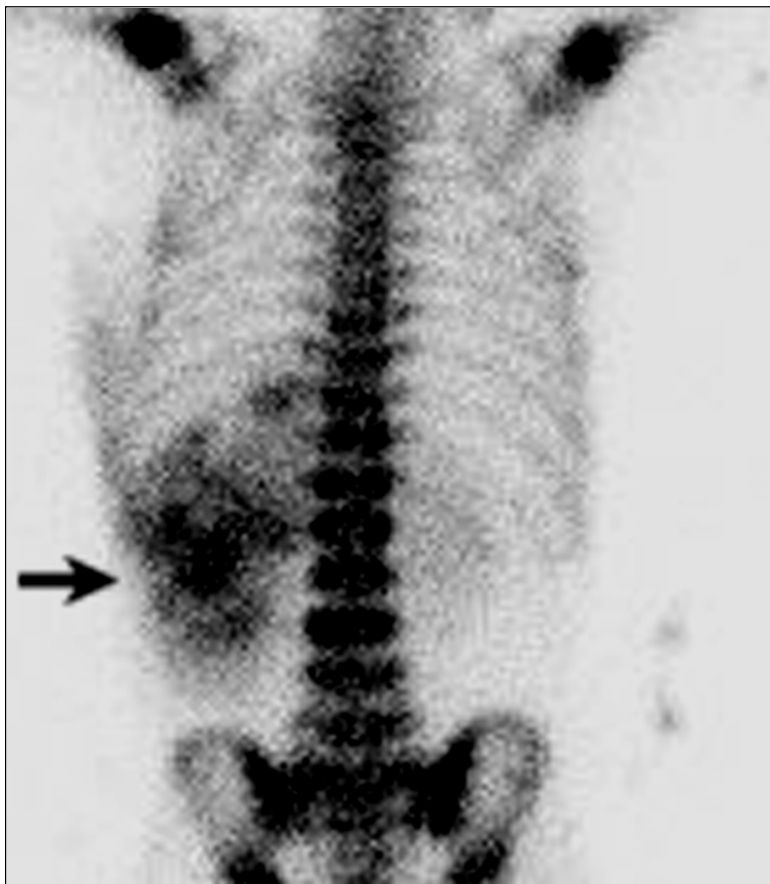
Figure 9. Neuroblastoma. Bone scan showing ^{99m}Tc-MDP uptake by the intra-abdominal primary (arrow).

twice daily for five days) before injecting the biliary radiopharmaceutical. This approach enhances the likelihood of biliary excretion in cases of neonatal hepatitis.

Clinical Role in Rectal Bleeding

The etiology of rectal bleeding in infants and children is often obscure. In a 10 year period from 1952 to 1962, 801 patients were admitted to our institution with a history of rectal bleeding. Sixty-one patients, in whom all examinations were negative, underwent a laparotomy. A Meckel's diverticulum was present in 24, of which 20 contained ectopic gastric mucosa. Meckel's diverticulum is a common congenital anomaly (0.3-3% in mature individuals); however, a relatively small number of these patients (approximately 20%) have ectopic gastric mucosa within their Meckel's diverticulum.
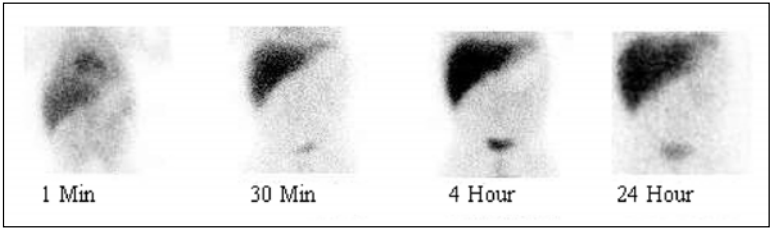
Figure 10. Biliary atresia. Anterior images following the injection of ^{99m}Tc-mebrofenin. While activity accumulates in the liver, the biliary tree is not visualized nor is there excretion into the gastrointestinal tract up to 24 hours. Faint activity in the left abdomen at 4 and 24 hours represents renal accumulation.

^{99m}Tc-pertechnetate accumulates in the mucus producing cells of the stomach. Following injection, there is a rapid increase in radioactivity in the stomach as the pertechnetate is extracted by the gastric mucosa. Renal and bladder activity is present as the kidneys excrete 20 percent of the injected pertechnetate. Early sequential views permit monitoring of the rate of accumulation of pertechnetate in the stomach during the first 15 min. The posterior views at 15 and 30 min demonstrate the location of the renal pelves. Other than these normal structures there should not be any focus of activity throughout the abdomen in the area of the small bowel, although ureters and the iliac vessels are sometimes seen.

In the child with a Meckel's diverticulum, the time sequence of radioactive concentration within the ectopic gastric mucosa parallels that in the normal gastric mucosa of the stomach (Fig. 11). This important feature helps differentiate ectopic gastric mucosa from inflammatory causes, which tend to accumulate the radioactivity at a slower rate, and can help to differentiate an extrarenal pelvis from a Meckel's diverticulum.

Problems can occur in interpreting this study. The early appearance of the radiopharmaceutical in the ureters may simulate a focal lesion posteriorly at the pelvic brim due to a slight holdup at this location while the child is supine. This fades with time and usually disappears during the prone and lateral imaging while on the subsequent anterior views there should not be much activity within the ureter. Occasionally a Meckel's diverticulum may overlie a normal structure containing radioactivity, such as the ureter. In this scenario, the diagnosis of Meckel's diverticulum is difficult unless the bowel moves during the study. If not, a repeat study may show the focal accumulation to have moved. In some patients there is rapid movement of the tracer into the duodenum, which causes confusion; however, the lateral and posterior views help to demonstrate the location of such increased activity. To minimize the excretion of pertechnetate into the lumen of the stomach and to promote retention of tracer by ectopic gastric mucosa, we suggest premedication one hour before the study with ranitidine 5 mg kg^{-1} to a maximum of 50 mg infused in 20 ml of saline over 20 minutes. Any other lesion which contains ectopic gastric mucosa, such as a duplication of the small bowel, can produce the same time sequence but may assume a different shape. Inflammatory bowel disease such as gastroenteritis or
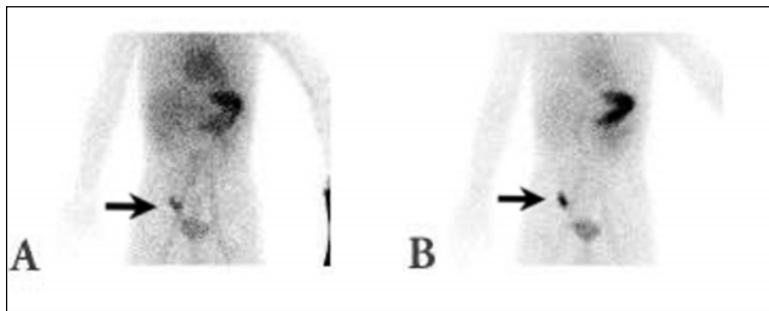
Figure 11. Meckel's diverticulum. Anterior images at (A) 5 minutes and (B) 30 minutes. 99mTc-pertechnetate is seen in the stomach as well as in the Meckel's diverticulum in the right lower quadrant (arrows).

regional enteritis produces abnormal scans but the distribution of activity is diffuse or the time sequence is different from that in the stomach.

Our results suggest that the pertechnetate abdominal scan detects ectopic gastric mucosa with an accuracy of at least 95 percent. This is a significant improvement over previously published reports, which we attribute to the combination of sequential early imaging, multiple views at 15 and 30 min, and the use of ranitidine.

Clinical Role in Genitourinary Disorders

Pelviureteric Obstruction

The child with pelvi-ureteric obstruction is usually evaluated pre- and post-operatively for the degree of relative renal function, absolute renal function and rate of egress of the radioactive urine from the kidneys. Interestingly, many young children with antenatal hydronephrosis have increased renal mass on the side of the hydronephrosis. This has been confirmed in 99mTc-DMSA studies carried out subsequent to the original diuretic washout study. In cases where an obstructive component to urine flow is suspected, a furosemide (Lasix®) stress test is begun between 10 and 30 minutes after the injection of 99mTc-DTPA or 99mTc-MAG3. Intravenous furosemide (1 mg kg^{-1} to a maximum of 20 mg) is given and images recorded for 20 min into the computer. The clearance rate is calculated using the computer. This provides a quantitative method for determining the effect of surgery and/or post-operative complications on the renal drainage system. Normally the time to empty one-half of the collecting system activity (T 1/2) is less than 8-10 min. This value may be higher (up to 20 minutes) in grossly dilated pelves or after surgery. In cases where the T1/2 is above 10 minutes, retention at 20 minutes is calculated (counts at 20 minutes divided by the counts at time '0') (Fig. 12). If the patient has a T1/2 of 20 minutes then the retention value at 20 minutes is 50%. The furosemide washout study appears to reflect the state of urinary flow better than the Whitaker test in the post-operative period.

In children who have had repair of a pelviureteric junction obstruction or reimplantation of the ureters as an antireflux surgical procedure, there may be a significant delay of about six months before there is a change in relative renal func-
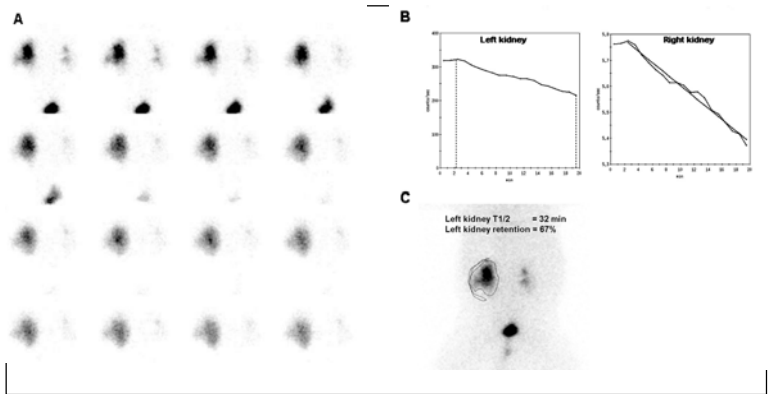
Figure 12. Diuretic renal scan. (A) delayed posterior images, (B) time activity curves of left renal pelvis and right renal pelvis and (C) ROI around left kidney. ^{99m}Tc-DTPA was injected and an initial set of images acquired (not shown). After a delay to allow for filling of the left renal pelvis, furosemide was injected. Visually, the right renal pelvis empties completely and the left renal pelvis partially. The left kidney T 1/2 is 32 minutes with 67% retention at 20 minutes—values that are in the obstructed range.

tion. When evaluated after that time, the kidneys usually function and drain normally.

Several important points have to be made regarding the assessment of diuretic washout curves. Firstly, the T1/2 is invalid when performed on normal kidneys that have already emptied their pelves. Secondly, when there is poor renal function, the kidneys cannot be evaluated as there may be little, if any, response to the furosemide stimulation. Lastly, in large hydronephrotic kidneys of greater than 70 ml capacity, there may be a significant delay in emptying even though there is no mechanical obstruction.

Urinary tract infection

Radionuclide techniques are the primary imaging modalities in evaluating children with suspected upper urinary tract infections (UTI). The direct radionuclide cystogram is the most sensitive method for detecting reflux—a condition which is often a prelude to an upper UTI. Direct radionuclide cystography entails bladder catheterization and instillation of saline mixed with a non-absorbable tracer such as ^{99m}Tc-MDP. The detection rate of reflux is as good as or better than that of the voiding cystourethrogram (VCUG) while the radiation dose is significantly less than that of the radiological study. In addition, the bladder and ureters are constantly monitored throughout both filling and emptying, something not feasible using fluoroscopy. Recently, computer analyzed antegrade voiding cystograms have been studied and appear to be almost as accurate as the retrograde version. In this indirect technique, a renal scan is performed and once the kidneys have emptied and bladder filled, continuous imaging is carried out during voiding. This may become the preferred procedure as it is more physiological. However, due to possible pelvic

17
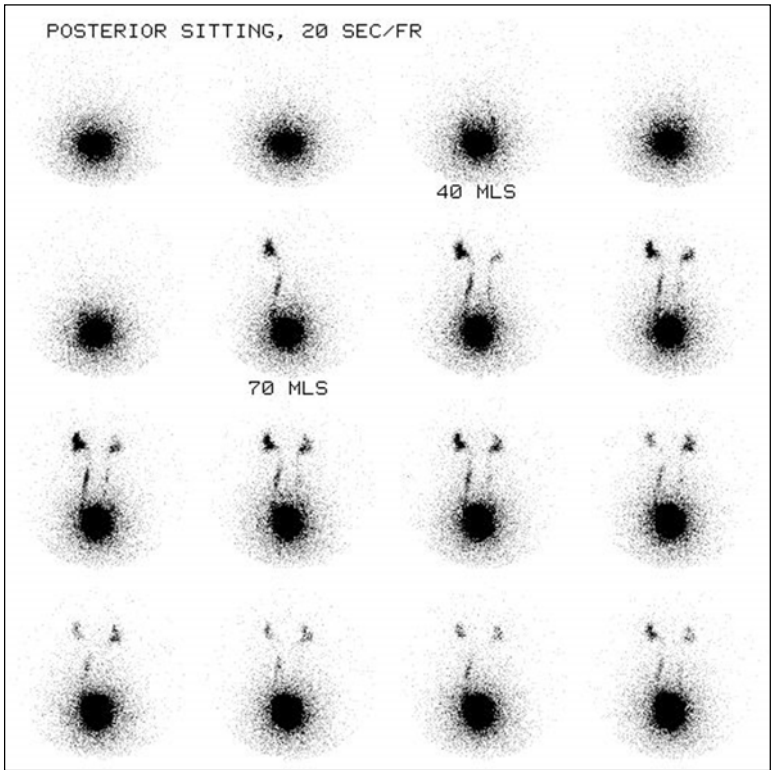
Figure 13. Bilateral vesico-ureteric reflux to the level of the renal pelves is clearly demonstrated.
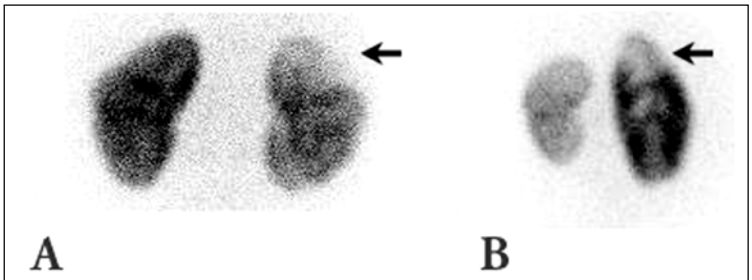
Figure 14. Pyelonephritis. ^{99m}Tc-DMSA study with planar imaging in the (A) posterior and (B) right posterior oblique projections. A defect is seen in the upper pole of the right kidney (arrows).

17
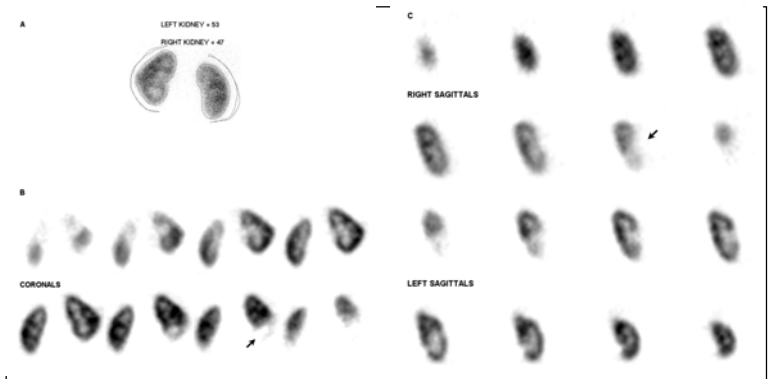
Figure 15. Renal scar. ^{99m}Tc-DMSA scan with (A) planar quantitation, (B) coronal SPECT and (C) sagittal SPECT images. Scarring is seen in the lower half of the kidney (arrows).

dilatation and thus retention of radioactive urine (which could mask reflux), the most widely accepted method is still direct radionuclide cystography (Fig. 13).

If an upper UTI is suspected, the child must be evaluated to determine whether or not acute pyelonephritis is present. If the child is sick enough to be admitted to hospital, then a ^{99m}Tc-DMSA SPECT study should be performed to determine whether or not pyelonephritis is present. Ultrasound should also be performed to see if there is dilatation of the renal pelvis. Finally, a cystogram should be performed to determine if reflux is present. If the child is suspected of having an upper UTI, but is not sufficiently ill to be admitted to hospital, the first study should be a cystogram and if reflux is demonstrated, this should be followed by ultrasound and DMSA studies. Similarly, if there are repeated UTIs at the time of presentation, this patient should be investigated in the same manner.

Acute pyelonephritis appears as a non-segmental single or multifocal reduction in cortical accumulation of the ^{99m}Tc-DMSA (Fig. 14). In the acute phase, it is sometimes difficult to do SPECT imaging and in these cases planar imaging with oblique views is a satisfactory substitute. Subsequent ^{99m}Tc-DMSA scans to monitor the progress of acute pyelonephritis should probably be done using SPECT imaging. Our experience is that while SPECT imaging does not increase the sensitivity of diagnosis in acute pyelonephritis, it is useful in defining the location, size and multiplicity of lesions. A major concern after an episode of acute pyelonephritis is the development of scars. In this case, SPECT imaging appears to be the method of choice. Not only is it easier to define whether scars are present or not, but location and definition are also enhanced (Fig. 15). In addition, it is much easier to determine whether an apparent defect toward the upper pole of the left kidney is a true scar or secondary to splenic impression. Cortical mantle thickness is also much more readily defined with SPECT.
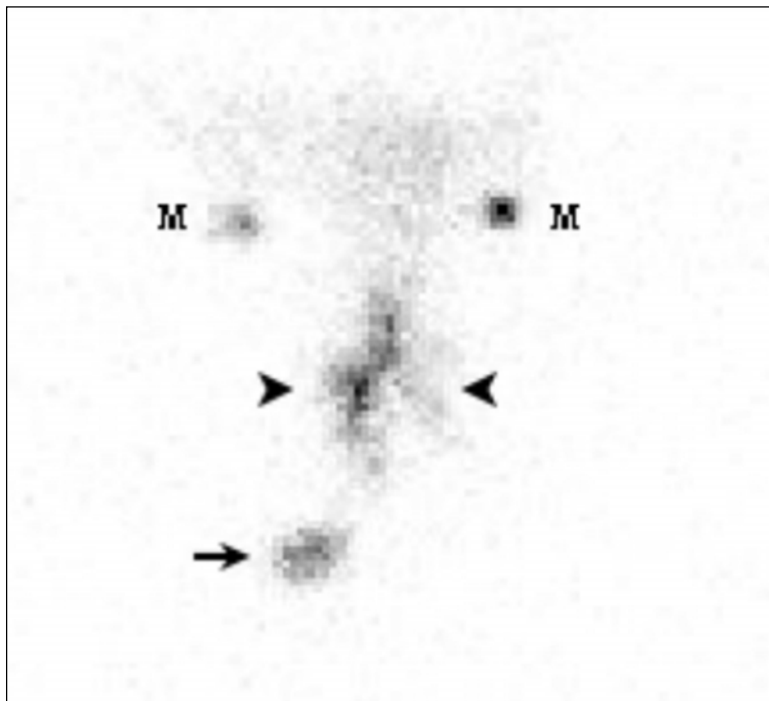
Figure 16. Aspiration demonstrated on a radionuclide salivagram with posterior imaging of the chest. For orientation purposes, markers are placed over the shoulders ('M'). A drop of ^{99m}Tc-MDP is administered orally with subsequent imaging. The "wishbone" shaped uptake in the chest represents aspiration into the trachea and both mainstem bronchi (arrowheads). Normal swallowed activity is seen in the stomach (arrow).

Frequently Asked Questions (FAQ's)

What technique is recommended to detect pulmonary aspiration?

The role of gastroesophageal reflux as the cause of symptoms and more specifically lung disease is well defined. However, it is difficult to determine whether or not the reflux is the cause of the repeated pulmonary infections. In the past the use of ^{99m}Tc-labeled milk to monitor reflux and aspiration in children has been used to see if refluxed gastric contents are aspirated. We have been much more successful using the salivogram, which is performed by instilling a drop of radiotracer (any ^{99m}Tc-radiopharmaceutical will do) in the mouth and letting the child swallow their radioactive saliva. This is carried out three times with dynamic imaging of the thorax and upper abdomen. After the three salivograms, a long exposure (2-3 minutes) image of the thorax is done to detect any aspiration (Fig. 16). This procedure is very

physiological as it depends upon the normal pharyngeal motility. In children with cerebral palsy or other neurological disorder that affects pharyngeal mechanics the study can show the presence of aspiration. It is an easy test to do and interpret.

Additional Reading

1. Conway JJ, ed. Pediatric nuclear medicine. Semin Nucl Med 1993; 23:3 and 23:4.
   These two issues were devoted to pediatric nuclear medicine. Topics of interest include the use of labeled RBCs and WBCs in abdominal disease (Miller JA. 23:219-230), MIBG in children (Gelfand MJ. 23:231-242), scintigraphic classification of Legg-Perthes disease (Conway JJ. 23:274-295), spine pain in children (Sty JR et al. 23:296-320) and bone scintigraphy in child abuse (Conway et al. 23:321-333).
2. Cooper JA. Kidney infection in children: Role of nuclear medicine. In: Nuclear Medicine Annual 1998. Philadelphia: Lippincott-Raven Publishers, 1998:225-246.
   This includes a discussion of radionuclide cystography as well as renal cortical scintigraphy.
3. Mandell GA. Nuclear medicine in pediatric orthopedics. Semin Nucl Med 1998; 28(1):95-115.
   Topics covered include painful hip, the limping preschool child, foot pain in older children, bone infections and back pain in adolescents.
4. Nadel HR. Hepatobiliary scintigraphy in children. Semin Nucl Med 1996; 26(1):25-42.
   A thorough discussion of the technical and clinical aspects of hepatobiliary scanning in children.
5. Piepsz A, Blaufox MD, Gordon I, Granerus G, Majd M, O'Reilly P et al. Consensus on renal cortical scintigraphy in children with urinary tract infection. Scientific Committee of Radionuclides in Nephrourology. Semin Nucl Med 1999; 29(2):160-74.
   A consensus document on technical and clinical issues related to DMSA imaging for urinary tract imaging in children.

Appendix I.   Half-lives and principal emissions from common radionuclides

Nuclide	Half Life	Mode of	Energy Decay*	Abundance
^{133}Xe	5.2 days	β-	101 keV†	90%
		γ	81 keV	37%
^{123}I	13.2 hours	EC	Tellurium x-rays (33 keV)†	
		γ	159 keV	83%
^{131}I	8.02 days	β	192 keV†	89%
		γ	364 keV	81%
^{99m}Tc	6.0 hours	IT	140 keV	89%
^{111}In	2.8 days	EC	Cadmium x-rays (26 keV)†	
		γ	171 and 245 keV	90%, 94%
^{67}Ga	3.3 days	EC	Zinc x-rays (10 keV)†	
		γ	93, 185, 300, and 394 keV	37%, 20%, 17%, 5%
^{201}Tl	3.1 days	EC	Mercury x-rays (80 keV)	100%
		γ	135 and 167 keV	3%, 10%
^{18}F	110 minutes	β	250 keV†	
		γ±	511 keV	200%

*EC = electron capture; IT = isomeric transition, γ± = annihilation photons.
†These emissions are not externally detectable. For β- and β+, energy is given as the average energy and is an indicator of path length.

Appendix 2. Effective dose from common radiologic and nuclear medicine procedures

Radiopharmaceutical (procedure) (mSv)*	Administered Activity (MBq)	Effective Dose (mSv)*
Normal annual background radiation		2.4
Transatlantic commercial airline flight		0.002
Lumbar spine DEXA (bone density)		< 0.01
PA chest x-ray		0.14
Mammogram		0.3
Lumbar spine x-ray		1.7
Single-slice abdominal CT		3.9
Upper GI barium contrast examination		6.7
Cerebral angiogram		7.0
Coronary angiogram		11.0
Coronary angioplasty		20.0
^{99m}Tc-DMSA (renal parenchyma scan)	80	0.7
^{99m}Tc-colloid (liver scan)	100	0.9
^{99m}Tc-MAA (lung perfusion scan)	100	1.1
^{99m}Tc-DTPA (renal function scan)	300	1.6
^{123}I-sodium iodide (thyroid scan)	7.4	1.6
^{111}In-leukocytes (inflammation scan)	40	1.9
^{99m}Tc-pertechnetate (thyroid scan)	185	2.2
^{99m}Tc-HIDA (biliary scan)	150	2.3
^{131}I-MIBG (adrenal medulla scan)	20	2.8
^{99m}Tc-MDP (bone scan)	600	3.5
^{99m}Tc-HMPAO (brain perfusion scan)	500	4.6
^{131}I-sodium iodide (thyroid uptake)	0.2	4.8
^{123}I-MIBG (adrenal medulla scan)	400	5.6
^{18}F-FDG (PET scan)	350	7.0
^{99m}Tc-MIBI (rest and stress myocardial scan)	1,500	12.0
^{67}Ga- gallium citrate (inflammation scan)	150	16.5
^{201}Tl-thallium chloride (myocardial perfusion scan)	80	18.4

* mRem = mSv x 100
Adapted from Johansson L, Mattsson S, Nosslin B, Leide-Svegborn S. Effective dose from radiopharmaceuticals. Eur J Nucl Med 1992; 19(11):933-938.